diagnostics

Special Issue Reprint

Lung Ultrasound

A Leading Diagnostic Tool

Edited by
Marcello Demi and Gino Soldati

mdpi.com/journal/diagnostics

MDPI

Lung Ultrasound: A Leading Diagnostic Tool

Lung Ultrasound: A Leading Diagnostic Tool

Editors

Marcello Demi
Gino Soldati

MDPI

Basel • Beijing • Wuhan • Barcelona • Belgrade • Novi Sad • Cluj • Manchester

Editors

Marcello Demi
Department of
Bioengineering
Fondazione Toscana Gabriele
Monasterio
Pisa
Italy

Gino Soldati
Diagnostic and Interventional
Ultrasound Unit
Ippocrate Medical Center
Lucca
Italy

Editorial Office
MDPI
St. Alban-Anlage 66
4052 Basel, Switzerland

This is a reprint of articles from the Special Issue published online in the open access journal *Diagnostics* (ISSN 2075-4418) (available at: www.mdpi.com/journal/diagnostics/special_issues/Lung_Ultrasound_Leading_Diagnostic_Tool).

For citation purposes, cite each article independently as indicated on the article page online and as indicated below:

Lastname, A.A.; Lastname, B.B. Article Title. *Journal Name* **Year**, *Volume Number*, Page Range.

ISBN 978-3-0365-8741-7 (Hbk)
ISBN 978-3-0365-8740-0 (PDF)
doi.org/10.3390/books978-3-0365-8740-0

Contents

About the Editors

Marcello Demi

Marcello Demi graduated in Electronic Engineering at the University of Florence, Italy, in 1985. Between 1986 and 1987, he carried out research at the Institute of Clinical Physiology (IFC) of the Italian National Research Council, with a grant from A.R.Med. (Association for Medical Research). From 1988 to 1990, he was a research fellow at Tesak Fas Ltd. From 1991 to 2010, he was a senior scientist at Esaote Ltd. and a research fellow at IFC, where he was the head of the Computer Vision Group. From 2002 to 2017, he taught a course on Medical Image Processing at the Faculty of Physics, University of Pisa. He is currently affiliated with the Fondazione Toscana Gabriele Monasterio (FTGM). He has 100 scientific publications and 4 patents under his name, and his research interests focus on filtering schemes inspired by the early stages of biological vision, ultrasound imaging, and lung ultrasound.

Gino Soldati

Gino Soldati graduated in Medicine from the University of Pisa, Italy, in 1985. From 1988 to 1992, he was an Assistant Doctor at the Emergency Medicine Division of the Lucca Hospital, and from 1992 to 2001, he was the Medical Director. From 2001 to 2006, he was the Medical Director of the Diagnostic and Interventional Ultrasound Division at the Valle del Serchio Hospital. In 2006, he was appointed the Director of the Emergency Medicine Division at the same hospital, where he worked in that capacity until 2022. He was a Founding Member of WINFOCUS (World Interactive Network Focused on Critical Ultrasound) and the President of the First National Congress on Ultrasound in Emergency and Critical Care. Since 2003, he has been teaching numerous courses on emergency ultrasound and thoracic ultrasound at the Università Cattolica in Rome, the University of Padova, the University of Pisa, and the University of Catania. He is currently working at the Ippocrate Medical Center. He has more than 100 scientific publications under his name, and his research interests focus on ultrasound imaging and lung ultrasound.

Preface

I remember the first time I met Dr. Soldati. He came into my lab and started talking about resonance and bridges collapsing when soldiers passed by. You can imagine my disorientation; I told Soldati that I had already taken several projects on board and could not commit to a new one. This was not true; I had just finished the analysis of a convincing mathematical model of retinal vision and was looking for new ideas to develop. However, the premises were not good and I declined the offer of collaboration. Obviously, Soldati did not give up and, over the following days, returned several times until he succeeded. I do not remember what clicked in my head, but, surely, curiosity got the better of me and his farfetched idea began to translate into more understandable engineering language. An engineer, however, is a bit like a doubtful St. Thomas, where seeing is believing. Therefore, the first thing to do was to reproduce those strange acoustic signs that Soldati observed in LUS (lung ultrasound) images. Imagine my surprise when, after a few attempts, I managed to reproduce those signs with simple objects (a steel rod and two aluminum blocks) immersed in water.

Since that time, we have never stopped investigating this phenomenon and the latter has slowly revealed its physical nature. Acoustic traps exist in pathological conditions that trap part of the energy of US pulses and gradually return it over time. Ultrasound scanners interpret what comes next as echoes of more distant structures, and this simple fact explains the nature of vertical signs: they are the visible representation of acoustic energy emitted from isolated, non aerated spaces located beneath the pleura. Since then, it has opened up new avenues of investigation because the shape of vertical signs (more appropriately, the response of acoustic traps) varies as the shape, size, and distribution of subpleural, non-aerated spaces vary. In short, a vertical sign is a bit like the signature of an acoustic trap that generates it, similar to footprints left by animals in the woods—we just have to learn to recognize these signs. When we began our collaboration, lung ultrasound was a tool with limited application by pulmonary physicians. Even the physicians at our institute (a medical research institute that is certainly on the cutting edge) practically ignored LUS. Today, the application of LUS is widespread, and medical and nonmedical doctors are collaborating to provide scientific answers to many questions that still arise when observing the aforementioned phenomenon. For this reason, we readily accepted the proposal of *Diagnostics* to be the Guest Editors of a Special Issue on lung ultrasound. We must never get tired of reiterating the importance of collaboration between medical and nonmedical doctors in the development of new diagnostic devices.

Marcello Demi
Editor

diagnostics

MDPI

Editorial

Lung Ultrasound: A Leading Diagnostic Tool

Marcello Demi [1,*] and Gino Soldati [2]

[1] Department of Bioengineering, Fondazione Toscana Gabriele Monasterio, 56126 Pisa, Italy
[2] Diagnostic and Interventional Ultrasound Unit, Ippocrate Medical Center, 55032 Lucca, Italy; soldatigino@yahoo.it
* Correspondence: demi@ftgm.it; Tel.: +39-3334763634

Thoracic ultrasound is an important diagnostic tool employed by many clinicians in well-defined applications. Over the last ten years, many technical, methodological, and clinical questions have been clarified, even though some problems await a response from the scientific medical and non-medical community. Its use is prominently clinical; that is, thoracic ultrasound is a diagnostic tool that combines classical semiotics and diagnostic reasoning. Equally evident is the content of the information provided by this tool, constituting a mix of classical anatomical information and information on the presence, distribution, and shape of acoustic traps that alter the physical state of the lung's surface. There is no doubt that the ultrasound manifestations of so-called interstitial syndrome represent a new field yet to be fully explored given the relationship between the superficial density of the lung when still aerated and under pleural histopathology.

Six research papers and two review papers on the clinical applications of lung ultrasound are presented in this Special Issue. In [1], 101 unselected pulmonary patients were evaluated blindly with ultrasound chest examinations. The obtained results show how chest ultrasound is an effective complementary diagnostic tool for pulmonologists. However, some discordances regarding the usefulness of LUS must also be considered. For example, the value of B-Line scores (BLSs) in guiding fluid management during critical illness [2] showed that daily BLS monitoring did not lead to a different cumulative fluid balance in surgical ICU patients compared to standard care. The B-line score, i.e., the simple counting of B lines, may not be a significant parameter. In [3], the authors show how a simple pulmonary assessment using LUS provides relevant information about pulmonary congestion in hemodialysis patients (outperforming chest radiography) and identifies patients at risk of complications. The authors suggest that dialysis units adopt LUS in their daily clinical practice as a bedside tool not only for fluid status assessment and dry weight prescription but also to prevent intradialytic hypotension and drive ultrafiltration prescription during the whole hemodialytic session. The authors of [4] show how US offers good sensitivity in the detection of pleural abnormalities localized in the costo-phrenic angle (CPA) and how an accurate ultrasound examination of CPA in patients affected by pleural effusion or suspected malignant pleural effusion could assess even millimetric pathological lesions not easily detectable by chest CT scan. In [5], the role of ultrasound in the diagnosis of pulmonary infection, caused by intracellular fungal pathogens or mycobacteria, is analyzed through a systematic review. Lung ultrasound can also be successfully used to examine children [6,7] and newborns [8]. The authors of [6] describe protocols for LUS examinations of children, discuss diagnostic criteria, and introduce methods for the diagnosis and classification of pulmonary diseases commonly encountered in pediatric cardiology. According to the authors' judgement, US is an easy, accurate, rapid, inexpensive, and radiation-free tool for the diagnosis and follow-up of major pulmonary complications in pediatric cardiac surgery, and they strongly encourage its use in routine practice. Cystic fibrosis (CF) lung disease is analyzed in [7]. The aim of the study was to evaluate a newly conceived LUS score by comparing it to the modified Bhalla CT score. The results show that LUS score can be used in the diagnosis and monitoring of CF lung disease in children.

Citation: Demi, M.; Soldati, G. Lung Ultrasound: A Leading Diagnostic Tool. *Diagnostics* **2023**, *13*, 1710. https://doi.org/10.3390/diagnostics13101710

Received: 3 May 2023
Accepted: 8 May 2023
Published: 12 May 2023

In [8], the use of lung ultrasonography and the LUS score is suggested not only for the initial diagnosis but also for the monitoring of newborns with respiratory problems. Lung ultrasonography appears to be a valuable tool for the real-time assessment of improvement in lung status after starting respiratory support. Therefore, it is an aid for the clinician to adjust management and subsequent support accordingly, increasing or decreasing the latter as needed.

Given the temporal context in which this Special Issue has been proposed, contributions regarding COVID-19 were expected. Three review papers and three research papers were submitted and accepted after revision. COVID-19-associated pneumonia can give rise to a variety of pathological pulmonary changes ranging from mild diffuse alveolar damage (DAD) to severe acute respiratory distress syndrome (ARDS), with the latter being characterized by peripheral bilateral patchy lung involvement. These findings have been well described in CT imaging and anatomopathological cases. Consequently, ultrasound artifacts and consolidations are expected signs in COVID-19 pneumonia because edema, DAD, lung hemorrhage, interstitial thickening, hyaline membranes, and infiltrative lung diseases, when they arise in a subpleural position, generate ultrasound findings. In [9], the structure of the ultrasound images in the normal and pathological lung is analyzed. Lung ultrasound is suggested to play an important role in this context due to its high diagnostic sensitivity, low cost, and simplicity of execution. Despite computed tomography being the gold standard of imaging, lung ultrasound is essential in every situation where CT is neither readily available nor applicable. In [10], the role of lung ultrasound (LUS) in the diagnosis and prognosis of SARS-CoV-2 pneumonia is discussed through a comparison with High-Resolution Computed Tomography (HRCT). In [11], the considerable versatility of LUS in diagnosis, the framing of the therapeutic route, and follow-up for SARS-CoV-2 interstitial syndrome is highlighted. In [12], the presence of LUS artifacts after SARS-CoV-2 infection in children were evaluated, and the associations between the time elapsed since infection and symptomatology during acute infection were analyzed. In a pilot study [13] of post-COVID syndrome patients, the usage of lung ultrasound in a follow-up was evaluated by identifying the variation of reverberation artifacts over the course of approximately one year. In [14], the utility of lung ultrasound with respect to neonates diagnosed with COVID-19 is assessed. The authors suggest that lung ultrasound is a useful diagnostic tool that offers a non-invasive, easy-to-use, and reliable method for lung lesion detection in neonates.

The challenges and potentialities correlated with the use of LUS as a leading diagnostic tool are also addressed by one research paper and two review papers. In [15], hospitalist perceptions of barriers to lung ultrasound adoption in diverse hospital environments are analyzed. The hospitalists interviewed perceive LUS as a tool offering important benefits for patients, clinicians, and health systems. However, the time required to master and perform LUS was perceived to be an important barrier to its adoption. In [16], the authors reveal how hand-held ultrasound devices, which are accessible and comparatively easy to decontaminate, could constitute a reliable tool for evaluating peripheral lung diseases. The study highlights how this tool can be successfully employed as an alternative to repeated X-ray examinations for peripheral lung disease monitoring. In [17], the authors show how current communication technologies can be exploited to allow patients to perform US assessments of their lung status.

Moreover, four research papers and two review papers focused their attention on the analysis and understanding of the acoustic information provided by LUS. A preliminary attempt to overcome the oversimplified B-Lines score uniquely based on the number of observed B-lines is illustrated in [18]. This study concerns the application of lung ultrasound for the evaluation of the significance of both vertical artifact changes with frequency and pleural line abnormalities in differentiating pulmonary edema from pulmonary fibrosis. The mechanisms underlying vertical artifacts in lung ultrasound and their potential use for differentiating cardiogenic pulmonary edema from lung diseases are discussed in [19] and in [20]. In [19], the authors recount the theory of the acoustic trap and the basic research

studies supporting the theory. In their contribution, the authors underline how published studies and pilot experiments indicate that the clarification of the relationship between the length and intensity of vertical artifacts and the physical or acoustic composition of sources may be useful for differentiating cardiogenic pulmonary edema from lung diseases. In [20], the author stresses a similar problem. This study highlights an important point: in order to derive further information from the visual inspection of vertical artifacts, the mechanisms that control artifact formation must be identified. In this paper, the link between the visual characteristics of the vertical artifacts (the observed effect) and the distribution of the aerated spaces at the pleural level (the cause) is addressed. Vertical artifacts are frequently seen in a variety of lung diseases, and they vary in length, width, shape, and internal reverberations. The reason for this diversity is still partially unknown and has generated debates between clinicians and physicists. In [21], the most common clinician observations are summarized and explained. The paper underscores the importance of the visual analysis of vertical artifacts along with the importance of strong collaboration between clinicians and physicists. In [22], a finite-element numerical model is proposed to simulate the radio frequency (RF) signals received by a probe when an US pulse is reflected by an acoustic trap that affects a normal lung surface. The RF signals give rise to images of horizontal A-lines and vertical B-lines that are reasonably similar to those observed in real images. The proposed model is useful for studying the impact of a specific lung infiltration on the appearance of LUS images. The authors of [23] describe a systematic working method that was used to comprehend the genesis of the vertical artifacts and their relationship with the surface histopathology of the lung. In this study, the acoustic trap theory is summarized, and the acoustic traps are seen as secondary sources of ultrasound. Moreover, the authors relate that they disagree with the term artifact since it does not adequately represent the informational content of acoustic signs, which, in their opinion, are not artifacts but pathological footprints and anatomical information.

When this Special Issue was proposed, the expected content was stratified into eight topics: (1) the essential physics of lung ultrasound imaging; (2) diagnostic signs provided by lung ultrasound; (3) guidelines in clinical care practice; (4) the biological effects of pulsed ultrasound; (5) theoretical and physical lung modeling; (6) visual and computer-aided image analysis; (7) spectral analysis of radiofrequency (RF) signals; and (8) clinical and open ultrasound platforms. Aside from biological effects and computer-aided image analysis, the received contributions address almost all these topics to varying degrees. On the one hand, many studies warn of the potential biological damage induced by the ultrasound-based examination of the lungs. However, on the other hand, physicians perform lung ultrasound examinations daily, and—to the best of our knowledge—lung damage has never been reported. In most papers reporting damage during lung ultrasound exams, hemorrhages were locally provoked on the lungs of small animals via static long expositions and often by locating the probe directly on the parietal pleura, i.e., by adopting working conditions that are never met in standard lung ultrasound exams. The submitted contributions have demonstrated the solid confidence of physicians to be using a safe [1,3,8,10,13,14] and harmless [8,10,13] imaging device that is free of adverse effects [5] and produces no side effects [12,17]. Computer-aided image analysis is a wide topic ranging from simple algorithms for the detection and counting of vertical artefacts in single-lung US images to convolutional neural networks for an explicit diagnosis of a pathology. Even though many papers in the literature follow this direction, in our opinion, the diagnostic utility of these tools is modest. The manuscripts published in this Special Issue strongly highlight the necessity of understanding the genesis of artefactual information as a unique method of completely and efficiently exploiting this information.

Author Contributions: Conceptualization, M.D. and G.S.; methodology, M.D.; formal analysis, M.D. and G.S.; investigation, M.D. and G.S.; writing—original draft preparation, M.D.; writing—review and editing, M.D and G.S.; supervision, G.S. All authors have read and agreed to the published version of the manuscript.

Institutional Review Board Statement: Not applicable.

Informed Consent Statement: Not applicable.

Data Availability Statement: Not applicable.

Acknowledgments: The authors wish to thank the Fondazione della Cassa di Risparmio di Lucca for its invaluable support.

Conflicts of Interest: The authors declare no conflict of interest.

References

1. Soldati, G.; Prediletto, R.; Demi, M.; Salvadori, S.; Pistolesi, M. Operative Use of Thoracic Ultrasound in Respiratory Medicine: A Clinical Study. *Diagnostics* **2022**, *12*, 952. [CrossRef] [PubMed]
2. Rusu, D.-M.; Grigora, I.; Blaj, M.; Siriopol, I.; Ciumanghel, A.-I.; Sandu, G.; Onofriescu, M.; Lungu, O.; Covic, A.C. Lung Ultrasound-Guided Fluid Management versus Standard Care in Surgical ICU Patients: A Randomised Controlled Trial. *Diagnostics* **2021**, *11*, 1444. [CrossRef] [PubMed]
3. Allinovi, M.; Palazzini, G.; Lugli, G.; Gianassi, I.; Dallari, L.; Laudicina, S.; Gregori, M.; Rossi, F.; Giannerini, D.; Cutruzzulà, R.; et al. Pre-Dialysis B-Line Quantification at Lung Ultrasound Is a Useful Method for Evaluating the Dry Weight and Predicting the Risk of Intradialytic Hypotension. *Diagnostics* **2022**, *12*, 2990. [CrossRef]
4. Conte, E.G.; Smargiassi, A.; Lococo, F. Giampietro Marchetti and Riccardo Inchingolo, Possible Role of Chest Ultrasound in the Assessment of Costo-Phrenic Angle Lesions Prior to Medical Thoracoscopy: A Retrospective Pilot Case Series. *Diagnostics* **2022**, *12*, 2587. [CrossRef] [PubMed]
5. Meli, M.; Spicuzza, L.; Comella, M.; La Spina, M.; Trobia, G.L.; Parisi, G.; Di Cataldo, A.; Russo, G. The role of ultrasound in the diagnosis of pulmonary infection caused by intracellular, fungal pa thogens and mycrobacteria: A systematic review. *Diagnostic* **2023**, *13*, 1612. [CrossRef]
6. Cantinotti, M.; Marchese, P.; Giordano, R.; Franchi, E.; Assanta, N.; Jani, V.; Kutty, S.; Gargani, L. Overview of Lung Ultrasound in Pediatric Cardiology. *Diagnostics* **2022**, *12*, 763. [CrossRef]
7. Ciuca, I.M.; Pop, L.L.; Dediu, M.; Stoicescu, E.R.; Marc, M.S. Aniko Maria Manea and Diana Luminita Manolescu, Lung Ultrasound in Children with Cystic Fibrosis in Comparison with Chest Computed Tomography: A Feasibility Study. *Diagnostics* **2022**, *12*, 376. [CrossRef]
8. Perri, A.; Fattore, S.; D'Andrea, V.; Sbordone, A.; Patti, M.L.; Nobile, S.; Tirone, C.; Giordano, L.; Tana, M.; Priolo, F.; et al. Lowering of the Neonatal Lung Ultrasonography Score after nCPAP Positioning in Neonates over 32 Weeks of Gestational Age with Neonatal Respiratory Distress. *Diagnostics* **2022**, *12*, 1909. [CrossRef]
9. Soldati, G.; Demi, M. What Is COVID 19 Teaching Us about Pulmonary Ultrasound? *Diagnostics* **2022**, *12*, 838. [CrossRef]
10. Lugarà, M.; Tamburrini, S.; Coppola, M.G.; Oliva, G.; Fiorini, V.; Catalano, M.; Carbone, R.; Saturnino, P.P.; Rosano, N.; Pesce, A.; et al. The Role of Lung Ultrasound in SARS-CoV-19 Pneumonia Management. *Diagnostics* **2022**, *12*, 1856. [CrossRef]
11. Maggi, L.; Biava, A.M.; Fiorelli, S.; Coluzzi, F.; Ricci, A.; Rocco, M. Lung Ultrasound: A Diagnostic Leading Tool for SARS-CoV-2 Pneumonia: A Narrative Review. *Diagnostics* **2021**, *11*, 2381. [CrossRef]
12. Altersberger, M.; Grafeneder, A.; Cho, Y.; Winkler, R.; Zwick, R.H.; Mathis, G.; Genger, M. One-year follow-up lung ultrasound of post-COVID syndrome—A pilot study. *Diagnostics* **2023**, *13*, 70. [CrossRef] [PubMed]
13. La Regina, D.P.; Pepino, D.; Nenna, R.; Iovine, E.; Mancino, E.; Andreoli, G.; Zicari, A.M.; Spalice, A.; Midulla, F.; on behalf of the Long COVID Research Group. Pediatric COVID-19 Follow-Up with Lung Ultrasound: A Prospective Cohort Study. *Diagnostics* **2022**, *12*, 2202. [CrossRef] [PubMed]
14. Stoicescu, E.R.; Ciuca, I.M.; Iacob, R.; Iacob, E.R.; Marc, M.S.; Birsasteanu, F.; Manolescu, D.L.; Iacob, D. Is Lung Ultrasound Helpful in COVID-19 Neonates? A Systematic Review. *Diagnostics* **2021**, *11*, 2296. [CrossRef] [PubMed]
15. Maw, A.M.; Ho, P.M.; Morris, M.A.; Glasgow, R.E.; Huebschmann, A.G.; Barnard, J.G.; Metter, R.; Tierney, D.M.; Mathews, B.K.; Havranek, E.P.; et al. Soni, Hospitalist Perceptions of Barriers to Lung Ultrasound Adoption in Diverse Hospital Environments. *Diagnostics* **2021**, *11*, 1451. [CrossRef]
16. Haji-Hassan, M.; Lenghel, L.M.; Bolboacă, S.D. Hand-Held Ultrasound of the Lung: A Systematic Review. *Diagnostics* **2021**, *11*, 1381. [CrossRef]
17. Kirkpatrick, A.W.; McKee, J.L.; Couperus, K.; Colombo, C.J. Patient Self-Performed Point-of-Care Ultrasound: Using Communication Technologies to Empower Patient Self-Care. *Diagnostics* **2022**, *12*, 2884. [CrossRef]
18. Buda, N.; Skoczylas, A.; Demi, M.; Wojteczek, A.; Cylwik, J.; Soldati, G. Clinical Impact of Vertical Artifacts Changing with Frequency in Lung Ultrasound. *Diagnostics*, 2021; 11, 401. [CrossRef]
19. Kameda, T.; Kamiyama, N.; Taniguchi, N. The Mechanisms Underlying Vertical Artifacts in Lung Ultrasound and Their Proper Utilization for the Evaluation of Cardiogenic Pulmonary Edema. *Diagnostics* **2022**, *12*, 252. [CrossRef]
20. Demi, M. On the Replica of US Pulmonary Artifacts by Means of Physical Models. *Diagnostics* **2021**, *11*, 1666. [CrossRef]
21. Demi, M.; Buda, N.; Soldati, G. Vertical Artifacts in Lung Ultrasonography: Some Common Clinician Questions and the Related Engineer Answers. *Diagnostics* **2022**, *12*, 215. [CrossRef]

22. da Silva, F.A.M.; Moreno, E.; de Albuquerque Pereira, W.C. B-Lines Lung Ultrasonography Simulation Using Finite Element Method. *Diagnostics* **2022**, *12*, 2751. [CrossRef]
23. Demi, M. Gino Soldati and Alessandro Ramalli, Lung Ultrasound Artifacts Interpreted as Pathology Footprints. *Diagnostics* **2023**, *13*, 1139. [CrossRef] [PubMed]

diagnostics

MDPI

Article

Operative Use of Thoracic Ultrasound in Respiratory Medicine: A Clinical Study

Gino Soldati [1], Renato Prediletto [2], Marcello Demi [3,*], Stefano Salvadori [4] and Massimo Pistolesi [5]

[1] Ippocrate Medical Center, 55032 Lucca, Italy; soldatigino@yahoo.it
[2] Pulmonology Unit, Fondazione Toscana Gabriele Monasterio and National Research Council, 56124 Pisa, Italy; predile@ftgm.it
[3] Department of Bioengineering, Fondazione Toscana Gabriele Monasterio, 56126 Pisa, Italy
[4] Clinical Physiology Institute, National Research Council, 56124 Pisa, Italy; stefsa@ifc.cnr.it
[5] Department of Respiratory Disease, University of Firenze, 50121 Firenze, Italy; massimo.pistolesi@unifi.it
* Correspondence: demi@ftgm.it

Abstract: For over 15 years, thoracic ultrasound has been applied in the evaluation of numerous lung diseases, demonstrating a variable diagnostic predictive power compared to traditional imaging techniques such as chest radiography and CT. However, in unselected pulmonary patients, there are no rigorous scientific demonstrations of the complementarity of thoracic ultrasound with traditional and standardized imaging techniques that use radiation. In this study 101 unselected pulmonary patients were evaluated blindly with ultrasound chest examinations during their hospital stay. Other instrumental examinations, carried out during hospitalization, were standard chest radiography, computed tomography (CT), and, when needed, radioisotopic investigation and cardiac catheterization. The operator who performed the ultrasound examinations was unaware of the anamnestic and clinical data of the patients. Diffuse fibrosing disease was detected with a sensitivity, specificity and diagnostic accuracy of 100%, 95% and 97%, respectively. In pleural effusions, ultrasound showed a sensitivity, specificity and diagnostic accuracy of 100%. In consolidations, the sensitivity, specificity and diagnostic accuracy were 83%, 98% and 93%, respectively. Low values of sensitivity were recorded for surface nodulations of less than one centimeter. Isolated subpleural ground glass densities were identified as White Lung with a sensitivity of 72% and a specificity of 86%. Only the associations Diffuse ultrasound findings/Definitive fibrosing disease, Ultrasound Consolidation/Definitive consolidation and non-diffuse ultrasound artefactual features/Definitive vascular pathology (pulmonary hypertension, embolism) were statistically significant with adjusted residuals of 7.9, 7 and 4.1, respectively. The obtained results show how chest ultrasound is an effective complementary diagnostic tool for the pulmonologist. When performed, as a complement to the patient's physical examination, it can restrict the diagnostic hypothesis in the case of pleural effusion, consolidation and diffuse fibrosing disease of the lung.

Keywords: diagnosis; lung; respiratory medicine; sonography; ultrasound

Citation: Soldati, G.; Prediletto, R.; Demi, M.; Salvadori, S.; Pistolesi, M. Operative Use of Thoracic Ultrasound in Respiratory Medicine: A Clinical Study. *Diagnostics* **2022**, *12*, 952. https://doi.org/10.3390/diagnostics12040952

Academic Editor: Chao-Min Cheng

Received: 10 March 2022
Accepted: 8 April 2022
Published: 11 April 2022

1. Introduction

Thoracic ultrasound (US) is a recently developed diagnostic tool [1,2]. Most literature deals with cardiogenic pulmonary edema, ARDS, bronchiolitis in children and pneumonia in adults [3–5]. Few studies, however, are aimed at studying focal, multifocal and diffuse lung diseases providing information on pleural signs, pulmonary artifacts morphology and pathological changes such as nodules and consolidations along with their surface distribution. Moreover, many works in the past based their attention on the artifacts numerical estimate for scoring the severity of a pathological state, but, to our knowledge, a rather limited number of clinical and technical papers investigated the meaning of their morphology [6–13].

This limits the ability to characterize and differentiate cardiac from pleuro-pulmonary pathological conditions, especially when these disorders overlap. It is worth noting that both pulmonologists and cardiologists hold the same view as regards thoracic ultrasound semeiotics in that it is mostly based on the classical "wet and dry" lung dichotomy. This work aims to clarify the diagnostic role of thoracic ultrasound on an unselected population of patients with pulmonary diseases and to provide clinical support to the hypotheses on the genesis of pulmonary ultrasound artifacts recently suggested [9,14,15]. The following points will be discussed: (1) the practical role of thoracic ultrasound, seen as a specific tool of the pulmonologist for "visiting" the patient and to restrict the field of the diagnostic options; (2) the associations between artefactual and anatomic ultrasound signs and CT findings; (3) the semeiotics and meaning of pulmonary artifacts based on the potential genesis of pleuro-pulmonary signs.

2. Materials and Methods

2.1. Clinical and Instrumentale Evaluation

We evaluated 101 subjects who had been admitted from November 2017 to December 2018 to the Pulmonary Medicine Unit of the Gabriele Monasterio Tuscany Foundation of Pisa, with 103 ultrasound chest examinations. Patients were studied in the Pulmonology Unit, either as an emergency or as a programmed hospitalization, on the basis of their pathological conditions and/or the onset of respiratory symptoms, such as recent dyspnea and chest pain in order to complete a diagnostic and therapeutic work-up. The exclusion criteria were pulmonary or cardiac acute decompensation during the evaluation, acute respiratory distress syndrome, heart and valvular diseases, fever, myocardial infarction, pneumothorax and thoracic trauma. All other pulmonary pathological conditions in patients older than 18 years were included. During the ultrasound examination all patients were in stable clinical conditions.

Every patient was informed in advance about the research content, and they provided signed informed consent. The investigation was authorized by the Institute's Ethics Committee CEAVNO (study number 1089, approved on 30 January 2017). All patients completed a thorough respiratory and cardiac evaluation by spirometry, gas exchange, single breath diffusion capacity, chest X-ray, CT scan, and perfusion lung scan evaluation. Chest CT findings were considered the gold standard for the anatomic evaluation of pleura and lung parenchyma. All chest high-resolution CT examinations were performed at our hospital's Department of Radiology using standard protocol. No intravenous contrast material was administered. CT images were evaluated by experienced radiologists and by a chest physician (RP) who is board certified in Radiology, using the traditional radiological lexicon. Discordance between radiologists and the chest physician were resolved by a consensus CT reading. The final diagnosis was drawn up by the chest physician following a thorough examination of the clinical and instrumental data.

The ultrasound examination was carried out by a single operator (GS) with more than twenty years' experience in chest ultrasound. The operator who performed the ultrasound examinations was unaware of the anamnestic and clinical data of the patients. We used a Toshiba Aplio V machine, equipped with convex (3.5–5 MHz) and linear (5–9 MHz) probes. Harmonic imaging was not used. With patients in a sitting position, posterior, basal, paravertebral and apical scans were obtained. Frontal and lateral scans, including supraclavicular regions were obtained in a supine position. Findings such as artifacts, consolidations, nodules, effusions, diaphragmatic position and kinetics were defined according to semeiotics described in the literature [1–3,5,8]. Table 1 lists the findings and the possible generic diagnoses which can be expected with the ultrasound and CT examination, respectively. These characteristics were recorded and stored in a database. The location of ultrasonographic findings on the thoracic surface was described for each patient through a graphic scheme with differently colored landmarks (Figure 1), to obtain a topography comparable to CT images.

Table 1. Observed/registered findings and possible generic diagnoses expected with the ultrasound and CT examination.

Ecographic Findings and Assumed Diagnosis	CT Findings and Assumed Diagnosis
Vertical artifacts	Septal thickening
B-lines	Reticular thickening
Hypermirror	Consolidation
Consolidation	Tree-in-bud
White Lung	Ground glass
Pleural effusion	Pleural thickening
Micronodules	Pleural effusion
Pleural thickening	Surface micronodules
Diaphragm kinetics	
Emphysema	Lung cancer
Focal interstitial syndrome	Pleural cancer
Diffuse interstitial syndrome	Diffuse interstitial syndrome
Cardiogenic contribution	Cardiogenic pulmonary edema
	Emphysema

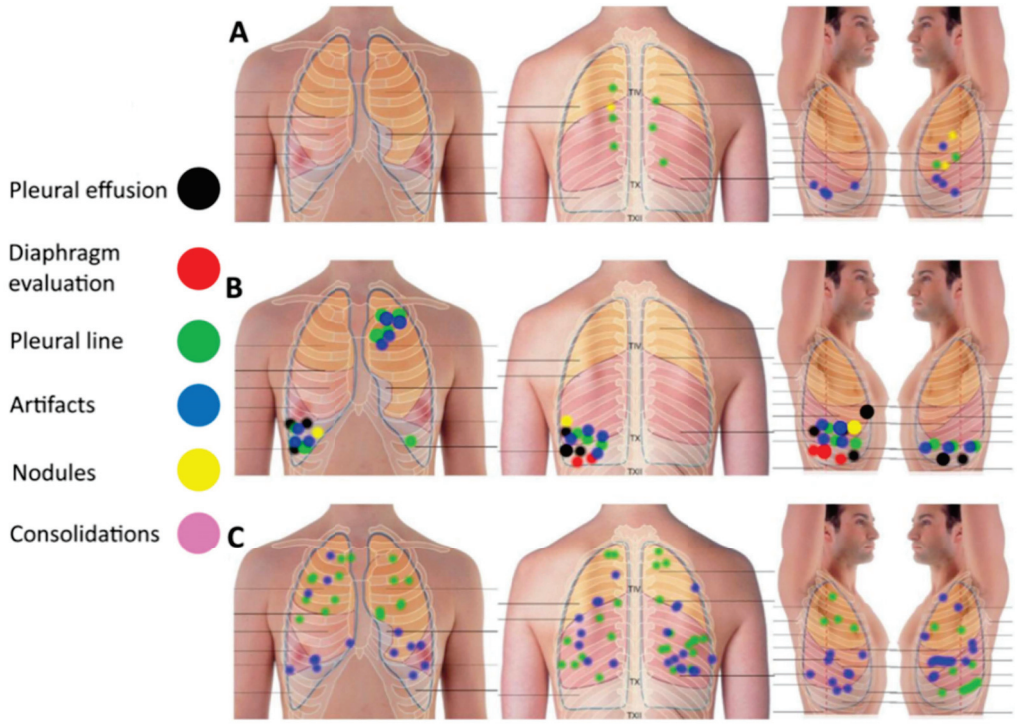

Figure 1. Example of the location of ultrasound (US) findings on the thoracic surface through a graphic scheme with differently colored landmarks, to obtain a superficial topography comparable to CT images. Three schemes of three different patients are shown in A, B and C.

Pleural effusions were identified on the basis of their classical ultrasound signs. Patients with pleural effusion were not considered as belonging to a specific subgroup since the effusion may be associated with different pathological conditions.

The distinction between pneumogenic and cardiogenic artifacts was made according to their structure and relative distribution and homogeneity along the pleural line [16]. Only the brightest artifacts with characteristics of full screen extension, pleural-point origin with or without internal modulation were considered "B-lines" [16,17]. All other artifacts were generically referred to as "vertical artifacts". White Lung [9,16] was identified as a focal or multifocal artifact characterized by an undifferentiated echogenic background, with the absence of A-lines and without evidence of vertical artifacts.

The presence of subpleural nodularities (consolidations with relatively defined contours with maximum size less than or equal to 1 cm) was simply reported. Subjects with dominant consolidations, single or multiple, mono or bilateral consolidations with a diameter greater than 1 cm, were assigned to a specific subgroup.

The term hypermirror, not mentioned in the literature, was arbitrarily introduced. It indicates a finding that covers at least a third of a lung field characterized by a regular pleural line and by the absence of vertical artifacts and B-lines. Its typical appearance is that of a pronounced mirror effect with an artefactual replica of the pleural line (two replicas at least). In presence of emphysema, the air content of the subpleural lung layers increases and, as a consequence, the reflection coefficient at the pleural plane also increases giving rise to more pronounced replica and mirror effects. Moreover, a suboptimal configuration of the diaphragm occurs in emphysema and the demand imposed by the pathology on this muscle increases due to both hyperinflation and air-flow obstruction. In certain types of emphysema (e.g., panlobular emphysema), a lower position and reduced dynamics of the hemidiaphragms is also expected. The hypermirror finding, along with both an objective reduction of the maximum diaphragmatic excursion (less than 3.5 cm in the middle axillary to the maximal inspiration in sitting position) and lowered hemidiaphragms, was considered as a sign of emphysema.

Based on the results of the ultrasound examination, the sonographer blindly assigned each subject to one of five groups (Table 2). This classification is based on the recognized non-specificity of many ultrasound signs. Therefore, it is more useful to refer to ultrasound patterns (typology and association of signs, topography, extension) rather than to single uncoordinated signs. While the terms "consolidation" and "nodule" have a real meaning (tissue without air), variable configurations of the artifacts assume a diagnostic power only through their distribution (focal, multifocal and diffuse). The groups were as follows:

Table 2. Characteristics of patient's subgroups.

Group	Male	Mean Age (y+/−sd)	Female	Mean Age (y+/−sd)	Total
No pathological findings	3	66+/−10	4	53.5+/−8.3	7
Limited findings	18	70.8+/−7.4	18	71.7+/−12.8	36
Diffuse findings	11	75.9+/−8.9	6	72.8+/−9.6	17
Consolidations	16	73.6+/−11.4	8	76.5+/−4	24
Non-diffuse features	9	73.2+/−8.4	10	63.6+/−16.3	19

Group 1: No pathological findings.

Group 2: Limited findings. Monofocal or multifocal artifacts, with or without nodularity (small consolidations abutting the pleura with a diameter $\leq$ 1 cm). This group was characterized by focal or multifocal findings whose characteristics did not allow us to hypothesize a specific pathological condition.

Group 3: Diffuse findings. Pathological artefactual signs (B-lines and/or vertical artifacts) spread bilaterally over two thirds of the lung fields.

Group 4: Consolidations. Single or multiple, mono or bilateral consolidations with a diameter > 1 cm, showing variable conditions of internal ventilation. The presence of vertical artifacts or perilesional White Lung was considered a related finding. Patients from other groups may present consolidations or nodules, but non-dominant with respect to other findings.

Group 5: Non-diffuse features. Presence of pathological artifacts, with or without nodularity (consolidations < 1 cm), configuring a pathological picture which extended up to two thirds of a pulmonary field.

2.2. Data Analysis

The anthropometric and clinical data of the patients including history, evolution and outcome US, CT findings, and other instrumental findings were coded and saved in a database. Descriptive statistics were expressed as mean +/− SD or as numbers with percentages. CT images with radiological descriptions were stored together with video clips from the ultrasound examinations and with the surface maps (Figure 1). The sonographer (GS) was unaware of any clinical and instrumental data and had access only to the ultrasound database. Both the clinical management and the organization and visualization of the clinical and CT database was assigned to and carried out by a single operator (RP). The attribution of patients to the US groups, described in Section 2.1, was carried out independently and blindly by the sonographer. Sonographic signs were interpreted and classified by the sonographer while the clinician was precluded from accessing the ultrasound database.

The primary endpoint of this study was to investigate the role of pattern-based chest ultrasound on an unselected population of patients admitted to a pulmonology department and undergoing a blinded ultrasound examination.

The secondary endpoint was to evaluate potential associations between established ultrasound findings and CT, and to discuss the role of selected findings as acoustic information related to the subpleural structure of the lung as seen in CT [9].

In order to evaluate the endpoints in the simplest way, two different evaluations were made:

(a) After a complete diagnostic work up, the subjects were divided into four groups of definitive pathologies: consolidative pathology, diffuse fibrosing disease, COPD, and vascular pathology (pulmonary hypertension, embolism). Descriptive analysis was performed and expected frequencies were reported within the contingency table of the distribution of "Group" by "Definitive pathology". To evaluate the structure of the association of the two variables, adjusted residuals were calculated for each cell, and p-values were adjusted as described by Beasley and Schumacker [18] in order to take multiple comparisons into account. A p-value < 0.00256 was considered statistically significant.

(b) Sensitivity and specificity of the ultrasound examination findings (vertical artifacts and B-lines, White Lung areas, consolidations, nodules) were calculated versus interstitial changes (septal and or reticular), ground glass density, consolidations and nodularities, respectively, using CT as the reference test. The specificity of the tests was defined as TN/(TN + FP), the sensitivity as TP/(TP + FN), the positive predictive value (PPV) as TP/(TP + FP), and the negative predictive value (NPV) as TN/(TN + FN).

3. Results

A total of 101 subjects, 55 males and 46 females ranging in age from 33–90 years, with an average age of 71, were evaluated with 103 ultrasound acquisitions. Two subjects had two acquisitions each. The chest ultrasound was carried out within 4 days of admission. Each ultrasound examination lasted no more than 15 min (range 8–15 min). A chest CT was carried out within 2 days of the ultrasound examination. The patients' subgroups are illustrated in Table 2. Seven subjects were free from pathological ultrasound findings and their final diagnoses are listed in Table 3. Table 4 illustrates the associations between the groups of the enrolled patients and the four groups of final pathologies described in Section 2.1. Only the association Diffuse findings/Fibrosing disease, Consolidation/Consolidation and Non-diffuse features/Vascular pathology (pulmonary hypertension, embolism) were statistically significant with adjusted residual of 7.9, 7 and 4.1, respectively.

Table 3. Final diagnosis in seven patients free from pathological ultrasound findings.

Patient	Sex	Final Diagnosis
1	F	Pulmonary Hypertension
2	F	Dyspnea in bronchial hyperreactivity
3	F	Syncope in a patient with susceptibility to the development of vaso-depressant syncopal episodes in response to prolonged orthostasis.
4	M	Type 1 respiratory failure secondary to right-left shunt from patent foramen ovale type ostium secundum
5	M	Type 1 respiratory failure of a nature to be determined with right saphenous small thrombophlebitis
6	F	Bronchitic exacerbation in patient with bronchiectasis
7	M	Respiratory insufficiency in pulmonary consolidations under diagnostic definition, resolved at the time of examination

Table 4. Associations between the groups of the patients according to the initial sonographic selection and the four groups of final pathologies described in methods.

Group		Definitive Pathology				Total
		Consolidation	COPD	Chronic Fibrosing Disease	Vascular Pathology	
Consolidations	Count	22	1	0	1	24
	Expected Count	7.9	6.3	3.5	6.3	
	% Within Group	91.7%	4.2%	0.0%	4.2%	
	Adjusted residual	7.0	−2.8	−2.3	−2.8	
Diffuse Findings	Count	0	3	13	1	17
	Expected Count	5.6	4.5	2.5	4.5	
	% Within Group	0.0%	17.6%	76.5%	5.9%	
	Adjusted residual	−3.2	−0.9	7.9	−2.1	
Limited Findings	Count	8	15	2	11	36
	Expected Count	11.9	9.4	5.2	9.4	
	% Within Group	22.2%	41.7%	5.6%	30.6%	
	Adjusted residual	−1.7	2.6	−1.9	0.7	
No pathological ultrasound findings	Count	1	4	0	2	7
	Expected Count	2.3	1.8	1.0	1.8	
	% Within Group	14.3%	57.1%	0.0%	28.6%	
	Adjusted residual	−1.1	1.9	−1.1	0.1	
Non-diffuse features	Count	3	4	0	12	19
	Expected Count	6.3	5.0	2.8	5.0	
	% Within Group	15.8%	21.1%	0.0%	63.2%	
	Adjusted residual	−1.8	−0.6	−2.0	4.1	
Total	Count	34	27	15	27	103
	% Within Group	33.0%	26.2%	14.6%	26.2%	

Thirty-nine pleural effusions were identified in 28 subjects (27.1%), 19 of which were minimal effusions (48.7%), i.e., only visible in the lateral costophrenic sinus. The effusions were bilateral in 11 patients (39.2% of the subjects with pleural effusion). All subjects without significant lung findings (Group 1) did not show any effusion. Among those with limited or monofocal findings (Group 2), diffuse findings (Group 3), consolidations (Group 4) and non-diffuse artefactual syndrome (Group 5), effusions were detected in 6, 2,

14 and 6 patients (17%, 12%, 64% and 17% of the subjects of each group), respectively. In pleural effusions, ultrasound showed a sensitivity, specificity and diagnostic accuracy of 100%.

Vertical artifacts and B-lines were detected in patients of all groups except in patients in Group 1. Furthermore, when considering the entire population studied, while the artifacts (B-lines and vertical artifacts) were present in 78 patients (75.7%), B-lines were present in 38 subjects only (36.8%). Only one patient showed B-Lines exclusively without vertical artifacts. All the other subjects with B-lines also showed vertical artifacts. Vertical artifacts in subjects without B-lines were present in 40 patients (52.2% of the entire population with artifacts).

B-lines were detected in all six patients whose CT findings were compatible with subpleural hydrostatic septal thickening. The sensitivity and specificity of B-lines in subjects with pulmonary edema was 100% and 68% respectively, as 31 subjects showed B-lines in the absence of CT findings of subpleural septal thickening.

Consolidations were detected in CT in 34 subjects and all subjects in Group 4 showed confirmation of the findings (Table 3). Six patients in Group 2 with CT consolidations turned out to be ultrasound false negative: three patients showed lesions which did not reach the pleura (two neoplasms and one inflammatory lesion) and three subjects showed findings which were compatible with atelectasis. Among the detected consolidations, a total of 11 neoplasms were diagnosed (10 lung tumors and one mesothelioma), 9 of which were visible on the ultrasound images. Mesothelioma was correctly detected.

In consolidations, the sensitivity, specificity and diagnostic accuracy were 83%, 98% and 93% respectively. Four of the six false negatives occurred in patients with central and non-subpleural lesions which were not visible on the ultrasound images. Sensitivity increases to 88% by excluding these patients.

Nodules were detected in 23 patients. CT showed superficial nodules in 55 patients. Sensitivity and specificity of ultrasound was 45% and 78%, respectively.

White Lung was detected in all groups except in Group 1. In order to compare isolated White Lung with CT ground glass findings, we selected those subjects who showed the White Lung artifact only (subjects without pleural effusion, consolidations or nodulations). Subjects with CT findings of ground glass not surfacing the pleura were not considered due to the limitation of ultrasounds to detect them. Among the 23 subjects whose CT showed subpleural isolated ground glass, 18 of them had corresponding areas of ultrasound White Lung. Sensitivity and specificity of ultrasound in detecting superficial ground glass were 72% and 86%, respectively. Positive and negative predictive values were 76% and 94%.

Of the forty-four subjects who were diagnosed with COPD or asthma, only 2 subjects did not show ultrasound signs. Forty-two subjects showed a variety of signs and were therefore included in the other groups (58.3% in Group 2, 29.4% in Group 3, 39.1% in Group 4 and 26.3% in Group 5).

The tree-in-bud CT pattern was detected in 13 subjects belonging to Groups 2 (7 subjects), 3 (2 subjects), 4 (2 subjects) and 5 (2 subjects), respectively. Among them, 4 subjects showed focal B-lines and vertical artifacts, 8 patients showed nodulations or microconsolidations.

The association of a hypermirror pattern with lowered hemidiaphragms and a reduction of the maximal diaphragmatic inspiratory excursion, showed a sensitivity, specificity and diagnostic accuracy of 45%, 96% and 86%, respectively, for the identification of subjects with pulmonary emphysema detected with CT.

Figures 2–6 show some examples of the main echographic signs which have been evaluated in this study.

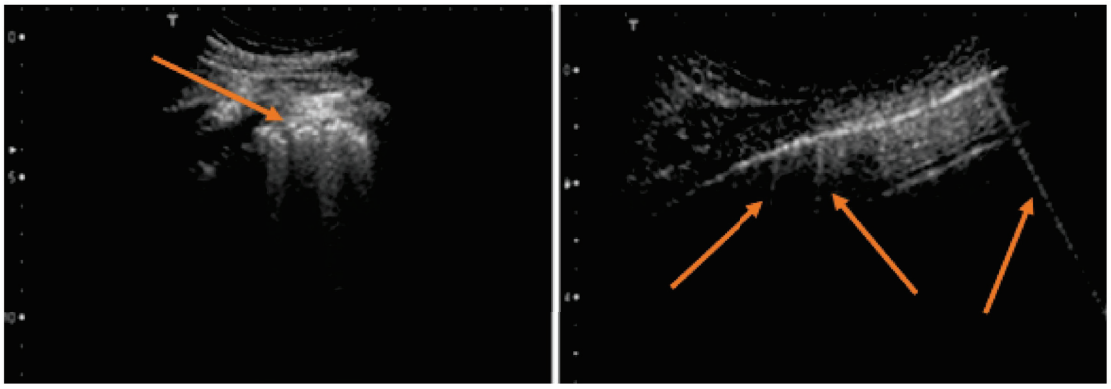

Figure 2. The image on the left shows vertical artifacts in a subject with idiopathic pulmonary fibrosis with a strongly irregular pleural line (red arrow). The image on the right shows B-lines (red arrows) with a regular pleural line in a subject with heart failure.

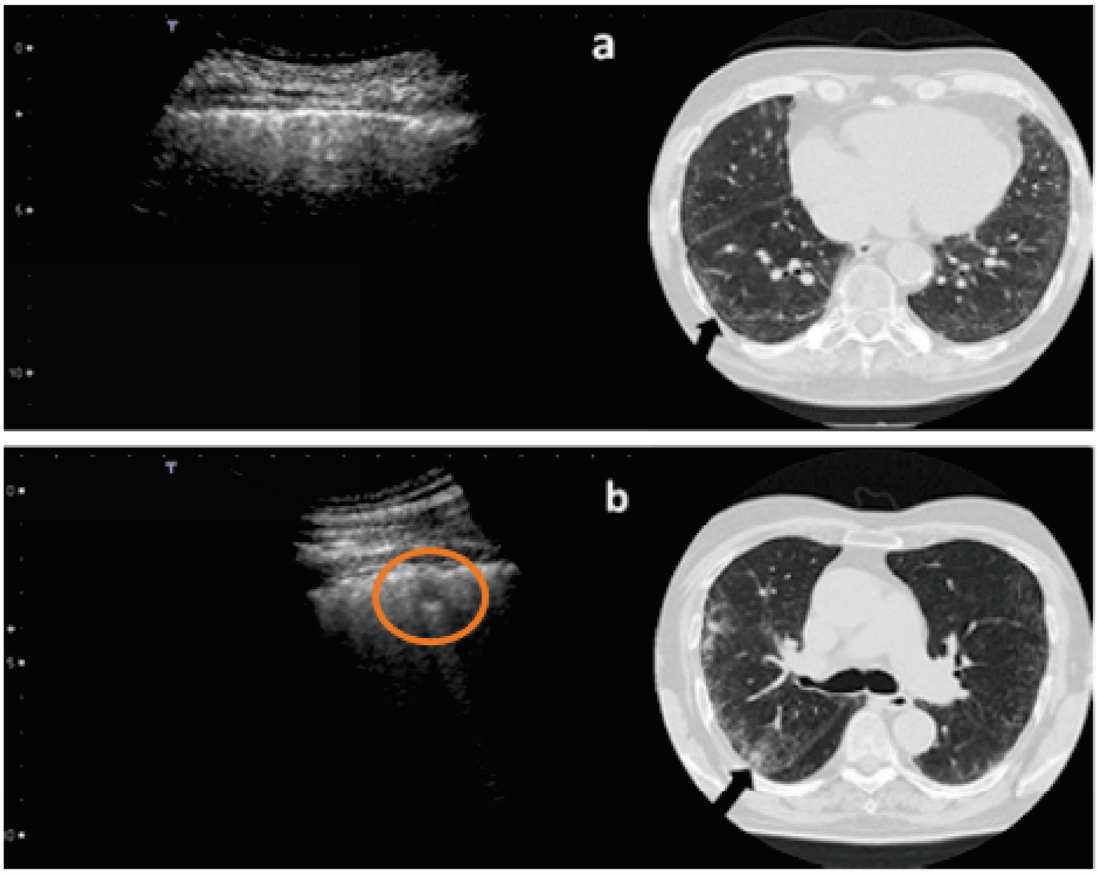

Figure 3. Ultrasound and CT scans of two patients with fibrosing lung disease. The black arrows indicate the position of the probe on the chest. The two CT and ultrasound scans are coplanar. In (**a**) a minor fibrotic involvement is present while in (**b**) a small nodulation (red circle) is evident.

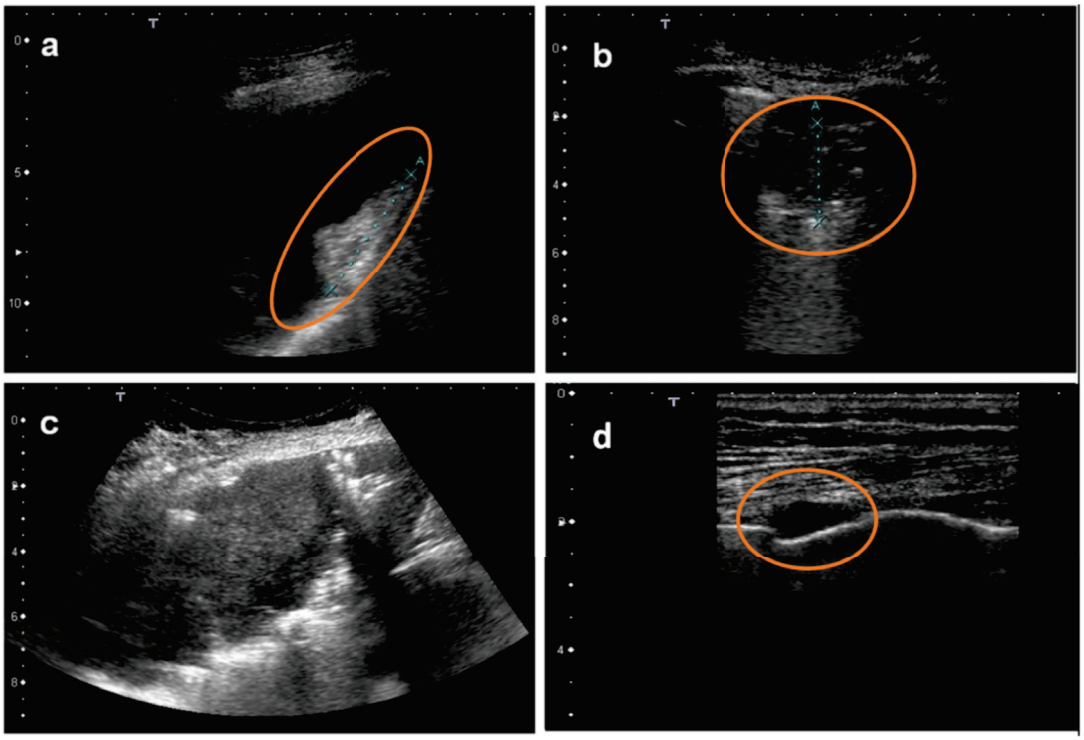

Figure 4. Image (**a**) shows an ultrasound scan of a patient with large pleural effusion and a coarse vegetation on the diaphragmatic surface (metastatic carcinoma in red circle). Image (**b**) shows lung consolidation with poor ventilation (pneumonia in red circle). Image (**c**) shows a large lung consolidation (lung cancer). Image (**d**) shows pleural neoplasia (mesothelioma in red circle).

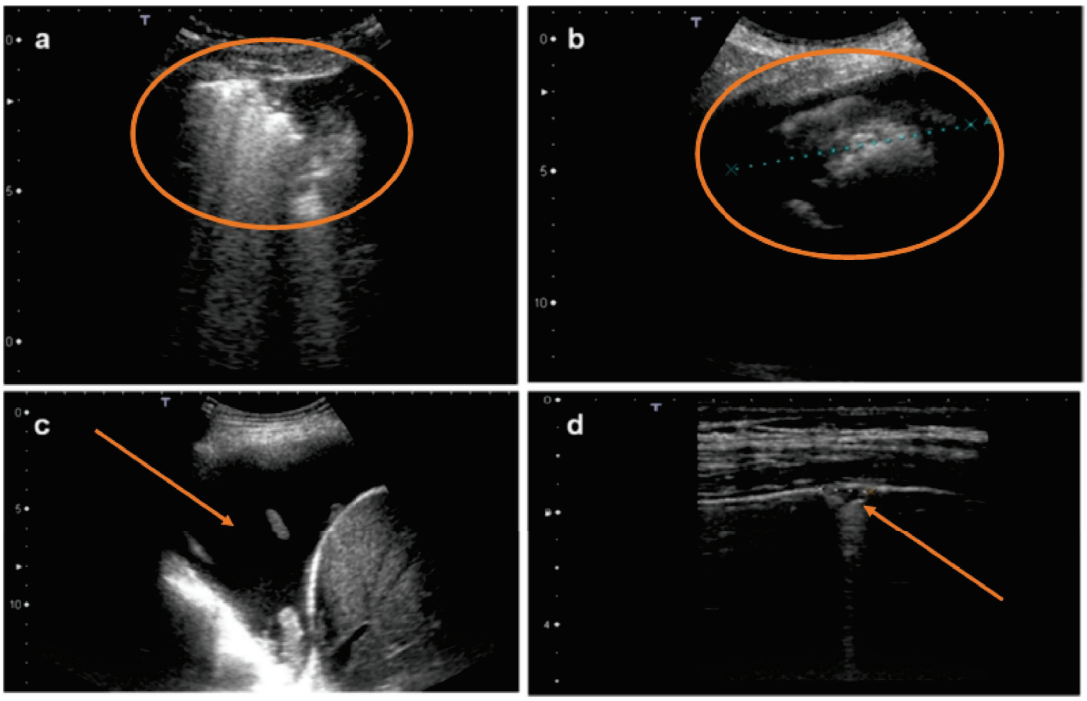

Figure 5. Image (**a**) shows lung consolidation with associated artifacts in a red circle (pneumonia). Image (**b**) shows lung consolidation with associated pleural effusion (lung cancer in red circle). The red arrow in image (**c**) shows a large finely corpuscular pleural effusion (mesothelioma). The red arrow in image (**d**) shows a single nodule emerging on the pleural surface with a regular pleural line.

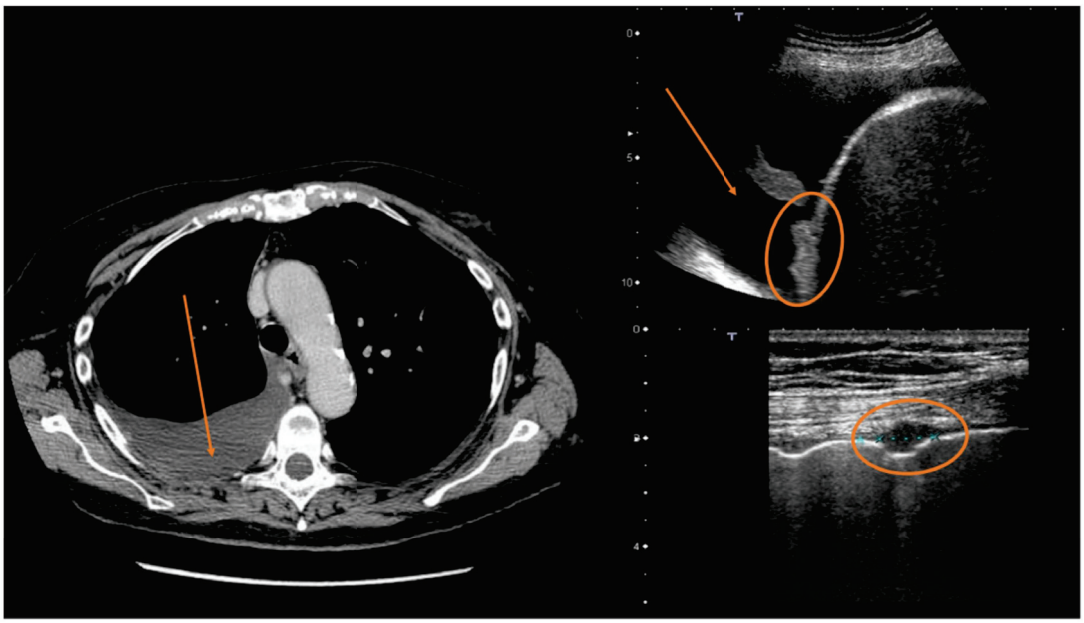

Figure 6. Ultrasound scans of a patient with mesothelioma. On the left, the CT scan shows only pleural effusion (red arrow). The upper right ultrasound scan clearly shows the pleural effusion (red arrow) and diaphragmatic nodulations (red circle). The lower right ultrasound scan shows a parietal pleural nodule (red circle).

4. Discussion

Pleuro-pulmonary ultrasound is widely reported in scientific literature. Although ultrasound semeiotics of pleural effusion and pulmonary surface consolidations are widely described and accepted [2], the sonographic patterns in non-consolidated pathological conditions are still under investigation and, in general, limited to the description of A-lines and (in quantitative terms) B-lines [19,20].

Most of the B-line literature regards cardiology patients with heart failure. In this context, the results are generally unique, and the B-lines were found to correlate with the increase of the extravascular pulmonary water and the severity of the pathology.

Recently, the increased interest in the ultrasound signs in ARDS, interstitial pulmonary diseases and COVID-19 pulmonary involvement has raised the need for a better classification of the artifacts to increase their specificity [15,16,21,22]. Some observations point out the great variability of the artifacts and suggest the use of their morphology and distribution pattern for a preliminary tissue characterization of the lung surface [10,11,23].

However, most of the published studies regard the settings of Emergency Medicine, Intensive Care, Cardiology, Pediatrics and Rheumatology. Only a few studies are available on Pulmonary Medicine patients [6,22,24]. Many patients have been selected according to specific pathological conditions (pulmonary edema, ARDS, pneumonia, bronchiolitis, collagen diseases) and to single sonographic findings. A few publications address the application of ultrasounds as an initial blind test in patients with the several pleuro-pulmonary pathological conditions encountered in a Respiratory Medicine Unit.

This paper evaluates an unselected series of non-critical patients admitted to a Pneumology Unit, and endeavors to represent the clinical workload of a pulmonologist's daily diagnostic activity. The great majority of our patients had more than one pathological condition, even though their prevailing clinical condition was of pulmonary origin.

By fixing an initial pattern evaluation of ultrasound findings (patient groups 1 to 5), it is possible to narrow down the diagnostic possibilities. This is particularly true for diagnosing consolidations and fibrosing lung diseases, appearing as deaerated lesions and diffuse pneumogenic artifacts, respectively [6,22].

Conversely, the absence of ultrasound signs, or the presence of artifacts with limited monofocal or multifocal distribution, with or without nodularity or non-diffuse artefactual features, remains non-specific outside a clinical context [25].

The association between non-diffuse features and vascular pathology (pulmonary hypertension, embolism) achieves statistical significance, but does not find a clear pathogenetic explanation. This probably merely reflects the non-specificity of non-diffuse pulmonary artifacts or the coexistence of multiple pathologies in the same patient.

When chest CT is used as a reference standard, pleuro-pulmonary sonography shows high accuracy for the detection of pleural effusion and pneumonia (sensitivity and specificity of 93–94% and 96–98% respectively) [5,26–29].

Our experience agrees with these data. The best diagnostic accuracy of ultrasound, compared with a set of diagnostic procedures including CT, was obtained for the detection of pleural effusions. Moreover, ultrasound is a useful tool for the evaluation of lung consolidations with a sensitivity of 83% and a high specificity (98%).

Its role is confirmed in pneumonia, atelectasis, inflammatory consolidations and neoplasms when they surface the pleura. 11 cases of pneumonia in 12 patients (91.6%) were correctly identified. Overall, 9 neoplastic lesions out of a total of 11 neoplasms (10 pulmonary and one pleural neoplasia) were detected by ultrasound since two of them (two pulmonary neoplasms) did not surface the pleura. Five neoplastic subjects presented pleural effusion that was fibrinous in two cases and corpuscular in one. Atelectasis was diagnosed by ultrasound in 9 cases, and all were confirmed by CT. Atelectasis was associated with neoplasia in two patients and to effusion or hypoventilation in the remaining 7 patients.

The performance of the US for cancer detection is limited only because US can show only the neoplasms which surface the pleura. The same problem exists for the definition of many pulmonary nodularities.

Lung artifacts (vertical artifacts and B-lines) were the most frequent pathological findings observed [15] (Figure 1). This study confirms the distinction described in literature between pneumogenic and cardiogenic artifacts based on their distribution and on the characteristics of the pleural line [16]. Artifacts in focal position and/or limited in their representation (Groups 5 and 2 respectively) appear non-specific outside a clinical context and generically indicate a pneumogenic origin, often related to COPD/asthma.

Many studies in literature have addressed the diagnostic role of artifacts. The Blue Protocol [30] applied to patients with acute dyspnea in the Emergency Room showed a sensitivity of 88% and a specificity of 96% of B-lines for the diagnosis of acute cardiogenic pulmonary edema. Moreover, if compared to chest radiography, ultrasound shows greater sensitivity in differentiating the dyspnea due to cardiogenic pulmonary edema from the dyspnea due to exacerbation of chronic obstructive pulmonary disease [31–33]. In a recently published review of patients with acute heart failure [34], ultrasound showed better diagnostic accuracy for pulmonary edema than chest radiography with a sensitivity of 88% and a specificity of 90%, respectively.

Vertical artifacts and B-lines report a non-consolidating increase in subpleural density which, through an interstitial expansion, opens acoustic channels which allow the transmission of acoustic energy to acoustic traps. Pairs of channels and traps with different shapes and sizes highlight specific harmonics of the pulse power spectrum which are subsequently represented visually by the scanner as artifacts with variable morphologies [14,15,20].

The evidence that three quarters of our patients showed pneumogenic artifacts associated with increased subpleural CT density (as in 17 cases with diffuse interstitial pathology) increases the plausibility of the hypotheses set out above. On the contrary, 23 subjects without vertical artifacts and B-lines had final diagnoses which excluded subpleural hyperdensity (12 patients with COPD/emphysema with pulmonary hypertension, 2 with heart disease without pulmonary congestion, 2 with pulmonary embolism, 3 with neoplasia and 1 with collagen disease without pulmonary involvement).

Vertical artifacts and B-lines have been described as being associated with consolidations [35]. Our findings indicate that neoplastic growth, contrary to pneumonia, can produce consolidations which are not surrounded by vertical artifacts or B-Lines and, on the other hand, that B-lines are more frequent in inflammatory consolidations where inflammatory edema is present. An inflammatory consolidation is usually surrounded by edematous tissue and, in this case, artifacts spreading from the borders of the consolidation are visible. This characteristic is usually absent or less evident at the borders of the neoplastic processes.

Six patients had ultrasound signs compatible with cardiogenic lung interstitial edema despite the absence of echocardiographic signs of heart decompensation. These subjects had B-lines associated with other vertical artifacts, which were probably justified by the concomitance of primary pulmonary pathology (COPD, interstitial lung disease and pneumonia). The wide distribution of the B-lines in the other groups and in subjects without heart failure testifies the low specificity of this finding for pulmonary edema (68%) which is lower than that mentioned in the literature in selected cases with low or no prevalence of primary lung disease [36]. However, the sensitivity of B-lines for pulmonary edema is 100%.

The presence of B-lines is not strictly related to cardiogenic components, and in our opinion, the presence of diffuse B-lines should be considered as a simple indication for the evaluation of the systolic and diastolic function of the left ventricle.

Different groups of patients give rise to different patterns and may also require different study protocols [37]. Different approaches to the patient may be required by critical subjects in intensive care or in the emergency room or by subjects with chronic pleuropulmonary pathologies. The pediatric and neonatal setting, although exploiting investigation methodologies and semiotics which are the same as those of the adult, may require specific methodologies. Finally, the recent COVID-19 pandemic, while validating some hypotheses on the origin of the artifacts, has also required special methods of investigation [38,39].

Vertical artifacts are observed in lung interstitial diseases. In these pathologies, the interstitium undergoes an irregular and dense expansion. Therefore, variable, irregular vertical artifacts arising from a blurred pleura are expected because of the presence of many different and irregular acoustic channels [11,14,15]. Diffuse fibrosing disease was detected with a high sensitivity and specificity. According to the final outcome, 15 subjects in group 3 (88.2%), and one subject in Group 5 were affected by interstitial fibrosis.

It has been speculated that the sonographic artifact called "White Lung" may represent a subpleural condition of homogeneous increased density that may strictly anticipate and progress to consolidation [15]. The most probable hypothesis of its genesis, echoes radiated by a subpleural distribution of small scatterers [9], suggests a correlation between the sonographic "White Lung" and the ground glass densities on CT. In our experience, the positive predictive value of US to detect White Lung was low (76%) compared with the detection of ground glass by CT, due to the limitation of ultrasound detection of artifacts (including White Lung) beyond the surface of the lung.

While classical teaching states that subjects with COPD and asthma do not show ultrasound changes [30,33], we rarely observed subjects with COPD or asthma without aspecific mono or oligofocal sonographic findings. Similar conclusions can be drawn for subjects with the tree-in-bud CT pattern. Patients with COPD, asthma and the tree-in-bud CT pattern can show mono or oligofocal findings with non-specific characteristics, probably related to hypoventilation, fibrosis, micro- consolidation or aspecific nodularities.

Finally, simple observations related to the hemidiaphragms with the evidence of hypernormal lung regions (hypermirror effect) can characterize subjects with emphysema. Preliminary results support this hypothesis. However, the role of ultrasound in emphysema has not been previously described and further studies are necessary to confirm this suggestion.

Our study has some limitations. The heterogeneity of the diseases is a limit to the definition of the ultrasound diagnostic accuracy for the single pathologies. Furthermore, the diagnostic framework with ultrasound was carried out by a single expert operator, and our results cannot be extended to all pneumology centers in the absence of skilled physicians.

5. Conclusions

Chest ultrasound is a safe and effective complementary diagnostic tool for the pulmonologist, and its role in an initial evaluation in unselected respiratory patients admitted to a Hospital Pulmonary Medicine Unit is important. The fact of not using ionizing energies and the simplicity of the US examinations makes this diagnostic tool directly accessible to all physicians in every situation. The high sensitivity of US to density increases of the lung surface is surely its most important strength. Another strength of US is its diagnostic accuracy in pleural pathology and lung consolidations. In these cases, a greater sensitivity than the chest X-ray is demonstrated. However, we believe that other applications may benefit from thoracic ultrasound. These include the screening and monitoring of diffuse interstitial pathologies (which are often imperceptible in chest X-ray images) and the diagnosis and monitoring of viral pneumonia. Finally, the interpretation of pulmonary hyperinflation and specifically pulmonary emphysema is a completely unexplored field. Conversely, the weaknesses of pulmonary ultrasound regard the limited field of view of the individual scans, the existence of areas that cannot be explored, and the impossibility of detecting lesions that do not affect the pleural surface. Moreover, the specificity of B-lines is still under study but is believed to be low if they are not included in a clinical evaluation of the patient. In patients with pleural effusion, consolidations, and diffuse interstitial diseases ultrasound can sensitively identify the generic pathology, its location and characteristics, thus achieving a higher diagnostic yield when compared with CT. In diffuse interstitial diseases the main factor favorably affecting the diagnostic yield is the subpleural location of the tissue hyperdensities, appearing in ultrasound as pneumogenic vertical artifacts. Our observations confirm the hypothesis that vertical artifacts (to which the known B-lines belong) are an extremely varied category of artifacts and we believe that an analysis of the latter, based on their visual characteristics and distribution, may be more useful than a mere quantitative count. In particular, recent evidence of the relationships between the internal structure of the vertical artifacts and the geometry of the acoustic trap/channel systems which have generated the artifacts opens new perspectives for increasing their specificity [9–11,15]. However, independently of its specificity, the artefactual ultrasound information of the lung must always be rationally integrated in a multiple district and multi-instrumental clinical context.

Author Contributions: Conceptualization, G.S. and M.D.; methodology, G.S.; software, S.S.; validation, R.P., M.P. and G.S.; formal analysis, S.S. and G.S.; investigation, G.S., R.P. and M.D.; resources, R.P. and M.P.; data curation, G.S. and S.S.; writing—original draft preparation, G.S., R.P. and S.S.; writing—review and editing, M.P. and M.D.; visualization, M.D. All authors have read and agreed to the published version of the manuscript.

Funding: This research received no external funding.

Institutional Review Board Statement: The study was conducted according to the guidelines of the Declaration of Helsinki, and approved by the Institute's Ethics Committee CEAVNO (study number 1089, approved on 30 January 2017).

Informed Consent Statement: Informed consent was obtained from all subjects involved in the study. Written informed consent has been obtained from the patients to publish this paper.

Acknowledgments: The authors wish to thank the Fondazione Cassa di Risparmio di Lucca for its valuable support which made this study possible.

Conflicts of Interest: The authors declare no conflict of interest.

References

1. Koegelenberg, C.F.; Von Groote-Bidlingmaier, F.; Bolliger, C.T. Transthoracic Ultrasonography for the Respiratory Physician. *Respiration* **2012**, *84*, 337–350. [CrossRef] [PubMed]
2. Volpicelli, G.; Elbarbary, M.; Blaivas, M.; Lichtenstein, D.A.; Mathis, G.; Kirkpatrick, A.W.; Melniker, L.; Gargani, L.; Noble, V.E.; Via, G.; et al. International Liaison Committee on Lung Ultrasound (ILC-LUS) for the International Consensus Conference on Lung Ultrasound (ICC-LUS). International evidence-based recommendations for point-of-care lung ultrasound. *Intensive Care Med.* **2012**, *38*, 577–591. [CrossRef]
3. Vignon, P.; Repessé, X.; Vieillard-Baron, A.; Maury, E. Critical care ultrasonography in acute respiratory failure. *Crit. Care* **2016**, *20*, 228. [CrossRef] [PubMed]
4. Picano, E.; Pellikka, P.A. Ultrasound of extravascular lung water: A new standard for pulmonary congestion. *Eur. Heart J.* **2016**, *37*, 2097–2104. [CrossRef] [PubMed]
5. Rambhia, S.H.; D'Agostino, C.A.; Noor, A.; Villani, R.; Naidich, J.J.; Pellerito, J.S. Thoracic Ultrasound: Technique, Applications, and Interpretation. *Curr. Probl. Diagn. Radiol.* **2017**, *46*, 305–316. [CrossRef] [PubMed]
6. Reissig, A.; Kroegel, C. Transthoracic sonography of diffuse parenchymal lung disease: The role of comet tail artifacts. *J. Ultrasound Med.* **2003**, *22*, 173–180. [CrossRef] [PubMed]
7. Kumar, I.; Siddiqui, Z.; Verma, A.; Chokhani, A.; Srivastava, G.N.; Shukla, R.C. Performance of semi-quantitative lung ul-trasund in the assessment of disease severity in interstial lung disease. *Ann. Thorac. Med.* **2021**, *16*, 110–117.
8. Mayo, P.H.; Copetti, R.; Feller-Kopman, D.; Mathis, G.; Maury, E.; Mongodi, S.; Mojoli, F.; Volpicelli, G.; Zanobetti, M. Thoracic ultrasonography: A narrative review. *Intensiv. Care Med.* **2019**, *45*, 1200–1211. [CrossRef]
9. Demi, M.; Prediletto, R.; Soldati, G.; Demi, L. Physical mechanisms providing clinical information from ultrasound lung images: Hypothesis and early confirmations. *IEEE Trans. Ultrason. Ferroelectr. Freq. Control.* **2020**, *67*, 612–623. [CrossRef]
10. Demi, M. The impact of multiple concurrent factors on the length of the US pulmonary vertical artifacts as illustrated through the experimental and numerical analysis of simple models. *J. Acoust. Soc. Am.* **2021**, *150*, 2106–2115. [CrossRef]
11. Demi, M. On the Replica of US Pulmonary Artifacts by Means of Physical Models. *Diagnostics* **2021**, *11*, 1666. [CrossRef] [PubMed]
12. Kameda, T.; Kamiyama, N.; Kobayashi, H.; Kanayama, Y.; Taniguchi, N. Ultrasonic B-Line–Like Artifacts Generated with Simple Experimental Models Provide Clues to Solve Key Issues in B-Lines. *Ultrasound Med. Biol.* **2019**, *45*, 1617–1626. [CrossRef]
13. Kameda, T.; Kamiyama, N.; Taniguchi, N. Simple Experimental Models for Elucidating the Mechanism Underlying Vertical Artifacts in Lung Ultrasound: Tools for Revisiting B-Lines. *Ultrasound Med. Biol.* **2021**, *47*, 3543–3555. [CrossRef] [PubMed]
14. Soldati, G.; Demi, M.; Inchingolo, R.; Smargiassi, A.; Demi, L. On the Physical Basis of Pulmonary Sonographic Interstitial Syndrome. *J. Ultrasound Med.* **2016**, *35*, 2075–2086. [CrossRef]
15. Soldati, G.; Demi, M.; Smargiassi, A.; Inchingolo, R.; Demi, L. The role of ultrasound lung artifacts in the diagnosis of res-piratory diseases. *Expert Rev. Respir. Med.* **2019**, *13*, 163–172. [CrossRef]
16. Copetti, R.; Soldati, G.; Copetti, P. Chest sonography: A useful tool to differentiate acute cardiogenic pulmonary edema from acute respiratory distress syndrome. *Cardiovasc. Ultrasound* **2008**, *6*, 16. [CrossRef] [PubMed]
17. Mathis, G.; Horn, R.; Morf, S.; Prosch, H.; Rovida, S.; Soldati, G.; Hoffmann, B.; Blaivas, M.; Dietrich, C.F. WFUMB position paper on reverberation artefacts in lung ultrasound: B-Lines or comet-tails? *Med. Ultrason.* **2021**, *23*, 70–73. [CrossRef] [PubMed]
18. Beasley, T.M.; Schumacker, R.E. Multiple Regression Approach to Analyzing Contingency Tables: Post Hoc and Planned Comparison Procedures. *J. Exp. Educ.* **1995**, *64*, 79–93. [CrossRef]
19. Lichtenstein, D.; Mezière, G.; Biderman, P.; Gepner, A.; Barré, O. The comet-tail artifact: An ultrasound sign of alveolar in-terstitial syndrome. *Am. J. Respir. Crit. Care Med.* **1997**, *156*, 1640–1646. [CrossRef]
20. Soldati, G.; Smargiassi, A.; Inchingolo, R.; Sher, S.; Nenna, R.; Valente, S.; Inchingolo, C.D.; Corbo, G.M. Lung Ultrasonography May Provide an Indirect Estimation of Lung Porosity and Airspace Geometry. *Respiration* **2014**, *88*, 458–468. [CrossRef]
21. Lacedonia, D.; Scioscia, G.; Giardinelli, A.; Quarato, C.M.I.; Sassani, E.V.; Barbaro, M.P.F.; Maci, F.; Sperandeo, M. The Role of Transthoracic Ultrasound in the Study of Interstitial Lung Diseases: High-Resolution Computed Tomography Versus Ultrasound Patterns: Our Preliminary Experience. *Diagnostics* **2021**, *11*, 439. [CrossRef] [PubMed]
22. Buda, N.; Piskunowicz, M.; Porzezińska, M.; Kosiak, W.; Zdrojewski, Z. Lung Ultrasonography in the Evaluation of Interstitial Lung Disease in Systemic Connective Tissue Diseases: Criteria and Severity of Pulmonary Fibrosis—Analysis of 52 Patients. *Ultraschall Der Med. Eur. J. Ultrasound* **2016**, *37*, 379–385. [CrossRef] [PubMed]
23. Mohanty, K.; Blackwell, J.; Egan, T.; Muller, M. Characterization of the Lung Parenchyma Using Ultrasound Multiple Scattering. *Ultrasound Med. Biol.* **2017**, *43*, 993–1003. [CrossRef]
24. Gasperini, M.L.; Gigante, A.; Iacolare, A.; Pellicano, C.; Lucci, S.; Rosato, E. The predictive role of lung ultrasound in pro-gression of scleroderma interstitial lung disease. *Clin. Rheumatol.* **2020**, *39*, 119–123. [CrossRef]
25. Lee, F.C.Y.; Jenssen, C.; Dietrich, C.F. A common misunderstanding in lung ultrasound: The comet tail artefact. *Med Ultrason.* **2018**, *20*, 379–384. [CrossRef] [PubMed]
26. Staub, L.J.; Biscaro, R.R.M.; Kaszubowski, E.; Maurici, R. Chest ultrasonography for the emergency diagnosis of traumat-ic pneumothorax and hemothorax: A systematic review and meta-analysis. *Injury* **2018**, *49*, 457–466. [CrossRef] [PubMed]
27. Reissig, A.; Copetti, R.; Mathis, G.; Mempel, C.; Schuler, A.; Zechner, P.; Aliberti, S.; Neumann, R.; Kroegel, C.; Hoyer, H. Lung ultrasound in the diagnosis and follow-up of community-acquired pneumonia: A prospective, multicenter, diagnostic accuracy study. *Chest* **2012**, *142*, 965–972. [CrossRef] [PubMed]

28. Orso, D.; Guglielmo, N.; Copetti, R. Lung ultrasound in diagnosing pneumonia in the emergency department: A systematic review and meta-analysis. *Eur. J. Emerg. Med.* **2018**, *25*, 312–321. [CrossRef] [PubMed]
29. Wang, L.; Song, W.; Wang, Y.; Han, J.; Lv, K. Lung ultrasonography versus chest radiography for the diagnosis of pediatric community acquired pneumonia in emergency department: A meta-analysis. *J. Thorac. Dis.* **2019**, *11*, 5107–5114. [CrossRef]
30. Lichtenstein, D.A.; Mezière, G.A. Relevance of Lung Ultrasound in the Diagnosis of Acute Respiratory Failure*: The BLUE Protocol. *Chest* **2008**, *134*, 117–125. [CrossRef]
31. Bekgoz, B.; Kilicaslan, I.; Bildik, F.; Keles, A.; Demircan, A.; Hakoglu, O.; Coskun, G.; Demir, H.A. BLUE proto-col ultrasonography in Emergency Department patients presenting with acute dyspnea. *Am. J. Emerg. Med.* **2019**, *37*, 2020–2027. [CrossRef] [PubMed]
32. Tierney, D.M.; Huelster, J.S.; Overgaard, J.D.; Plunkett, M.B.; Boland, L.L.; Hill, C.A.S.; Agboto, V.K.; Smith, C.S.; Mikel, B.F.; Weise, B.E.; et al. Comparative Performance of Pulmonary Ultrasound, Chest Radiograph, and CT Among Patients with Acute Respiratory Failure. *Crit. Care Med.* **2020**, *48*, 151–157. [CrossRef] [PubMed]
33. Lichtenstein, D.; Mezière, G. A lung ultrasound sign allowing bedside distinction between pulmonary edema and COPD: The comet-tail artifact. *Intensiv. Care Med.* **1998**, *24*, 1331–1334. [CrossRef] [PubMed]
34. Maw, A.M.; Hassanin, A.; Ho, P.M.; McInnes, M.D.F.; Moss, A.; Juarez-Colunga, E.; Soni, N.J.; Miglioranza, M.H.; Platz, E.; DeSanto, K.; et al. Diagnostic Accuracy of Point-of-Care Lung Ultrasonography and Chest Radiography in Adults with Symptoms Suggestive of Acute Decompensated Heart Failure: A Systematic Review and Meta-analysis. *JAMA Netw. Open* **2019**, *2*, e190703. [CrossRef]
35. Lichtenstein, D.A. Lung Ultrasound in the Critically Ill. *Ann. Intensive Care* **2014**, *4*, 1–12. [CrossRef] [PubMed]
36. Agricola, E.; Bove, T.; Oppizzi, M.; Marino, G.; Zangrillo, A.; Margonato, A.; Picano, E. "Ultrasound comet-tail images": A marker of pulmonary edema—A comparative study with wedge pressure and extravascular lung water. *Chest* **2005**, *127*, 1690–1695. [CrossRef]
37. Mongodi, S.; De Luca, D.; Colombo, A.; Stella, A.; Santangelo, E.; Corradi, F.; Gargani, L.; Rovida, S.; Volpicelli, G.; Bouhemad, B.; et al. Quantitative Lung Ultrasound: Technical Aspects and Clinical Applications. *Anesthesiology* **2021**, *134*, 949–965. [CrossRef]
38. Senter, R.; Capone, F.; Pasqualin, S.; Cerruti, L.; Molinari, L.; Basso, E.F.; Zan-forlin, N.; Previato, L.; Toffolon, A.; Sensi, C.; et al. Lung Ultrasound Patterns and Clinical-Laboratory Correlates during COVID-19 Pneumonia: A Retrospective Study from North East Italy. *J. Clin. Med.* **2021**, *10*, 1288. [CrossRef]
39. Buda, N.; Cylwik, J.; Mróz, K.; Rudzińska, R.; Dubik, P.; Malczewska, A.; Oraczewska, A.; Skoczyński, S.; Suska, A.; Górecki, T.; et al. Lung Ultrasound Examination in Patients with SARS-CoV-2 Infection: Multicenter Study. *J. Clin. Med.* **2021**, *10*, 3255. [CrossRef]

diagnostics

MDPI

Article

Lung Ultrasound-Guided Fluid Management versus Standard Care in Surgical ICU Patients: A Randomised Controlled Trial

Daniel-Mihai Rusu [1,2], Ioana Grigoraș [1,2,*], Mihaela Blaj [1,3], Ianis Siriopol [1,2], Adi-Ionut Ciumanghel [3], Gigel Sandu [3], Mihai Onofriescu [4,5], Olguta Lungu [1,2] and Adrian Constantin Covic [4,5]

1 Anaesthesia and Intensive Care Department, Grigore T. Popa University of Medicine and Pharmacy, 700115 Iasi, Romania; rusu.daniel.ro@gmail.com (D.-M.R.); mihaela.blaj@umfiasi.ro (M.B.); ianismarian-sn-siriopol@umfiasi.ro (I.S.); olguta.lungu@umfiasi.ro (O.L.)
2 Anaesthesia and Intensive Care Department, Regional Institute of Oncology, 700483 Iasi, Romania
3 Anaesthesia and Intensive Care Department, Sf. Spiridon University Hospital, 700111 Iasi, Romania; adi.ionut80@yahoo.com (A.-I.C.); gigelsandu@ymail.com (G.S.)
4 Nephrology Department, Grigore T. Popa University of Medicine and Pharmacy, 700115 Iasi, Romania; onomihai@yahoo.com (M.O.); adrian.covic@umfiasi.ro (A.C.C.)
5 Nephrology Department, Dr. C.I. Parhon University Hospital, 700503 Iasi, Romania
* Correspondence: ioana.grigoras@umfiasi.ro; Tel.: +40-7-4530-7196

Abstract: The value of lung ultrasound (LU) in assessing extravascular lung water (EVLW) was demonstrated by comparing LU with gold-standard methods for EVLW assessment. However, few studies have analysed the value of B-Line score (BLS) in guiding fluid management during critical illness. The purpose of this trial was to evaluate if a BLS-guided fluid management strategy could improve fluid balance and short-term mortality in surgical intensive care unit (ICU) patients. We conducted a randomised, controlled trial within the ICUs of two university hospitals. Critically ill patients were randomised upon ICU admission in a 1:1 ratio to BLS-guided fluid management (active group) or standard care (control group). In the active group, BLS was monitored daily until ICU discharge or day 28 (whichever came first). On the basis of BLS, different targets for daily fluid balance were set with the aim of avoiding or correcting moderate/severe EVLW increase. The primary outcome was 28-day mortality. Over 24 months, 166 ICU patients were enrolled in the trial and included in the final analysis. Trial results showed that daily BLS monitoring did not lead to a different cumulative fluid balance in surgical ICU patients as compared to standard care. Consecutively, no difference in 28-day mortality between groups was found (10.5% vs. 15.6%, $p = 0.34$). However, at least 400 patients would have been necessary for conclusive results.

Keywords: lung ultrasound; B-line score; extravascular lung water; fluid management; intensive care; randomised controlled trial

Citation: Rusu, D.-M.; Grigoraș, I.; Blaj, M.; Siriopol, I.; Ciumanghel, A.-I.; Sandu, G.; Onofriescu, M.; Lungu, O.; Covic, A.C. Lung Ultrasound-Guided Fluid Management versus Standard Care in Surgical ICU Patients: A Randomised Controlled Trial. *Diagnostics* **2021**, *11*, 1444. https://doi.org/10.3390/diagnostics11081444

Academic Editors: Marcello Demi, Gino Soldati and Byeong-Ho Jeong

Received: 8 June 2021
Accepted: 28 July 2021
Published: 10 August 2021

1. Introduction

Despite increasing awareness of the deleterious effects of fluid overload (FO) [1] and the advances made in guiding fluid therapy [2–5], avoiding FO in intensive care unit (ICU) patients remains challenging. Consequently, the number of patients with positive fluid balance (FB) and FO during ICU stay is still worryingly high [6]. FO leads to tissue and organ oedema [7] and has been associated with increased risk of postoperative complications [8], acute kidney injury (AKI) [9], prolonged mechanical ventilation [10], and prolonged ICU and hospital length of stay (LOS) [11,12]. Moreover, a meta-analysis summarizing current evidence related to FO's impact on mortality in 31 observational studies reported an increased risk of mortality in the general ICU population with FO or positive cumulative FB (CFB) [1]. FO is multifactorial [13], but the challenge of finding the right moment to start fluid de-escalation is a major contributor; for instance, clinical examination, FB, chest X-ray, and patients' oxygen requirements are often used by clinicians

to trigger fluid de-escalation over more reliable (but more invasive) volume assessment methods [14]. In this context, the possible value of monitoring extravascular lung water (EVLW) with lung ultrasound (LU) in order to individualise fluid management and improve outcome has recently come into question [15].

EVLW increase is an early marker of pulmonary oedema [15]; thus, its assessment may be used to limit fluid administration or trigger fluid de-escalation, as pulmonary oedema may be further worsened in the context of a positive FB. Transpulmonary thermodilution is the method currently used for EVLW measurement [16]. This method requires central venous and arterial cannulation, time, expertise, and resources [17,18], and is usually reserved for the most complex ICU cases. Computed tomography (CT) and nuclear magnetic-performed resonance imaging (MRI) may also be used for EVLW assessment [19,20]. However, despite their great value in diagnosing several pulmonary and extrapulmonary conditions, CT and MRI scans of the chest are impractical for daily monitoring of EVLW as they are costly, time-consuming, and they expose patients to transportation hazards or high doses of radiation. LU can detect increases in EVLW [21,22] and its dynamic changes [23,24] noninvasively at the bedside, with minimal distress for the patient and using minimal resources [25]. B-lines are the ultrasonographic signs of EVLW increase [26]. The close correlation between the number of B-lines on LU and EVLW volume has already been demonstrated by comparing LU with gold-standard methods for EVLW evaluation [27–29]. Moreover, B-lines can be easily detected [30] using various ultrasound systems and probes [31] with good intra- and inter-evaluator reliability [32–35]. Nonetheless, LU is infrequently used to guide fluid therapy, as its added value in fluid management is still a matter of debate.

This study's primary aim was to evaluate the impact of a B-Line score (BLS) fluid management strategy on ICU patients' short-term mortality. Our central hypothesis was that the daily assessment of BLS, coupled with active fluid removal in cases of moderate or severe EVLW increase (as reflected by the BLS value), might improve CFB and decrease 28-day mortality as compared to standard care. The secondary hypotheses were that BLS-guided fluid management would decrease 90-day mortality, ICU and hospital LOS, AKI recovery time, and the duration of vasopressor therapy and mechanical ventilation.

2. Materials and Methods

2.1. Study Design and Settings

From November 2017 to November 2019, we conducted a randomised, controlled trial within two tertiary hospitals' ICUs to determine whether BLS-guided fluid management could decrease 28-day mortality in critically ill patients, as compared to standard care. The study was approved by the Research Ethics Committees of the Grigore T. Popa University of Medicine and Pharmacy Iași (No 26261/14 November 2017) and was conducted under the principles of the Declaration of Helsinki. Written informed consent was obtained from all subjects/legal representatives.

The trial was retrospectively registered on ClinicalTrials.gov (https://clinicaltrials.gov/ct2/show/NCT03393065) accessed on 8 January 2018.

The study protocol has been published elsewhere [36].

2.2. Participants

During the trial, study investigators performed a daily screening of all ICU admissions to identify patients who fulfilled one of the following inclusion criteria: major surgery, major comorbid conditions in surgical patients, polytrauma with an Injury Severity Score (ISS) $\geq$ 15, an Acute Physiology and Chronic Health Evaluation II (APACHE II) score on admission $\geq$ 10 or a Sequential Organ Failure Assessment (SOFA) score on admission $\geq$ 6. Major surgery included: Esophagectomy, Total Gastrectomy, Total Colectomy, Duodenopancreatectomy, Major Hepatectomy, Multi-Organ Resection, Aorto-Bifemoral Bypass, Aortic Interposition Tube Graft. Major comorbid conditions included: Chronic Obstructive Pulmonary Disease (COPD) Global Initiative for Obstructive Lung Disease (GOLD) stage

III or IV, Heart Failure New York Heart Association (NYHA) Class III or IV, Heart Valve Disease grade III or IV, Cirrhosis Child-Pugh score B or C, Chronic Kidney Disease (CKD) stage 1–4.

Patients fulfilling any of the following criteria were excluded: trial participation refusal, age < 18 years, pregnancy, known pulmonary conditions that can interfere with LU interpretation (pneumectomy, pulmonary fibrosis, pulmonary lymphangitis, persistent pleural effusion), CKD stage 5, or indication for emergency renal replacement therapy (RRT), previous prolonged resuscitation ($\geq$10 min) for cardiorespiratory arrest.

2.3. Randomisation and Blinding

After enrolment, patients were randomly assigned to BLS-guided fluid management (active group) or standard care (control group) in a 1:1 ratio, using block randomisation. The randomised sequence was created using a computerised random-number generator and concealed at the coordinating centre. The allocation group was provided each time a new patient was enrolled using a 24-h phone service. Patients and healthcare providers were not blinded, but the outcome assessors were blinded to the patient's group assignment. Data analysis was performed before the allocation sequence code was broken.

2.4. Lung Ultrasound Performance

In the active group, LU was performed daily, from ICU admission to ICU discharge, or day 28 (whichever came first). In the control group, LU was only performed once on admission, and the treating physician remained blinded to LU data. All LU examinations were made by trained ICU physicians at the bedside, with the patient in the supine position; the focus of the image was set at the pleural line level and the depth of penetration set between 40 and 80 mm. The ultrasound equipment used was the GE LOGIQ V2® ultrasound system and the GE 3Sc-RS Cardiac Sector Probe® (General Electric Healthcare, Chicago, IL, USA). The BLS assessment protocol consisted of a complete scan of 28 chest sites, as described by Jambrik et al. [37]. The sum of all B-lines seen on LU defined the BLS. A map of chest sites scans is provided in Figure 1.

RIGHT					LEFT			
MA	AA	MC	PS	IC	PS	MC	AA	MA
R2MA	R2AA	R2MC	R2PS	II	L2PS	L2MC	L2AA	L2MA
R3MA	R3AA	R3MC	R3PS	III	L3PS	L3MC	L3AA	L3MA
R4MA	R4AA	R4MC	R4PS	IV	L4PS	L4MC	L4AA	L4MA
R5MA	R5AA	R5MC	R5PS	V				

Figure 1. A map of chest site scans for BLS assessment. The figure shows the 28 chest sites scanned for the BLS calculation. The code of each site describes its space alignment: R: Right Chest; L: Left Chest; 1 to 5: the number of the intercostal space (IC); MA: Mid-Axillary Line; AA: Anterior-Axillary Line; MC: Mid-Clavicular Line; PS: Parasternal Line.

2.5. Fluid Management

In the active group, with every LU examination, patients were stratified into four classes: no EVLW increase (BLS = 0–4), mild increase (BLS = 5–14), moderate increase (BLS = 15–29), or severe EVLW increase (BLS $\geq$ 30), based on BLS severity grading system proposed by Frassi et al. [38]. In patients with no or mild EVLW increase (BLS = 0–14), a zero FB was targeted if no signs of shock were present. In patients with a moderate or severe increase in EVLW (BLS $\geq$ 15), a daily negative FB of -250 to -1000 mL was targeted until BLS dropped under 15. To reach daily targeted FB, furosemide-induced diuresis and RRT were used. Furosemide was administrated in a stepwise manner considering the previous furosemide dose and the FB achieved. If the targeted FB was achieved from the

first day of diuretic administration, the furosemide dose was maintained. If FB was outside the targeted range, the furosemide dose was progressively reduced or increased until the goal was achieved. RRT was used in patients with moderate and severe EVLW increase (BLS $\geq$ 15) if the targeted FB could not be reached despite using the maximum furosemide dose of 800 mg/day. Outside trial interventions, overall ICU patients' management was at the treating physicians' discretion.

In the control group, fluid management was guided by the Enhanced Recovery after Surgery (ERAS) principles. Within the ERAS protocol, the aim was to maintain an adequate intravascular volume while minimising weight gain. Various parameters were used to attain this goal based on case-by-case clinical judgment: lung sounds, heart rate, blood pressure, temperature, urine output, FB, lactate, haemoglobin, haematocrit, serum urea, creatinine, sodium, potassium, chloride, and bicarbonate values. Additionally, central venous oxygen saturation, pulse pressure variation and stroke volume variation were used to assess fluid responsiveness in patients with shock.

The trial algorithm is presented in Figure 2. The recommended furosemide regimens are provided in Table 1.

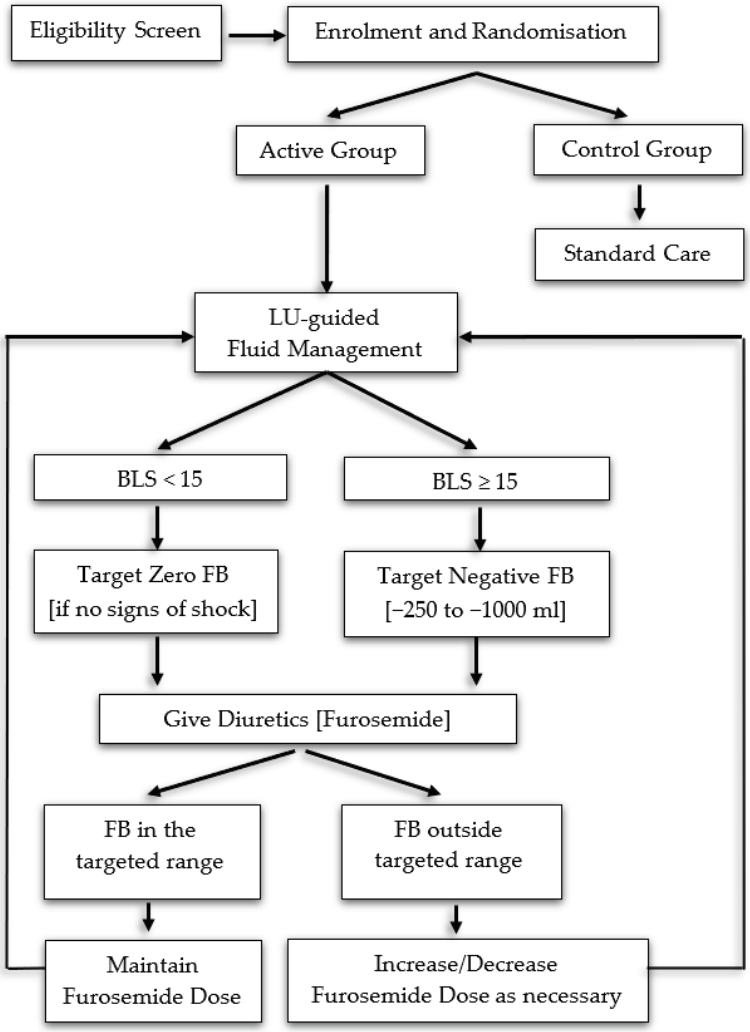

Figure 2. Trial algorithm.

Table 1. The recommended Furosemide regimens to attain targeted fluid balance.

Previous Furosemide Dose (mg/day)		Recommended Furosemide Dose (mg/day)
1	≤80 mg	40 mg iv bolus + 5 mg/h
2	81–160 mg	80 mg iv bolus + 10 mg/h
3	161–240 mg	80 mg iv bolus + 20 mg/h
4	>240 mg	80 mg iv bolus + 30 mg/h

2.6. Collected Variables

Data were collected from the ICU charts and hospital medical records. Survival was assessed via a phone call to the patient or the patient's legal representative. On ICU admission, age, gender, body mass index (BMI), primary diagnosis, surgery type, infectious status, organ dysfunctions, comorbid conditions, severity scores, BLS, and main laboratory data were collected. During the ICU stay, data regarding fluid management, BLS (active group), organ dysfunctions and organ support therapies were collected. Outcome data were 28-day and 90-day mortality, ICU and hospital LOS, AKI, vasopressor therapy, and mechanical ventilation duration.

2.7. Study Sample Size

We estimated that, with a sample size of 199 patients in each group, the study would have 80% power to detect an absolute difference of 10% in the primary outcome, assuming a 28-day mortality rate of 20% in the control group, at a two-sided 5% level of significance. The choice of 10% expected difference in the primary outcome was based on mortality rates in patients with and without FO, observed in a large cohort study of ICU patients [11]. To account for potential withdrawals of consent, the recruitment target was set at 250 patients in each arm. For circumstantial reasons (the COVID-19 pandemic), the study was not able to reach the targeted sample size.

2.8. Statistical Analysis

Data were analysed using MedCalc Statistical Software version 19.1.7 (MedCalc Software Ltd., Ostend, Belgium, 2020). All analyses were conducted on an intention-to-treat basis. The intention-to-treat population was formed by all trial participants, except those who withdrew consent. No assumptions for missing data were made. Variables distribution was tested for normality using histograms and the Shapiro-Wilk test. Comparisons between continuous variables were performed using Student's *t*-test (for normally distributed data) or Mann-Whitney U-test (for non-normally distributed data). Comparisons between categorical variables were performed using Chi-square ($\chi 2$) test or Fisher's exact test, as appropriate. Hazard ratios (HRs) and risk ratios (RRs) with 95% confidence intervals (CIs) were used to evaluate the effect size of BLS-guided fluid management on the primary outcome and 90-day mortality. Cohen's kappa and Cliff's delta statistics were used for estimating the effect size (ES) of active vs. control group allocation on continuous secondary outcomes.

An exploratory analysis of the effect of active group allocation on the primary outcome was performed across non-prespecified subgroups of patients.

Continuous variables are presented as means and standard deviations (sd) if normally distributed or as medians and 25–75% interquartile ranges (IQRs) if non-normally distributed. Categoric variables are presented as number (*n*) and percentage (%). Data are presented by group allocation. For all analyses, a p-value < 0.05 was considered statistically significant.

3. Results

3.1. Study Patients

Over the study period, 208 patients were eligible, based on the inclusion criteria. Informed consent was obtained from 176 patients who were further randomised in a

1:1 ratio to intervention or standard care. A total of 10 patients withdrew consent after randomisation. Hence, 166 patients were included in the final analysis. Patients flow through the trial is presented in a Consolidated Standards of Reporting Trials (CONSORT) diagram in Figure 3.

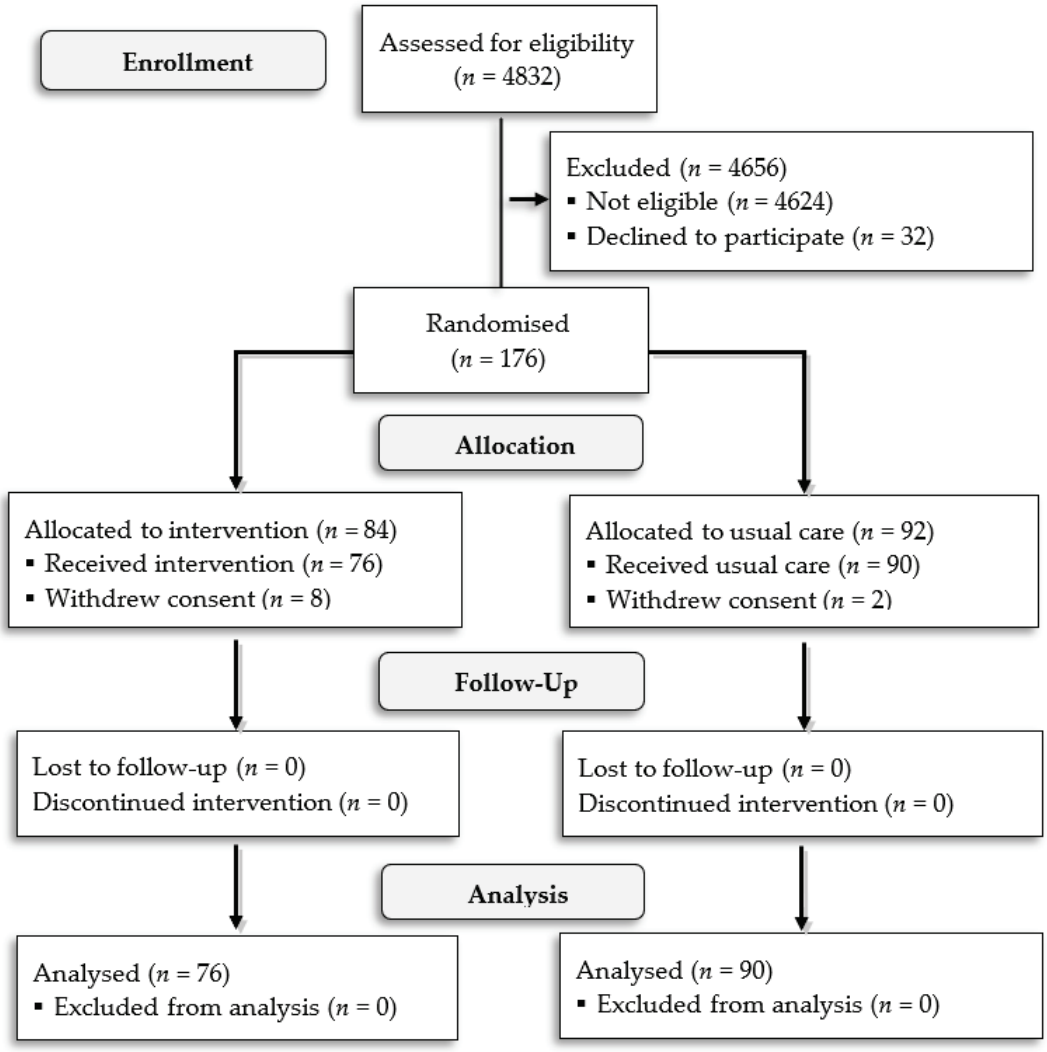

Figure 3. CONSORT diagram showing patient flow through the trial.

3.2. Baseline Data

The median age of the study population was 64 (IQR 59–70) years. The male-female ratio was 2:1. Mean BMI was 25.6 (sd 4.2) kg/m^2. The majority of patients (162 patients, 97.6%) were admitted to the ICU following surgery: 30 (18.1%) patients after emergency surgery and 132 (79.5%) patients after elective surgery. The primary diagnosis was cancer in 112 (67.5%) patients. Forty-one (24.7%) patients had sepsis or septic shock. Ninety-five (57.2%) patients had organ dysfunction. The leading comorbidities were cardiovascular diseases (117 patients, 70.5%), diabetes mellitus (48 patients, 28.9%) and CKD (42 patients, 25.3%). Anaemia was present in 145 (87.3%) patients. Hyperchloremia and hypokalaemia were the main imbalances found in serum electrolytes. Moderate/severe EVLW volume increase, as reflected by the BLS value, was observed on ICU admission in 32 (19.3%) patients. The median APACHE II score on admission was 8.5 (IQR 7–12), and the median SOFA score was 4 (IQR 2–6). The trial arms were well balanced, with no significant differences in baseline characteristics between groups. See Tables 2 and 3.

Table 2. Baseline characteristics of patients.

Variable	Active Group (n = 76)	Control Group (n = 90)	p
Age (years)	63.5 (58–71)	64.5 (60–70)	0.94
Male Gender	51 (67.1)	63 (70.0)	0.69
BMI (kg/m^2)	25.8 (3.9)	25.4 (4.5)	0.58
Surgery			
Emergency	14 (18.4)	16 (17.8)	0.91
Elective	62 (81.6)	70 (77.8)	0.55
Primary diagnosis			
Cancer	52 (68.4)	60 (66.7)	0.81
Nononcologic Disease	24 (31.6)	30 (33.3)	0.81
Comorbid Conditions	65 (85.5)	77 (85.6)	0.99
COPD/Asthma	12 (15.8)	8 (8.9)	0.17
Cardiovascular Diseases	54 (71.0)	63 (70.0)	0.88
Hepatitis/Cirrhosis	10 (13.2)	14 (15.6)	0.66
CKD	19 (25.0)	23 (25.6)	0.81
Previous Stroke	4 (5.3)	3 (3.3)	0.54
Diabetes Mellitus	21 (27.6)	27 (30.0)	0.74
Autoimmune Diseases	1 (1.3)	4 (4.4)	0.24
Major comorbidities	22 (28.9)	32 (35.6)	0.37
Sepsis/Septic shock	20 (26.3)	21 (23.3)	0.66
Organ dysfunction	43 (56.6)	52 (57.8)	0.88
Anaemia	64 (84.2)	81 (90.0)	0.26
Electrolytes' imbalances			
Hyperkalaemia	1 (1.3)	0 (0.0)	0.40
Hypokalaemia	10 (13.2)	14 (15.6)	0.62
Hypernatremia	6 (7.9)	7 (7.8)	0.98
Hyponatremia	2 (2.6)	4 (4.4)	0.53
Hyperchloremia	16 (21.0)	18 (20.0)	0.87
Hypochloraemia	1 (1.3)	1 (1.1)	0.90
EVLW on LU			
normal (BLS 0–4)	24 (31.6)	29 (32.2)	0.93
mild increase (BLS 5–14)	38 (44.7)	43 (47.8)	0.78
moderate increase (BLS 15–29)	12 (15.8)	10 (11.1)	0.38
severe increase (BLS $\geq$ 30)	2 (2.6)	8 (8.9)	0.09
Severity Scores			
Charlson Comorbidity Index	6.4 (2.7)	6.0 (2.2)	0.32
APACHE II	8 (6–12)	9 (7–14)	0.08
SOFA	4 (2–6)	4 (1–7)	0.61

Data are given as number (%), mean (standard deviation) or median (quartile 25–75%). Abbreviations: APACHE II: Acute Physiology and Chronic Health Evaluation II score; BLS: B-Line score; BMI: Body Mass Index; CKD: Chronic Kidney Disease; COPD: Chronic Obstructive Pulmonary Disease; EVLW: Extravascular Lung Water; SOFA: Sequential Organ Failure Assessment score.

Table 3. Surgical procedures performed on the studied patients.

Surgery Type	Active Group (n = 76)	Control Group (n = 90)	p
Esophagectomy	2 (2.6)	1 (1.1)	0.46
Total Gastrectomy	18 (23.7)	15 (16.7)	0.26
Duodeno-pancreatectomy	11 (14.5)	21 (23.3)	0.15
Hepatectomy	5 (6.6)	4 (4.4)	0.55
Total Colectomy	1 (1.3)	0 (0.0)	0.28
Multi-organ Resection	10 (13.2)	11 (12.2)	0.86
Aorto-bifemoral Bypass	11 (14.5)	13 (14.4)	0.99
Aortic interposition tube graft	2 (2.6)	2 (2.2)	0.86
Damage control surgery	14 (18.4)	16 (17.8)	0.91
Other type	2 (2.6)	3 (3.3)	0.79

Data are given as number (%).

3.3. Lung Ultrasound Data and Fluid Balance

Four hundred forty LU exams were performed in the active group, with an average of six exams/patient. Cohen's kappa for the inter-rater agreement was 0.91 (95% CI 0.84 to 0.98). From all of the LU exams, 97 (22%) did not reveal signs of EVLW increase (BLS < 5), 231 (52.5%) revealed a mild EVLW increase (BLS = 5–14), 79 (11.9%) revealed a moderate increase (BLS = 15–29), and 33 (7.5%) revealed a severe EVLW increase (BLS $\geq$ 30). Following admission, the number of patients without LU signs of EVLW increase (BLS < 5) dropped from 24 (31.6%) to 12 (15.8%) (p = 0.02), while the number of those with severe EVLW increase (BLS $\geq$ 30) rose from 2 (2.6%) to 9 (11.8%) (p = 0.03); see Figure 4. Overall, of the 76 patients in the active group, 67 (88.2%) had LU signs of EVLW increase (BLS $\geq$ 5) at least once during their ICU stay, of which 23 (30.3%) demonstrated a moderate/severe EVLW increase (BLS $\geq$ 15).

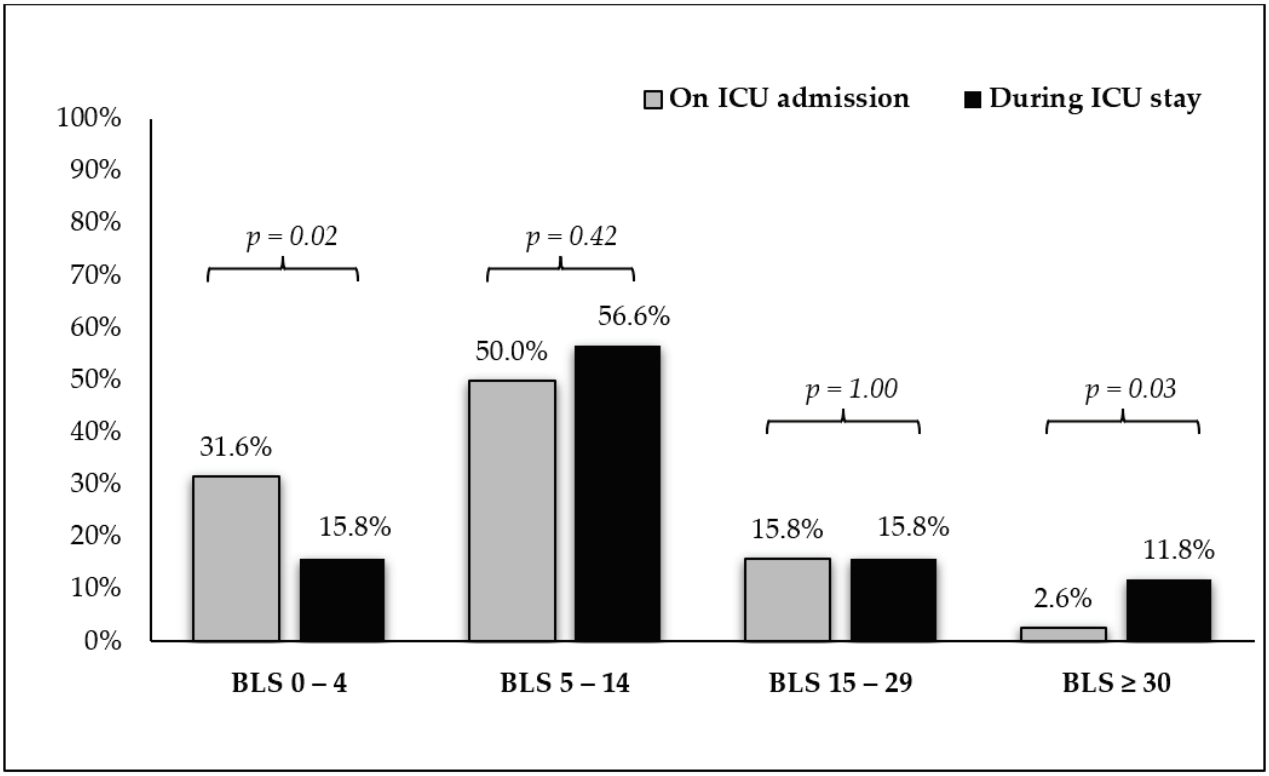

Figure 4. B-Line score dynamics in the active group. The figure shows the percentages of patients with no (BLS = 0–4), mild (BLS = 5–14), moderate (BLS = 15–29), and severe (BLS $\geq$ 30) EVLW increase on ICU admission and during ICU stay. Abbreviations: BLS: B-Line score; EVLW: Extravascular Lung Water; ICU: Intensive Care Unit.

Fluid de-escalation measures, defined as furosemide prescription to obtain a zero or negative FB, were taken early in both groups, and by ICU discharge, more than 90% of patients received furosemide at least once, with no major differences between trial arms (Table 4). The cumulative furosemide dose at ICU discharge was similar in both groups (120 vs. 110 mg, p = 0.74). Two patients (2.6%) from the active group and four from the control group (4.4%) required RRT to rebalance their volume status (p = 0.53).

The percentages of patients with zero or negative CFB at 24 h, 48 h, 72 h, and at ICU discharge were not significantly different between the active and control group. Similarly, there were no significant differences regarding the median CFB at 24 h, 48 h, 72 h, and at ICU discharge between the active and control group (Table 4).

Table 4. Fluid de-escalation measures and CFB across groups.

Variable	Active Group	Control Group	*p*
Fluid De-escalation, pts (%)			
day 1	57/76 (75.0)	71/90 (78.9)	0.55
day 2	58/74 (78.4)	61/84 (72.6)	0.40
day 3	44/56 (78.6)	53/67 (79.1)	0.94
overall	70/76 (92.1)	82/90 (91.1)	0.82
Cumulative Furosemide dose, mg	120 (60–270)	110 (65–220)	0.74
RRT, pts (%)	2 (2.6)	4 (4.4)	0.53
Zero or Negative CFB, pts (%)			
at 24 h	21/76 (27.6)	21/90 (23.3)	0.53
at 48 h	18/74 (24.3)	20/84 (23.8)	0.94
at 72 h	14/56 (25.0)	23/67 (34.3)	0.26
at ICU discharge	21/76 (27.6)	29/90 (32.2)	0.52
Median CFB, mL			
at 24 h	630 (−139–1430)	680 (115–1366)	0.52
at 48 h	1320 (1–2406)	1379 (47–2157)	0.86
at 72 h	1580 (−56–3079)	1150 (−515–2593)	0.27
at ICU discharge	1027 (−374–2690)	1027 (−430–2875)	0.97

Data are given as the number of cases/total number of patients (%) or as median (quartile 25–75%). Abbreviations: CFB: Cumulative Fluid Balance; Pts: Patients; RRT: Renal Replacement Therapy.

3.4. Outcome Data

During the trial, there was no cross over between the groups and all the patients completed follow-up. The primary outcome analysis showed no significant difference in 28-day mortality in the active vs. control group (10.5% vs. 15.6%, $p = 0.34$, RR 0.68, 95% CI 0.30 to 1.53). Mean survival time by day 28 was similar in the two trial arms (26 vs. 25 days, HR 0.66, 95% CI 0.28 to 1.52, reference control group, $p = 0.33$). Secondary outcomes analyses revealed no significant differences between the active and control group in 90-day mortality (11.8% vs. 17.8%, $p = 0.29$, RR 0.67, 95% CI 0.31 to 1.42), ICU LOS (4 vs. 4 days, $p = 0.78$), hospital LOS (12 vs. 10 days, $p = 0.17$), AKI recovery time (6 vs. 5 days, $p = 0.22$), or vasopressor therapy duration (3 vs. 3 days, $p = 0.97$). We noticed that the hours on mechanical ventilation were significantly lower in the active vs. the control group (22 vs. 44 h, ES 0.67, $p = 0.02$), but ventilator-free days were not significantly different (26 vs. 20 days, $p = 0.32$). Mean survival time by day 90 was 81 days in the active group and 76 days in the control group (HR 0.64, 95% CI 0.29 to 1.42, reference control group, $p = 0.28$). Outcome data are presented in Table 5.

Table 5. Primary and secondary outcomes.

	Group Allocation		RR/ES (95% CI)	*p*
	Active (*n* = 76)	Control (*n* = 90)		
28-day mortality	8 (10.5)	14 (15.6)	0.68 (0.30 to 1.53)	0.34
90-day mortality	9 (11.8)	16 (17.8)	0.67 (0.31 to 1.42)	0.29
ICU LOS, days	4 (2–6)	4 (2–6)	0.04	0.78
ICU-free days	24 (20–26)	24 (21–25)		0.62
Hospital LOS, days	12 (9–18)	10 (7–16)	0.23	0.17
Hospital-free days	76 (69–81)	77 (66–81)		0.84
Patients with AKI	11 (14.5)	23 (25.6)		0.08
AKI recovery time, days	6 (4–11)	5 (3–6)	0.43	0.22
AKI-free days	18 (3–23)	22 (0–24)		0.98
Patients on Vasopressors	40 (52.6)	48 (53.3)		0.93
Vasopressors use, days	3 (2–5)	3 (1–5)	0.01	0.97
Vasopressors-free days	25 (22–26)	25 (0–27)		0.57
Patients on MV	21 (27.6)	30 (33.3)		0.43
MV duration, hours	22 (6–48)	44 (22–107)	0.67	0.02
Ventilator-free days	26 (0–27)	20 (0–27)		0.32

Data are given as number (%) and RR (95% CI) or median (quartile 25–75%) and ES. Abbreviations: AKI: Acute Kidney Injury; CI: Confidence Interval; ES: Effect Size; LOS: Length-Of-Stay; MV: Mechanical Ventilation; RR: Risk Ratio.

In the explorative analyses, we found that the BLS-guided fluid management effect on the primary outcome was significantly different across subgroups of patients with emergency surgery and sepsis/septic shock. The results showed a decreased mortality in emergency surgery patients and patients with sepsis/septic shock that received BLS-guided fluid management in the postoperative period as compared with the standard care group (Table 6).

Table 6. Primary outcome across non-prespecified subgroups.

	28-Day Mortality		RR (95% CI)	*p*
	Active	Control		
Surgery				
emergency	1/14 (7.1)	10/16 (62.5)	0.11 (0.02 to 0.78)	<0.01
elective	7/62 (11.3)	3/70 (4.3)	2.63 (0.71 to 9.75)	0.13
Sepsis/septic shock				
yes	1/20 (5.0)	8/21 (38.1)	0.13 (0.02 to 0.96)	0.01
no	7/56 (12.5)	6/69 (8.7)	1.44 (0.51 to 4.03)	0.49
AKI or CKD				
yes	3/25 (12.0)	12/37 (32.4)	0.37 (0.12 to 1.18)	0.06
no	5/51 (9.8)	2/53 (3.8)	2.60 (0.53 to 12.79)	0.22
AHF or CHF				
yes	7/46 (15.2)	14/55 (25.4)	0.60 (0.26 to 1.35)	0.21
no	1/30 (3.3)	0/35 (0.0)	3.48 (0.15 to 82.48)	0.28

Data are given as the number of patients with negative outcome/total number of exposed patients (%) and RR (95% CI). Abbreviations: AHF: Acute Heart Failure; AKI: Acute Kidney Injury; CHF: Chronic Heart Failure; CI: Confidence Interval; CKD: Chronic Kidney Disease; RR: Risk Ratio.

4. Discussion

To our knowledge, this is the first study to analyse the potential outcome effects of a fluid management strategy based on BLS assessment in a population of surgical critically ill patients. The concept of using B-lines dynamics to guide fluid therapy is not new. It was developed in 2012 by Lichtenstein, who proposed fluid administration limited by lung ultrasonography (the FALLS protocol) in patients with acute circulatory failure [39]. However, this concept has never been tested in a controlled clinical trial. Our study showed no significant difference in the short-term mortality of patients receiving BLS-guided fluid management and those receiving standard care. The 90-day mortality, ICU and hospital LOS, duration of vasopressor therapy and AKI recovery time were similar in the two trial arms. We noticed a significantly lower mechanical ventilation duration in the active vs. control group, but the overall ventilator-free days were not significantly different between groups.

Several other studies that compared restrictive or active fluid de-escalation strategies with standard care reported similar results. In the Fluid and Catheter Treatment Trial, 1000 patients with acute lung injury were randomised to a conservative or a liberal fluid strategy [40]. The trial reported a decreased mechanical ventilation duration in the conservative group, but no significant difference in the 60-day mortality [40]. In a single-centre randomised trial, Richard et al. analysed the effects of fluid administration based on preload dependence indices in 60 septic shock patients [41]. In this study, no significant differences were noted regarding the 28-day mortality, ICU LOS, and vasopressor therapy duration in the preload dependence group as compared to standard care group [41]. Chen and Kollef randomised 82 septic shock patients under vasoactive therapy following the initial fluid resuscitation phase to fluid management guided by daily assessments of fluid responsiveness or standard care [42]. Their study results showed no significant differences regarding in-hospital mortality and vasopressor therapy duration between groups [42]. Moreover, Chen and Kollef did not report a significant difference in mechanical ventilation duration between groups [42]. Hjortrup et al. analysed a conservative fluid strategy effect on outcome vs. standard care in 151 septic shock patients [43]. They found

no differences in the 90-day mortality between groups, but a higher risk for worsening AKI in the control group [43]. Recently, in a randomised pilot study, Corl et al. compared a restrictive fluid resuscitation strategy with standard care in 109 patients with severe sepsis and septic shock and found similar 30-day mortality rates, ICU and hospital LOS, and duration of vasopressors use [44]. The duration of ventilatory support was shorter in the restrictive fluid group, but the number of patients requiring new mechanical ventilation was only 32 [44].

In our study, a possible explanation for the lack of significant difference in CFB and short-term mortality between groups is that we examined BLS-guided fluid management within the context of ERAS pathways. Thus, increased efforts to attain a zero or negative FB were taken in both groups. These efforts are reflected in the increased number of patients that received diuretics early in their ICU stay, in both groups. Moreover, no significant difference was found between cumulative furosemide doses used in the active and control group. A recent survey of ICU physicians' practices also pointed towards the increased use of several preventive and treatment strategies to attain a zero FB in standard care [45]. A few years ago, fluids were often prescribed in patients who develop hypotension, and ICU physicians were less willing to give diuretics to patients requiring vasopressors. At present, they favour the use of vasopressors for isolated hypotension treatment while continuing fluid removal in patients with signs of FO [45]. It also seems that in the presence of FO, ICU physicians target a negative 24 h FB of −500 to −1500 mL [45].

Another possible explanation is that we used the same diuretic protocol in all patients, while the varying situations that led to EVLW increase would have required different diuretic regimens to attain the same therapeutic response.

Finally, we enrolled a heterogeneous population of critically ill surgical patients in which B-lines may not have reflected only pulmonary congestion. While some studies point towards an accurate evaluation of EVLW with the BLS [46], others suggest that the accuracy of EVLW assessment with BLS depends on the studied population [47]. For instance, Seibel et al., in a large heterogeneous population of critically ill patients, found that the correlation coefficient between BLS on LU and EVLW assessed by transpulmonary thermodilution was highly variable, with the highest sensitivity and specificity of BLS to predict EVLW increase being in the subgroup of patients with a PaO_2/FiO_2 ratio <200 mmHg [47]. Furthermore, in a recent study, Buda et al. showed that subpleural small consolidations might be responsible for at least some of the B-lines seen on LU [48]. Interestingly, by increasing ultrasound frequency from 2 MHz to 6 MHz, Buda et al. showed that most B-lines caused by lung surface abnormalities convert to Z-lines [48]. Mutually, most patients (97%) in whom B-lines were converted to Z-lines by increasing ultrasound frequency had pleural line abnormalities [48]. These recent findings indicate that the lung surface should also be checked for abnormalities in order to differentiate between the different possible aetiologies of B-lines [48]. In this context, our study results may reflect the futility of adding BLS data in fluid management decision-making without using additional parameters to increase BLS specificity. Future studies should establish whether the BLS alone yields any value or needs to be correlated with B-lines distribution patterns, cardiac ultrasound, PaO_2/FiO_2 ratio, or other parameters to increase its specificity.

The lower duration of mechanical ventilation observed in the active group is the single positive outcome in our study. However, in our trial, the number of patients on mechanical ventilation was too small to support any strong conclusions. It is possible that the clinicians felt more confident to extubate patients earlier simply by having a daily LU evaluation, but this may also be a spurious finding. If LU can indeed help decrease the duration of mechanical ventilation, it deserves further investigation in the future.

In the explorative analyses, we found a lower mortality in emergency surgery patients and patients with sepsis/septic shock that received LU-guided fluid management in the postoperative period. These hypotheses should be verified in future trials.

Study Strengths and Limitations

Our results must be interpreted in light of certain strengths and limitations. The primary limitation is the lack of power, as a result of failing to achieve the desired sample size. Nevertheless, many other trials investigating different fluid management strategies have similar or smaller cohorts. A second limitation concerns the criteria used for participant selection. We targeted the recruitment of patients prone to positive FB, or even FO, following major surgery. We also enrolled surgical patients with major comorbidities, in which fluid retention may worsen their condition due to impaired respiratory, cardiovascular, kidney, or hepatic function. These inclusion criteria led to a heterogeneous study population that may have altered the results. Another limitation is that ICU physicians in the study were not blinded to patient group assignment, thus we cannot exclude the Hawthorne effect. Being aware that their patient's outcome will be assessed, ICU physicians may have increased their efforts to improve FB in the control group by limiting the amount of prescribed fluids or by prescribing higher doses of diuretics.

A lack of clear guidelines for education in clinical LU [49] and a lack of consensus on the various methodological aspects and scoring systems used to assess EVLW [31] are common limitations of any fluid management protocol design based on LU, including ours. Several studies report that B-lines can be accurately identified by examiners with different levels of expertise [30,33,50], using different types of ultrasound machines and probes [31]. However, counting B-lines may be challenging [51]. In our trial, trained ICU physicians performed all LU exams, and the inter-rater agreement was high. Moreover, all patients were examined in a supine position using the same cardiac sector probe. Current evidence shows that patient positioning may influence LU findings, at least in patients with heart failure [52]. Regarding probe selection for B-lines detection, no advice is provided in the 2012 consensus guideline [53]. Nevertheless, according to various reports, the cardiac and convex probes are slightly more accurate in B-lines detection than other types of ultrasound transducers [54–56]. To quantify the degree of pulmonary congestion, we used a comprehensive approach, in which 28 predefined points were scanned for B-lines. This approach, first used by Jambrik et al. [37], seems to have a better diagnostic accuracy for EVLW assessment than others [57]. However, we did not analyse the relationship between B-lines and lung surface abnormalities, which might have caused at least some of the B-lines seen on LU [48].

In our study, different targets for daily FB were set using a BLS cut-off value of 15. This cut-off value was based on the severity grading system used by Frassi et al. to show the correlation between different BLS classes and survival in patients with dyspnoea, chest pain, or both [38]. In another study, Zoccali et al. reported an increased risk of mortality in end-stage CKD patients with a BLS $\geq$ 15 [58]. More recently, Yin et al. found that a high BLS on ICU admission was associated with an increased 28-day mortality in critically ill patients [59]. On the basis of these findings, we assumed that maintaining a BLS < 15 would improve the outcome. However, it is not clear what "the safe range" is for BLS in a surgical ICU population and how BLS should be maintained in that range to improve outcome.

In the active group, we used a protocol for fluid removal to attain the targeted FB. The protocol was based on diuretic therapy and ultrafiltration. In patients with moderate and severe EVLW increase (BLS $\geq$ 15), the aim was to obtain a predefined -250 to -1000 mL/24 h negative FB until BLS dropped under 15. However, this strategy may not be appropriate for all patients, as some evidence indicates an average decrease of only 2.7 B-lines per 500 mL fluid removed [23]. Furthermore, we did not use LU to assess fluid responsiveness and titrate fluid input, but only to count B-lines and establish daily FB targets. A combined approach might have been more efficient in affecting FB and outcome.

In the explorative analyses of the primary outcome, the subgroups were not prespecified. Therefore, the risk of spurious findings should not be ignored.

Finally, we believe that important LU data may be lost when summarised in a single value such as the BLS. This needs to be highlighted as bedside LU is rapidly becoming a highly valued method for EVLW assessment. Learning to identify B-lines is easy, and previ-

ous studies showed a quick learning curve [60]. Moreover, other studies showed promising results regarding automatic B-line detection using image-processing algorithms [61]. However, the majority of the studies that found LU-guided fluid management to be associated with lower CFB as compared to standard care used LU in combination with cardiac ultrasound or inferior vena cava ultrasonography [62–64]. Thus, the utility or futility of BLS assessment may depend on additional ultrasound data, which should be considered when designing LU-based fluid management strategies.

5. Conclusions

Within its limitations, this trial suggests that daily BLS monitoring, with the aim of avoiding and correcting moderate/severe EVLW increase, does not improve CFB in surgical ICU patients compared to standard care. Moreover, it does not improve 28-day or 90-day survival, ICU or hospital LOS, AKI recovery time, or duration of vasopressors use. Daily BLS assessment might help decrease mechanical ventilation duration, but this result needs to be verified in a larger trial. Future studies should also establish whether BLS alone yields any value in a heterogeneous population of critically ill surgical patients or needs to be correlated with B-lines distribution patterns, cardiac ultrasound, PaO_2/FiO_2 ratio, or other parameters to increase its specificity in EVLW assessment.

Author Contributions: Conceptualisation: A.C.C.; methodology: A.C.C., I.G. and M.B.; software: D.-M.R.; validation: A.C.C., I.G. and M.B.; formal analysis: D.-M.R.; investigation: A.-I.C., D.-M.R., G.S., I.S. and O.L.; resources: M.O.; data curation: D.-M.R. and M.O.; writing—original draft: D.-M.R.; writing—review & editing: A.C.C. and I.G.; visualisation: D.-M.R.; supervision: A.C.C., I.G. and M.B.; project administration: A.C.C.; funding acquisition: A.C.C. All authors have read and agreed to the published version of the manuscript.

Funding: This research was funded by The Romanian Ministry of Education, The Executive Unit for Funding for Higher Education, Research, Development, and Innovation. The funding body had no role in study design, analysis, and interpretation of data.

Institutional Review Board Statement: The study was conducted according to the guidelines of the Declaration of Helsinki and approved by the Research Ethics Committees of the Grigore T. Popa University of Medicine and Pharmacy Iasi (26261/14 November 2017) and by the research ethic boards of all participating hospitals. The trial was retrospectively registered on ClinicalTrials.gov (https://clinicaltrials.gov/ct2/show/NCT03393065) accessed on 8 January 2018.

Informed Consent Statement: Informed consent was obtained from all subjects involved in the study.

Data Availability Statement: The datasets used and/or analysed during the current study are available from the corresponding author on reasonable request.

Conflicts of Interest: The authors declare no conflict of interest.

References

1. Messmer, A.S.; Zingg, C.; Müller, M.; Gerber, J.L.; Schefold, J.C.; Pfortmueller, C.A. Fluid Overload and Mortality in Adult Critical Care Patients-A Systematic Review and Meta-Analysis of Observational Studies. *Crit. Care Med.* **2020**, *48*, 1862–1870. [CrossRef] [PubMed]
2. Hoste, E.A.; Maitland, K.; Brudney, C.S.; Mehta, R.; Vincent, J.L.; Yates, D.; Kellum, J.A.; Mythen, M.G.; Shaw, A.D. Four phases of intravenous fluid therapy: A conceptual model. *Br. J. Anaesth.* **2014**, *113*, 740–747. [CrossRef]
3. Finfer, S.; Myburgh, J.; Bellomo, R. Intravenous fluid therapy in critically ill adults. *Nat. Rev. Nephrol.* **2018**, *14*, 541–557. [CrossRef]
4. Vincent, J.L. Fluid management in the critically ill. *Kidney Int.* **2019**, *96*, 52–57. [CrossRef]
5. Malbrain, M.L.N.G.; Langer, T.; Annane, D.; Gattinoni, L.; Elbers, P.; Hahn, R.G.; De Laet, I.; Minini, A.; Wong, A.; Ince, C.; et al. Intravenous fluid therapy in the perioperative and critical care setting: Executive summary of the International Fluid Academy (IFA). *Ann. Intensive Care* **2020**, *10*, 64. [CrossRef] [PubMed]
6. Silversides, J.A.; Fitzgerald, E.; Manickavasagam, U.S.; Lapinsky, S.E.; Nisenbaum, R.; Hemmings, N.; Nutt, C.; Trinder, T.J.; Pogson, D.G.; Fan, E.; et al. Deresuscitation of patients with iatrogenic fluid overload is associated with reduced mortality in critical illness. *Crit. Care Med.* **2018**, *46*, 1600–1607. [CrossRef]
7. Claure-Del Granado, R.; Mehta, R.L. Fluid overload in the ICU: Evaluation and management. *BMC Nephrol.* **2016**, *17*, 109. [CrossRef]

8. Sim, J.; Kwak, J.Y.; Jung, Y.T. Association between postoperative fluid balance and mortality and morbidity in critically ill patients with complicated intra-abdominal infections: A retrospective study. *Acute Crit. Care* **2020**, *35*, 189–196. [CrossRef]
9. Zhang, J.; Crichton, S.; Dixon, A.; Seylanova, N.; Peng, Z.Y.; Ostermann, M. Cumulative fluid accumulation is associated with the development of acute kidney injury and non-recovery of renal function: A retrospective analysis. *Crit. Care* **2019**, *23*, 392. [CrossRef] [PubMed]
10. Van Mourik, N.; Metske, H.A.; Hofstra, J.J.; Binnekade, J.M.; Geerts, B.F.; Schultz, M.J.; Vlaar, A.P.J. Cumulative fluid balance predicts mortality and increases time on mechanical ventilation in ARDS patients: An observational cohort study. *PLoS ONE* **2019**, *14*, e0224563. [CrossRef]
11. Child, D.L.; Cao, Z.; Seiberlich, L.E.; Brown, H.; Greenberg, J.; Swanson, A.; Sewall, M.R.; Robinson, S.B. The costs of fluid overload in the adult intensive care unit: Is a small-volume infusion model a proactive solution? *Clin. Outcomes Res.* **2014**, *7*, 1–8. [CrossRef] [PubMed]
12. RENAL Replacement Therapy Study Investigators; Bellomo, R.; Cass, A.; Cole, L.; Finfer, S.; Gallagher, M.; Lee, J.; Lo, S.; McArthur, C.; McGuiness, S.; et al. An observational study fluid balance and patient outcomes in the randomized evaluation of normal vs. augmented level of replacement therapy trial. *Crit. Care Med.* **2012**, *40*, 1753–1760. [CrossRef]
13. Gong, Y.C.; Liu, J.T.; Ma, P.L. Early fluid loading for septic patients: Any safety limit needed? *Chin. J. Traumatol.* **2018**, *21*, 1–3. [CrossRef]
14. O'Connor, M.E.; Jones, S.L.; Glassford, N.J.; Bellomo, R.; Prowle, J.R. Defining fluid removal in the intensive care unit: A national and international survey of critical care practice. *J. Intensive Care Soc.* **2017**, *18*, 282–288. [CrossRef]
15. Nair, S.; Sauthoff, H. Assessing Extravascular Lung Water with Ultrasound: A Tool to Individualize Fluid Management? *J. Intensive Care Med.* **2020**, *35*, 1356–1362. [CrossRef]
16. Jozwiak, M.; Teboul, J.L.; Monnet, X. Extravascular lung water in critical care: Recent advances and clinical applications. *Ann. Intensive Care* **2015**, *5*, 1–13. [CrossRef]
17. Bendjelid, K.; Giraud, R.; Siegenthaler, N.; Michard, F. Validation of a new transpulmonary thermodilution system to assess global end-diastolic volume and extravascular lung water. *Crit. Care* **2010**, *14*, R209. [CrossRef]
18. Kiefer, N.; Hofer, C.K.; Marx, G.; Geisen, M.; Giraud, R.; Siegenthaler, N.; Hoeft, A.; Bendjelid, K.; Rex, S. Clinical validation of a new thermodilution system for the assessment of cardiac output and volumetric parameters. *Crit. Care* **2012**, *16*, R98. [CrossRef]
19. Kuzkov, V.V.; Suborov, E.V.; Kirov, M.Y.; WÆrhaug, K.; Mortensen, R.; Kuklin, V.N.; Nordhus, K.C.; BjertnÆs, L.J. Radiographic lung density assessed by computed tomography is associated with extravascular lung water content. *Acta Anaesthesiol. Scand.* **2010**, *54*, 1018–1026. [CrossRef] [PubMed]
20. Hayes, C.E.; Case, T.A.; Ailion, D.C.; Morris, A.H.; Cutillo, A.; Blackburn, C.W.; Durney, C.H.; Johnson, S.A. Lung water quantitation by nuclear magnetic resonance imaging. *Science* **1982**, *216*, 1313–1315. [CrossRef] [PubMed]
21. Pingitore, A.; Garbella, E.; Piaggi, P.; Menicucci, D.; Frassi, F.; Lionetti, V.; Piarulli, A.; Catapano, G.; Lubrano, V.; Passera, M.; et al. Early subclinical increase in pulmonary water content in athletes performing sustained heavy exercise at sea level: Ultrasound lung comet-tail evidence. *Am. J. Physiol. Heart Circ. Physiol.* **2011**, *301*, H2161–H2167. [CrossRef] [PubMed]
22. Gargani, L.; Lionetti, V.; Di Cristofano, C.; Bevilacqua, G.; Recchia, F.A.; Picano, E.; Cristofano, C.; Bevilacqua, G.; Recchia, F.A.; Picano, E. Early detection of acute lung injury uncoupled to hypoxemia in pigs using ultrasound lung comets. *Crit. Care Med.* **2007**, *35*, 2769–2774. [CrossRef] [PubMed]
23. Noble, V.E.; Murray, A.F.; Capp, R.; Sylvia-Reardon, M.H.; Steele, D.J.R.R.; Liteplo, A. Ultrasound assessment for extravascular lung water in patients undergoing hemodialysis: Time course for resolution. *Chest* **2009**, *135*, 1433–1439. [CrossRef]
24. Platz, E.; Merz, A.A.; Jhund, P.S.; Vazir, A.; Campbell, R.; McMurray, J.J. Dynamic changes and prognostic value of pulmonary congestion by lung ultrasound in acute and chronic heart failure: A systematic review. *Eur. J. Heart Fail.* **2017**, *19*, 1154–1163. [CrossRef] [PubMed]
25. Bouhemad, B.; Zhang, M.; Lu, Q.; Rouby, J.J. Clinical review: Bedside lung ultrasound in critical care practice. *Crit. Care* **2007**, *11*, 205. [CrossRef] [PubMed]
26. Picano, E.; Frassi, F.; Agricola, E.; Gligorova, S.; Gargani, L.; Mottola, G. Ultrasound lung comets: A clinically useful sign of extravascular lung water. *J. Am. Soc. Echocardiogr.* **2006**, *19*, 356–363. [CrossRef]
27. Agricola, E.; Bove, T.; Oppizzi, M.; Marino, G.; Zangrillo, A.; Margonato, A.; Picano, E. "Ultrasound comet-tail images": A marker of pulmonary edema—A comparative study with wedge pressure and extravascular lung water. *Chest* **2005**, *127*, 1690–1695. [CrossRef] [PubMed]
28. Jambrik, Z.; Gargani, L.; Adamicza, Á.; Kaszaki, J.; Varga, A.; Forster, T.; Boros, M.; Picano, E. B-lines quantify the lung water content: A lung ultrasound versus lung gravimetry study in acute lung injury. *Ultrasound Med. Biol.* **2010**, *36*, 2004–2010. [CrossRef] [PubMed]
29. Anile, A.; Russo, J.; Castiglione, G.; Volpicelli, G. A simplified lung ultrasound approach to detect increased extravascular lung water in critically ill patients. *Crit. Ultrasound J.* **2017**, *9*, 13. [CrossRef]
30. Chiem, A.T.; Chan, C.H.; Ander, D.S.; Kobylivker, A.N.; Manson, W.C. Comparison of expert and novice sonographers' performance in focused lung ultrasonography in dyspnea (FLUID) to diagnose patients with acute heart failure syndrome. *Acad. Emerg. Med.* **2015**, *22*, 564–573. [CrossRef]

31. Neuteboom, O.B.; Heldeweg, M.L.; Pisani, L.; Smit, M.R.; Lagrand, W.K.; Cherpanath, T.G.; Dondorp, A.M.; Schultz, M.J.; Tuinman, P.R. Assessing Extravascular Lung Water in Critically Ill Patients Using Lung Ultrasound: A Systematic Review on Methodological Aspects in Diagnostic Accuracy Studies. *Ultrasound Med. Biol.* **2020**, *46*, 1557–1564. [CrossRef]
32. Volpicelli, G.; Mussa, A.; Garofalo, G.; Cardinale, L.; Casoli, G.; Perotto, F.; Fava, C.; Frascisco, M. Bedside lung ultrasound in the assessment of alveolar-interstitial syndrome. *Am. J. Emerg. Med.* **2006**, *24*, 689–696. [CrossRef]
33. Pivetta, E.; Goffi, A.; Lupia, E.; Tizzani, M.; Porrino, G.; Ferreri, E.; Volpicelli, G.; Balzaretti, P.; Banderali, A.; Iacobucci, A.; et al. Lung ultrasound-implemented diagnosis of acute decompensated heart failure in the ED: A SIMEU multicenter study. *Chest* **2015**, *148*, 202–210. [CrossRef]
34. Liteplo, A.S.; Marill, K.A.; Villen, T.; Miller, R.M.; Murray, A.F.; Croft, P.E.; Capp, R.; Noble, V.E. Emergency thoracic ultrasound in the differentiation of the etiology of shortness of breath (ETUDES): Sonographic B-lines and N-terminal Pro-brain-type natriuretic peptide in diagnosing congestive heart failure. *Acad. Emerg. Med.* **2009**, *16*, 201–210. [CrossRef]
35. Anderson, K.L.; Fields, J.M.; Panebianco, N.L.; Jenq, K.Y.; Marin, J.; Dean, A.J. Inter-rater reliability of quantifying pleural B-lines using multiple counting methods. *J. Ultrasound Med.* **2013**, *32*, 115–120. [CrossRef]
36. Rusu, D.-M.; Siriopol, I.; Grigoras, I.; Blaj, M.; Ciumanghel, A.-I.; Siriopol, D.; Nistor, I.; Onofriescu, M.; Sandu, G.; Cobzaru, B.; et al. Lung Ultrasound Guided Fluid Management Protocol for the Critically Ill Patient: Study protocol for a multi-centre randomized controlled trial. *Trials* **2019**, *20*, 236. [CrossRef]
37. Jambrik, Z.; Monti, S.; Coppola, V.; Agricola, E.; Mottola, G.; Miniati, M.; Picano, E. Usefulness of ultrasound lung comets as a nonradiologic sign of extravascular lung water. *Am. J. Cardiol.* **2004**, *93*, 1265–1270. [CrossRef] [PubMed]
38. Frassi, F.; Gargani, L.; Tesorio, P.; Raciti, M.; Mottola, G.; Picano, E. Prognostic Value of Extravascular Lung Water Assessed With Ultrasound Lung Comets by Chest Sonography in Patients With Dyspnea and/or Chest Pain. *J. Card. Fail.* **2007**, *13*, 830–835. [CrossRef]
39. Lichtenstein, D. Fluid administration limited by lung sonography: The place of lung ultrasound in assessment of acute circulatory failure (the FALLS-protocol). *Expert Rev. Respir. Med.* **2012**, *6*, 155–162. [CrossRef]
40. Wiedemann, H.; Wheeler, A.; Bernard, G.; Thompson, B.; Hayden, D.; DeBoisblanc, B.; Connors, A.; Hite, R.; Harabin, A. Comparison of Two Fluid-Management Strategies in Acute Lung Injury. *N. Engl. J. Med.* **2006**, *354*, 2564–2575. [CrossRef]
41. Richard, J.C.; Bayle, F.; Bourdin, G.; Leray, V.; Debord, S.; Delannoy, B.; Stoian, A.C.; Wallet, F.; Yonis, H.; Guerin, C. Preload dependence indices to titrate volume expansion during septic shock: A randomized controlled trial. *Crit. Care* **2015**, *19*, 5. [CrossRef]
42. Chen, C.; Kollef, M.H. Targeted fluid minimization following initial resuscitation in septic shock a pilot study. *Chest* **2015**, *148*, 1462–1469. [CrossRef]
43. Hjortrup, P.B.; Haase, N.; Bundgaard, H.; Thomsen, S.L.; Winding, R.; Pettilä, V.; Aaen, A.; Lodahl, D.; Berthelsen, R.E.; Christensen, H.; et al. Restricting volumes of resuscitation fluid in adults with septic shock after initial management: The CLASSIC randomised, parallel-group, multicentre feasibility trial. *Intensive Care Med.* **2016**, *42*, 1695–1705. [CrossRef] [PubMed]
44. Corl, K.A.; Prodromou, M.; Merchant, R.C.; Gareen, I.; Marks, S.; Banerjee, D.; Amass, T.; Abbasi, A.; Delcompare, C.; Palmisciano, A.; et al. The Restrictive IV Fluid Trial in Severe Sepsis and Septic Shock (RIFTS): A Randomized Pilot Study. *Crit. Care Med.* **2019**, *47*, 951–959. [CrossRef]
45. Silversides, J.A.; McAuley, D.F.; Blackwood, B.; Fan, E.; Ferguson, A.J.; Marshall, J.C. Fluid management and deresuscitation practices: A survey of critical care physicians. *J. Intensive Care Soc.* **2020**, *21*, 111–118. [CrossRef]
46. Mayr, U.; Lukas, M.; Habenicht, L.; Wiessner, J.; Heilmaier, M.; Ulrich, J.; Rasch, S.; Schmid, R.M.; Lahmer, T.; Huber, W.; et al. B-Lines Scores Derived from Lung Ultrasound Provide Accurate Prediction of Extravascular Lung Water Index: An Observational Study in Critically Ill Patients. *J. Intensive Care Med.* **2020**, 885066620967655. [CrossRef]
47. Seibel, A.; Zechner, P.M.; Berghold, A.; Holter, M.; Braß, P.; Michels, G.; Leister, N.; Gemes, G.; Donauer, R.; Giebler, R.M.; et al. B-Lines for the assessment of extravascular lung water: Just focused or semi-quantitative? *Acta Anaesthesiol. Scand.* **2020**, *64*, 953–960. [CrossRef]
48. Buda, N.; Skoczylas, A.; Demi, M.; Wojteczek, A.; Cylwik, J.; Soldati, G. Clinical Impact of Vertical Artifacts Changing with Frequency in Lung Ultrasound. *Diagnostics* **2021**, *11*, 401. [CrossRef]
49. Pietersen, P.I.; Madsen, K.R.; Graumann, O.; Konge, L.; Nielsen, B.U.; Laursen, C.B. Lung ultrasound training: A systematic review of published literature in clinical lung ultrasound training. *Crit. Ultrasound J.* **2018**, *10*, 23. [CrossRef]
50. Bedetti, G.; Gargani, L.; Corbisiero, A.; Frassi, F.; Poggianti, E.; Mottola, G. Evaluation of ultrasound lung comets by hand-held echocardiography. *Cardiovasc. Ultrasound.* **2006**, *4*, 34. [CrossRef]
51. Haaksma, M.E.; Smit, J.M.; Heldeweg, M.L.A.; Pisani, L.; Elbers, P.; Tuinman, P.R. Lung ultrasound and B-lines: B careful! *Intensive Care Med.* **2020**, *46*, 544–545. [CrossRef]
52. Frasure, S.E.; Matilsky, D.K.; Siadecki, S.D.; Platz, E.; Saul, T.; Lewiss, R.E. Impact of patient positioning on lung ultrasound findings in acute heart failure. Eur Hear. *J. Acute Cardiovasc. Care* **2015**, *4*, 326–332. [CrossRef] [PubMed]
53. Volpicelli, G.; Elbarbary, M.; Blaivas, M.; Lichtenstein, D.A.; Mathis, G.; Kirkpatrick, A.W.; Melniker, L.; Gargani, L.; Noble, V.E.; Via, G.; et al. International evidence-based recommendations for point-of-care lung ultrasound. *Intensive Care Med.* **2012**, *38*, 577–591. [CrossRef] [PubMed]

54. Sperandeo, M.; Varriale, A.; Sperandeo, G.; Polverino, E.; Feragalli, B.; Piattelli, M.L.; Maggi, M.M.; Palmieri, V.O.; Terracciano, F.; De Sio, I.; et al. Assessment of ultrasound acoustic artifacts in patients with acute dyspnea: A multicenter study. *Acta Radiol.* **2012**, *53*, 885–892. [CrossRef]
55. Tasci, O.; Hatipoglu, O.N.; Cagli, B.; Ermis, V. Sonography of the chest using linear-array versus sector transducers: Correlation with auscultation, chest radiography, and computed tomography. *J. Clin. Ultrasound.* **2016**, *44*, 383–389. [CrossRef] [PubMed]
56. Bobbia, X.; Chabannon, M.; Chevallier, T.; de La Coussaye, J.E.; Lefrant, J.Y.; Pujol, S.; Claret, P.G.; Zieleskiewicz, L.; Roger, C.; Muller, L. Assessment of five different probes for lung ultrasound in critically ill patients: A pilot study. *Am. J. Emerg. Med.* **2018**, *36*, 1265–1269. [CrossRef] [PubMed]
57. Pirompanich, P.; Karakitsos, D.; Alharthy, A.; Gillman, L.; Blaivas, M.; Buchanan, B.; Brindley, P.; Wattanathum, A. Evaluating extravascular lung water in sepsis: Three lung-ultrasound techniques compared against transpulmonary thermodilution. *Indian J. Crit. Care Med.* **2018**, *22*, 650–655. [CrossRef]
58. Zoccali, C.; Torino, C.; Tripepi, R.; Tripepi, G.; D'Arrigo, G.; Postorino, M.; Gargani, L.; Sicari, R.; Picano, E.; Mallamaci, F. Pulmonary congestion predicts cardiac events and mortality in ESRD. *J. Am. Soc. Nephrol.* **2013**, *24*, 639–646. [CrossRef]
59. Yin, W.; Zou, T.; Qin, Y.; Yang, J.; Li, Y.; Zeng, X.; Kang, Y. Poor lung ultrasound score in shock patients admitted to the ICU is associated with worse outcome. *BMC Pulm. Med.* **2019**, *19*, 1. [CrossRef] [PubMed]
60. Scali, M.C.; Ciampi, Q.; Picano, E.; Bossone, E.; Ferrara, F.; Citro, R.; Colonna, P.; Costantino, M.F.; Cortigiani, L.; Andrea, A.D.; et al. Quality control of B-lines analysis in stress Echo 2020. *Cardiovasc. Ultrasound.* **2018**, *16*, 20. [CrossRef] [PubMed]
61. Brattain, L.J.; Telfer, B.A.; Liteplo, A.S.; Noble, V.E. Automated B-line scoring on thoracic sonography. *J. Ultrasound Med.* **2013**, *32*, 2185–2190. [CrossRef]
62. Öhman, J.; Harjola, V.P.; Karjalainen, P.; Lassus, J. Focused echocardiography and lung ultrasound protocol for guiding treatment in acute heart failure. *ESC Heart Fail.* **2018**, *5*, 120–128. [CrossRef] [PubMed]
63. Wang, L.; Qiu, C.; Guan, X.; Chen, M.; Chen, J.; Si, X.; Du, Z.; Liu, Y.; Ouyang, B. Fluid Removal with Ultrasound Guided Protocol Improves the Efficacy and Safety of Dehydration in Post-Resuscitated Critically Ill Patients: A Quasi-Experimental, Before and After Study. *Shock* **2018**, *50*, 401–407. [CrossRef] [PubMed]
64. Pontet, J.; Yic, C.; Díaz-Gómez, J.L.; Rodriguez, P.; Sviridenko, I.; Méndez, D.; Noveri, S.; Soca, A.; Cancela, M. Impact of an ultrasound-driven diagnostic protocol at early intensive-care stay: A randomized-controlled trial. *Ultrasound J.* **2019**, *11*, 24. [CrossRef] [PubMed]

diagnostics

MDPI

Article

Pre-Dialysis B-Line Quantification at Lung Ultrasound Is a Useful Method for Evaluating the Dry Weight and Predicting the Risk of Intradialytic Hypotension

Marco Allinovi [1,*], Giulia Palazzini [1,2], Gianmarco Lugli [2,3], Iacopo Gianassi [1], Lorenzo Dallari [1,2], Selene Laudicina [1,2], Marco Gregori [4], Francesco Rossi [1], Daniele Giannerini [1], Roberta Cutruzzulà [1], Egrina Dervishi [1], Maria Biagini [1] and Calogero Lino Cirami [1]

[1] Nephrology, Dialysis and Transplantation Unit, Careggi University Hospital, Largo Brambilla, 3, 50134 Florence, Italy
[2] Department of Biomedical Experimental and Clinical Sciences "Mario Serio", University of Florence, 50121 Florence, Italy
[3] Nephrology Unit, Meyer Children's Hospital, 50139 Florence, Italy
[4] Department of Nephrology, Transplantation, Dialysis and Apheresis, Pellegrin University Hospital, 33076 Bordeaux, France
* Correspondence: marco.allinovi@gmail.com

Abstract: Intradialytic hypotension (IDH) is a frequent and well-known complication of hemodialysis, occurring in about one third of patients. An integrated approach with different methods is needed to minimize IDH episodes and their complications. In this prospective observational study, recruited patients underwent a multiparametric evaluation of fluid status through a lung ultrasound (LUS) with the quantification of B-lines, a physical examination, blood pressure, NT-proBNP and chest X-rays. The evaluation took place immediately before and at the end of the dialysis session, and the patients were divided into IDH and no-IDH groups. We recruited a total of 107 patients. A pre-dialysis B-line number $\geq$ 15 showed a high sensitivity in fluid overload diagnosis (94.5%), even higher than a chest X-ray (78%) or physical examination (72%) alone. The identification at the beginning of dialysis of <8 B-lines in the overall cohort or <20 B-lines in patients with NYHA 3–4 class are optimal thresholds for identifying those patients at higher risk of experiencing an IDH episode. In the multivariable analysis, the NYHA class, a low pre-dialysis systolic BP and a low pre-dialysis B-line number were independent risk factors for IDH. At the beginning of dialysis, the B-line quantification at LUS is a valuable and reliable method for evaluating fluid status and predicting IDH episodes. A post-dialysis B-line number <5 may allow for an understanding of whether the IDH episode was caused by dehydration, probably due to due to an overestimation of the dry weight.

Keywords: lung ultrasound; B-lines; dry weight; intradialytic hypotension; fluid overload

Citation: Allinovi, M.; Palazzini, G.; Lugli, G.; Gianassi, I.; Dallari, L.; Laudicina, S.; Gregori, M.; Rossi, F.; Giannerini, D.; Cutruzzulà, R.; et al. Pre-Dialysis B-Line Quantification at Lung Ultrasound Is a Useful Method for Evaluating the Dry Weight and Predicting the Risk of Intradialytic Hypotension. *Diagnostics* **2022**, *12*, 2990. https://doi.org/10.3390/diagnostics12122990

Academic Editors: Gino Soldati and Marcello Demi

Received: 29 September 2022
Accepted: 26 November 2022
Published: 29 November 2022

1. Introduction

Intradialytic hypotension (IDH) is a serious, well-known complication of hemodialysis (HD). The National Kidney Foundation's Kidney Disease Outcomes Quality Initiative (KDOQI) guidelines define IDH as a decrease in either systolic BP $\geq$20 mmHg or mean arterial pressure $\geq$10 mmHg associated with symptoms or need for intervention [1]. IDH and other hypovolemia-related symptoms are common in HD, occurring in 15% to 50% of ambulatory HD sessions [2,3]. This high range in prevalence reported is due to the different hypotension definitions used. When symptom-based definitions of hypotension are used, the IDH is underestimated because these symptoms (such as dizziness, nausea, headache and muscle cramp) are frequently not reported by patients, but even asymptomatic IDH is a predictor of mortality and non-fatal cardiovascular disease [4,5]. IDH occurs owing to an imbalance between the ultrafiltration rate and the normal compensatory mechanisms,

including the plasma refilling rate and a reduction in venous capacity [6]. Moreover, structural and functional abnormalities of the heart and blood vessels (such as those due to a dysautonomic neuropathy, diabetes, being elderly or heart failure) increase the sensitivity of the patient to changes in fluid status [1–5]. Regardless of the definition, IDH has been associated with subsequent vascular access thrombosis, inadequate dialysis dose, cardiac arrhythmias, major adverse cardiac events, dementia, and mortality [3,7–14]. Even when asymptomatic, IDH is associated with a lower white matter and hippocampus volume and reduced global cognitive functioning [15]. Therefore, any IDH episode should prompt a reassessment of fluid status and dry weight estimation, including an evaluation of the UF rate, dialysis treatment time, interdialytic weight gain, and antihypertensive medication use. Every strategy used in hypotension management must be tightly balanced in light of the risk of generating secondary opposite side effects and complications such as fluid overload, interdialytic hypertension, edema, congestive heart failure, inadequate blood purification and the discontinuation of antihypertensive medication. Therefore, an integrated approach to IDH management is needed to resolve acute hypotension crises and to minimize complications. From this perspective, a personalized approach should be applied with a global view to ensuring a management tailored to the individual's characteristics.

In this complex setting, a deeper knowledge about the main hypotension risk factors is needed. Critical issues include target weight, residual renal kidney function protection, hemodialysate composition, temperature biofeedback and the hemodialysis technique used, since convective therapies lead to major intradialytic stability [16–19]. Moreover, given the complexity of the involved factors, the dry weight assessment of dialysis patients remains a challenge and predicting an IDH episode using conventional parameters and models may be difficult. Among several approaches, lung ultrasound (LUS) is increasingly being used at the bedside to integrate the clinical assessment of patients on dialysis [20]. The pre-dialysis number of B-lines showed a direct correlation with interdialytic weight gain and the quantification of B-lines is a widely recognized method for assessing the dry weight, decreasing ambulatory blood pressure (BP) values, recurrent episodes of decompensated heart failure and cardiovascular events of patients on dialysis [21–25]. However, comprehensive data regarding the potential role of LUS in predicting the risk of IDH are lacking. In two different randomized clinical trials, an LUS-guided strategy for dry weight assessment reported conflicting results: the first showed a marginal (almost significant) decrease in the percentage of patients experiencing one or more IDH episodes (34.3% vs. 55.6%, $p = 0.072$), while the other showed a 26% higher relative risk of intradialytic cramps (HR 1.26) [23,26].

This prospective cohort study aimed to evaluate the potential role of LUS, in particular that of B-line quantification, in predicting IDH episodes and detecting patients at a greater risk of developing IDH because of their fluid status or an overestimation of their dry weight. We also evaluated the relationship between IDH episodes and different parameters to help clarify the most important predictive factors of IDH.

2. Materials and Methods

2.1. Study Cohort

This was a prospective observational single-center study performed between 1 January 2020 and 1 January 2021 at Careggi University Hospital, a tertiary hospital facility in Florence, Italy. The primary outcome was the development of an IDH episode, defined as a decrease in systolic BP of $\geq$20 mmHg and/or a decrease in mean arterial pressure of $\geq$10 mmHg from pre-dialysis levels [1], associated with intradialytic or post-dialytic symptoms (abdominal discomfort, yawning, sighing, nausea, vomiting, muscle cramps, restlessness, dizziness or fainting and anxiety), a need for nursing interventions and/or a failure to meet a prescribed ultrafiltration goal. In relation to the achievement of the primary outcome (an IDH episode) experienced on the same day as the multiparametric evaluation, patients were divided into a hypotension group (IDH) and non-hypotension group (no-IDH). Each patient underwent a single multiparametric evaluation of their fluid status immediately before and at the end of a midweek dialysis session, using the following

methods: LUS, physical examination, blood pressure measurement, NT-proBNP and chest X-rays. At the time of patient recruitment, before the hemodialysis session, it was not possible to predict which group the patient would be included in, and in order not to create selection bias, all patients of our Dialysis Center were progressively recruited. No patient refused to complete the pre-dialysis and post-dialysis multiparametric evaluation of fluid status. Inclusion criteria were as follows: (1) age > 18 years; (2) treatment by intermittent hemodialysis, performed 3 times a week; (3) a history of hemodialysis of more than 3 months; and (4) the ability to provide consent. Exclusion criteria were as follows: (1) A pre-dialysis systolic BP < 90 mmHg. (2) A history of pneumonia in the previous weeks, co-existent lung fibrosis or interstitial lung disease, which are diseases that appear as multiple B-lines during an LUS regardless of the fluid status. In particular, patients affected by COVID-19 were excluded for 6 months after infection due to the potential persistence of B-lines [27]. (3) Insufficient clinical information and no, or lacking, laboratory findings. Demographic data and medical history were extracted from the participants' clinical records. Laboratory parameters and any other dialysis data, such as the UF rate and dialysis prescription, were collected. Data were immediately recorded on individual case report forms. The pre-dialysis systolic BP was measured in a seated position after 5 min of rest, and either every 60 min or in the case of the onset of symptoms. Data on left ventricular hypertrophy (LVH) were derived from our institution's periodic echocardiography, which is performed every year. Dry weight was assessed according to clinical criteria (blood pressure, presence of peripheral edema or pulmonary crackles, previous IDH episodes and cramps) which represent the gold standard ("trial and error") approach. The nephrologist in charge of the dialysis service performed a physical examination for the fluid status assessment. The prescribed UF volume was determined based on the patient's medical history, physical examination and the difference between the pre-dialysis weight and dry weight. The nephrologists who performed LUS were blinded to the health status of the subjects, their interdialytic weight gain, laboratory values and physical examination. Intermittent hemodialysis was performed with 5008 (Fresenius Medical Care, Waltham, MA, USA) or Artis (Baxter Healthcare Corp., Deerfield, IL, USA) hemodialysis machines, and dialysate concentrate solutions with a 1.5 mmol/L calcium concentration. Symptomatic IDH episodes, as well as any other disorder, were recorded during dialysis sessions, together with the administration of fluids or drugs.

2.2. Ultrasound Evaluation

LUS was chosen because it is a non-invasive, radiation-free and inexpensive technique, it is easy to learn and interpret and can be performed at the bedside with a portable device and does not depend on acoustic windows or patient position [28]. Although the potential harmlessness of LUS was questioned in preclinical studies, LUS is nowadays widely validated, recommended by the guidelines and its role in reducing numerous strong outcomes has been demonstrated, with no safety issues raised so far in humans. Ultrasound examinations were performed at the bedside immediately before and after dialysis sessions using an ultrasound machine (MyLab Class C-Esaote®, Genoa, Italy) with a 6–18 MHz linear probe (LA435). Various transducers (convex, microconvex, linear and phased array) have been used to quantify B-lines in adult patients. We used the linear one because it is thought to be the best for studying the pleural line. A single B-line appears as a hyperechoic, laser-like, vertical line originating from the pleura and extending to the bottom of the field of view, moving in synchrony with the patient's breathing. There are several different B-line shapes (e.g., a single thin line, a single comet-shaped line, a double or triple line converging to a single point on the pleural line), but all of them should be considered as a single B-line. B-line identification and quantification were performed by physicians with long-term expertise in LUS. A standardized 28-position B-line score was adopted to calculate the cumulative number of B-lines as an expression of interstitial pulmonary congestion, with the patient in the semi-supine position [29]. This approach consists of scanning from the second to fifth intercostal spaces on the right side and from the second

to fourth spaces on the left side, in the parasternal, midclavicular, anterior axillary and midaxillary positions, for a total of 28 positions. At every scanning site in each intercostal space, B-lines were counted from 0 to 10. It is currently accepted that, with a 28-position LUS score, a B-line score ≤ 5 is indicative of euvolemia and a B-line score > 15 reflects hypervolemia [30].

2.3. Chest X-ray

A chest radiograph, obtained in the orthostatic posteroanterior and lateral projections, gives valuable information for fluid assessment. The presence of enlargement of the azygos vein, enlargement and loss of definition of hilar structures, septal lines in the lower lung (namely, Kerley A- and B-lines), peribronchial and perivascular cuffing with widening and blurring of the margins, thickening of interlobar fissures with subpleural fluid accumulation and/or pleural effusion during chest X-ray imaging was considered as suggestive of lung congestion and hypervolemia [31,32]. Each patient underwent a chest X-ray before the dialysis session.

2.4. Blood Volume Monitoring

Blood volume monitoring is routinely performed in all patients undergoing HD in our unit. Nowadays, most manufacturers have incorporated a relative blood volume (RBV) monitor in their dialysis apparatus in order to monitor the RBV slope. In our cohort, the blood volume change during dialysis was monitored using a HEMOcontrol BV sensor (Baxter Healthcare Corp., Deerfield, IL, USA) or Blood Volume Management (BVM®) technology (Fresenius Medical Care, Concord, Hopkins, MN, USA). During ultrafiltration, as fluid is removed from an hemodialysis patient's vascular space, the RBV slope (%) continuously correlates with the increase of hematocrit or total proteins. Trained dialysis nurses recorded the BV reduction every hour during the session.

2.5. Statistical Analysis

Parametric data were reported as the mean $\pm$ standard deviation (SD) and non-parametric data as the median and interquartile range (IQR) from the 25th to 75th percentile. Continuous variables were compared using a non-parametric Mann–Whitney test, while proportions were compared using a Chi-square test. Multiple variables were compared between groups of sessions (with IDH vs. no-IDH). The IDH was considered a dummy variable, where 0 means "no IDH" and 1 means "presence of IDH". As appropriate, relationships between variables were tested with the Pearson product-moment correlation coefficient, or the Spearman's rank correlation coefficient. Logistic regression with both categorical and continuous independent variables was used to build predictive models for the occurrence of hypotension. Univariate receiver operating characteristic (ROC) curve analysis was used to calculate the area under the curve (AUC) with a 95% confidence interval (CI). The maximum value of Youden's index was applied to ROC curves as a criterion to select the optimum cut-off point both for sensitivity and specificity. A p-value < 0.05 was considered statistically significant. Statistical analysis was performed using the SPSS 22.0 software package (IBM, Armonk, NY, USA).

3. Results

3.1. Baseline Characteristics

From January 2020 to January 2021, a total of 107 patients on chronic hemodialysis received a single multiparametric evaluation characterized by a physical examination, LUS, chest X-ray, NT-proBNP and other laboratory tests. The duration of ultrasound bedside assessments ranged from 5 to 8 min. The main demographic, anthropometric, clinical, biochemical and ultrasound characteristics of the three patient groups (all patients, IDH and no-IDH) are detailed in Table 1. The IDH and no-IDH groups were not significantly different in terms of the prevalence of diabetes, left ventricular hypertrophy (LVH), age and dialysis vintage. Although two of the most important determinants of IDH are the

interdialytic weight gain and impaired compensatory mechanisms (especially reduced venous refilling because of hypoalbuminemia), neither an interdialytic weight gain nor hypoalbuminemia resulted in significant differences in the IDH group (Table 1). The IDH group had significantly fewer patients with ≥15 B-lines at pre-dialysis LUS assessment (30.3% vs. 60.8%, $p = 0.004$) and more patients with ≤5 B-lines (42.4% vs. 16.2%, $p = 0.004$), compared to no-IDH patients. Moreover, the IDH group was characterized by a lower pre-dialysis systolic BP (126 mmHg vs. 137 mmHg; $p = 0.003$).

Table 1. Clinical characteristics of the study population: patients on hemodialysis who underwent multiparametric assessment.

	All	No Intradialytic Hypotension Group	Intradialytic Hypotension Group	*p*-Value
Number of patients	107	74	33	
Males, n (%)	68 (63.6)	48 (64.9)	20 (60.6)	0.672
Age [years, median (IQR)]	69.1 (58.2–81.3)	68.2 (58.1–79.6)	75.8 (59.1–82.1)	0.324
Comorbidities:				
Diabetes, n (%)	28 (26.7%)	18 (24.3)	10 (30.3)	0.516
Hypertension, n (%)	99 (92.5)	70 (94.6)	29 (87.9)	0.124
Dialysis vintage [years, median (IQR)]	1.7 (0.2–3.5)	1.6 (0.5–3.7)	1.8 (0.2–4.9)	0.589
Oligoanuria, n (%)	60 (56.1)	41 (55.4)	19 (57.6)	0.835
LVH, n (%)	87 (81.3)	63 (85.1)	24 (72.7)	0.128
NYHA ≥ 3, n (%)	26 (24.3)	13 (17.6)	13 (39.4)	**0.015**
Anemia, n (%)	43 (40.1)	29 (39.2)	14 (42.4)	0.753
Hypoalbuminemia, n (%)	43 (40.1)	27 (36.5)	16 (48.5)	0.242
Pre-dialysis fluid status assessment:				
SBP before dialysis [mmHg, median (IQR)]	135 (120–147)	137 (130–150)	126 (110–138)	**0.003**
Peripheral oedema-pulmonary crackles, n (%)	42 (39.3)	31 (41.9)	11 (33.3)	0.632
Lung congestion at chest X-ray, n (%)	52 (47.7)	43 (58.1)	9 (27.3)	**0.006**
NT-proBNP [pg/mL, median (IQR)]	8896 (3545–34,500)	22,249 (3888–63,809.8)	6306 (2899–20,310.5)	**0.019**
Interdialytic weight gain [kg, median (IQR)]	2.3 (1.3–3.5)	2.4 (1.5–3.5)	1.8 (1.0–2.9)	0.2
Interdialytic weight gain [%, median (IQR)]	3.3 (1.9–5.1)	3.6 (2.0–5.3)	2.6 (1.5–4.2)	0.117
UF rate [mL/Kg/hr, median (IQR)]	10.5 (7.3–12.7)	10.5 (6.9–13.5)	10.5 (7.4–11.4)	0.684
B-lines before dialysis [n, median (IQR)]	15.0 (6.0–35.0)	18 (6.9–13.5)	7.0 (3.0–15.5)	**<0.001**
B-lines ≤ 5 before dialysis, n (%)	26 (24.3)	12 (16.2)	14 (42.4)	**0.004**
B-lines ≥ 15 before dialysis, n (%)	55 (51.4)	45 (60.8)	10 (30.3)	**0.004**
Fluid status assessment all along the dialysis session:				
B-lines after dialysis [n, median (IQR)]	3.0 (1.0–17.0)	4.5 (1.0–22.8)	1.0 (0–3.0)	**0.006**
% slope in RBV during first hour of dialysis [n, median (IQR)]	−5.5 (−2.8–−8.5)	−4.6 (−4.2–−6.7)	−7.6 (−4.2–−10)	**<0.001**
Follow-up				
12-month mortality, n (%)	31/92 (33.7)	17/60 (28.3)	14/32 (43.8)	0.14

Legend: RBV, relative blood volume; LVH, left ventricular hypertrophy; NYHA, New York Heart Association; IQR, interquartile range; Hb, hemoglobin; UF, ultrafiltration; SBP, systolic blood pressure.

3.2. LUS Yields a High Sensitivity in Fluid Overload Diagnosis

In patients with a pre-dialysis B-line score $\geq$ 15, LUS demonstrated 94.5% sensitivity in fluid overload diagnosis (defined through a clinical evaluation and chest X-ray), while clinical evaluation alone demonstrated 72% sensitivity, and chest X-ray alone demonstrated 78% sensitivity. Patients without B-lines or with a low pre-dialysis B-line score ($\leq$5 B-lines) experienced an IDH episode more commonly ($p = 0.004$).

A binomial logistic regression was performed to ascertain the effects of the pre-dialysis B-line score on the likelihood that participants presented fluid overload (Figure 1B). The logistic regression was statistically significant ($\chi^2 = 114.344$, $p < 0.001$). An increase in the B-lines score of one conferred 1693-times higher odds of exhibiting fluid overload (95% CI 1.328–2.159, $p < 0.001$). ROC analysis was conducted, and the area under the ROC curve was 0.983 (95% CI 0.964–1.000), which was an outstanding level of discrimination according to Hosmer et al. [33].

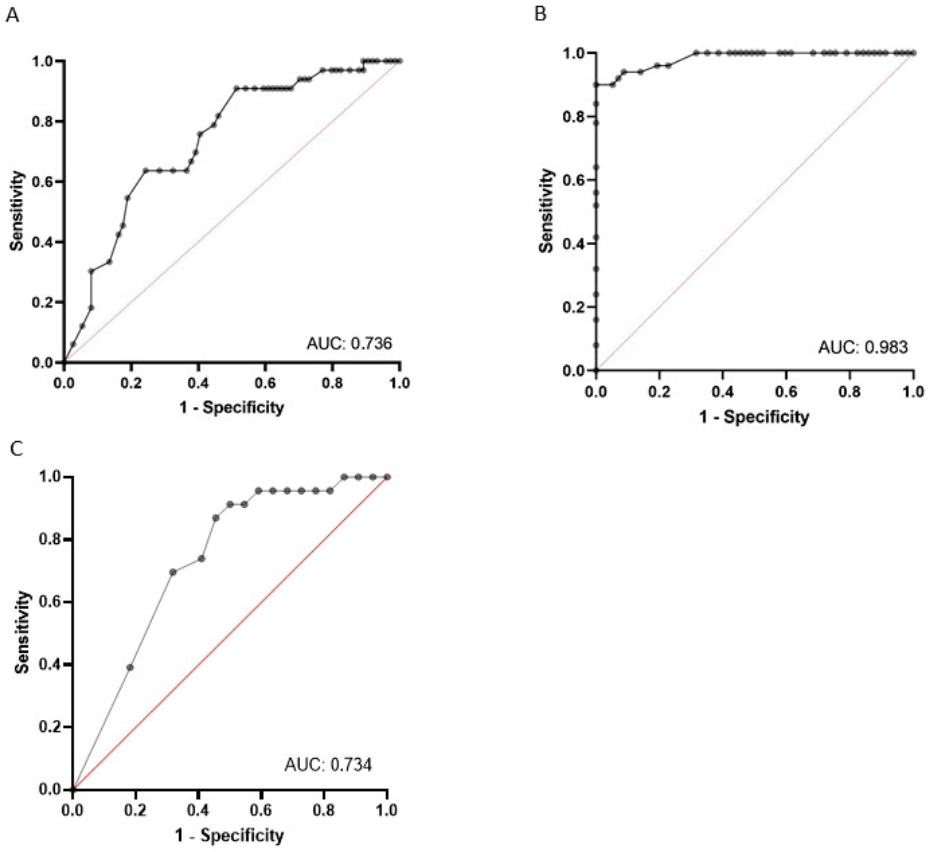

Figure 1. ROC curves in the overall cohort. (**A**) ROC curve plotting number of B-lines with the likelihood that participants had intradialytic hypotension; (**B**) ROC curve plotting number of B-lines with the likelihood that participants had overall fluid overload; (**C**) ROC curve plotting number of post-dialytic B-lines with the likelihood that participants had intradialytic hypotension.

3.3. The Number of B-Lines Predicts the Risk of IDH

A binomial logistic regression was performed to ascertain the effects of the pre-dialysis number of B-lines on the likelihood that participants had an IDH episode. The logistic regression model was statistically significant ($\chi^2 = 15.98$, $p < 0.001$). An increase in the number of B-lines of one conferred a 0.946-times lower odds of experiencing an IDH episode (95% CI 0.913–0.979, $p = 0.003$), indicating that a higher B-line score was associated with a decreased likelihood of IDH. ROC analysis was conducted, and the area under the ROC curve was 0.736 (95% CI 0.637–0.835), which was an acceptable level of discrimination according to Hosmer et al. [33] (Figure 1A). According to the Youden index method, the optimal threshold was reached when eight B-lines were detected, with a sensitivity of

63.6% and a specificity of 75.7%. With regard to the post-dialysis number of B-lines, a lower number of B-lines was detectable in patients who experienced IDH (OR 0.895, 95% CI 0.7830–0.9684). ROC analysis retrieved an AUC that showed an acceptable level of discrimination (AUC = 0.734, 95% IC 0.5843–0.8841), with an optimal threshold of five B-lines (Figure 1C).

3.4. The Number of B-Lines Predicts the Risk of IDH, Even in Patients with Heart Failure

A subgroup analysis was conducted according to the NYHA class (see Supplementary Figure S1). Notably, in NYHA classes 0–2, the optimal threshold to predict an IDH episode was reached when 8 B-lines were detected (sensitivity 70.5%, specificity 75%), but in NYHA classes 3–4, a threshold as high as 20 B-lines was reached (sensitivity 92.3%, specificity 84.6%).

In our cohort of 26 patients with heart failure (defined as NYHA class $\geq$ 3), only a chest X-ray, the NT-proBNP value and the number of B-lines before dialysis appeared to be promising fluid status assessment methods that were able to predict an IDH episode (Table 2).

Table 2. Clinical characteristics of patients with heart failure (defined as NYHA class $\geq$3) on hemodialysis who underwent multiparametric assessment.

	All	No intradialytic Hypotension Group	Intradialytic Hypotension Group	*p*-Value
Number of patients	26	13	13	
Males, n (%)	20 (77)	10 (77)	10 (77)	1.0
Age [years, median (IQR)]	76.6 (71.7–84.2)	73.6 (66.5–84.9)	79.6 (76.0–83.9)	0.41
Different methods for fluid status assessment before dialysis:				
SBP before dialysis [mmHg, median (IQR)]	128 (114–138)	130 (114–138)	126 (114–138)	0.84
Peripheral oedema-pulmonary crackles, n (%)	15 (57.7)	9 (69.2)	6 (46.2)	0.43
Lung congestion at chest X-ray, n (%)	18 (69.2)	12 (92.3)	6 (46.2)	**0.03**
NT-proBNP [pg/mL, median (IQR)]	49,895 (11,681–82,920)	76,293 (48,141–84,818)	21,097 (6279–23,784)	**<0.001**
B-lines before dialysis [n, median (IQR)]	28.6 (12.8–47.5)	41.8 (37–51)	15.4 (3–18)	**0.001**
Different methods for fluid status assessment during the dialysis session:				
% slope in RBV during first hour of dialysis [n, median (IQR)]	−5.1 (−7.7–−3.0)	−4.1 (−5.5–−2.8)	−6.2 (−9.5–−3.0)	0.24
B-lines after dialysis [n, median (IQR)]	9 (3–18)	24 (10–28)	3 (0–6)	**<0.001**

Legend: RBV, relative blood volume; NYHA, New York Heart Association; IQR, interquartile range; SBP, systolic blood pressure.

3.5. The Number of B-Lines Correlates with NT-proBNP and Serum Albumin

Correlation analysis was run to assess the relationship between the number of B-lines and the other variables. Preliminary analyses showed that only the weight difference (weight—dry weight) in Kg and weight difference in %, the two variables which describe the interdialytic weight gain, were normally distributed, as assessed using Shapiro–Wilk's tests ($p > 0.05$). Thus, a Pearson's product-moment correlation was run to assess the relationship between the number of B-lines and these variables, showing in both cases a positive statistically significant correlation (r(107) = 0.529, $p < 0.001$; r(107) = 0.586, $p < 0.001$). A Spearman's rank-order correlation was run to assess the relationship between the number of B-lines and the other variables measured. A preliminary analysis showed that the

relationship with the NT-proBNP plasma concentration, albuminemia and NYHA class was monotonic, as assessed by a visual inspection of scatter plots. There was a statistically significant, strong positive correlation between the number of B-lines and the NT-proBNP plasma concentration ($r_s(77) = 0.628$, $p < 0.001$) and a positive correlation with the NYHA class ($r_s(107) = 0.301$, $p = 0.002$) and hypoalbuminemia ($r_s(107) = -0.194$, $p = 0.046$).

3.6. Hypoalbuminemia, Low Pre-Dialysis Systolic BP and a Low Number of B-Lines Are Independent Risk Factors for IDH

Table 3 summarizes the results of the multivariable logistic regression analysis of 12 factors in relation to IDH. We decided to include all these variables in this analysis (Model 1) without testing each one in univariable logistic regression models to preserve all the possible clinical information related to IDH. In the multivariable analysis (Table 3, Model 1), a low pre-dialysis systolic BP (OR 0.964; 95% CI 0.933–0.996) and a low pre-dialysis B-line score (OR 0.877; 95% CI 0.817–0.942) were independent risk factors for IDH (p for the model < 0.01). Model 2 was built including only independent risk factors derived from Model 1, with the inclusion of NYHA class and hypoalbuminemia, both of which had $p < 0.1$ in Model 1. A low pre-dialysis systolic BP, low number of B-lines, and NYHA class, but not hypoalbuminemia, were independent risk factors for developing IDH (p for the model < 0.01).

Table 3. Multivariable analysis of different risk factors predicting an intradialytic hypotension episode.

	Model 1				**Model 2**			
	OR	**95% CI**		***p***	**OR**	**95% CI**		***p***
Age (years)	0.989	0.950	1.029	0.579	-	-	-	-
Gender (M)	0.666	0.211	2.100	0.487	-	-	-	-
NYHA class	2.334	0.989	5.509	0.053	2.06	1.027	4.132	**0.042**
Previous cardiovascular events (yes/no)	0.809	0.199	3.298	0.768	-	-	-	-
Residual diuresis (mL)	0.999	0.998	1.00	0.192	-	-	-	-
SBP before dialysis (mmHg)	0.964	0.933	0.996	**0.030**	0.965	0.938	0.994	**0.017**
Delta weight gain/dry weight (%)	1.149	0.781	1.689	0.480	-	-	-	-
UF rate (mL/kg/h)	1.018	0.832	1.246	0.863	-	-	-	-
Peripheral oedema-pulmonary crackles (yes/no)	4.476	0.980	21.369	0.53	-	-	-	-
Hypoalbuminemia (yes/no)	0.319	0.091	1.122	0.075	0.471	0.164	1.352	0.162
B-lines before dialysis (n)	0.877	0.817	0.942	**<0.001**	0.920	0.881	0.962	**<0.001**
Hb (g/dL)	1.364	0.397	4.69	0.622	-	-	-	-

Model 1: all the variables included in the model. Model 2: NYHA class, SBP before dialysis, hypoalbuminemia, B-lines before dialysis included. Legend: NYHA, New York Heart Association; IQR, interquartile range; Hb, hemoglobin; UF, ultrafiltration per hour; SBP, systolic blood pressure.

3.7. IDH and Pre-Dialysis B-Lines Are Not Associated with a Higher Mortality

Among patients with at least one year of follow-up, the overall one-year mortality rate was 33.7% and it did not differ between IDH and no-IDH patients (43.8% vs. 28.3%, $p = 0.136$). Moreover, neither the number of pre-dialysis B-lines nor belonging to the IDH group were significant predictors of one-year mortality (binary logistic regression: $p = 0.554$ and $p = 0.480$).

3.8. Overall Performance of Selected Items to Predict IDH

We then decided to assess the performance of single variables for the prediction of IDH. We tested LUS (in terms of number of B-lines before dialysis), the BVM values (in terms of % slope in RBV during first hour of dialysis), the clinical evaluation (based on

the physical examination), the chest X-rays and the NT-proBNP values in relation to the likelihood that participants had intradialytic hypotension (Figure 2A). In the ROC analysis, the number of B-lines performed significantly better than all the other variables, with the exception of BVM (Figure 2B). Taken together, these results highlighted the feasibility of using LUS to predict IDH and its superiority to chest X-rays and physical examination, which are widely used.

A

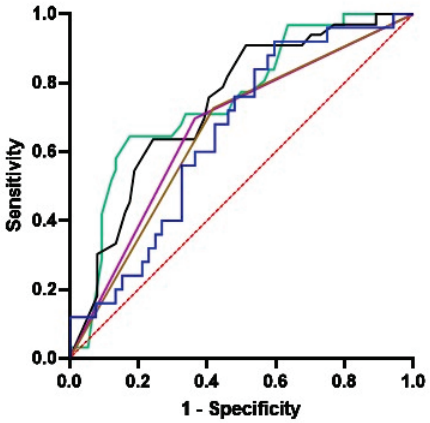

B

	AUC	95% IC	Pairwise comparisons
B-lines	0.736	0.6373 to 0.8348	ref
BVM	0.747	0.6457 to 0.8487	0.428
Clinical evaluation	0.666	0.5548 to 0.7773	**0.009**
Chest X-Ray	0.654	0.5431 to 0.7652	**0.05**
NT-proBNP	0.650	0.5257 to 0.7758	**0.024**

Figure 2. Comparative analysis of different fluid status assessment methods to predict IDH episodes. ROC curve analysis for the overall cohort. (**A**) ROC curves plotting number of B-lines, BVM values, clinical evaluation, chest X-ray and the NT-proBNP values in relation to the likelihood that participants had an IDH. (**B**) Table shows AUC values and pairwise comparisons with B-lines score.

With regard to RBV changes during the first hour of dialysis, and according to the Youden index method, the optimal diagnostic threshold was reached when a −7.9% reduction in RBV during first hour of dialysis was detected, with a sensitivity of 82.7% and a specificity of 62.5%. With regard to the Nt-proBNP values, and according to the Youden index method, the optimal diagnostic threshold was reached when a Nt-proBNP value of 33713.5 was detected, with a sensitivity of 40.4% and a specificity of 91.7%.

4. Discussion

IDH is a frequent complication in hemodialysis and its importance is shown by the important adverse clinical outcomes it determines, both in the short- and long-term. In our study, 33/107 (30.4%) patients on three-weekly hemodialysis experienced an IDH episode. This prevalence was in line with previously published articles, in which IDH was documented in 5–77.7% of patients [34]. This huge range depends on the definition of IDH used, but the majority of the studies confirmed a prevalence between 15 and 30% of all sessions [35]. Several risk factors of IDH have been identified by different studies over the years, such as age, hypoalbuminemia, ultrafiltration rate (mL/h/kg) and pre-dialysis SBP, and all of them were confirmed in our study [3,36,37]. From a recent meta-analysis, diabetes, high interdialytic weight gain, female gender, and lower body weight were described in association with IDH across studies, but we did not confirm these associations in our cohort [34]. We also demonstrated that an NYHA class ≥ 3, a low number of B-lines before dialysis, and a low pre-dialysis systolic BP were independent risk factors for IDH. The use of LUS as a tool for assessing patients' hydration status has been spreading for some years, and it was established that a finding of $\leq$5 B-lines was indicative of euvolemia and that >15 B-lines reflected hypervolemia, considering a 28-position LUS score [30]. By applying this approach to dialysis patients, for whom the hydration state is so variable, we demonstrated that LUS is a valuable technique for fluid overload assessment. We found a higher incidence of IDH in patients with fewer pre-dialysis B-lines and a lower risk of IDH in cases where pre-dialysis there was $\geq$15 B-lines. A similar study showed that there was

an increased risk of IDH in critically ill patients on intermittent HD with <14 pre-dialysis B-lines only if they presented a concomitant vena cava collapsibility $\leq$ 11.5 mm m^{-2} [38]. Another study, again on patients undergoing HD in an intensive care setting, showed that patients with documentation of an A-line pattern (indicating a dry lung) had a higher incidence of IDH than those with an overriding B-line pattern, although the authors did not provide a prognostic threshold in the B-line score [39]. In our study, a significantly lower number of B-lines post-dialysis was identified in patients who experienced IDH, with $\leq$5 B-lines in most patients, highlighting the central role of hypovolemia in IDH etiopathogenesis. Altogether, we demonstrated that, both pre-dialysis and post-dialysis, the number of B-lines was inversely related to the risk of an IDH episode. The identification of <8 B-lines using LUS at the beginning of dialysis was an optimal threshold for identifying those patients at higher risk of experiencing an IDH episode, with a sensitivity of 63.6% and specificity of 75.7%, and well-designed prospective studies are required to validate this observation. Although these values were not excellent, we should also consider that the pathophysiology of IDH events is very complex and not completely predictable. Not all hypotension is due to hypovolemia, and not all hypovolemia causes significant hypotension. This happens because there are compensatory mechanisms that try to maintain a stable BP. Consequently, LUS before dialysis cannot aspire to predict all IDH episodes and we consider the results obtained as satisfactory. Conversely, a post-dialysis B-lines quantification may provide an understanding of whether the IDH episode was due to dehydration, probably due to an overestimation of the dry weight, as demonstrated by <5 B-lines, or due to other reasons (e.g., autonomic dysfunction, high UF rate, non-dialyzable antihypertensive drugs, hypoalbuminemia and/or anemia).

Even considering the multifactorial nature of IDH in hemodialysis and the great heterogeneity of dialysis patients, a multiparametric approach to predict IDH is needed. Consequently, nephrologists should also be careful about UF rate prescription (in particular for >13 mL/kg/hour), and be more vigilant about RBV changes (in particular for an RBV decline below $-$7.9% during the first hour of dialysis).

Each method (physical examination, B-line score, blood pressure measurement, NT-proBNP and RBV decline) suffers from several shortcomings, and, consequently, we should adopt different methods or different thresholds for each method in the presence of comorbidities associated with autonomic dysfunction. For example, in patients with severe heart failure (defined as NYHA class $\geq$ 3), the loss of compensation from increased contractility predisposes them to the development of IDH even with >8 B-lines pre-dialysis or with physical signs of fluid overload. In these patients, pulmonary congestion (identified using a chest X-ray or the number of B-lines) did not appear to be representative of systemic fluid status, and this was likely related to the concomitant left ventricular dysfunction. Interestingly, the identification of <20 B-lines pre-dialysis in patients with NYHA class 3–4 was the optimal threshold for predicting an IDH episode, with a sensitivity of 92.3% and specificity 84.6%, suggesting that the extent of pulmonary congestion in these patients was not representative of the overall volume status. A certain amount of pulmonary congestion remained, even when the patient had reached the dry weight (Table 2). As a result of left ventricular dysfunction, we should be very careful to avoid systemic dehydration (and, therefore, IDH) in an attempt to dry out the lung congestion.

Although the development of IDH is recognized as a risk factor for mortality in dialysis patients, in our study, we only found a correlation between IDH and one-year mortality (Table 1). Statistical significance was probably not reached due to the relatively small number of patients enrolled with an adequate follow-up.

Changes in the B-line score were apparent in real-time with fluid removal during dialysis, reflecting the degree of interstitial imbibition of lung tissue, with a progressive B-line score reduction over the hemodialysis session [40,41]. This versatility of LUS makes it a useful tool, not only at the beginning of dialysis, but also during or at the end of the session, to guide a progressive reduction in post-dialysis weight in order to optimize patients' baseline fluid status, even considering that IDH generally occurs at a median

time interval of 120–149 min [42]. We recommend LUS as a routine exam in patients on dialysis in order to obtain a more accurate volemic status evaluation, but also to prevent IDH episodes. In particular, LUS can be used as a first-level exam before dialysis sessions in patients at a high risk of developing IDH, such as those with (1) frequent or recent IDH episodes, (2) fluctuations in dry weight, (3) recent surgery or infections, (4) malnutrition, (5) a recent period of fasting or an increased appetite and (6) glucocorticoid therapy.

In this study, we also demonstrated that a simple pulmonary assessment using LUS provided relevant information about pulmonary congestion in hemodialysis patients (outperforming chest radiography [43]) and identified patients at risk of complications. This new element can help an integrated clinical evaluation (B-line quantification together with BVM and a physical examination) and guide physicians in the selection of an appropriate ultrafiltration profile. We propose that dialysis units adopt LUS in their daily clinical practice as a bedside tool not only for fluid status assessment and dry weight prescription, but also to prevent IDH and drive the ultrafiltration prescription during the whole hemodialytic session (Figure 3). The risk of an IDH episode can be reduced at the beginning of any dialysis session with treatment of the modifiable risk factors, for example, by administering colloids (serum albumin) during the dialysis session, modulating antihypertensive therapies (for patients with a low pre-dialysis systolic BP) and by assessing the number of B-lines pre-dialysis (as a sensitive method with which to evaluate fluid status).

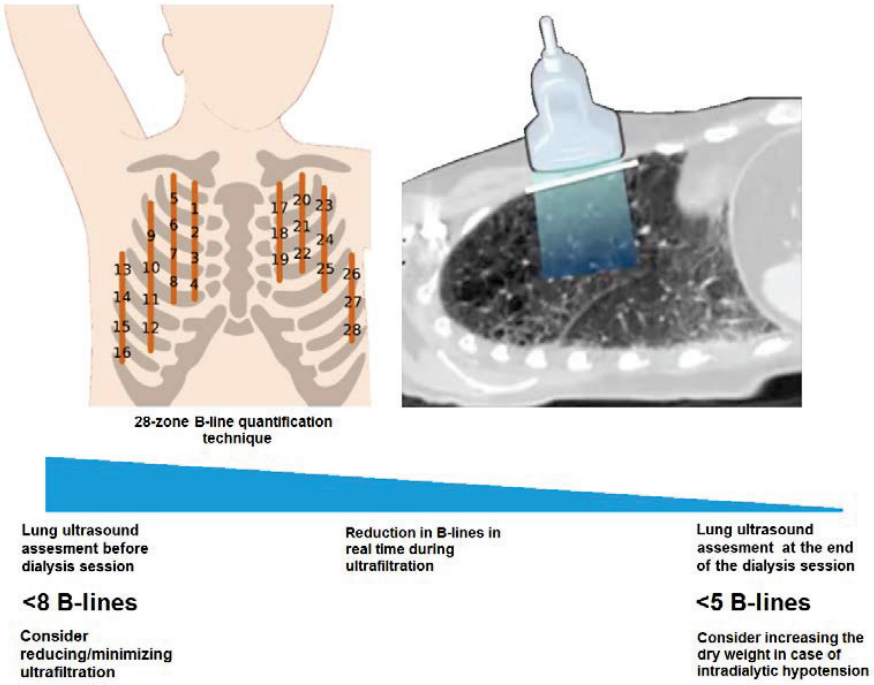

Figure 3. A proposed lung ultrasound approach in hemodialysis in order to drive ultrafiltration prescriptions. Nephrologists should adopt B-line quantification by LUS as a bedside approach to prevent IDH and drive the ultrafiltration prescription during the whole hemodialytic session. The identification of <8 B-lines at the beginning of dialysis can be helpful for identifying those patients at higher risk of experiencing an IDH episode, and consequently nephrologists might consider reducing/minimizing ultrafiltration. Conversely, the identification of <5 B-lines at the end of a dialysis session complicated by an IDH episode is highly suggestive of dehydration, probably due to an overestimation of the dry weight, and consequently nephrologists might consider increasing the dry weight.

The small number of patients enrolled from one single center represents an important limitation of this study, and it was not sufficiently powered to detect clinically relevant changes in strong outcomes, such as mortality or cardiovascular events. Due to its observational nature and the lack of a follow-up, this study could not establish whether the routine use of LUS could improve efficiency in terms of preventing IDH episodes, but it

does serve as a pilot study for future studies. Last, we recruited consecutive patients who needed a multiparametric evaluation of fluid status and, consequently, we might have selected patients more prone to fluid status abnormalities, including both hypovolemia or hypervolemia. Despite this, patients' characteristics were similar between the two groups.

5. Conclusions

In summary, IDH occurs in response to a reduction in blood volume as an expression of different independent risk factors, such as abnormal cardiac function (NYHA class ≥ 3), lower pre-dialysis systolic BP and lower fluid status (quantified by LUS as a lower number of B-lines). Using LUS at the beginning of dialysis is a valuable method for fluid status assessment, showing a high sensitivity in fluid overload diagnosis, even higher than a chest X-ray and physical examination. The pre-dialysis number of B-lines at LUS assessment was able to predict an IDH episode independently from the NYHA class, UF rate and physical signs/symptoms of fluid status. A low B-line score (<8 B-lines) at the beginning of dialysis may predict IDH and its quantification should be integrated with other clinical and laboratory parameters in order to drive the prescription of ultrafiltration. A low B-line score ($\leq$5 B-lines) at the end of dialysis may suggest that IDH was associated with hypovolemia due to an overestimation of the dry weight. In patients with low B-line scores, nephrologists should be careful about UF prescription and more vigilant about RBV changes during a dialysis session.

Supplementary Materials: The following supporting information can be downloaded at: https://www.mdpi.com/article/10.3390/diagnostics12122990/s1.

Author Contributions: Conceptualization, M.A.; methodology, M.A. and G.L.; software, E.D.; validation, C.L.C. and M.B.; formal analysis, G.L.; investigation, G.P., I.G., L.D., S.L., M.G., F.R., D.G. and R.C.; resources, M.A.; data curation, G.L.; writing—original draft preparation, M.A., G.P. and G.L.; writing—review and editing, M.A. and C.L.C.; visualization, I.G.; supervision, L.D.; project administration, M.G. All authors have read and agreed to the published version of the manuscript.

Funding: This research received no external funding.

Institutional Review Board Statement: The study protocol conformed to the Declaration of Helsinki and was approved by a local research ethics committee (study approval number 18217/OSS).

Informed Consent Statement: Informed consent was obtained from all subjects involved in the study.

Data Availability Statement: The datasets used and/or analyzed during the current study are available from the corresponding author on reasonable request.

Conflicts of Interest: The authors declare no conflict of interest.

References

1. K/DOQI Workgroup. K/DOQI clinical practice guidelines for cardiovascular disease in dialysis patients. *Am. J. Kidney Dis. Off. J. Natl. Kidney Found.* **2005**, *45*, S1–S153.
2. Orofino, L.; Marcen, R.; Quereda, C.; Villafruela, J.; Sabater, J.; Matesanz, R.; Pascual, J.; Ortuño, J. Epidemiology of Symptomatic Hypotension in Hemodialysis: Is Cool Dialysate Beneficial for All Patients? *Am. J. Nephrol.* **1990**, *10*, 177–180. [CrossRef] [PubMed]
3. Chou, J.A.; Kalantar-Zadeh, K.; Mathew, A.T. A brief review of intradialytic hypotension with a focus on survival. *Semin. Dial.* **2017**, *30*, 473–480. [CrossRef]
4. Meredith, D.J.; Pugh, C.W.; Sutherland, S.; Tarassenko, L.; Birks, J. The relationship between symptoms and blood pressure during maintenance hemodialysis. *Hemodial. Int. Int. Symp. Home Hemodial.* **2015**, *19*, 543–552. [CrossRef]
5. Cedeño, S.; Vega, A.; Macías, N.; Sánchez, L.; Abad, S.; López-Gómez, J.M.; Luño, J. Intradialytic hypotension definitions with mortality prediction capacity in a cohort of haemodialysis patients. *Nefrología* **2020**, *40*, 402–412. [CrossRef]
6. Daugirdas, J.T. Pathophysiology of dialysis hypotension: An update. *Am. J. Kidney Dis. Off. J. Natl. Kidney Found.* **2001**, *38*, S11–S17. [CrossRef] [PubMed]
7. Chang, T.I.; Paik, J.; Greene, T.; Desai, M.; Bech, F.; Cheung, A.K.; Chertow, G.M. Intradialytic Hypotension and Vascular Access Thrombosis]. *J. Am. Soc. Nephrol.* **2011**, *22*, 1526–1533. [CrossRef]
8. Ronco, C.; Brendolan, A.; Milan, M.; Rodeghiero, M.P.; Zanella, M.; La Greca, G. Impact of biofeedback-induced cardiovascular stability on hemodialysis tolerance and efficiency. *Kidney Int.* **2000**, *58*, 800–808. [CrossRef]

9. Mc Causland, F.R.; Tumlin, J.A.; Roy-Chaudhury, P.; Koplan, B.A.; Costea, A.I.; Kher, V.; Williamson, D.; Pokhariyal, S.; Charytan, D.M. Intradialytic Hypotension and Cardiac Arrhythmias in Patients Undergoing Maintenance Hemodialysis: Results from the Monitoring in Dialysis Study. *Clin. J. Am. Soc. Nephrol. CJASN* **2020**, *15*, 805–812. [CrossRef] [PubMed]
10. Stefánsson, B.V.; Brunelli, S.M.; Cabrera, C.; Rosenbaum, D.; Anum, E.; Ramakrishnan, K.; Jensen, D.E.; Stålhammar, N.O. Intradialytic hypotension and risk of cardiovascular disease. *Clin. J. Am. Soc. Nephrol.* **2014**, *9*, 2124–2132. [CrossRef]
11. Assimon, M.M.; Wang, L.; Flythe, J.E. Cumulative Exposure to Frequent Intradialytic Hypotension Associates With New-Onset Dementia Among Elderly Hemodialysis Patients. *Kidney Int. Rep.* **2019**, *4*, 603–606. [CrossRef]
12. Shoji, T.; Tsubakihara, Y.; Fujii, M.; Imai, E. Hemodialysis-associated hypotension as an independent risk factor for two-year mortality in hemodialysis patients. *Kidney Int.* **2004**, *66*, 1212–1220. [CrossRef] [PubMed]
13. Jansen, M.A.; Hart, A.A.; Korevaar, J.C.; Dekker, F.W.; Boeschoten, E.W.; Krediet, R.T. Predictors of the rate of decline of residual renal function in incident dialysis patients. *Kidney Int.* **2002**, *62*, 1046–1053. [CrossRef]
14. Mizumasa, T.; Hirakata, H.; Yoshimitsu, T.; Hirakata, E.; Kubo, M.; Kashiwagi, M.; Tanaka, H.; Kanai, H.; Fujimi, S.; Iida, M. Dialysis-related hypotension as a cause of progressive frontal lobe atrophy in chronic hemodialysis patients: A 3-year prospective study. *Nephron* **2004**, *97*, c23–c30. [CrossRef]
15. Cedeño, S.; Desco, M.; Aleman, Y.; Macías, N.; Fernández-Pena, A.; Vega, A.; Abad, S.; López-Gómez, J.M. Intradialytic hypotension and relationship with cognitive function and brain morphometry. *Clin. Kidney J.* **2021**, *14*, 1156–1164. [CrossRef] [PubMed]
16. Flythe, J.E.; Assimon, M.M.; Overman, R.A. Target weight achievement and ultrafiltration rate thresholds: Potential patient implications. *BMC Nephrol.* **2017**, *18*, 185. [CrossRef]
17. Daugirdas, J.T.; Greene, T.; Rocco, M.V.; A Kaysen, G.; Depner, T.A.; Levin, N.W.; Chertow, G.M.; Ornt, D.B.; Raimann, J.G.; Larive, B.; et al. Effect of frequent hemodialysis on residual kidney function. *Kidney Int.* **2013**, *83*, 949–958. [CrossRef]
18. Odudu, A.; Eldehni, M.T.; McCann, G.P.; McIntyre, C.W. Randomized Controlled Trial of Individualized Dialysate Cooling for Cardiac Protection in Hemodialysis Patients. *Clin. J. Am. Soc. Nephrol. CJASN* **2015**, *10*, 1408–1417. [CrossRef]
19. Locatelli, F.; Altieri, P.; Andrulli, S.; Bolasco, P.; Sau, G.; Pedrini, L.A.; Basile, C.; David, S.; Feriani, M.; Montagna, G.; et al. Hemofiltration and hemodiafiltration reduce intradialytic hypotension in ESRD. *J. Am. Soc. Nephrol. JASN* **2010**, *21*, 1798–1807. [CrossRef] [PubMed]
20. Alexandrou, M.E.; Theodorakopoulou, M.P.; Sarafidis, P.A. Lung Ultrasound as a Tool to Evaluate Fluid Accumulation in Dialysis Patients. *Kidney Blood Press Res.* **2022**, *47*, 163–176. [CrossRef]
21. Ross, D.W.; Abbasi, M.M.; Jhaveri, K.D.; Sachdeva, M.; Miller, I.; Barnett, R.; Narasimhan, M.; Mayo, P.; Merzkani, M.; Mathew, A.T. Lung ultrasonography in end-stage renal disease: Moving from evidence to practice—A narrative review. *Clin. Kidney J.* **2017**, *11*, 172–178. [CrossRef]
22. Zoccali, C. Lung Ultrasound in the Management of Fluid Volume in Dialysis Patients: Potential Usefulness. *Semin. Dial.* **2017**, *30*, 6–9. [CrossRef]
23. Loutradis, C.; Sarafidis, P.A.; Ekart, R.; Papadopoulos, C.; Sachpekidis, V.; Alexandrou, M.E.; Papadopoulou, D.; Efstratiadis, G.; Papagianni, A.; London, G.; et al. The effect of dry-weight reduction guided by lung ultrasound on ambulatory blood pressure in hemodialysis patients: A randomized controlled trial. *Kidney Int.* **2019**, *95*, 1505–1513. [CrossRef]
24. Loutradis, C.; Papadopoulos, C.E.; Sachpekidis, V.; Ekart, R.; Krunic, B.; Karpetas, A.; Bikos, A.; Tsouchnikas, I.; Mitsopoulos, E.; Papagianni, A.; et al. Lung Ultrasound–Guided Dry Weight Assessment and Echocardiographic Measures in Hypertensive Hemodialysis Patients: A Randomized Controlled Study. *Am. J. Kidney Dis. Off. J. Natl. Kidney Found.* **2020**, *75*, 11–20. [CrossRef]
25. Zoccali, C.; Torino, C.; Mallamaci, F.; Sarafidis, P.; Papagianni, A.; Ekart, R.; Hojs, R.; Klinger, M.; Letachowicz, K.; Fliser, D.; et al. A randomized multicenter trial on a lung ultrasound–guided treatment strategy in patients on chronic hemodialysis with high cardiovascular risk. *Kidney Int.* **2021**, *100*, 1325–1333. [CrossRef]
26. Siriopol, D.; Onofriescu, M.; Voroneanu, L.; Apetrii, M.; Nistor, I.; Hogas, S.; Kanbay, M.; Sascau, R.; Scripcariu, D.; Covic, A. Dry weight assessment by combined ultrasound and bioimpedance monitoring in low cardiovascular risk hemodialysis patients: A randomized controlled trial. *Int. Urol. Nephrol.* **2017**, *49*, 143–153. [CrossRef]
27. Fortini, A.; Torrigiani, A.; Sbaragli, S.; Forte, A.L.; Crociani, A.; Cecchini, P.; Bruni, G.I.; Faraone, A. COVID-19: Persistence of symptoms and lung alterations after 3–6 months from hospital discharge. *Infection* **2021**, *49*, 1007–1015. [CrossRef]
28. Basso, F.; Manani, S.M.; Cruz, D.N.; Teixeira, C.; Brendolan, A.; Nalesso, F.; Zanella, M.; Ronco, C. Comparison and Reproducibility of Techniques for Fluid Status Assessment in Chronic Hemodialysis Patients. *Cardiorenal Med.* **2013**, *3*, 104–112. [CrossRef]
29. Jambrik, Z.; Monti, S.; Coppola, V.; Agricola, E.; Mottola, G.; Miniati, M.; Picano, E. Usefulness of ultrasound lung comets as a nonradiologic sign of extravascular lung water. *Am. J. Cardiol.* **2004**, *93*, 1265–1270. [CrossRef]
30. Zoccali, C.; Torino, C.; Tripepi, R.; Tripepi, G.; D'Arrigo, G.; Postorino, M.; Gargani, L.; Sicari, R.; Picano, E.; Mallamaci, F.; et al. Pulmonary congestion predicts cardiac events and mortality in ESRD. *J. Am. Soc. Nephrol. JASN* **2013**, *24*, 639–646. [CrossRef]
31. Heitzman, E.R.; Ziter, F.M., Jr. Acute interstitial pulmonary edema. *Am. J. Roentgenol. Radium Ther. Nucl. Med.* **1966**, *98*, 291–299. [CrossRef]
32. Milne, E.N.; Pistolesi, M.; Miniati, M.; Giuntini, C. The radiologic distinction of cardiogenic and noncardiogenic edema. *AJR Am. J. Roentgenol.* **1985**, *144*, 879–894. [CrossRef]
33. Hosmer, D.W.; Lemeshow, S.; Sturdivant, R.X. *Applied Logistic Regression*; John Wiley & Sons, Inc.: Hoboken, NJ, USA, 2013. [CrossRef]

34. Kuipers, J.; Verboom, L.M.; Ipema, K.J.; Paans, W.; Krijnen, W.P.; Gaillard, C.A.; Westerhuis, R.; Franssen, C.F. The Prevalence of Intradialytic Hypotension in Patients on Conventional Hemodialysis: A Systematic Review with Meta-Analysis. *Am. J. Nephrol.* **2019**, *49*, 497–506. [CrossRef]
35. Sands, J.J.; Usvyat, L.A.; Sullivan, T.; Segal, J.H.; Zabetakis, P.; Kotanko, P.; Maddux, F.W.; Diaz-Buxo, J.A. Intradialytic hypotension: Frequency, sources of variation and correlation with clinical outcome. *Hemodial. Int. Int. Symp. Home Hemodial.* **2014**, *18*, 415–422. [CrossRef]
36. Hryciw, N.; Joannidis, M.; Hiremath, S.; Callum, J.; Clark, E.G. Intravenous Albumin for Mitigating Hypotension and Augmenting Ultrafiltration during Kidney Replacement Therapy. *Clin. J. Am. Soc. Nephrol. CJASN* **2021**, *16*, 820–828. [CrossRef]
37. Correa, S.; Pena-Esparragoza, J.K.; Scovner, K.M.; Mc Causland, F.R. Predictors of Intradialytic Symptoms: An Analysis of Data From the Hemodialysis Study. *Am. J. Kidney Dis. Off. J. Natl. Kidney Found.* **2020**, *76*, 331–339. [CrossRef]
38. Passos, R.D.H.; Caldas, J.; Ramos, J.G.R.; Melo, E.B.D.S.G.D.; Ribeiro, M.P.D.; Alves, M.F.C.; Batista, P.B.P.; Messeder, O.H.C.; Farias, A.M.D.C.D.; Macedo, E.; et al. Ultrasound-based clinical profiles for predicting the risk of intradialytic hypotension in critically ill patients on intermittent dialysis: A prospective observational study. *Crit. Care Soc. Crit. Care Med.* **2019**, *23*, 389.
39. Khanin, Y.; Hirsch, J.S.; Stalbow, D.; Zhang, M.; Hasan, Z.; Ross, D.W. Intradialytic Hypotension in Critically Ill Patients on Hemodialysis With A-Line versus B-Line Pattern on Lung Ultrasonography. *Kidney Int. Rep.* **2021**, *6*, 1969–1972. [CrossRef]
40. Picano, E.; Pellikka, P.A. Ultrasound of extravascular lung water: A new standard for pulmonary congestion. *Eur. Heart J.* **2016**, *37*, 2097–2104. [CrossRef]
41. Trezzi, M.; Torzillo, D.; Ceriani, E.; Costantino, G.; Caruso, S.; Damavandi, P.T.; Genderini, A.; Cicardi, M.; Montano, N.; Cogliati, C. Lung ultrasonography for the assessment of rapid extravascular water variation: Evidence from hemodialysis patients. *Intern. Emerg. Med.* **2013**, *8*, 409–415. [CrossRef]
42. Keane, D.F.; Raimann, J.G.; Zhang, H.; Willetts, J.; Thijssen, S.; Kotanko, P. The time of onset of intradialytic hypotension during a hemodialysis session associates with clinical parameters and mortality. *Kidney Int.* **2021**, *99*, 1408–1417. [CrossRef] [PubMed]
43. Vizioli, L.; Ciccarese, F.; Forti, P.; Chiesa, A.M.; Giovagnoli, M.; Mughetti, M.; Zompatori, M.; Zoli, M. Integrated Use of Lung Ultrasound and Chest X-Ray in the Detection of Interstitial Lung Disease. *Respir. Int. Rev. Thorac. Dis.* **2017**, *93*, 15–22. [CrossRef] [PubMed]

diagnostics

MDPI

Article

Possible Role of Chest Ultrasound in the Assessment of Costo-Phrenic Angle Lesions Prior to Medical Thoracoscopy: A Retrospective Pilot Case Series

Emanuele Giovanni Conte [1], Andrea Smargiassi [2,*], Filippo Lococo [3], Giampietro Marchetti [4] and Riccardo Inchingolo [2]

[1] Pulmonology Unit, "C.&G. Mazzoni" Hospital, 63100 Ascoli Piceno, Italy
[2] UOC Pneumologia, Dipartimento Scienze Mediche e Chirurgiche, Fondazione Policlinico Universitario A. Gemelli IRCCS, 00168 Rome, Italy
[3] Thoracic Surgery Unit, Dipartimento Scienze Mediche e Chirurgiche, Fondazione Policlinico Universitario A. Gemelli IRCCS, 00168 Rome, Italy
[4] Respiratory Medicine Department, ASST Spedali Civili, 25123 Brescia, Italy
* Correspondence: andrea.smargiassi@policlinicogemelli.it; Tel.: +39-0630-156-062

Abstract: Background: Pleural malignancy (PM) and malignant pleural effusion (MPE) represent an increasing burden of diseases. Costo-phrenic angle (CPA) could be involved by malignant small nodularities or thickenings in the case of MPE. The aim of this study was to evaluate whether lung ultrasound (LUS), performed prior to medical thoracoscopy (MT), could detect pleural abnormalities in CPA not easily detectable by chest computed tomography scan (CCT). Methods: Patients suspected for PM and MPE were retrospectively recruited. Patients underwent both LUS examination with a linear array and CCT prior to diagnostic medical thoracoscopy. LUS pathological findings in CPA were compared with pathological findings detected by CCT. Findings were confirmed by subsequent MT, the gold standard for PMs. Results: Twenty-eight patients were recruited. LUS detected 23 cases of pleural abnormalities in CPA. CCT was detected 12 pleural abnormalities. Inter-rater agreement between the two techniques was minimal (Cohen's Kappa: 0.28). MT detected PMs in CPA in 22 patients. LUS had a sensitivity of 100% and specificity of 83%. CCT had a sensitivity of 54% and specificity of 100%. A better sensitivity for CCT was reached analysing only all abnormalities > 5 mm (64.3%). Conclusions: LUS examination, in the case of PMs, could change and speed up diagnostic workup.

Keywords: chest ultrasound; medical thoracoscopy; pleural effusion; pleural malignancy

Citation: Conte, E.G.; Smargiassi, A.; Lococo, F.; Marchetti, G.; Inchingolo, R. Possible Role of Chest Ultrasound in the Assessment of Costo-Phrenic Angle Lesions Prior to Medical Thoracoscopy: A Retrospective Pilot Case Series. *Diagnostics* **2022**, *12*, 2587. https://doi.org/10.3390/diagnostics12112587

Academic Editor: Philippe A. Grenier

Received: 16 September 2022
Accepted: 20 October 2022
Published: 25 October 2022

1. Introduction

Pleural effusion (PE) is a common medical problem in patients hospitalized in pneumology or internal medicine departments, and aetiology varies according to geographical area, healthcare setting, patient age and other factors. An important category of PE is malignant pleural effusion (MPE). Epidemiological data suggest that MPE is one of the top three causes of pleural effusion, along with heart failure and para-pneumonic effusions [1]. The majority of MPE is caused by metastatic disease, most commonly lung cancer in men and breast cancer in women. These two cancers account for 50–65% of all MPE [1]. Mesothelioma is the most common type of primary pleural tumour and is associated with MPE in more than 90% of cases [2].

Nowadays, the gold standard in pleural disease assessment is medical thoracoscopy [2,3]. Currently, the diagnostic yield in patients with malignant pleural disease is reaching 94–97% [4,5].

Chest CT scan is considered as the most important radiological technique in evaluating pleural surface. Pleural Diseases BTS guidelines recommend performing this exam in the case of exudative pleural effusion without diagnosis after thoracentesis [6]. Anyway, several

studies reported contrasting data on CT scan sensitivity and specificity [7–9]. The work published by Tsim and coworkers reported CT sensitivity of 58% and specificity of 80% in detecting pleural malignancies, concluding that radiological examination is not sufficient to exclude or confirm presence of primary or secondary pleural malignancies [10], thus requiring invasive procedures.

Another important technique in assessing pleural disease is chest ultrasonography. Nowadays, respiratory physicians routinely use thoracic ultrasound, mainly for the guidance of pleural interventions to minimise complications [11]. International guidelines strongly recommend the utility of this technique [12]. Chest US can discriminate features highly specific for malignancy and may therefore help to expedite correct investigations in those with these high-risk features [12,13]. In the case of pleural effusions, Chest US is able to assess, with high sensibility, pleural abnormalities especially at the costo-phrenic angle (CPA) [14].

It is crucial to study CPA. This region is the most caudal area of the thorax, it is delimitated by parietal, diaphragmatic and visceral pleura, each one characterized by different lymphatic drainage. It is rich of lymphatic stomata [15] being pulled open by inspiratory movements of lung and thoracic cage. Francisco Rodriguez-Panadero and colleagues detected that the majority of the pleural malignancies are caused by tumour emboli to the visceral pleura with subsequent secondary seeding to the parietal pleura [16].

It has been demonstrated that malignant seeding can be influenced by gravitational effects for intra-abdominal distribution [17]. Similarly, it has been described an increased prevalence of pleural abnormalities in the lower posterior area of thorax [18]. Pleural seeding and stasis of pleural fluid in this region lead us to focus our research to this anatomical area to find neoplastic lesions.

Moreover, chest ultrasound has been reported to have an excellent diagnostic accuracy for small pleural lesions, guiding percutaneous pleural needle biopsy. Percutaneous ultrasound guided pleural biopsy has high diagnostic yield and low complication rate [19]. Park J and colleagues [20] reported that ultrasound guided pleural biopsy is highly likely diagnostic for small pleural lesions with nodular morphology on either CT or US or with a pleural thickness of 4.5 mm or greater.

Aim of this study is to provide a picture of real life in a Pleural Unit, evaluating whether lung ultrasound (US), performed prior to medical thoracoscopy, could detect pleural abnormalities in CPA sometimes not easily detectable by chest computed tomography (CT) scan, previously performed and brought for viewing in the outpatient visit.

2. Materials and Methods

2.1. Study Population

In this retrospective case series, we included patients referred to Pleural Unit (Spedali Civili, Brescia, Italy) during a 38-month period who underwent Medical Thoracoscopy for suspected PMs, pleural effusions, or pleural abnormalities, already subject to chest ultrasonography with at least one chest CT scan. Patients were selected through a pleural disease database. The inclusion criteria were: (1) age $\geq$ 18 years; (2) suspect of pleural malignancies, pleural effusions or pleural abnormalities less than 10 mm; (3) chest ultrasound evaluation of costo-phrenic angle prior to medical thoracoscopy; (4) chest CT scan evaluation in the 30 days prior to medical thoracoscopy. Written informed consent was obtained from all patients retrospectively involved. This study was approved by the ethics committee of the Spedali Civili of Brescia (CE133/2017).

2.2. Chest Ultrasonography

Ultrasonographic assessment was performed using MyLabTM 30 CV machine (Esaote, Genova, Italy) equipped with convex (2–5 MHz) and linear (7–13 MHz) probes. All ultrasonographic evaluations were performed by a pneumologist (GM) with a consolidated expertise in lung ultrasonography.

Each patient was asked initially to stay seated for dorsal sonographic scans, then to lie in a supine position for anterior and lateral scans and finally in the lateral thoracoscopic decubitus position. A bilateral ultrasonographic evaluation was performed.

The convex probe was used firstly to look for pleural effusions, large lung consolidations and curtain signs. Secondly, the linear probe (7.5 MHz) was used to detect sliding sign, adherences, pleural thickenings, and small pleural abnormalities. CPA was constantly evaluated searching for small pleural thickenings and subcentrimetric nodules. Images and videos of costo-phrenic angle pleural lesions were acquired and stored.

Videos of the sonographic assessment of CPA were recorded and stored. A subsequent evaluation by 3 pneumologists (EGC, AS and RI) with high expertise in lung ultrasonography was performed for this retrospective study.

Pleural findings were classified, according to previous studies [21,22], in pleural thickenings and pleural nodules. Each lesion was measured and categorized.

2.3. Chest CT Scan

We reviewed all chest CT scans reports and images performed on enrolled patients. Chest CT scans have already been performed previously and brought for viewing in the visit at the Pleural Unit. Radiological examinations were not performed in the same centre and different CT scanner, parameters and protocols were reported. Contrast enhancement evaluation was not undertaken in all examinations.

We searched for description of pleural lesions in the costo-phrenic angle. The presence or absence of lesions was reported.

2.4. Medical Thoracoscopy (MT)

All MT procedures were performed in the Pleural Unit of ASST Spedali Civili (Brescia, Italy) by pulmonologists in a dedicated Endoscopy Room. Anaesthetists assisted patients during procedures providing conscious sedation.

Patients were placed in the lateral decubitus position with the ipsilateral arm abducted to maximize access to the hemi thorax. Chest ultrasonography was also performed immediately before the MT with the patient already in the lateral decubitus in order to detect sliding sign and the best entry site [23,24].

Local anaesthesia was induced with mepivacaine (200 mg) and after making a small skin incision, blunt dissection was performed with a curved blunt-point scissors in the chest wall until penetration of parietal pleura. Subsequently, a blunt-point trocar was carefully introduced through the chest wall, reaching pleural cavity. After aspiration of pleural fluid, a rigid 7-mm thoracoscopy set (Karl Storz GmbH & Co., Tuttlingen, Germany) was introduced in the pleural cavity. A complete assessment of pleural cavity was performed, and images and videos were acquired and stored in a local hard-disk. At least eight pleural biopsy specimens for each patient were then collected. A detailed report of the procedure, with description of macroscopic features of lesions, was stored in the Pleural Unit database.

2.5. Statistical Analysis

A descriptive analysis was accomplished by computing mean values and standard deviations. Kappa statistic was used to assess agreement between ultrasound and computed tomography technique. Linear weighted kappa was calculated for the ordered categories [25]. Finally, we calculated sensitivity, specificity, and receiver operating characteristic (ROC) curve by comparing the results that were obtained from chest US and chest CT scan respect to gold standard MT. Data analysis was performed using MedCalc Statistical Software version 17.6 (MedCalc Software bvba, Ostend, Belgium; http://www.medcalc.org (accessed on 8 December 2017)).

3. Results

The study population (Table 1) consisted of 28 patients, 21 males and 7 females, with a mean age of 64 $\pm$ 5 years (range 19–81). Malignancies were detected in final diagnosis in

22 cases (78.5%). Benign or infectious diseases were found in six cases. Pleural effusion was present in 25 cases (89% of subjects) and it was most frequently right sided (15 cases).

Table 1. Patients' characteristics.

Patient	Age	Sex	Effusion Side	Final Diagnosis
Patient 1	81	M	Right	Unspecified pleural inflammation
Patient 2	76	F	Right	Epithelioid mesothelioma
Patient 3	66	M	No pleural effusion	Lung Adenocarcinoma
Patient 4	66	M	Right	Unspecified pleural inflammation
Patient 5	75	M	Right	Epithelioid mesothelioma
Patient 6	76	F	Right	Breast Cancer
Patient 7	60	M	Right	Epithelioid mesothelioma
Patient 8	21	M	Right	Tuberculosis
Patient 9	78	M	Left	Biphasic mesothelioma
Patient 10	72	M	Right	Lung Adenocarcinoma
Patient 11	56	M	Left	Other malignancy
Patient 12	63	F	No pleural effusion	Epithelioid mesothelioma
Patient 13	68	M	Right	Lung Squamous cell carcinoma
Patient 14	68	F	Right	Epithelioid mesothelioma
Patient 15	75	M	Left	Epithelioid mesothelioma
Patient 16	49	M	Left	Tuberculosis
Patient 17	73	F	No pleural effusion	Epithelioid mesothelioma
Patient 18	64	M	Left	Epithelioid mesothelioma
Patient 19	48	M	Right	Lung Adenocarcinoma
Patient 20	49	F	Left	Breast Cancer
Patient 21	62	M	Right	Other malignancy
Patient 22	19	M	Left	Other malignancy
Patient 23	79	M	Right	Unspecified pleural inflammation
Patient 24	61	M	Left	Other malignancy
Patient 25	81	F	Right	Other malignancy
Patient 26	62	M	Left	Unspecified pleural inflammation
Patient 27	77	M	Left	Lung Adenocarcinoma
Patient 28	65	M	Right	Epithelioid mesothelioma
Patients, n				28
Male/Female				21/7
Mean age (range), years				64 ± 5 (19–81)
Effusion side (Ultrasound)				
Left				10
Right				15
Absent				3
Final diagnosis				
Benign				*6*
Unspecified pleural inflammation				4
Tuberculosis				2
Malignant				*22*
Mesothelioma				10
Epithelioid mesothelioma				9
Biphasic mesothelioma				1
Lung cancer				5
Adenocarcinoma				4
Squamous cell carcinoma				1
Breast cancer				2
Other malignancies				5

All patients underwent chest US examination. Pleural abnormalities in CPA were detected in 23 patients (82%). These abnormalities (Figure 1) were classified in: pleural thickenings (12 cases), nodularities (seven cases) and a combination pattern of nodules and

thickenings (four cases). Each pattern was divided into two categories based on dimension: up to 5 mm, and ranging from 5 to 10 mm. (Table 2).

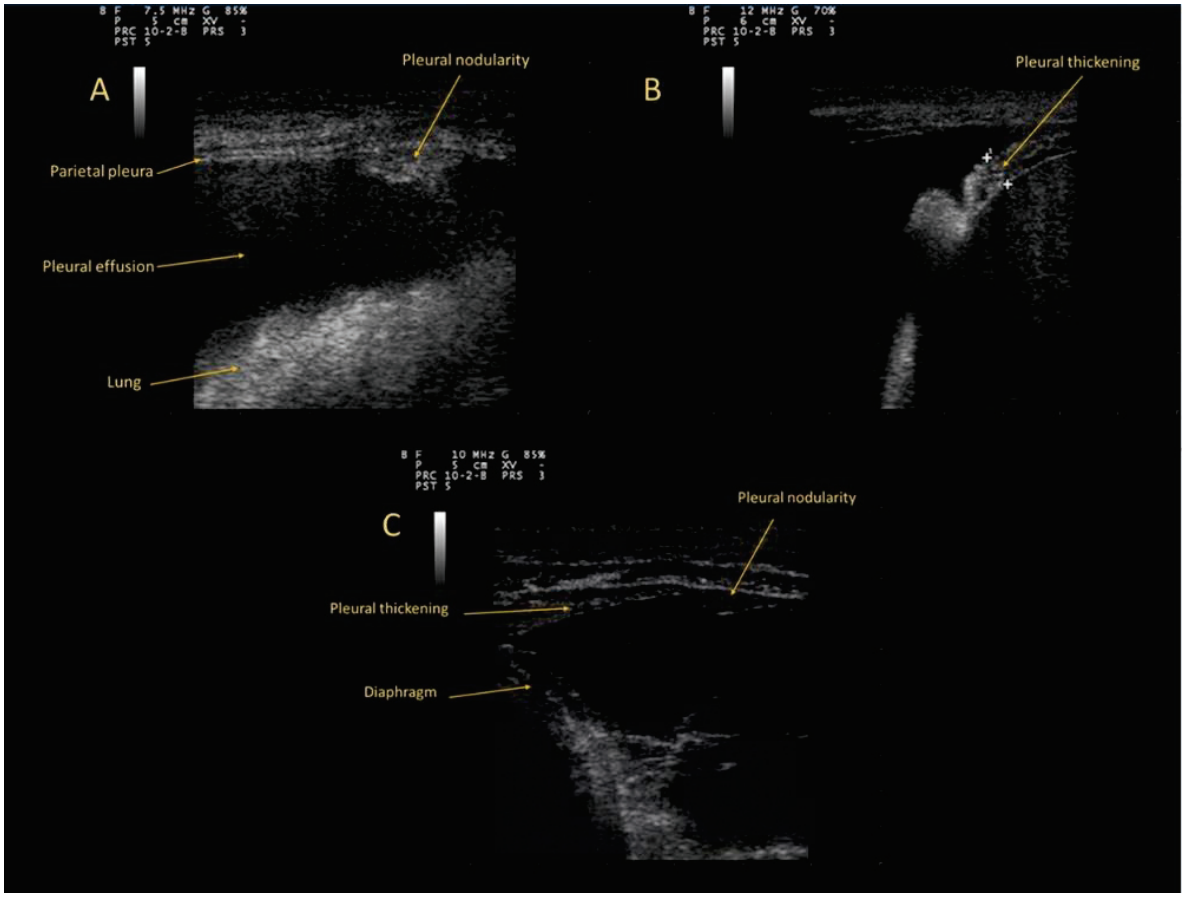

Figure 1. (**A**): Pleural nodularity; (**B**): Pleural thickening; (**C**): pattern of nodules and thickenings.

Table 2. Chest US findings in CPA.

CPA US Findings	Values
No abnormalities	5
Nodularities 5–10 mm	7
Pleural thickening	12
<5 mm	5
5–10 mm	7
Nodularities and pleural thickening	4
<5 mm	3
5–10 mm	1

Chest CT scan was performed with and without contrast enhancement in 28.6% (8) and 71.4% (20) of patients, respectively. Pleural abnormalities in CPA were detected by chest CT scan in 12 patients (43%).

3.1. Chest US and Chest CT Scan Inter-Rater Agreement

Inter-rater agreement between chest US and chest CT scan findings was evaluated (Table 3).

Table 3. Comparison of chest US and chest CT scan findings in CPA.

	Chest Ultrasound		
Chest CT scan	**Positive**	**Negative**	
Positive	12	0	12 (43%)
Negative	11	5	16 (57%)
	23 (82%)	5 (18%)	28

Both techniques detected pleural abnormality in CPA in 12 patients. Agreement for the absence of pathological findings was reported in 5 patients.

In 11 cases, only US evaluation detected pleural abnormalities. No cases were reported for which CPA abnormalities, detected by chest CT scan, were non detectable with chest US evaluation.

Inter-rater agreement between the two techniques was assessed by linear weighted kappa values. Cohen's Kappa was 0.28 (95% CI 0.050–0.51). This result described a minimal concordance between chest US and chest CT scan.

3.2. Comparison with Gold-Standard MT

Medical thoracoscopy detected pleural abnormalities in the CPA in 22 patients (79%). From macroscopic point of view, 10 patients had nodularities, nine pleural thickenings, and three patients both abnormalities.

Concerning pleural biopsies, a final diagnosis of pleural malignancy was achieved in 22 patients (79%). Ten patients suffered from mesothelioma (35%), five lung cancer (18%), two pleural metastasis of breast cancer (7%), and five other malignancies (ovarian; bone; kidney; solitary fibrous tumor; myoepithelial (Table 1).

Six patients (21%) had a final non-malignant diagnosis: two cases of pleural tuberculosis (7%) and four cases of unspecified pleural inflammation (14%).

Comparing ultrasound findings to medical thoracoscopy (Figure 2), MT confirmed the presence of pleural abnormalities in 22 of 23 cases detected by chest US. Only one false-positive was reported, resulting to be diaphragmatic pillars at MT examination. In the remaining five patients, no abnormalities were found by MT in agreement with chest US (Table 4).

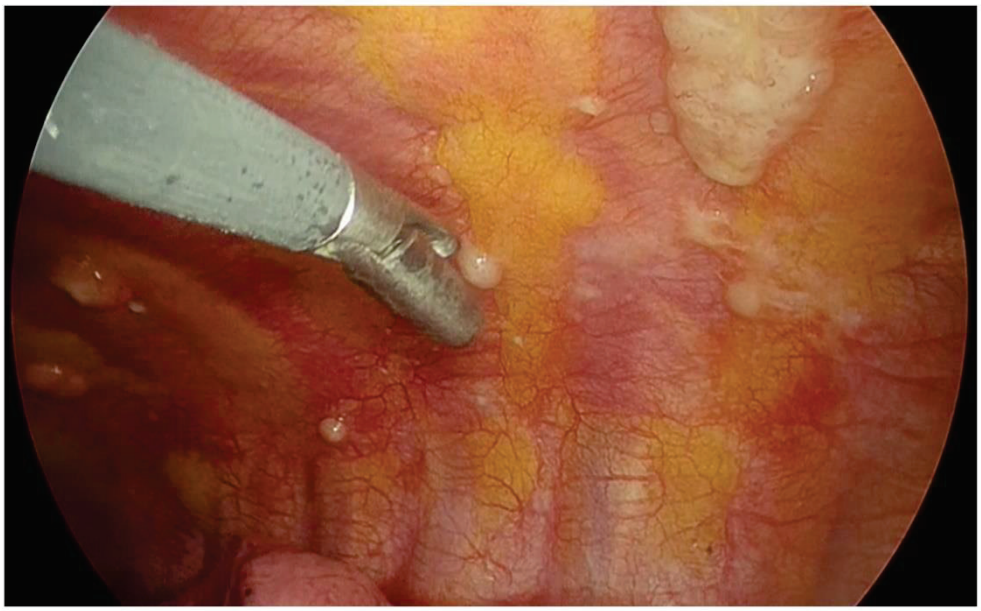

Figure 2. Thoracoscopic view: small pleural lesions on the surface of parietal pleura. After biopsy, pathological examination confirmed a pleural carcinosis from NSCLC.

Table 4. Chest US and CT findings compared with MT gold standard.

	Disease Present (MT)	Disease Absent (MT)
Chest US positive	22	1
Chest US negative	0	5
Chest CT positive	12	0
Chest CT negative	10	6

Comparing radiological findings to MT, CT scan correctly detected presence of abnormalities in 12 cases, absence of abnormalities in six cases, but in 10 cases it was falsely negative (Table 4).

A comparison of sensitivity, specificity for both chest US and chest CT scan versus MT findings in CPA is reported in Table 5.

Table 5. Sensitivity, Specificity, AUC-ROC analysis of Chest US and Chest CT scan vs. gold standard MT.

Diagnostic Test	Sensitivity	Specificity	AUC
Chest ultrasound	100%	83%	0.92
Chest CT	54%	100%	0.77

When compared to MT, chest CT scan had a sensitivity of 54% (95% CI 32.2% to 75.6%) and specificity of 100% (95% CI 54% to 100%).

Similarly, chest US had instead a sensitivity of 100% (95% CI 84.5% to 100%) and specificity of 83% (95% CI 36% to 99.6%).

We calculated the ROC curve for each of the two techniques (Figure 3), showing an area under the curve (AUC) for chest US of 0.92 and for chest CT scan of 0.77 (p = 0.148).

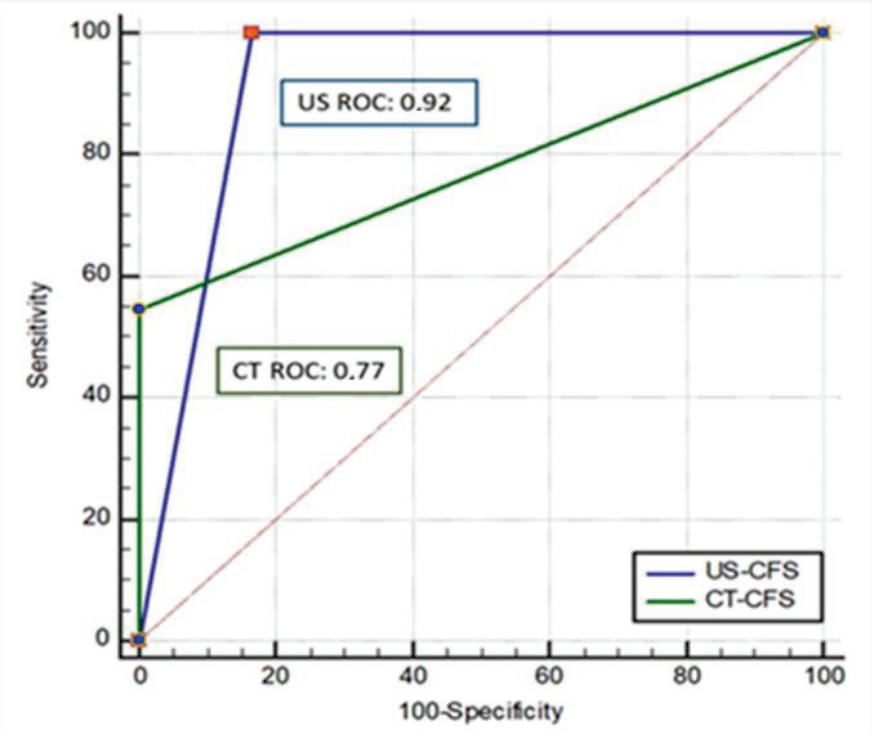

Figure 3. ROC curves for chest US and chest CT scan.

In order to explain differences between chest US and chest CT scan in terms of sensitivities versus gold standard, we compared chest CT to medical thoracoscopy in a subgroup analysis of patients according to dimension of abnormalities detected by Chest US (Table 6).

Table 6. Comparison between Chest CT scan vs. gold standard MT according to subgroup analysis of Ultrasonographic findings.

All abnormalities < 5 mm	8	37.5%	100%
All abnormalities > 5 mm	14	64.3%	100%

When all patients with pleural abnormalities <5 mm (8 patients) were included in the analysis, chest CT scan demonstrated 37.5% of sensitivity, instead in patients with pleural abnormalities >5 mm (14 patients), CT scan demonstrated 64.3% of sensitivity.

Finally, considering the two subgroups separately, when the first CT scan of the chest was performed with (eight cases) and without (20 cases) iodine contrast of mean, it was possible to compute sensitivities and specificities differentiating cases.

Although low number of cases are reported, for the eight cases with contrast enhanced CT scan of the chest, sensitivity versus gold standard MT, was 87% for CT scan and 100% for chest US, respectively. It is not possible to report specificities because all eight cases were positive for CPA at MT (Table 7).

Table 7. Subgroup of 8 cases with contrast enhanced (c.e.) CT scan of the chest. Chest US and CT scan compared with MT gold standard for pleural abnormalities in CPA.

	Disease Present (MT)	**Disease Absent (MT)**
Chest US positive	8	0
Chest US negative	0	0
c.e. CT scan positive	7	0
c.e. CT scan negative	1	0
Diagnostic test	**Sensitivity**	**Specificity**
Chest ultrasound	100%	N.A.
c.e. CT scan	87%	N.A.

On the other hand, for the 20 cases without contrast enhanced CT scan of the chest, sensitivity versus gold standard MT, was 36% for CT scan and 100% for chest US. In these cases, specificities versus gold standard MT were 100% for CT scan and 83% for chest US, respectively (Table 8).

Table 8. Subgroup of 20 cases without contrast enhanced (c.e.) CT scan of the chest. Chest US and CT scan compared with MT gold standard for pleural abnormalities in CPA.

	Disease Present (MT)	**Disease Absent (MT)**
Chest US positive	14	1
Chest US negative	0	5
CT scan positive	5	0
CT scan negative	9	6
Diagnostic test	**Sensitivity**	**Specificity**
Chest ultrasound	100%	83%
CT scan	36%	100%

4. Discussion

This case series showed how chest US is able to help physicians for the assessment of CPA in case of suspected pleural malignancies. It is able to detect pleural abnormalities in CPA not easily detectable by first chest CT scan, especially in the case of absence of iodine mean of contrast. These abnormalities have been confirmed by MT which can be considered the referral technique.

Studying CPA, chest US detected all cases (22 out of 22) of pleural abnormalities identified by medical thoracoscopy (Table 4). Only one false-positive case has been reported: an apparent nodular lesion on the diaphragmatic surface of the CPA, resulting in an

abnormal diaphragmatic pillar at thoracoscopic evaluation. In five cases chest US reported the absence of alterations, confirmed by MT. Chest US, when compared to MT, showed an overall sensitivity of 100% and a specificity of 83%.

As to chest CT scan, it detected only 12 cases out 22 reported by MT. However, no false-positive case has been reported. These results are similar to other described in current medical literature [8,9].

Chest CT scan in our series demonstrated a high specificity in detecting pleural abnormalities in the CPA (100%), but a low level of sensitivity (54%).

ROC analysis for chest US and CT scan showed higher accuracy for the ultrasound evaluation of CPA if compared to chest CT, although the difference between AUCs was not significant. Comparison between chest US and chest CT scan resulted in a minimal concordance, assessed by the Cohen's Kappa. Discordance was detected in 11 cases. In all cases, chest US was positive for pleural abnormalities in CPA and chest CT scan negative. In 10 out of these 11 cases, MT actually identified abnormalities. One case confirmed the absence of pathology according to chest CT scan. Therefore, radiological examination was unable to detect 10 cases, correctly identified by chest US.

The majority of these cases were represented by small pleural abnormalities in CPA (usually less than 5 mm). Among these cases, we reported pleural malignancies, but also one patient with a histological diagnosis of unspecified pleural inflammation and two patients with pleural tuberculosis.

Based on these findings, we compared chest CT scan to medical thoracoscopy in a subgroup analysis of patients according to dimension of abnormalities detected by chest US. We found that CT scan detected with lower sensitivity abnormalities <5 mm (37.5%). A better sensitivity was reached for all abnormalities >5 mm (64.3%).

Our results could be explained by the different spatial resolution of US examination [23] with a high frequency probe compared to chest CT scan performed without high resolution protocol, not required in the study of suspected pleural malignant effusion or pleural malignancies [6].

Our study has several limitations. The first one is the retrospective model of our study. We could include in our work only patients who underwent a lung ultrasonography and a chest CT scan prior medical thoracoscopy and we excluded all patients whose images and videos were not recorded and all patients who performed a chest CT scan, with or without iodine contrast mean, after the procedure. Moreover, chest CT scan examinations were not performed in the same centre, with same protocols and all with contrast enhancement phase. Most of the exams were performed without contrast enhancement because of patients either with renal failure or with known adverse reactions to iodine contrast mean or because the first chest CT scan has been usually performed without contrast enhancement. Another limitation is the small population of our study and the higher proportion of patient affected by mesothelioma compared to other malignant diseases, above all lung cancer. This can be due to the high incidence of mesothelioma in the part of Italy that refers patients to the Pleural Unit of ASST Spedali Civili, Brescia [26].

Despite these limitations, our original observation suggests that the absence of pleural abnormalities detected by first chest CT scan is not sufficient to exclude pleural involvements especially in case of malignancy.

Chest US could improve detection of even millimetric pleural abnormalities localized in the costo-phrenic angle, not detected by chest CT scan, with high sensitivity and specificity when compared with gold standard medical thoracoscopy.

Even if diagnostic performance of chest CT scan is not sufficient to exclude or confirm small pleural abnormalities, it is crucial to assess mediastinal and diaphragmatic pleural surface, pleura behind ribs or shoulder blades, lung fissures, lung parenchyma, central nodules, or peripheral lung abnormalities not reaching pleural surface.

The aim of this work, presenting a picture of real life in pleural unit, was not to suggest chest US in substitution of chest CT scan, but to provide pulmonologists with a useful tool

to assess pleural surface [27] and chest wall [28], in addition to ionizing radiations [29–31], in order to indicate and guide diagnostic MT.

Finally, this retrospective case series represents the first step towards a prospective study, enrolling patients with a standardized protocol, focusing on the role of chest US in the assessment of costo-phrenic angle prior to MT with the final goal to make this technique common in clinical practice.

5. Conclusions

According to our results, US showed a good sensitivity in the detection of pleural abnormalities localized in the costo-phrenic angle. An accurate ultrasound examination of CPA in patients affected by pleural effusion or suspected malignant pleural effusion could assess even millimetric pathological lesions, sometimes not easily detectable by chest CT scan.

US examination, in the presence of a suspected pleural pathology, could change and speed up diagnostic workup (Figure 4) [13,14,32–35], aiding malignancy characterization and therapeutic care.

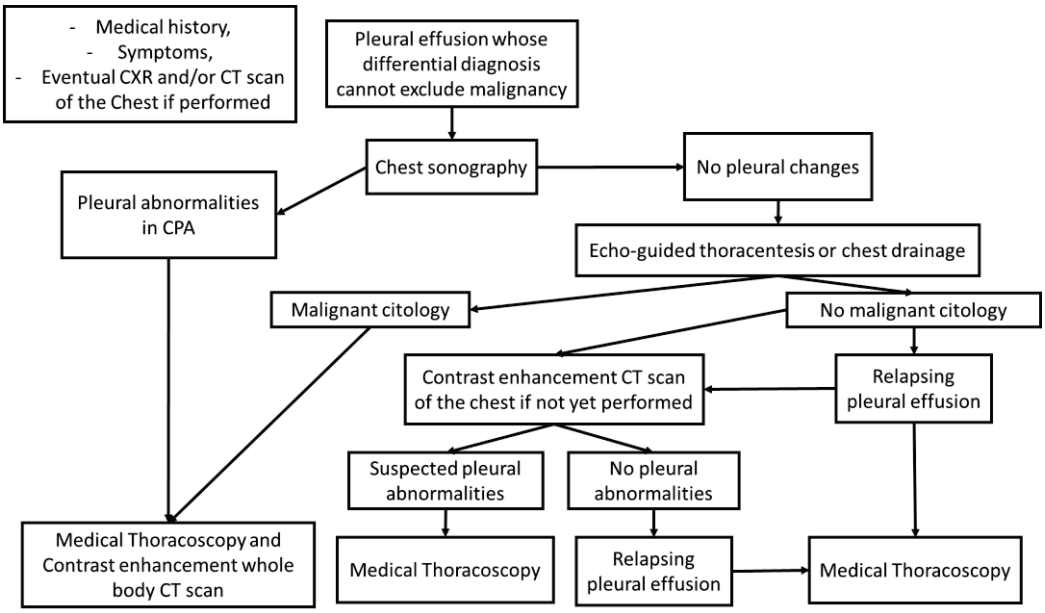

Figure 4. Proposal of diagnostic algorithm.

Author Contributions: Conceptualization, A.S. and E.G.C.; methodology, R.I.; software, G.M.; validation, G.M., E.G.C. and F.L.; formal analysis, E.G.C.; investigation, R.I.; resources, G.M.; data curation, E.G.C.; writing—original draft preparation, E.G.C.; supervision, A.S. and R.I. All authors have read and agreed to the published version of the manuscript.

Funding: This research received no external funding.

Institutional Review Board Statement: The study was conducted in accordance with the Declaration of Helsinki and approved by the Ethics Committee of the Spedali Civili of Brescia (CE133/2017).

Informed Consent Statement: Informed consent was obtained from all subjects involved in the study.

Data Availability Statement: The data presented in this study are available on request at emanuele.conte_86@hotmail.it.

Conflicts of Interest: The authors declare no conflict of interest.

References

1. Light, R.W. *Pleural Diseases*, 6th ed.; Lippincott Williams & Wilkins: Philadelphia, PA, USA, 2013.
2. Woolhouse, I.; Bishop, L.; Darlison, L.; De Fonseka, D.; Edey, A.; Edwards, J.; Faivre-Finn, C.; Fennell, D.A.; Holmes, S.; Kerr, K.M.; et al. British Thoracic Society Guideline for the investigation and management of malignant pleural mesothelioma. *Thorax* **2018**, *73* (Suppl. 1), i1–i30. [CrossRef] [PubMed]
3. Roberts, M.E.; Neville, E.; Berrisford, R.G.; Antunes, G.; Ali, N.J. Management of a malignant pleural effusion: British Thoracic Society pleural disease guideline 2010. *Thorax* **2010**, *65* (Suppl. 2), ii32–ii40. [CrossRef] [PubMed]
4. Froudarakis, M.E. New Challenges in Medical Thoracoscopy. *Respiration* **2011**, *82*, 197–200. [CrossRef] [PubMed]
5. Loddenkemper, R. Thoracoscopy—State of the art. *Eur. Respir. J.* **1998**, *11*, 213–221. [CrossRef] [PubMed]
6. Hooper, C.; Lee, Y.C.G.; Maskell, N.; BTS Pleural Guideline Group. Investigation of a unilateral pleural effusion in adults: British Thoracic Society pleural disease guideline 2010. *Thorax* **2010**, *65* (Suppl. 2), ii4–ii17. [CrossRef]
7. Metintas, M.; Ak, G.; Dundar, E.; Yildirim, H.; Ozkan, R.; Kurt, E.; Erginel, S.; Alatas, F.; Metintas, S. Medical thoracoscopy vs. CT scan-guided abrams pleural needle biopsy for diagnosis of patients with pleural effusions: A randomized, controlled trial. *Chest* **2010**, *137*, 1362–1368. Available online: http://linkinghub.elsevier.com/retrieve/pii/S0012369210602899 (accessed on 15 June 2018). [CrossRef]
8. Traill, Z.C.; Davies, R.J.O.; Gleeson, F.V. Thoracic Computed Tomography in Patients with Suspected Malignant Pleural Effusions. *Clin. Radiol.* **2001**, *56*, 193–196. [CrossRef]
9. Hallifax, R.J.; Haris, M.; Corcoran, J.P.; Leyakathalikhan, S.; Brown, E.; Srikantharaja, D.; Manuel, A.; Gleeson, F.V.; Munavvar, M.; Rahman, N.M. Role of CT in assessing pleural malignancy prior to thoracoscopy. *Thorax* **2015**, *70*, 192–193. [CrossRef]
10. Tsim, S.; Stobo, D.B.; Alexander, L.; Kelly, C.; Blyth, K.G. The diagnostic performance of routinely acquired and reported computed tomography imaging in patients presenting with suspected pleural malignancy. *Lung Cancer* **2017**, *103*, 38–43. [CrossRef]
11. Gordon, C.E.; Feller-Kopman, D.; Balk, E.M.; Smetana, G.W. Pneumothorax following thoracentesis: A systematic review and meta-analysis. *Arch. Intern. Med.* **2010**, *170*, 332–339. [CrossRef]
12. Havelock, T.; Teoh, R.; Laws, D.; Gleeson, F. Pleural procedures and thoracic ultrasound: British Thoracic Society pleural disease guideline 2010. *Thorax* **2010**, *65* (Suppl. 2), i61–i76. [CrossRef] [PubMed]
13. Qureshi, N.R.; Rahman, N.M.; Gleeson, F.V. Thoracic ultrasound in the diagnosis of malignant pleural effusion. *Thorax* **2009**, *64*, 139–143. [CrossRef] [PubMed]
14. Bugalho, A.; Ferreira, D.; Dias, S.S.; Schuhmann, M.; Branco, J.C.; Gomes, M.K.M.; Eberhardt, R. The diagnostic value of transthoracic ultrasonographic features in predicting malignancy in undiagnosed pleural effusions: A prospective observational study. *Respiration* **2014**, *87*, 270–278. [CrossRef] [PubMed]
15. Shinohara, H. Distribution of lymphatic stomata on the pleural surface of the thoracic cavity and the surface topography of the pleural mesothelium in the golden hamster. *Anat. Rec.* **1997**, *249*, 16–23. [CrossRef]
16. Rodrîguez-Panadero, F.; Borderas Naranjo, F.; López Mejîas, J. Pleural metastatic tumours and effusions. Frequency and pathogenic mechanisms in a post-mortem series. *Eur. Respir. J.* **1989**, *2*, 366–369.
17. Meyers, M.A. Distribution of intra-abdominal malignant seeding: Dependency on dynamics of flow of ascitic fluid. *Am. J. Roentgenol.* **1973**, *119*, 198–206. [CrossRef]
18. Araki, T.; Yanagawa, M.; Sun, F.J.; Dupuis, J.; Nishino, M.; Yamada, Y.; Washko, G.R.; Christiani, D.C.; Tomiyama, N.; O'Connor, G.T.; et al. Pleural abnormalities in the Framingham Heart Study: Prevalence and CT image features. *Occup. Environ. Med.* **2017**, *74*, 756–761. [CrossRef]
19. Portela-Oliveira, E.; Souza, C.A.; Gupta, A.; Bayanati, H.; Inacio, J.; Rakhra, K. Ultrasound-guided percutaneous biopsy of thoracic lesions: High diagnostic yield and low complication rate. *Clin. Radiol.* **2021**, *76*, 281–286. [CrossRef]
20. Park, J.; Park, B.; Lim, J.K.; Shin, K.M.; Lee, J.; Kim, C.H.; Seo, H.; Lee, Y.H.; Heo, J.; Do, Y.W. Ultrasound-Guided Percutaneous Needle Biopsy for Small Pleural Lesions: Diagnostic Yield and Impact of CT and Ultrasound Characteristics. *Am. J. Roentgenol.* **2021**, *217*, 699–706. [CrossRef]
21. Zanforlin, A.; Giannuzzi, R.; Nardini, S.; Testa, A.; Soldati, G.; Copetti, R.; Marchetti, G.; Valente, S.; Inchingolo, R.; Smargiassi, A. The role of chest ultrasonography in the management of respiratory diseases: Document I. *Multidiscip. Respir. Med.* **2013**, *8*, 54. [CrossRef]
22. Smargiassi, A.; Inchingolo, R.; Soldati, G.; Copetti, R.; Marchetti, G.; Zanforlin, A.; Giannuzzi, R.; Testa, A.; Nardini, S.; Valente, S. The role of chest ultrasonography in the management of respiratory diseases: Document II. *Multidiscip. Respir. Med.* **2013**, *8*, 55. [CrossRef]
23. Medford, A.R.L.; Agrawal, S.; Bennett, J.A.; Free, C.M.; Entwisle, J.J. Thoracic ultrasound prior to medical thoracoscopy improves pleural access and predicts fibrous septation. *Respirology* **2010**, *15*, 804–808. [CrossRef]
24. Marchetti, G.; Valsecchi, A.; Indellicati, D.; Arondi, S.; Trigiani, M.; Pinelli, V. Ultrasound-guided medical thoracoscopy in the absence of pleural effusion. *Chest* **2015**, *147*, 1008–1012. [CrossRef]
25. Mandrekar, J.N. Measures of Interrater Agreement. *J. Thorac. Oncol.* **2011**, *6*, 6–7. [CrossRef]
26. Ng, A.; Swanevelder, J. Resolution in ultrasound imaging. *Contin. Educ. Anaesth. Crit. Care Pain* **2011**, *11*, 186–192. [CrossRef]
27. Mensi, C.; De Matteis, S.; Catelan, D.; Dallari, B.; Riboldi, L.; Pesatori, A.C.; Consonni, D. Geographical patterns of mesothelioma incidence and asbestos exposure in Lombardy, Italy. *Med. Lav.* **2016**, *107*, 340–355.

28. Smargiassi, A.; Pasciuto, G.; Pedicelli, I.; Lo Greco, E.; Calvello, M.; Inchingolo, R.; Schifino, G.; Capoluongo, P.; Patriciello, P.; Manono, M.; et al. Chest ultrasonography in health surveillance of asbestos-related lung diseases. *Toxicol. Ind. Health* **2017**, *33*, 537–546. [CrossRef]
29. Bandi, V.; Lunn, W.; Ernst, A.; Eberhardt, R.; Hoffmann, H.; Herth, F.J.F. Ultrasound vs. CT in Detecting Chest Wall Invasion by Tumor. *Chest* **2008**, *133*, 881–886. [CrossRef]
30. Raju, S.; Ghosh, S.; Mehta, A.C. Chest CT Signs in Pulmonary Disease: A Pictorial Review. *Chest* **2017**, *151*, 1356–1374. [CrossRef]
31. Demi, L.; Wolfram, F.; Klersy, C.; De Silvestri, A.; Ferretti, V.V.; Muller, M.; Miller, D.; Feletti, F.; Wełnicki, M.; Buda, N.; et al. New International Guidelines and Consensus on the Use of Lung Ultrasound. *J. Ultrasound Med.* **2022**. Epub ahead of print. [CrossRef]
32. Leung, A.N.; Muller, N.L.; Miller, R.R. CT in differential diagnosis of diffuse pleural disease. *AJR Am. J. Roentgenol.* **1990**, *154*, 487–492. [CrossRef] [PubMed]
33. Metintas, M.; Ucgun, I.; Elbek, O.; Erginel, S.; Metintas, S.; Kolsuz, M.; Harmanci, E.; Alatas, F.; Hillerdal, G.; Ozkan, R.; et al. Computed tomography features in malignant pleural mesothelioma and other commonly seen pleural diseases. *Eur. J. Radiol.* **2002**, *41*, 1–9. [CrossRef]
34. Yilmaz, U.; Polat, G.; Sahin, N.; Soy, O.; Gulay, U. CT in differential diagnosis of benign and malignant pleural disease. *Monaldi Arch. Chest Dis.* **2005**, *63*, 17–22. [CrossRef] [PubMed]
35. McDonald, C.M.; Pierre, C.; de Perrot, M.; Darling, G.; Cypel, M.; Pierre, A.; Waddell, T.; Keshavjee, S.; Yasufuku, K.; Czarnecka-Kujawa, K. Efficacy and Cost of Awake Thoracoscopy and Video-Assisted Thoracoscopic Surgery in the Undiagnosed Pleural Effusion. *Ann. Thorac. Surg.* **2018**, *106*, 361–367. [CrossRef]

diagnostics

MDPI

Review

The Role of Ultrasound in the Diagnosis of Pulmonary Infection Caused by Intracellular, Fungal Pathogens and Mycobacteria: A Systematic Review

Mariaclaudia Meli [1,†], Lucia Spicuzza [2,†], Mattia Comella [1,†], Milena La Spina [1], Gian Luca Trobia [3], Giuseppe Fabio Parisi [4], Andrea Di Cataldo [1,†] and Giovanna Russo [1,*,†]

1 Pediatric Hematology and Oncology Unit, Department of Clinical and Experimental Medicine, University of Catania, 95123 Catania, Italy; mclaudiameli@gmail.com (M.M.); mattiacomella@gmail.com (M.C.); mlaspina@unict.it (M.L.S.); adicata@unict.it (A.D.C.)
2 Pulmology Unit, Department of Clinical and Experimental Medicine, University of Catania, 95123 Catania, Italy; lucia.spicuzza@unict.it
3 Pediatrics and Pediatric Emergency Room, Cannizzaro Emergency Hospital, 95126 Catania, Italy; trobia@tin.it
4 Pediatric Pulmology Unit, Department of Clinical and Experimental Medicine, University of Catania, 95123 Catania, Italy; giuseppe.parisi@policlinico.unict.it
* Correspondence: diberuss@unict.it
† These authors contributed equally to this work.

Abstract: Background: Lung ultrasound (LUS) is a widely available technique allowing rapid bedside detection of different respiratory disorders. Its reliability in the diagnosis of community-acquired lung infection has been confirmed. However, its usefulness in identifying infections caused by specific and less common pathogens (e.g., in immunocompromised patients) is still uncertain. Methods: This systematic review aimed to explore the most common LUS patterns in infections caused by intracellular, fungal pathogens or mycobacteria. Results: We included 17 studies, reporting a total of 274 patients with *M. pneumoniae*, 30 with fungal infection and 213 with pulmonary tuberculosis (TB). Most of the studies on *M. pneumoniae* in children found a specific LUS pattern, mainly consolidated areas associated with diffuse B lines. The typical LUS pattern in TB consisted of consolidation and small subpleural nodes. Only one study on fungal disease reported LUS specific patterns (e.g., indicating "halo sign" or "reverse halo sign"). Conclusions: Considering the preliminary data, LUS appears to be a promising point-of-care tool, showing patterns of atypical pneumonia and TB which seem different from patterns characterizing common bacterial infection. The role of LUS in the diagnosis of fungal disease is still at an early stage of exploration. Large trials to investigate sonography in these lung infections are granted.

Keywords: lung ultrasound; pneumonia; pulmonary infection

Citation: Meli, M.; Spicuzza, L.; Comella, M.; La Spina, M.; Trobia, G.L.; Parisi, G.F.; Di Cataldo, A.; Russo, G. The Role of Ultrasound in the Diagnosis of Pulmonary Infection Caused by Intracellular, Fungal Pathogens and Mycobacteria: A Systematic Review. *Diagnostics* **2023**, *13*, 1612. https://doi.org/10.3390/diagnostics13091612

Academic Editor: Chao-Min Cheng

Received: 6 March 2023
Revised: 11 April 2023
Accepted: 13 April 2023
Published: 2 May 2023

1. Introduction

Since its first introduction in clinical practice, lung ultrasound (LUS) has been acknowledged as a potential first-line imaging modality to recognize common lung pathology [1–3]. Among a number of acute conditions, the accuracy and reliability of LUS for the diagnosis of community acquired pneumonia (CAP), has been explored with promising results in both adults and children [4–6]. There is now evidence that LUS may have greater sensitivity, similar specificity, and better inter-operator reliability in the diagnosis of pneumonia when compared with standard chest X-ray (CXR) [4,7–10]. Moreover, LUS has the advantage of being free of ionizing radiation, has lower cost and easier bedside availability than CXR and is subject to fewer regulatory requirements. This makes the technique particularly appealing as a point-of-care tool in the acute clinical setting, especially for children.

Indeed, although LUS has been under evaluation for over a decade, the important role played during the recent COVID-19 pandemic, has greatly increased the interest of

clinicians from multiple disciplines toward this technique and many efforts have been done to standardize its use [11].

It is a paradigm that, to be detected from LUS, a parenchymal lesion must be close enough to the pleura. In patients with typical bacterial pneumonia, the parenchymal consolidation usually appears as a sub-pleural hypo-echoic area associated with hyperechoic dynamic spots called "air bronchograms", representing air-filled bronchi within the density of surrounding alveoli [12,13]. The pleural line above the consolidation is less echogenic or even non-visible. At the rear, the presence of compact vertical artifacts, called B lines, is a frequent expression of wall reinforcements typically produced by areas with fluid content [14,15].

Differently from bacterial pneumonia, interstitial pneumonia (e.g., viral) sonographycally appears as a pattern characterized by three or more B lines (vertical hyperechoic reverberations) in the same scansion between two ribs, either isolated or confluent. These features are similar to those described in the interstitial-alveolar syndrome and may form, in more severe cases, a "white lung pattern" [16].

As mentioned, a large number of studies have shown the accuracy of LUS in the diagnosis of the most common lung infections affecting children and adults, mainly bacterial pneumonia [4,10,17]. Conversely, few studies have explored the usefulness of LUS for the detection of less common lung infections such as those caused by atypical and fungal pathogens or mycobacteria.

Atypical pneumonia caused by intracellular pathogens such as Mycoplasma Pneumoniae (*M. pneumoniae*) and Chlamydia Pneumoniae (*C. pneumoniae*) distinctively cause lung interstitial involvement and are insensitive to common antibiotics used for the treatment of bacterial pneumonia [18]. Lung infections caused by mycobacteria, mainly *Mycobacterium tuberculosis* or fungal pathogens are rare in immunocompetent patients, but increasingly diagnosed in immunocompromised patients [19]. In addition, TB remains highly prevalent in low- and middle-income countries [20]. When a lung infection is suspected in immunocompromised patients, it is crucial to reach an early diagnosis in order to start promptly a specific treatment. CXR and computerized tomography (CT) are often required in febrile patients with cancer to make diagnosis. However, CXR, especially during neutropenia, is hampered by a low specificity and hardly differentiates bacteria from a non-bacterial pneumonia, making essential a chest CT scan that has both higher sensitivity and specificity [21]. The role of lung ultrasound as a point-of-care tool may therefore be decisive in the diagnosis and follow-up of these infections, particularly in children and severely ill patients.

This systematic review aimed to explore the most common findings reported at lung ultrasound in patients with infection caused by intracellular, fungal pathogens or mycobacteria, and to discuss a putative role for this technique in the diagnosis of these lung infections.

2. Materials and Methods

A search strategy was developed in order to recognize the most significant literature on the topic. An exhaustive search was performed on the main scientific libraries including PubMed, Embase, Google Scholar and Cochrane. We used the following keywords: lung/thoracic ultrasound/ultrasonography, atypical pneumonia, *Mycoplasma pneumoniae*, *Chlamydia pneumoniae*, fungal pneumonia, fungal invasive disease, lung Aspergillosis, tuberculosis/mycobacterium. A combination of MeSH and associated terms with other methodological terms (Mycoplasma or Chlamydia or atypical pneumonia or pneumonitis and LUS or lung or thoracic and ultrasound or ultrasonography; fungal or fungal invasive or Aspergillosis and pneumonia or pneumonitis and LUS or lung or thoracic and ultrasound or ultrasonography; Tuberculosis or Mycobacterium and pneumonia or pneumonitis and LUS or lung or thoracic and ultrasound or ultrasonography).

Study Selection and Data Extraction

The search was limited to articles published in English peer-reviewed journals between January 1990 and January 2023. We included original studies, retrospective or prospective, case reports and case series reporting detailed lung ultrasound findings for the diagnosis or follow-up of pulmonary infection by atypical, fungal pathogens and mycobacteria. We included studies on adults, children and infants reporting a microbiologically confirmed lung infection. We excluded: (1) studies reporting data from endoscopic ultrasound; (2) studies reporting "suspected infection" without clear microbiology data; (3) study in which the prevalence of any ultrasound finding in the population was not well specified; (4) review articles and meta-analyses; (5) qualitative studies; (6) not English articles.

For data processing, the document management tool Mendeley and the program Microsoft Excel were used. The cumulative selection of articles was evaluated and screened independently by two researchers. In case of disagreement between investigators, a third investigator was involved. To select eligible studies for full text review, we used an evidence-based algorithmic approach, Preferred Reporting Items for Systematic Reviews and Meta-Analyses (PRISMA) (Figure 1) [22].

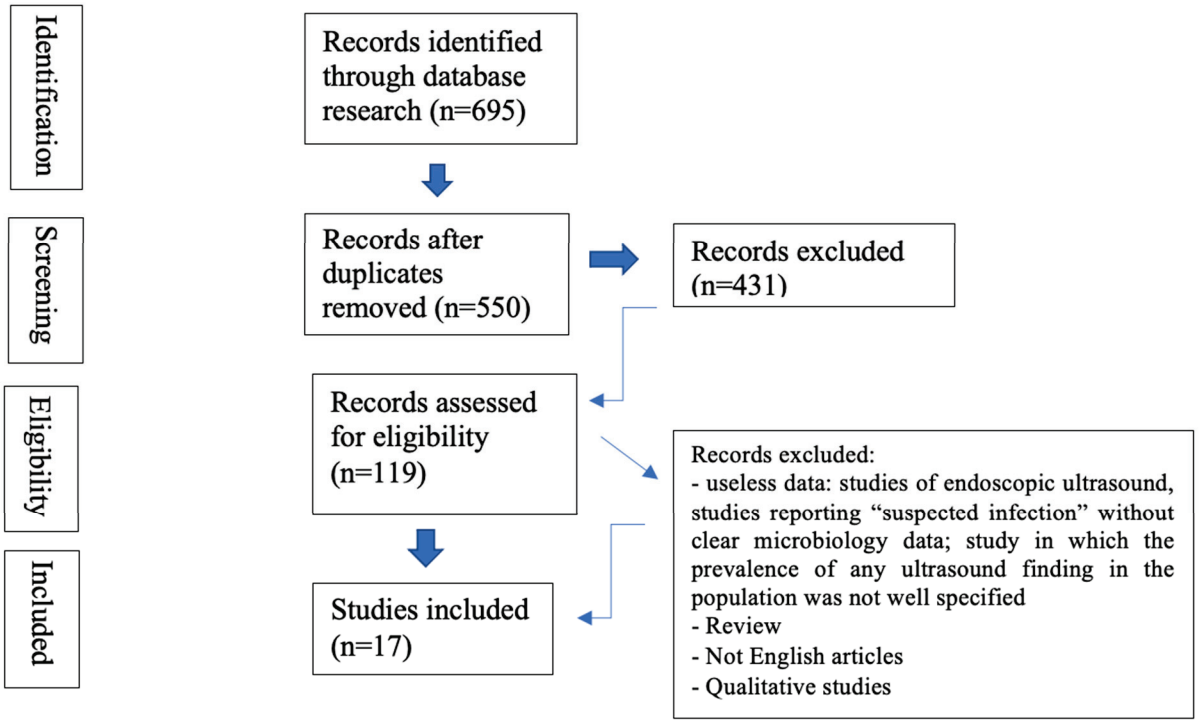

Figure 1. PRISMA flow-chart [22].

For each study we collected the following information: (1) author and year of publication; (2) sample size; age; (3) specific pathogen; (4) LUS findings.

3. Results

3.1. Study Selection and LUS Definitions

The initial search included a total of 695 studies. Duplicates found in different databases were excluded. From the remaining 550 we excluded 431 articles for being review, not in English or qualitative studies. Of 119 studies assessed for eligibility, only 17 articles were useful for the purpose of this review. These included four studies on atypical pneumonia, seven on fungal infection and six on pulmonary tuberculosis. Although sometimes a different terminology was used in the studies to describe lung patterns, definitions of the main signs observed from LUS are shown in Table 1.

Table 1. Definitions of the main lung ultrasound findings.

	Definition
Consolidation	Area in which lung tissue is de-aerated with density similar to parenchymal tissues [23]
Atelectasis	Type of consolidation shown as hyperechogenic tissue structure visualized as solid parenchyma with static air bronchogram [11,24]
Cavitation	Solid, hypoechoic, heterogeneous lesions with sharp lobulated margins [11,25]
Pleural effusion	Hypo- or anechogenic structure, delineated by the chest wall and the diaphragm [11,26]
B-lines	Vertical reverberation artefacts from the pleural line to the edge of the scree; laserlike, vertical hyperechogenic artefacts synchronized with pleural line [11,23,27]
Pleural irregularities	Reduction or interruption of pleural line [11,28]
Sub-pleural nodes/granularities	Hyperechogenic subcentimetric granularities or consolidation under the pleural line [29,30]

3.2. Primary Results

3.2.1. Intracellular Pathogens Lung Infection

All eligible studies on pneumonia caused by intracellular pathogens focused on *M. pneumoniae* except one study also including some cases of *C. pneumoniae*. As this infection is more common at a pediatric age, not surprisingly all studies were performed in children with an age range from 2 months to 15 years (Table 2). A total of four studies, two prospective and two retrospective were analyzed, including a total of 274 patients with a diagnosis of atypical pneumonia confirmed by microbiology and conventional imaging.

Table 2. Lung ultrasonographic findings in bacterial intracellular pathogens infection.

	N. of Patients	**Age**	**Pleural Effusion**	**Consolidation**		**B-Lines**			**Atelectasias**
				Total	**>1–1.5 cm**	**Total**	**Scattered**	**Confluent**	
Li, 2021 [31]	30	Mean 9 yrs	16 (53%)	30 (100%)	NS	30 (100%)	30 (100%)	30 (100%)	18 (60%)
Tripaldi, 2021 [32]	40	Mean 4 yrs	6 (15%)	34 (85%)	31 (77%)	13 (32%)	NS	NS	NS
Buonsenso, 2022 [33]	43	Mean 7 yrs	7 (16%)	38 (88%)	19 (44%)	28 (65%)	28 (65%)	0	26 (60%)
Liu G., 2022 [34]	161	Median 4 yrs	48 (29%)	136 (84%)	NS	161 (100%)	3 (1%)	154 (95%)	NS
Total	274		77 (28%)	238 (86%)	50 (60%)	232 (84%)	61 (26%)	184 (79%)	44 (60%)

All patients with *M. pnuemonia* infectin; Buonsenso 2022 included also *Chlamydia pneumonia* infection. NS: the exact number is not specified in the study, thus excluded from calculation of total (%).

Overall, the sonographic patterns described were consistent among studies (Figures 2–4). The most common LUS feature was consolidation reported in 84–100% of the patients (Table 2). Of the two studies analyzing the consolidation's dimension, one reported most commonly a dimension < 1.5 cm, while another described largest consolidated areas up to 4 cm (Figure 2). Only in a few cases of severe atypical pneumonia did the consolidation reach the dimension of 6 cm. Atelectasis, characterized by a hyperechoic static air bronchograms, was also common (60%). In most of the cases consolidation was associated with subpleural effusions (Figure 3) and a diffuse interstitial pattern. B lines were in fact extremely common, being present in 85% of all cases (Figure 4). Although both scattered

and confluent B lines were described, in most cases, the B lines were confluent and so dense in more severe disease that they formed the so-called "white lung".

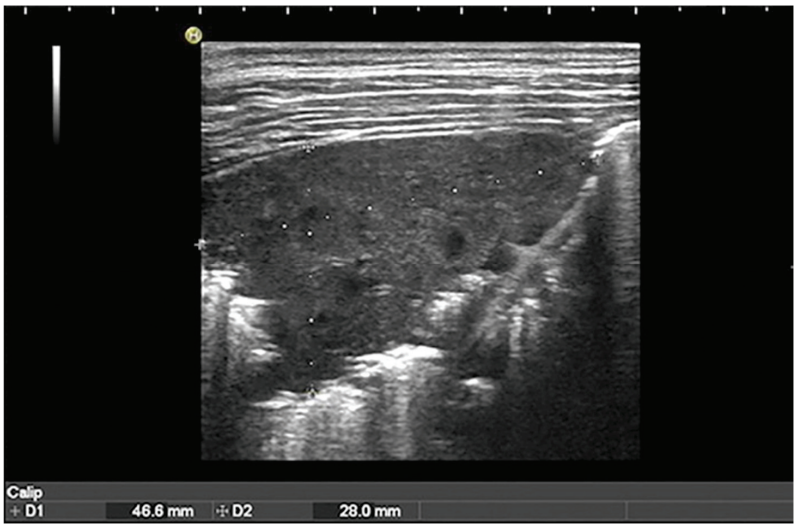

Figure 2. Cosolidation and air bronchogram in *Mycoplasma pneumonia* [31].

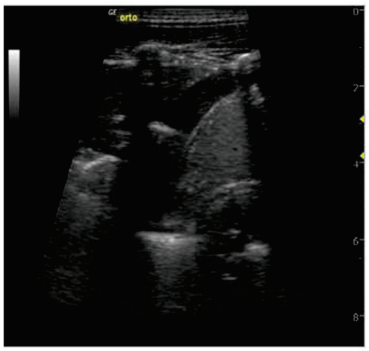

Figure 3. Subpleural effusions in *Mycoplasma pneumonia* [32].

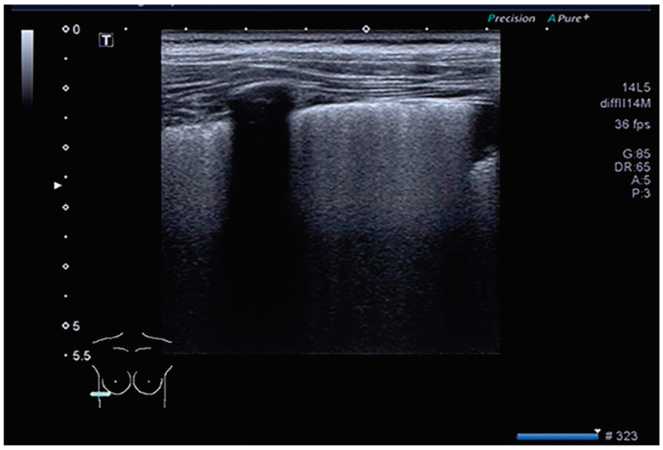

Figure 4. B lines in *Mycoplasma pneumonia* [31].

3.2.2. Fungal Lung infection

Studies on pneumonia caused by fungal pathogens, also known as invasive fungal disease, were rare and extremely heterogeneous in terms of age range, disease manifestation, patients' comorbidities (e.g., immune status) and specific pathogen (Table 3).

Table 3. Lung ultrasonographic findings in fungal invasive pneumonia.

	N. of Patients	Age	Microorganism	Consolidation	Atelectasis	Cavitation	Hyper–Echoic Nodule with Hypo–Echoic Rim	Hypo–Echoic Nodule with Hyper–Echoic Rim	Pleural Effusion	B–lines
				Children						
Trinavarat 2012 [35]	1	6 weeks	Aspergillus	1 (100%)		1 (100%)				
Alamdara, 2021 [36]	6	5-11 yrs	1 Mucurmicosis, 5 Aspegillus	5 (83%)		2 (33%)	2 (33%)	4 (66%)		
Liu J., 2022 [37]	7	Premature newborns	5 C. albicans, 1 C. parapsilosis, 1 Aspergillus	7 (100%)	2 (33%)				2 (33%)	7 (100%)
Total	14			13 (93%)	2 (14%)	3 (21%)	2 (14%)	4 (28%)	2 (14%)	7 (50%)
				Adults						
Tikkakoski, 1995 [38]	4	49-79 yrs	4 Aspergillus (1 A.niger, 2 A.fumigatus)	4 (100%)		4 (100%)			1 (25%)	
Grabala, 2017[39]	1	41 yrs	1 Mucurmicosis	1 (100%)						1 (100%)
Greco, 2019 [40]	10	Mean 44 yrs	Not specified	10 (100%)	4 (40%)				4 (40%)	8 (80%)
Ruby, 2021 [41]	1	45 yr	1 Aspergillus	1 (100%)		1 (100%)	1 (100%)			
Total	16			16 (100%)	4 (25%)	5 (31%)	1 (6%)		5 (31%)	9 (56%)

A total of seven studies were analyzed which included a total of 30 patients. These studies were mainly case reports describing between one and four patients. The three largest studies available included, respectively, 10 adults, 6 children (6–11 years) and 7 premature infants (Table 3). In most of the cases lung fungal disease was caused by Aspergillus, five cases of Candida Albicans and two cases of rare Mucormycosis were also described.

Among 10 cases of invasive fungal diseases, in patients treated with allogenic hematopoietic stem cell transplantation, the most common LUS feature was sub-pleural consolidation with an inhomogeneous echotexture and indistinct margins, usually bilateral (Figure 5). Atelectasis and pleural effusion were present in 40% of the patients, whereas B lines, expression of an interstitial pattern, were extremely common (80%) (Figure 6, Table 3).

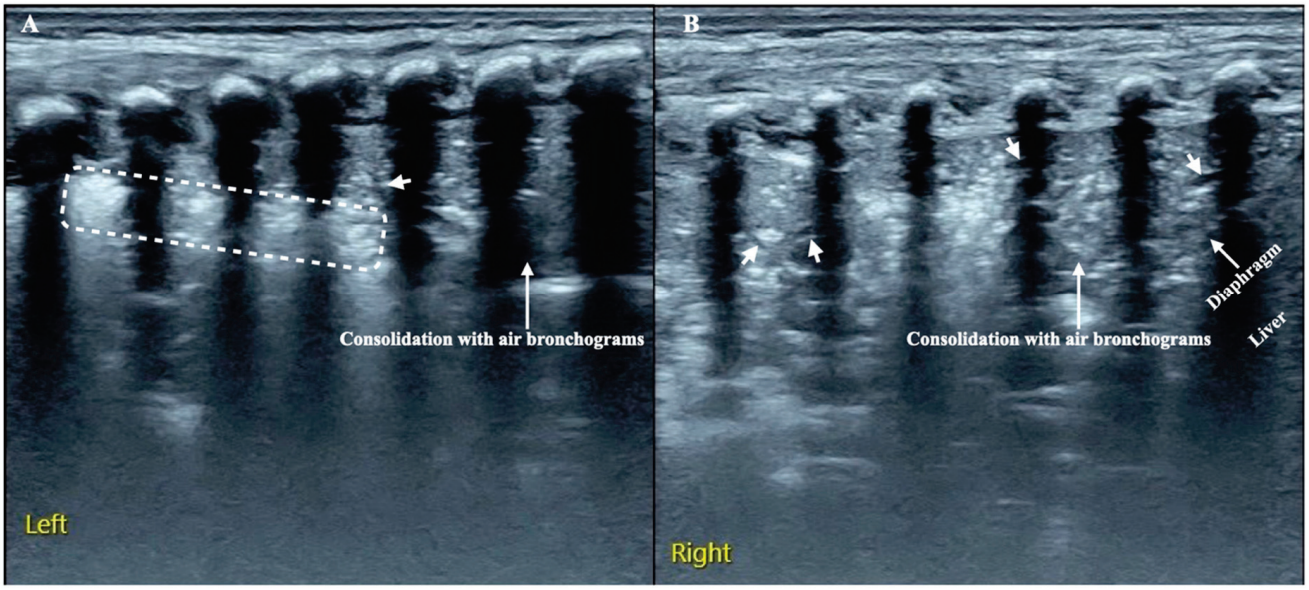

Figure 5. Consolidation with air bronchogram in fungal pneumonia [37].

Cavitations, a common feature of pulmonary Aspergillosis observed in lung CT scan, were reported in all four adults (age 49–79 years) belonging to a group with invasive aspergillosis and in two out of five children, aged 7–11 years, with Aspergillosis and Mucormycosis (Figure 7, Table 3).

In a group of seven premature newborns the sonographic pattern of lung invasive fungal disease was typical, characterized by bilateral lung consolidation with air bronchogram and irregular boundaries (Table 3). Different patterns of B lines, reflecting a different degree of lung edema, were observed in all non-consolidated areas.

In a group of older children (5–11 years), more typical lesions were described, including hypo-echoic nodules with hyperechoic rims or hyper-echoic nodules with hypo/anechoic rims (Figures 8–10). In a few cases, the "fungus ball" was evidenced as a hyper-echoic area in the center of the main lesion (Figure 8).

3.2.3. *Mycobacterium tuberculosis* Lung Infection

We selected six studies, including a total of 213 patients affected by pulmonary TB. Of these, one study included only children (40 cases, with a mean age of 2 years old) and one study specifically selected 10 adults with miliary TB (Table 4). The studies were performed either in Western countries including patients at high risk for TB or in countries that have a high risk of TB.

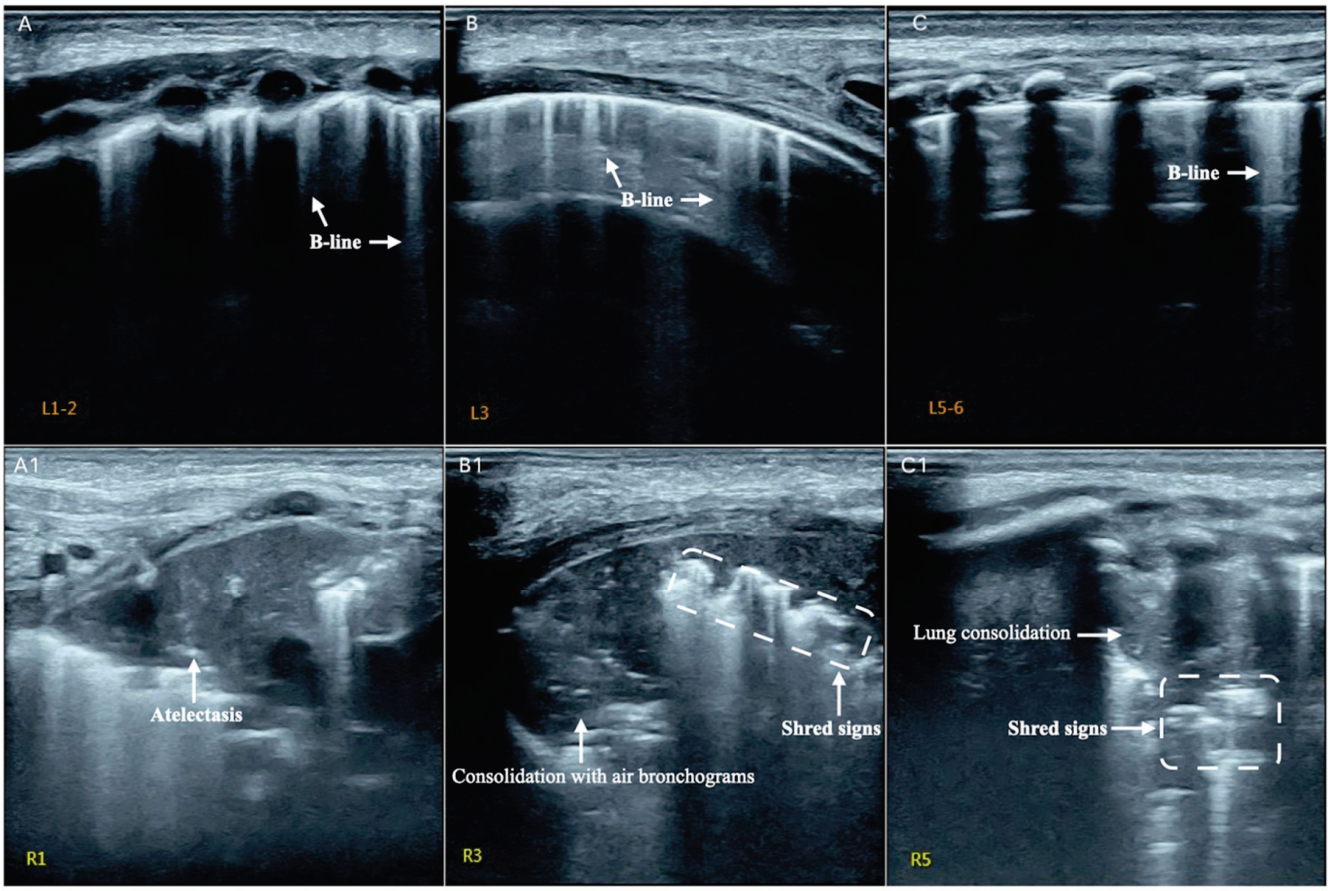

Figure 6. B-lines (**A**–**C**), Atelectasias, consolidation with air bronchogram, shred signs in fungal pneumonioa [37].

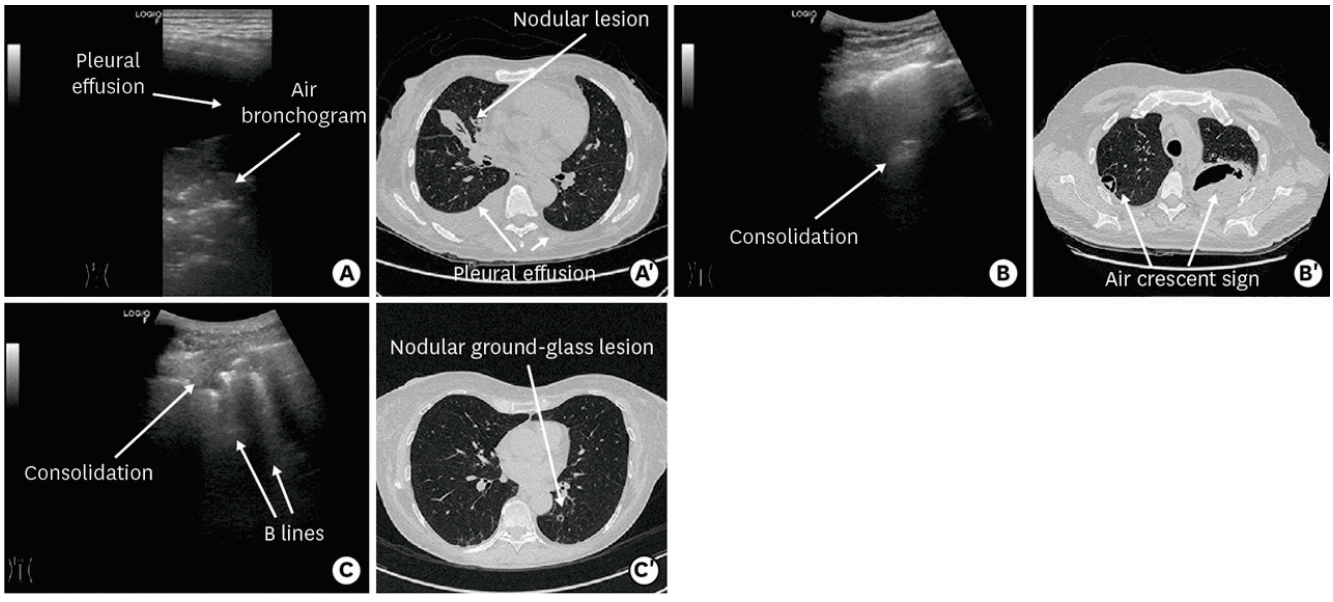

Figure 7. Comparison between LUS images and CT images in fungal pneumonia [40].

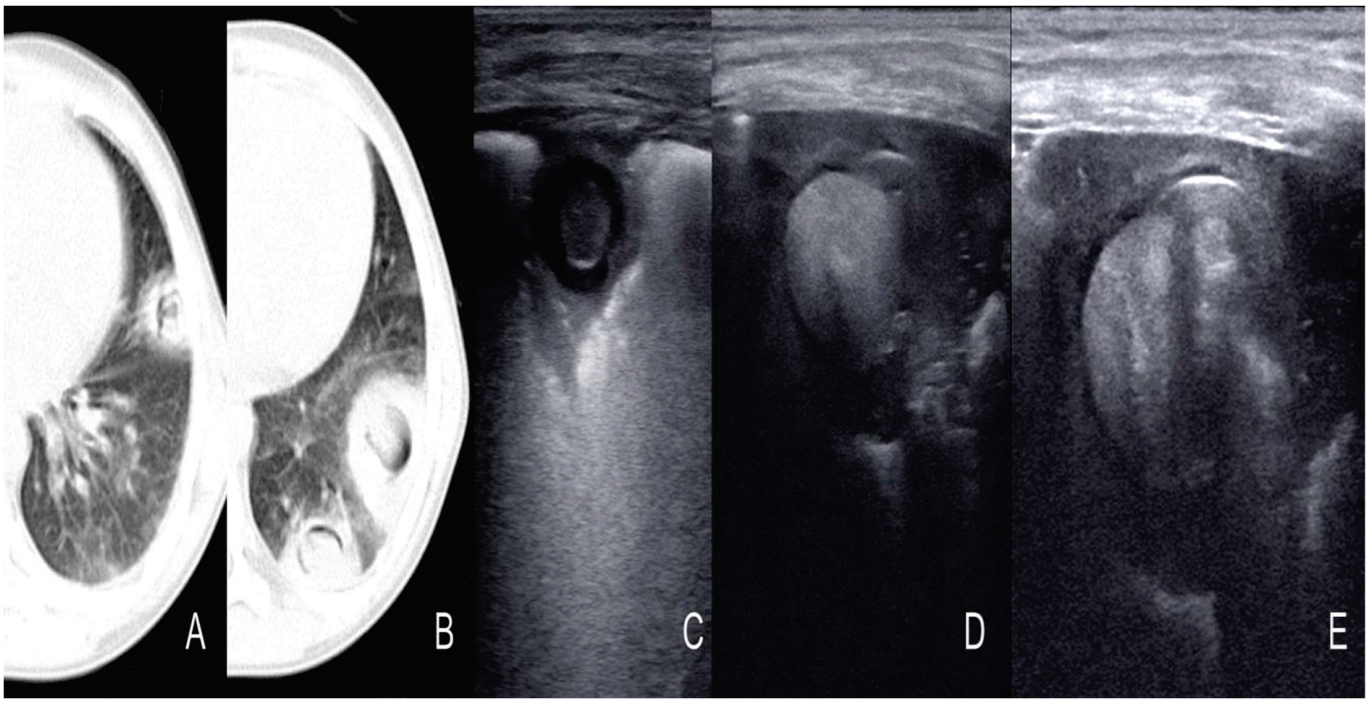

Figure 8. (**A**,**B**) Multiple nodular lesions with peripheral ground-glass opacity or halo sign, reverse halo sign, and air crescent sign. (**C**) The target lesions; a hyper-echoic central nodule with a hypo-echoic rim. (**D**) Hyper-echoic nodule (fungus ball) within consolidaion. (**E**) Hyper-echoic fungus ball with air exension at the peripheral hup-echoic rim [36].

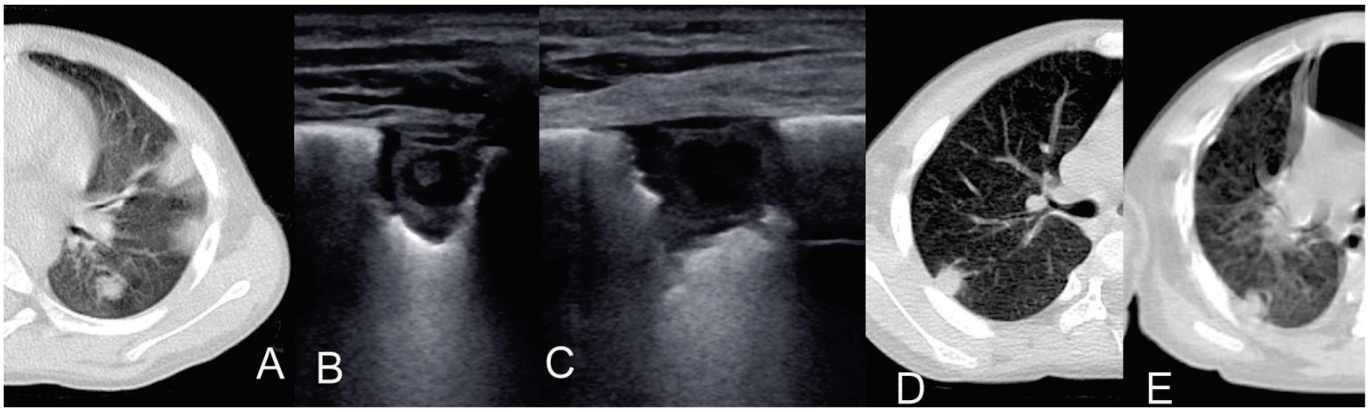

Figure 9. (**A**) Multiple nodular lesions with ground-glass opacity or halo sign, without air crescent sign. Two target lesions in ultrasound. (**B**) Hyper-echoic central nodule with a hypo-echoic rim. Figure (**C**) Hypo-echoic center with a hyper-echoic rim. (**D**,**E**) A nodular lesion of the right lung that has developed and air crescent sign in control HRCT [36].

Sonographic consolidations, often multiples and mainly apical, where commonly described in both children (55%) and adults (from 77% to 80%), with the exception of cases of miliary TB. None of the studies, except a single case report, reported the occurrence of atelectasis in the context of consolidated areas.

In adult TB, the most common and peculiar findings were circular or ellipsoidal hypo-echoic sub-pleural lesion, generally <1.5 cm, defined as "sub-pleural nodes". These were reported in up to 90% of adults, mainly in the superior quadrants of the lung (Table 4, Figures 11 and 12).

Pleural effusion was most commonly found in children (30%) than in adults (on average 15% of the cases). However, pleural irregularities were common findings in all groups. Sonographic cavitation was absent in children and was reported in a small number of adults (5 to 30%) (Figure 13 and Table 4).

In 10 adults with miliary TB, a quite precise sonographic pattern was shown, invariably characterized by B lines and echogenic bright "granular" artifacts in the sub-pleural areas, defined as "sub-pleural granularities".

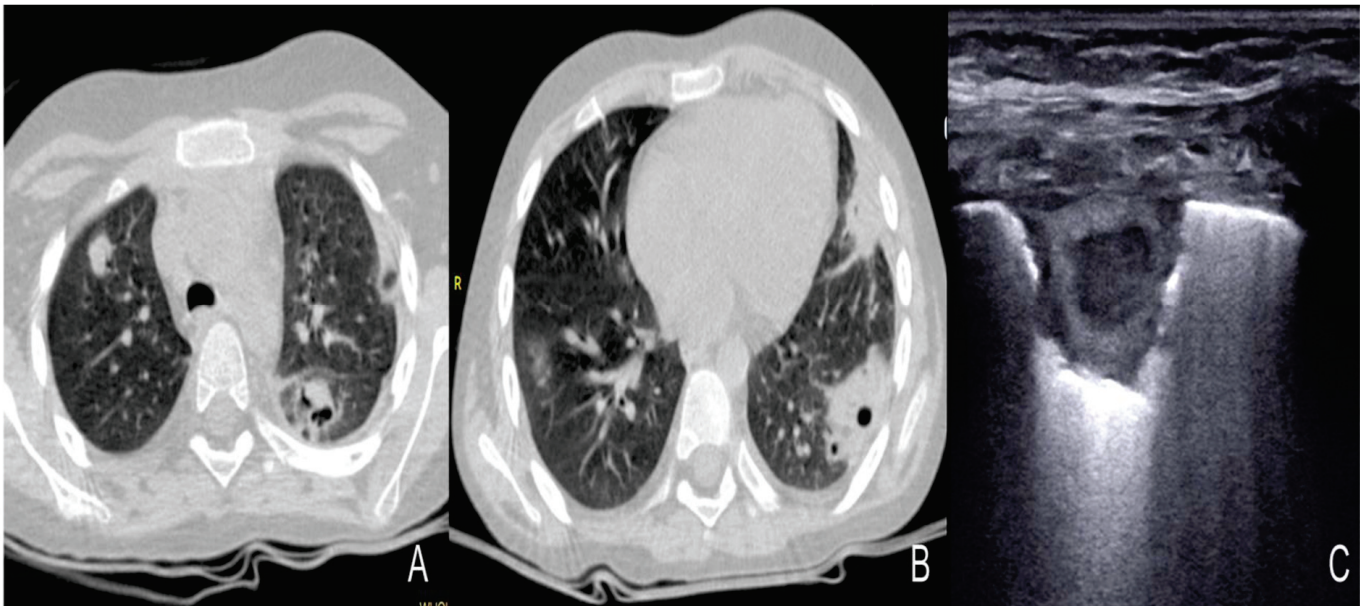

Figure 10. (**A**,**B**) Multiple nodular lesions with cavitation. (**C**) The target lesion in ultrasound has a Hypo-echoic center with a hyper-echoic rim [36].

Table 4. Ultrasonographic findings in *Mycobacterium tuberculosis*.

	N. of Patients	Mean Age	Pleural Effusion	Pleural Irregularities	Consolidation	Cavitation	Subpleural Nodes	Subpleural Granularities	B-Lines
Children									
Heuvelings, 2019 [42]	40	2 yrs	12 (30%)	31 (78%)	22 (55%)	0	0	0	13 (33%)
Adults									
Hunter, 2016 [30] *	10	33 yrs median	0	0	0	0	0	10 (100%)	10 (100%)
Agostinis, 2017 [29]	60	32 yrs	11 (18%)	NS	28 (46%)	3 (5%)	58 (98%)	4 (6%)	NS
Montuori, 2019 [43]	51	34 yrs	10 (20%)	37 (73%)	40 (77%)	9 (30%)	37 (73%)	0	0
Fentress, 2020 [44]	51	34 yrs	4 (7%)	NS	41 (80%)	3 (6%)	41 (80%)	0	20 (39%)
Cocco, 2022 [45]	1	36 yrs	1 (100%)	0	1 (100%)	1 (100%)	0	0	0
Total (adults)	173		26 (15%)	37 (59%)	110 (63%)	16 (9%)	136 (78%)	14 (8%)	30 (26%)

* Only cases of miliary tuberculosis included. NS: the exact number is not specified in the study, thus excluded from calculation of total (%).

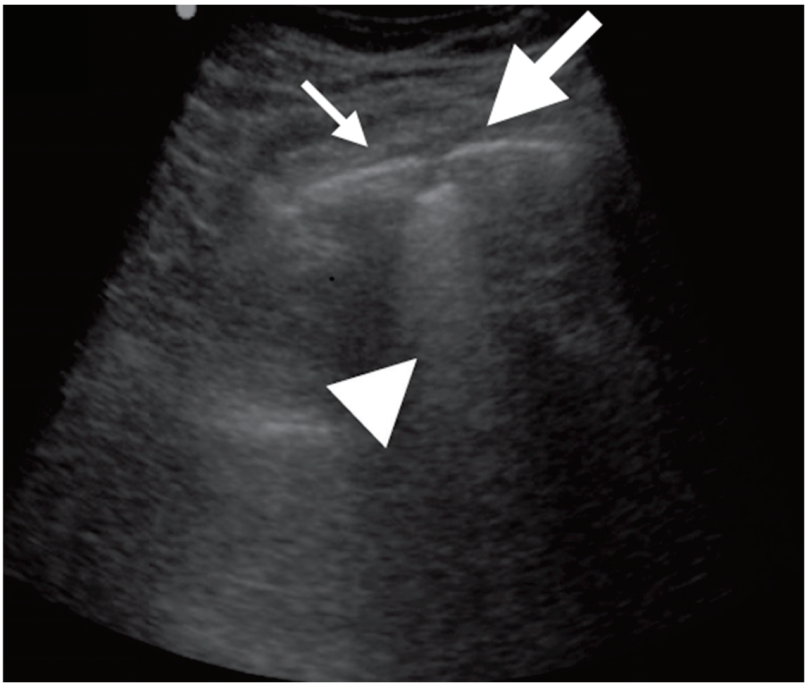

Figure 11. Subpleural consolidation (thick arrow), characterized by subpleural hypo-echoic region < 1 × 1 cm, with distinct borders and trailing artifact (arrowhead), next to the normal white pleural line (thin arrow) [44].

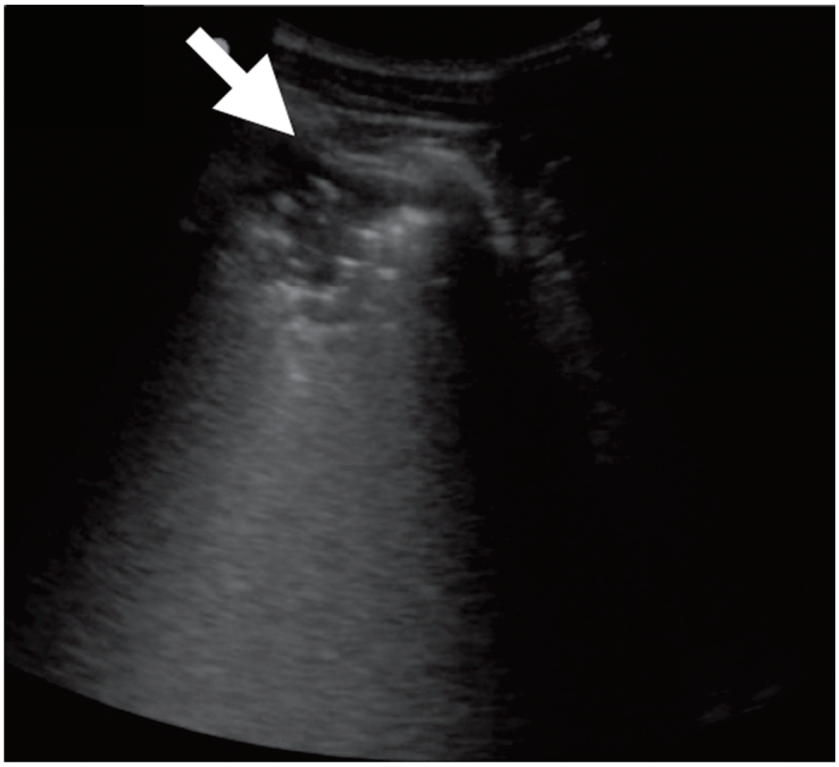

Figure 12. Consolidation (thick arrow), characterized by echo-poor region > 1 × 1 cm, with air bronchograms [44].

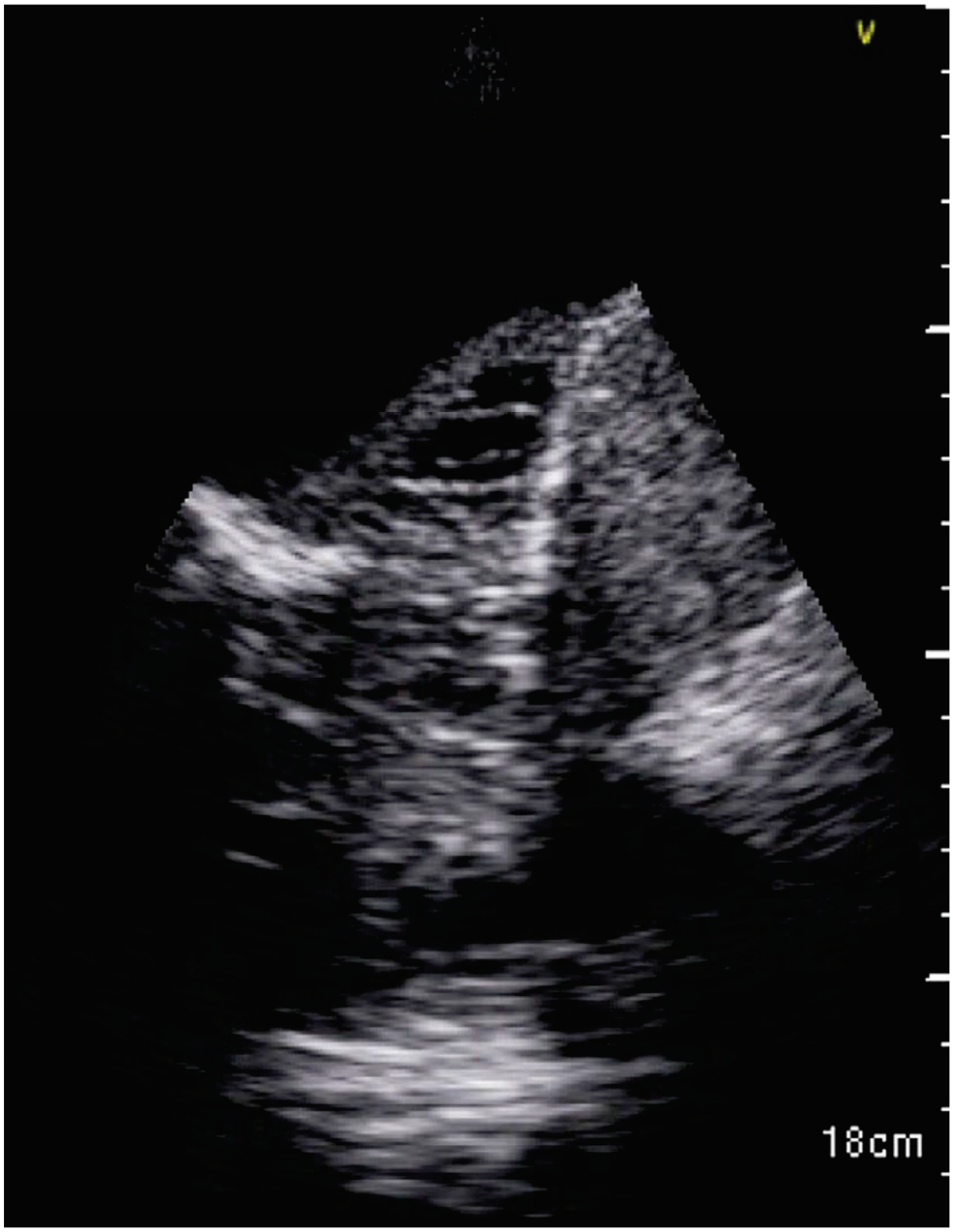

Figure 13. Cavitation in mycobacterial pneumonia [45].

4. Discussion

4.1. General Considerations

Over the last decade, a considerable amount of work has been performed to define the role of LUS as point-of-care diagnostic tool [46–55]. While most of the studies focused on CAP, with pathogens rarely microbiologically distinguished, LUS has also been proposed as a tool for etiological diagnosis [33]. This systematic revision explored cases of lung infection caused by pathogens which are rare in the immunocompetent population (Mycobacteria and fungi) or by intracellular pathogens. These infections are common in children but are mainly included in the group of community acquired infections, without any distinction from the most common etiologies such as *S. pneumoniae*. We found a limited number of studies, particularly for fungal infection. These studies presented several limitations including mainly a small sample size and heterogeneous definitions of lung sonographic patterns. This is not surprising, as LUS is still an emerging technique and is currently in the

process of standardization. For this reason, the studies were difficult to compare and the study populations difficult to merge. However, we found that some interesting and specific LUS patterns have been described in association with these infections and can represent a good starting point for further investigations.

4.2. Intracellular Pathogens Lung Infection

As expected, data on the accuracy of LUS in atypical pneumonia focused on children, and indeed the role of this technique in pediatrics may be crucial, given the extent they are free of ionizing radiation [56–67]. A recent meta-analysis showed a 96% sensitivity and 93% specificity of LUS in detecting pneumonia in children [68]. The peculiar feature of atypical, as well as of viral pneumonia, is the involvement of lung interstitium with characteristic edema and inflammatory cellular infiltrate. These pathological changes correlate with specific radiographic features such as ground-glass and reticular/nodular patterns [69].

A mentioned above, the identification of a lung interstitial pattern linked to non-bacterial infection through the detection of B lines from LUS has been widely reported during the observation of COVID-19-related pneumonias [70].

Indeed, we found that the presence of an interstitial pattern, characterized by scattered or most commonly confluent B lines is a main feature in children with atypical pneumonia in all age groups [31–34,37,71–73].

Most of the studies that we examined aimed to correlate LUS and traditional imaging findings and to assess the possibility to rapidly differentiate the etiology of lung infection by bedside LUS.

In one of the largest prospective studies, Buonsenso et al. found that in children with pneumonia, LUS findings were more helpful than clinical presentation, laboratory data and CXR in distinguishing bacterial, viral or atypical pneumonia [33]. They showed that multiple consolidations were related to viral and atypical pneumonia, whereas larger and solitary consolidations with bacterial pneumonia. Moreover, deep air bronchogram was more typical of bacterial and viral pneumonia, whereas a superficial air bronchogram was almost always present in atypical pneumonia. B lines were more common in atypical/viral pneumonia, generally diffused to the lung, while in bacterial pneumonia B lines were mainly located in continuity with the solid mass. It is noteworthy that the same group has previously shown that LUS pattern recognition at diagnosis may help the predict early antibiotic response better than clinical and laboratory data [72].

The relevance of the dimension of the consolidation and distribution of B lines has been suggested earlier by studies on CAP, although these could not be included in this review since the exact prevalence of the findings was not reported. Data from Buonsenso et al. were in agreement with earlier data from Berce and co-workers. The data showed that in children with bacterial pneumonia consolidations, B lines were commonly solitary, larger, and unilateral compared to those with viral/atypical pneumonia. In bacterial pneumonia, B lines were in proximity to the consolidation, whereas in viral/atypical pneumonia, they were diffuse [17].

Interestingly, Iorio and co-workers describe some small sub-pleural consolidations in children with CAP and consider these “satellites” of the main consolidation, when they are located in the lower or upper anterior district of the contralateral lung [73]. They speculate that this phenomenon could be linked to the lymphatic drainage, being peculiar of atypical pneumonia in which the involvement of lymphatic network is part of the pathogenesis of the interstitial disease [73].

The patterns described so far have been further confirmed by Liu and co-workers in the a large and most recent study [34,37]. In all children with atypical pneumonia, an interstitial pattern was reported, which in some cases, formed the “white lung” pattern. Interestingly, these authors measured the ratio of consolidation size/body surface area and suggested that the dimension of the consolidation may depend on the age of the child [34,37]. They also found that the presence of pleural effusion, which can be detected even in a tiny quantity by LUS is a negative prognostic factor in pediatric atypical pneumonia [34,37].

The predictive value of LUS findings has also been explored by Li et al. [31]. They found that the evaluation of consolidation and atelectasis through LUS may predict the effect of bronchoalveolar lavage in the treatment of children with severe *M. pneumoniae* infection [31].

However, it has to be mentioned that other studies failed to find specific LUS findings for atypical pneumonia. As an example, Tripaldi et al. describe large consolidations in both bacterial and atypical CAP in 4-year-old children and state that the interstitial pattern is not so common in atypical pneumonia [32].

4.3. Fungal Lung Infection

Fungal pulmonary infection, also known as invasive fungal infection, encompasses a broad spectrum of conditions affecting patients who are immunocompromised for different reasons (e.g., chemotherapy, organ transplantation, blood cancer) [71,74–76]. These pathogens are a major threat as they are becoming increasingly common and resistant to treatment, causing high mortality. Although a number of fungal pathogens may infect the lung, infection by different species of Aspergillus is the most common [77–80].

The gold standard imaging for invasive fungal infection is lung CT showing a large variety of lesions including areas of consolidation, cavitation, abscess, nodule or infarction associated with the angio-invasive nature of the fungal pathogens [81–85]. In this wide range of lesions some signs at lung CT can be considered more specific, including: (1) "halo sign", a crescent or complete ring of ground-glass opacity surrounding a focal rounded area of consolidation; (2) "reverse-halo" sign, a focal rounded area of ground-glass opacity surrounded by a crescent/complete ring of consolidation [81]. Although these signs may be present in other bacterial or viral infections, they are strongly suggestive of fungal infection in immunocompromised patients [86–89].

In many cases, these lesions are located in close proximity to the pleura, leading to speculation about the possible role of LUS in their detection. In fact, dealing with patients that are generally severely ill, and given that laboratory data are slow to obtain, the use of a point-of-care diagnostic tool could be crucial for a prompt management of the disease. In addition, it should also be considered that CRX has a low specificity for these infections [21]. Unfortunately, the literature on the topic is scarce. In addition, as lung CT scan may present a variety of different patterns, it might be more difficult to detect these patterns on LUS.

In one of the first studies on LUS-guided fine-needle aspiration biopsies in adults with pulmonary Aspergillosis, abscesses were described as both round, hypo-echoic areas with irregular margins and as difficult to differentiate from bacterial abscesses. However, with the help of LUS biopsies, they were diagnosed in three out of four patients [38].

Perhaps, the most representative study on the topic is the report by Alamdaran et al., describing ten children with hematological cancer and fungal lung infection (mainly Aspergillosis) all undergoing CT scan and LUS [36]. In the CT scan, the most common findings were nodules with halo-sign or reverse halo sign or crescent sign, wedge-shaped consolidation and cavitation. In the LUS, these patterns had a peculiar appearance as either hyper-echoic nodules with hypo-anecoic rims or hypo-echoic nodules with hyperechoic rims. The presence of a mycetoma in an existent cavitation is particular in chronic conditions. In the CT scan, it appears as a crescent sign, airspace between the mycetoma and the cavitation. The mycetoma can be detected by LUS and appears as a central hyperechoic roundish area with air extension to the peripheral anechoic rim, often described as the air crescent sign or cavitation [36,39]. In another cohorts of adults with invasive fungal disease, after hematopoietic stem cell transplantation, LUS showed a good sensitivity compared to CT for the detection of fungal infection, showing hypo-echoic areas with positive air bronchogram [40].

It has been suggested that the evaluation of the vascular component of the lesion with color-coded Doppler may help to discriminate a fungal pneumonia from other causes of consolidation [7,35,39].

Finally, it is worth mentioning a brief report showing the presence of consolidations with air bronchogram and B lines from LUS in premature newborn infants with fungal infection [37]. If confirmed, the latest data might be of great relevance given the difficulty diagnosing early onset pneumonia in newborn infants via traditional imaging.

4.4. Mycobacterium tuberculosis Infection

TB is still a major of cause of death worldwide and to achieve a global reduction of the disease, a prompt diagnosis and treatment initiation is fundamental [20,90–92]. The diagnosis of active TB is based on microbiology and traditional radiology; however, facilities for diagnosis are often lacking in countries with low resources where the prevalence of TB is significantly high. In this context, the use of ultrasonography as an affordable point-of-care diagnostic tool is extremely attractive. Indeed, given that LUS is becoming increasingly popular its use for suspected TB cases, it has been explored by a number of studies [45,62,93–95].

The three largest studies on adults TB included in this review showed that the most common LUS features were sub-pleural nodules, <1 cm, often multiple and diffuse, and areas of consolidation, generally on apical or middle fields. In a recent systematic review in adult TB, it was shown that these sub-pleural nodules and lung consolidations were the LUS findings with the highest sensitivities, ranging from 72 to 100% and 46% to 80%, respectively [62].

According to one study, although sub-pleural consolidations may be present in other conditions, in TB, these may appear patchier and more irregular and contiguous with pleura [44].

However, in some cases, the consolidation in LUS has been described as indistinguishable from bacterial pneumonia [29].

The specificity of LUS findings has been reported only by one study showing that in the presence of suggestive symptoms, the combination of apical consolidations and sub-pleural oval or round nodules, can reach a specificity of 96% [43]. There is agreement among authors that for TB, LUS has a poor ability to screen radiographically identified cavities [29,41,43].

Although differences exist among studies, considering that the sensitivity of CXR for TB has been estimated around 87%, it is reasonable to expect that LUS, with a sensitivity ranging from 72% to 100%, has the potential to become a valid alternative point-of-care diagnostic tool. A recent study further supports this consideration, showing that in a cohort of 82 patients with suspected TB, the overall sensitivity was 80% for LUS and 81% for CXR [96]. It is also noteworthy that in some patients with TB, pleural effusion is more commonly evidenced by LUS than a CT scan [97]. One limitation of using LUS is that in many cases, TB lesions are localized in the posterior-superior regions of the lung, which may not be visible to LUS due to the presence of the scapula [96].

One of the first studies on LUS in TB explored the features of miliary manifestation, which is characterized by tiny (1–2 mm) diffuse granulomatous lesions appearing in CXR as multiple small opacities diffuse in all lung zones [30,98]. The recent interest toward this "old" disease has been raised due to the common occurrence of this miliary form in patients with HIV or in patients undergoing immunosuppressive therapy [98]. Sonographic findings in this form of TB consist invariably in an interstitial pattern typically present in all lung zones together with subpleural granularities [30]. While the interstitial pattern in immunocompromised patients may be shared by the rare Pneumocystis Jirovecii or Cytomegalovirus infections, sub-pleural granular changes may add specificity [30].

Finally, little can be concluded on the role of LUS in pediatric TB, as only one study was published showing that consolidation was commonly associated with pleural effusion and enlarged mediastinal lymph nodes [42]. Our review focused on identifying parenchymal and pleural patterns using sonography. However, in children with TB, there has been more exploration into sonographic detection of enlarged mediastinal lymph nodes, with the aim of performing mediastinal biopsies [99,100].

5. Conclusions

Lung sonography is a rapid, widely available, free-of-adverse effects and point-of-care diagnostic tool. LUS has been considered equal or even superior to chest X-ray for the detection of pneumonia in both adults and children. Although chest X-ray remains unsurpassed for the detection of central lesions, sonography can detect peripheral lesions, even small ones that can escape a chest X-ray. The use of LUS for less common lung infections has raised interest, although the literature is still insufficient to draw a definitive conclusion. In addition, available studies present acute limitations including (1) low number of patients, (2) methodological limitations, (3) poor standardization of the technique, and (4) a lack of common definitions for LUS findings. However, aside from these limitations, some aspects have emerged from this review that deserve consideration.

The role of ultrasonography has been explored in children with atypical pneumonia caused by M.pneumoniae, and certainly some specific patterns have been described. If these were to be confirmed by larger trial, it may position LUS as a point-of-care tool for distinguishing the etiology of community-acquired pneumonia and predicting outcomes and responses to therapy. In atypical pneumonia, consolidations where described in 84–100% of cases; in most of these cases, consolidation was associated with a diffuse interstitial pattern characterized by scattered or most frequently confluent B lines. Studies focusing on the role of LUS in the diagnosis of pulmonary TB have shown a good sensitivity of this technique compared with standard imaging. The most common LUS features were sub-pleural nodules, <1 cm, often multiple and diffuse, and consolidations, often multiples and mainly apical. Although scant data are available, it is common opinion that further investigation is worthy in this field. In fact, LUS might be a more easily affordable diagnostic tool in low-income countries where traditional imaging is not promptly available.

Sonographic imaging of lung invasive fungal infection has received less attention, and several reports have presented inconsistent data. The most common LUS feature was sub-pleural consolidation with an inhomogeneous echotexture and indistinct margins, which were usually bilateral. In cases of diffuse Aspergillosis infection, cavitations were also detected by LUS. However, given the poor outcomes and mortality associated with this disease, particularly in patients with malignancies, a bedside tool for the follow-up and treatment strategy is important. Therefore, large trials on the use of LUS for the differentiation between bacterial and fungal pneumonia are needed.

Author Contributions: M.M., M.C., L.S., A.D.C. and G.R. contributed equally. M.M., L.S. and M.C. are co-first authors. M.L.S. and G.L.T. and G.F.P. collected the most significant literature on the topic. All authors have read and agreed to the published version of the manuscript.

Funding: This research received no external funding. APC was founded by AOU Policlinico-San Marco, Progetto Obiettivo PSN Anno 2016.

Data Availability Statement: No new data were created.

Conflicts of Interest: The authors declare no conflict of interest.

References

1. Joyner, C.; Herman, R.J.; Reid, J.M. Reflected ultrasound in the detection and localization of pleural effusion. *JAMA* **1967**, *200*, 399–402. [CrossRef] [PubMed]
2. Lichtenstein, D.; Mézière, G.; Biderman, P.; Gepner, A.; Barrè, O. The comettail artifact. An ultrasound sign of alveolar-interstitial syndrome. *Am. J. Respir. Crit. Care Med.* **1997**, *156*, 1640–1646. [CrossRef] [PubMed]
3. Soldati, G.; Testa, A.; Silva, F.R.; Carbone, L.; Portale, G.; Silveri, N.G. Chest ultrasonography in lung contusion. *Chest* **2006**, *130*, 533–538. [CrossRef] [PubMed]
4. Chavez, M.A.; Shams, N.; Ellington, L.E.; Naithani, N.; Gilman, R.H.; Steinhoff, M.C.; Santosham, M.; Black, R.E.; Price, C.; Gross, M.; et al. Lung ultrasound for the diagnosis of pneumonia in adults: A systematic review and meta-analysis. *Respir. Res.* **2014**, *15*, 50. [CrossRef]
5. Iorio, G.; Capasso, M.; De Luca, G.; Prisco, S.; Mancusi, C.; Laganà, B.; Comune, V. Lung Ultrasound in the Diagnosis of Pneumonia in Children: Proposal for a New Diagnostic Algorithm. *Peer J.* **2015**, *3*, e1374. [CrossRef]

6. Ticinesi, A.; Lauretani, F.; Nouvenne, A.; Mori, G.; Chiussi, G.; Maggio, M.; Meschi, T. Lung ultrasound and chest x-ray for detecting pneumonia in an acute geriatric ward. *Medicine* **2016**, *95*, e4153. [CrossRef]
7. Volpicelli, G.; Elbarbary, M.; Blaivas, M.; Lichtenstein, D.A.; Mathis, G.; Kirkpatrick, A.W.; Melniker, L.; Gargani, L.; Noble, V.E.; Via, G.; et al. International Liaison Committee on Lung Ultrasound (ILC-LUS) for International Consensus Conference on Lung Ultrasound (ICC-LUS). International evidence-based recommendations for point-of-care lung ultrasound. *Intensive Care Med.* **2012**, *38*, 577–591. [CrossRef]
8. Urbankowska, E.; Krenke, K.; Drobczyński, Ł.; Korczyński, P.; Urbankowski, T.; Krawiec, M.; Kraj, G.; Brzewski, M.; Kulus, M. Lung ultrasound in the diagnosis and monitoring of community acquired pneumonia in children. *Respir. Med.* **2015**, *109*, 1207–1212. [CrossRef]
9. Balk, D.S.; Lee, C.; Schafer, J.; Welwarth, J.; Hardin, J.; Novack, V.; Yarza, S.; Hoffmann, B. Lung ultrasound compared to chest-X-ray for diagnosis of pediatric pneumonia: A meta-analysis. *Pediatr. Pulmonol.* **2018**, *53*, 1130–1139. [CrossRef]
10. Najgrodzka, P.; Buda, N.; Zamojska, A.; Marciniewicz, E.; Lewandowicz-Uszyńska, A. Lung Ultrasonography in the Diagnosis of Pneumonia in Children—A Metaanalysis and a Review of Pediatric Lung Imaging. *Ultrasound Q.* **2019**, *35*, 157–163. [CrossRef]
11. Laursen, C.B.; Clive, A.; Hallifax, R.; Pietersen, P.I.; Asciak, R.; Davidsen, J.R.; Bhatnagar, R.; Bedawi, E.O.; Jacobsen, N.; Coleman, C.; et al. European Respiratory Society statement on thoracic ultrasound. *Eur. Respir. J.* **2021**, *57*, 2001519. [CrossRef]
12. Soldati, G.; Copetti, R. *Ecografia Toracica*, 2nd ed.; Edizioni Medico Scientifiche: Pavia, Italy, 2012.
13. Lichtenstein, D.A.; Meziere, G.; Lascols, N.; Biderman, P.; Courret, J.P.; Gepner, A.; Goldstein, I.; Tenoudji-Cohen, M. Ultrasound diagnosis of occult pneumothorax. *Crit. Care Med.* **2005**, *33*, 1231–1238. [CrossRef]
14. Cox, M.; Soudack, M.; Podberesky, D.J.; Epelman, M. Pediatric chest ultrasound: A practical approach. *Pediatr. Radiol.* **2017**, *47*, 1058–1068. [CrossRef]
15. Riccabona, M. Ultrasound of the chest in children (mediastinum excluded). *Eur. Radiol.* **2008**, *18*, 390–399. [CrossRef]
16. Volpicelli, G.; Mussa, A.; Garofalo, G.; Cardinale, L.; Casoli, G.; Perotto, F.; Fava, C.; Frascisco, M. Bedside lung ultrasound in the assessment of alveolar-interstitial syndrome. *Am. J. Emerg. Med.* **2006**, *24*, 689–696. [CrossRef]
17. Berce, V.; Tomazin, M.; Gorenjak, M.; Berce, T.; Lovrenčič, B. The Usefulness of Lung Ultrasound for the Aetiological Diagnosis of Community-Acquired Pneumonia in Children. *Sci. Rep. Nat. Res.* **2019**, *9*, 17957. [CrossRef]
18. Miyashita, N. Atypical pneumonia: Pathophysiology, diagnosis, and treatment. *Respir. Investig.* **2022**, *60*, 56–67. [CrossRef]
19. Dropulic, L.K.; Lederman, H.M. Overview of Infections in the Immunocompromised Host. *Microbiol. Spectr.* **2016**, *4*, 1–50. [CrossRef]
20. Harding, E. WHO global progress report on tuberculosis elimination. *Lancet Respir. Med.* **2020**, *8*, 19. [CrossRef]
21. Meli, M.; La Spina, M.; Lo Nigro, L.; Trobia, G.L.; Russo, G.; Di Cataldo, A. Pleuro-pulmonary ultrasound in the diagnosis and follow-up of lung infections in children with cancer: A pilot study. *J. Ultrasound* **2022**, *25*, 865–875. [CrossRef]
22. Stewart, L.A.; Clarke, M.; Rovers, M. Preferred reporting items for systematic review and meta-analyses of individual participant data: The PRISMA-IPD statement. *JAMA* **2015**, *313*, 1657–1665. [CrossRef] [PubMed]
23. Gargani, L.; Volpicelli, G. How I do it: Lung ultrasound. *Cardiovasc. Ultrasound* **2014**, *12*, 25. [CrossRef] [PubMed]
24. Mento, F.; Khan, U.; Faita, F.; Smargiassi, A.; Inchingolo, R.; Perrone, T.; Demi, L. State of the Art in Lung Ultrasound, Shifting from Qualitative to Quantitative Analyses. *Ultrasound Med. Biol.* **2022**, *48*, 2398–2416. [CrossRef] [PubMed]
25. Stassen, J.; Bax, J.J. How to do lung ultrasound. *Eur. Heart J. Cardiovasc. Imaging* **2022**, *23*, 447–449. [CrossRef] [PubMed]
26. Havelock, T.; Teoh, R.; Laws, D.; Gleeson, F.; BTS Pleural Disease Guideline Group 2010. Pleural procedures and thoracic ultrasound: British Thoracic Society Pleural Disease Guideline 2010. *Thorax* **2010**, *65*, ii61–ii76. [CrossRef]
27. Hallifax, R.J.; Corcoran, J.P.; Ahmed, A.; Nagendran, M.; Rostom, H.; Hassan, N.; Maruthappu, M.; Psallidas, I.; Manuel, A.; Gleeson, F.V.; et al. Physician-based ultrasound-guided biopsy for diagnosing pleural disease. *Chest* **2014**, *146*, 1001–1006. [CrossRef]
28. Laursen, C.B.; Sloth, E.; Lassen, A.T.; Christensen, R.D.; Lambrechtsen, J.; Madsen, P.H.; Henriksen, D.P.; Davidsen, J.R.; Rasmussen, F. Point-of-care ultrasonography in patients admitted with respiratory symptoms: A single-blind, randomised controlled trial. The Lancet. *Respir. Med.* **2014**, *2*, 638–646. [CrossRef]
29. Agostinis, P.; Copetti, R.; Lapini, L.; Badona Monteiro, G.; N'Deque, A.; Baritussio, A. Chest ultrasound findings in pulmonary tuberculosis. *Trop. Dr.* **2017**, *47*, 320–328. [CrossRef]
30. Hunter, L.; Bélard, S.; Janssen, S.; van Hoving, D.J.; Heller, T. Miliary tuberculosis: Sonographic pattern in chest ultrasound. *Infection* **2016**, *44*, 243–246. [CrossRef]
31. Li, S.; Zhang, Q.L.; Guo, R.J.; Lv, X.Z.; Yang, X. Quantitative evaluation and significance of ultrasound in bronchoalveolar lavage for lung consolidation in children with severe mycoplasma pneumonia. *Transl. Pediatr.* **2021**, *10*, 2325–2334. [CrossRef]
32. Tripaldi, C.; Polito, M.; Iacoviello, O.; Basile, V.; De Bellis, T.; Fortunato, M.; Laforgia, F.; Scalini, E.; Silletti, M.; Lofù, I. Ultrasound Studies on Mycoplasma Bronchopneumonia. *J. Curr. Med. Res. Opin.* **2021**, *5*, 1301–1315. [CrossRef]
33. Buonsenso, D.; Musolino, A.; Ferro, V.; De Rose, C.; Morello, R.; Ventola, C.; Liotti, F.M.; De Sanctis, R.; Chiaretti, A.; Biasucci, D.G.; et al. Role of lung ultrasound for the etiological diagnosis of acute lower respiratory tract infection (ALRTI) in children: A prospective study. *J. Ultrasound* **2022**, *25*, 185–197. [CrossRef]
34. Liu, G.; Wang, G.; Yang, Z.; Liu, G.; Ma, H.; Lv, Y.; Ma, F.; Zhu, W. A Lung Ultrasound-Based Nomogram for the Prediction of Refractory *Mycoplasma pneumoniae* Pneumonia in Hospitalized Children. *Infect. Drug. Resist.* **2022**, *31*, 6343–6355. [CrossRef]

35. Trinavarat, P.; Chatchatri, P.; Chandtranuwatana, P. Color Doppler sonography of pulmonary aspergillosis in infants with chronic granulomatous disease. *Asian Biomed.* **2012**, *6*, 129–133.
36. Alamdaran, S.A.; Heidarzadeh, H.; Zavvar, N.; Badlee, Z.; Jaberi, M.; Ghasemi, A. Presentation of Sonographic Features of Pulmonary Invasive Fungal Disease in Six Children with Leukemia. *Int. J. Pediatr.* **2021**, *9*, 13203–13211. [CrossRef]
37. Liu, J.; Ma, H.R.; Fu, W. Lung Ultrasound to Diagnose Pneumonia in Neonates with Fungal Infection. *Diagnostics* **2022**, *12*, 1776. [CrossRef]
38. Tikkakoski, P.; Lohela, M.; Paivansalo, T.; Kerola, T. Pleuro-pulmonary aspergillosis: US and US-guided biopsy as an aid to diagnosis. *Acta Radiol.* **1995**, *36*, 122–126. [CrossRef]
39. Grabala, J.; Grabala, M.; Onichimowski, D.; Grabala, P. Possibilities of using ultrasound for diagnosis of invasive pulmonary mucormycosis—A case study. *Pol. Ann. Med.* **2017**, *24*, 224–227. [CrossRef]
40. Greco, R.; Lazzari, L.; Xue, E.; Assanelli, A.; Marktel, S.; Giglio, F.; Clerici, D.; Lupo Stanghellini, M.T.; Corti, C.; Bernardi, M.; et al. Lung ultrasound to evaluate invasive fungal diseases after allogeneic hematopoietic stem cell transplantation. *Infect. Chemother.* **2019**, *51*, 386–392. [CrossRef]
41. Ruby, L.C.; Kadavigere, R.; Sheshadri, S.; Saravu, K.; Bélard, S. Pulmonary aspergilloma on transthoracic ultrasound. *Infection* **2021**, *49*, 1337–1340. [CrossRef]
42. Heuvelings, C.C.; Bélard, S.; Andronikou, S.; Jamieson-Luff, N.; Grobusch, M.P.; Zar, H.J. Chest ultrasound findings in children with suspected pulmonary tuberculosis. *Pediatr. Pulmonol.* **2019**, *54*, 463–470. [CrossRef] [PubMed]
43. Montuori, M.; Casella, F.; Casazza, G.; Franzetti, F.; Pini, P.; Invernizzi, C.; Torzillo, D.; Rizzardini, G.; Galli, M.; Cogliati, C. Lung ultrasonography in pulmonary tuberculosis: A pilot study on diagnostic accuracy in a high-risk population. *Eur. J. Intern. Med.* **2019**, *66*, 29–34. [CrossRef] [PubMed]
44. Fentress, M.; Ugarte-Gil, C.; Cervantes, M.; Rivas, D.; Moore, D.; Caliguiri, P.; Bergman, K.; Noazin, S.; Padovani, A.; Gilman, R.H. Lung Ultrasound Findings Compared with Chest X-Ray Findings in Known Pulmonary Tuberculosis Patients: A Cross-Sectional Study in Lima, Peru. *Am. J. Trop. Med. Hyg.* **2020**, *103*, 1827–1833. [CrossRef] [PubMed]
45. Cocco, G.; Boccatonda, A.; Rossi, I.; D'Ardes, D.; Corvino, A.; Delli Pizzi, A.; Ucciferri, C.; Falasca, K.; Vecchiet, J. Early detection of pleuro-pulmonary tuberculosis by bedside lung ultrasound: A case report and review of literature. *Clin. Case Rep.* **2022**, *10*, e05739. [CrossRef]
46. Parlamento, S.; Copetti, R.; Di Bartolomeo, S. Evaluation of lung ultrasound for the diagnosis of pneumonia in the ED. *Am. J. Emerg. Med.* **2009**, *27*, 379–384. [CrossRef]
47. Reali, F.; Sferrazza Papa, G.F.; Carlucci, P.; Fracasso, P.; Di Marco, F.; Mandelli, M.; Soldi, S.; Riva, E.; Centanni, S. Can lung ultrasound replace chest radiography for the diagnosis of pneumonia in hospitalized children? *Respiration* **2014**, *88*, 112–115. [CrossRef]
48. Reissig, A.; Copetti, R.; Mathis, G.; Mempel, C.; Schuler, A.; Zechner, P.; Aliberti, S.; Neumann, R.; Kroegel, C.; Hoyer, H. Lung ultrasound in the diagnosis and follow-up of community-acquired pneumonia: A prospective, multicenter, diagnostic accuracy study. *Chest* **2012**, *142*, 965–972. [CrossRef]
49. Blaivas, M. Lung ultrasound in evaluation of pneumonia. *J. Ultrasound Med. Off. J. Am. Inst. Ultrasound Med.* **2012**, *31*, 823–826. [CrossRef]
50. Caiulo, V.A.; Gargani, L.; Caiulo, S.; Fisicaro, A.; Moramarco, F.; Latini, G.; Picano, E.; Mele, G. Lung ultrasound characteristics of community-acquired pneumonia in hospitalized children. *Pediatr. Pulmonol.* **2013**, *48*, 280–287. [CrossRef]
51. Copetti, R.; Cattarossi, L. Ultrasound diagnosis of pneumonia in children. *Radiol. Med.* **2008**, *113*, 190–198. [CrossRef]
52. Corradi, F.; Brusasco, C.; Garlaschi, A.; Paparo, F.; Ball, L.; Santori, G.; Pelosi, P.; Altomonte, F.; Vezzani, A.; Brusasco, V. Quantitative analysis of lung ultrasonography for the detection of community-acquired pneumonia: A pilot study. *BioMed Res. Int.* **2015**, *2015*, 868707. [CrossRef]
53. Cortellaro, F.; Colombo, S.; Coen, D.; Duca, P.G. Lung ultrasound is an accurate diagnostic tool for the diagnosis of pneumonia in the emergency department. *Emerg. Med. J.* **2012**, *29*, 19–23. [CrossRef]
54. Iuri, D.; De Candia, A.; Bazzocchi, M. Evaluation of the lung in children with suspected pneumonia: Usefulness of ultrasonography. *Radiol. Med.* **2009**, *114*, 321–330. [CrossRef]
55. Nazerian, P.; Volpicelli, G.; Vanni, S.; Gigli, C.; Betti, L.; Bartolucci, M.; Zanobetti, M.; Ermini, F.R.; Iannello, C.; Grifoni, S. Accuracy of lung ultrasound for the diagnosis of consolidations when compared to chest computed tomography. *Am. J. Emerg. Med.* **2015**, *33*, 620–625. [CrossRef]
56. Bhalla, D.; Naranje, P.; Jana, M.; Bhalla, A.S. Pediatric lung ultrasonography: Current perspectives. *Pediatr. Radiol.* **2022**, *52*, 2038–2050. [CrossRef]
57. Principi, N.; Esposito, A.; Giannitto, C.; Esposito, S. Lung ultrasonography to diagnose community-acquired pneumonia in children. *BMC Pulm. Med.* **2017**, *17*, 212. [CrossRef]
58. Ambroggio, L.; Sucharew, H.; Rattan, M.S.; O'Hara, S.M.; Babcock, D.S.; Clohessy, C.; Steinhoff, M.C.; Macaluso, M.; Shah, S.S.; Coley, B.D. Lung Ultrasonography: A Viable Alternative to Chest Radiography in Children with Suspected Pneumonia? *J. Pediatr.* **2016**, *176*, 93–98.e7. [CrossRef]
59. Joshi, P.; Vasishta, A.; Gupta, M. Ultrasound of the pediatric chest. *Br. J. Radiol.* **2019**, *92*, 20190058. [CrossRef]
60. Goh, Y.; Kapur, J. Sonography of the Pediatric Chest. *J. Ultrasound Med.* **2016**, *35*, 1067–1080. [CrossRef]

61. Rea, G.; Sperandeo, M.; Di Serafino, M.; Vallone, G.; Tomà, P. Neonatal and pediatric thoracic ultrasonography. *J. Ultrasound* **2019**, *22*, 121–130. [CrossRef] [PubMed]
62. Bigio, J.; Kohli, M.; Klinton, J.S.; MacLean, E.; Gore, G.; Small, P.M.; Ruhwald, M.; Weber, S.F.; Jha, S.; Pai, M. Diagnostic accuracy of point-of-care ultrasound for pulmonary tuberculosis: A systematic review. *PLoS ONE* **2021**, *16*, e0251236. [CrossRef] [PubMed]
63. Bloise, S.; La Regina, D.P.; Pepino, D.; Iovine, E.; Laudisa, M.; Di Mattia, G.; Nicolai, A.; Nenna, R.; Petrarca, L.; Mancino, E.; et al. Lung ultrasound compared to chest X-ray for the diagnosis of CAP in children. *Pediatr. Int.* **2021**, *63*, 448–453. [CrossRef] [PubMed]
64. Lichosik, M.; Rustecka, A.; Placzyńska, M.; Wawrzyniak, A.; Kalicki, B. Transthoracic lung ultrasound in children with signs of acute lower respiratory infection. *Pediatr. Med. Rodz.* **2020**, *16*, 87–92. [CrossRef]
65. Stadler, J.A.M.; Andronikou, S.; Zar, H.J. Lung ultrasound for the diagnosis of community-acquired pneumonia in children. *In Pediatr. Radiol.* **2017**, *47*, 1412–1419. [CrossRef]
66. Sansone, F.; Attanasi, M.; Di Filippo, P.; Sferrazza Papa, G.F.; Di Pillo, S.; Chiarelli, F. Usefulness of Lung Ultrasound in Paediatric Respiratory Diseases. *Diagnostics* **2021**, *11*, 1783. [CrossRef]
67. Man, M.A.; Dantes, E.; Domokos Hancu, B.; Bondor, C.I.; Ruscovan, A.; Parau, A.; Motoc, N.S.; Marc, M. Correlation between Transthoracic Lung Ultrasound Score and HRCT Features in Patients with Interstitial Lung Diseases. *J. Clin. Med.* **2019**, *8*, 1199. [CrossRef]
68. Pereda, M.A.; Chavez, M.A.; Hooper-Miele, C.C.; Gilman, R.H.; Steinhoff, M.C.; Ellington, L.E.; Gross, M.; Price, C.; Tielsch, J.M.; Checkley, W. Lung ultrasound for the diagnosis of pneumonia in children: A meta-analysis. *Pediatrics* **2015**, *135*, 714–722. [CrossRef]
69. Reynolds, J.H.; McDonald, G.; Alton, H.; Gordon, S.B. Pneumonia in the immunocompetent patient. *Br. J. Radiol.* **2010**, *83*, 998–1009. [CrossRef]
70. Lerchbaumer, M.H.; Lauryn, J.H.; Bachmann, U.; Enghard, P.; Fischer, T.; Grune, J.; Hegemann, N.; Khadzhynov, D.; Kruse, J.M.; Lehner, L.J.; et al. Point-of-care lung ultrasound in COVID-19 patients: Inter- and intra-observer agreement in a prospective observational study. *Sci. Rep.* **2021**, *11*, 10678. [CrossRef]
71. Li, Z.; Lu, G.; Meng, G. Pathogenic Fungal Infection in the Lung. *Front. Immunol.* **2019**, *3*, 1524. [CrossRef]
72. Buonsenso, D.; Brancato, F.; Valentini, P.; Curatola, A.; Supino, M.; Musolino, A.M. The use of lung ultrasound to monitor the antibiotic response of community-acquired pneumonia in children: A preliminary hypothesis. *J. Ultrasound Med.* **2020**, *39*, 817–826. [CrossRef]
73. Iorio, G.; Capasso, M.; Prisco, S.; De Luca, G.; Mancusi, C.; Laganà, B.; Piscopo, M.A.; Comune, V. Lung Ultrasound Findings Undetectable by Chest Radiography in Children with Community-Acquired Pneumonia. *Ultrasound Med. Biol.* **2018**, *44*, 1687–1693. [CrossRef]
74. Panigrahi, M.K.; Manju, R.; Kumar, S.V.; Toi, P.C. Pulmonary mucormycosis presenting as nonresolving pneumonia in a patient with diabetes mellitus. *Respir. Care* **2014**, *59*, e201–e205. [CrossRef]
75. Tedder, M.; Spratt, J.A.; Anstadt, M.P.; Hegde, S.S.; Tedder, S.D.; Lowe, J.E. Pulmonary mucormycosis: Results of medical and surgical therapy. *Ann. Thorac. Surg.* **1994**, *57*, 1044–1050. [CrossRef]
76. Chamilos, G.; Marom, E.M.; Lewis, R.E.; Lionakis, M.S.; Kontoyiannis, D.P. Predictors of pulmonary zygomycosis versus invasive pulmonary Aspergillosis in patients with cancer. *Clin. Infect. Dis. Off. Publ. Infect. Dis. Soc. Am.* **2005**, *4*, 60–66. [CrossRef]
77. Kousha, M.; Tadi, R.; Soubani, A.O. Pulmonary aspergillosis: A clinical review. *Eur. Respir. Rev. Off. J. Eur. Respir. Soc.* **2011**, *20*, 156–174. [CrossRef]
78. Gao, Y.; Soubani, A. Advances in the diagnosis and management of pulmonary aspergillosis. *Adv. Respir. Med.* **2019**, *87*, 231–243. [CrossRef]
79. El-Baba, F.; Gao, Y.; Soubani, A.O. Pulmonary Aspergillosis: What the Generalist Needs to Know. *Am. J. Med.* **2020**, *133*, 668–674. [CrossRef]
80. Kanj, A.; Abdallah, N.; Soubani, A.O. The spectrum of pulmonary aspergillosis. *Respir. Med.* **2018**, *141*, 121–131. [CrossRef]
81. Garg, M.; Prabhakar, N.; Gulati, A.; Agarwal, R.; Dhooria, S. Spectrum of imaging findings in pulmonary infections. Part 2: Fungal, mycobacterial, and parasitic. *Pol. J. Radiol.* **2019**, *22*, 214–223. [CrossRef]
82. Katragkou, A.; Fisher, B.T.; Groll, A.H.; Roilides, E.; Walsh, T.J. Diagnostic Imaging and Invasive Fungal Diseases in Children. *J. Pediatr. Infect. Dis. Soc.* **2017**, *6*, S22–S31. [CrossRef] [PubMed]
83. Aquino, S.L.; Kee, S.T.; Warnock, M.L.; Gamsu, G. Pulmonary Aspergillosis: Imaging findings with pathologic correlation. *Am. J. Roentgenol.* **1994**, *163*, 811–815. [CrossRef] [PubMed]
84. Pesle, G.D.; Monod, O. Bronchiectasis due to asperigilloma. *Dis. Chest* **1954**, *25*, 172–183. [CrossRef] [PubMed]
85. Rodrigues-Pinto, E.; Lopes, S.; Principe, F.; Costa, J.; Macedo, G. Pulmonary Aspergillosis diagnosed by endoscopic ultrasound fine-needle aspiration. *Endosc. Ultrasound* **2016**, *5*, 58–60. [CrossRef] [PubMed]
86. Panse, J.; von Schwanewede, K.; Jost, E.; Dreher, M.; Müller, T. Pulmonary infections in patients with and without hematological malignancies: Diagnostic yield and safety of flexible bronchoscopy—A retrospective analysis. *J. Thorac. Dis.* **2020**, *12*, 4860–4867. [CrossRef]
87. Panse, P.; Smith, M.; Cummings, K.; Jensen, E.; Gotway, M.; Jokerst, C. The many faces of pulmonary aspergillosis: Imaging findings with pathologic correlation. *Radiol. Infect. Dis.* **2016**, *3*, 192–200. [CrossRef]

88. Ruhnke, M.; Behre, G.; Buchheidt, D.; Christopeit, M.; Hamprecht, A.; Heinz, W.; Heussel, C.P.; Horger, M.; Kurzai, O.; Karthaus, M.; et al. Diagnosis of invasive fungal diseases in haematology and oncology: 2018 update of the recommendations of the infectious diseases working party of the German society for hematology and medical oncology (AGIHO). *Mycoses* **2018**, *61*, 796–813. [CrossRef]
89. Davda, S.; Kowa, X.Y.; Aziz, Z.; Ellis, S.; Cheasty, E.; Cappocci, S.; Balan, A. The development of pulmonary aspergillosis and its histologic, clinical, and radiologic manifestations. *Clin. Radiol.* **2018**, *73*, 913–921. [CrossRef]
90. Sotgiu, G.; Sulis, G.; Matteelli, A. Tuberculosis—A World Health Organization Perspective. *Microbiol. Spectr.* **2017**, *5*, 211–228. [CrossRef]
91. Pai, M.; Behr, M.A.; Dowdy, D.; Dheda, K.; Divangahi, M.; Boehme, C.C.; Ginsberg, A.; Swaminathan, S.; Spigelman, M.; Getahun, H.; et al. Tuberculosis. *Nat. Rev. Dis. Prim.* **2016**, *2*, 16076. [CrossRef]
92. Chen, X.; Hu, T.Y. Strategies for advanced personalized tuberculosis diagnosis: Current technologies and clinical approaches. *Precis. Clin. Med.* **2021**, *4*, 35–44. [CrossRef]
93. Rea, G.; Sperandeo, M.; Lieto, R.; Bocchino, M.; Quarato, C.M.I.; Feragalli, B.; Valente, T.; Scioscia, G.; Giuffreda, E.; Foschino Barbaro, M.P.; et al. Chest Imaging in the Diagnosis and Management of Pulmonary Tuberculosis: The Complementary Role of Thoracic Ultrasound. *Front. Med.* **2021**, *8*, 753821. [CrossRef]
94. Di Gennaro, F.; Pisani, L.; Veronese, N.; Pizzol, D.; Lippolis, V.; Saracino, A.; Monno, L.; Huson, M.A.M.; Copetti, R.; Putoto, G.; et al. Potential Diagnostic Properties of Chest Ultrasound in Thoracic Tuberculosis-A Systematic Review. *Int. J. Environ. Res. Public Health* **2018**, *15*, 2235. [CrossRef]
95. Morello, R.; De Rose, C.; Ferrari, V.; Valentini, P.; Musolino, A.M.; Biasucci, D.G.; Vetrugno, L.; Buonsenso, D. Utility and Limits of Lung Ultrasound in Childhood Pulmonary Tuberculosis: Lessons from a Case Series and Literature Review. *J. Clin. Med.* **2022**, *11*, 5714. [CrossRef]
96. Giannelli, F.; Cozzi, D.; Cavigli, E.; Campolmi, I.; Rinaldi, F.; Giachè, S.; Rogasi, P.G.; Miele, V.; Bartolucci, M. Lung ultrasound (LUS) in pulmonary tuberculosis: Correlation with chest CT and X-ray findings. *J. Ultrasound* **2022**, *25*, 625–634. [CrossRef]
97. Akhan, O.; Demirkazik, F.B.; Ozmen, M.N.; Balkanci, F.; Ozkara, S.; Cöplü, L.; Emri, A.; Besim, A. Tuberculous pleural effusions: Ultrasonic diagnosis. *J. Clin. Ultrasound* **1992**, *20*, 461–465. [CrossRef]
98. Sharma, S.K.; Mohan, A.; Sharma, A.; Mitra, D.K. Miliary tuberculosis: New insights into an old disease. *Lancet Infect. Dis.* **2005**, *5*, 415–430. [CrossRef]
99. Bosch-Marcet, J.; Serres-Créixams, X.; Zuasnabar-Cotro, A.; Codina-Puig, X.; Català-Puigbó, M.; Simon-Riazuelo, J.L. Comparison of ultrasound with plain radiography and CT for the detection of mediastinal lymphadenopathy in children with tuberculosis. *Pediatr. Radiol.* **2004**, *34*, 895–900. [CrossRef]
100. Bosch-Marcet, J.; Serres-Créixams, X.; Borrás-Pérez, V.; Coll-Sibina, M.T.; Guitet-Juliá, M.; Coll-Rosell, E. Value of sonography for follow-up of mediastinal lymphadenopathy in children with tuberculosis. *J. Clin. Ultrasound* **2007**, *35*, 118–124. [CrossRef]

diagnostics

MDPI

Review

Overview of Lung Ultrasound in Pediatric Cardiology

Massimiliano Cantinotti [1,2,*], Pietro Marchese [1], Raffaele Giordano [3], Eliana Franchi [1], Nadia Assanta [1], Vivek Jani [4], Shelby Kutty [4] and Luna Gargani [5]

1 Fondazione G. Monasterio CNR-Regione Toscana, 54100 Massa, Italy; pitrino91@gmail.com (P.M.); eliana.franchi@ftgm.it (E.F.); assanta@ftgm.it (N.A.)
2 Institute of Clinical Physiology, National Research Council, 56124 Pisa, Italy
3 Adult and Pediatric Cardiac Surgery, Department of Advanced Biomedical Sciences, University of Naples "Federico II", 80131 Napoli, Italy; r.giordano81@libero.it
4 Taussig Heart Center, Department of Pediatrics, Johns Hopkins Hospital, Baltimore, MD 21205, USA; vpjani@ucsd.edu (V.J.); shelby.kutty@gmail.com (S.K.)
5 Department of Surgical, Medical and Molecular Pathology and Critical Care Medicine, University of Pisa, 56124 Pisa, Italy; lunagargani@gmail.com
* Correspondence: cantinotti@ftgm.it; Tel.: +39-05-8549-3622; Fax: +39-05-8549-3616

Abstract: Lung ultrasound (LUS) is increasing in its popularity for the diagnosis of pulmonary complications in acute pediatric care settings. Despite the high incidence of pulmonary complications for patients with pediatric cardiovascular and congenital heart disease, especially in children undergoing cardiac surgery, the use of LUS remains quite limited in these patients. The aim of this review is to provide a comprehensive overview and list of current potential applications for LUS in children with congenital heart disease, post-surgery. We herein describe protocols for LUS examinations in children, discuss diagnostic criteria, and introduce methods for the diagnosis and classification of pulmonary disease commonly encountered in pediatric cardiology (e.g., pleural effusion, atelectasis, interstitial edema, pneumothorax, pneumonia, and diaphragmatic motion analysis). Furthermore, applications of chest ultrasounds for the evaluation of the retrosternal area, and in particular, systematic search criteria for retrosternal clots, are illustrated. We also discussed the potential applications of LUS, including the guidance of interventional procedures, namely lung recruitment and drainage insertion. Lastly, we analyzed current gaps in knowledge, including the difficulty of the quantification of pleural effusion and atelectasis, and the need to differentiate different etiologies of B-lines. We concluded with future applications of LUS, including strain analysis and advanced analysis of diaphragmatic mechanics. In summary, US is an easy, accurate, fast, cheap, and radiation-free tool for the diagnosis and follow-up of major pulmonary complications in pediatric cardiac surgery, and we strongly encourage its use in routine practice.

Keywords: congenital; pediatric; echo; ultrasound; cardiac

Citation: Cantinotti, M.; Marchese, P.; Giordano, R.; Franchi, E.; Assanta, N.; Jani, V.; Kutty, S.; Gargani, L. Overview of Lung Ultrasound in Pediatric Cardiology. *Diagnostics* **2022**, *12*, 763. https://doi.org/10.3390/diagnostics12030763

Academic Editor: Po-Hsiang Tsui

Received: 14 December 2021
Accepted: 18 March 2022
Published: 21 March 2022

1. Background

Lung ultrasound (LUS) is an ideal tool for the diagnosis and follow-up of pulmonary complications after pediatric cardiac surgery. LUS offers the possibility to monitor lung disease progression easily and quickly at the patient's bedside, and it allows us to evaluate the response to medical therapy (i.e., diuretics) and physiotherapy [1–4]. In addition, several potential applications of LUS exist, particularly for children after cardiac surgery. In this setting, LUS can be employed for the diagnosis of post-op lung complications, including atelectasis, effusion, lung congestion, pneumonia, pneumothorax, obstructive pulmonary disease, and diaphragmatic motion anomalies [1–4]. Compared to traditional chest radiography, LUS allows for the differential diagnosis of many common pulmonary complications after pediatric cardiac surgery [1–4]. For instance, LUS easily differentiates between effusion and atelectasis, both of which are common sequelae of cardiac surgery, and importantly, require different therapeutic approaches [1–4]. LUS also allows us to

differentiate among different types of effusion, to quantify the effusion size, and to follow up on the response to medical therapy [2,3]. In addition, LUS does not expose patients to ionizing radiation, providing yet another advantage [1–4].

Despite these advantages, the role of LUS in children undergoing cardiac surgery remains surprisingly limited [2] compared to other pediatric settings [5–10], probably due to cultural inheritance mostly relying on chest radiography. The aim of this review is to provide a comprehensive overview and list of current potential applications for LUS in children with congenital heart disease (CHD), post-surgery, with the hope of encouraging its use for this important patient population.

2. LUS Examination Protocols

LUS examinations are performed with either phased array probes or linear/convex probes. In neonates and children, linear and convex probes are preferred, however, as they offer a quick and comprehensive view of the entire lung field.

LUS examinations in adult patients should include the evaluation of different pulmonary areas and be performed in different views and positions. According to standardized protocols [11], for each hemithorax, 2 or 3 major areas (anterior, lateral, and sometimes posterior) delineated by the parasternal, anterior axillary, and posterior axillary line, respectively, should be identified and scanned. Each area can be further divided into an upper and lower half, creating 4 to 6 different quadrants for each hemithorax, namely anterior superior, anterior inferior, lateral superior, lateral inferior, posterior superior, and posterior inferior [11] (Figure 1).

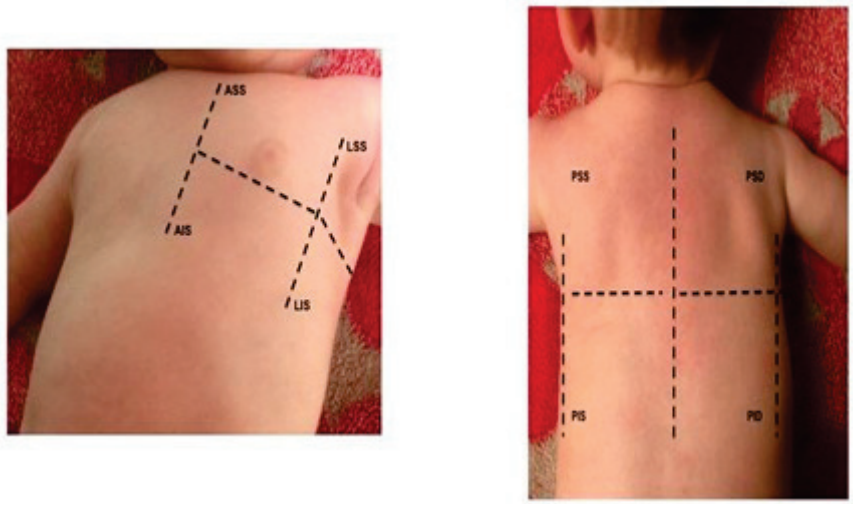

(**A**) (**B**)

Figure 1. Six segments score. Each hemithorax is divided into 3 major quadrants (anterior, lateral, and posterior). Each quadrant is further subdivided into the upper and the lower half. (**A**) anterior and lateral, (**B**) posterior quadrants.

In children undergoing cardiac surgery for CHD, the posterior view is crucial for the diagnosis of atelectasis/effusion, the most common post-surgical, pulmonary complications. In a study of over 138 examinations at different post-operative times in 79 children (median age 9.3 months), the posterior areas were found to be more sensitive than the anterior and lateral areas in the diagnosis of effusion or atelectasis [12]. Lungs may be scanned posteriorly starting from the diaphragm to differentiate the lung from the liver, with a continuous brush up to the apex. The posterior view, however, may be not feasible to acquire in unstable children, particularly those with an open sternum, poorly cooperative children, or children with poor mobilization. In studies from our group, the posterior area was precluded in 7% of cases, while the anterior area could not be assessed in 11% due to bandages and medications covering a substantial part of the hemithorax. In contrast, the lat-

eral area, despite the frequent presence of drainage tubes and other physical impediments, was almost always accessible (e.g., feasibility 98%) for LUS examination [12,13].

3. When and Who Should Perform LUS

There has been great debate on which members of the care team should perform LUS. Theoretically, LUS should be performed by any physician who oversees the patient (e.g., anesthetist, cardiologist, surgeon). Some recent works [14,15] suggest that LUS can be performed by mid-level healthcare professionals, including nurses [15] and physiotherapists [14] for whom LUS represents a unique tool to guide treatment and monitor results [14].

4. Common Findings

4.1. B-Lines

B-lines are the sonographic sign of partial deaeration of the lung parenchyma [11]. In CHD patients with left-to-right, or bidirectional shunt, LUS has a high sensitivity (94%), specificity (96%), and diagnostic accuracy (95%) for the assessment of lung congestion from pulmonary overflow, compared to CT [16]. Furthermore, neonates with CHD more B-lines compared to their healthy counterparts [17]. The presence of B-lines is almost universal after pediatric cardiac surgery due to extravascular fluid accumulation (particularly after cardiopulmonary bypass) and other effects of the main cardiac defect and post-surgical imbalance on the lung [4,12,13].

4.2. Classification of Lung Congestion in Children

In each scanning area, B-lines are counted, and a score can be assigned for either single quadrants or for the entire hemithorax, the latter quantified by summing partial scores for each single scanning area. In adults, the main scores for the classification of lung congestion in heart failure are either the sum of B-lines in each area or the number of areas with more than three B-lines [18]; lung involvement is commonly classified into four categories (none, mild, moderate, and severe) [18,19]. In children, however, we use simplified scores; either qualitative or semiquantitative scores have been adopted. Some authors have proposed semiquantitative scores [13,17] (Table 1), while others [1,20] have proposed a qualitative score identifying three different patterns: (A) white lung, defined as the presence of confluent B-lines in two or more of the four areas; (B) the prevalence of B-lines in two or more areas; and (C) the prevalence of A-lines, or no significant congestion/normal lung (Figure 2).

Table 1. Major semiquantitative scores for lung congestion classification in children.

Authors	Classifications
Wu (34)	(I) Normal: A lines (II) Mild: fewer than 3 B lines in 2 rip spaces with spared areas (III) Moderate: between 3 and 7 B lines between 2 rip spaces (IV) Severe: more than 7 or coalescent B-lines from the base to the apex without spared area
Cantinotti (12,13)	(I) trivial-none (LUS-score = 0–6), (II) mild (LUS-Score = 6–12), (III) moderate (LUS-Score = 13–24) (IV) severe (LUS-Score > 24)
Raimondi, Vitale (15,20)	(I) Type 1- full hyperechoic image of the lung fields or 'white lung'; (II) Type 2- prevalence of B lines, that is, vertical, comet-tail artifacts. (III) Type 3- predominance of A lines

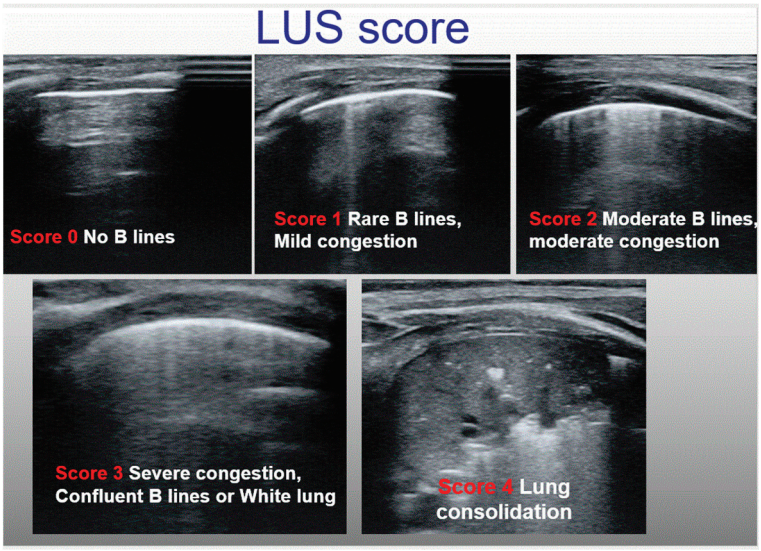

Figure 2. An example of semiquantitative LUS score that we have recently validated.

4.3. Pleural Effusion

The evaluation of pleural effusion is one of the most employed applications of LUS. LUS has high sensitivity and specificity (93%) for the diagnosis of pleural effusion, comparable to computed tomography (CT), which remains the diagnostic gold standard but is invasive, time consuming, expensive, and exposes the children to dangerous radiations [2,3]. In addition, LUS may allow us to differentially diagnose the nature of post-surgical pleural effusion, highlighting yet another advantage. For instance, while anechoic effusion may be either a transudate or an exudate, the presence of internal echoes is highly suggestive of an exudate or a hemothorax [21–28]. Despite these advantages, the application of LUS for pleural effusion is often qualitative, classified as mild, moderate, or severe. Furthermore, there is lack of consensus for the quantitative measurement of pleural effusion by LUS. In adults, various algorithms, each using different projections and measurement methods, have been proposed for pleural effusion quantification [21–28], though none of these have been validated for infants and children (Table 2 and Figure 3).

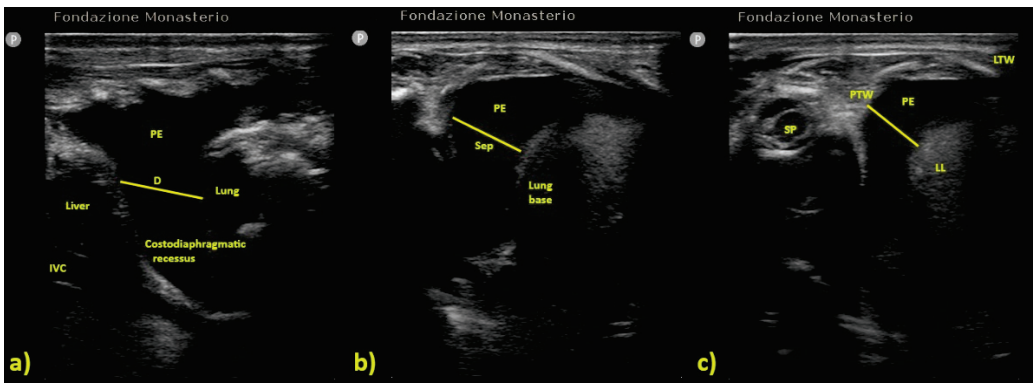

Figure 3. Formulas for pleural effusion quantification according to different authors: (**a**) Usta et al. [24], PEV is calculated by the formula D (mm) × 16, (**b**) Balik et al. [23] PEV is calculated by the formula Sep (mm) × 20; (**c**) Eibenberger [25] the major effusion's diameter (D) is associated with PEV on a progressive scale (e.g., 10 mm correspond to 50–300 mL of PEV, 20 mm to 150–310 mL, etc.). (Table 2) D = distance; IVC = Inferior Vena Cava; LL = Lung Lower Lobe; LTW = Lateral Thoracic Wall; PE = Pleural Effusion; PEV = Pleural Effusion Volume; PTW = Posterior Thoracic Wall; Sep = maximal distance between parietal and visceral pleura; SP = Spine.

4.4. Atelectasis, Pneumonia, Consolidations, and Others

One of the main advantages of LUS over chest X-ray (CXR) is the ability to differentiate between effusion and atelectasis, which, as emphasized, are the most common pulmonary complications after pediatric cardiac surgery. Atelectasis is a universal complication after general anesthesia, either with tracheal intubation or laryngeal mask, occurring in about 68–100% of all types of surgery [29–34], with varying degrees of severity, ranging from small atelectasis to complete lung collapse. In these cases, the etiology of atelectasis is multifactorial and includes surgical compression, cardiopulmonary bypass, consequences on the lung of cardiac defect, and inappropriate ventilation. In children without cardiac defects or with no history of pulmonary disease undergoing minor surgery [29–34], atelectasis tends to resolve spontaneously, though it may persist after 3 days in about 70% of patients undergoing pediatric cardiac surgery [29].

LUS allows for the precise identification of regions of atelectasis. In several studies employing LUS after pediatric cardiac surgery, atelectasis was found to occur much more frequently in the inferior-posterior region (60–92.7%) than in the anterior (5–20.7%) or lateral regions (5–13.8%) [12,34]. LUS further helps in the differentiation of different types of consolidations and masses. Consolidations may be due to infection, infraction from pulmonary embolism, primary or metastatic cancer, compressive or obstructive atelectasis, or a contusion from thoracic trauma, all of which can potentially be differentiated by LUS [12,34]. For instance, the use of LUS for the diagnosis of pneumonia is today accepted in many NICUs, with diagnostic criteria based on major signs, including consolidation, air bronchograms, and pleural effusion. A recent (2020) meta-analysis [35] of over 22 studies with a total of 2470 patients demonstrated that LUS has high sensitivity (0.95; 95% CI: 0.94 to 0.96), specificity (0.90; 95% CI: 0.87 to 0.92), and diagnostic odds ratio (137.49; 95% CI: 60.21 to 313.98) for the diagnosis of pneumonia in children.

4.5. Pneumothorax

Pneumothorax is a common complication in cardiac surgery. Pneumothorax is diagnosed by LUS based on three major findings, namely the absence of lung sliding and lung pulse, the absence of B-lines, and evidence of the 'lung point' [1,36]. The first two signs are required, whereas the lung point may not always be detectable. LUS revealed optimal diagnostic accuracy, with superior sensitivity and similar specificity compared to CXR for the detection of pneumothorax, and it was found to be superior to CT in the classification of pneumothorax size [1,36]. Thus, LUS may be extremely useful for the diagnosis of pneumothorax in a pediatric cardiac surgery setting [13,37]. LUS may be used to monitor the occurrence of pneumothorax after drainage removal, avoiding serial CXRs as is routine practice in many centers [37] (Figure 4 and Video S1).

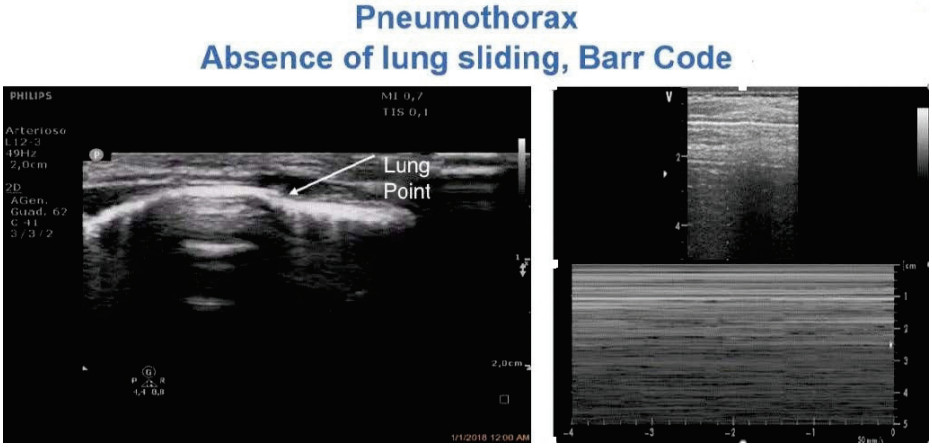

Figure 4. And Video S1: Diagnosis of pneumothorax. The lung pointy (e.g., the point where the pleura stops its movement) is highlighted on the left side. On the right side, the typical Barcode sign on M-mode is shown.

Table 2. Major studies proposing formula for pleural effusion quantification.

Authors	Population	Protocol of Examination	Formula	
Remérand et al. [22], France	58 (45 M) Age 58 ± 17 years	SUPINE Transverse views positioning the transducer in each IS. The transducer was slipped between the patient's back and mattress. The lower and upper IS where PE was detected were drawn on the patient's skin PE length measured in paravertebral regions between the apical and caudal limits. Cross-sectional area measured at the mid-length of PE	PEV (mL) = ACT (cm^2) × LCT (mm)	
Usta [24], Germany	135 (90 M) Age 60 (45–67) years	SITTING The transducer was moved in a cranial direction in the mid-scapular line. PE diameter: maximal distance between mid-height of the diaphragm and visceral pleura	PEV (mL) = D (mm) × 16	
Balik et al. [23], Czech Republic	81 (47 M) m. ventilated patients Age 60 ± 15 years	SUPINE The transducer was moved in the cranial direction in the posterior axillary line PE diameter: maximal distance between parietal and visceral pleura at the lung base	PEV (mL) = 20 × Sep (mm)	
Eibenberger [37], Austria	51 (21 M) Age 28–82 years	SITTING Latero-dorsal wall of the chest PE diameter: the maximal perpendicular distance between the posterior wall of the lung and the posterior chest wall	D (mm) 0 10 20 30 40 50 >60	PEV (mL) 0–90 50–300 150–310 160–660 490–1670 650–1840 950–251
Vignon et al. [21], France	97 (61 M) age 59 ± 20 years	SUPINE From the base to the apex of the chest, along the dorso-lateral part of the chest wall, as far as possible posterior between the mattress and the patient's back without lifting the hemithorax. PE diameter: the maximal distance from the leading edge of the dependent surface of the lung to the trailing edge of the posterior chest wall, on transverse views of pleural spaces. Measurements were made at the base and at the apex of the pleural space	D > 45 mm at the RTB D > 50 mm at the LTB base predicted a PEV ≥ 800 mL sensitivity of 94% and 100 and specificity of 76 and 67%, respectively	

ACT: pleural effusion cross-sectional area; EE: end-expiration; EI: end-inspiration; IS: inter-costal space; LCT: pleural effusion length; LTB: left thoracic base; m.: mechanical; PEV: pleural effusion volume; RTB: right thoracic base; Sep: separation; V: volume; D: diameter; PE: pleural effusion; BMI: body mass index. A Typically, the inter-pleural distance was greater at end-expiration in ventilated patients and on inspiration in spontaneously breathing patients.

4.6. The Retrosternal Area: Diagnosis of Clots

To conclude our discussion of the LUS examination, we found it useful to explore the inspection of the parasternal region for the evaluation of the retrosternal area, a zone where clots are commonly known to form after pediatric cardiac surgery [2,28,38].

By placing the probe close to the parasternal line, the anterior segments can be scanned up and down. If a clot or hematoma is detected, the probe should be placed over it and freely tilted in various planes or orientations for visualization.

There is no standardized system to measure and classify clot dimensions. In a recent series, we defined clot size according to the maximal diameter on an axis perpendicular to the cardiac wall as follows. We specifically defined four classes of clot size, namely

(1) large clots: >3 cm; (2) moderate sized clots: >2 to <3 cm; (3) small to moderate sized clots >1 to <2 cm; and (4) small clots: <1 cm.

Among 37 children undergoing total cavopulmonary connection (mean age 5.5 ± 1.8 years, (range 2.4–11.7) (2.38) mean body surface area 0.7 ± 0.1 m^2 (range 0.3–1.6 m^2)), retrosternal clots were detected in 18 children (48.6%). Of these, seven (13.5%) had small clots (<1 cm), two (5.4%) had small to moderately sized clots (>1–<2 cm), three (8.1%) had moderately sized clots (>2–<3 cm), and six (16.2%) had large clots (>3 cm). Four of the six detected large clots required surgical revision, and the other two clots were not treated because the patients were clinically stable.

Furthermore, exploring the retrosternal area may be helpful for the diagnosis of serious complications after cardiac surgery such as mediastinitis [28], which is typically characterized by retrosternal fluid collection and parasternal hyperconvexity. Hematoma and infections may have similar finding and may overlap [28]; thus, echographic findings should always be correlated clinically (Figure 5).

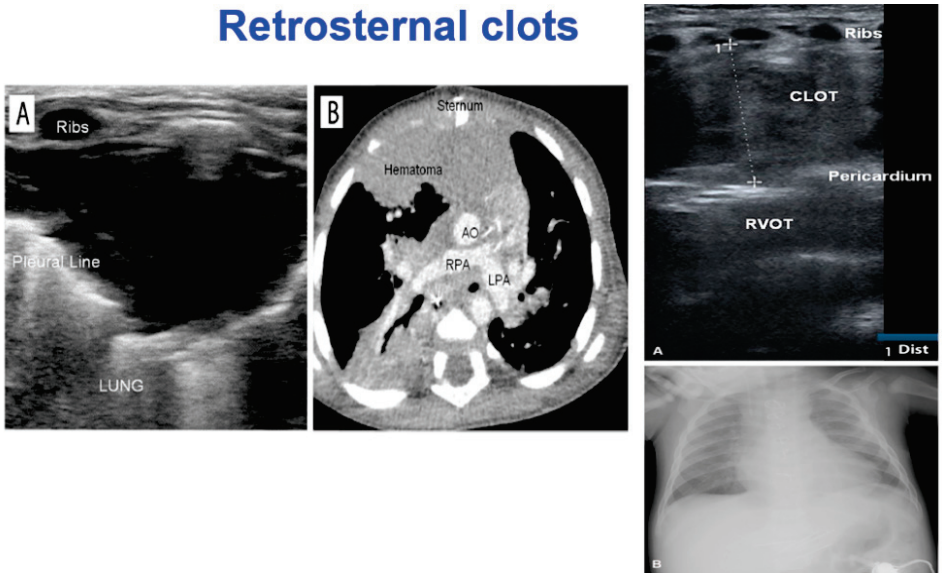

Figure 5. Retrosternal clot. (**Left**) In (**A**), a retrosternal clot is visualized by LUS and confirmed (**B**) by CT scan. Using LUS, it is possible to appreciate how the clot is interposed among the sternum and the plural line. (**Right**) A retrosternal clot among the strum and the right ventricular outflow tract (RVOT) is visualized by LUS (**A**). On chest X-ray and enlargement of right mediastinum can be observed (**B**).

4.7. Diaphragmatic Motion Anomalies

Diaphragmatic paralysis is a serious complication after pediatric cardiac surgery and occurs in 0.3–12.8% of patients. Consequences of diaphragmatic paralysis include respiratory insufficiency, pulmonary infections, and the prolongation of hospital stay. Diaphragmatic paralysis is usually associated with concomitant atelectasis [12,39,40] and may be easily diagnosed either with LUS or with conventional echocardiography by subcostal view. Diagnosis is confirmed by comparing each hemidiaphragm in subxiphoid view and evaluating their respective movements using M-mode. Diaphragmatic motion can be classified as normal (towards the transducer in inspiration with a difference of excursion between the hemidiaphragms of <50%), decreased (difference in the amplitude between the hemidiaphragms >50%), absent (flat line at M-mode), or paradoxical (with absent and paradoxical motion away from the transducer in inspiration), the latter indicating diaphragmatic paralysis [12,39] (Figure 6 and Video S2).

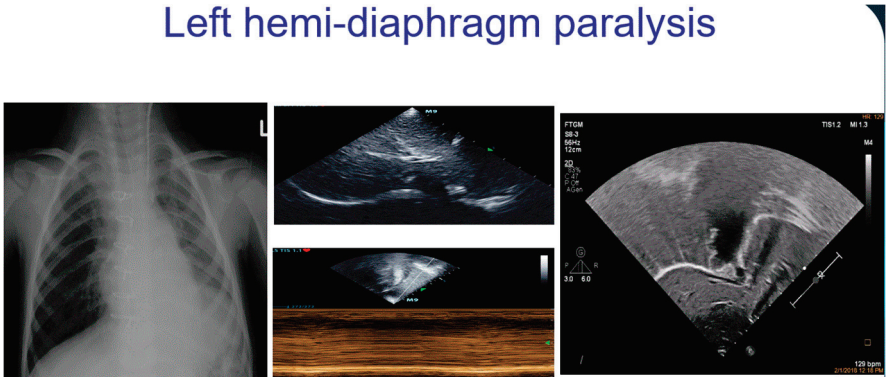

Figure 6. And Video S2: A left hemidiaphragm paralysis can be visualized by chest X-ray (left side) and confirmed by echographic analysis of diaphragm by subcostal view. In the middle, a paradoxical motion of the diaphragm can be appreciated in M-mode, and on the right image, the left hemidiaphragm lifted can be appreciated (Video S2).

4.8. LUS Guidance of Interventional Procedures

LUS may be used to guide common interventional procedures in pediatric cardiology, including drainage insertion for pleural effusion and pneumothorax [41]. Adult studies have demonstrated that the routine use of LUS may drastically reduce the risk of pneumothorax in thoracentesis from 8.8% to 0.97% ($p < 0.0001$) [41]. The utility of LUS extends to tracheal tube verification in the NICU [42,43]. The echographic visualization of the tracheal tube tip by LUS was found to be feasible (i.e., 83% to 100%) and had good sensitivity (i.e., 0.91 to 1.00) with sufficient specificity (i.e., 5 to 1.0) for appropriate tracheal tube depth verification. Furthermore, LUS may be used for echo-guided lung recruitment [3].

4.9. Chest X-ray Reduction in Pediatric Cardiac Surgery

In a previous study, we analyzed [44] the medical records of 1487 children and adolescents (7.09 ± 12.34 years, range 0–17 years) who underwent cardiac surgery over a 6-year period (2013–2018) at our Center, to assess whether the systematic use of LUS reduces the use of CXR. We retrospectively compared CXR use between 2013–2015, where LUS was not routinely employed, with CXR utilization between 2016–2018, after the introduction of systematic LUS use. We found a significant reduction in the number of chest radiographs (10.68 ± 10.31, $p < 0.005$), corresponding to a radiation dose reduction of 0.032 mSv for each individual patient.

4.10. Prognostic Utility of LUS

More recently, several studies evaluated not only the diagnostic capabilities but also the prognostic potential of LUS in pediatric cardiac surgery [1,13,45]. Vitale et al. showed that 20 children (<20 kg; 3–7.25 months) with higher pulmonary congestion on day one post-op had longer times on cardiopulmonary bypass (CPB), longer cross clamp times, longer need of mechanical ventilation, and lengthened stay in ICU [1]. In another study of 61 children (3 days–7.4 years), the percentage of B-lines 1–6 h postoperatively predicted the length of mechanical ventilation and PICU stay [45]. The incremental prognostic value of a new LUS score post-cardiac surgery has been demonstrated. In one study of 237 children undergoing cardiac surgery (0–17 years) at a single center, the use of a new LUS score 12–36 h post-surgery better predicted the intensive care length of stay (beta 0.145; $p = 0.047$) and extubation time (beta 1.644; $p = 0.024$), compared with conventional risk factors. Of note, when single quadrants were analyzed, only the anterior LUS score had significant prognostic value (ICU stay beta, 0.471; $p = 0.020$; extubation time beta 5.530; $p = 0.007$).

5. Current Gaps of Knowledge

5.1. Why Is the Lung White?

In several cases, deaeration, or white lung, can occur due to extravascular water content in response to hypoxia. Many children with CHD, both before and after surgery, present cases of pulmonary edema, due to increased pulmonary blood flow, ventricular dysfunction, valve defects, etc., and deaeration from chronic hypoxia or recovery from atelectasis [2,3]. Pulmonary atelectasis commonly occurs after pediatric surgery and/or in the ICU, and if scanned during post-operative recovery, it is difficult to differentiate from severe pulmonary congestion. Characteristic B-lines help to differentiate cardiogenic lung congestion from other forms of lung deaeration. In cardiogenic lung congestion, B-lines are uniformly present on either hemithorax with a gravity-dependent distribution, with thin and regular pleural lines [11,18] (Figure 7A and Video S3). A patchy, irregular distribution of B-lines, often with irregular pleural lines, is more characteristic of non-cardiogenic pulmonary edemas, such as is observed in acute respiratory distress syndrome (ARDS) or pulmonary fibrosis [11,18] (Figure 7B).

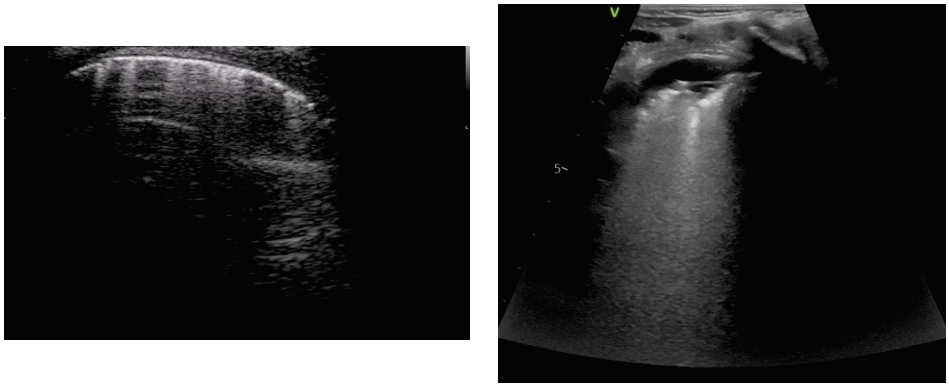

(**A**) (**B**)

Figure 7. (**A**) B-lines due to cardiogenic lung congestion (regular, uniformly distributed along the lungs, with a regular pleural line) and (**B**) B-lines typical of a lung disease (irregular, patchy, with altered pleural line) (Video S3).

5.2. Future Perspectives

Studies on adult patients suggest that the use of speckle tracking may improve the accuracy for the diagnosis of pneumothorax [46,47]; however, as mentioned above, the data on such applications in pediatric populations are lacking.

Preliminary observations in children suggest that the use of contrast agents is feasible and may increase the accuracy for the diagnosis of complicated pneumonia, accurately differentiating necrotizing pneumonia from complex parapneumonic effusion [48]. The use of contrast agents may further allow us to accurately visualize the drainage tubes during invasive maneuvers such as drain insertion.

Studies of diaphragmatic structure and motion, including the quantification of diaphragm thickness, diaphragm excursion, and diaphragm thickening, are increasing in relevance for both the diagnosis of post-surgical paralysis and the monitoring of pulmonary recovery and response to therapy [49,50].

6. Conclusive Remarks

LUS is an accurate, fast, cheap, and radiation-free tool that may be employed for the diagnosis and follow-up of major pulmonary complications in pediatric cardiac surgery. The systematic use of LUS in pediatric cardiology should be encouraged to reduce serial CXR examinations that are not only expensive but also expose children to potentially high doses of radiation.

Further studies are warranted to establish a consensus classification system for the evaluation of disease severity and to further assess the prognostic potential of LUS in children undergoing cardiac surgery for CHD.

Supplementary Materials: The following supporting information can be downloaded at: https://www.mdpi.com/article/10.3390/diagnostics12030763/s1, Video S1: pneumothorax, Video S2: diaphragmatic paralysis, Video S3: A lines cardiogenic.

Author Contributions: Conceptualization, M.C., P.M., R.G. and L.G.; Methodology, M.C. and R.G.; software, P.M.; validation, M.C., S.K., V.J. and L.G.; formal analysis, P.M.; investigation, M.C., E.F., N.A. and P.M.; data curation, M.C., P.M., E.F. and N.A.; writing—original draft preparation, M.C.; writing—review and editing, M.C.; supervision, M.C., S.K., V.J., R.G. and L.G. All authors have read and agreed to the published version of the manuscript.

Funding: This research received no external funding.

Conflicts of Interest: The authors declare no conflict of interest.

References

1. Vitale, V.; Ricci, Z.; Cogo, P. Lung ultrasonography and pediatric cardiac surgery: First experience with a new tool for postoperative lung complications. *Ann. Thorac. Surg.* **2014**, *97*, e1214. [CrossRef] [PubMed]
2. Cantinotti, M.; Giordano, R.; Assanta, N.; Murzi, B.; Gargani, L. Chest Ultrasound: A New, Easy, and Radiation-Free Tool to Detect Retrosternal Clot after Pediatric Cardiac Surgery. *J. Cardiothorac. Vasc. Anesth.* **2015**, *29*, e59–e60. [CrossRef] [PubMed]
3. Cantinotti, M.; Giordano, R.; Volpicelli, G.; Kutty, S.; Murzi, B.; Assanta, N.; Gargani, L. Lung ultrasound in adult and paediatric cardiac surgery: Is it time for routine use? *Interact. Cardiovasc. Thorac. Surg.* **2016**, *22*, 208–215. [CrossRef]
4. Hasan, T.; Bonetti, S.; Gioachin, A.; Bulgarelli, A.; Bartolacelli, Y.; Ragni, L.; Gargiulo, G.D.; Donti, A. Lung ultrasound compared with bedside chest radiography in a paediatric cardiac intensive care unit. *Acta Paediatr.* **2021**, *110*, 1335–1340. [CrossRef]
5. Conlon, T.W.; Himebauch, A.S.; Fitzgerald, J.C.; Chen, A.E.; Dean, A.J.; Panebianco, N.; Darge, K.; Cohen, M.S.; Greeley, W.J.; Berg, R.A.; et al. Implementation of a pediatric critical care focused bedside ultrasound training program in a large academic PICU. *Pediatr. Crit. Care Med.* **2015**, *16*, 219–226. [CrossRef]
6. Chen, S.W.; Fu, W.; Liu, J.; Wang, Y. Routine application of lung ultrasonography in the neonatal intensive care unit. *Medicine* **2017**, *96*, e5826. [CrossRef]
7. Claes, A.S.; Clapuyt, P.; Menten, R.; Michoux, N.; Dumitriu, D. Performance of chest ultrasound in pediatric pneumonia. *Eur. J. Radiol.* **2017**, *88*, 82–87. [CrossRef]
8. Gao, Y.Q.; Qiu, R.X.; Liu, J.; Zhang, L.; Ren, X.L.; Qin, S.J. Lung ultrasound completely replaced chest X-ray for diagnosing neonatal lung diseases: A 3-year clinical practice report from a neonatal intensive care unit in China. *J. Matern. Fetal Neonatal Med.* **2020**, *9*, 1–8. [CrossRef]
9. Liu, J.; Ren, X.L.; Fu, W.; Liu, Y.; Xia, M.-R. Bronchoalveolar lavage for the treatment of neonatal pulmonary atelectasis under lung ultrasound monitoring. *J. Matern. Fetal Neonatal Med.* **2017**, *30*, 2362–2366. [CrossRef]
10. Soldati, G.; Smargiassi, A.; Inchingolo, R.; Sher, S.; Valente, S.; Corbo, G.M. Ultrasound-guided pleural puncture in supine or recumbent lateral position—feasibility study. *Multidiscip. Respir. Med.* **2013**, *8*, 18. [CrossRef]
11. Volpicelli, G.; Elbarbary, M.; Blaivas, M.; Lichtenstein, D.A.; Mathis, G.; Kirkpatrick, A.W.; Melniker, L.; Gargani, L.; Noble, V.E.; Via, G.; et al. International Liaison Committee on Lung Ultrasound (ILC-LUS) for International Consensus Conference on Lung Ultrasound (ICC-LUS). International evidence-based recommendations for point-of-care lung ultrasound. *Intensive Care Med.* **2012**, *38*, 577–591. [CrossRef] [PubMed]
12. Cantinotti, M.; Ait Ali, L.; Scalese, M.; Giordano, R.; Melo, M.; Remoli, E.; Franchi, E.; Clemente, A.; Moschetti, R.; Festa, P.; et al. Lung ultrasound reclassification of chest X-ray data after pediatric cardiac surgery. *Paediatr. Anaesth.* **2018**, *28*, 421–427. [CrossRef] [PubMed]
13. Cantinotti, M.; Giordano, R.; Scalese, M.; Marchese, P.; Franchi, E.; Viacava, C.; Molinaro, S.; Assanta, N.; Koestenberger, M.; Kutty, S.; et al. Prognostic Value of a New Lung Ultrasound Score to Predict Intensive Care Unit Stay in Pediatric Cardiac Surgery. *Ann. Thorac. Surg.* **2020**, *109*, 178–184. [CrossRef] [PubMed]
14. Leech, M.; Bissett, B.; Kot, M.; Ntoumenopoulos, G. Lung ultrasound for critical care physiotherapists: A narrative review. *Physiother. Res. Int.* **2015**, *20*, 69–76. [CrossRef] [PubMed]
15. Vitale, J.; Mumoli, N.; Giorgi-Pierfranceschi, M.; Cresci, A.; Cei, M.; Basile, V.; Cocciolo, M.; Dentali, F. Comparison of the Accuracy of Nurse-Performed and Physician-Performed Lung Ultrasound in the Diagnosis of Cardiogenic Dyspnea. *Chest* **2016**, *150*, 470–471. [CrossRef]
16. Wu, L.; Hou, Q.; Lu, Y.; Bai, J.; Sun, L.; Huang, Y.; Zhang, M.; Zheng, J. Feasibility of lung ultrasound to assess pulmonary overflow in congenital heart disease children. *Pediatr. Pulmonol.* **2018**, *53*, 1525–1532. [CrossRef]

17. Rodríguez-Fanjul, J.; Llop, A.S.; Balaguer, M.; Bautista-Rodriguez, C.; Hernando, J.M.; Jordan, I. Usefulness of Lung Ultrasound in Neonatal Congenital Heart Disease (LUSNEHDI): Lung Ultrasound to Assess Pulmonary Overflow in Neonatal Congenital Heart Disease. *Pediatr. Cardiol.* **2016**, *37*, 1482–1487. [CrossRef]
18. Gargani, L.; Volpicelli, G. How I do it: Lung ultrasound. *Cardiovasc. Ultrasound* **2014**, *12*, 25. [CrossRef]
19. Buda, N.; Kosiak, W.; Wełnicki, M.; Skoczylas, A.; Olszewski, R.; Piotrkowski, J.; Skoczyński, S.; Radzikowska, E.; Jassem, E.; Grabczak, E.M. Recommendations for Lung Ultrasound in Internal Medicine. *Diagnostics* **2020**, *10*, 597. [CrossRef]
20. Raimondi, F.; Migliaro, F.; Sodano, A.; Umbaldo, A.; Romano, A.; Vallone, G.; Capasso, L. Can neonatal ultrasound monitor fluid clearence and preditc the need of respiratory support? *Crit. Care* **2012**, *16*, R220. [CrossRef]
21. Vignon, P.; Chastagner, C.; Berkane, V.; Chardac, E.; François, B.; Normand, S.; Bonnivard, M.; Clavel, M.; Pichon, N.; Preux, P.-M.; et al. Quantitative assessment of pleural effusion in critically ill patients by means of ultrasonography. *Crit. Care Med.* **2005**, *33*, 1757–1763. [CrossRef] [PubMed]
22. Remérand, F.; Dellamonica, J.; Mao, Z.; Ferrari, F.; Bouhemad, B.; Jianxin, Y.; Arbelot, C.; Lu, Q.; Ichaï, C.; Rouby, J.J. Multiplane ultrasound approach to quantify pleural effusion at the bedside. *Intensive Care Med.* **2010**, *36*, 656–664. [CrossRef]
23. Balik, M.; Plasil, P.; Waldauf, P.; Pazout, J.; Fric, M.; Otahal, M.; Pachl, J. Ultrasound estimation of volume of pleural fluid in mechanically ventilated patients. *Intensive Care Med.* **2006**, *32*, 318–321. [CrossRef] [PubMed]
24. Usta, E.; Mustafi, M.; Ziemer, G. Ultrasound estimation of volume of postoperative pleural effusion in cardiac surgery patients. *Interact. Cardiovasc. Thorac. Surg.* **2010**, *10*, 204–207. [CrossRef] [PubMed]
25. Eibenberger, K.; Dock, W.; Ammann, M. Quantification of pleural effusions: Sonography versus radiography. *Radiology* **1994**, *191*, 681–684. [CrossRef]
26. Lorenz, J.; Börner, N.; Nikolaus, H.P. Sonographic volumetry of pleural effusions. *Ultraschall Med.* **1988**, *9*, 212–215. [CrossRef]
27. Yang, P.C.; Luh, K.T.; Chang, D.B.; Wu, H.D.; Yu, C.J.; Kuo, S.H. Value of sonography in determining the nature of pleural effusion: Analysis of 320 cases. *AJR Am. J. Roentgenol.* **1992**, *159*, 29–33. [CrossRef]
28. Hosokawa, T.; Shibuki, S.; Tanami, Y.; Sato, Y.; Ko, Y.; Nomura, K.; Oguma, E. Extracardiac Complications in Intensive Care Units after Surgical Repair for Congenital Heart Disease: Imaging Review with a Focus on Ultrasound and Radiography. *J. Pediatr. Intensive Care* **2021**, *10*, 85–105. [CrossRef]
29. Kane, J.M.; Friedman, M.; Mitchell, J.B.; Wang, D.; Huang, Z.; Backer, C.L. Association between postoperative Fever and atelectasis in pediatric patients. *World J. Pediatr. Congenit. Heart Surg.* **2011**, *2*, 359–363. [CrossRef]
30. Acosta, C.M.; Maidana, G.A.; Jacovitti, D.; Belaunzarán, A.; Cereceda, S.; Rae, E.; Molina, A.; Gonorazky, S.; Bohm, S.H.; Tusman, G. Accuracy of transthoracic lung ultrasound for diagnosing anesthesia-induced atelectasis in children. *Anesthesiology* **2014**, *120*, 1370–1379. [CrossRef]
31. Östberg, E.; Auner, U.; Enlund, M.; Zetterström, H.; Edmark, L. Minimizing atelectasis formation during general anaesthesia-oxygen washout is a non-essential supplement to PEEP. *Ups. J. Med. Sci.* **2017**, *122*, 92–98. [CrossRef]
32. Monastesse, A.; Girard, F.; Massicotte, N.; Chartrand-Lefebvre, C.; Girard, M. Lung ultrasonography for the assessment of perioperative atelectasis: A pilot feasibility study. *Anesth. Analg.* **2017**, *124*, 494–504. [CrossRef] [PubMed]
33. Magnusson, L.; Spahn, D.R. New concepts of atelectasis during general anaesthesia. *Br. J. Anaesth.* **2003**, *91*, 61–72. [CrossRef] [PubMed]
34. Wu, L.; Hou, Q.; Bai, J.; Zhang, J.; Sun, L.; Tan, R.; Zhang, M.; Zheng, J. Modified Lung Ultrasound Examinations in Assessment and Monitoring of Positive End-Expiratory Pressure-Induced Lung Reaeration in Young Children with Congenital Heart Disease Under General Anesthesia. *Pediatr. Crit. Care Med.* **2019**, *20*, 442–449. [CrossRef] [PubMed]
35. Yan, J.H.; Yu, N.; Wang, Y.H.; Gao, Y.B.; Pan, L. Lung ultrasound vs. chest radiography in the diagnosis of children pneumonia: Systematic evidence. *Medicine* **2020**, *99*, e23671. [CrossRef] [PubMed]
36. Volpicelli, G.; Boero, E.; Sverzellati, N.; Cardinale, L.; Busso, M.; Boccuzzi, F.; Tullio, M.; Lamorte, A.; Stefanone, V.; Ferrari, G.; et al. Semi-quantification of pneumothorax volume by lung ultrasound. *Intensive Care Med.* **2014**, *40*, 1460–1467. [CrossRef]
37. Eisenberg, R.L.; Khabbaz, K.R. Are chest radiographs routinely indicated after chest tube removal following cardiac surgery? *AJR Am. J. Roentgenol.* **2011**, *197*, 122–124. [CrossRef]
38. Urvoas, E.; Pariente, D.; Fausser, C.; Lipsich, J.; Taleb, R.; Devictor, D. Diaphragmatic paralysis in children: Diagnosis by TM-mode ultrasound. *Pediatr. Radiol.* **1994**, *24*, 564–568. [CrossRef]
39. Joho-Arreola, A.L.; Bauersfeld, U.; Stauffer, U.G.; Baenziger, O.; Bernet, V. Incidence and treatment of diaphragmatic paralysis after cardiac surgery in children. *Eur. J. Cardiothorac. Surg.* **2005**, *27*, 53–57. [CrossRef]
40. Cavanna, L.; Mordenti, P.; Bertè, R.; Palladino, M.A.; Biasini, C.; Anselmi, E.; Seghini, P.; Vecchia, S.; Civardi, G.; di Nunzio, C.; et al. Ultrasound guidance reduces pneumothorax rate and improves safety of thoracentesis in malignant pleural effusion: Report on 445 consecutive patients with advanced cancer. *World J. Surg. Oncol.* **2014**, *12*, 139. [CrossRef]
41. Sharma, D.; Tabatabaii, S.A.; Farahbakhsh, N. Role of ultrasound in confirmation of endotracheal tube in neonates: A review. *J. Matern. Fetal Neonatal Med.* **2019**, *32*, 1359–1367. [CrossRef]
42. Jaeel, P.; Sheth, M.; Nguyen, J. Ultrasonography for endotracheal tube position in infants and children. *Eur. J. Pediatr.* **2017**, *176*, 293–300. [CrossRef] [PubMed]
43. Cantinotti, M.; Giordano, R.; Gargani, L.; Marchese, P.; Franchi, E.; Koestenberger, M.; Kutty, S.; Ait-Ali, L.; Assanta, N. Could judicious use of lung ultrasound reduce radiographic examinations in pediatric cardiac surgery patients? *J. Clin. Anesth.* **2020**, *61*, 109638. [CrossRef] [PubMed]

44. Kaskinen, A.K.; Martelius, L.; Kirjavainen, T.; Rautiainen, P.; Andersson, S.; Pitkänen, O.M. Assessment of extravascular lung water by ultrasound after congenital cardiac surgery. *Pediatr. Pulmonol.* **2017**, *52*, 345–352. [CrossRef]
45. Fissore, E.; Zieleskiewicz, L.; Markarian, T.; Muller, L.; Duclos, G.; Bourgoin, M.; Michelet, P.; Leone, M.; Claret, P.G.; Bobbia, X. Pneumothorax diagnosis with lung sliding quantification by speckle tracking: A prospective multicentric observational study. *Am. J. Emerg. Med.* **2021**, *49*, 14–17. [CrossRef] [PubMed]
46. Duclos, G.; Bobbia, X.; Markarian, T.; Muller, L.; Cheyssac, C.; Castillon, S.; Resseguier, N.; Boussuges, A.; Volpicelli, G.; Leone, M.; et al. Speckle tracking quantification of lung sliding for the diagnosis of pneumothorax: A multicentric observational study. *Intensive Care Med.* **2019**, *45*, 1212–1218. [CrossRef] [PubMed]
47. Rafailidis, V.; Andronikou, S.; Mentzel, H.J.; Piskunowicz, M.; Squires, J.H.; Barnewolt, C.E. Contrast-enhanced ultrasound of pediatric lungs. *Pediatr. Radiol.* **2021**, *51*, 2340–2350. [CrossRef]
48. Lewińska, A.; Shahnazaryan, K. The Use of Diaphragm Ultrasonography in Pulmonary Physiotherapy of COPD Patients: A Literature Review. *J. Clin. Med.* **2020**, *9*, 3525. [CrossRef]
49. Weber, M.D.; Lim, J.K.B.; Glau, C.; Conlon, T.; James, R.; Lee, J.H. A narrative review of diaphragmatic ultrasound in pediatric critical care. *Pediatr. Pulmonol.* **2021**, *56*, 2471–2483. [CrossRef]
50. Ait-Ali, L.; Andreassi, M.G.; Foffa, I.; Spadoni, I.; Vano, E.; Picano, E. Cumulative patient effective dose and acute radiation-induced chromosomal DNA damage in children with congenital heart disease. *Heart* **2010**, *96*, 269–274. [CrossRef]

diagnostics

MDPI

Article

Lung Ultrasound in Children with Cystic Fibrosis in Comparison with Chest Computed Tomography: A Feasibility Study

Ioana Mihaiela Ciuca [1], Liviu Laurentiu Pop [1], Mihaela Dediu [1], Emil Robert Stoicescu [2,3], Monica Steluta Marc [4,*], Aniko Maria Manea [5] and Diana Luminita Manolescu [2]

[1] Pediatric Department, "Victor Babes" University of Medicine and Pharmacy Timisoara, Eftimie Murgu Square No. 2, 300041 Timisoara, Romania; ciuca.ioana@umft.ro (I.M.C.); liviupop@umft.ro (L.L.P.); dediu.mihaela@umft.ro (M.D.)

[2] Radiology Department, "Victor Babes" University of Medicine and Pharmacy Timisoara, Eftimie Murgu Square No. 2, 300041 Timisoara, Romania; stoicescu.emil@umft.ro (E.R.S.); dmanolescu@umft.ro (D.L.M.)

[3] Research Center for Pharmaco-Toxicological Evaluations, "Victor Babes" University of Medicine and Pharmacy Timisoara, Eftimie Murgu Square No. 2, 300041 Timisoara, Romania

[4] Pulmonology Department, "Victor Babes" University of Medicine and Pharmacy Timisoara, Eftimie Murgu Square No. 2, 300041 Timisoara, Romania

[5] Neonatology and Puericulture Department, "Victor Babes" University of Medicine and Pharmacy, Eftimie Murgu Square No. 2, 300041 Timisoara, Romania; manea.aniko@umft.ro

* Correspondence: marc.monica@umft.ro; Tel.: +40-721434044

Abstract: Background: Cystic fibrosis (CF) lung disease determines the outcome of this condition. For lung evaluation processes, computed tomography (CT) is the gold standard, but also causes irradiation. Lately, lung ultrasound (LUS) has proven to be reliable for the diagnosis of consolidations, atelectasis, and/or bronchiectasis. The aim of our study was to evaluate the value of a newly conceived LUS score by comparing it to the modified Bhalla CT score. A further aim was to evaluate the correlation between the score and the lung clearance index (LCI). Methods: Patients with CF were screened by LUS, followed by a CT scan. Spearman's test was used for correlations. Results: A total of 98 patients with CF were screened, and 57 were included in the study; their mean age was 11.8 ± 5.5 (mean ± SD) years. The mean LUS score was 5.88 ± 5.4 SD. The LUS CF score had a very strong correlation with the CT score of rs = 0.87 (p = 0.000). LUS showed a good sensibility for detecting atelectasis (Se = 83.7%) and consolidations (Se = 94.4%). A lower Se (77.7%) and Sp (9%) were found for cylindrical bronchiectasis. Conclusion: Our study shows that LUS and the lung CF score are parameters that can be used with a complementary role in the diagnosis and monitoring of CF lung disease in children.

Keywords: lung ultrasound; cystic fibrosis; computed tomography comparison; CT

Citation: Ciuca, I.M.; Pop, L.L.; Dediu, M.; Stoicescu, E.R.; Marc, M.S.; Manea, A.M.; Manolescu, D.L. Lung Ultrasound in Children with Cystic Fibrosis in Comparison with Chest Computed Tomography: A Feasibility Study. *Diagnostics* **2022**, *12*, 376. https://doi.org/10.3390/diagnostics12020376

Academic Editors: Marcello Demi and Gino Soldati

Received: 20 December 2021
Accepted: 30 January 2022
Published: 1 February 2022

1. Introduction

Cystic fibrosis is a complex disease characterized by significant clinical polymorphism, a special evolution, and severe complications that raise problems in the individual monitoring and management of the disease [1]. The pulmonary condition remains the most important issue that dictates the prognosis of the disease [2]. Therefore, an early diagnosis of pulmonary complications and the preservation of the lung function are essential. For the diagnosis and monitoring of CF lung disease, many investigations are used, from widely accessible chest X-ray examinations (CXR) [3]—which have lower sensitivity—to computed tomography (CT), the current gold standard [4]. HRCT is very sensitive for the detection of any structural changes, but its repeatability is restricted because of its significant irradiating potential. On the other hand, lung ultrasound is a non-irradiating, easy-to-use method, reliable for the detection of severe childhood pulmonary diseases, from pneumonia [5] to

pulmonary fibrosis [6]; therefore, it is important to evaluate its potential in the accurate detection of CF lung disease.

Presently, lung ultrasound has demonstrated efficiency in the diagnosis of child pneumonia [5,7] and other frequent childhood diseases, such as bronchiolitis, pneumothorax, atelectasis [8], pleural effusion, and pulmonary contusion [9]. It is important to note that lung ultrasound is more sensitive for the detection of smaller lesions [10]. LUS is also valuable for the examination of children diagnosed with tuberculosis, as it seems to be more sensitive than CXR [11]—especially for sickle cell disease [12], or rare diseases such as NEHI [13].

Studies have shown that LUS value in CF exacerbations [14] correlates with lung function tests [15], and reliable correlations between LUS and Chrispin–Norman X-ray score [16] or modified Bhalla CT score have been published [17].

The progression of structural lung deterioration requires objective measurements, such as CT scores [18–21], which offer the necessary support for correct monitoring and the possibility of a follow-up—a mandatory procedure for accurate lung evaluation.

Numerous lung ultrasound scores were developed as consistent, non-invasive tools for numerous diagnoses, such as respiratory COVID-19 in adults [22–24], pneumonia in elders [25], ARDS [26], and lung recruitment ventilation [27,28], with significant practical results. Similarly, for children's respiratory pathology, important achievements have been made by the use of LUS scores to evaluate COVID-19 pneumonia in neonates, pneumonia in children [29], and to predict the need for surfactants in neonates [30], or ventilation requirements in neonatal respiratory distress syndrome [31].

Therefore, in this study, we aimed to assess the value of a newly conceived lung ultrasound (LUS) score by comparing it to the HRCT modified Bhalla score, and to evaluate the correlation between the LUS score and the lung function expressed by the lung clearance index (LCI), which is the most accurate parameter for CF lung function evaluation [32,33].

The LUS scoring system is useful for the detection of multiple respiratory diseases, including features that can be found in CF, in addition to pneumonia [34] or COVID-19 [24].

Chest CT is the gold standard for the structural evaluation of CF lung disease, and the need of an objective marker led to creation of CT scores, which are able to estimate the severity and degree of the specific features that appear in CF [33]. The modified Bhalla score is an accurate and feasible way to assess the severity of CF—a lung parenchymal disease—as it is closely correlated with lung functions [33], severe genotype, and chronic Pseudomonas infections [32,33,35]. In the study conducted by Leung A. et al. [35], modified Bhalla score included the evaluation of the presence, severity, and extent of bronchiectasis, bronchial wall thickening, mucus plugging, atelectasis/consolidation, and air trapping, using a 0–3 severity scale [35], thus simplifying the original Bhalla scale [20].

Even CT scores are used as a surrogate outcome in the evaluation of cystic fibrosis lung disease. In terms of sensitivity, it seems that LCI is comparable with CT. LCI is an indicator of irregular ventilation distribution that sensibly detects abnormal lung structure and early changes in the lungs with CF [32,33]; its practical usefulness lies in its applicability in younger children who cannot be subjected to spirometry, as only tidal breathing is necessary for performing multiple-breath washout (MBW)—the method through which LCI is obtained [32]. Several studies have demonstrated that LCI is better correlated with CT scores than spirometry parameters, and is very sensitive for the detection of early changes in CF lungs [32,33], suggesting that "LCI may be even more sensitive than HRCT scanning for detecting lung involvement in CF" [32].

Therefore, we conclude that the comparison between our new LUS-CF score and a CT examination—the gold standard for structural CF changes—and LCI—the most accurate lung function parameter—is the right premise for this feasibility study.

2. Materials and Methods

2.1. Study Population

The study population was aged between 6 months and 18 years, diagnosed with typical cystic fibrosis and monitored at our CF center. They were invited to participate in the study, starting from October 2016 until March 2020. The study was approved by the Ethics Committee of the Clinical County Hospital (no.8/2016).

Each parent and, in cases over 12 years old, each child, signed the informed consent agreement regarding the agreement to participate in the study, in accordance with the Declaration of Helsinki.

2.2. Study Protocol

2.2.1. Lung Ultrasound

LUS was performed at the first clinical evaluation, before the biological tests and the computer scanning.

We used an Alpinion E-CUBE 9 ultrasound system, scanning with a linear probe of 7–12 MHz frequency and a 3.5–5 MHz convex probe, corresponding to the thoracic wall dimensions. The lung ultrasound was performed by a pediatric pulmonologist with 7 years of experience in LUS, blinded to previous CT examinations, and the stored images were checked by a senior radiologist with 8 years of expertise in lung ultrasound.

Most of the compliant children were evaluated in supine and prone positions, and then in their mothers' arms or in an upright position, if pleurisy was detected, for volume estimation.

The ultrasound evaluation protocol included scanning of the lung areas by longitudinal sections: right and left parasternal, medio-clavicular, anterior and posterior axillary, posterior by paravertebral, medio-scapular and posterior axillar lines. Moreover, the probe transversally scanned each intercostal space, in addition to the transabdominal approach through the liver and spleen window for costal diaphragmatic angles and retrocardiac consolidations. Separately, the hemithorax was virtually divided into 6 areas: 2 anterior—anterosuperior and anteroinferior; 2 lateral—superior and inferior lateral; and 2 posterior—superior and inferior [6,34]. The splenic ultrasound window was also used to evaluate the lower lobes of the left lung and the left costodiaphragmatic angle, as well as the hepatic window for the lower right lung artefacts.

LUS-CF scores were quantified as normal (0–1), mild (2–6), moderate (6–10), or severe (>10).

2.2.2. CT

After the LUS examinations were performed, the patients underwent a CT scan every two years, as part of their regular evaluation, according to our national standards.

The CT scans were performed with a Philips MX 16 EVO 16-slice CT with dedicated pediatric protocols and a Neusoft NeuViz 16 Essence 16-slice CT in the Radiology Department of "Pius Brînzeu" County Emergency Clinical Hospital, Timisoara. The CT scans were optimally performed at 120 kVp, according to international standards. CT scans were acquired at a 2.5 mm and 5 mm slice thickness, with reconstruction images at 1.25 mm. The images were stored in the workstation, the hospital's PACS system, and on CDs, and were interpreted by an experienced radiologist with CT competence and 16 years of experience.

The CT images were analyzed and scored using a modified Bhalla cystic fibrosis score for HRCT [35]. For evaluating the lung lesions, the score considered the quantification of the injuries to the respiratory tract: type (cylindrical, varicose, and saccular) and extension of bronchiectasis, the thickening of the bronchial walls in different stages (mild, moderate, and severe) and the extent of mucus plugging. The quantification of air-trapping zones and the extension of the lung parenchymal lesions (a consolidation area with air bronchogram, consolidation zones, and atelectasis) were also examined.

The scores were achieved for all five lung regions corresponding to the right upper, middle, and lower lung zones, as well as the left upper and left lower lung zones. The

final lesion score was obtained by summing up the five-lobe score. According to the total severity score, CT scores were classified as mild (0–33), moderate (34–66), or severe (> 66) [35].

2.2.3. Lung Function

Spirometry was performed in all patients over the age of 5 years old, as part of the biannual or 3-monthly evaluation, according to their age and infection status. The standards imposed by the American Thoracic Society/European Respiratory Society [36], along with the Global Lung Function Initiative 2012 reference equations [37], were used to calculate the percentage of the predicted parameter values, using a CareFusion machine.

LCI obtained by tidal breathing and by multiple-breath nitrogen (N2) washout was determined using Quark PFT (COSMED, Italy). The LCI was calculated as the number of lung volume turnovers (i.e., the cumulative expired volume divided by the functional residual capacity) needed to lower the end-tidal tracer gas concentration below 2.5% (1/40 of starting level), with the normal values considered below 7 [38].

2.3. Statistical Analysis

For the descriptive statistics, the percentage values for categorical variables and continuous variables were expressed as the mean ± standard deviation. The Shapiro–Wilk test was used to establish the distribution of our quantitative data. The data were investigated using IBM SPSS Statistics version 26.0. Spearman's correlation coefficient was used for the evaluation of the relationships between the quantitative variables. The coefficient Spearman's rho < 0.2 was significant for showing the lack of relationship between the variables. The correlation was considered weak if Spearman's rho was between 0.2 and 0.29, moderate with Spearman's rho 0.3–0.39, strong relationship if Spearman's rho had a value in the 0.4–0.67 interval, and very strong when Spearman's rho > 0.7 [39]. The Kruskal–Wallis test was applied to compare the medians between the groups. The specificity and sensitivity rates were calculated, in addition to the positive and negative predictive values, while p-values were considered significant if $p < 0.005$.

3. Results

3.1. Descriptive Data

A total of 98 patients with CF were screened, and 57 were included in the study, as CT was performed at their biannual evaluation. Their mean age was 11.8 ± 5.5 SD years (ranging between 3.3 and 21.8 years old), and 42.1% were females. Most of the patients had a severe genotype, almost half of them (49.1%) being f508 del homozygous; the f 508 del allele was present in 71.05% of the cases, followed by G542X in 6.1%. The percentage of chronically infected patients was = 49.12% (33.3% with *Pseudomonas aeruginosa* 15.7% with *Staphylococcus* strains, and 7% were polymicrobial).

3.2. LUS CF Score

The artefacts used to define the pathological elements were as follows (Table 1): the presence of A lines—normal aspect = 0 points; less than 3 B lines, thin (< 2 mm in width)/intercostal space = 0 points; more than 3 distinctive B lines or 1 coalescent B line = 1 point, quantifying interstitial inflammation or small bronchiectasis (Figure 1) confirmed by CT (Figure 2); more than 2 coalescent B lines = 2 points, suggestive of alveolo-interstitial inflammation or mucus plugging with loss of aeration; either bronchial wall thickening or subpleural consolidation < 1 cm = 3 points, associated with the absence of A lines quantified either as small atelectasis or cystic bronchiectasis with mucus plugging; subpleural lung consolidation > 1 cm, without bronchogram = 4 points; quantified atelectasis (Figure 3)/consolidation with bronchogram = 5 points.

Table 1. LUS-CF artefacts score.

LUS Artefact	Lung CF Score
Presence of A lines-normal aspect Distinctive B lines < 3/ic space	0
Distinctive B lines > 3/space or 1 coalescent B line	1
Coalescent B lines > 2/ic space	2
Consolidation < 1 cm	3
Consolidation > 1 cm, with bronchogram	4
Atelectasis/consolidation without bronchogram, > 1 cm	5

Figure 1. LUS image shows B lines > 3, LUS score = 2. The corresponding CT image (Figure 2) shows bronchiectasis.

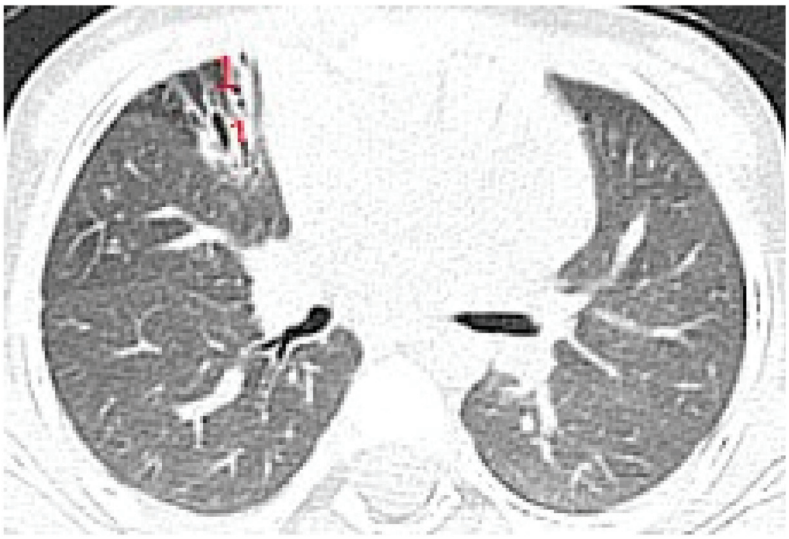

Figure 2. CT reveals (1) peripheral cylindrical bronchiectasis with mucus plugging.

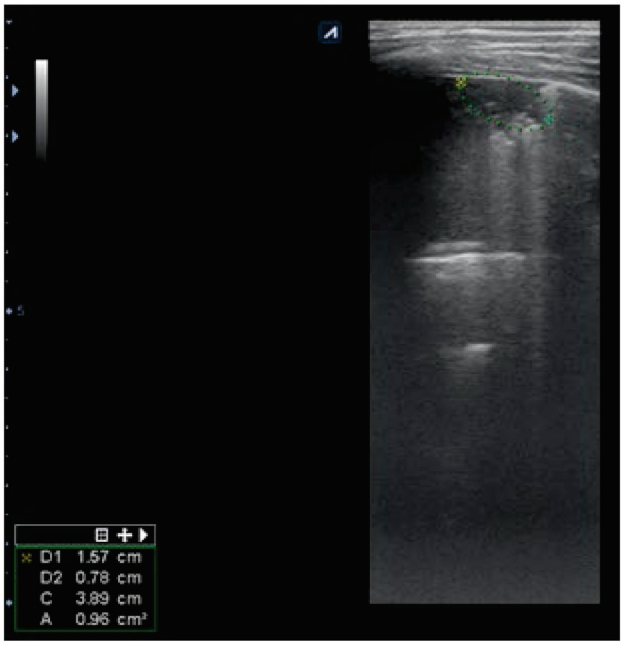

Figure 3. LUS: subpleural consolidation of 1.75 cm/0.78 cm, surface of 0.96 cm^2 (score 4), without bronchogram, with adjacent B lines (2 points); A lines also present, examination of left posterior hemithorax.

Subpleural consolidation were detected by CT scan (Figure 4) in 33.3% of patients, and confirmed by LUS in 31.5% (Figure 3).

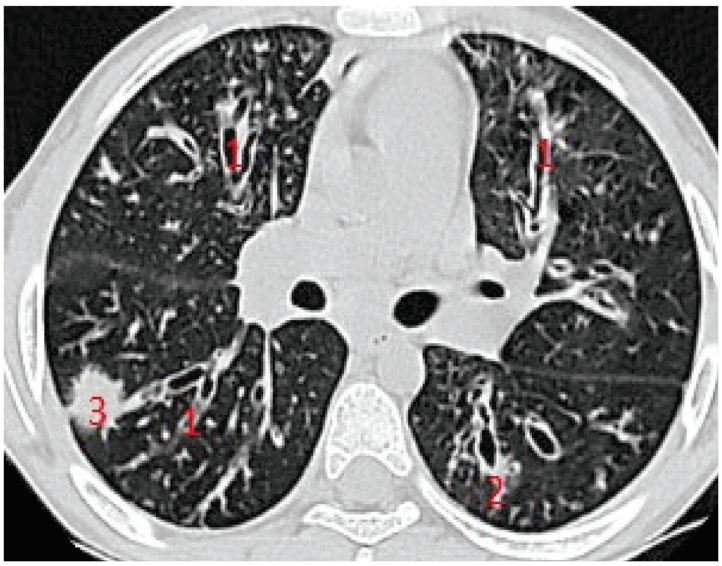

Figure 4. CT scan of the same patient, with various types of bronchiectasis: (1) cylindrical bronchiectasis with moderate bronchial wall thickening; (2) varicose bronchiectasis; and (3) a round/spiculated consolidation, corresponding to previous LUS consolidation. CT score = 62.

The right hemithorax of the same patients revealed the presence of B lines for cylindrical bronchiectasis via LUS (Figure 5).

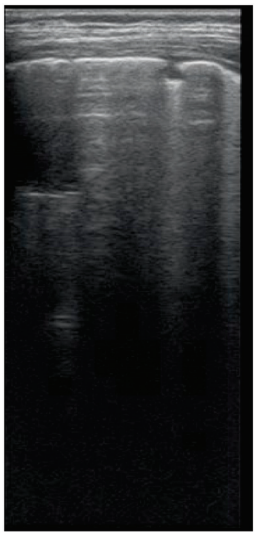

Figure 5. LUS: coalescent B lines, with a very small subpleural consolidation (2 points) and 2 coalescent B lines (2 points), corresponding to mucus-filled varicose bronchiectasis; examination of the same patient's right posterior hemithorax.

The calculation of the score was done by summing up the lesions detected in the six zones of every corresponding hemithorax. The mean LUS score was 5.88 ± 5.4 SD, ranging from 0–21. The mean CT score was 38.14 ± 11.1, consistent with the moderate structural lung damage, ranging from 4 points to a maximum of 82 points.

3.3. Spearman's Correlation Test

Taking into consideration the fact that our data have a nonparametric distribution, we used Spearman's rho coefficient in order to evaluate the correlation between LUS score and CT score, FEV1, FEF 25–75, and LCI.

3.3.1. LUS-CF Score and CT Score

The LUS-CF score had a very strong correlation with the CT score of rs = 0.87, showing important statistical significance (p = 0.000), suggesting a good reliability of the LUS-CF score in the evaluation of CF lung parenchymal deterioration.

We divided the patients according to their CT score: mild disease (0–33), moderate disease (34–66), and severe disease (> 67) (Figure 6). The correlation in patients with mild disease, expressed by an LUS-CF score from 0 to 7, was weak (rs = 0.439) (p = 0.014), while in patients with moderate disease, the correlation coefficient strongly increased to rs = 0.57, with good statistical significance (p = 0.01). By applying the Kruskal–Wallis test, we found a statistical difference between the median LUS values in the categories of the CT score (H = 39.845, p = 0.000; Table 2).

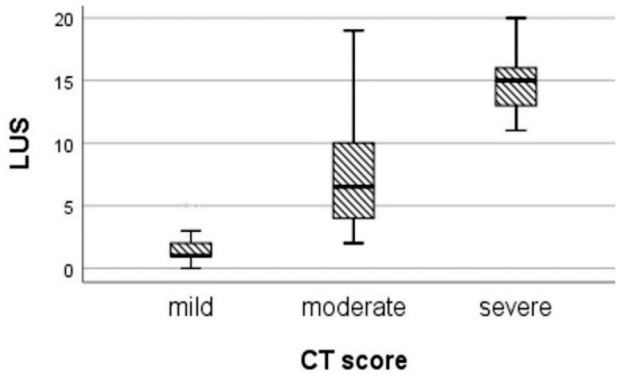

Figure 6. Median LUS scores in patients classified by CT score.

Table 2. Median LUS scores in CT score categories.

	Mild CT Score	Moderate CT Score	Severe CT Score	H	*p*
LUS					
Median (IQR)	1 (1; 2)	6.5 (4; 11)	15 (12.75; 16.5)	39.845	0.000
Mean of rank	16.07	38.14	50.05		

In patients with important structural lung damage (Figure 7), quantified as severe disease, expressed by a CT score > 66, the correlation was strong (rs = 0.83), with statistical significance (p = 0.002).

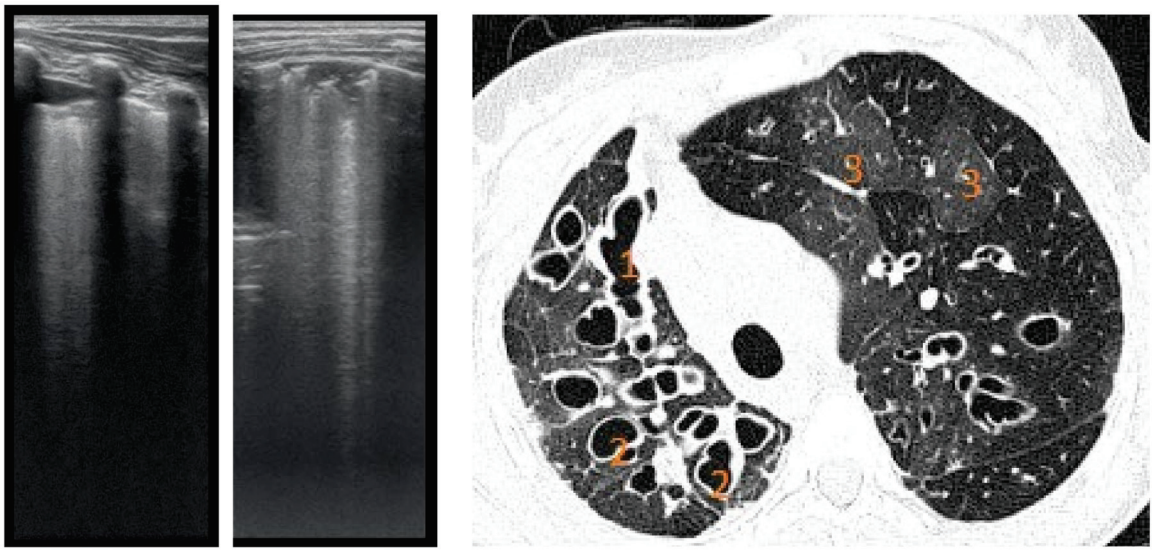

(**A**) (**B**) (C)

Figure 7. (**A**) LUS: coalescent B lines, erased A profile, loss of aeration, left hemithorax. (**B**) LUS image with subpleural consolidations, coalescent B lines, and left hemithorax. (**C**) CT scan of the same patients: (1) varicose bronchiectasis with middle 1/3 of lung extended and moderate bronchial wall thickening; (2) saccular bronchiectasis with mild and moderate wall thickening; and (3) zones with increased attenuation of pulmonary parenchyma (alveolar infiltrates).

3.3.2. LUS-CF Score with Lung Function Parameters

Evaluating the relationship between the LUS score and LCI, the Spearman's correlation coefficient rs = 0.8 revealed a strong, statistically significant correlation (p = 0.000)—an encouraging significant association between the structural lung disease and lung function. Additionally, the relationship between the LUS-CF score and the spirometry parameters was evaluated, and a strong negative correlation was found with FEV1 rs = −0.65 (p = 0.000) and FEF 25–75 rs = −0.542 (p = 0.000).

3.4. LUS Sensitivity and Specificity

The assessment of LUS sensitivity and specificity in bronchiectasis detection varied with the form of bronchiectasis: for cylindrical bronchiectasis(Figure 8A,B), LUS Se = 77.7%, Sp = 9%, PPV = 80.7%, and NPV = 76.9%, while for saccular bronchiectasis (Figure 7), a moderate Se = 68.4%, with good Sp = 94.9%, PPV = 88.8%, and NPV = 94.7% were found.

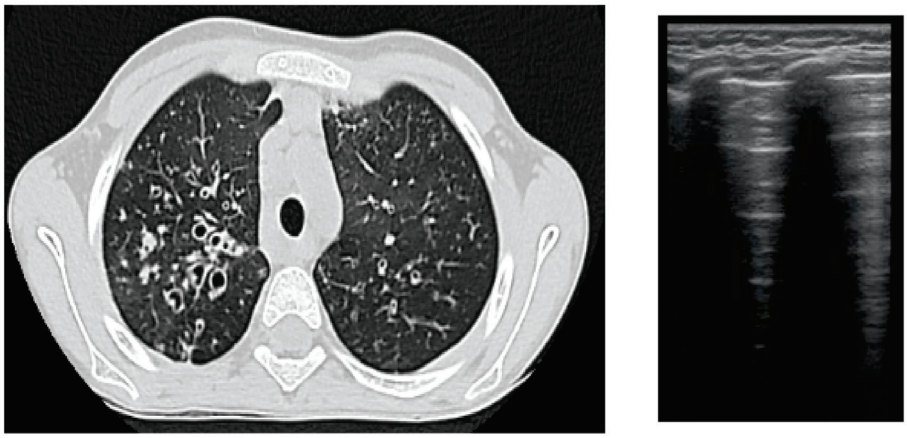

(**A**) (**B**)

Figure 8. (**A**) CT scan: cylindrical bronchiectasis with mucus plugs (**B**) LUS: A lines, normal LUS aspect, score = 0.

As for varicose bronchiectasis (Figure 9 A,B), a very low Sp = 25% and NPV = 16.6% were calculated, with a satisfactory PPV = 88.8% and Se = 68.4%.

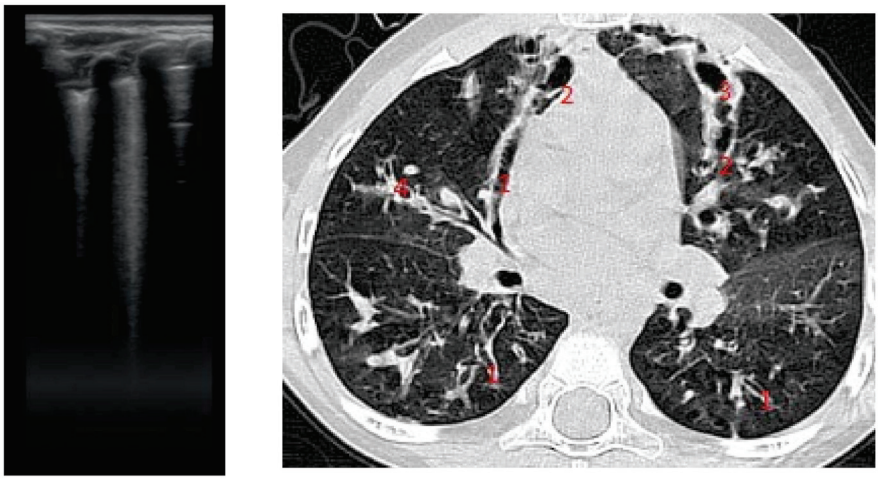

(**A**) (**B**)

Figure 9. (**A**) LUS: coalescent B lines, loss of A lines. (**B**) CT image: (1) cylindrical bronchiectasis with moderate wall thickening; (2) varicose bronchiectasis; (3) saccular bronchiectasis with moderate wall thickening; and (4) several bronchiectasis with mucus plugging.

The results regarding atelectasis (Figures 10 and 11) and consolidation detection were significant. LUS showed good sensitivity and specificity in detecting atelectasis (Figure 10)—Se = 83.7%, Sp = 94.5%, PPV = 92.5%, NPV = 72.3%—and consolidations—Se = 94.4%, Sp = 93.02%, PPV = 89.4%, NPV = 97.3%.

As for bronchial thickening, low sensitivity and specificity were found: Se = 31.7%, Sp = 35.2%, PPV = 54.1, NPV = 14.2%.

We could not calculate the reliability of LUS for air trapping or for mucus plugging because of a lack of specific artefacts.

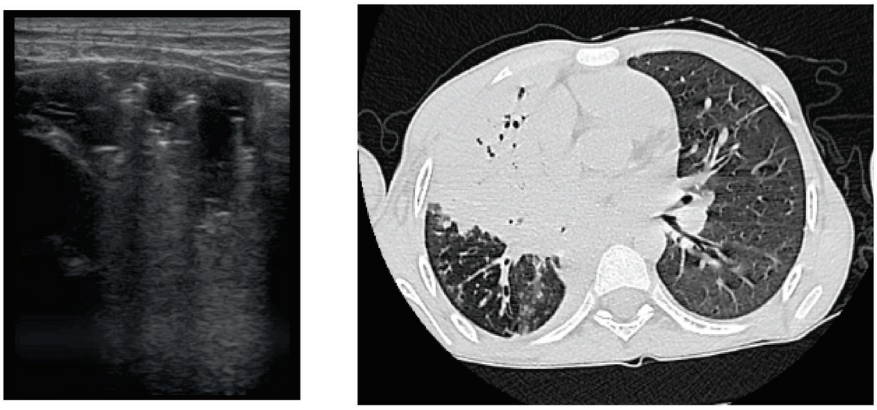

(**A**) (**B**)

Figure 10. (**A**) LUS image of atelectasis, hypoechoic image with air inside. (**B**) CT scan reveals atelectasis, bronchiectasis, and partial bronchogram.

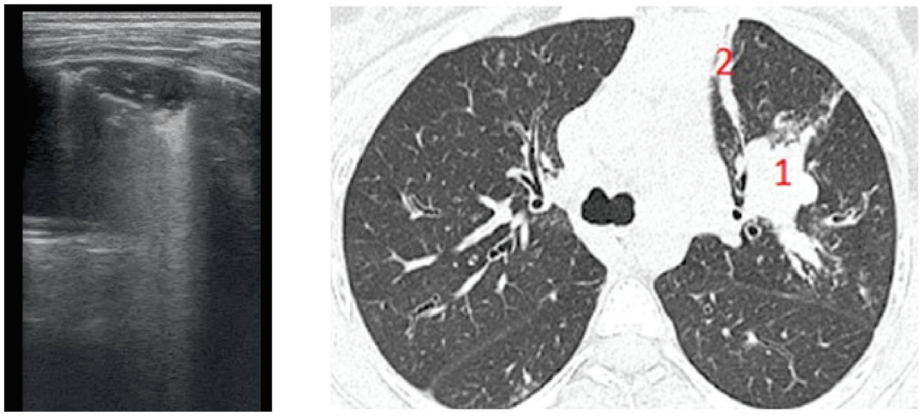

(**A**) (**B**)

Figure 11. (**A**) LUS image of atelectasis, consolidation without bronchogram. (**B**) CT exam illustrates (1) a peribronchovascular consolidation without air bronchogram, and (2) a lamellar (band) atelectasis.

4. Discussion

The literature on LUS-CF is limited, as CF is a rare disease with few patients, and a small number of specialists in LUS.

In this study, we found that the LUS-CF score is a valuable instrument not only to reveal the presence and quantification of parenchymal injury in CF, but also for expressing the relationship with lung clearance index—the most accurate CF functional parameter.

LUS can show many ultrasound abnormalities, such as B lines, pleural line abnormalities, important consolidations, and atelectasis. In addition to its diagnostic practicality, LUS also seems to be effective for detection of exacerbations [40], showing good correlation with lung function [17,41]. Few studies have investigated the significance of LUS in CF [15–17,40,41], but emerging evidence remains to be shown. Our study is the first to describe the LUS artefacts corresponding to CT lung lesions, quantifying all lung injuries potentially detected by LUS. Furthermore, this is the first study to evaluate the relationship between lung structural damage expressed by LUS scoring and functional issues expressed by LCI, as we previously noted this correlation between structure and function [41].

The first study that presented the CF lung ultrasound artefacts in cystic fibrosis described the presence of interstitial syndrome, bronchiectasis, alveolar consolidation, and pleural signs, but was published only in abstract, by our group [41]. Strzelczuk-Judka subsequently reported the CF-USS (cystic fibrosis ultrasound score), which evaluated the presence and extent of pleural irregularities, focal or coalescent ”lung rockets” B lines,

subpleural consolidations, and pleural fluid, showing a positive correlation with Chrispin–Norman CXR scoring systems (r = 0.52, p = 0.0002) [16]. As in our study, they acknowledged an important limitation in the inability to visualize the respiratory airway deterioration, e.g., bronchiectasis and mucus plugs.

Peixoto et al. reported a score that included A pattern and B pattern and C pattern (consolidation), stratifying patients into A profile, B profile, C profile, or mixed profiles compared to CT, and reported a good correlation between LUS and CT [17]. The presence of pleural effusion was not scored (declared as very rare), nor were the pleural irregularities (only describing the finding) [17], similar to our study. The choice of excluding pleural effusion from our LUS-CF score was based on the fact that pleural effusion is not a specific feature of CF.

Hassanzad et al. noted in LUS the presence of pleural thickening, atelectasis, air bronchogram, B lines, and consolidation, compared the findings with corresponding CXR and HRCT, and evaluated the diagnostic performance of LUS and CXR for every artefact, with satisfactory results [40]. Similar to our discoveries, a good diagnostic performance for the detection of consolidation was reported in this paper.

Regarding pleural irregularities, Strzelczuk-Judka noted pleural irregularities similar to bronchiolitis in one patient [16]; Peixoto described this feature, but did not quantify it [17]. We did not take into consideration the presence of the pleural irregularities for this 2016 starting study, because CT did not show a specific corresponding finding; therefore, we considered it normal appearance at the time of our LUS-CF score's development. Neither of the others studies stated that pleural irregularities or thickening would correspond to a specific modification in CT.

With previous experience of our group on LUS in CF [41], we noted that LUS artefacts may quantify different pathological expression. As exemplified in the results of the present paper, B lines can also quantify interstitial inflammation or small bronchiectasis, as confirmed by CT in our study. Similarly, the coalescent B lines can be suggestive of alveolo-interstitial inflammation or mucus plugging with loss of aeration, or bronchial wall thickening. We observed that subpleural consolidation with absence of A lines quantified small atelectasis, but also cystic bronchiectasis filled with mucus. The lack of specificity for mentioned artefacts led us to be cautious in asserting the specificity of LUS for CF lung disease. However, the LUS-CF score showed a very good correlation with CT, as mentioned, and was highly sensitive in detecting parenchymal abnormalities. Other studies suggest the role of LUS in CF exacerbations [42], showing its superiority to CXR in terms of the detection of consolidations, pleural effusion and irregularities compared to CT examination [40] in exacerbations of CF in patients. In previously published papers, a good correlation was found between the LUS and Chrispin–Norman CXR score [16], and also with the modified Bhalla CT score [17], which is also reflected in our own findings.

Our findings reveal a very strong positive linear correlation between the LUS-CF score and LCI (rs = 0.87, p = 0.000), suggesting the reliability of the LUS-CF score in the detection of functional impairment in CF patients. The correlation coefficient between LUS and LCI was superior to the correlation with spirometry parameters, which can be explained by the increased sensitivity of LCI in the detection of lung function impairment and the specificity of the LUS-CF score that included all B line spectra, consolidations with or without bronchiectasis, and loss of aeration.

A strong negative correlation was found with CF-specific parameters for obstructions such as FEV1 (rs = −0.65 (p = 0.000) and FEF 25–75 (rs = −0.542 (p = 0.000). These findings are similar to those of another study that evaluated LUS patterns in CF, and which showed a correlation with lung function expressed by pre-BD FVC r = 0.538 and pre-BD FEV1 r = 0.536 [17].

Descriptive data on LUS artefacts in a number of conditions have been published, but the development of LUS scores has opened the door to objective evaluation. These studies show a correlation between LUS scores and inflammation [29], lung function in CF, and even mortality prognosis [43] in several diseases.

The reliability of LUS in CF lung disease is sustained by its very good sensitivity and specificity in detecting consolidations (Se = 94.4%, Sp = 93.02%), a reliable positive predictive value of 89.4%, and an important NPV = 97.3%. LUS detected atelectasis with a good sensitivity of 83.7% and a significant specificity of 94.5%. The positive predictive value was important for atelectasis (PPV = 92.5%), and NPV = 72.3%. These findings are similar to those of other studies [16,17,40].

As for LUS sensitivity and sensibility in bronchiectasis, detection varied with the type of bronchiectasis, with a decent sensitivity for detecting cylindrical bronchiectasis (77.7%) and saccular bronchiectasis (Se = 68.4%, Sp = 94.9%), but a lower specificity of 9% for cylindrical bronchiectasis, explained by the fact that they were quantified by B lines which, as stated, suggest several diseases [44].

The results regarding atelectasis detection were significant; LUS showed good sensibility and specificity in detecting atelectasis: Se = 83.7%, Sp = 94.5%, PPV = 92.5%, NPV = 72.3%. As for bronchial thickening, low sensitivity and specificity were found: Se = 31.7%, Sp = 35.2%, PPV = 54.1, NPV = 14.2%.

This study has a few limitations. Lung ultrasound was performed by a single practitioner, and while the number of patients included in the study was satisfactory, it is possible that a larger study would have offered more consistency. Another limitation is that important artefacts such as air trapping/emphysema—one of the premature signs of lung damage in CF—has no US correspondence. No artefact for emphysema quantification was found, nor has any been published previously. Furthermore, small mucus plugging or mild bronchial wall thickening was not detected by LUS, as no LUS artefacts for these changes have been identified to date.

An additional important issue is related to the lack of specificity of B lines, which can quantify a number of diseases [44], ranging from interstitial lung disease or bronchiolitis to acute respiratory distress syndrome or bronchiectasis [45]. We specifically quantified different extensions of bronchiectasis (i.e., cylindrical, varicose, cystic) by the presence of B lines to increase the accuracy of our study, and we eliminated the patients in exacerbations in order to decrease the misinterpretations of interstitial inflammation that can occur in exacerbations with bronchiectasis. As bronchiectasis is the hallmark of CF lung disease, special attention was given to its detection via LUS, and we found LUS to be reliable for the detection of bronchiectasis—a finding that is similar to those of recent studies in adult pathology [46]. The presence of more than three individual B lines per intercostal space, in longitudinal sections, detected before CT examination, suggested certain structural changes. In some of the patients, the above-mentioned studies quantified bronchiectasis to different degrees; in others, bronchial wall thickening or small mucus plugging—specific features identified on CT; therefore, they are not specific to a single lesion, but their presence definitely indicates a lung lesion.

The validation of our score is expressed by the strong correlation found with the modified Bhalla CT score—especially in severely altered lung diseases. However, CT remains the gold standard for CF lung morphological evaluation, as it can accurately detect alterations that are not encryptable via LUS so far, such as air trapping and mucus plugging, considering that bronchiectasis and air trapping are important validated outcome parameters [47].

Even if HRCT is the gold standard for lung disease in CF, it cannot be used as often as necessary—especially in children diagnosed with CF, who require sedation when being exposed to repetitive irradiating scans, even if a low dosage is used.

LUS can be a reliable instrument for screening and monitoring children with CF—especially in the advanced forms of the disease—reducing the levels of exposure to CT radiation.

The strength of this study is the presentation of the LUS-CF score as a non-invasive and reliable tool for the screening of advanced structural damage in CF.

5. Conclusions

LUS in the monitoring of CF patients' lung disease is reliable for advanced lung disease and for lesions of moderate severity, but for the detection of early changes LUS is not a consistent method of lung investigation, with CT remaining the gold standard.

Our study has shown that the LUS-CF score is a parameter that can be used for an associated evaluation, and can play a complementary role in the diagnosis and monitoring of CF lung disease in children.

Author Contributions: Conceptualization, I.M.C.; data curation, I.M.C., E.R.S., A.M.M., and D.L.M.; formal analysis, I.M.C., L.L.P., M.D., E.R.S., M.S.M., A.M.M., and D.L.M.; investigation, M.D., E.R.S., M.S.M., A.M.M., and D.L.M.; methodology, L.L.P., M.D., and E.R.S.; project administration, L.L.P. and M.S.M.; software, A.M.M.; supervision, L.L.P. and D.L.M.; validation, A.M.M. and D.L.M.; visualization, I.M.C., L.L.P., M.D., E.R.S., M.S.M., and A.M.M.; writing—original draft preparation, I.M.C.; writing—review and editing, I.M.C., L.L.P., M.D., M.S.M., and D.L.M. All authors have read and agreed to the published version of the manuscript.

Funding: This research received no external funding.

Institutional Review Board Statement: This study was conducted according to the guidelines of the Declaration of Helsinki, and approved by the Ethics Committee of Clinical County Hospital Timisoara, Romania (No.8/11.01.2016).

Informed Consent Statement: Informed consent was obtained from all subjects involved in the study; patients and their parents signed the informed consent and agreed to the study.

Data Availability Statement: Data available on request from the corresponding author.

Acknowledgments: The authors acknowledge the colleagues from the Pediatric Clinic Pulmonology Unit and National Cystic Fibrosis Center of Clinical County Hospital who participated in the care of the patients.

Conflicts of Interest: The authors declare no conflict of interest.

References

1. Bell, S.C.; Mall, M.A.; Gutierrez, H.; Macek, M.; Madge, S.; Davies, J.C.; Burgel, P.-R.; Tullis, E.; Castaños, C.; Castellani, C.; et al. The future of cystic fibrosis care: A global perspective. *Lancet Respir. Med.* **2020**, *8*, 65–124. [CrossRef]
2. Goss, C.H. Acute Pulmonary Exacerbations in Cystic Fibrosis. *Semin. Respir. Crit. Care Med.* **2019**, *40*, 792–803. [CrossRef] [PubMed]
3. Cleveland, R.H.; Neish, A.S.; Zurakowski, D.; Nichols, D.P.; Wohl, M.E.B.; Colin, A.A. Cystic fibrosis: A system for assessing and predicting progression. *Am. J. Roentgenol.* **1998**, *170*, 1067–1072. [CrossRef]
4. Tiddens, H.A.W.M. Chest computed tomography scans should be considered as a routine investigation in cystic fibrosis. *Paediatr. Respir. Rev.* **2006**, *7*, 202–208. [CrossRef] [PubMed]
5. Pereda, M.A.; Chavez, M.A.; Hooper-Miele, C.C.; Gilman, R.H.; Steinhoff, M.C.; Ellington, L.E.; Gross, M.; Price, C.; Tielsch, J.M.; Checkley, W. Lung ultrasound for the diagnosis of pneumonia in children: A meta-analysis. *Pediatrics* **2015**, *135*, 714–722. [CrossRef] [PubMed]
6. Volpicelli, G.; Elbarbary, M.; Blaivas, M.; Lichtenstein, D.A.; Mathis, G.; Kirkpatrick, A.W.; Melniker, L.; Gargani, L.; Noble, V.E.; Via, G.; et al. International evidence-based recommendations for point-of-care lung ultrasound. *Intensive Care Med.* **2012**, *38*, 577–591. [CrossRef]
7. Esposito, S.; Papa, S.S.; Borzani, I.; Pinzani, R.; Giannitto, C.; Consonni, D.; Principi, N. Performance of lung ultrasonography in children with community-acquired pneumonia. *Ital. J. Pediatrics* **2014**, *40*, 37. [CrossRef]
8. Heuvelings, C.C.; Bélard, S.; Familusi, M.A.; Spijker, R.; Grobusch, M.P.; Zar, H.J. Chest ultrasound for the diagnosis of paediatric pulmonary diseases: A systematic review and meta-analysis of diagnostic test accuracy. *Br. Med. Bull.* **2019**, *129*, 35–51. [CrossRef]
9. Kharasch, S.; Duggan, N.M.; Cohen, A.R.; Shokoohi, H. Lung ultrasound in children with respiratory tract infections: Viral, bacterial or covid-19? A narrative review. *Open Access Emerg. Med.* **2020**, *12*, 275–285. [CrossRef]
10. Urbankowska, E.; Krenke, K.; Drobczyński, Ł.; Korczyński, P.; Urbankowski, T.; Krawiec, M.; Kraj, G.; Brzewski, M.; Kulus, M. Lung ultrasound in the diagnosis and monitoring of community acquired pneumonia in children. *Respir. Med.* **2015**, *109*, 1207–1212. [CrossRef]
11. Heuvelings, C.C.; Bélard, S.; Andronikou, S.; Lederman, H.; Moodley, H.; Grobusch, M.P.; Zar, H.J. Chest ultrasound compared to chest X-ray for pediatric pulmonary tuberculosis. *Pediatric Pulmonol.* **2019**, *54*, 1914–1920. [CrossRef] [PubMed]

12. Daswani, D.D.; Shah, V.P.; Avner, J.R.; Manwani, D.G.; Kurian, J.; Rabiner, J.E. Accuracy of Point-of-care Lung Ultrasonography for Diagnosis of Acute Chest Syndrome in Pediatric Patients with Sickle Cell Disease and Fever. *Acad. Emerg. Med.* **2016**, *23*, 932–940. [CrossRef] [PubMed]
13. Sansone, F.; Attanasi, M.; di Filippo, P.; Sferrazza Papa, G.F.; di Pillo, S.; Chiarelli, F. Usefulness of lung ultrasound in paediatric respiratory diseases. *Diagnostics* **2021**, *11*, 1783. [CrossRef] [PubMed]
14. Ciuca, I.M.; Pop, L.L. 145 Lung ultrasound in CF children's exacerbation—one center experience. *J. Cyst. Fibros.* **2015**, *14* (Suppl. 1), S95. [CrossRef]
15. Ciuca, I.M.; Dediu, M.; Pop, L.L. Lung clearance index and lung ultrasound in cystic fibrosis children. *Eur. Respir. J.* **2018**, *52*, OA4988.
16. Strzelczuk-Judka, L.; Wojsyk-Banaszak, I.; Zakrzewska, A.; Jończyk-Potoczna, K. Diagnostic value of chest ultrasound in children with cystic fibrosis—Pilot study. *PLoS ONE* **2019**, *14*, e0215786. [CrossRef]
17. Peixoto, A.O.; Al Marson, F.; Dertkigil, S.S.J.; Dertkigil, R.P.; Souza, T.H.; Fraga, A.M.A.; Ribeiro, A.F.; Toro, A.A.; Ribeiro, J.D. The use of ultrasound as a tool to evaluate pulmonary disease in cystic fibrosis. *Respir. Care* **2020**, *65*, 293–303. [CrossRef]
18. Folescu, T.W.; de Andrade Marques, E.; Boechat, M.C.B.; Daltro, P.; Higa, L.Y.S.; Cohen, R.W.F. High-resolution computed tomography scores in cystic fibrosis patients colonized with Pseudomonas aeruginosa or Staphylococcus aureus. *J. Bras. Pneumol.* **2012**, *38*, 41–49. [CrossRef]
19. Brody, A.S.; Sucharew, H.; Campbell, J.D.; Millard, S.P.; Molina, P.L.; Klein, J.S.; Quan, J. Computed tomography correlates with pulmonary exacerbations in children with cystic fibrosis. *Am. J. Respir. Crit. Care Med.* **2005**, *172*, 1128–1132. [CrossRef]
20. Bhalla, M.; Turcios, N.; Aponte, V.; Jenkins, M.; Leitman, B.; McCauley, D.I.; Naidich, D. Cystic fibrosis: Scoring system with thin-section CT. *Radiology* **1991**, *179*, 783–788. [CrossRef]
21. Rosenow, T.; Oudraad, M.C.J.; Murray, C.P.; Turkovic, L.; Kuo, W.; de Bruijne, M.; Ranganathan, S.C.; Tiddens, H.A.W.M.; Stick, S. PRAGMA-CF. A Quantitative Structural Lung Disease Computed Tomography Outcome in Young Children with Cystic Fibrosis. *Am. J. Respir. Crit. Care Med.* **2015**, *191*, 1158–1165. [CrossRef] [PubMed]
22. Soldati, G.; Smargiassi, A.; Inchingolo, R.; Buonsenso, D.; Perrone, T.; Briganti, D.F.; Perlini, S.; Torri, E.; Mariani, A.; Mossolani, E.E.; et al. Proposal for international standardization of the use of lung ultrasound for COVID-19 patients; a simple, quantitative, reproducible method. *J. Ultrasound Med. Off. J. Am. Inst. Ultrasound Med.* **2020**, *39*, 1413–1419.
23. Dargent, A.; Chatelain, E.; Kreitmann, L.; Quenot, J.-P.; Cour, M.; Argaud, L.; The COVID-LUS Study Group. Lung ultrasound score to monitor COVID-19 pneumonia progression in patients with ARDS. *PLoS ONE* **2020**, *15*, e0236312. [CrossRef]
24. Volpicelli, G.; Lamorte, A.; Villén, T. What's new in lung ultrasound during the COVID-19 pandemic. *Intensive Care Med.* **2020**, *46*, 1445–1448. [CrossRef] [PubMed]
25. Linsalata, G.; Okoye, C.; Antognoli, R.; Guarino, D.; Ravenna, V.; Orsitto, E.; Calsolaro, V.; Monzani, F. Pneumonia Lung Ultrasound Score (PLUS): A New Tool for Detecting Pneumonia in the Oldest Patients. *J. Am. Geriatr. Soc.* **2020**, *68*, 2855–2862. [CrossRef]
26. Costamagna, A.; Pivetta, E.; Goffi, A.; Steinberg, I.; Arina, P.; Mazzeo, A.T.; Del Sorbo, L.; Veglia, S.; Davini, O.; Brazzi, L.; et al. Clinical performance of lung ultrasound in predicting ARDS morphology. *Ann. Intensive Care* **2021**, *11*, 51. [CrossRef]
27. Bouhemad, B.; Brisson, H.; Le-Guen, M.; Arbelot, C.; Lu, Q.; Rouby, J.-J. Bedside ultrasound assessment of positive end-expiratory pressure-induced lung recruitment. *Am. J. Respir. Crit. Care Med.* **2011**, *183*, 341–347. [CrossRef]
28. Enghard, P.; Rademacher, S.; Nee, J.; Hasper, D.; Engert, U.; Jörres, A.; Kruse, J.M. Simplified lung ultrasound protocol shows excellent prediction of extravascular lung water in ventilated intensive care patients. *Crit. Care* **2015**, *19*, 36. [CrossRef]
29. Ciuca, I.M.; Dediu, M.; Pop, L.L. Pediatric pneumonia (PedPne) lung ultrasound score and inflammatory markers: A pilot study. *Pediatric Pulmonol.* **2022**, *57*, 576–582. [CrossRef]
30. De Martino, L.; Yousef, N.; Ben-Ammar, R.; Raimondi, F.; Shankar-Aguilera, S.; de Luca, D. Lung ultrasound score predicts surfactant need in extremely preterm neonates. *Pediatrics* **2018**, *142*, e20180463. [CrossRef]
31. Szymański, P.; Kruczek, P.; Hożejowski, R.; Wais, P. Modified lung ultrasound score predicts ventilation requirements in neonatal respiratory distress syndrome. *BMC Pediatrics* **2021**, *21*, 17. [CrossRef] [PubMed]
32. Gustafsson, P.M.; de Jong, P.A.; Tiddens, H.A.W.M.; Lindblad, A. Multiple-breath inert gas washout and spirometry versus structural lung disease in cystic fibrosis. *Thorax* **2008**, *63*, 129–134. [CrossRef] [PubMed]
33. Fretzayas, A.; Loukou, I.; Moustaki, M.; Douros, K. Correlation of computed tomography findings and lung function in children and adolescents with cystic fibrosis. *World J. Pediatrics* **2021**, *17*, 221–226. [CrossRef] [PubMed]
34. Copetti, R.; Cattarossi, L. Ultrasound diagnosis of pneumonia in children. *La Radiol. Med.* **2008**, *113*, 190–198. [CrossRef]
35. Robinson, T.E.; Leung, A.N.; Chen, X.; Moss, R.B.; Emond, M.J. Cystic fibrosis HRCT scores correlate strongly with pseudomonas infection. *Pediatric Pulmonol.* **2009**, *44*, 1107–1117. [CrossRef]
36. Miller, M.R.; Hankinson, J.; Brusasco, V.; Burgos, F.; Casaburi, R.; Coates, A.; Crapo, R.; Enright, P.; Van Der Grinten, C.P.M.; Gustafsson, P.; et al. Standardisation of spirometry. *Eur. Respir. J.* **2005**, *26*, 319–338. [CrossRef]
37. Quanjer, P.H.; Stanojevic, S.; Cole, T.J.; Baur, X.; Hall, G.L.; Culver, B.H.; Enright, P.L.; Hankinson, J.L.; Ip, M.S.M.; Zheng, J.; et al. Multi-ethnic reference values for spirometry for the 3-95-yr age range: The global lung function 2012 equations. *Eur. Respir. J.* **2012**, *40*, 1324–1343. [CrossRef]
38. Fuchs, S.I.; Eder, J.; Ellemunter, H.; Gappa, M. Lung clearance index: Normal values, repeatability, and reproducibility in healthy children and adolescents. *Pediatr. Pulmonol.* **2009**, *44*, 1180–1185. [CrossRef]

39. Dancey, C.P.; Reidy, J. *Statistics without Maths for Psychology: Using Spss for Windows*; Prentice-Hall, Inc.: Edinburgh, UK, 2004.
40. Hassanzad, M.; Kiani, A.; Abedini, A.; Ghaffaripour, H.; Emami, H.; Alizadeh, N.; Zoghi, G.; Hashemi, S.; Velayati, A.A. Lung ultrasound for the diagnosis of cystic fibrosis pulmonary exacerbation. *BMC Pulm. Med.* **2021**, *21*, 353. [CrossRef]
41. Ciuca, I.; Dediu, M.; Margau, E.; Pop, L. P114 Lung ultrasound score correlation with lung clearance index. *Thorax* **2018**, *73*, A163.
42. Ciuca, I.; Pop, L.; Marc, M.; Oancea, C. How useful is the lung ultrasound in cystic fibrosis? *Eur. Respir. Soc.* **2016**, *48* (Suppl. 60), PA1261.
43. Tana, C.; Ricci, F.; Coppola, M.G.; Mantini, C.; Lauretani, F.; Campanozzi, D.; Renda, G.; Gallina, S.; Lugará, M.; Cipollone, F.; et al. Prognostic Significance of Chest Imaging by LUS and CT in COVID-19 Inpatients: The ECOVID Multicenter Study. *Respiration* **2021**, *101*, 122–131. [CrossRef] [PubMed]
44. Dietrich, C.F.; Mathis, G.; Blaivas, M.; Volpicelli, G.; Seibel, A.; Wastl, D.; Atkinson, N.S.; Cui, X.-W.; Fan, M.; Yi, D. Lung B-line artefacts and their use. *J. Thorac. Dis.* **2016**, *8*, 1356–1365. [CrossRef] [PubMed]
45. Barakat, M. B lines: Role of chest sonography in assessment of bronchiectasis. In: 13 Imaging. *Eur. Respir. Soc.* **2016**, *48*, PA3797.
46. Ghany, M.F.A. Transthoracic ultrasound in the diagnosis of bronchiectasis: Is it valuable? *Egypt. J. Bronchol.* **2019**, *13*, 303–308. [CrossRef]
47. Loeve, M.; Krestin, G.P.; Rosenfeld, M.; de Bruijne, M.; Stick, S.M.; Tiddens, H.A. Chest computed tomography: A validated surrogate endpoint of cystic fibrosis lung disease? *Eur. Respir. J.* **2013**, *42*, 844–857. [CrossRef]

diagnostics

MDPI

Article

Lowering of the Neonatal Lung Ultrasonography Score after nCPAP Positioning in Neonates over 32 Weeks of Gestational Age with Neonatal Respiratory Distress

Alessandro Perri [1], Simona Fattore [1], Vito D'Andrea [1,*], Annamaria Sbordone [1], Maria Letizia Patti [1], Stefano Nobile [1], Chiara Tirone [1], Lucia Giordano [1], Milena Tana [1], Francesca Priolo [1], Francesca Serrao [1], Riccardo Riccardi [2], Giorgia Prontera [1] and Giovanni Vento [1]

[1] Department of Woman and Child Health and Public Health, Fondazione Policlinico Universitario Agostino Gemelli IRCCS, 00168 Rome, Italy
[2] Neonatal Intensive Care Unit, "San Giovanni Calibita Fatebenefratelli" Hospital, Isola Tiberina, 00186 Rome, Italy
* Correspondence: dandrea.vito@gmail.com; Tel.: +39-0630154357; Fax: +39-063383211

Abstract: Respiratory distress (RD) is one of the most common causes of admission to the neonatal intensive care unit. Correct diagnosis and timely intervention are crucial. Lung ultrasonography (LU) is a useful diagnostic tool for the neonatologist in the diagnosis of RD; the neonatal lung ultrasonography score (nLUS) can be used in the diagnostic process, but some authors hypothesise that it is also useful for the management of some neonatal RD. The aim of this study is to analyse the changes in nLUS score before (T0) and after (T1) the start of respiratory support with nasal CPAP in neonates over 32 weeks of age with RD. Thirty-three newborns were enrolled in this retrospective study. LU was performed before and after the start of CPAP. The median nLUS scores at T0 and T1 were 9 (IQR 7–12) and 7 (IQR 4–10), respectively, and showed a significant difference ($p < 0.001$). The magnitude of reduction in nLUS score, expressed as a percentage, was inversely related to the need for subsequent administration of exogenous surfactant. The study suggests the usefulness of the nLUS score in assessing the response to CPAP in neonates over 32 weeks gestational age.

Keywords: lung ultrasonography; respiratory distress syndrome; preterm infants

Citation: Perri, A.; Fattore, S.; D'Andrea, V.; Sbordone, A.; Patti, M.L.; Nobile, S.; Tirone, C.; Giordano, L.; Tana, M.; Priolo, F.; et al. Lowering of the Neonatal Lung Ultrasonography Score after nCPAP Positioning in Neonates over 32 Weeks of Gestational Age with Neonatal Respiratory Distress. *Diagnostics* **2022**, *12*, 1909. https://doi.org/10.3390/diagnostics12081909

Academic Editors: Marcello Demi and Gino Soldati

Received: 17 June 2022
Accepted: 3 August 2022
Published: 7 August 2022

1. Introduction

Respiratory distress (RD) is one of the most common causes of neonatal intensive care unit (NICU) admission in preterm and term infants and is associated with acute and chronic adverse outcomes.

The underlying causes can vary; transient tachypnoea of the newborn (TTN), respiratory distress syndrome (RDS), pneumonia, meconium aspiration syndrome (MAS) and persistent pulmonary hypertension (PPHN) are among the most common [1].

Overall, RD occurs in up to 7% of newborns [2], more commonly in preterm infants, with incidence inversely proportional to gestational age [3–5].

In infants with a gestational age of over 32 weeks (GA), the differential diagnosis between TTN and RDS is difficult. TTN can be treated with oxygen therapy, RDS must be treated with respiratory assistance (RA), although non-invasive ventilation is preferable. Continuous positive airway pressure (CPAP) is mandatory, especially in the acute phase of RDS [6–9]. In addition, treatment of the severe form of this condition includes the administration of exogenous surfactant [10,11].

The need for ICU admission may complicate the management of these neonates, especially if transfer from a spoke centre to a hub centre is required [12]. Predicting the course of RD in neonates over 32 weeks GA is difficult. An objective diagnostic tool capable

of detecting RD early in this particular group of neonates and monitoring treatment would be a useful tool for the neonatologist.

Lung ultrasonography (LU) in NICU is a safe, harmless, bedside diagnostic tool that has been shown to be more accurate than chest X-ray in diagnosing the major neonatal lung diseases. It is also a safe tool that does not use ionising radiation and can be repeated several times if necessary to provide timely information on the progression of the underlying pathology [13,14]. Its use has increased exponentially in recent years [15]. The standardisation of this examination, which by definition depends on the operator, has increased owing to the introduction of protocols and guidelines [16,17]. The main ultrasound signs of the different causes of neonatal respiratory disease are now widely described and allow accurate differentiation between them [18,19]. Lung ultrasonography has a high accuracy in the diagnosis of TTN [20]. The typical ultrasound image of TTN is represented by a symmetrical B-line distribution with a regular pleural line. The double lung point, the transition point between the normal part of the lung and the fluid-filled part, has high specificity for the diagnosis of TTN [21,22].

In contrast, neonates with RDS have an irregular and thickened pleural line, multiple hyperechoic subpleural consolidations, and widespread B-lines. In severe RDS, the lungs may appear completely white due to confluence of B-lines [23–26].

The neonatal lung ultrasonography score (nLUS) is a simple tool that has been shown to accurately predict the need for exogenous surfactant administration [27–29]. It assigns a severity score to pulmonary pathology based on ultrasound patterns of the anterior superior, anterior inferior, and lateral regions. For each area examined, a score of 0 is assigned if only A-lines are present; 1 if A-lines are present in the upper part of the lung and coalescent B-lines are present in the lower part of the lung or at least three B-lines are present; 2 if coalescent B-lines are present; 3 if extensive consolidations are present [28]. The approach does not include examination of the posterior lung areas, as the LUS score aims to screen critically ill patients with an examination that can be performed as quickly as possible and does not necessarily require mobilisation with the associated risk of destabilisation.

The LUS score, performed in the first hour of life, also appears to be able to predict admission to the neonatal intensive care unit (NICU) for transient neonatal tachypnoea or respiratory distress syndrome in term and late-preterm infants [30].

To our knowledge, there are currently no studies comparing the nLUS score before and after the initiation of non-invasive respiratory support in patients with these characteristics. The aim of this study is to analyse the changes in nLUS score in neonates before initiation of respiratory support and during support with nasal CPAP (nCPAP) in order to improve neonatal care. The description of a possible pattern of worsening or improvement of the score may lead to early detection of neonates with a milder or more severe form of RDS and consequently to early treatment.

2. Materials and Methods

This is a retrospective study analysing a group of patients born at Fondazione Policlinico Universitario "A. Gemelli" IRCCS (Rome, Italy) and Fatebenefratelli Isola Tiberina-Ospedale San Giovanni Calibita (Rome, Italy) from December 2019 to January 2021.

The primary aim of this study is to analyse changes in the nLUS score in neonates before the start of respiratory support and during support with nasal CPAP. The secondary aims are to analyse the relation between nLUS, oxygen requirement, clinical course of the underlying pulmonary pathology and to identify and analyse the difference in changes in nLUS score in infants intended to receive replacement therapy with exogenous surfactant versus those who will not need it.

We considered eligible for inclusion in the study every infant of gestational age over 32 weeks presenting respiratory distress at birth (Silverman score ≥ 3) and with nasal CPAP (nCPAP) needed in the first six hours of life, with an oxygen requirement greater than 25%. Exclusion criteria were: genetic or chromosomal abnormalities or major congenital malformations, congenital lung pathologies, congenital heart disease, absence of written

informed consent to participate from parents/legal guardians, timing of ultrasound scans not respected. Within the first 3 h of life (T0), before the start of respiratory support with nCPAP, for any eligible infant, a lung ultrasonography was performed and the nLUS score was calculated. We repeated the exam at 4–6 h of life (T1), during respiratory support, according to our protocols. We reported and analysed the nLUS score, calculated at T0 and T1 (Figure 1). Any infants who needed respiratory assistance before the first scan was excluded from the study. For any eligible infants, written informed consent was obtained from parents or from legal guardians before enrolment. We collected data from clinical record about gestational age, LUS score at T0 and T1, difference between nLUS score at T0 and T1 (nLUS at T0–nLUS at T1) expressed as absolute number and percentage, level of nCPAP used, oxygen requirement, exogenous surfactant administration. We also collected and analysed data about sex, birth weight and antenatal steroids administration.

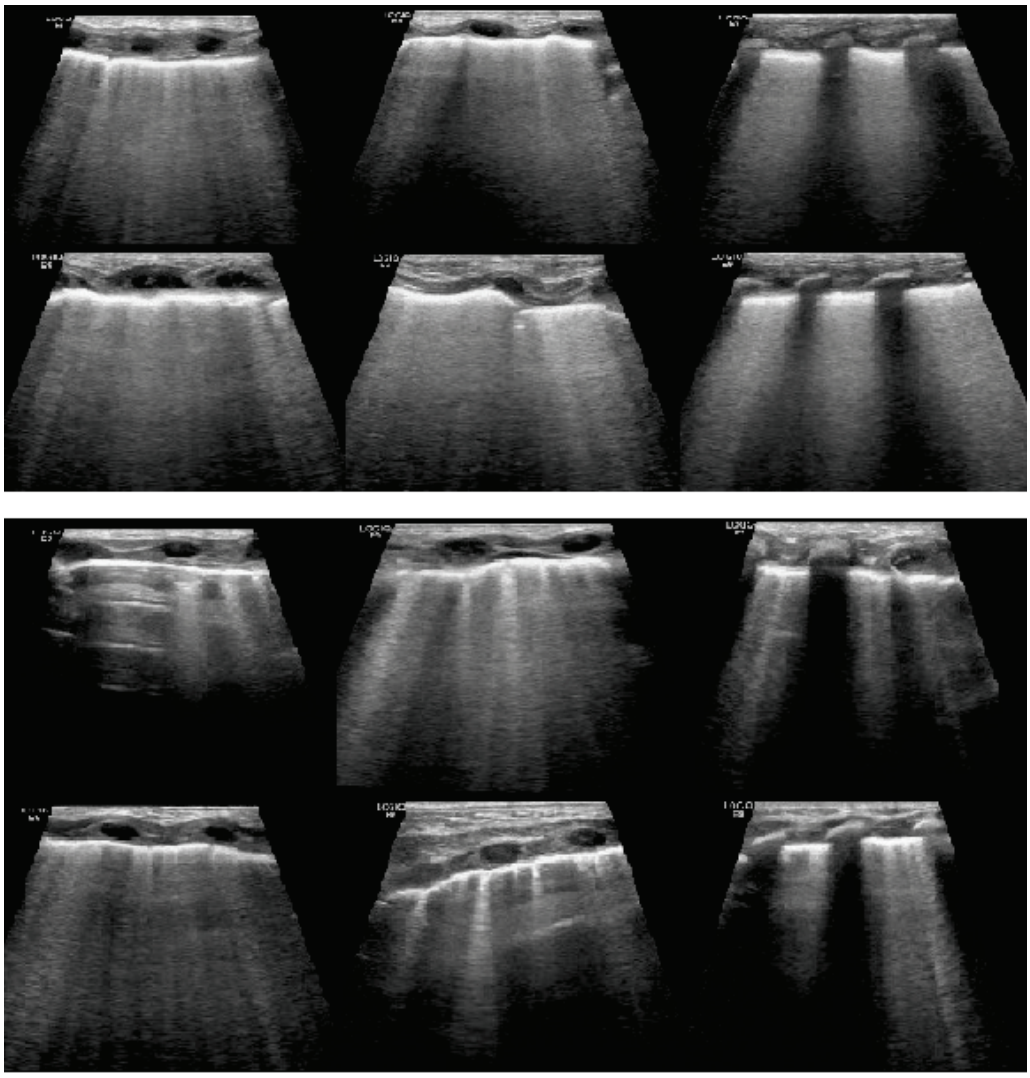

Figure 1. Sonograms at T0 and at T1 of a patient diagnosed with RD. After the positioning of the nCPAP the nlus score has lowered accordingly with the reduction of the coalescent b lines areas. In the second sonogram, the appearance of A lines can easily be noticed.

Non-invasive respiratory assistance and the possible need to administer exogenous surfactant therapy were managed according to European Guidelines [31] and standardised internal protocols. The decision to start support with nCPAP was made in the presence of one of the following criteria: dyspnoea with Silvermann > 3, polypnea with respiratory rate > 75 breaths per minute, oxygen requirement of at least 30% to maintain saturation

in the appropriate range, episodes of apnoea and bradycardia [32]. For all neonates, endotracheal surfactant was administered when oxygen requirements were greater than 30% despite optimisation of non-invasive respiratory care with nCPAP [33].

The nLUS has been previously validated in the neonatal field. Each lung was divided into three areas (upper anterior, lower anterior, lateral) and examined using a linear probe, frequency 12 MHz, through both transverse and longitudinal scans. Images were obtained using a LOGIQ E9 General Electrics ultrasound machine. For each lung area (upper anterior, lower anterior and lateral), a 0–3 score was given relating to lung's echogenicity patterns Figure 2. The total nLUS (between 0 and 18) was obtained from the sum of the scores of the six areas studied. The execution of the ultrasound scans and the assignment of the relative LUS score were carried out by trained physicians. In order to minimise the discomfort of the infants during the examination, ultrasound scans were performed using pre-heated ultrasound gel. Non-pharmacological measures, such as non-nutritive sucking and gentle physical containment, were used to prevent patient agitation. All examinations were performed using sterile disposable probe covers, as established by internal protocols.

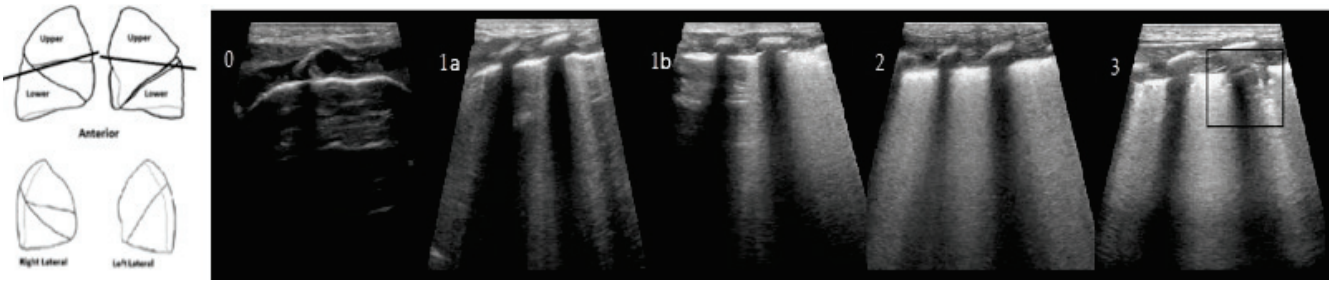

Figure 2. The lung ultrasonography score (nLUS). Lungs are divided into three areas: upper anterior; lower anterior; lateral. Each area is scored. Score values are related to the patterns that are shown in the upper part of the figure. Scores is given as follows: 0, only A-lines; 1a,b, presence at least 3 B-lines or A-lines in the upper part of the lung, coalescent B-lines in the lower part of the lung; 2, coalescent B lines with or without consolidations limited to sub-pleural space; 3, extended consolidation.

Statistical Analysis

Data were analysed using IBM Statistical Package for Social Science 25.0 version (SPSS, Inc., Chicago, IL, USA). Normality of continuous data was evaluated using Shapiro–Wilk test. Because the data distribution was not normal, continuous data are expressed as median and interquartile range (IQR). The dichotomous variables are reported as absolute numbers and percentage. The nLUS score at T0 and T1 were compared using Wilcoxon test for related samples. We obtained the difference between nLUS score at T0 and T1 as absolute number and percentage. Oxygen requirement at T0 and T1 were also compared using Wilcoxon test for related samples. We tested correlation between CPAP level and improvement of nLUS score and between CPAP and oxygen requirement using Spearman correlation. Lastly, we divided the enrolled neonates into two groups, based on the need for therapy with exogenous surfactant, in order to compare the extent of the reduction in the nLUS score in the two groups. The numerical variation of the nLUS score was expressed as absolute number and as percentage and was compared using the Mann Whitney U test. A p-value < 0.05 was considered statistically significant.

3. Results

Thirty-three (33) neonates were included; median GA was 35 (IQR 34–37) and the median of their birth weight was 2530 g (IQR 2230–2993). About 20 neonates (60.6%) had a diagnosis of RDS, 6 neonates had TTN (18.2%), 7 neonates had pneumonia (21.2%). About 13 neonates (39.4%) received exogenous surfactant (Table 1), none of them needed a second dose of surfactant. A total of 13 (39.4%) were infants of diabetic mother.

Table 1. Study population details.

	N = 33
GA (weeks)	35.4 (34.2–37.3)
Birth weight (grams)	2530 (2230–2993)
Vaginal delivery	11 (33.3%)
AGA SGA LGA	29 (87.9%) 2 (6.1%) 2 (6.1%)
Female Male	8 (24.2%) 25 (75.8%)
Antenatal steroids No antenatal steroids	4 (12.1%) 29 (87.9%)
RDS TTN Pneumonia	20 (60.6%) 6 (18.2%) 7 (21.2%)
Exogenous surfactant	13(39.4%)

Data are expressed as number (percentage) or median (IQR).

Only 3 neonates (9.1%) showed worsening lung ultrasonography; 10 neonates (30.3%) remained stable and 20 (60.6%) showed improvement in lung ultrasonography, with significant changes in LUS score after the start of respiratory support with CPAP: the median of nLUS score at T0 was 9 (IQR 7–12), the median of nLUS score at T1 was 7 (IQR 4–10). Wilcoxon test showed a *p*-value < 0.001.

The median of the differences between nLUS at T0 and nLUS at T1 (nLUS T0-nLUS T1) was 2 (IQR 0–3). Levels of CPAP used were between 4 and 8 cm H_2O, depending on the extent of respiratory distress and oxygen requirement.

Median of oxygen requirement was 30% at T0 (IQR 25–30%) and 25% at T1 (22–30%). 19 neonates (58%) had a reduction in oxygen requirements at T1 compared to T0. The difference between oxygen requirement before and during respiratory assistance with CPAP was not significant: Wilcoxon test showed a *p* value of 0.48 (Table 2).

Table 2. nLUS, oxygen requirement before (T0) and after CPAP (T1).

	T0	**T1**	**Z (Wilcoxon)**	***p*-Value**
nLUS	9 (7–12)	7 (4–10)	−3.66	<0.001
FiO_2	30% (25–30%)	25% (22–30%)	−7	0.48

Data are expressed as median (IQR).

Spearman's correlation showed an inverse relation between nLUS T0-nLUS T1 and oxygen requirement at T1, with a coefficient of −0.6 (*p* value 0.001). The extent of the reduction in the nLUS score expressed as a percentage was found to be inversely correlated with the need for subsequent administration of exogenous surfactant with a Spearman coefficient of −0.48 (*p* value 0.005).

About 20 neonates had diagnosis of RDS and 13 received exogenous surfactant. Their gestational age was 34 (IQR 35–37), 6 (46%) were born from diabetic mothers and 8 (62%) were born from caesarean section. Their LUS score was 12 (IQR 7–12) at T0 and 10 (8–12) at T1. Neonates who needed surfactant therapy showed a change in the LUS from T0 and T1 equal to 0 (median; IQR 0–2); those who did not receive surfactant had a variation of 3 (median; IQR 0–6); Mann Whitney U test showed a significant difference between the groups (*p* 0.02) (Table 3). In Table 4 we reported the nLUS score related to underlying pathology.

Table 3. nLUS reduction.

	Exogenous Surfactant (n = 13)	No Exogenous Surfactant (n = 20)	U (Mann Whitney)	*p*-Value
nLUSt0-nLUSt1	0 (0–2)	3 (0–6)	67.5	0.02
nLUSt0-nLUSt1(%)	0% (0–16%)	28%(4–77%)	58	0.007

Data are expressed as median (IQR).

Table 4. nLUS and diagnosis.

	LUS T0	LUS T1	DeltaLUS
RDS	10 (7–12)	8 (6–11)	1.5 (0–2.5)
TTN	8 (7–9)	2 (0–2)	5 (3.25–7)
Pneumonia	9 (7–10)	9 (7–10)	0 (0–0)

4. Discussion

Our results showed an association between the short-term clinical improvement achieved by the use of early CPAP treatment for respiratory distress in neonates and the nLUS score. The majority of patients studied (60.6%) experienced a reduction in nLUS score and clinical improvement, as evidenced by a reduction in oxygen demand (58%) after initiation of respiratory support with CPAP. Current knowledge suggests that the improvement in oxygenation and respiratory mechanics can be explained physio-pathologically by greater alveolar distension with a consequent improvement in the ventilation-perfusion ratio and by the prevention of alveolar collapse. According to recent evidence, early CPAP treatment appears to have several advantages in the treatment of neonatal distress syndrome: By opening the lungs, residual functional capacity can be restored and maintained, reducing airway fatigue and preventing alveolar collapse and re-expansion (atelectotrauma). Early CPAP could also improve surfactant deficit [34]. The nLUS score appears to be effective in monitoring changes in the lungs after the start of respiratory support with CPAP, and we found that the score decreases significantly after the start of CPAP treatment. It also correlates with changes in the trend of oxygen demand.

The level of CPAP does not seem to correlate with the reduction in nLUS score: This seems to indicate a positive effect of non-invasive respiratory support independent of the level of pressure applied. However, with increasing pressure, oxygen demand is significantly reduced, showing a greater clinical benefit for higher pressure values in the range considered (4–8 cm H_2O).

The nLUS score differed according to the underlying pathology: infants with RDS had higher nLUS score values than the others, especially in the group receiving therapy with exogenous surfactant. This confirms what has already been reported in the literature, namely that the nLUS score is able to predict the need for exogenous surfactant with good accuracy. Although the small sample size does not allow the development of a ROC curve and the consistent establishment of a cut-off, the infants receiving surfactant had higher LUS score values than the infants treated with non-invasive respiratory support.

The magnitude of the reduction in nLUS score, expressed as a percentage, was inversely correlated with the need for subsequent administration of exogenous surfactant.

We found an inverse relationship between nLUS T0-nLUS T1 and oxygen demand at T1.

This is useful information to assist the clinician in making decisions about the management of the neonate with respiratory distress, especially when the decision involves transfer from a spoke centre to a hub centre, hospitalisation in the NICU and administration of exogenous surfactant. An objective diagnostic tool capable of early detection and monitoring of the progression of RD in this population of neonates would be a useful tool for the neonatologist and could reduce the time between the onset of the patient's symptoms and their treatment.

The main limitations of the study are the retrospective study design, the small sample size and the heterogeneity of the characteristics (gestational age, neonatal weight, pathology, level of assistance needed) of the patients studied. In addition, a modified nLUS score has recently been proposed [35]. In the new score, the examination of the posterior lung fields is added. It would be interesting to repeat these data in a prospective study using the modified nLUS score.

In summary, these are promising results suggesting the serial use of lung ultrasonography and the LUS score not only in the initial diagnosis but also in the monitoring of newborns with respiratory problems. Indeed, lung ultrasonography could be a valuable tool to assess in real time the actual improvement in lung status after starting respiratory support. It is an aid for the clinician to adjust management and subsequent support accordingly, increasing or decreasing as needed. In addition, lung ultrasonography can help the clinician to select patients who do or do not require administration of exogenous surfactant. In the last decade, some concerns have been raised about the harmfulness of ultrasound. However, these concerns should be taken with a grain of salt. There are only a few studies on this topic, mostly based on animal models. One of the most interesting is by Schneider-Kolsky et al. [36]. In this paper, pulsed Doppler ultrasound was found to be harmful to the brain of chicks and may impair cognitive functions. To our knowledge, these data have not been confirmed in any study on human models. In any case, it is right to limit the use of Doppler ultrasound on the brain to selected patients and diseases. No harmful effects have been found with ultrasound of the lungs. On the other hand, the ionising effect of X-rays on the chest is very well-known. At present, it is imperative to limit neonatal exposure to X-rays [37], and this goal can be achieved thanks to the increasing use of ultrasound and wireless ultrasound probes [38], which offer the highest level of safety in the diagnostic treatment of neonates, including those isolated for SARS-CoV-2.

5. Conclusions

The study suggests the usefulness of the nLUS score for assessing response to CPAP in neonates over 32 weeks GA. The nLUS score appears to decrease in infants who respond to CPAP; little or no decrease in nLUS score after CPAP may identify infants who require early administration of exogenous surfactant. Further studies are needed to confirm these findings.

Author Contributions: Conceptualisation, A.P. and S.F.; methodology, F.P.; software, G.P.; validation, V.D. and G.V.; formal analysis, L.G.; investigation, C.T., R.R. and S.N.; resources, F.S. and M.L.P.; data curation, A.S.; writing—original draft preparation, A.P. and S.F.; writing—review and editing, V.D.; visualisation, M.T.; supervision, V.D., S.N. and A.P.; project administration, G.V. All authors have read and agreed to the published version of the manuscript.

Funding: This research received no external funding.

Institutional Review Board Statement: The study was conducted in accordance with the Declaration of Helsinki, and approved by the Institutional Ethics Committee Ethics Committee of the Fondazione Policlinico Universitario A. Gemelli IRCCS, Rome, Italy (N. 50294/19 ID2898, 11-06-2020).

Informed Consent Statement: Informed consent was obtained from all subjects involved in the study. Written informed consent has been obtained from the parents to publish this paper.

Data Availability Statement: The data presented in this study are available on request from the corresponding author.

Acknowledgments: Ministero della Salute–Ricerca Corrente 2022.

Conflicts of Interest: The authors declare no conflict of interest.

References

1. Reuter, S.; Moser, C.; Baack, M. Respiratory distress in the newborn. *Pediatr. Rev.* **2014**, *35*, 417–428. [CrossRef] [PubMed]
2. Edwards, M.O.; Kotecha, S.J.; Kotecha, S. Respiratory distress of the term newborn infant. *Paediatr. Respir. Rev.* **2013**, *14*, 29–36. [CrossRef] [PubMed]

3. Pramanik, A.K.; Rangaswamy, N.; Gates, T. Neonatal respiratory distress: A practical approach to its diagnosis and management. *Pediatr. Clin. N. Am.* **2015**, *62*, 453–469. [CrossRef] [PubMed]
4. Hogden, L.; Munger, K.; Duffek, S. Neonatal Respiratory Distress. *S D Med.* **2021**, *74*, 28–35.
5. Liszewski, M.C.; Stanescu, A.L.; Phillips, G.S.; Lee, E.Y. Respiratory Distress in Neonates: Underlying Causes and Current Im-aging Assessment. *Radiol. Clin. N. Am.* **2017**, *55*, 629–644. [CrossRef]
6. Mahoney, A.D.; Jain, L. Respiratory Disorders in Moderately Preterm, Late Preterm, and Early Term Infants. *Clin. Perinatol.* **2013**, *40*, 665–678. [CrossRef]
7. Chowdhury, O.; Wedderburn, C.J.; Duffy, D.; Greenough, A. CPAP review. *Eur. J. Pediatr.* **2012**, *171*, 1441–1448. [CrossRef]
8. Behnke, J.; Lemyre, B.; Czernik, C.; Zimmer, K.-P.; Ehrhardt, H.; Waitz, M. Non-Invasive Ventilation in Neonatology. *Dtsch. Arztebl. Int.* **2019**, *116*, 177–183. [CrossRef]
9. Schmölzer, G.M.; Kumar, M.; Pichler, G.; Aziz, K.; O'Reilly, M.; Cheung, P.-Y. Non-invasive versus invasive respiratory support in preterm infants at birth: Systematic review and meta-analysis. *BMJ* **2013**, *347*, f5980. [CrossRef]
10. Jha, K.; Nassar, G.N.; Makker, K. *Transient Tachypnea of the Newborn*; StatPearls Publishing: Treasure Island, FL, USA, 2022.
11. Alhassen, Z.; Vali, P.; Guglani, L.; Lakshminrusimha, S.; Ryan, R.M. Recent Advances in Pathophysiology and Management of Transient Tachypnea of Newborn. *J. Perinatol.* **2021**, *41*, 6–16. [CrossRef]
12. Neonatal Respiratory Distress in the Community Hospital: When to Transport, When to Keep. Available online: https://www.thefreelibrary.com/Neonatal+respiratory+distress+in+the+community+hospital%3A+when+to...-a020582095 (accessed on 15 June 2022).
13. Corsini, I.; Parri, N.; Ficial, B.; Dani, C. Lung ultrasound in the neonatal intensive care unit: Review of the literature and future perspectives. *Pediatr. Pulmonol.* **2020**, *55*, 1550–1562. [CrossRef] [PubMed]
14. Perri, A.; Riccardi, R.; Iannotta, R.; Di Molfetta, D.V.; Arena, R.; Vento, G.; Zecca, E. Lung ultrasonography score versus chest X-ray score to predict surfactant administration in newborns with respiratory distress syndrome. *Pediatr. Pulmonol.* **2018**, *53*, 1231–1236. [CrossRef] [PubMed]
15. Miller, L.E.; Stoller, J.; Fraga, M.V. Point-of-care ultrasound in the neonatal ICU. *Curr. Opin. Pediatr.* **2020**, *32*, 216–227. [CrossRef]
16. Liu, J.; Copetti, R.; Sorantin, E.; Lovrenski, J.; Rodriguez-Fanjul, J.; Kurepa, D.; Feng, X.; Cattaross, L.; Zhang, H.; Yeh, T.F.; et al. Protocol and Guidelines for Point-of-Care Lung Ultrasound in Diagnosing Neonatal Pulmonary Diseases Based on International Expert Consensus. *J. Vis. Exp.* **2019**, e58990. [CrossRef] [PubMed]
17. Kurepa, D.; Zaghloul, N.; Watkins, L.; Liu, J. Neonatal lung ultrasound exam guidelines. *J. Perinatol.* **2017**, *38*, 11–22. [CrossRef] [PubMed]
18. Ramaswamy, V.V.; More, K.; Roehr, C.C.; Bandiya, P.; Nangia, S. Efficacy of noninvasive respiratory support modes for primary respiratory support in preterm neonates with respiratory distress syndrome: Systematic review and network meta-analysis. *Pediatr. Pulmonol.* **2020**, *55*, 2940–2963. [CrossRef] [PubMed]
19. Ma, H.-R.; Liu, J.; Yan, W.-K. Accuracy and Reliability of Lung Ultrasound to Diagnose Transient Tachypnoea of the Newborn: Evidence from a Meta-analysis and Systematic Review. *Am. J. Perinatol.* **2020**, *39*, 0973–0979. [CrossRef]
20. Ruoss, J.L.; Bazacliu, C.; Cacho, N.; De Luca, D. Lung Ultrasound in the Neonatal Intensive Care Unit: Does It Impact Clinical Care? *Children* **2021**, *8*, 1098. [CrossRef]
21. He, L.; Sun, Y.; Sheng, W.; Yao, Q. Diagnostic performance of lung ultrasound for transient tachypnea of the newborn: A me-ta-analysis. *PLoS ONE* **2021**, *16*, e0248827. [CrossRef]
22. Li, C.-S.; Chu, S.-M.; Lien, R.; Mok, T.-Y.; Hsu, K.-H.; Lai, S.-H. Prospective investigation of serial ultrasound for transient tachypnea of the newborn. *Pediatr. Neonatol.* **2021**, *62*, 64–69. [CrossRef]
23. Gregorio-Hernández, R.; Arriaga-Redondo, M.; Pérez-Pérez, A.; Ramos-Navarro, C.; Sánchez-Luna, M. Lung ultrasound in preterm infants with respiratory distress: Experience in a neonatal intensive care unit. *Eur. J. Pediatr.* **2020**, *179*, 81–89. [CrossRef] [PubMed]
24. Zong, H.F.; Guo, G.; Liu, J.; Yang, C.Z.; Bao, L.L. Wet lung leading to RDS: The lung ultrasound findings and possible mechanisms—A pilot study from an animal mode. *J. Matern.-Fetal Neonatal Med.* **2021**, *34*, 2197–2205. [CrossRef]
25. Ibrahim, M.; Omran, A.; AbdAllah, N.; El-Sharkawy, S. Lung ultrasound in early diagnosis of neonatal transient tachypnea and its differentiation from other causes of neonatal respiratory distress. *J. Neonatal-Perinat. Med.* **2018**, *11*, 281–287. [CrossRef]
26. Oktem, A.; Yigit, S.; Oğuz, B.; Celik, T.; Haliloğlu, M.; Yurdakok, M. Accuracy of lung ultrasonography in the diagnosis of respiratory distress syndrome in newborns. *J Matern.-Fetal Neonatal Med.* **2021**, *34*, 281–286. [CrossRef] [PubMed]
27. De Martino, L.; Yousef, N.; Ben-Ammar, R.; Raimondi, F.; Shankar-Aguilera, S.; De Luca, D. Lung Ultrasound Score Predicts Surfactant Need in Extremely Preterm Neonates. *Pediatrics* **2018**, *142*, e20180463. [CrossRef] [PubMed]
28. Brat, R.; Yousef, N.; Klifa, R.; Reynaud, S.; Aguilera, S.; De Luca, D. Lung Ultrasonography Score to Evaluate Oxygenation and Surfactant Need in Neonates Treated with Continuous Positive Airway Pressure. *JAMA Pediatr.* **2015**, *169*, e151797. [CrossRef] [PubMed]
29. Raimondi, F.; Migliaro, F.; Corsini, I.; Meneghin, F.; Pierri, L.; Salomè, S.; Perri, A.; Aversa, S.; Nobile, S.; Lama, S.; et al. Neonatal Lung Ultrasound and Surfactant Administration: A Pragmatic, Multicenter Study. *Chest* **2021**, *160*, 2178–2186. [CrossRef]
30. Poerio, A.; Galletti, S.; Baldazzi, M.; Martini, S.; Rollo, A.; Spinedi, S.; Raimondi, F.; Zompatori, M.; Corvaglia, L.; Aceti, A. Lung ultrasound features predict admission to the neonatal intensive care unit in infants with transient neonatal tachypnoea or respiratory distress syndrome born by caesarean section. *Eur. J. Pediatr.* **2020**, *180*, 869–876. [CrossRef]

31. Sweet, D.G.; Carnielli, V.; Greisen, G.; Hallman, M.; Ozek, E.; Te Pas, A.; Plavka, R.; Roehr, C.C.; Saugstad, O.D.; Simeoni, U.; et al. European Consensus Guidelines on the Management of Respiratory Distress Syndrome—2019 Update. *Neonatology* **2019**, *115*, 432–450. [CrossRef]
32. Ng, E.H.; Shah, V. Guidelines for surfactant replacement therapy in neonates. *Paediatr. Child Health* **2021**, *26*, 35–41. [CrossRef]
33. Ho, J.J.; Subramaniam, P.; Davis, P.G. Continuous positive airway pressure (CPAP) for respiratory distress in preterm infants. *Cochrane Database Syst Rev.* **2020**, *10*, CD002271. [PubMed]
34. Ho, J.J.; Subramaniam, P.; Sivakaanthan, A.; Davis, P.G. Early versus delayed continuous positive airway pressure (CPAP) for respiratory distress in preterm infants. *Cochrane Database Syst. Rev.* **2020**, *10*, CD002975. [CrossRef] [PubMed]
35. Szymański, P.; Kruczek, P.; Hożejowski, R.; Wais, P. Modified lung ultrasound score predicts ventilation requirements in neonatal respiratory distress syndrome. *BMC Pediatr.* **2021**, *21*, 17. [CrossRef] [PubMed]
36. Schneider-Kolsky, M.E.; Ayobi, Z.; Lombardo, P.; Brown, D.; Kedang, B.; Gibbs, M.E. Ultrasound exposure of the foetal chick brain: Effects on learning and memory. *Int. J. Dev. Neurosci.* **2009**, *27*, 677–683. [CrossRef]
37. Komatsu, C.V.; Silva, C.C.; De Souza, L.R.M.F.; Gonçalves, L.F. Excess Radiation to Newborns Hospitalized in the Intensive Care Unit. *Radiat. Prot. Dosim.* **2017**, *177*, 331–341. [CrossRef]
38. Prontera, G.; Perri, A.; Vento, G.; D'Andrea, V. Use of Wireless Ultrasound Probe in Isolated Infants: A Case Report of Two SARS-CoV-2-Positive Mothers' Newborns. *Neonatology* **2022**, *119*, 129–132. [CrossRef]

diagnostics

MDPI

Review

What Is COVID 19 Teaching Us about Pulmonary Ultrasound?

Gino Soldati [1] and Marcello Demi [2,*]

[1] Ippocrate Medical Center, 55032 Lucca, Italy; soldatigino@yahoo.it
[2] Department of Bioengineering, Fondazione Toscana Gabriele Monasterio, 56126 Pisa, Italy
* Correspondence: demi@ftgm.it; Tel.: +39-050-3152618

Abstract: In lung ultrasound (LUS), the interactions between the acoustic pulse and the lung surface (including the pleura and a small subpleural layer of tissue) are crucial. Variations of the peripheral lung density and the subpleural alveolar shape and its configuration are typically connected to the presence of ultrasound artifacts and consolidations. COVID-19 pneumonia can give rise to a variety of pathological pulmonary changes ranging from mild diffuse alveolar damage (DAD) to severe acute respiratory distress syndrome (ARDS), characterized by peripheral bilateral patchy lung involvement. These findings are well described in CT imaging and in anatomopathological cases. Ultrasound artifacts and consolidations are therefore expected signs in COVID-19 pneumonia because edema, DAD, lung hemorrhage, interstitial thickening, hyaline membranes, and infiltrative lung diseases when they arise in a subpleural position, generate ultrasound findings. This review analyzes the structure of the ultrasound images in the normal and pathological lung given our current knowledge, and the role of LUS in the diagnosis and monitoring of patients with COVID-19 lung involvement.

Keywords: COVID-19; clinical review; lung ultrasound imaging

Citation: Soldati, G.; Demi, M. What Is COVID 19 Teaching Us about Pulmonary Ultrasound?. *Diagnostics* **2022**, *12*, 838. https://doi.org/10.3390/diagnostics12040838

Academic Editor: Koichi Nishimura

Received: 3 February 2022
Accepted: 26 March 2022
Published: 29 March 2022

1. Introduction

Chest ultrasonography is gaining ever more consideration among physicians as a useful diagnostic tool. In recent years, cardiologists, intensivists, and many pulmonologists have explored the diagnostic capability of ultrasound in chest diseases.

Novel aspects in clinical methodology regarding how to approach respiratory patients with the help of ultrasound have already been discussed in literature [1,2].

Moreover, recent studies have furthered our knowledge of the physical mechanisms underlying the formation of the images in lung ultrasound (LUS) [3–10].

The recent COVID-19 pandemic has contributed to expanding the indications for the use of ultrasound to assess and monitor viral lung lesions. However, problems have also emerged relating to the poor specificity of the ultrasound findings reported in the pulmonary involvement of COVID-19 [11] and the need for better knowledge of the ultrasound signs connected to the interstitial diseases (which are notoriously represented by artifacts) strongly emerged.

Similarly to what has been already done to distinguish between primary pulmonary and secondary cardiogenic lung pathology [12], a valuable strategy is that of integrating the morphological data related to ultrasound and data derived from both the clinical examination and the epidemiological context.

Knowledge of the relationship between artefactual images and the superficial histology of the lung, in terms of airspace distribution [5], represents a field of extreme interest since this can improve the low specificity of ultrasound signs of sonographic interstitial syndrome (SIS).

Ultimately, the ultrasound semeiotics of the lung are based on artefactual findings and anatomical images (consolidations) [13].

Lung artifacts carry important information on the subpleural density and subpleural structural disorder [5,14,15]. The more the lung is similar to air, the more evident the

replicas of the pleural line (generically called A-Lines) and the replica and mirror effects of the thoracic wall structures will be. Conversely, the denser the pulmonary subpleural layer is, the more vertical artifacts (known as B-Lines) and white lung will be visualized.

B-lines represent a large variety of vertical artifacts that identify a wide range of superficial lung diseases that do not consolidate the organ. The pathology is represented by edema (cardiogenic and non), non-consolidating pneumonia, and interstitial lung diseases and by all those conditions that are able to modify the subpleural ratio between full and empty, in favor of the former. Lung consolidations appear when the lung is severely air-deprived [13].

Based on current knowledge, in this review we will synthetize the physical basis of the artifacts and consolidations that are observed in LUS images and the relationships of these findings with the explored histopathology in COVID-19 pulmonary damage.

COVID-19 pneumonia has a macro/micromorphology and histopathological pattern of which we have sufficient knowledge through CT images and postmortem examinations, and its prevailing anatomical picture is an inhomogeneous increase of subpleural density (due to interstitial thickening and consolidation). Consequently, the experience acquired in the laboratory along with the clinical use of LUS can be used for the LUS interpretation of a COVID-19 pulmonary injury.

1.1. Historical Perspective of Ultrasound (US) Vertical Artifacts

While the meaning and genesis of A-Lines and consolidations are well known, in this section special emphasis will be given to the significance of vertical lung artifacts, generally known as B-Lines.

References to vertical artifacts in ultrasound imaging date back to the 1980s. "Comet-tail artifacts" were described in abdominal and thoracic ultrasound images even though a clear explanation regarding their origin was not provided [16,17].

In 1985 Avruch explained the origin of vertical artifacts in experimental models as a "resonance" phenomenon occurring when the ultrasound enters a fluid film surrounded by a tetrahedral disposition of bubbles. These artifacts were named "ring-down artifacts" [18].

In their seminal work, Lichtenstein and co-workers described pulmonary "comet-tail artifacts" related to pulmonary edema [19,20]. By comparing ultrasound images with chest CT scans at the same level, an association between these artifacts (subsequently called B-Lines) and thickened interlobular septa was observed. With these observations as a starting point an association between the "comet-tail artifacts" or B-Lines and increased pulmonary extravascular water was speculated. Many studies observed a correlation between the number of vertical artifacts and the severity or the evolution of the cardiogenic pulmonary edema [21].

In many cardiological and critical care settings, the presence of "comet-tail artifacts" was considered synonymous with the presence of pulmonary extravascular water, even if the evidence showed that these artifacts were present in many pathological conditions of the pulmonary interstitium [22].

More recently, the hypothesis that the US vertical artifacts do not represent discrete anatomical structures of the lung, but are the expression of the ultrasound interaction on a lung surface (the immediately subpleural tissue), which is denser than normal but not yet consolidated [3,7], has been proposed.

In other words, several anatomic structures may be responsible for the genesis of the artifacts. The requirement for this is essentially the existence of acoustically permissive structures (acoustic channels and traps) surrounded by aerated spaces and linked to the pleura. In this sense, not only may the thickened interlobular septa be responsible for the vertical artifacts [23,24], but micronodules, groups of collapsed alveoli, neo production of collagen, and so on, could also be responsible.

A clear demonstration of this is the possibility of reproducing similar artifacts in non-biological materials [10,24] and in healthy lungs when deflated to a critical, non-physiological level of density [14].

1.2. An Introduction to the Clinical Use of Artifacts

Traditionally, the most important artefactual patterns in LUS are A-lines, B-lines, and white lung [12,13].

A-lines are horizontal artifacts related to a normal pleural plane. A-lines are a replica of the pleural line and a blurred superposition of the parietal acoustic discontinuities appears between the pleura line and the first A-line (as well as between every pair of subsequent A-lines) due to the mirror and replica effects caused by the strong reflection of the pleural line [7], (Figure 1). This pattern represents how ultrasound scanners visualize the echo signals that are bouncing between the probe, the chest wall planes, and the lung surface.

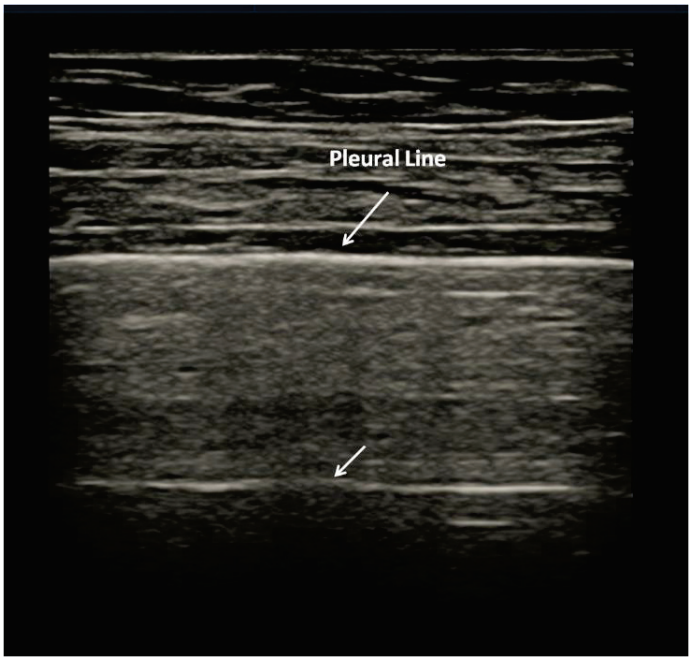

Figure 1. Normal lung. Pleural line is regular. The first artefactual replica of the pleural line is clearly seen (deeper arrow). Between the pleural line and the first A-line, a blurred superposition of the parietal acoustic discontinuities appears due to the mirror and replica effects caused by the strong reflection of the pleural line. Linear probe, 8 MHz.

The expression of the A-lines is however closely linked to the acoustic energy incident on the pleural plane and to its reflectivity, and introduces further useful elements for better ultrasound semeiotics of the lung, as it is possible that in many lung pathologies the reflectivity of the pleural line may be impaired (see later) [4,7,10].

As already mentioned, the so-called B-Lines are linked to the existence of acoustic traps distributed along the pleural surface, which are capable of capturing the acoustic energy among the aerated spaces and returning it as a prolonged signal over time. According to this view, acoustic energy can be partially trapped and subsequently re-radiated towards the probe after multiple reflections between the separated aerated spaces, giving rise to vertical artifacts [4,7,9,10].

Some recent studies have validated this hypothesis and introduced further elements for a more accurate definition of the relationships between the morphology of the artifacts and the distribution of the air spaces within the subpleural interstitium. In essence, this links the distribution and visual appearance of the different B-lines to the subpleural histology [5] (Figures 2 and 3).

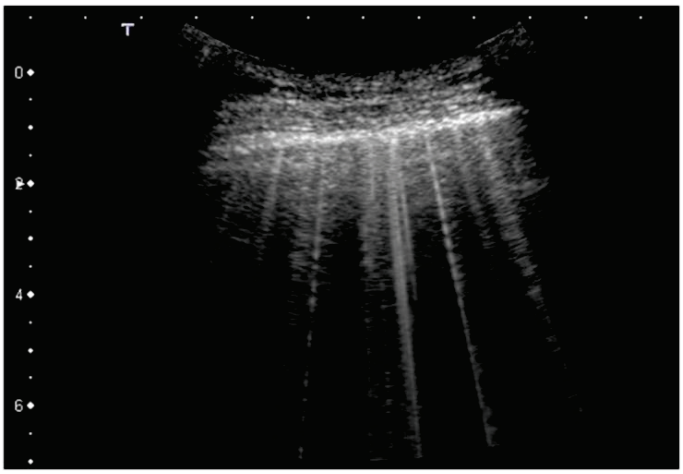

Figure 2. B-lines with variable appearance (cardiogenic pulmonary edema). B-lines are qualitatively characterized by their brightness, the full screen extension, the pleural origin, and the presence or absence of internal modulation. Convex probe, 6 MHz.

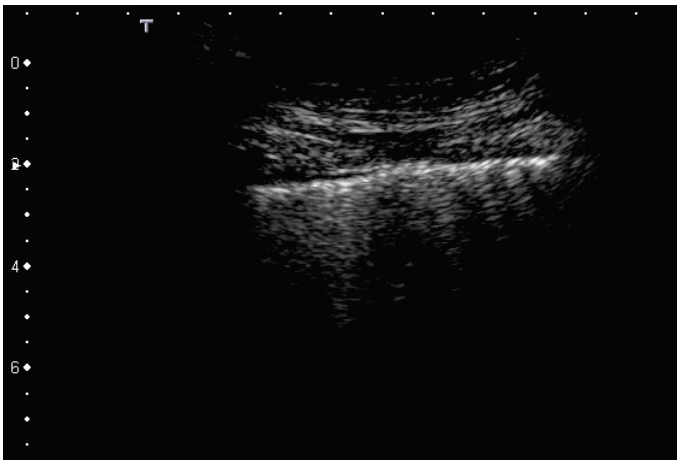

Figure 3. Vertical artifacts from a patient with scleroderma and pulmonary fibrosis. They show variable brightness, width, and length. Convex probe, 3 MHz.

In our opinion, therefore, considerable importance is assumed by the morphology of the artifacts as it is shown that the configuration of the acoustic traps determines the appearance of the individual artifacts. A large list of phenomena and configurations acting as active acoustic channels along the pleural surface may play a crucial role in producing many different types of artifacts in many diffuse and localized superficial interstitial diseases, which depend on different re-arrangements of the air spaces. Therefore, every pair of acoustic channel and acoustic trap has its own spectral signature, which is related to the shape, size, and nature of the medium that constitutes the channel and the trap [6,7,10]. In practical terms, a visual inspection can show different vertical artifacts with respect to their pleural origin. Every vertical artifact has its own structure [5,20]. It can show a sequence of alternating white and black/gray horizontal bands (Figure 3) or a constant gray level, or it can appear more or less confused as has been illustrated by mathematical and physical models [7,9]. The width of the vertical artifacts is variable and this can even change from the start to the end point.

The imaging parameters play a fundamental role in the formation of the artifacts, and the visibility of a vertical artifact depends on multiple non-orthogonal factors. Therefore, given the intrinsic variability of the artifacts as a function of multiple factors, making an

objective diagnosis on the basis of the artefactual information is a difficult task when using the usual ultrasound devices [6].

Differences in the appearance of vertical artifacts between hydrostatic (cardiogenic) lung edema and adult respiratory distress syndrome (ARDS) were described some years ago [12] (Table 1). In light of recent evidence [25], the differences can be determined by the distribution and morphology of the acoustic traps generated in the two pathologies. A review on the ultrasound differential diagnosis of pulmonary and cardiac interstitial pathology reiterated some of these important concepts in light of current knowledge regarding the response of the pleural plane to ultrasound waves [26].

Table 1. Differences between acute cardiogenic pulmonary edema (ACPE) and ARDS (pneumogenic) sonographic interstitial syndrome (SIS).

Cardiogenic	Pneumogenic
Diffuse homogenous SIS	Diffuse inhomogeneous SIS, and spared areas
Smooth, linear, and regular pleural line	Coarse, irregular, and cobbled pleural line
Bright (laser-like), and modulated artifacts	Rough attenuated vertical artifacts
Normal sliding sign	Reduced sliding sign

In some cases of particular subpleural echogenicity, the term "vertical artifacts" or B-Lines is not appropriate, even if the echogenic aspect may recall the coalescence of several vertical artifacts.

White lung [3,7,12] is a focal or multifocal LUS artifact, characterized by an undifferentiated echogenic background, with the absence of A-lines, and without clear evidence of vertical artifacts. This pattern suggests the presence of a relatively random scatterer distribution (many small airspaces close to each other which contribute to the formation of many small acoustic traps) which gives rise to a complex multiple scattering phenomenon. It appears to correlate with CT ground-glass attenuation.

In conclusion, from a clinical point of view, lung pathological artifacts indicate a physical state of the subpleural lung that is denser, but which has not yet consolidated, caused by: (1) interstitial pathology enlarging the interstitial tissue but sparing residual peripheral air spaces; (2) pathological deflations of a normal healthy lung or pathological subversion of peripheral air spaces; or (3) mixed situations. In this way, the anatomic term "interstitial syndrome", used to describe the presence of vertical artifacts could be changed to "hyperdense not-consolidated subpleural lung". The spatial distribution and the variations in the morphology of the vertical artifacts can provide information on the structure of the subpleural lung at infra-millimeter dimensional levels. In the next sections the generic term of sonographic interstitial syndrome (SIS) is still used for historical reasons.

2. Clinical Interpretation of SIS

SIS is a non-specific echographic pattern. As it appears in various pathologies of the lung, its interpretation must include further information relating to its appearance and clinical context. Similarly, ultrasound COVID-19 findings, being also based on the presence of SIS, are not specific in themselves. To increase the specificity of ultrasound, when approaching SIS, it is important to focus on four steps in every situation:

1. Characteristics of the pleural line;
2. Characteristics of the artifacts;
3. Extension and distribution of SIS;
4. Relationships with clinical data and integrated multi-district sonography.

2.1. Characteristics of the Pleural Line

Once an US pulse reaches the visceral pleural surface it is near-totally reflected by the non-diseased lung because the size of the intra and interalveolar septa are relatively

thin (with respect to the wave length of the carrier frequency). In these cases, the US pulse meets a sort of air wall, it is near-totally reflected towards the probe and the outer lung surface is represented as a thick white line where the thickness of this line is related to the length of the US pulse. It is necessary, here, to highlight that the perceived thickness of the pleural line is, in theory, equal to the length of the US pulse. However, this is true only if the direction of the wave propagation is orthogonal to the pleural plane. When the insonation is not orthogonal, and, even more importantly, when the visceral pleura is not "healthy" (in the presence of slightly thickened interstitial spaces, for example), it can appear blurred and apparently thickened.

In cases where the pleura is not a good acoustic reflector, even in the absence of vertical artifacts, the signs to be taken into consideration are the blurred and thickened appearance of the pleural line and, as a consequence, the less evident replica and mirror effects of the parietal structures below it.

The above is in agreement with known clinical experience. In ACPE, the pleural line is regular, smooth, linear, and with normal sliding. Generally, in primitive pulmonary interstitial diseases, the pleura contributes to the generation of artifacts, and is stably irregular, cobbled or even finely interrupted, especially in the basal regions [26–28]. Typical signs of ARDS are spared areas, and a normal or poorly altered pleural line with normal sliding next to areas with irregular pleura, which shows reduced or absent movements [29–31]. The pleural line is slight and focally irregular in score 1 (see Section 4) COVID-19, and becomes progressively more irregular as the disease progresses.

2.2. Artifacts' Characteristics

Different vertical artifacts are observed in acute cardiogenic pulmonary edema (ACPE), and acute respiratory distress syndrome (ARDS) or pulmonary fibrosis [3,29] (see Figure 3 and Table 1).

In the case of ACPE (especially early ACPE), the lung architecture remains unchanged and shows only septal enlargement by transudate. The artifacts in early pulmonary edema are B-lines with their characteristic pleural point-like origin and brightness. In contrast, in pulmonary fibrosis, vertical artifacts are variable in morphology and distribution, and are often distinguishable by their low level of brightness and rapid attenuation.

In ARDS, the artefactual pattern is pneumogenic, inhomogeneous, and typically gravitational, with the most aerated lung in an elevated position and the denser or consolidated lung in the sloping position [32].

In COVID-19, a distribution of artifacts similar to that seen in early ARDS is present, but many single B-lines are brighter, and patchy columnar areas of white lung can be seen.

2.3. Extension and Distribution

SIS can be either focal, multifocal, or diffuse [27]. Mono- or oligofocal SIS is often seen around monolateral pulmonary consolidation, representing a denser but not consolidated tissue. This finding is suggestive of bacterial pneumonia.

When SIS is diffuse and bilateral, it is indicative of a diffuse pulmonary pathology. It can be either homogeneous or inhomogeneous. Homogeneous SIS can show a gravitational distribution, without spared areas. This could be indicative of cardiogenic pulmonary edema [12]. When SIS is bilateral and inhomogeneous, with spared areas, it could be indicative of non-cardiogenic pathology [22,26]. SIS in COVID-19 patients is typically pneumogenic and appears inhomogeneous and patchy, and is more prevalent in the basal portions of the lungs.

2.4. Relationships with Clinical Data and Integrated Multi-District Sonography

Given the non-specificity of vertical artifacts, it is only possible to suspect that one condition is more probable than another through an inferential abductive process of reasoning, which allows clinicians to make a more accurate diagnosis [1].

Knowledge of the clinical history and the preclinical probability of disease is useful and becomes crucial in the event of a COVID-19 epidemic. In the case of suspected cardiogenic SIS, echocardiography can add much information (cardiac signs of diastolic/systolic heart failure) [29]. Inferior caval vein dynamics give a rough preload estimate. A multi-district approach is useful when many diseases co-occur to establish a clinical picture or when cardiac or renal complications occur in COVID-19 patients.

In the case of diffuse pneumogenic SIS associated with fibrotic interstitial lung diseases (ILDs), a typical appearance and distribution of artifacts with a congruent clinical picture (non-epidemic, subacute, or chronic onset) can aid in the diagnosis. Creating an acoustic pulmonary map is useful for narrowing down the diagnostic options, especially in diffuse ILDs [31].

3. Clinical Basis of COVID-19 Lung Ultrasound Imaging

Coronavirus disease 2019 (COVID-19) appeared in Wuhan, China, in December 2019, and rapidly increased to a pandemic level around the world. Its etiological agent is a novel coronavirus named severe acute respiratory syndrome coronavirus 2 (SARS-CoV-2) [33]. In the previous two decades, coronaviruses have caused other epidemic diseases—SARS-CoV-1 and Middle East respiratory syndrome (MERS-CoV). In SARS-CoV-1 coronavirus pneumonia, peripheral lung involvement was common but unifocal involvement was more common than multifocal or bilateral involvement. On CT images, GGOs with consolidations were the main findings, and reticulation was noted after the second week [34]. On CT images, MERS-CoV pneumonia showed subpleural and basilar airspace lesions, with extensive subpleural GGO and consolidation. Studies concerning the use of US in SARS-CoV-1 and in MERS-CoV are lacking. However, on the basis of the CT findings, we can suppose that the ultrasound signs in these pathologies would have been similar to those in patients with COVID-19. COVID-19, SARS-CoV-1, and MERS-CoV cause lung damage and, in their final stages, also multiorgan failure [35].

In general, in COVID-19 the most serious initial symptoms are related to pneumonia, while the evolution towards respiratory failure is similar to ARDS [36]. In light of our current knowledge regarding COVID-19, this picture may be too simplistic.

Many viruses cause pneumonia. Histopathology of viral pneumonia varies, and is related to the pathogenesis of pulmonary infection. Consequently, a computed tomographic (CT) pattern of viral pneumonia reports, at best, the fine pathology at the lobular level. Generally, interstitial viral pneumonitis shows a thickened interstitium with lymphocytic infiltration, and viral particles can be seen in both the bronchial and alveolar epithelium. Hyperplasia and desquamation of the alveolar lining cells and hemorrhage are the result of the harmful action of some viruses [37]. Histopathological findings in cases of SARS-CoV-1 and influenza infection (H1N1, H5N1) are characterized by diffuse alveolar damage (DAD), hemorrhage, edema, and hyaline membrane [31].

The histopathological picture of initial COVID-19 involvement is characterized by patchy DAD, interstitial thickness, and pneumocyte hyperplasia. Late stages show alveolar congestion, desquamation, organizing pneumonia, and hemorrhage [38–40]. More recent papers pay attention to the thickening of alveolar capillaries surrounded by edema, intraluminal fibrin thrombi, and CD61+ megakaryocytes in association with platelets [41]. Despite a direct viral infection of the endothelial cells being reported, other mechanisms of vascular involvement have been proposed. Magro et al. [42] examined lung tissue from five COVID-19 patients with respiratory failure. Histopathological patterns were characterized by significant capillary fibrin deposition. Vascular deposits of terminal complement components (C5-b9, C4d, MASP2) were noted, suggesting a systemic activation of a lectin-based complement pathway. Therefore, a complement-mediated coagulative dysregulation is possible. The proportion of COVID-19 patients with abnormal initial radiographic findings is low (50% or less). In these patients, chest computed tomography (CT) has a high sensitivity (97%) but a lower specificity (56%) for lung involvement, showing subpleural patchy ground-glass opacities (GGO), reticular and crazy paving patterns, and

finally consolidations. A study demonstrated that lung involvement gradually increased to consolidation up to two weeks after the onset of the disease (72%, half of these with subsegmental appearance). In general, consolidations are considered an indication of disease progression [43,44].

When interpreting the lung ultrasound findings related to COVID-19, both the structural variations of the superficial lung tissue and CT findings are important. The former defines the appearance of the ultrasound images while the latter their sonographic visibility (only superficial alterations are visible with LUS).

In CT, GGO are present in 100% of cases, appearing in peripheral locations in 89% of cases. While 93% of patients have multilobar and posterior lung involvement, 91% of patients have bilateral findings [43]. These characteristics allow us to indicate ultrasound as a diagnostic tool in COVID-19 lung involvement. In accordance with the physical basis of the formation of ultrasound images, reticular and ground-glass opacities appear as artifacts, while the consolidative ones are anatomical tissue images [13,45].

Ultrasound reproduces superficial consolidations in explorable thoracic regions with excellent accuracy, including the presence of air and fluid bronchograms. Consolidations, that are evident in CT, appear on ultrasound if they emerge from the pleura. CT superficial interstitial thickenings appear on ultrasound as small consolidations or as vertical artifacts with variable lengths and modulations in relation to their shape and size. Ground-glass CT typically appears as white lung [3,4,13].

4. SIS in COVID-19

SIS is an expected finding in COVID-19 because edema, DAD, lung hemorrhage, interstitial thickening, hyaline membranes, and non-consolidative infiltrative lung diseases (if abutting the pleura) generate artefactual signs in LUS. In physical terms, the common denominator of these conditions is an increase in the density of the involved lung areas compared to the healthy lung [15]. The topographical distribution of COVID-19 findings, as visible in CT, justifies their appearance and the typically bilateral, multilobar, and patchy pattern [1]. The most affected lung areas are the posteroinferior (93.8%) followed by the lateral (88.7%) [46].

Many studies have addressed lung ultrasound findings in COVID-19 patients. Most of these adapted past experiences in other fields (intensive-care medicine and ARDS-CoV-1) to COVID-19 cases. In clinical practice, there are various ways to assess the extent of pulmonary involvement in COVID-19. In general, the larger the number of the explored areas, the greater the likelihood of a significant picture of overall lung involvement.

A total of 12 areas over the chest, namely the anterosuperior, anteroinferior, laterosuperior, lateroinferior, posterosuperior, and posteroinferior lung regions on each side, showed an optimal accuracy [47]. In agreement with this method, scoring (generally from 0 to 3) each area in accordance with the most severe lung ultrasound finding gives a total gravity score (for example, when exploring six regions on each hemithorax a maximum of 36 is reached).

Clinical and experimental evidence concerning the relationships between pulmonary ultrasound signs and changes in the subpleural histology [5,7,48] allowed the formulation of a specific gravity score of COVID-19, which was initially computed in 14 areas, and published at the beginning of the pandemic [49,50]. This score is synthetized in Table 2 and in Figure 4.

This specific methodology was subsequently validated by two studies attributing a prognostic validity to the US COVID-19 score, and proposing an evidence-based approach through a specific methodology [51,52].

Similarly, using different practical approaches, much literature data supports these original suggestions, showing both the utility of chest ultrasonography in pulmonary COVID-19 and the correlations between the diagnostic CT and ultrasound findings, whether this be at the level of a first diagnosis or as predictive tools in COVID-19 patients.

Table 2. COVID-19 Scores.

Score	Description
0	Pleural line is regular. Horizontal artifacts and mirror effects are present. Normal lung.
1	Pleural line has slight alterations with sporadic vertical bright artifacts. The presence of relatively small acoustic channels due to focal interstitial thickening is speculated.
2	Pleural line has relevant alterations. Progression of subversion of peripheral air space geometry causes a predominance of vertical artifacts. Small subpleural consolidations, related to deaeration, can be present.
3	Pleural line is irregular and cobbled. Subpleural lung is denser and more disordered. White lung with or without larger consolidations may be present. Small and large consolidations are subpleural regions minimally or completely deprived of air.

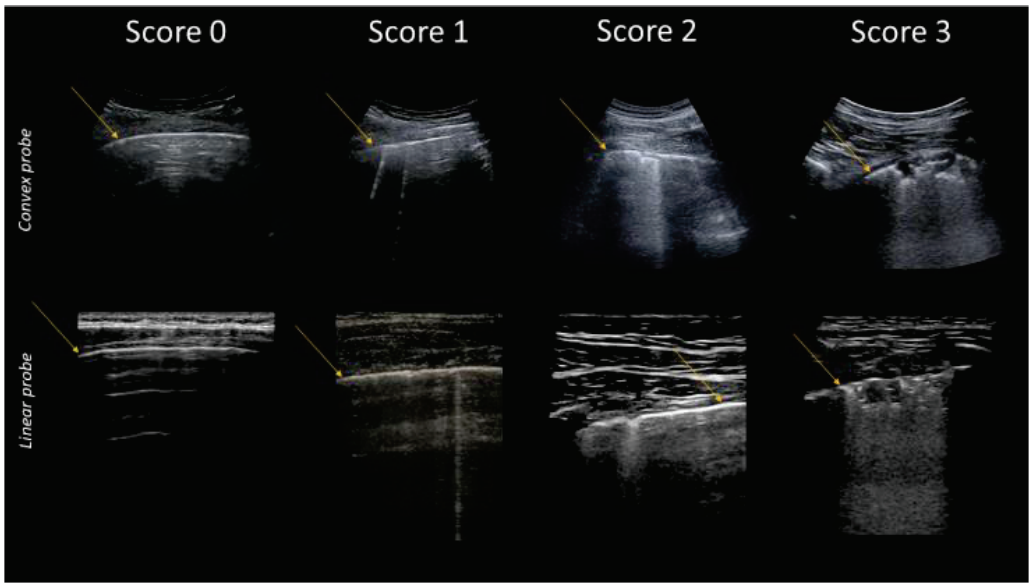

Figure 4. Classification of pathological lung ultrasound findings in COVID-19 patients. Arrows indicate the pleural line. Top: convex probe. Bottom: linear probe.

All in all, LUS represents a valuable tool in symptomatic patients with high negative predictive value for ruling out the disease.

As compared to HRCT, LUS is characterized by a very high sensitivity and specificity in detecting signs of interstitial pneumonia in COVID-19 patients (77–97% and 77–100%, respectively) [53–55].

From a technical point of view CT and US provide completely different assessments (CT scans lung parenchymal volumes, while in SIS, ultrasound generates a surface density map) and for this reason the diagnostic agreement between LUS and CT in terms of score was not always adequate.

However, in practical terms, LUS can be considered as an equally accurate alternative for CT in many situations where CT is not easily accessible or when molecular tests are not available. The use of lung ultrasound (LUS) as a triage tool has been proposed since the beginning of the COVID-19 pandemic [49] and subsequent studies have confirmed its role [56]. The high sensitivity of ultrasound for the superficial lesions of the lung from the interstitial stages represents its great value. Despite not showing pathognomonic COVID-19-signs, LUS is an established point-of-care tool for the evaluation of patients in the emergency department [57]. Every trained physician evaluating the admitted patients can perform an LUS to make a primary discrimination between subjects with pneumonia and subjects without pneumonia, and to monitor its pulmonary status.

Other aspects are worthy of mention. Asymptomatic carriers represent 17.9–33.3% of patients with COVID-19 [58,59] and they may contribute to the spread of the infection. The yield of screening for COVID-19 with LUS in asymptomatic patients is not known. In a retrospective study 22% of the asymptomatic patients with positive COVID-19 RT-PCR showed LUS findings. In comparison, LUS showed a positive predictive value of 100% [60].

The usefulness of LUS to predict complications in COVID-19 pneumonia has been described and sonography seems a powerful predictor of in-hospital mortality, playing a crucial role in risk stratification of patients with COVID-19.

Lung ultrasound score measured at the time of inclusion of the patients was independently associated with admission to the intensive care unit, the need for supplemental oxygen and respiratory support, and mortality. Conversely, a normal scan within 24 h of admission is indicative of a positive evolution of the pathology [61–63].

Moreover, LUS involvement in COVID-19 patients correlated with IL-6 levels and with the P/F ratio [64]. In hospitalized COVID-19 patients, pathological LUS was associated with venous thromboembolism [65].

Finally, using the score proposed in [50], a median value higher than 24 was associated with an almost 6-fold increase in the odds of worsening, defined as a combination of high-flow oxygen support, intensive care unit admission, or 30-day mortality as the primary end-point [51].

The worsening of pneumonia in patients with COVID-19 appears in echography with the spatial diffusion of signs of interstitial disease and consolidations. This is in accordance with the proposed grading system. On the contrary, the clinical improvement coincides with the regression of these findings (vertical artifacts, white lung, and consolidations), which leads to a downstaging of the score. Mild signs of interstitial pathology (vertical artifacts) may persist for a long time or indefinitely (see Section 7).

Beyond its use as a diagnostic and prognostic tool, LUS can be used to define optimal PEEP, guide recruitment, or monitor recruitment and should be part of the diagnostic toolset in intensive care units [66]. Ultrasound-guided recruitment is generally carried out according to the principles set out by Bouhemad et al. [67].

US signs of COVID-19 pneumonia are not specific, as they are also present to various degrees in other pathologies. Therefore, the diagnostic accuracy of pulmonary ultrasound in this pathology is strongly influenced by the pretest probability of belonging to an exposed population in a particular epidemiological context, and showing compatible symptoms.

As for any etiology of acute respiratory distress, lung ultrasound must incorporate examinations of the pleura, and of the cardiovascular system, so as to detect myocarditis, for example, and to acquire some hemodynamic data at least.

Five SARS-CoV-2 variants are known—alpha, beta, gamma, delta, and omicron. The delta variant was dominant in the summer of 2021 and the omicron variant was identified in November 2021. There are currently no data demonstrating differences in ultrasound appearance between COVID-19 variants in cases of pneumonia [68].

5. Why Does COVID-19 Consolidate the Lung?

Radiographic and ultrasound lung consolidations are characteristic findings in bacterial pneumonia and atelectasis. In viral pneumonia, CT ground-glass opacities (GGO) are usual, while consolidations can be present. These, however, are rare in varicella zoster, Epstein-Barr, paramyxo- and hantavirus pulmonary involvement [37]. Peripheral GGOs are typical in COVID-19, explaining the frequency of SIS in this disease. Consolidations are observed with CT in 72% of COVID-19 patients [43]. Subsegmental consolidative peripheral involvement is present in half of the subjects. Gravitational consolidations, on the other hand, are characteristic of ARDS patients. In ARDS microatelectasis are seen in the early phase. Atelectasis, reduced lung compliance, organizing pneumonia, bacterial infections, and pulmonary fibrosis develop in the fibroproliferative or reparative phases. The distribution of densities results from the generalized increase in weight of the overlying lung causing compression in a sponge like manner [65].

The nature of the lung consolidation in COVID-19 is complex, and theoretically, all the mechanisms described are possible. However, knowledge of the nature of these lesions would have a positive impact on the pharmacological and ventilatory treatment of these subjects.

Gattinoni et al. [69] noted that COVID-19 subjects with respiratory failure showed different patterns of pneumonia with different pathophysiology. At the beginning a "Type L" of pulmonary involvement, characterized by a nearly normal compliance, low pulmonary weight, CT GGO, and low lung recruitability may be seen. The evolution of this phenotype, if it occurs, is towards a "Type H" pattern, showing low compliance, high pulmonary weight, non-aerated tissue, and high lung recruitability.

In COVID-19 the transition between different pulmonary phenotypes probably depends on the interaction of many factors, one of the most important of which could be a maladaptive immune response rather than an increased viral load.

An immune overreaction was described in SARS-CoV-1 and MERS-CoV and in severe influenza (H1N1, H5N1) [70,71]. Cytokine storm causing severe capillary damage and organ dysfunction was supposed. Systemic vasculitis was observed in one report of SARS-CoV-1 [72].

Considering the relationships between inflammation, immunity, and coagulation, the evidence of endothelial activation, upregulation of adhesion molecules, endothelial disruption, and activation of coagulation pathways in many bacterial, viral, and parasitic (malaria) diseases is not surprising. In all these situations, an activation of complement component C3 could exacerbate vascular damage. It is interesting to note that excessive complement activation may lead to the activation of a clotting pathway and diffuse thrombotic microangiopathy, and is responsible for a massive local release of pro-inflammatory cytokines [42,73].

In ultrasound, COVID-19 consolidations have the appearance of small cuneiform lesions abutting the pleura, often containing a central echogenic spot of residual air (Score 3), surrounded by white lung (see Figure 5).

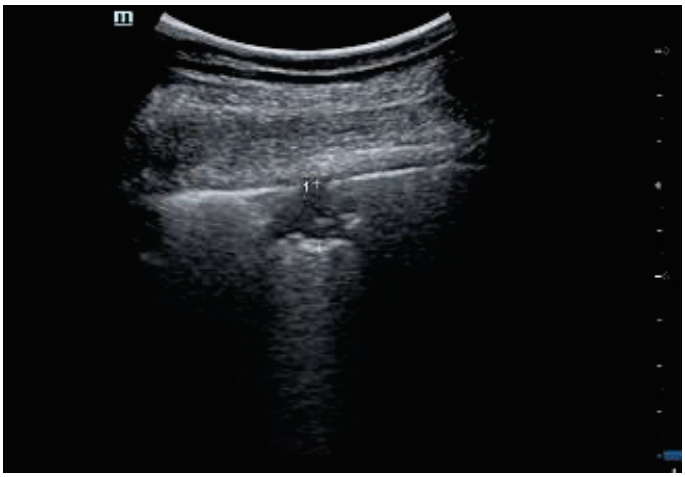

Figure 5. Patient with COVID-19 lung involvement. A small consolidation under the pleura, surrounded by white lung.

The major consolidations are generally seen in a posterobasal, laterobasal, or superior position, with or without air bronchograms. Observations related to histopathological findings of hemorrhage, vascular fibrin, and cell deposition and clotting have already been discussed. Recently, Tang et al. [74] showed that in 183 patients with confirmed COVID-19, the non-survivors revealed significantly higher D-dimer and fibrin degradation product (FDP) levels compared to the survivors. Therefore, despite atelectasis-organizing pneumonia and complete alveolar exudation maybe being the cause of consolidations, the hypotheses of vascular, thrombotic, or ischemic lung damage which are at the base of

some of these findings, should be considered. A published report on three patients with confirmed COVID-19 pneumonia, in which contrast-enhanced ultrasound (CEUS) imaging was conducted to study lung consolidations [75], showed an abnormal early, inhomogeneous, and partial arterial enhancement without evidence of a segmentary arrangement of pulmonary arteries. Consolidations of less than 2 cm did not show enhancement.

These observations suggest the existence of a further pattern of COVID-19 lung involvement in which some consolidations do not represent atelectasis or easily recruitable areas, but rather tissue with large perfusion defects. Further confirmations of these observations would imply a complete review of the therapies for COVID-19, which should be finely tuned not only as regards the antiviral approach, but also regarding the selective ventilation methods and valid treatments to interrupt the many targets of the maladaptive immune response.

In this context, ultrasound (B-mode and CEUS) can play a key role as a predictive instrument of aggravation by detecting and characterizing the consolidations, and as a tool for managing a targeted therapy and ventilation.

6. COVID-19 in Pediatrics

During the COVID-19 pandemic, LUS played an important role in screening affected individuals and also, to a lesser extent, the pediatric population [76]. The clinical COVID-19 manifestations in children are mild or moderate compared to adults. Dong et al. [77] reported that approximately 4% of children were asymptomatic, 51% had a mild illness, 39% had a moderate illness, and 6% had a severe or critical illness. In those pediatric patients who contracted COVID-19, vertical artifacts, pleural irregularities, subpleural consolidations, and patchy white lung were described. Musolino et al. [78] confirmed the presence of bilateral lung involvement in 70% of the patients and pleural irregularities in 60% of the patients. Children with a moderate disease presented more vertical artifacts than patients with a mild disease (85.7% vs. 36.4%, respectively). No pleural effusion was detected. Denina et al. [79] noted subpleural consolidations in 25% of cases and confluent B-lines in 62%. The existing studies confirm that LUS findings in children are similar to those described in adults and are not specific for the COVID-19 disease.

7. Post-Acute Sequelae of COVID-19 Pneumonia

Little is known about the possible clinical complications persisting after the resolution of acute COVID-19. Among hospitalized patients with COVID-19 respiratory impairment, over 50% show abnormalities on CT and the latter are more common in subjects with a more severe pulmonary disease [80].

The most common abnormalities are ground-glass opacity, densities in the form of subpleural bands, reticular thickening, and evidence of fibrotic changes with air trapping. It has been speculated that some patients could progress to advanced lung fibrosis or post-COVID interstitial lung disease [81].

In view of the high sensitivity of pulmonary ultrasound in detecting parenchymal alterations in primary and secondary fibrosing diseases of the lung [3], it is conceivable that LUS may have a role in post-COVID patient surveillance. In some studies LUS showed an outstanding discrimination ability compared to CT in identifying fibrotic changes in the post-COVID-19 follow-up [82]. LUS should be proposed as the first-line tool in follow-up programs, while chest CT could be performed based on LUS findings.

8. Conclusions

Lung ultrasound is nowadays a rapidly evolving field. The COVID-19 pandemic has contributed to a better understanding of its technical basis and its clinical use. In this review we highlighted known clinical applications, as well as US findings and applications of lung US in the context of the current COVID-19 pandemic.

Chest US is used to a great extent in the bedside management of COVID-19 pneumonia (home, emergency department, ward, and ICU) and for monitoring the evolution

of lung lesions. Lung US is comparable to CT for detecting the superficial parenchymal involvement in COVID-19 and its severity. Moreover, based on the ultrasound findings, a prognostic stratification of the patients can be implemented.

In the face of a general poor specificity of ultrasound signs in COVID-19 pneumonia, there is a need for a better understanding of the physical mechanisms that determine the image formation starting from the received ultrasound signals, together with the use of a dedicated methodology and signal-processing procedures.

Author Contributions: Conceptualization, G.S.; methodology, G.S. and M.D.; validation, G.S. and M.D.; writing—original draft preparation, G.S.; writing—review and editing, M.D.; supervision, project administration, G.S. and M.D. All authors have read and agreed to the published version of the manuscript.

Funding: This research received no external funding.

Institutional Review Board Statement: Not applicable.

Acknowledgments: The authors wish to thank the Fondazione della Cassa di Risparmio di Lucca for its invaluable support.

Conflicts of Interest: The authors declare no conflict of interest.

References

1. Soldati, G.; Smargiassi, A.; Mariani, A.A.; Inchingolo, R. Novel aspects in diagnostic approach to respiratory patients: Is it the time for a new semiotics? *Multidiscip. Respir. Med.* **2017**, *12*, 15. [CrossRef] [PubMed]
2. Narula, J.; Chandrashekhar, Y.; Braunwald, E. Time to Add a Fifth Pillar to Bedside Physical Examination: Inspection, Palpation, Percussion, Auscultation, and Insonation. *JAMA Cardiol.* **2018**, *1*, 346–350. [CrossRef] [PubMed]
3. Soldati, G.; Demi, M.; Smargiassi, A.; Inchingolo, R.; Demi, L. The role of ultrasound lung artifacts in the diagnosis of respiratory diseases. *Expert Rev. Respir. Med.* **2019**, *13*, 163–172. [CrossRef] [PubMed]
4. Soldati, G.; Demi, M.; Inchingolo, R.; Smargiassi, A.; Demi, L. On the physical basis of pulmonary sonographic interstitial syndrome. *J. Ultrasound Med.* **2016**, *35*, 2075–2086. [CrossRef]
5. Soldati, G.; Smargiassi, A.; Demi, L.; Inchingolo, R. Artefactual lung ultrasonography: It is a matter of traps, order, and disorder. *Appl. Sci.* **2020**, *10*, 1570. [CrossRef]
6. Demi, L.; Egan, T.; Muller, M. Lung Ultrasound Imaging, a Technical Review. *Appl. Sci.* **2020**, *10*, 462. [CrossRef]
7. Demi, M.; Prediletto, R.; Soldati, G.; Demi, L. Physical Mechanisms Providing Clinical Information From Ultrasound Lung Images: Hypotheses and Early Confirmations. *IEEE Trans. Ultrason. Ferroelectr. Freq. Control* **2020**, *67*, 612–623. [CrossRef]
8. Mohanty, K.; Blackwel, J.; Egan, T.; Muller, M. Characterization of the Lung Parenchyma Using Ultrasound Multiple Scattering. *Ultrasound Med. Biol.* **2017**, *43*, 993–1003. [CrossRef]
9. Demi, M. The impact of multiple concurrent factors on the length of the US pulmonary vertical artifacts as illustrated through the experimental and numerical analysis of simple models. *J. Acoust. Soc. Am.* **2021**, *150*, 2106–2115. [CrossRef]
10. Demi, M. On the Replica of US Pulmonary Artifacts by Means of Physical Models. *Diagnostics* **2021**, *11*, 1666. [CrossRef]
11. De Carvalho, L.S.; Da Silva Júnior, R.T.; Oliveira, B.V.S.; De Miranda, Y.S.; Rebouças, N.L.F.; Loureiro, M.S.; Pinheiro, S.L.R.; da Silva, R.S.; Correia, P.V.S.L.M.; Maria José Souza Silva, M.J.S.; et al. What the imaging exams show about the disease. *World J. Radiol.* **2021**, *13*, 122–136. [CrossRef] [PubMed]
12. Copetti, R.; Soldati, G.; Copetti, P. Chest sonography: A useful tool to differentiate acute cardiogenic pulmonary edema from acute respiratory distress syndrome. *Cardiovasc. Ultrasound* **2008**, *6*, 16. [CrossRef] [PubMed]
13. Volpicelli, G.; Elbarbary, M.; Blaivas, M.; Lichtenstein, D.A.; Mathis, G.; Kirkpatrick, A.W.; Melniker, L.; Gargani, L.; Noble, V.E.; Via, G.; et al. International Liaison Committee on Lung Ultrasound (ILC-LUS) for International Consensus Conference on Lung Ultrasound (ICC-LUS). International evidence-based recommendations for point-of-care lung ultrasound. *Intensive Care Med.* **2012**, *38*, 577–591. [CrossRef] [PubMed]
14. Soldati, G.; Inchingolo, R.; Smargiassi, A.; Sher, S.; Nenna, R.; Inchingolo, C.D.; Valente, S. Ex vivo lung sonography: Morphologic-ultrasound relationship. *Ultrasound Med. Biol.* **2012**, *38*, 1169–1179. [CrossRef]
15. Soldati, G.; Smargiassi, A.; Inchingolo, R.; Sher, S.; Nenna, R.; Valente, S.; Inchingolo, C.D.; Corbo, G.M. Lung ultrasonography may provide an indirect estimation of lung porosity and airspace geometry. *Respiration* **2014**, *88*, 458–468. [CrossRef]
16. Ziskin, M.C.; Thickman, D.I.; Goldenberg, N.J.; Lapayowker, M.S.; Becker, J.M. The comet tail artifact. *J. Ultrasound Med.* **1982**, *1*, 1–7. [CrossRef]
17. Thickman, D.I.; Ziskin, M.C.; Goldenberg, N.J.; Linder, B.E. Clinical manifestations of the comet tail artifact. *J. Ultrasound Med.* **1983**, *2*, 225–230. [CrossRef]
18. Avruch, L.; Cooperberg, P.L. The ring-down artifact. *J. Ultrasound Med.* **1985**, *4*, 21–28. [CrossRef]

19. Lichtenstein, D.; Mezière, G.; Biderman, P.; Gepner, A.; Barré, O. The comet-tail artifact: An ultrasound sign of alveolar interstitial syndrome. *Am. J. Respir. Crit. Care Med.* **1997**, *156*, 1640–1646. [CrossRef]
20. Dietrich, C.F.; Mathis, G.; Blaivas, M.; Volpicelli, G.; Seibel, A.; Wastl, D.; Atkinson, N.S.S.; Cui, X.W.; Fan, M.; Yi, D. Lung B-line artifacts and their use. *J. Thorac. Dis.* **2016**, *8*, 1356–1365. [CrossRef]
21. Picano, E.; Frassi, F.; Agricola, E.; Gligorova, S.; Gargani, L.; Mottola, G. Ultrasound lung comets: A clinically useful sign of extravascular lung water. *J. Am. Soc. Echocardiogr.* **2006**, *19*, 356–363. [CrossRef] [PubMed]
22. Reissig, A.; Kroegel, C. Transthoracic sonography of diffuse parenchymal lung disease: The role of comet tail artifacts. *J. Ultrasound Med.* **2003**, *22*, 173–180. [CrossRef]
23. Soldati, G.; Giunta, V.; Sher, S.; Melosi, F.; Dini, C. "Synthetic" comets: A new look at lung sonography. *Ultrasound Med. Biol.* **2011**, *37*, 1762–1770. [CrossRef] [PubMed]
24. Soldati, G.; Copetti, R.; Sher, S. Sonographic interstitial syndrome: The sound of lung water. *J. Ultrasound Med.* **2009**, *28*, 163–174. [CrossRef] [PubMed]
25. Demi, L.; van Hoeve, W.; van Sloun, R.J.G.; Soldati, G.; Demi, M. Determination of a potential quantitative measure of the state of the lung using lung ultrasound spectroscopy. *Sci. Rep.* **2017**, *7*, 12746. [CrossRef] [PubMed]
26. Soldati, G.; Demi, M. The use of lung ultrasound images for the differential diagnosis of pulmonary and cardiac interstitial pathology. *J. Ultrasound* **2017**, *20*, 91–96. [CrossRef] [PubMed]
27. Smargiassi, A.; Inchingolo, R.; Soldati, G.; Copetti, R.; Marchetti, G.; Zanforlin, A.; Giannuzzi, R.; Testa, A.; Nardini, S.; Valente, S. The role of chest ultrasonography in the management of respiratory diseases: Document II. *Multidiscip. Respir. Med.* **2013**, *8*, 55. [CrossRef]
28. Demi, L.; Demi, M.; Smargiassi, A.; Inchingolo, R.; Faita, F.; Soldati, G.; Task Force Group. Ultrasonography in lung pathologies: New perspectives. *Multidiscip. Respir. Med.* **2014**, *9*, 27. [CrossRef]
29. Soldati, G.; Demi, M.; Demi, L. Ultrasound patterns of pulmonary edema. *Ann. Transl. Med.* **2019**, *7* (Suppl. 1), S16. [CrossRef]
30. Koegelenberg, C.F.; von Groote-Bidlingmaier, F.; Bolliger, C.T. Transthoracic ultrasonography for the respiratory physician. *Respiration* **2012**, *84*, 337–350. [CrossRef]
31. Smargiassi, A.; Inchingolo, R.; Calandriello, C.; Lombardi, F.; Calabrese, A.; Siciliano, M.; Larici, A.R.; Demi, L.; Richeldi, L.; Soldati, G. Possible Role of Chest Ultrasonography for the Evaluation of Peripheral Fibrotic Pulmonary Changes in Patients Affected by Idiopathic Pulmonary Fibrosis-Pilot Case Series. *Appl. Sci.* **2020**, *10*, 1617. [CrossRef]
32. Pesenti, A.; Musch, G.; Lichtenstein, D.; Mojoli, F.; Amato, M.B.P.; Cinnella, G.; Gattinoni, L.; Quintel, M. Imaging in acute respiratory distress syndrome. *Intensive Care Med.* **2016**, *42*, 686–698. [CrossRef] [PubMed]
33. Chen, N.; Zhou, M.; Dong, X.; Qu, J.; Gong, F.; Han, Y.; Qiu, Y.; Wang, J.; Liu, Y.; Wei, Y.; et al. Epidemiological and clinical characteristics of 99 cases of 2019 novel coronavirus pneumonia in Wuhan, China: A descriptive study. *Lancet* **2020**, *395*, 507–513. [CrossRef]
34. Muller, N.L.; Ooi, G.C.; Kong, P.L.; Nicolaou, S. Severe Acute Respiratory Syndrome: Radiographic and CT Findings. *AJR Am. J. Roentgenol.* **2003**, *181*, 3–8. [CrossRef]
35. Ajlan, A.M.; Ahyad, R.A.; Jamjoom, L.G.; Alharthy, A.; Madani, T.A. Middle East Respiratory Syndrome Coronavirus (MERS-CoV) Infection: Chest CT Findings. *AJR Am. J. Roentgenol.* **2014**, *203*, 782–787. [CrossRef]
36. Zhu, N.; Zhang, D.; Wang, W.; Li, X.; Yang, B.; Song, J.; Zhao, X.; Huang, B.; Shi, W.; Lu, R.; et al. A novel coronavirus from patients with pneumonia in China, 2019. *N. Engl. J. Med.* **2020**, *382*, 727–733. [CrossRef]
37. Koo, H.J.; Lim, S.; Choe, J.; Choi, S.H.; Sung, H.; Do, K.H. Radiographic and CT features of viral pneumonia. *Radiographics* **2018**, *38*, 719–739. [CrossRef]
38. Ruuskanen, O.; Lathi, E.; Jennings, L.C.; Murdoch, D.R. Viral pneumonia. *Lancet* **2011**, *377*, 1264–1275. [CrossRef]
39. Tian, S.; Hu, W.; Niu, L.; Liu, H.; Xu, H.; Xiao, S.Y. Pulmonary pathology of early phase 2019 novel coronavirus (COVID-19) pneumonia in two patients with lung cancer. *J. Thorac. Oncol.* **2020**, *15*, 700–704. [CrossRef]
40. Fox, S.E.; Akmatbekov, A.; Harbet, J.L.; Li, G.; Brown, J.Q.; Heide, R.S.V. Pulmonary and cardiac pathology in COVID-19: The first autopsy series from New Orleans. *Lancet Respir. Med.* **2020**, *8*, 681–686. [CrossRef]
41. Caramaschi, S.; Kapp, M.E.; Miller, S.E.; Eisemberg, R.; Johnson, J.; Epperly, G.; Maiorana, A.; Silvestri, G.; Giannico, G.A. Histopathological findings and clinicopathologic correlation in COVID-19: A systematic review. *Mod. Pathol.* **2021**, *34*, 1614–1633. [CrossRef] [PubMed]
42. Magro, C.; Mulvey, J.J.; Berlin, D.; Nuovo, G.; Salvatore, S.; Harp, J.; Baxter-Stoltzfus, A.; Laurence, J. Complement associated microvascular injury and thrombosis in the pathogenesis of severe COVID-19 infection: A report of five cases. *Transl. Res.* **2020**, *220*, 1–13. [CrossRef] [PubMed]
43. Caruso, D.; Zerunian, M.; Polici, M.; Pucciarelli, F.; Polidori, T.; Rucci, C.; Guido, G.; Bracci, B.; De Dominicis, C.; Laghi, A. Chest Ct features of COVID-19 in Rome, Italy. *Radiology* **2020**, *296*, 79–85. [CrossRef] [PubMed]
44. Shi, H.; Han, X.; Jiang, N.; Cao, Y.; Alwalid, O.; Gu, J.; Fan, Y.; Zheng, C. Radiological findings from 81 patients with COVID-19 in Wuhan, China: A descriptive study. *Lancet Infect. Dis.* **2020**, *20*, 425–434. [CrossRef]
45. Kianzad, A.; Meijboom, L.J.; Nossent, E.J.; Roos, E.; Schurink, B.; Bonta, P.I.; van den Berk, I.A.H.; Britstra, R.; Stoker, J.; Noordegraaf, A.V.; et al. COVID-19: Histopathological correlates of imaging patterns on chest computed tomography. *Respirology* **2021**, *26*, 869–877. [CrossRef]

46. Hernández-Píriz, A.; Tung-Chen, Y.; Juménez-Virumbrales, D.; Ayala-Larrañaga, I.; Barba-Martín, R.; Canora-Lebrato, J.; Zapatero-Gaviria, A.; De Casasola-Sánchez, G.G. Importance of lung Ultrasound follow-up in patients who had recovered from Coronavirus Disease 2019: Results from a Prospective Study. *J. Clin. Med.* **2021**, *10*, 3196. [CrossRef]
47. Mento, F.; Perrone, T.; Macioce, V.N.; Tursi, F.; Buonsenso, D.; Torri, E.; Smargiassi, A.; Inchingolo, R.; Soldati, G.; Demi, L. On the inpact of different lung ultrasound imaging protocols in the evaluation of patients affected by Coronavirus Disease 2019. How many acquisitions are needed? *J. Ultrasound Med.* **2021**, *40*, 2235–2238. [CrossRef]
48. Pal, A.; Ali, A.; Young, T.R.; Oostenbrink, J.; Prabhakar, A.; Prabhakar, A.; Deacon, N.; Arnold, A.; Eltayeb, A.; Yap, C.; et al. Comprehensive literature review on the radiographic findings, imaging modalities, and the role of radiology in the COVID-19 pandemic. *World J. Radiol.* **2021**, *13*, 258–282. [CrossRef]
49. Soldati, G.; Smargiassi, A.; Inchingolo, R.; Buonsenso, D.; Perrone, T.; Briganti, D.F.; Perlini, S.; Torri, E.; Mariani, A.; Mossolani, E.E.; et al. Is There a Role for Lung Ultrasound During the COVID-19 Pandemic? *J. Ultrasound Med.* **2020**, *39*, 1459–1462. [CrossRef]
50. Soldati, G.; Smargiassi, A.; Inchingolo, R.; Buonsenso, D.; Perrone, T.; Briganti, D.F.; Perlini, S.; Torri, E.; Mariani, A.; Mossolani, E.E.; et al. Proposal for International Standardization of the Use of Lung Ultrasound for Patients with COVID-19: A Simple, Quantitative, Reproducible Method. *J. Ultrasound Med.* **2020**, *39*, 1413–1419. [CrossRef]
51. Perrone, T.; Soldati, G.; Padovini, L.; Fiengo, A.; Lettieri, G.; Sabatini, U.; Gori, G.; Lepore, F.; Garolfi, M.; Palumbo, I.; et al. A new Lung Ultrasound Protocol able to predict worsening in Patients affected by Severe Acute Respiratory Syndrome Coronavirus 2 pneumonia. *J. Ultrasound Med.* **2021**, *40*, 1627–1635. [CrossRef] [PubMed]
52. Demi, L.; Mento, F.; Di Sabatino, A.; Fiengo, A.; Sabatini, U.; Macioce, V.N.; Marco Robol, M.; Tursi, F.; Sofia, C.; Di Cienzo, C.; et al. Lung Ultrasound in COVID-19 and Post-COVID-19 patients, an Evidence-Based Approach. *J. Ultrasound Med.* **2021**. *ahead of print*. [CrossRef] [PubMed]
53. Wang, M.; Luo, X.; Wang, L.; Estil, J.; Lv, M.; Zhu, Y.; Wang, Q.; Xiao, X.; Song, Y.; Lee, M.S.; et al. A comparison of lung Ultrasound and Computed Tomography in the diagnosis of patients with COVID-19: A systematic Review and Meta-Analysis. *Diagnostics* **2021**, *11*, 1351. [CrossRef] [PubMed]
54. Portale, G.; Ciolina, F.; Arcari, L.; Di Lazzaro Giraldi, G.; Danti, M.; Pietropaolo, L.; Camastra, G.; Cordischi, C.; Urbani, L.; Proietti, L.; et al. Lung Ultrasound in COVID-19: Clinical Correlates and Comparison with Chest Computed Tomography. *SN Compr. Clin. Med.* **2021**, *3*, 2075–2081. [CrossRef] [PubMed]
55. Buda, N.; Cylwik, J.; Mróz, K.; Rudzinska, R.; Dubik, P.; Malczewska, A.; Oraczewska, A.; Skoczyński, S.; Suska, A.; Górecki, T.; et al. Lung Ultrasound examination in patients with SARS-CoV-2Infection: Multicenter study. *J. Clin. Med.* **2021**, *10*, 3255. [CrossRef]
56. Smith, M.J.; Hayward, S.A.; Innes, S.M.; Miller, A.S.C. Point-of-care lung ultrasound in patients with COVID-19—A narrative review. *Anaesthesia* **2020**, *24*, 2776. [CrossRef]
57. Schmid, B.; Feuerstein, D.; Lang, C.N.; Fink, K.; Steger, R.; Rieder, M.; Duerschmied, D.; Busch, H.J.; Damjanovic, D. Lung ultrasound in the emergency department—A valuable tool in the management of patients presenting with respiratory symptoms during the SARS-CoV-2 pandemic. *BMC Emerg. Med.* **2020**, *20*, 96. [CrossRef]
58. Nishiura, H.; Kobayashi, T.; Miyama, T.; Suzuki, A.; Jung, S.M.; Hayashi, K.; Kinoshita, R.; Yang, Y.; Yuan, B.; Akhmetzhanov, A.R.; et al. Estimation of the asymptomatic ratio of novel coronavirus infections (COVID-19). *Int. J. Infect. Dis.* **2020**, *94*, 154–155. [CrossRef]
59. Mizumoto, K.; Kagaya, K.; Zarebski, A.; Chowell, G. Estimating the asymptomatic proportion of coronavirus disease 2019 (COVID-19) cases on board the Diamond Princess cruise ship, Yokohama, Japan, 2020. *Eurosurveillance* **2020**, *25*, 2000180. [CrossRef]
60. Puylaert, C.A.J.; Scheijmans, J.C.G.; Borgstein, A.B.J.; Andeweg, C.S.; Bartels-Rutten, A.; Beets, G.I.; van Berge Henegouwen, M.I.; Braak, S.J.; Couvreur, R.; Daams, F.; et al. Yield of Screening for COVID-19 in Asymptomatic Patients Before Elective or Emergency Surgery Using Chest CT and RT-PCR (SCOUT). *Ann. Surg.* **2020**, *272*, 919–924. [CrossRef]
61. Kumar, A.; Weng, I.; Graglia, S.; Lew, T.; Gandhi, K.; Lalani, F.; Chia, D.; Duanmu, Y.; Jensen, T.; Lobo, V.; et al. Point-of-Care Ultrasound predicts clinical outcomes in patients with COVID-19. *J. Ultrasound Med.* **2021**. *ahead of print*. [CrossRef] [PubMed]
62. Stecher, S.S.; Anton, S.; Fraccaroli, A.; Götschke, J. Lung ultrasound predicts clinical course but not outcome in COVID-19 ICU patients: A retrospective single-center analysis. *BMC Anesthesiol.* **2021**, *21*, 178. [CrossRef] [PubMed]
63. Hoffmann, T.; Bulla, P.; Dicke, L.; Klein, C.; Bott, S.; Keller, R.; Malek, N.; Fröhlich, E.; Göpel, S.; Blumenstock, G.; et al. Can follow up lung ultrasound in Coronavirus Disease-19 patients indicate clinical outcome? *PLoS ONE* **2021**, *16*, e0256359. [CrossRef] [PubMed]
64. Fratianni, G.; Malfatto, G.; Perge, E.; Facchetti, L.; Pini, L.; Bosco, M.; Cernigliaro, F.; Perego, G.B.; Facchini, M.; Badano, L.P.; et al. Lung Ultrasound in patients with SARS-CoV-2 pneumonia: Correlations with chest computed tomography, respiratory impairment, and inflammatory cascade. *J. Ultrasound Med.* **2021**. *ahead of print*. [CrossRef]
65. Sheard, S.; Rao, P.; Devaraj, A. Imaging of acute respiratory distress syndrome. *Respir. Care* **2012**, *57*, 607–612. [CrossRef]
66. Magnani, E.; Mattei, L.; Paolucci, E.; Magalotti, G.; Giacalone, N.; Praticò, C.; Praticò, B.; Zani, M.C. Lung Ultrasound in Severe COVID-19 Pneumonia in the Sub-Intensive Care Unit: Beyond the Diagnostic Purpose. *Respir. Med. Case Rep.* **2020**, *31*, 101307. [CrossRef]

67. Bouhemad, B.; Brisson, H.; Le-Guen, M.; Arbelot, C.; Lu, Q.; Rouby, J.J. Bedside Ultrasound assessment of Positive End-Expiratory Pressure–induced lung recruitment. *Am. J. Respir. Crit. Care Med.* **2011**, *183*, 341–347. [CrossRef]
68. Prü, B.M. Variants of SARS-CoV-2: Mutations, transmissibility, virulence, drug resistance, and antibody/vaccine sensitivity. *Front. Biosci.* **2022**, *27*, 65. [CrossRef]
69. Gattinoni, L.; Chiumello, D.; Caironi, P.; Busana, M.; Romitti, F.; Brazzi, L.; Camporota, L. COVID-19 pneumonia: Different respiratory treatment for different phenotypes? *Intensive Care Med.* **2020**, *46*, 1099–1102. [CrossRef]
70. Tisoncik, J.R.; Korth, M.J.; Simmons, C.P.; Farrar, J.; Martin, T.R.; Katze, M.G. Into the eye of the cytokine storm. *Microbiol. Mol. Biol. Rev.* **2012**, *76*, 16–32. [CrossRef]
71. Shy, Y.; Wang, Y.; Shao, C.; Huang, J.; Gan, J.; Huang, X.; Bucci, E.; Piacentini, M.; Ippolito, G.; Melino, G. COVID-19 infection: The perspective on immune responses. *Cell Death Differ.* **2020**, *27*, 1451–1454. [CrossRef]
72. Franks, T.J.; Chong, P.Y.; Chui, P.; Galvin, J.R.; Lourens, R.M.; Reid, A.H.; Selbs, E.; McEvoy, C.P.L.; Hayden, C.D.L.; Fukuoka, J.; et al. Lung pathology of severe acute respiratory syndrome (SARS): A study of 8 autopsy cases from Singapore. *Hum. Pathol.* **2003**, *34*, 743–748. [PubMed]
73. Risitano, A.M.; Mastellos, D.C.; Huber-Lang, M.; Yancopoulou, D.; Garlanda, C.; Ciceri, F.; Lambris, J.D. Complement as a target in COVID-19? *Nat. Rev. Immunol.* **2020**, *20*, 343–344. [CrossRef] [PubMed]
74. Tang, N.; Dengju, L.; Wang, X.; Sun, Z. Abnormal coagulation parameters are associated with poor prognosis in patients with novel coronavirus pneumonia. *J. Thromb. Haemost.* **2020**, *18*, 844–847. [CrossRef] [PubMed]
75. Soldati, G.; Giannasi, G.; Smargiassi, A.; Inchingolo, R.; Demi, L. Contrast-Enhanced Ultrasound in patients with COVID-19: Pneumonia, Acute Respiratory Distress Syndrome, or something else. *J. Ultrasound Med.* **2020**, *39*, 2483–2489. [CrossRef]
76. Buonsenso, D.; Pata, D.; Chiaretti, A. COVID-19 outbreak: Less stethoscope, more ultrasound. *Lancet Respir. Med.* **2020**, *8*, e27. [CrossRef]
77. Dong, Y.; Mo, X.; Hu, Y.; Qi, X.; Jiang, F.; Jiang, Z.; Tong, S. Epidemiology of COVID-19 among children in China. *Pediatrics* **2020**, *145*, e20200702. [CrossRef]
78. Musolino, A.M.; Supino, M.C.; Buonsenso, D.; Papa, R.E.; Chiurchiù, S.; Magistrelli, A.; Barbieri, M.A.; Raponi, M.; D'Argenio, P.; Villani, A.; et al. Lung ultrasound in the diagnosis and monitoring of 30 children with coronavirus disease 2019. *Pediatr. Pulmonol.* **2021**, *56*, 1045–1052. [CrossRef]
79. Denina, M.; Scolfaro, C.; Silvestro, E.; Pruccoli, G.; Mignone, F.; Zoppo, M.; Ramenghi, U.; Garazzino, S. Lung ultrasound in children with COVID-19. *Pediatrics* **2020**, *146*, e20201157.
80. Caruso, D.; Guido, G.; Zerunian, M.; Polidori, T.; Lucertini, E.; Pucciarelli, F.; Polici, M.; Rucci, C.; Bracci, B.; Nicolai, M.; et al. Post-Acute sequelae of COVID-19 pneumonia: Six-month chest CT Follow-up. *Radiology* **2021**, *301*, 396–405. [CrossRef]
81. Udwadia, Z.F.; Koul, P.A.; Richeldi, L. Post-COVID lung fibrosis: The tsunami that will follow the earthquake. *Lung India* **2021**, *38* (Suppl. S1), 41–47. [CrossRef] [PubMed]
82. Ambardar, S.R.; Hightower, S.L.; Huprikar, N.A.; Chung, K.K. Post-COVID-19 pulmonary fibrosis: Novel sequelae of the current pandemic. *J. Clin. Med.* **2021**, *10*, 2452. [CrossRef] [PubMed]

diagnostics 2022, 12, 1856

Article

The Role of Lung Ultrasound in SARS-CoV-19 Pneumonia Management

Marina Lugarà [1,*], Stefania Tamburrini [2], Maria Gabriella Coppola [1], Gabriella Oliva [1], Valeria Fiorini [2], Marco Catalano [2], Roberto Carbone [2], Pietro Paolo Saturnino [2], Nicola Rosano [2], Antonella Pesce [2], Raffaele Galiero [3], Roberta Ferrara [3], Michele Iannuzzi [4], D'Agostino Vincenzo [5], Alberto Negro [5], Francesco Somma [5], Fabrizio Fasano [5], Alessandro Perrella [6], Giuseppe Vitiello [7], Ferdinando Carlo Sasso [3], Gino Soldati [8] and Luca Rinaldi [3]

1 U.O.C. Internal Medicine, ASL Center Naples 1, P.O. Ospedale del Mare, 80147 Naples, Italy; gabry.cop@libero.it (M.G.C.); gably@libero.it (G.O.)
2 U.O.C. Radiology, ASL Center Naples 1, P.O. Ospedale del Mare, 80147 Naples, Italy; tamburrinistefania@gmail.com (S.T.); valeria.fiorini@libero.it (V.F.); marco26catalano@yahoo.it (M.C.); robcarbone@alice.it (R.C.); pietropsaturnino@libero.it (P.P.S.); nicola.rosano89@gmail.com (N.R.); antonellapesce1986@libero.it (A.P.)
3 Department of Advanced Medical and Surgical Sciences, University of Campania Luigi Vanvitelli, 80121 Naples, Italy; raffaele.galiero@gmail.com (R.G.); roberta.ferrara@libero.it (R.F.); ferdinandocarlo.sasso@unicampania.it (F.C.S.); lucarinaldi@hotmail.it (L.R.)
4 Department of Anesthesia and Intensive care Medicine, ASL Center Naples 1, P.O. Ospedale del Mare, 80147 Naples, Italy; michele.iannuzzi@aslnapoli1centro.it
5 U.O.C. Neurodiology, ASL Center Naples 1, P.O. Ospedale del Mare, 80147 Naples, Italy; vincenzo-dagostino@libero.it (D.V.); alberto.negro@hotmail.it (A.N.); fra1585@hotmail.it (F.S.); fabriziodoc@gmail.com (F.F.)
6 Infectious Diseases at Health Direction, AORN A. Cardarelli, 80131 Naples, Italy; alessandro.perrella@aocardarelli.it
7 Healt Direction, ASL Center Naples 1, P.O. Ospedale del Mare, 80147 Naples, Italy; giuseppe.vitiello@aslnapoli1centro.it
8 Diagnostic and Interventional Ultrasound Unit, Valle del Serchio General Hospital, Castelnuovo Garfagnana, 55032 Lucca, Italy; soldatigino@yahoo.it
* Correspondence: marinalugara82@gmail.com

Citation: Lugarà, M.; Tamburrini, S.; Coppola, M.G.; Oliva, G.; Fiorini, V.; Catalano, M.; Carbone, R.; Saturnino, P.P.; Rosano, N.; Pesce, A.; et al. The Role of Lung Ultrasound in SARS-CoV-19 Pneumonia Management. *Diagnostics* **2022**, *12*, 1856. https://doi.org/10.3390/diagnostics12081856

Academic Editor: Philippe A. Grenier

Received: 3 July 2022
Accepted: 27 July 2022
Published: 31 July 2022

Abstract: Purpose: We aimed to assess the role of lung ultrasound (LUS) in the diagnosis and prognosis of SARS-CoV-2 pneumonia, by comparing it with High Resolution Computed Tomography (HRCT). Patients and methods: All consecutive patients with laboratory-confirmed SARS-CoV-2 infection and hospitalized in COVID Centers were enrolled. LUS and HRCT were carried out on all patients by expert operators within 48–72 h of admission. A four-level scoring system computed in 12 regions of the chest was used to categorize the ultrasound imaging, from 0 (absence of visible alterations with ultrasound) to 3 (large consolidation and cobbled pleural line). Likewise, a semi-quantitative scoring system was used for HRCT to estimate pulmonary involvement, from 0 (no involvement) to 5 (>75% involvement for each lobe). The total CT score was the sum of the individual lobar scores and ranged from 0 to 25. LUS scans were evaluated according to a dedicated scoring system. CT scans were assessed for typical findings of COVID-19 pneumonia (bilateral, multi-lobar lung infiltration, posterior peripheral ground glass opacities). Oxygen requirement and mortality were also recorded. Results: Ninety-nine patients were included in the study (male 68.7%, median age 71). 40.4% of patients required a Venturi mask and 25.3% required non-invasive ventilation (C-PAP/Bi-level). The overall mortality rate was 21.2% (median hospitalization 30 days). The median ultrasound thoracic score was 28 (IQR 20–36). For the CT evaluation, the mean score was 12.63 (SD 5.72), with most of the patients having LUS scores of 2 (59.6%). The bivariate correlation analysis displayed statistically significant and high positive correlations between both the CT and composite LUS scores and ventilation, lactates, COVID-19 phenotype, tachycardia, dyspnea, and mortality. Moreover, the most relevant and clinically important inverse proportionality in terms of P/F, i.e., a decrease in P/F levels, was indicative of higher LUS/CT scores. Inverse proportionality P/F levels and LUS and TC scores were evaluated by univariate analysis, with a P/F–TC score correlation

coefficient of -0.762, $p < 0.001$, and a P/F–LUS score correlation coefficient of -0.689, $p < 0.001$. Conclusions: LUS and HRCT show a synergistic role in the diagnosis and disease severity evaluation of COVID-19.

Keywords: lung ultrasound; high resolution computed tomography; SARS-CoV-19; interstitial pneumonia; ARDS

1. Introduction

COVID-19 is an infectious disease with a wide range of clinical symptoms, ranging from asymptomatic to mildly symptomatic and severe forms, pointing to a major role of the host response to SARS-CoV-2 (severe acute respiratory syndrome coronavirus 2) [1]. The clinical spectrum of SARS-CoV-2 infection is broad, ranging from asymptomatic infection to flu-like illness, to severe and diffuse viral pneumonia with a life-threating course, related to cytopathic and immune-mediated injury in the pulmonary parenchymal. Patients may show symptoms that include fever, high temperature, cough, myalgia, sputum production, headache, hemoptysis, diarrhea, dyspnea, and, in some cases, acute respiratory distress syndrome (ARDS), acute cardiac injury, or secondary infection. Most of infections are not severe, 81% are mild, 14% of the cases are severe (with dyspnea, hypoxia, or >50% lung involvement on diagnostic imaging), and 5% develop a critical disease with respiratory failure, shock, or multiorgan dysfunction [2]. The risk of death from COVID-19 strongly depends on the patient's age and previous health status. Older patients are much more prone to critical and fatal disease outcomes, especially with comorbidities, including cardiovascular diseases, hypertension, chronic kidney disease, diabetes, and pulmonary disease [3]. Thrombotic microangiopathy and complement activation, pulmonary embolism, and elevated D-dimer levels have also been reported with high frequency in patients with COVID-19 [4–7]. Numerous previous studies, including the paper by Giannini and al. [8,9], have already discussed the significance of the D-dimer level as an independent predictor of mortality in severe cases of ARDS during SARS-CoV-2. COVID-19 laboratory diagnosis is based on real-time polymerase chain reaction (RT-PCR) assay obtained by oro-nasopharyngeal swab sample, bronchoalveolar lavage, or tracheal aspirate, while imaging plays a major role in the early diagnosis of the pleuropulmonary complications [8–10]. The pathophysiology of severe COVID-19 infection is marked by elevated numbers of neutrophils in the nasopharyngeal epithelium, in the distal parts of the lungs, and in blood. The experience gained during the Italian epidemic pointed to patients' age as one of the most important risk factors for COVID-19 mortality [11]. However, a recent study demonstrated that patients who died of COVID-19 appear to have lost considerable lifetime, independent of their age. Imaging findings significantly support clinical judgement to ensure effective and timely management and prognosis; indeed, the identification of disease severity allows appropriate selection for early involvement of intensive care [10–12]. Contrary to X-ray, chest computed tomography (CT) plays a pivotal role in the diagnosis and monitoring of interstitial pneumonia [13,14]. Typical CT patterns of COVID-related pneumonia include multifocal bilateral peripheral ground glass opacities associated with subsegmental patchy consolidations, commonly subpleural and predominantly involving lower lung lobes and posterior segments [15,16]. Likewise, lung ultrasound (LUS) shows certain advantages for detecting and monitoring COVID-19 "pneumonia" [17]. This diagnostic technique is safe, repeatable, and can be used with low cost at the bedside in absence of radiation exposure [16–18]. Moreover, it is useful for rapid assessment of the severity of SARS-CoV-2 pneumonia/ARDS (acute respiratory distress syndrome) in diagnosis and follow-up settings, and for monitoring lungs during recruitment maneuvers and in prone positions [19,20]. The use of LUS for patients with suspected COVID-19 may reduce the risk associated with transporting unstable patients to

CT rooms, which is especially important for preventing nosocomial outbreaks due to high contagiousness of virus [21,22].

Thoracic ultrasound has been employed for the diagnosis of many thoracic diseases and is an accepted detection tool for pleural effusions, atelectasis, pneumothorax, and pneumonia. However, the use of ultrasound for the evaluation of parenchymal lung disease, when the organ is still aerated, is a relatively new application. The diagnosis of a normal lung and the differentiation between a normally aerated lung and a lung with interstitial pathology are based on the interpretation of ultrasound artifacts universally known as A- and B-Lines. Even though the practical role of lung ultrasound artifacts is accepted by many clinicians, their physical basis and the correlations between these signs and the causal pathology is not understood in detail [23]. The utility of a lung ultrasound (LUS) in the diagnosis of interstitial lung disease (ILD in very early SSc has also been described including, more recently, its potential for the detection of SSc-ILD in asymptomatic preclinical stages. Recent research has focused on the predictive value of LUS [24,25], which is promising for the application of LUS as a screening method for SSc-ILD in clinical practice. Although these are strong arguments in favor of the application of LUS in SSc, to date there is no unanimous consensus on the role LUS plays in the diagnosis and/or prognosis of SSc-ILD [26].

The use of LUS for patients with suspected COVID-19 may reduce the risk associated with transporting unstable patients to CT rooms, which is especially important for preventing nosocomial outbreaks, due to the high contagiousness of the virus. The purpose of our study was to determine the role of LUS in the diagnosis and prognosis of SARS-CoV-2 pneumonia, considering high-resolution computed tomography (HRTC) as the gold standard.

2. Materials and Method

2.1. Patients

From March 2020 to October 2020, all patients who had been diagnosed with COVID-19 infection by RT-PCR on nasopharyngeal swab samples and throat swabs, and subsequently hospitalized at our COVID Centre, were enrolled in the study. Patients underwent LUS and CT within 48–72 h of admission to our emergency department. Anamnestic, epidemiological, and demographic data were collected either from the patients themselves or from their families, and were recorded. All the results, clinical and laboratory data, and pulmonary CT and LUS were analyzed retrospectively and aggregated anonymously. Comorbidities and related therapies, including obesity, chronic kidney disease, hypertension, type 2 diabetes mellitus, atrial fibrillation, coronary artery disease, dementia, chronic obstructive pulmonary disease (COPD), chronic hepatitis, history of cancer in the last 5 years, and smoking were also recorded.

Clinical phenotypes were classified into four groups as follows:

1. pauci-symptomatic subjects (fever, no hypoxemia);

2. mildly symptomatic patients (fever, mild hypoxemia with pO_2 40–60 mmhg, need of oxygen therapy with nasal cannula and vent-mask);

3. moderately symptomatic patients (fever, moderate to severe respiratory failure with $pO_2 < 40$ mmhg, need of CPAP/NIV);

4. patients with severe disease (severe respiratory failure with $pO_2 < 40$ mmhg, ARDS, with or without invasive ventilation).

2.2. Statement of Ethics

The study protocol was approved by the Institutional Ethics Committee of Ancona (ID 0179104/I, 28 July 2021). The study was conducted in accordance with the principles of the Declaration of Helsinki. Due to the retrospective design of the study and anonymous collection of data, informed consent signature was waived, in compliance with Italian law.

2.3. Laboratory Data

Venous blood samples were collected from all patients to assess complete blood counts, with differentiation, fibrinogen, D-dimer, NT pro-bnp, troponin, and biochemistry tests (creatinine, LDH, C-reactive protein, ferritin, procalcitonin, glycemia, lymphocytes, PT, PTT, INR).

All patients underwent blood gas analysis on admission, by radial artery cannulation or puncture. The oxygenation status was assessed by O_2 partial pressure value (pO_2), $CO_{2\ partial}$ pressure value (pCO_2) and hemoglobin oxygen saturation (SO_2). We used the P/F ratio to compare different values of arterial pO_2 in patients receiving different fractions of inspired oxygen (FiO_2) by non-invasive ventilation. PaO_2/FiO_2 (P/F) ratio was used to classify the severity of ARDS, according to the Berlin definition, even though most of the evidence derived from intensive care settings.

According to the 2012 Berlin definition by the ARDS Definition Taskforce, a ratio of the partial pressure of arterial oxygen (PaO_2) to the fraction of inspired oxygen (FiO_2) (P/F ratio) of $\leq$100, 101–200 or 201–300 mmHg is deemed as severe, moderate, or mild, respectively.

Lactate levels were also recorded to evaluate any possible degree of tissue perfusion.

2.4. Oxygen Requirement

Ventilatory support was categorized into three groups: nasal cannula, Venturi mask and, non-invasive ventilation (CPAP and b-pap). Patients admitted to intensive care required tracheal intubation.

2.5. LUS Protocol

Lung ultrasound examinations were performed at the bedside by trained sonographers (three internists and two radiologists) using portable ultrasound machines (Alpinion E cube i7 and Mindray DP10), equipped with a convex probe (3.5 MHz) and a linear probe (7.5–10 MHz). No harmonic filter was used. The linear and convex probes were each used in every patient. A reduced mechanical index was used as often as possible to obtain interpretable images. The depth was set to provide a clear view of the pleural line and 3–4 cm of the field below it. The gain was set in the intermediate position. The focus was placed at the level of the pleural line.

All the devices, the US scanner, probes, and cables, were wrapped in single-use plastic covers to reduce the risk of contamination and to facilitate the sterilization procedures.

Lung Ultrasound Scoring System

The thorax was explored in twelve areas, six on each hemithorax, by intercostal scans (Figure 1). In critically ill patients who could not maintain the sitting position, paravertebral scans were acquired and moved as posteriorly as possible and towards the lowest and apical points, by placing the patient in an oblique position. Each area was assessed with the probe perpendicular to the chest wall, searching for the following signs: pleural line (a horizontal hyperechoic line between the ribs), A-lines (horizontal replica artifacts repeated at a constant distance equal to the distance between the pleural line and probe surface), vertical artifacts (vertical hyperechoic artefacts spreading from the pleural line towards the bottom of the screen), white lung (focal or multifocal artifacts characterized by an undifferentiated echogenic background, with the absence of A-lines and without evidence of vertical artifacts), and consolidation (presence of a tissue-like pattern) [23–25].

A standardized and COVID-19-dedicated four-level scoring system was used to categorize the ultrasound examination, according to published papers [26,27]:

Score 0: The pleural line is regular. Horizontal reverberant artifacts (A-Lines) and mirror effects are present. Absence of visible alterations with ultrasound.

Score 1: The pleural line has slight alterations with sporadic vertical bright artifacts. These are often grouped and separated by the absence of visible alterations of the lung.

Score 2: The pleural line is broken at many points. Vertical artifacts are more numerous. Small subpleural consolidations may be present, often showing a cuneiform shape.

Score 3: The pleural line is irregular and cobbled. The subpleural lung is denser and more disordered. White lung with or without larger consolidations may be present. Small and large consolidations are evident in the scanned parts of the lung.

For each patient, the total score was computed by adding the scores for each area explored. The total scores ranged from 0 (best) to 36 (worst).

Severity of US pulmonary involvement was classified as mild (1–5), moderate (>5–15), or severe (>15).

The presence of pleural effusion and lung sliding was recorded. Ultrasound images and videos were stored and numbered from the right posterior basal regions.

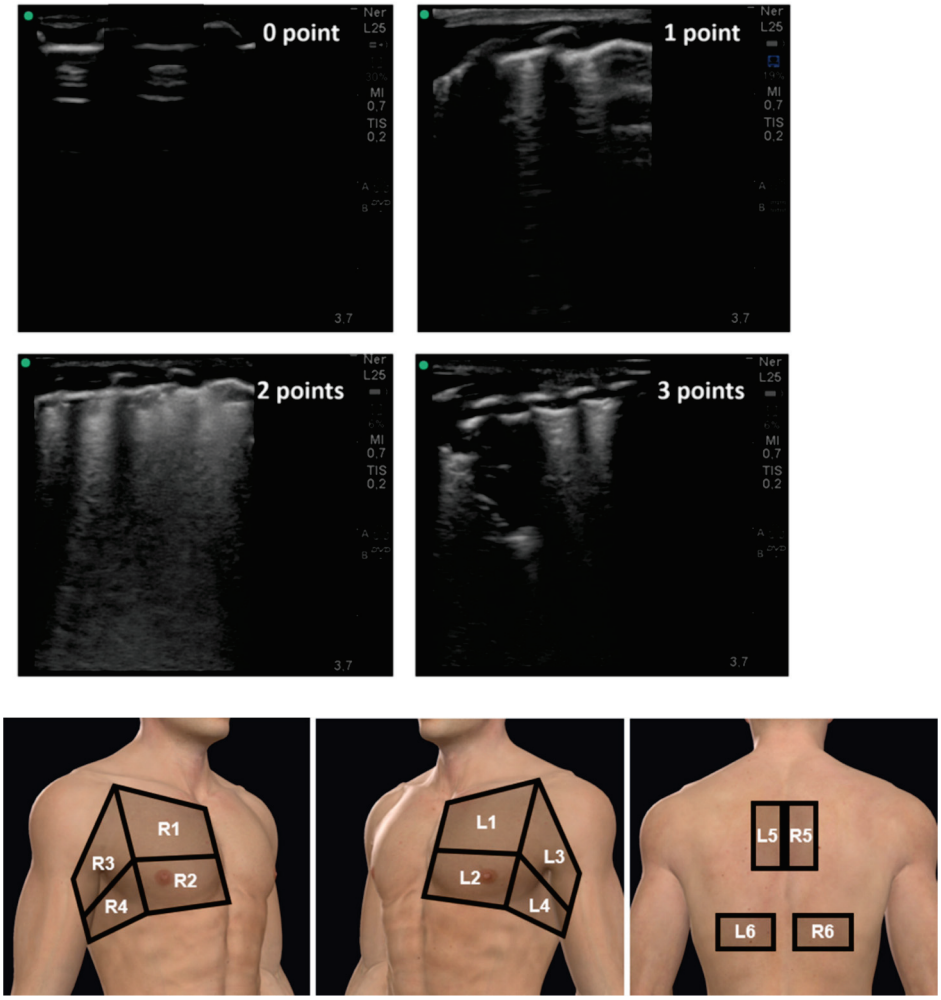

Figure 1. 12-zone method; anterior, lateral, and posterior chest. In each zone a score was assigned; 0 = no B-lines; 1 = multiple spaced or isolated B-lines; 2 = diffused coalescent B-lines; 3 = lung consolidation.

2.6. High Resolution CT (HRCT)

All patients had an initial chest HRCT scan within 48 h of hospitalization, using a multidetector 64-channel CT machine (Toshiba Aquilion PRIME). The detailed parameters for CT acquisition were as follows: tube voltage, 120 kVp; tube current, standard (reference mAs, 60–120); slice thickness, 1.0 mm; reconstructed interval, 1.0 mm. Patients were placed in a supine position. To minimize motion artifacts, patients were instructed on breath-holding and images were acquired during a single breath-hold. The scanning range was from the apex to the lung base. All the images were stored in a picture archive and

communication system. Image analysis was performed using the institutional digital database system.

Two radiologists with more than 10 years' experience evaluated the images in consensus, to determine the disease pattern, distribution, stage, and severity score for each patient. When discordant, the final decision was reached collegially. No negative control cases were examined.

The scans were first assessed, whether negative or positive, for typical findings of COVID-19 pneumonia (bilateral, multi-lobar lung infiltration, posterior peripheral ground glass opacities) as defined by the RSNA consensus statement and peer-reviewed literature on viral pneumonia. Recorded findings included ground glass opacity (GGO), crazy-paving pattern, and consolidation [16]. Atypical COVID-19 CT patterns were recorded.

CT findings were described as follows: (1) ground-glass opacities; (2) Consolidation; (3) ground-glass opacity with consolidation (assessing their respective predominance); (4) crazy-paving patterns; (5) no abnormalities.

Ground-glass opacification was defined as hazy increased lung attenuation with preservation of bronchial and vascular margins, and consolidation was defined as opacification with obscuration of vessel margins and airway walls. Crazy paving represented GGO opacity with superimposed inter- and intralobular septal thickening [10,11]. Consolidation consisted of parenchyma deprived of air.

For each pulmonary lobe (five lobes), the volumetric parenchymal involvement was estimated with a score system as follows: 0 = no involvement; 1 = <5% involvement; 2 = 5–25% involvement; 3 = 26–49% involvement; 4 = 50–74% involvement; 5 = >75%.

The total CT score was the sum of the individual lobar scores, and ranged from 0 (no involvement) to 25 (maximum involvement) [11,15–28]. A correlation between the total LUS score and a Pan score of 0 to 24 was shown to be significant in a previous work [29–31].

In addition, CT scans were evaluated according to their distribution, side, and lobe involvement predominance. Finally, the presence of underlying non-related lung disease such as emphysema or fibrosis was recorded.

2.7. End Points of the Study

The primary endpoint was to compare the lung ultrasound severity score and chest CT severity in COVID-19 clinical management. Furthermore, we wanted to explore the correlation between the imaging severity score and COVID-19 phenotypes, clinical and laboratory parameters, and oxygen requirements, thus establishing a prognostic role for lung ultrasound in COVID-19 patients.

2.8. Statistical Analysis

Categorical data were expressed as numbers and percentages, and continuous variables either as mean and standard deviation (SD) or median and interquartile range (IQR), according to their distribution, and were tested by the Shapiro–Wilk test.

The sample size was 79 patients for a confidence level of 95%.

The ultrasound thoracic score and the CT score were tested for correlation by a linear regression analysis, and a dispersion graph was reported to describe the degree of correlation. The respective correlations of the CT and ultrasound thoracic (US) scores with several outcomes were assessed, as well as the respiratory and laboratory parameters, by calculating the Spearman correlation coefficient. The ROC curve analysis was used to evaluate mortality as a function of the LUS score, and to identify an optimal cut-off value. A p-value < 0.05 was considered as statistically significant. All the analyses were performed by STATA software (StataCorp. College Station, TX: StataCorp LLC), version 15.5.

3. Results

Ninety-nine patients were included in the study, with a median age of 71 years (IQR 58–78 years); within the study group the incidence of SARS-CoV-2 was higher in males 68.7% than in females 31.3% (Table 1). All patients underwent a CT scan and a US scan.

Table 1. Anthropometric, demographic, clinical, and biochemical characteristics of the study cohort (*n* = 99).

Parameters	**Values**
Age (years), median [IQR]	71 [58–78]
Sex, *n* (%) M F	 68 (68.7) 31 (31.3)
Signs and Symptoms	
Presence of fever, *n* (%)	90 (90.9)
Presence of cough, *n* (%)	90 (90.9)
Pharyngeal hyperemia, *n* (%)	63 (63.6)
Asthenia, *n* (%)	76 (76.8)
Vomiting, *n* (%)	5 (5.1)
Diarrhea, *n* (%)	11 (11.1)
Dyspnea, *n* (%)	89 (89.9)
Tachycardia, *n* (%)	67 (67.7)
Phenotype, *n* (%) type 1 type 2 type 3 type 4	 7 (7.1) 21 (21.2) 60 (60.6) 11 (11.1)
Pre-existing Comorbidities	**Values**
Hypertension, *n* (%)	85 (85.9)
Diabetes, *n* (%)	34 (34.3)
Atrial fibrillation, *n* (%)	13 (13.1)
Ischemic heart disease, *n* (%)	33 (33.3)
Ictus, *n* (%)	14 (14.1)
Dementia, *n* (%)	31 (31.3)
Chronic obstructive pulmonary disease (COPD), *n* (%)	56 (56.6)
Active cancer in the last five years, n (%)	14 (14.1)
Hyperinflammatory syndrome %	84 (84.8)
Smoke, *n* (%)	66 (66.7)
Obesity, *n* (%) No Grade I Grade II Grade III	 58 (59.6) 30 (30.3) 8 (8.1) 2 (2)
Chronic liver disease, *n* (%)	7 (7.1)
Chronic kidney disease, *n* (%)	31 (31.3)
Mortality, *n* (%)	21 (21.2)
Days of hospitalization, median [IQR]	30 [20–40]
Ventilation, median [IQR]	0.50 [0.28–0.60]

Table 1. *Cont.*

Parameters	Values
Oxygen interface, *n* (%)	
None	14 (14.1)
Nasal cannula	18 (18.2)
Venturi Mask	40 (40.4)
CPAP/Bi-level	25 (25.3)
Orotracheal Intubation	2 (2)
Therapy	
Anticoagulants, *n* (%)	72 (72.7)
Antiplatelets, *n* (%)	35 (35.4)
ACE Inhibitors, *n* (%)	32 (32.3)
Ultrasound thoracic, median [IQR]	28 [20–36]
Ultrasound score, *n* (%)	
Score 0	2 (2)
Score 1	18 (18.2)
Score 2	47 (47.6)
Score 3	32 (32.2)
CT score, mean (SD)	12.63 (5.72)
CT score, *n* (%)	
Score 1	20 (20.2)
Score 2	59 (59.6)
Score 3	20 (20.2)

Abbreviations: IQR: interquartile range; SD: standard deviation; M: male; F: female; BMI: body mass index. The biochemical parameters and the blood-gas analysis results are shown in Table 2. In general, patients were characterized by hyper-inflammation syndrome, lymphopenia, high levels of C-reactive protein, neutrophils, and ferritin, and abnormal coagulation parameters (fibrinogen, d-dimer).

Table 2. Laboratory characteristics of the study population ($n = 99$).

Laboratory	Values
Hb (mg/dL), mean (SD)	12.2 (2.2)
White blood cells ($\times 10^3$), mean (SD)	9.73 (4.38)
Lymphocytes (a.v.), median [IQR]	0.8 [0.6–1.3]
Neutrophils (a.v.), mean (SD)	7.56 (3.15)
Platelets, mean (SD)	282,098 (141,397)
Azotemia (mg/dL), mean (SD)	54.7 (34.85)
Creatinine (mg/dL), median [IQR]	0.9 [0.8–1.2]
Sodium (mmol/L), mean (SD)	138.8 (4.2)
Potassium (mmol/L), mean (SD)	4.8 (3.9)
AST (U/L), mean (SD)	42.6 (124.6)
ALT (U/L), mean (SD)	48.8 (136.8)
Glycemia (mg/dL), median [IQR]	110 [88.3–175]
CRP (mg/dL), median [IQR]	5 [2.6–12]
INR, median [IQR]	1.12 [1.10–1.20]
aPTT (s), mean (SD)	31 (6.8)
Fibrinogen (mg/dL), mean (SD)	483.3 (141.4)
Nt-pro-bnp (pg/mL), median [IQR]	1578 [600–3500]
D-Dimer (pg/mL), median [IQR]	2300 [782.5–4210]
LDH (mU/mL), mean (SD)	361.5 (138.4)
Troponin (ng/mL), median [IQR]	0.032 [0.014–0.090]
Procalcitonin (ng/mL), median [IQR]	0.2 [0.03–0.90]
Ferritin (ng/mL), median [IQR]	450 [280–700]

Table 2. *Cont.*

Laboratory	Values
Blood Gas Analysis	
pH, median [IQR]	7.45 [7.40–7.47]
pO_2 (mmHg), median [IQR]	68 [58.3–84.8]
pCO_2 (mmHg), median [IQR]	35 [33–42]
HCO^{3-} (mmol/L), median [IQR]	25 [23–26]
spO_2 (%), median [IQR]	93.1 [90–96]
Lactates (mmol/L), median [IQR]	2.25 (1.02)
P/F, median [IQR]	231 [136.3–295.3]
FiO_2 admission, median [IQR]	0.30 [0.21–0.50]

Abbreviations: IQR: interquartile range; SD: standard deviation; Hb: hemoglobin; PLT: platelets; AST: aspartate aminotransferase; ALT: alanine aminotransferase; CRP: C-reactive protein; LDH: lactate dehydrogenase; CPK: creatine phosphokinase. Reference ranges: [Hb] F = 12–16/M = 12–18 g/dL; WBCs: 4500–11,000, Neutrophils: 1500–7000; Lymphocytes: 1500–7000; PLT: 150,000–450,000; Azotemia: 15–50 mg/dL; Serum Creatinine: 0.51–0.95 mg/dL; Sodium: 135–145 mmol/L; Potassium: 3.5–5 mEq/L; AST (F = 8–43 U/L; M = 8–48 U/L); ALT (F = 7–45 U/L, M = 7–55 U/L); Glycemia: 60–110 mg/dL; CRP: 5–10 mg/dL; INR: 0.9–1.3; aPTT: 28–40 s; Fibrinogen: 200–400 mg/dL; NT-proBNP: ≤900 pg/mL; D-Dimer: <500 pg/mL; LDH: 80–300 mU/mL; Troponin: <0.1; procalcitonin: 0–1; ferritin: M: 20–200 ng/mL, F: 20–120 ng/mL; Iron: M: 31–144 µg/dL, F: 25–156 µg/dL; CPK: 60–190 U/L. Blood gas ranges: pH: 7.35–7.45; pO_2: 80–100 mmHg; pCO_2: 35–45 mmHg; HCO^{3-}: 22–26 mmol/L; spO_2: 95–100%; Lactates: <2 mmol/L.

Table 1 synthetizes the anthropometric, demographic, clinical, and biochemical characteristics of the study cohort.

The main symptoms on admission were fever and cough, detected in 90.9% of patients, and dyspnea in 89.9%, whilst asthenia was present in 76.8% of patients and pharyngeal hyperemia in 63.6%.

Table 2 illustrates the pre-existing diseases of the patients and their therapies, while Table 3 shows the patients' phenotypes and their clinical evolution during their hospital stay. Among pre-existing diseases, the most prevalent was hypertension (85.9%), while chronic obstructive pulmonary disease (COPD) was present in more than half of the patients (56.6%). Hyper-inflammation syndrome, due to the excessive production of proinflammatory cytokines and the dysfunction of the immune response, was found in 84.8% of patients.

Table 3. Univariate analysis of relationships between ultrasound thoracic score and other parameters in patients infected by COVID-19.

Parameters	Correlation Coefficient	*p*
Age (years)	0.289	0.034
Dyspnoea	0.319	0.051
Tachycardia	0.457	0.002
COVID-19 phenotype	0.589	<0.001
Dementia	0.197	0.256
Platelets	−0.118	0.286
Prothrombin time	0.057	0.917
NT-proBNP	0.174	0.419
D-dimer	0.218	0.047
pH	−0.469	0.008
pO_2	−0.486	0.003
spO_2	−0.226	0.467
P/F	−0.689	<0.001
Death of patients	0.492	0.008
Ventilation	0.562	<0.001
Lactates	0.479	0.001

The clinical phenotype 3 was the most prevalent, which was characterized by fever, and moderate to severe respiratory failure, with pO_2 < 40 mmhg and need of Nnon -invasive ventilation (CPAP/NIV).

Oxygen support was needed for 66% (65%) of patients, specifically nasal cannulas (CN) 7%, venturi mask (VM) 24%, high flows (HFNC) 10%, and non-invasive ventilation—biPap 15% and CPAP 10%.

The LUS and CT scores were analyzed for correlation with the mortality outcomes, coagulation, and respiratory parameters using the Spearman correlation coefficient. As reported in Tables 3 and 4, the results were for both scores similar. Table 3 shows negative correlation of P/F and LUS score (r = −0.689), and pO_2–LUS score (r = −0.486), and positive correlation of ventilation–LUS score (r = 0.562), and lactates–LUS score (r = 0.479). Table 4 shows negative correlation of P/F with TC score (r = −0.689) and pO_2 (r = −0.470) and positive correlation with type of ventilation (0.530).

Table 4. Univariate analysis of the relationships between CT score and other parameters in patients infected by COVID-19.

Parameters	Correlation Coefficient	*p*
Age (years)	0.369	0.029
Dyspnoea	0.488	<0.001
Tachycardia	0.321	0.007
COVID-19 phenotype	0.639	<0.001
Dementia	0.124	0.298
Platelets	−0.189	0.321
Prothrombin time	0.025	0.874
NT-proBNP	0.098	0.513
D-dimer	0.289	0.041
pH	−0.396	0.019
pO_2	−0.470	<0.001
spO_2	−0.199	0.148
P/F	−0.762	<0.001
Death of patients	0.466	0.001
Ventilation	0.503	<0.001
Lactates	0.442	0.001

The LUS signs of COVID-19 in every patient were B-lines. The frequencies of irregular or blurred pleural lines were 45% and 15%, respectively. Sub-centimetric lung consolidation was seen in 18 patients (18%).

The median ultrasound thoracic score was 28 (IQR 20–36) and the most frequent scores per single scan were 2 and 3 (47.6% and 32.2%, respectively) (Table 1).

The mean CT score was 12.63 (SD 5.72), with most of the patients showing a score 2 pattern (59.6%).

Patients with clinical phenotypes 3 or 4 (71% of the patients enrolled) presented higher rates of bilateral involvement, with more involved zones, B-lines, pleural line abnormalities, and consolidation.

The relationship between the LUS scores and the CT scores was assessed by a linear regression analysis and dispersion graph (Figure 2), showing a positive linear relationship between the two evaluation scoring systems, which despite not being high (rho = 0.352), did however reach statistical significance (p = 0.008) (Figure 3).

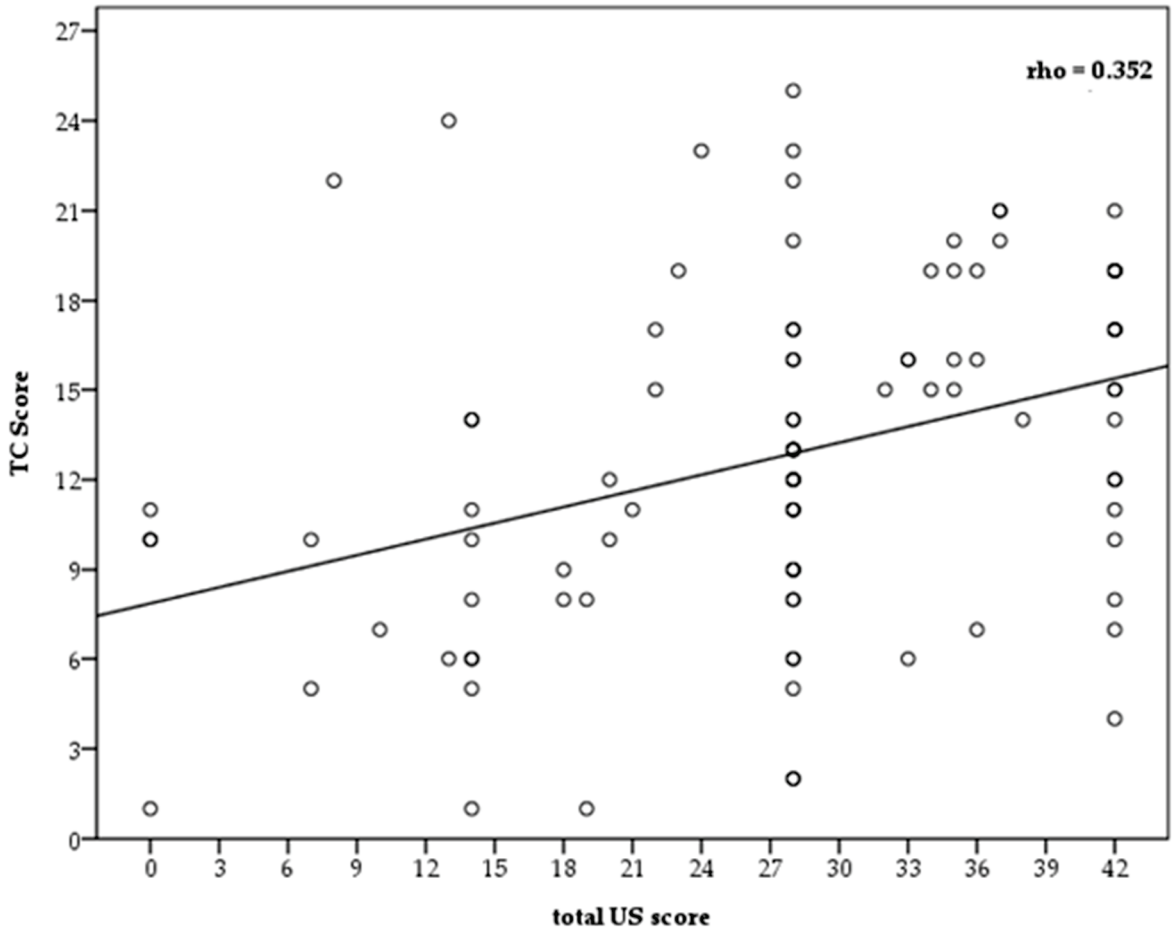

Figure 2. Linear regression analysis and dispersion graph.

Using the Spearman correlation coefficient, use LUS and CT scores were analyzed for correlation with the mortality outcome, coagulation, and respiratory parameters. As reported in Tables 3 and 4, the results were almost similar for both scoring systems. Table 3 showed negative correlation for P/F and LUS score (r = −0.689), and pO_2–LUS score (r = −0.486), positive correlation for ventilation–LUS Score (r = 0.562), and lactates–LUS Score (r = 0.479). Table 4 showed negative correlation for P/F and TC score (r = −0.689), and pO_2 (r = −0.470), and positive correlation by type of ventilation (0.530).

The bivariate correlation analysis displayed statistically significant and high positive correlations for the CT scores as well as the LUS scores with the following parameters: ventilation, lactates, COVID-19 phenotype, tachycardia, dyspnea, and mortality.

The LUS scores showed a significant association with in-hospital mortality (OR 0.7, 0.95% CI 0.59–0.82) Table 5; $p < 0.001$), with the risk of invasive respiratory support increasing with a greater LUS score measured on patient arrival.

Table 5. ROC-AUC value of the LUS score compared to the different factor.

AUC of LUS Score	AUC (95% CI)
Dyspnea	0.77 (0.61–0.92)
Tachycardia	0.79 (0.68–0.879
Dementia	0.57 (0.45–0.69)
Mortality	0.70 (0.59–0.82)

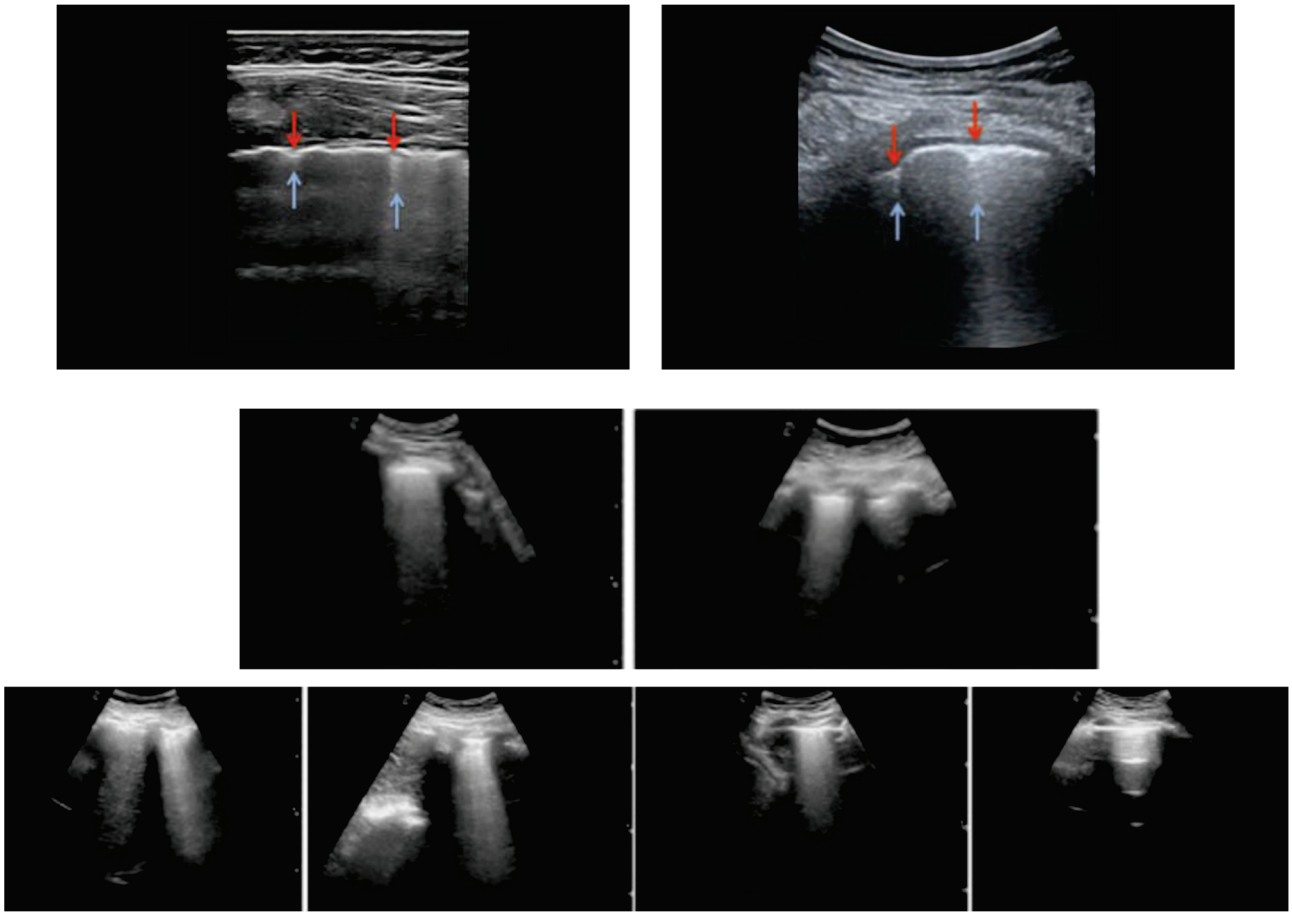

(**a**)

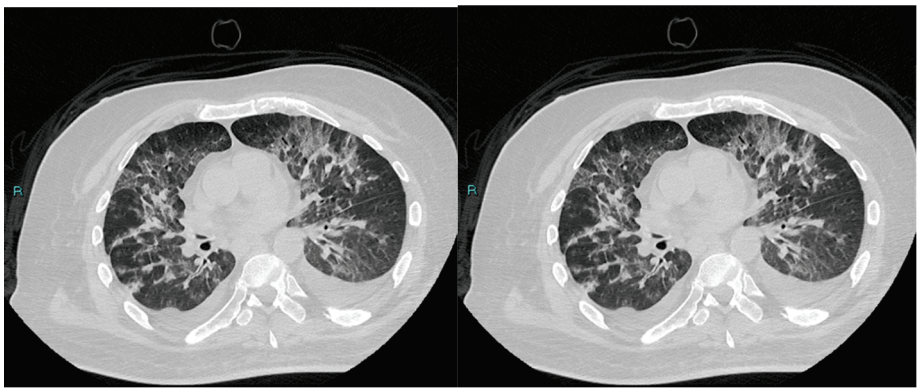

(**b**) (**c**)

Figure 3. CT and LUS imaging scans of different scores. In these figures the pleural line (indicated by red arrows) is indented, and vertical areas of white (blue arrows) are visible below the indent, which reflect local alterations in the acoustical properties of the lung caused by replacement of air with water, blood, or collapsed tissue. A typical case of a COVID-19 pneumonia patient. (**a**) B-lines at the right and left of the lower lateral lung reflecting pneumonia (score 2); (**b**) B-lines at the right and left of the lower lateral lung reflecting pneumonia (score 3); (**c**) chest CT showing multiple infiltrations.

These positive correlations demonstrate that a higher composite LUS or CT score corresponded to a higher mortality rate and a more severe COVID-19 phenotype. Furthermore, there was a direct proportionality between increased CT and LUS scores on one

hand and elevated lactate levels and a need for ventilation on the other. Remarkably lower correlations, though still statistically significant, were found for age and d-dimer.

4. Discussion

Lung CT is currently the standard for comparison of other imaging methods for anatomical definition down to the level of the secondary lung lobule.

The most important radiology societies [11–16] recommend the use of CT in the presence of moderate and severe features of COVID-19 when RT-PCR results are negative or not available, when there is high pre-test probability, and in the management of patients with worsening or severe respiratory symptoms.

The possibility of using ultrasound to evaluate pulmonary changes in COVID-19 has been proposed since the beginning of the pandemic [26]. Two factors indicated this possibility; first, the prevailing sub-cortical distribution of the injuries, necessary for their US visibility, shown by the Computed Tomography (CT); and second, the histopathology of COVID-19 pulmonary involvement, which generates different degrees of physical density (de-aeration) within the lung, ranging from diffuse patchy alveolar damage to consolidations. Subpleural hyper densities are detectable by ultrasound [30,31], and COVID-19 histopathology (expressed by hyperdensities) represents a measure of the injury of the respiratory tissue which, in the most severe cases, can lead to respiratory failure.

The most frequently observed anatomical feature of COVID-19 is diffuse alveolar damage (DAD), characterized by high levels of proinflammatory cytokines. Later, a proliferative phase develops, involving fibroblasts, myofibroblast, lymphocytes, and extracellular matrix, with intra-alveolar fibrin accumulation. Finally, large vessel thrombosis and microthrombi containing fibrin and platelets may be detected in arteries smaller than 1 mm. In short, ultrasound consolidation corresponds to a lung region deprived of air, therefore without gas exchange. Alternatively, consolidations can represent ischemic regions. This overlap of viral, inflammatory, immune, and vascular events is clinically expressed by disease phenotypes with different prognostic weight [32].

This non-homogeneity was highlighted by Gattinoni et al. [33]. They noted that COVID-19 subjects with respiratory failure showed different clinical patterns of "pneumonia" with different pathophysiology. The transition between different pulmonary COVID-19 phenotypes probably depends on the interaction of many factors, also affecting the ventilation modes and contributing to respiratory injury.

If ultrasound allows bedside assessment of the subpleural lung in terms of density, i.e., absolute or relative reduction of the air spaces and interstitial ratio, or de-aeration, it is reasonable to expect correlations between ultrasound signs and the clinical picture in patients with COVID-19 lung involvement [34].

Although LUS is not currently included in the main international guidelines for COVID-19 patient management, some authors have proposed semi-quantitative LUS scores, which can be used to quantify lung aeration [35]. This approach has recently been used in patients with COVID-19 pneumonia. [36,37].

In the light of recent evidence regarding the genesis of pulmonary signs in ultrasound [35], and their possible relationship with the superficial histopathology of the lung in terms of density and de-structuring, it can be theorized that ultrasound can help define a stratification of tissue damage in COVID-19 patients.

The four-level ultrasound score used in this paper is based on the concept of disease severity, with consideration given to extension of findings on the lung and the nature of tissue densities [38].

Despite the profound difference between CT (tomographic) and ultrasound (exploring only superficial densities), LUS and CT scores showed a weak (but statistically significant) positive linear relationship. This agrees with other observations [39–41]. A plausible explanation can be found in the prevalent peripheral, subpleural expression of COVID-19 pulmonary injuries [11,15], which can minimize the differences between the two methods (axial and superficial estimates).

Results of this study and other observations agree with this hypothesis. In practical terms, LUS can be considered an equally accurate alternative to CT in cases of COVID-19, particularly in situations where CT is not easily accessible or when molecular tests are not available [42,43].

In our study, a significant positive correlation was demonstrated between LUS score and CT score, and certain strategic parameters (COVID-19 phenotype, need for non-invasive ventilation, hematic lactate level, and mortality) (Tables 3 and 4). As expected, P/F, pH, and pO_2, displayed significant negative correlations. However, the most relevant and clinically important inverse proportionality was found in relation to P/F, i.e., higher LUS/CT scores were indicative of a decrease in P/F ratio.

This study reinforces the results presented by Perrone et al [37], which demonstrated a significant correlation between an equivalent US scoring system (of 12 fields), and established end points of clinical worsening, including high-flow oxygen support, ICU admission, and death. This is important, because their methodology of ultrasound exploration of the chest and the score used in their study (specifically proposed for COVID-19 patients) were the same as those we used.

Many other studies showed that the extent of lung abnormalities evaluated by the LUS score is a predictor of a worse outcome, ETI, or death [44,45]. However, the scoring systems used, and, above all, the number of regions explored are often not comparable to each other. For example, it has been assumed that a very marked reduction in the number of regions explored may decrease the accuracy of LUS, as demonstrated by Falster et al. [46] using the Mongodi score with analysis of only eight thoracic areas.

From a practical point of view, our results justify the attribution of an LUS score to every COVID-19 patient, from the early stages of management and during monitoring in the various settings. LUS may have a potential role in Emergency department for triaging symptomatic patients, managing ventilation, weaning ICU patients, and monitoring COVID-19 pneumonia and its evolution toward ARDS in critically ill patients. Moreover, it may be considered a first-line alternative to chest X-ray and CT scan in critically ill patients.

Even though asymptomatic carriers may comprise 17.9–33.3% of patients with COVID-19 [47,48], and can contribute to the spread of the infection, the role of screening these asymptomatic carriers is not known. Ultrasonography could help identify infected people with signs and symptoms at the onset [49]. Compared to its sensitivity, the specificity of US to pathological artifacts of the lung in COVID-19 and other diseases is generally considered low.

US signs of COVID-19 are present in various degrees in other pathologies (diffuse pneumonia, pulmonary edema, interstitial lung diseases). The diagnostic accuracy of pulmonary ultrasound in COVID-19 is based on the diffuse and bilateral aspect of lung involvement, on the prevalence of artefactual components, and on a typically patchy distribution. Of course, the pretest probability of having contracted the infection assumes significance [34]. At present, to our knowledge, very few lung diseases with a large epidemic diffusion show these aspects.

In this study, we found that the most common CT findings were GGO, consolidation, and crazy-paving patterns, including "spider web sign" (defined as a triangular or angular GGO in the subpleural lung with the internal interlobular septa thickened like a net). A differential diagnosis between COVID 19 and systemic sclerosis (SSc) with interstitial lung is made possible by employing CT images; the presence of consolidations and fibrosis inside GGO in the lower lobes are independent CT diagnostic features for COVID-19 [50]. As expected, the most common ultrasound signs were vertical artifacts and white lung. A quantitative LUS score for lung aeration assessment has been proposed, based on the identification of four patterns in number and type of visualized artifacts: normal aeration, moderate, severe, and complete loss of aeration [51]. Baldi et al. [52] reported a relationship between the number of B-lines and lung density in mechanically ventilated patients. In patients with VAP, changes in LUS score before and after antibiotics predicted improvement in lung aeration. These findings are consistent with the fact that CT scan computes lung

density, which is also the main determinant of appearance, number, and coalescence of LUS artifacts.

In agreement with recent evidence that connects the vertical artifacts to acoustic traps that can capture acoustic energy and restore it over time, and white lung with a relatively random scattered distribution, a relationship between CT and US features can be speculated [53]; for example, between septal enlargement and vertical artifacts, or between ground glass opacity in CT and white lung. Equally probable is a deteriorating progression, in terms of ventilation, from less dense vertical artifacts to white lung and consolidations.

Consolidations were significantly more frequent in severe and critical patients. In consolidations, the alveoli are filled by inflammatory exudation, and/or collapsed. If the role of consolidations in causing a shunt effect is recognized, it can be speculated that consolidations are aggravating factors and indicators of cytokine storm, vascular damage, ARDS, or bacterial superinfection.

As regards the laboratory indicator, we found a difference between the ordinary and severe and critical phenotypes. The decrease of lymphocytes in the severe and critical patients indicated that many immune cells had been consumed, and the immune function was inhibited. Damage to lymphocytes may be critical in-patient exacerbation, and the decreased lymphocytes could be used as an important index in the evaluation of disease severity. The increased values of neutrophil ratio, C-reactive protein, and procalcitonin in severe and critical patients may have been related to cytokine storm induced by virus invasion, and to comorbidity with other kinds of infections, which has been supported by recent studies [29]. The timely prevention of infection may help reduce complications and mortality.

The strength of this study concerns the robustness of the data obtained from a large, real-life, general adult population, where COVID-19-positive individuals with pneumonia were included. Moreover, all patients were evaluated by the same CT and US methodology, including the score used.

However, the study has some limitations. Ultrasound scans were performed by different operators and the inter-operator agreement was not assessed, due to the technical difficulties imposed by the emergency clinical context.

Moreover, in our study there was no control group, as its purpose was not to validate the test nor to provide a differential diagnosis with other diseases based on ultrasound imaging, but to evaluate how useful ultrasound can be in the management of a COVID setting.

It is also important to consider that our results were linked to the prevalence of the disease, which was particularly high during the first wave of the pandemic. With a lower prevalence, the significance of our analysis should be revisited.

5. Conclusions

LUS score was independently able to predict a higher risk of adverse events in patients with COVID-19. Indeed, patients with higher LUS scores were more likely to have higher levels of cardiac injury, coagulopathy, and inflammatory biomarkers, more non-invasive ventilation with c-pap or b-level, higher incidence of respiratory failure, ARDS, and sepsis, and higher mortality. The US does not replace the CT examination gold standard for interstitial pneumonia, and US has poor capacity for risk stratification compared to CT. More interesting is the role of US for monitoring patients at the bedside every day during hospitalization, for clinical and instrumental correlation, for follow-up, and for reducing the risk of radiation. Likewise, chest CT has played a crucial role in characterizing pulmonary lesions during the COVID-19 pandemic. It can accurately evaluate the type and extent of lung lesions and could be used to evaluate the severity of the disease. LUS allows only a superficial mapping of the lung, and the LUS score in theory is not perfectly comparable to the CT score (a volumetric estimate of injury). It is conceivable that a certain congruence of results is linked to the superficial expression of lesions, and that therefore in COVID-19 relative symmetry between volume and surface of the pulmonary lesions is maintained. In

conclusion, LUS and chest CT have been shown to play a synergistic role in the diagnosis and severity evaluation of COVID-19.

Author Contributions: M.L., S.T. and L.R.: study design, data analysis, data interpretation, and writing and reviewing the paper. G.O., M.G.C. and V.F.: data collection, data interpretation, and reviewing the paper. M.C., R.C., P.P.S., N.R. and A.P. (Antonella Pesce): data collection, and reviewing the final version of the paper. G.S., F.C.S., R.G., R.F., M.I., A.P. (Alessandro Perrella), G.V., D.V., F.F., F.S. and A.N., reviewing the paper. All authors have read and agreed to the published version of the manuscript.

Funding: This research received no external funding.

Institutional Review Board Statement: The study protocol was approved by the Institutional Ethics Committee of Ancona (ID 0179104/I, 28 July 2021).

Informed Consent Statement: Informed consent was obtained from all subjects involved in the study.

Data Availability Statement: The raw data supporting this study will be made available by the authors if requested.

Acknowledgments: We are grateful to the patients who participated in the study.

Conflicts of Interest: The authors declare that the research was conducted in the absence of any commercial or financial relationships that could be construed as a potential conflict of interest.

References

1. WHO. Coronavirus (COVID-19) Dashboard. Available online: https://covid19.who.int/ (accessed on 16 February 2022).
2. Valdenassi, L.; Franzini, M.; Ricevuti, G.; Rinaldi, L.; Galoforo, A.C.; Tirelli, U. Letter to the Editor: Potential mechanisms by which the oxygen-ozone (O_2–O_3) therapy could contribute to the treatment against the coronavirus COVID-19. *Eur. Rev. Med. Pharmacol. Sci.* **2020**, *24*, 4059–4061. [CrossRef] [PubMed]
3. Zhou, F.; Yu, T.; Du, R.; Fan, G.; Liu, Y.; Liu, Z.; Xiang, J.; Wang, Y.; Song, B.; Gu, X.; et al. Clinical Course and Risk Factors for Mortality of Adult Inpatients with COVID-19 in Wuhan, China: A Retrospective Cohort Study. *Lancet* **2020**, *395*, 1054–1062. [CrossRef]
4. Kudlinski, B.; Zgoła, D.; Stolińska, M.; Murkos, M.; Kania, J.; Nowak, P.; Noga, A.; Wojciech, M.; Zaborniak, G.; Zembron-Lacny, A. Systemic Inflammatory Predictors of In-Hospital Mortality in COVID-19 Patients: A Retrospective Study. *Diagnostics* **2022**, *12*, 859. [CrossRef] [PubMed]
5. Léonard-Lorant, I.; Delabranche, X.; Séverac, F.; Helms, J.; Pauzet, C.; Collange, O.; Ohana, M. Acute Pulmonary Embolism in Patients with COVID-19 at CT Angiography and Relationship to d-Dimer Levels. *Radiology* **2020**, *296*, E189–E191. [CrossRef]
6. Poyiadji, N.; Cormier, P.; Patel, P.Y.; Hadied, M.O.; Bhargava, P.; Khanna, K.; Nadig, J.; Keimig, T.; Spizarny, D.; Reeser, N.; et al. Acute Pulmonary Embolism and COVID-19. *Radiology* **2020**, *297*, E335–E338. [CrossRef] [PubMed]
7. Grillet, F.; Behr, J.; Calame, P.; Aubry, S.; Delabrousse, E. Acute Pulmonary Embolism Associated with COVID-19 Pneumonia Detected with Pulmonary CT Angiography. *Radiology* **2020**, *296*, E186–E188. [CrossRef]
8. Kermali, M.; Khalsa, R.K.; Pillai, K.; Ismail, Z.; Harky, A. The Role of Biomarkers in Diagnosis of COVID-19—A Systematic Review. *Life Sci.* **2020**, *254*, 117788. [CrossRef]
9. Rodrigues, T.S.; de Sá, K.S.; Ishimoto, A.Y.; Becerra, A.; Oliveira, S.; Almeida, L.; Gonçalves, A.V.; Perucello, D.B.; Andrade, W.A.; Castro, R.; et al. Inflammasomes are activated in response to SARS-CoV-2 infection and are associated with COVID-19 severity in patients. *Exp. Med.* **2021**, *218*, e20201707. [CrossRef]
10. Bernheim, A.; Mei, X.; Huang, M.; Yang, Y.; Fayad, Z.A.; Zhang, N.; Diao, K.; Lin, B.; Zhu, X.; Li, K.; et al. Chest CT Findings in Coronavirus Disease-19 (COVID-19): Relationship to Duration of Infection. *Radiology* **2020**, *295*, 200463. [CrossRef] [PubMed]
11. Fumagalii, C.; Rozzini, R.; Vannini, M.; Coccia, F.; Cesaroni, G.; Mazzeo, F.; Cola, M.; Bartoloni, A.; Fontanari, P.; Lavorini, F.; et al. Clinical risk score to predict in-hospital mortality in COVID-19 patients: A retrospective cohort study. *BMJ Open* **2020**, *10*, e040629. [CrossRef]
12. Leonardi, A.; Scipione, R.; Alfieri, G.; Petrillo, R.; Dolciami, M.; Ciccarelli, F.; Perotti, S.; Cartocci, G.; Scala, A.; Imperiale, C.; et al. Role of computed tomography in predicting critical disease in patients with COVID-19 pneumonia: A retrospective study using a semiautomatic quantitative method. *Eur. J. Radiol.* **2020**, *130*, 109202. [CrossRef] [PubMed]
13. Liu, H.; Luo, S.; Zhang, Y.; Jiang, Y.; Jiang, Y.; Wang, Y.; Li, H.; Huang, C.; Zhang, S.; Li, X.; et al. Chest CT Features of 182 Patients with Mild Coronavirus Disease 2019 (COVID-19) Pneumonia: A Longitudinal, Retrospective and Descriptive Study. *Infect. Dis. Ther.* **2020**, *9*, 1029–1041. [CrossRef] [PubMed]
14. Zhan, J.; Li, H.; Yu, H.; Liu, X.; Zeng, X.; Peng, D.; Zhang, W. 2019 novel coronavirus (COVID-19) pneumonia: CT manifestations and pattern of evolution in 110 patients in Jiangxi, China. *Eur. Radiol.* **2021**, *31*, 1059–1068. [CrossRef] [PubMed]
15. Chung, M.; Bernheim, A.; Mei, X.; Zhang, N.; Huang, M.; Zeng, X.; Cui, J.; Xu, W.; Yang, Y.; Fayad, Z.; et al. CT Imaging Features of 2019 Novel Coronavirus (2019-nCoV). *Radiology* **2020**, *295*, 202–207. [CrossRef] [PubMed]

16. Soldati, G.; Smargiassi, A.; Inchingolo, R.; Buonsenso, D.; Perrone, T.; Briganti, D.F.; Perlini, S.; Torri, E.; Mariani, A.; Mossolani, E.E.; et al. Proposal for International Standardization of the Use of Lung Ultrasound for Patients with COVID-19: A Simple, Quantitative, Reproducible Method. *J. Ultrasound Med.* **2020**, *39*, 1413–1419. [CrossRef]
17. Mayo, P.H.; Copetti, R.; Feller-Kopman, D.; Mathis, G.; Maury, E.; Mongodi, S.; Mojoli, F.; Volpicelli, G.; Zanobetti, M. Thoracic ultrasonography: A narrative review. *Intensive Care Med.* **2019**, *45*, 1200–1211. [CrossRef]
18. Rinaldi, L.; Milione, S.; Fascione, M.C.; Pafundi, P.C.; Altruda, C.; Di Caterino, M.; Monaco, L.; Reginelli, A.; Perrotta, F.; Porta, G.; et al. Relevance of lung ultrasound in the diagnostic algorithm of respiratory diseases in a real-life setting: A multicentre prospective study. *Respirology* **2020**, *25*, 535–542. [CrossRef]
19. Jalil, B.A.; Khan, A.; Kugasia, I.R.; Ijaz, M. Lung ultrasound in early SARS-CoV-2 pneumonia and the LUS-CoV criteria. In *Baylor University Medical Center Proceedings*; Taylor & Francis: Oxfordshire, UK, 2020; Volume 34, pp. 1–4. [CrossRef]
20. Lugara, M.; Oliva, G.; Pafundi, P.C.; Tamburrini, S.; Nevola, R.; Gjeloshi, K.; Rinaldi, L. Clinical application of lung ultrasound score on COVID-19 setting: A regional experience in Southern Italy. *Eur. Rev. Med. Pharmacol. Sci.* **2021**, *25*, 3623–3631. [CrossRef] [PubMed]
21. Pivetta, E.; Goffi, A.; Tizzani, M.; Locatelli, S.M.; Porrino, G.; Losano, I.; Leone, D.; Calzolari, G.; Vesan., M.; Steri, F.; et al. Lung Ultrasonography for the Diagnosis of SARS-CoV-2 Pneumonia in the Emergency Department. *Ann. Emerg. Med.* **2021**, *77*, 385–394. [CrossRef]
22. Buonsenso, D.; Piano, A.; Raffaelli, F.; Bonadia, N.; de Gaetano Donati, K.; Franceschi, F. Point-of-Care Lung Ultrasound findings in novel coronavirus disease-19 pnemoniae: A case report and potential applications during COVID-19 outbreak. *Eur. Rev. Med. Pharmacol. Sci.* **2020**, *24*, 2776–2780. [CrossRef] [PubMed]
23. Soldati, G.; Demi, M.; Smargiassi, A.; Inchingolo, R.; Demi, L. The role of ultrasound lung artifacts in the diagnosis of respiratory diseases. *Expert. Rev. Respir. Med.* **2019**, *13*, 163–172. [CrossRef] [PubMed]
24. Delle Sedie, A.; Carli, L.; Cioffi, E.; Bombardieri, S.; Riente, L. The promising role of lung ultrasound in systemic sclerosis. *Clin. Rheumatol.* **2012**, *31*, 1537–1541. [CrossRef] [PubMed]
25. Gutierrez, M.; Salaffi, F.; Carotti, M.; Tardella, M.; Pineda, C.; Bertolazzi, C.; Bichisecchi, E.; Filippucci, E.; Grassi, W. Utility of a simplified ultrasound assessment to assess interstitial pulmonary fibrosis in connective tissue disorders–preliminary results. *Arthritis Res. Ther.* **2011**, *13*, R134. [CrossRef] [PubMed]
26. Ruaro, B.; Baratella, E.; Confalonieri, P.; Confalonieri, M.; Vassallo, F.G.; Wade, B.; Geri, P.; Pozzan, R.; Caforio, G.; Marrocchio, C.; et al. High-Resolution Computed Tomography and Lung Ultrasound in Patients with Systemic Sclerosis: Which One to Choose? *Diagnostics* **2021**, *11*, 2293. [CrossRef]
27. Lokuge, A.; Alexander, J.; Land, B.; McAllister, A. Lung ultrasound in a respiratory pandemic. *Emerg. Med. Australas.* **2020**, *32*, 883–889. [CrossRef]
28. Burkert, J.; Jarman, R.; Deol, P. Evolution of Lung Abnormalities on Lung Ultrasound in Recovery from COVID-19 Disease—A Prospective, Longitudinal Observational Cohort Study. *J. Ultrasound. Med.* **2022**. [CrossRef]
29. Soldati, G.; Smargiassi, A.; Inchingolo, R.; Buonsenso, D.; Perrone, T.; Briganti, D.F.; Perlini, S.; Torri, E.; Mariani, A.; Mossolani, E.E.; et al. Is There a Role for Lung Ultrasound During the COVID-19 Pandemic? *J. Ultrasound. Med.* **2020**, *39*, 1459–1462. [CrossRef]
30. Soldati, G.; Smargiassi, A.; Inchingolo, R.; Sher, S.; Nenna, R.; Valente, S.; Inchingolo, C.D.; Corbo, G.M. Lung Ultrasonography may Provide an Indirect Estimation of Lung Porosity and Airspace Geometry. *Respiration* **2014**, *88*, 458–468. [CrossRef]
31. Soldati, G.; Smargiassi, A.; Demi, L.; Inchingolo, R. Artifactual lung ultrasonography: It is a matter of traps, order, and disorder. *Appl. Sci.* **2020**, *10*, 1570. [CrossRef]
32. Shafqat, A.; Shafqat, S.; Salameh, S.A.; Kashir, J.; Alkattan, K.; Yaqinuddin, A. Mechanistic insights into the immune pathophysiology of COVID-19; an in-depth review. *Front. Immunol.* **2022**, *13*, 835104. [CrossRef]
33. Gattinoni, L.; Gattarello, S.; Steinberg, I.; Busana, M.; Palermo, P.; Lazzari, S.; Romitti, F.; Quintel, M.; Meissner, K.; Marini, J.J.; et al. COVID-19 pneumonia: Pathophysiology and management. *Eur. Respir. Rev.* **2021**, *30*, 210138. [CrossRef] [PubMed]
34. Soldati, G.; Demi, M. What Is COVID 19 Teaching Us about Pulmonary Ultrasound? *Diagnostics* **2022**, *12*, 838. [CrossRef] [PubMed]
35. Mongodi, S.; De Luca, D.; Colombo, A.; Stella, A.; Santangelo, E.; Corradi, F.; Gargani, L.; Rovida, S.; Volpicelli, G. Quantitative Lung Ultrasound: Technical aspects and clinical applications. *Anesthesiology* **2021**, *134*, 949–965. [CrossRef] [PubMed]
36. Nguyen, M.; Gaujard, G.; Guinot, P.G.; Bouhemad, B.; L.U. S. Study Group. Using the lung ultrasound score to monitor disease progression for COVID-19-associated ARDS. *Intensive Care Med.* **2021**, *47*, 1329–1331. [CrossRef] [PubMed]
37. Perrone, T.; Soldati, G.; Padovini, L.; Fiengo, A.; Lettieri, G.; Sabatini, U.; Gori, G.; Lepore, F.; Garolfi, M.; Palumbo, I.; et al. A New Lung Ultrasound Protocol Able to Predict Worsening in Patients Affected by Severe Acute Respiratory Syndrome Coronavirus 2 Pneumonia. *J. Ultrasound Med.* 2020; *in press*. [CrossRef] [PubMed]
38. Demi, M.; Prediletto, R.; Soldati, G.; Demi, L. Physical Mechanisms Providing Clinical Information from Ultrasound Lung Images: Hypotheses and Early Confirmations. *IEEE Trans. Ultrason. Ferroelectr. Freq. Control* **2020**, *67*, 612–623. [CrossRef]
39. Kumar, A.; Weng, I.; Graglia, S.; Lew, T.; Gandhi, K.; Lalani, F.; Chia, D.; Duanmu, Y.; Jensen, T.; Lobo, V.; et al. Point-of-Care Ultrasound predicts clinical outcomes in patients with COVID-19. *J. Ultrasound Med.* **2022**, *67*, 1367–1375. [CrossRef]
40. Stecher, S.S.; Anton, S.; Fraccaroli, A.; Götschke, G. Lung ultrasound predicts clinical course but not outcome in COVID-19 ICU patients: A retrospective single-center analysis. *BMC Anesthesiol.* **2021**, *21*, 178. [CrossRef]

41. Hoffmann, T.; Bulla, P.; Jödicke, L.; Klein, C.; Bott, S.M.; Keller, R.; Malek, N.; Fröhlich, E.; Göpel, S.; Blumenstock, G.; et al. Can follow up lung ultrasound in Coronavirus Disease-19 patients indicate clinical outcome? *PLoS ONE* **2021**, *16*, e0256359. [CrossRef]
42. Wang, M.; Luo, X.; Wang, L.; Estill, J.; Lv, M.; Zhu, Y.; Wang, Q.; Xiao, X.; Song, Y.; Lee, M.S.; et al. A comparison of lung Ultrasound and Computed Tomography in the diagnosis of patients with COVID-19: A systematic Review and Meta-Analysis. *Diagnostics* **2021**, *11*, 1351. [CrossRef]
43. Buda, N.; Cylwik, J.; Mróz, K.; Rudzińska, R.; Dubik, P.; Malczewska, A.; Oraczewska, A.; Skoczyński, S.; Suska, A.; Górecki, T.; et al. Lung Ultrasound examination in patients with SARS-CoV-2 Infection: Multicenter study. *J. Clin. Med.* **2021**, *10*, 3255. [CrossRef] [PubMed]
44. Lichter, Y.; Topilsky, Y.; Taieb, P.; Banai, A.; Hochstadt, A.; Merdler, I.; Oz, A.G.; Vine, J.; Goren, O.; Cohen, B.; et al. Lung ultrasound predicts clinical course and outcomes in COVID-19 patients. *Intensive Care Med.* **2020**, *46*, 1873–1883. [CrossRef] [PubMed]
45. Zhao, L.; Yu, K.; Zhao, Q.; Tian, R.; Xie, H.; Xie, L.; Deng, P.; Xie, G.; Bao, A.; Du, J. Lung Ultrasound Score in Evaluating the Severity of Coronavirus Disease 2019 (COVID-19) Pneumonia. *Ultrasound Med. Biol.* **2020**, *46*, 2938–2944. [CrossRef] [PubMed]
46. Falster, C.; Jacobsen, N.; Wulff Madsen, L.; Dahlerup Rasmussen, L.; Davidsen, J.R.; Christie Knudtzen, F.; Nielsen, S.L.; Johansen, I.S.; Laursen, C.B. Lung ultrasound may be a valuable aid in decision making for patients admitted with COVID-19 disease. *Eur. Clin. Respir. J.* **2021**, *8*, 1909521. [CrossRef]
47. Nishiura, H.; Kobayash, T.; Miyama, T.; Suzuki, A.; Jung, S.M.; Hayashi, K.; Kinoshita, R.; Yang, Y.; Yuan, B.; Akhmetzhanov, A.R.; et al. Estimation of the asymptomatic ratio of novel coronavirus infections (COVID-19). *Int. J. Infect. Dis.* **2020**, *94*, 154–155. [CrossRef]
48. Mizumoto, K.; Kagaya, K.; Zarebski, A.; Chowell, G. Estimating the asymptomatic proportion of coronavirus disease 2019 (COVID-19) cases on board the Diamond Princess cruise ship, Yokohama, Japan, 2020. *Eurosurveillance* **2020**, *25*, 2000180. [CrossRef]
49. Puylaert, C.A.J.; Scheijmans, J.C.G.; Borgstein, A.B.J.; Andeweg, C.S.; Bartels-Rutten, A.; Beets, G.L.; van Berge Henegouwen, M.I.; Braak, S.J.; Couvreur, R.; Daams, F.; et al. Yield of Screening for COVID-19 in Asymptomatic patients before Elective or Emergency Surgery Using Chest CT and RT-PCR (SCOUT). *Ann. Surg.* **2020**, *272*, 919–924. [CrossRef]
50. Pelosi, P.; Tonelli, R.; Torregiani, C.; Baratella, E.; Confalonieri, M.; Battaglini, D.; Marchioni, A.; Confalonieri, P.; Clini, E.; Salton, F.; et al. Different Methods to Improve the Monitoring of Noninvasive Respiratory Support of Patients with Severe Pneumonia/ARDS Due to COVID-19: An Update. *J. Clin. Med.* **2022**, *11*, 1704. [CrossRef] [PubMed]
51. Bouhemad, B.; Liu, Z.H.; Arbelot, C.; Zhang, M.; Ferarri, F.; Le-Guen, M.; Girard, M.; Lu, Q.; Rouby, J.-J. Ultrasound assessment of anti- biotic-induced pulmonary reaeration in ventilator-associated pneumo-nia. *Crit. Care Med.* **2010**, *38*, 84–92.
52. Baldi, G.; Gargani, L.; Abramo, A.; D'Errico, L.; Caramella, D.; Picano, E.; Giunta, F.; Forfori, F. Lung water assessment by lung ultrasonography in intensive care: A pilot study. *Intensive Care Med.* **2013**, *39*, 74–84. [CrossRef]
53. Demi, M.; Buda, N.; Soldati, G. Vertical Artifacts in Lung Ultrasonography: Some Common Clinician Questions and the Related Engineer Answers. *Diagnostics* **2022**, *12*, 215. [CrossRef] [PubMed]

diagnostics

MDPI

Review

Lung Ultrasound: A Diagnostic Leading Tool for SARS-CoV-2 Pneumonia: A Narrative Review

Luigi Maggi [1,*], Anna Maria Biava [2], Silvia Fiorelli [2], Flaminia Coluzzi [3], Alberto Ricci [2] and Monica Rocco [2]

[1] Department of Central Prevention Police, Ministry of Interior, 00198 Rome, Italy
[2] Department of Medical-Surgical Sciences and Translational Medicine, Via di Grottarossa 1035, Sapienza University of Rome, 00189 Rome, Italy; annamariabiava@gmail.com (A.M.B.); silvia.fiorelli@uniroma1.it (S.F.); alberto.ricci@uniroma1.it (A.R.); monica.rocco@uniroma1.it (M.R.)
[3] Department Medical and Surgical Sciences and Biotechnologies, Piazzale Aldo Moro 5, Sapienza University of Rome, 00185 Rome, Italy; flaminia.coluzzi@uniroma1.it
* Correspondence: maggi.medicina@libero.it

Abstract: Severe acute respiratory syndrome coronavirus 2 (SARS-CoV-2) has spread worldwide causing a global pandemic. In this context, lung ultrasound (LUS) has played an important role due to its high diagnostic sensitivity, low costs, simplicity of execution and radiation safeness. Despite computed tomography (CT) being the imaging gold standard, lung ultrasound point of care exam is essential in every situation where CT is not readily available nor applicable. The aim of our review is to highlight the considerable versatility of LUS in diagnosis, framing the therapeutic route and follow-up for SARS-CoV-2 interstitial syndrome.

Keywords: lung ultrasound; COVID-19; SARS-CoV-2; pneumonia; point of care; interstitial syndrome; chest ultrasound

Citation: Maggi, L.; Biava, A.M.; Fiorelli, S.; Coluzzi, F.; Ricci, A.; Rocco, M. Lung Ultrasound: A Diagnostic Leading Tool for SARS-CoV-2 Pneumonia: A Narrative Review. *Diagnostics* **2021**, *11*, 2381. https://doi.org/10.3390/diagnostics11122381

Academic Editors: Marcello Demi and Gino Soldati

Received: 8 November 2021
Accepted: 15 December 2021
Published: 17 December 2021

1. Introduction

At the end of 2019, a new coronavirus called SARS-CoV-2, emerged in China, which was first caused an epidemic illness in Wuhan and then spread worldwide causing a global pandemic [1]. SARS-CoV-2 has high affinity for upper and lower respiratory tract illnesses [2].

Clinical presentation of SARS-CoV-2 infection has an extremely heterogeneous spectrum of severity ranging from self-limiting infection to acute respiratory failure [3].

The diagnostic gold standard of coronavirus lung involvement is chest tomography with a 97% sensitivity to detect SARS-CoV-2 pneumonia [4].

Typical CT findings of COVID-19 related to pneumonia are bilateral involvement in 100% of cases, with evidence of ground glass opacities, crazy paving signs, subpleural lines and fat vessel signs, which involve all lung lobes in 88% of cases. CT findings suggestive of SARS-CoV-2 pneumonia correlate with abnormalities seen on chest ultrasounds [5]. Contrarily, chest X-rays have a poor ability to detect SARS-CoV-2 lung lesions [6] compared to CT and chest ultrasounds [7].

Although CT scan is the imaging gold standard, it is expensive and includes some disadvantages such as the need to move patients, risk of spreading infections and use of human resources [8].

Ultrasound assessment for COVID-19 pneumonia to date has been clear since the beginning of the pandemic [3,9,10]. LUS was also used during the previous H1N1 viral pandemic, showing a good sensitivity and specificity [11]. Compared to CT, lung ultrasound is cost effective, radiation free, repeatable and performable bedside by a single operator [12].

In the context of the SARS-CoV-2 pandemic, the high sensitivity of thoracic ultrasound and its manageability should have numerous applications; however, has been extensively

used mostly in the emergency department (3) and intensive care unit (ICU) [13]. It could also be a valuable tool in the pre-hospital phase to identify those SARS-CoV-2 patients who are at high risk of developing respiratory failure requiring hospitalization.

Furthermore, it allows clinicians to monitor the long-term COVID-19 patients [14].

About 14% of SARS-CoV-2 positive patients require hospitalization and oxygen support and 5% require intensive care. Early identification of severe pneumonia allows for a more appropriate therapeutic approach to be initiated promptly in a designated hospital setting or intensive care unit. For this purpose, chest imaging (radiography, CT or LUS) is essential [15]. As compared to HRCT, LUS has the ability to detect interstitial syndrome with a sensitivity of 100% and a specificity of 97% [16]. LUS can be used in predicting outcome of SARS-CoV-2 pneumonia. It could guide the choice of different ventilatory strategies, from high flow nasal cannula to mechanical ventilation. Finally, LUS has a high predictive power of severity and fatality of SARS-CoV-2 pneumonia [17].

The role of chest ultrasound in the management of critically ill patient with respiratory symptoms has been extensively demonstrated, showing its diagnostic value, higher than chest X-ray and similar to chest CT scan in a wide range of pulmonary diseases [18]. LUS is particularly accurate in diagnosing dyspnea, differentiating between "wet" causes (cardiogenic pulmonary edema and acute inflammation) and "dry" causes (chronic obstructive pulmonary disease and asthma) [19].

Currently in this pandemic, LUS examination allows a complete evaluation of the patient with COVID-19 related interstitial pneumonia [20].

However, in this paper we underline the clear definition of the clinical context, and positive swab test in the management of the SARS-CoV-2 patient to define possible differential diagnosis of interstitial patterns as acute respiratory distress syndrome (ARDS) [21], pulmonary edema [22] and contusion [23].

2. Lung Ultrasound in COVID-19 Pneumonia: Technique

LUS for COVID-19 can be performed by most ultrasound machines available. A lung preset is available for many recent machines but operators can adjust settings to provide good quality images [18].

The feasibility of a lung scan does not provide a predefined scheme for the evaluation and can be adapted to the needs of the clinician.

However, we suggest depth should be set between 8 and 10 cm and modulated according to the height of the patient and the thickness of his chest wall.

Focus should be positioned on the pleural line when available. It might be necessary to adjust the post processing settings to acquire the best image.

The ultrasound chest exploration should be systematic, starting from the anterior to the inferior areas along the intercostal spaces from medial to lateral.

If the patient is in the supine position, it is advisable to scan the anterior and lateral thorax dividing each hemithorax into 6 zones with diagnostic accuracy comparable to the 12-zone scanning scheme [24]. When the patient is in forced supine position, it may also be convenient to use an 8-zone scan scheme. In this approach, 4 zones, 2 anterior and 2 lateral, are examined for each hemithorax. The anterior zones are between the mid-clavicular line medially and the anterior axillary line laterally, while the lateral zones are between the anterior axillary line medially and the posterior axillary line laterally [25].

Regarding the ultrasound analysis of posterior regions of the thorax, which can be scanned if the patient is able to maintain the sitting position, the detection is performed along the paravertebral line, the scapular line and the posterior axillary line [26].

The ultrasound probe can be positioned transversely along the intercostal space or longitudinally perpendicular to the ribs. This last approach makes it possible to identify "the bat sign" (Figure 1), in which the bat's wings are represented by the upper and lower ribs while the outline of the bat's body is the pleural line [27].

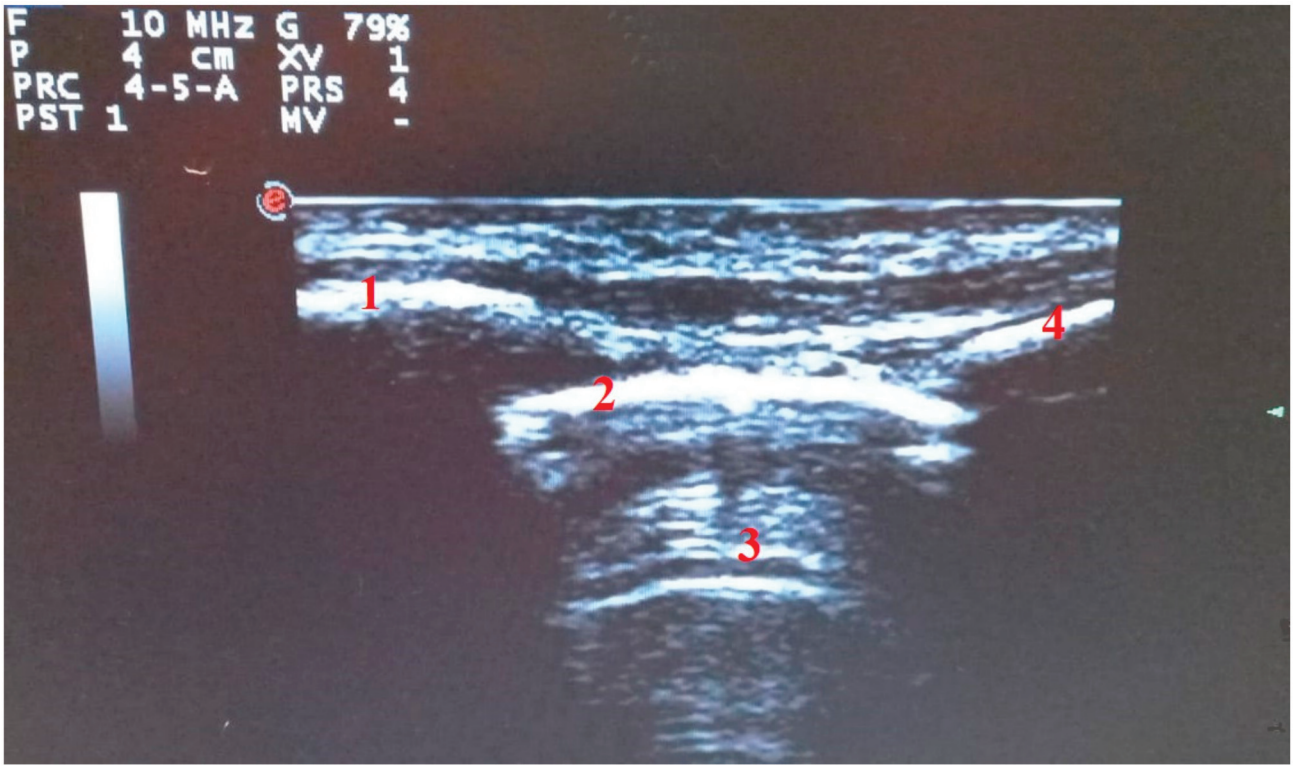

Figure 1. Longitudinal scan with linear probe: "the bat sign". (1) Upper rib. (2) Pleural line. (3) A Lines. (4) Lower rib.

It is possible to choose any transducer: cardiac, convex, micro convex or linear. Usually, the convex probe is the most used because it allows a better visualization of the pleural line and subpleural space. Moreover, it guarantees a better evaluation of the diaphragmatic recess. Alternatively, using a phased array for both cardiac and lung ultrasound can reduce costs [27].

3. Lung Ultrasound in COVID-19 Pneumonia: Findings

LUS Assessment for SARS-CoV-2 Pneumonia is a Clinically Driven "Point of Care" Method.

LUS detects changes in the relationship between air and tissue at the surface of the lung [12].

Ultrasound cannot be transmitted through air and allows for air-filled lungs to create artifacts.

In a normally aerated lung, a pleural line appears as a hyperechoic horizontal line that moves synchronously with breaths [28]. Moreover, we recognize several hyperechoic lines parallel to the pleura named A lines. Those are repetition artifact that indicates a normally aerated parenchyma [29]. However, in patients with chronic obstructive pulmonary disease (COPD), atelectasis of the lung and asthma, the A lines are present and well represented in the presence of normal lung sliding, while in patients with pneumothorax, the only visible artifacts are the A lines in the absence of lung sliding [25]. The Z lines are also non-pathological vertical hyperechoic artifacts that originate from the pleural line but do not reach the border of the screen, do not move with the lung sliding and do not cancel the A lines. These features allow to differentiate the Z lines from the B lines, which are also hyperechoic lines and instead can take on pathological significance.

SARS-CoV-2 pneumonia is an interstitial pneumonia with a typically peripheral distribution.

It is characterized by progressive reduction of air-filled lungs and LUS acts as a densitometer. It detects changes in the abnormal ventilated parenchyma due to lung density increasing and air content decreasing [30].

The sonographic findings suggestive of SARS-CoV-2 pneumonia are B-line, fuse B-line (white lung), abnormalities of pleural line, small and large peripherical consolidations with or without bronchogram [31].

B lines are vertical hyperechoic artifacts originating from the pleural line and extending to the bottom of the image erasing the A lines [3].

B line move synchronously with lung sliding and are indicative of interstitial syndrome [32]. Cluster of B- lines are the ultrasound sign of the subpleural interlobular thickening. In the scanned fields, more than three B lines or their confluence, configuring the "white lung", suggests an interstitial pneumonia SARS-CoV-2 and the number of B lines is associated with a greater severity of pulmonary involvement [33] (Figure 2).

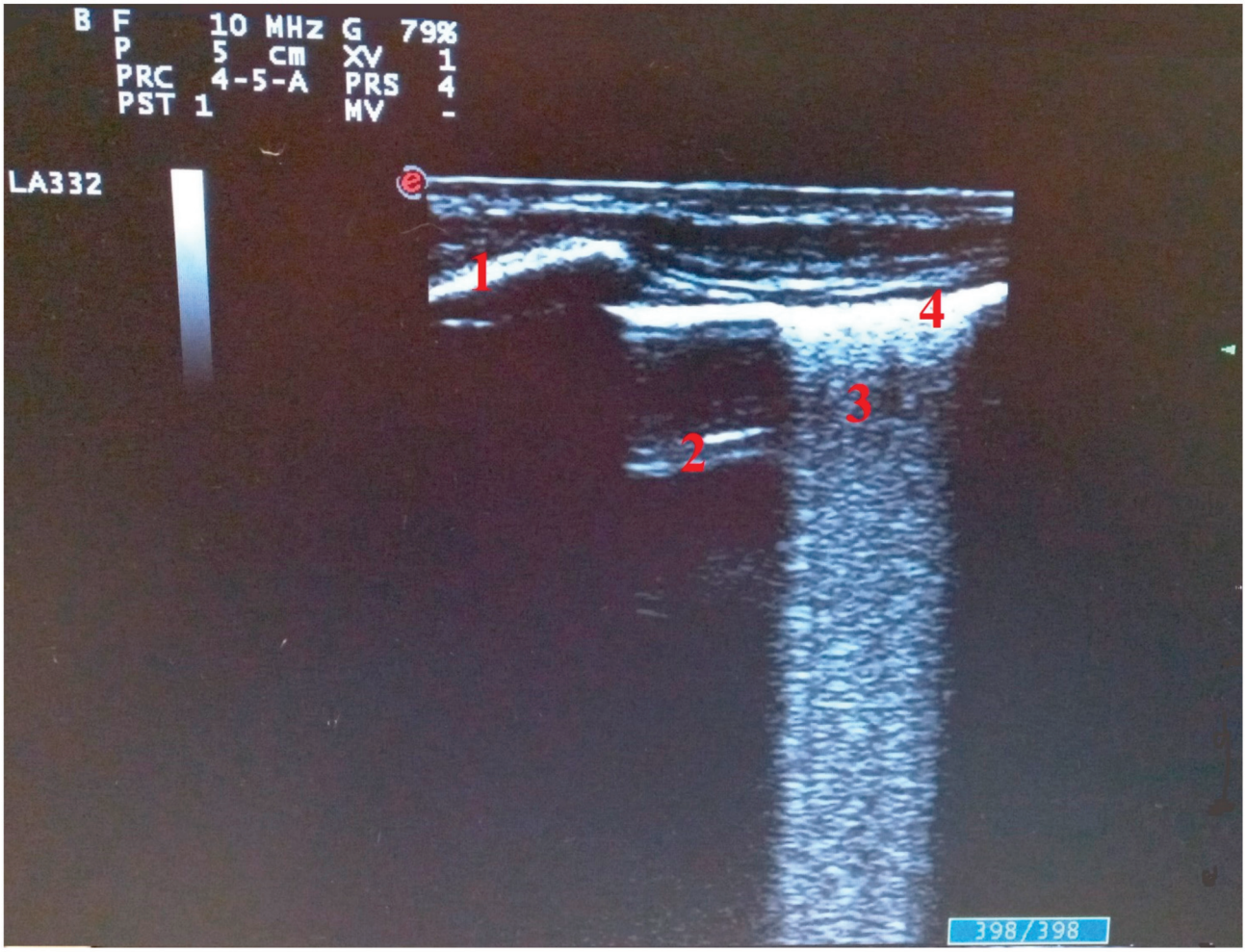

Figure 2. Ultrasound findings in SARS-CoV-2 pneumonia: (1) ribs, (2) A line, (3) cluster of B lines, (4) pleural line.

The Kerley B-lines visible on chest X-ray, which are the expression of the thickening of the interlobular septa in the interstitial syndrome, correlate with the ultrasound finding of B-lines in numbers greater than 3 per field [25]. In the initial phase, B lines have a focal distribution and there is a separation between them. As the disease progresses, B lines tend to merge and their distribution increases. In the resolution phase, they gradually disappear [26]. Consequently, ultrasound allows us to identify the different evolutionary stages of SARS-CoV-2 pneumonia [34].

The white lung is a multiple coalescent B line that completely occupies the lung field. It is due to alveolar de-aeration [3] and it correlates with ground glass on HRCT in SARS-CoV-2 pneumonia [3,33] (Figure 3).

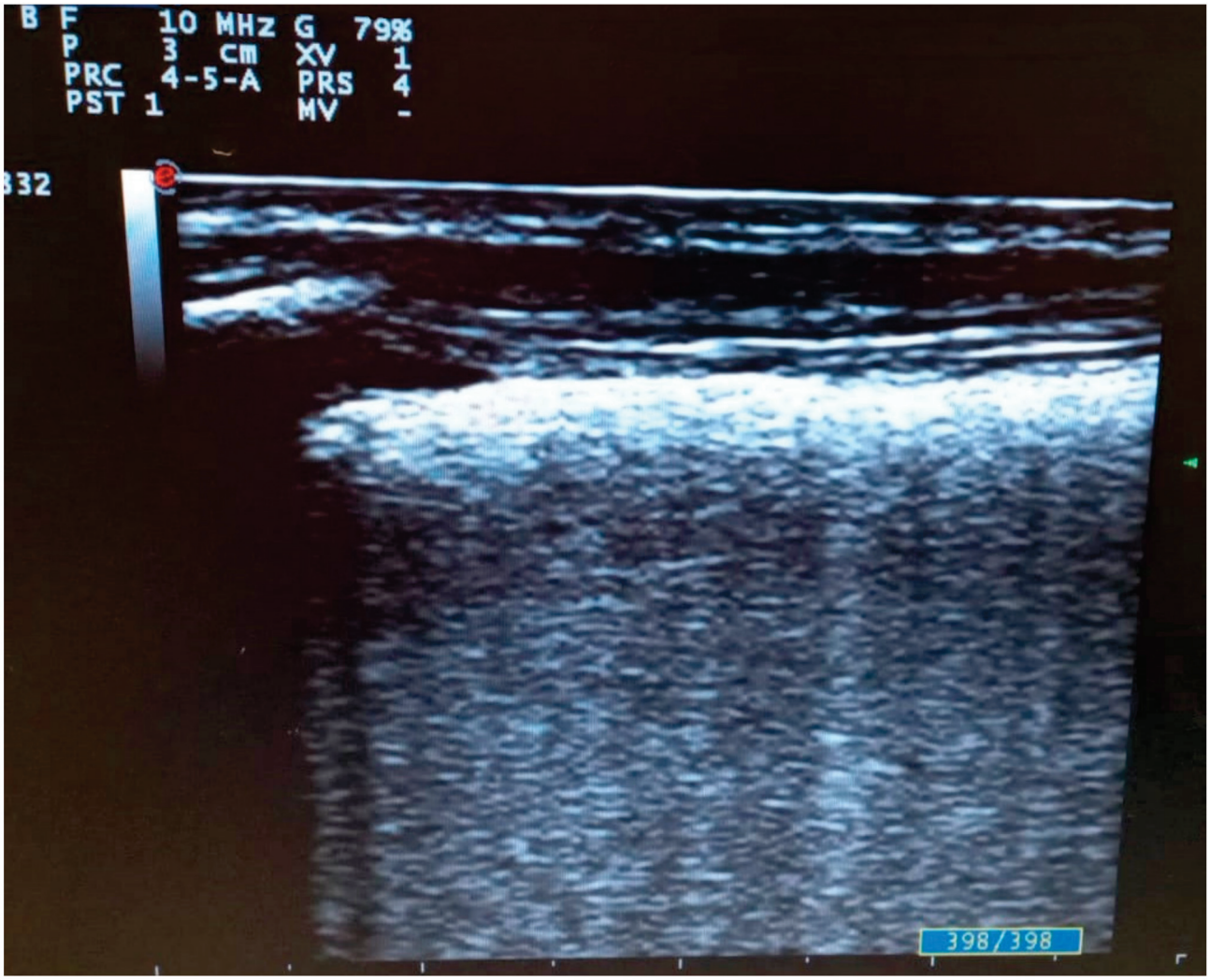

Figure 3. Transversal scan with linear probe of COVID-19 pneumonia: fused B lines configuring "white lung".

Among vertical artifacts of SARS-CoV-2 pneumonia, "the light beam", a bright vertical artifact that moves rapidly with sliding, correlates with the early phase "ground glass" observed on chest CT scan. It arises from a normal pleural line, goes within areas of normal pattern or with separate B lines and disappears quickly from the screen with an "on-off" effect [35].

Another suggestive ultrasound sign is abnormalities of the pleural line [36] (Figure 4). In the initial phase of the disease, small and diffuse irregular thickening of the pleural line appears. This artifact becomes more nodular in the appearance as the disease progresses, with areas of discontinuity that usually disappear if the disease progresses favorably [26].

In the subpleural space, consolidations can be found and appear on the ultrasound as areas of hepatization with irregular edges and air bronchogram [32].

Parenchymal consolidations increase with disease severity [37], while large consolidations with air bronchogram in the lower lobes raise the suspicion of bacterial superinfection [35] (Figure 5).

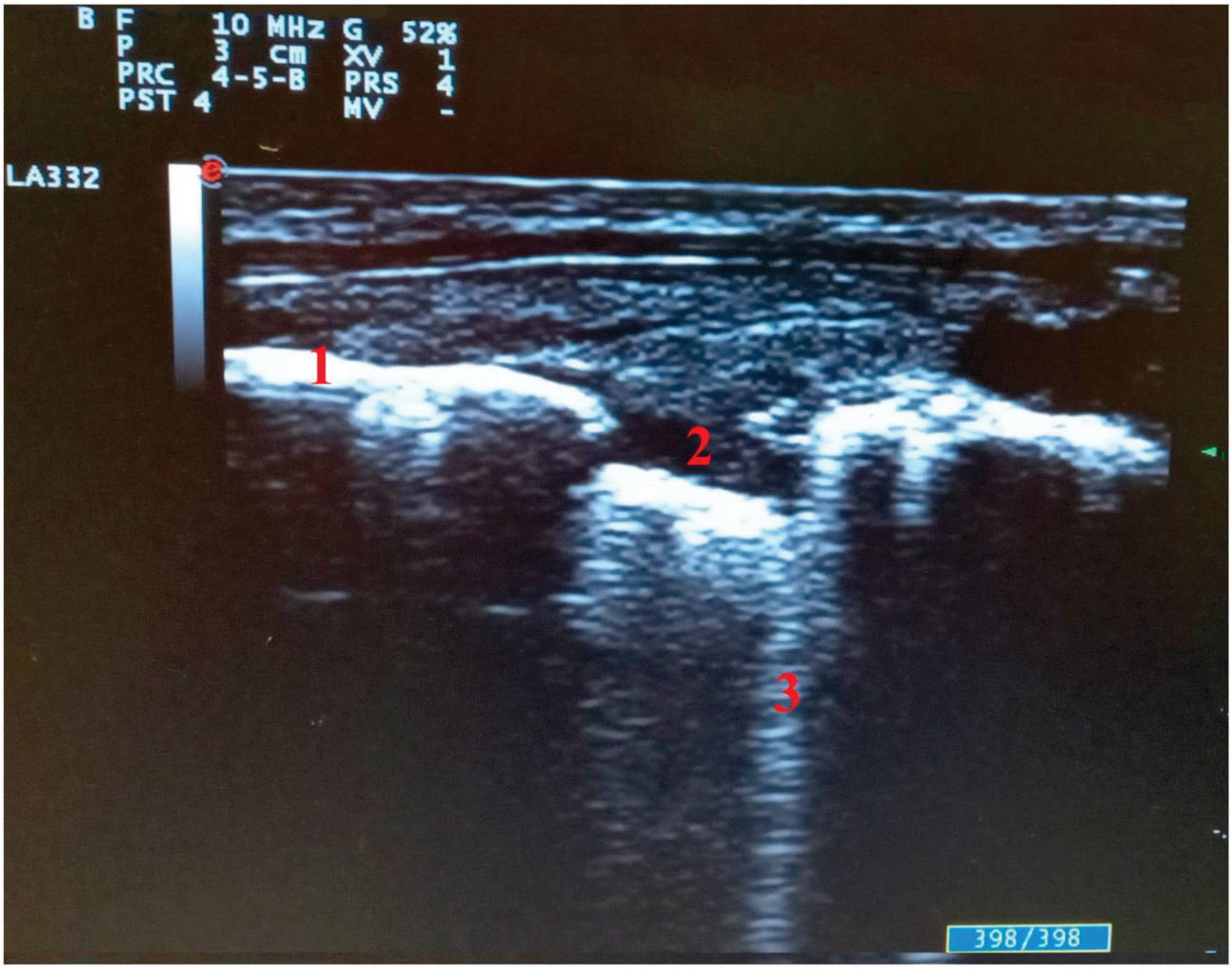

Figure 4. Abnormalities of pleural line in transversal scan: (1) pleural line, (2) pleural line interruption with subpleural consolidation, (3) single B line arising from subpleural consolidation.

The pulmonary lesions are preferentially located in the posterior zone with bilateral distribution [38], while in severe forms it could progress to affect all lung fields [36], and have a patchy bilateral distribution of multiform cluster with sparing areas [39].

Complications of severe forms of SARS-CoV-2 pneumonia are pneumomediastinum and pneumothorax eventually associated with subcutaneous emphysema [40].

If pneumothorax (PNX) is present, there is no B line, lung pulse and sliding. If these absences are highlighted on the ultrasound scan, it is necessary to perform another scan along the middle axillary line. If the lung point is visible, the diagnosis of PNX will be probable with a sensitivity between 75% and 100% and a specificity between 94% and 100% [41].

If subcutaneous emphysema is present, on chest ultrasound it will be possible to visualize only B lines arising from the subcutaneous tissue and not from the pleural line that will not be visible as well as the subpleural space.

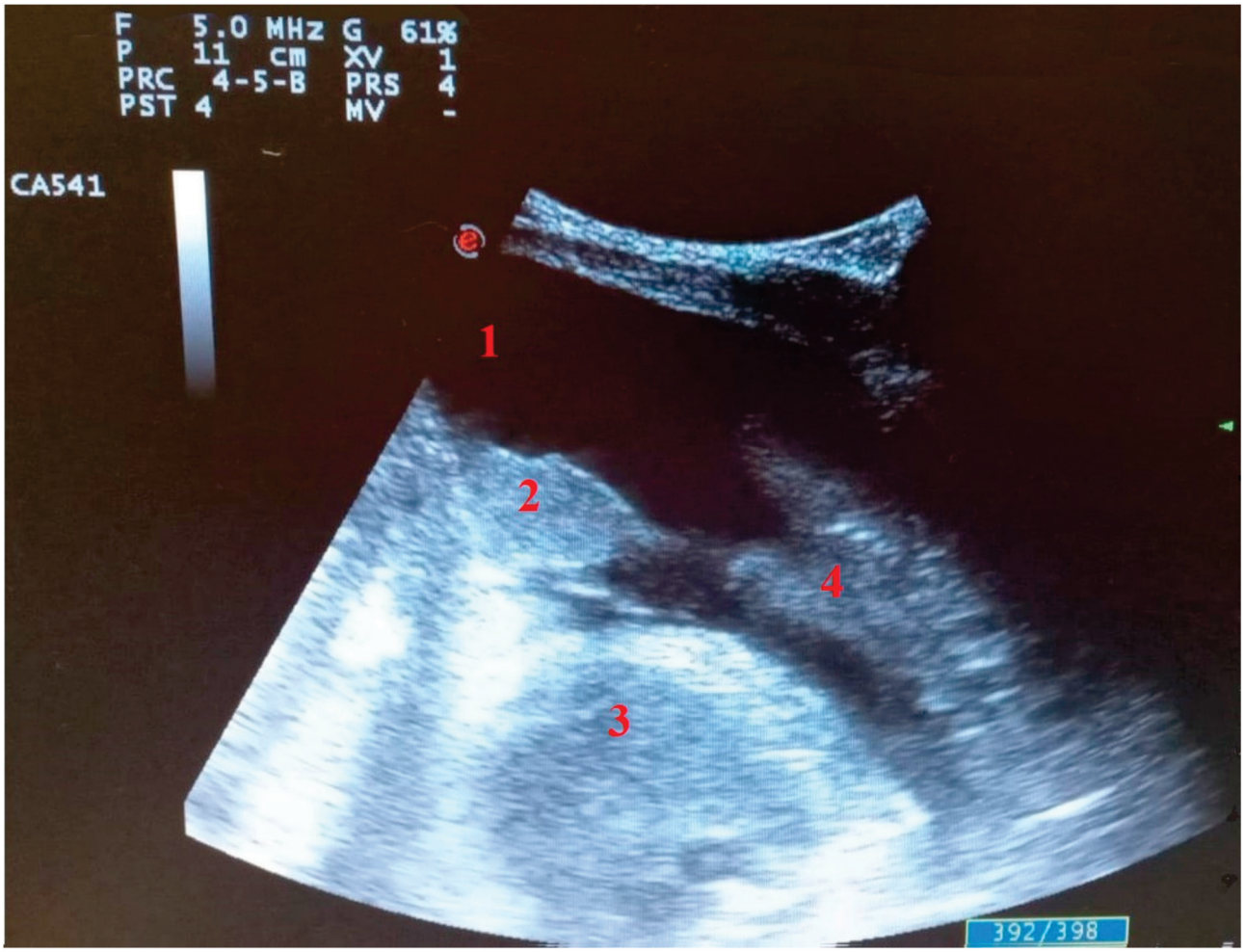

Figure 5. Longitudinal scan with convex probe in COVID-19 patient on mechanical ventilation with bacterial superinfection: (1) pleural effusion, (2) parenchymal consolidation without air bronchogram, (3) heart, (4) parenchymal consolidation with air bronchogram.

Scores

Many scores have been evaluated to assess thoracic ultrasound but the most commonly used is the lung ultrasound score (LUSS).

This score is widely used to assess patients in several clinical contexts. It allows evaluation of loss of aeration in the scanned area with a numeric outcome [42]. LUSS numerically describes the spread and progressive severity of pulmonary involvement. Moreover, numerical value is reduced in the successfully extubated patient. The 12 scanning zones are evaluated and a score from 0 to 3 is assigned for each one: 0 is assigned to a normal ultrasound pattern, 1 to the presence of the B lines, 2 to the white lung and 3 to consolidations [43]. The total score goes from 0 to 36 and it correlates with increasing lung involvement severity.

Correlation between LUSS and lung weight has been extensively demonstrated [44] and it could be a useful tool for assessing severity of SARS-CoV-2 pneumonia and monitoring the progression of lung involvement [45].

LUSS evaluation for SARS-CoV-2 has been shown to be a valuable choice for ICU patients [43,45]. Furthermore SARS-CoV-2 pneumonia and SARS-CoV-2 ARDS have specific features. In fact, posterior consolidations are preponderant in SARS-CoV-2 pneumonia and this feature weakens LUSS accuracy [46].

A specific ultrasound approach for SARS-CoV-2 pneumonia has been proposed since 2020 [47].

This new score evaluates the scan of seven areas in each hemithorax (three posterior, two lateral, two anterior). The scanned are located:

- On the paravertebral line upon the curtain sign.
- On the para-vertebral line at the inferior angle of the scapula.
- On the para-vertebral line at the spine of the scapula.
- On the mid-axillary line below the inter-nipple line.
- On the mid-axillary line above the inter-nipple line.
- On the mid-clavicular line below the inter-nipple line.
- On the mid-clavicular line above the inter-nipple line.

This proposal needs two skilled operators and pocket devices to perform ultrasound. The aim is to minimize risk to health workers operators and reduce the ultrasound operator-dependance. The limits of this score are shortage of skilled operators and the small number of pocket devices readily available.

4. Application Setting

In the context of the SARS-CoV-2 pandemic, the high sensitivity of thoracic ultrasound and its manageability has numerous application settings.

These settings include the triage of patients with flu symptoms in the emergency department, monitoring of hospitalized patients in both low-intensity care wards and ICU and in the follow-up of long COVID-19 patients [14,17,48]. It could also be a valuable tool in the pre-hospital phase to identify those SARS-CoV-2 positive patients who are at high risk of developing respiratory failure requiring hospitalization.

Chest ultrasound is a non-invasive, patient-safe (radiation free) exam that can quickly rule out COVID-19 pneumonia with good diagnostic accuracy, making it particularly useful for triage of the symptomatic patient with suspicion of COVID-19 infection [3].

It has been shown that there is a correlation between ultrasound results, clinical severity, and the trend over time [36]. In the hospital, patients who need and therefore receive respiratory support must be carefully monitored in order to identify early clinical worsening and thus well timed treatment/escalation [37].

4.1. Emergency Department

The SARS-CoV-2 pandemic has revolutionized the medical approach to patients arriving in the emergency room with respiratory symptoms. In the current context, it is essential while awaiting swab test results, to define the severity and consequently to refer the patient to the intensive care unit or intermediate ward as needed. Lung ultrasound is therefore a first level examination that can be quickly performed bedside and that provides information about the severity of lung involvement.

Furthermore, in the event a patient is in a critical condition that requires life-saving interventions, lung ultrasound together with blood gas analysis allows the assessment of severity without wasting precious time to move the patient to perform chest CT scan, which can be performed once the patient is stabilized. On the other hand, some authors have highlighted the predictive value of LUS to detect worsening in patients, admitted to the emergency department without severe symptoms of SARS-CoV-2 [49]. In confirmed positive patients with mild–moderate symptoms, lung ultrasound allows an initial evaluation, which together with anamnesis, stable clinical condition, blood gas analysis and chest CT, defines the appropriate care management of the patient with possible admission to an intermediate ward or discharge at home with the recommendation of isolation [3].

4.2. Intensive Care Unit

In an ICU setting, lung ultrasound, due to the simplicity of execution and prompt availability, is particularly useful in documenting any improvement or worsening without the need to move the patient. Bedside evaluation reduces the risk associated with transporting the unstable patient to CT, the infectious risk for healthcare personnel and possible

spread of the virus during transports. Consequently, ultrasound evaluation helps in the saving of human and economic resources [50].

LUS is also known as a valid tool to optimize ventilatory therapy and its use as a guide for recruitment maneuvers [35,51].

Furthermore, thoracic ultrasound can be a valuable complementary tool in assessing the need for pronation as it is a good predictor of oxygenation response in the prone position as has been demonstrated in ARDS patients with a normal LUS pattern in anterior and basal zones bilaterally [52].

It is also a useful tool for monitoring regional aeration changes during prone ventilation [53]; unfortunately, lung ultrasound cannot detect over-distention (51).

Weaning mechanical ventilation is a crucial point in intensive care unit patient treatment. In this context, it is essential to have diagnostic techniques to verify ventilator weaning and ultrasounds are a tool to monitor the cardiorespiratory system during weaning, and in particular, the weakness of the respiratory muscles, especially the diaphragm, which can contribute to weaning failure [54].

Lung ultrasound is also useful in predicting post-extubation distress as it is able to assess loss of regional lung aeration during a spontaneous breathing trial [55].

4.3. Pediatric Patients

The pediatric population, particularly children under 6 months, are more susceptible to infections than adults and the mortality rate from seasonal flu is much higher. However, SARS-CoV-2 infection appears to be less severe in children than adults, presenting more frequently in mild or moderate form, unlike SARS-CoV-2 infection, which occurs in more severe form [56]. However, it has recently emerged a new spectrum of SARS-CoV-2 disease characterized by multi-organ inflammation and cardiovascular compromise among children, although respiratory failure is currently still the main cause of admission to the pediatric intensive care unit [57].

Radiation exposure, the requirement of sedation and infectious risk reduction are the main advantages in using lung ultrasound in pediatric population [58].

In children, half of all patients have neither symptoms nor radiological findings [59]; moreover, chest ultrasound has a greater sensitivity than chest X-ray in detecting pneumonia and avoids exposure to ionizing radiation [27].

In children with SARS-CoV-2 pneumonia, CT scan is mainly used to define the severity disease [59]. Pediatric patients have an increased risk to radiation exposure and often requires sedation during CT scan.

LUS findings in the pediatric age are similar to those found in adulthood and include pleural line abnormalities, B line, white lung and subpleural consolidations. LUS could be an integrative tool complementary to the CT scan in the diagnosis and monitoring of SARS-CoV-2 pneumonia in children [58]. Nevertheless, current literature in children still considers diagnosis mainly based on typical findings obtained with CT scan, epidemiology and contact tracing [56].

4.4. Out-Patients

In hospitalized patients with SARS-CoV-2 pneumonia, LUS plays an important role in care management.

However, some authors suggest LUS utilization, performed with pocket/portable sized ultrasound, in the out-patient therapeutic route, management and follow-up [3].

In mild–moderate forms of SARS-CoV-2 pneumonia that do not require hospitalization, it is essential to monitor the evolution of the disease and promptly identify worsening of symptoms.

In home management of COVID-19 pneumonia, use of imaging techniques such as CT and chest X-ray is not readily available. In this setting, lung ultrasound, due to its high sensitivity, ease of execution at the patient's home and cost effectiveness, can be used as a

screening method for pulmonary involvement [33,60] and could have a potential role in early hospitalization. Further study should clarify it.

Moreover, is known that patients with severe SARS-CoV-2 pneumonia often have sequelae that needs follow-up and pulmonary rehabilitation [61]. Muscle impairment could have a potential role [62].

Some authors suggest an early follow up assessment four to six week after discharge and a further follow up at twelve weeks in severe SARS-CoV-2 pneumonia. In this route the recommended imaging method is Chest-X-ray [61].

In our knowledge in Long Term Covid patients LUS could be a potential perfect methodology to follow those patients due to cost effectiveness and radiation safeness.

5. Conclusions

During this pandemic, point of care lung ultrasound has demonstrated a key role in the management of patients with COVID-19 associated lung injury.

LUS provides supplemental imaging information. It shows cost effectiveness, radiation safety, reduction of the infectious risk of healthcare personnel as well as savings in human resources. It is an examination that can be performed at the patient's bedside by a single operator, easily repeated at any time and shows a good correlation with HRCT and is better suited than the chest X-ray.

Its high sensitivity and specificity, together with its flexibility, allows it to be used for the triage of patients with flu symptoms and the monitoring of hospitalized patients in order to identify early clinical worsening and thus timely treatment.

LUS can be integrated into the diagnostic and therapeutic pathway of COVID-19 pneumonia by informing the initiation of respiratory support as well as escalation, titration and weaning from mechanical ventilation. Further study should be considered to better explain the potential role of LUS for early admission to hospital and in follow-up.

Author Contributions: Conceptualization: L.M., A.M.B. and M.R.; writing: L.M., A.M.B., S.F. and A.R.; review and editing: S.F., A.R. and F.C.; supervision: M.R. and F.C. All authors have read and agreed to the published version of the manuscript.

Funding: This research received no external funding.

Institutional Review Board Statement: Not applicable.

Informed Consent Statement: Not applicable.

Data Availability Statement: Not applicable.

Conflicts of Interest: The authors declare no conflict of interest.

References

1. Alhazzani, W.; Møller, M.H.; Arabi, Y.M.; Loeb, M.; Rhodes, A. Surviving Sepsis Campaign: Guidelines on the Management of Critically Ill Adults with Coronavirus Disease 2019 (COVID-19). *Intensive Care Med.* **2020**, *46*, 854–887. [CrossRef] [PubMed]
2. Antonelli, G.; Carosi, G.; Pession, A.; Cauda, R. *Harrison Principles of Internal Medicine*, 20th ed.; 2021-CEA-Rev. 20-05-2021; AccessMedicine; ISBN 978-88-08-82037-2. Available online: https://accessmedicine.mhmedical.com/book.aspx?bookid=2129 (accessed on 8 November 2021).
3. Boccatonda, A.; Cocco, G.; Ianniello, E.; Montanari, M.; D'Ardes, D.; Borghi, C.; Giostra, F.; Copetti, R.; Schiavone, C. One year of SARS-CoV-2 and lung ultrasound: What has been learned and future perspectives. *J. Ultrasound* **2021**, *24*, 115–123. [CrossRef] [PubMed]
4. Ai, T.; Yang, Z.; Hou, H.; Zhan, C.; Chen, C.; Lv, W. Correlation of chest CT and RTPCR testing in coronavirus disease 2019 (COVID-19) in China: A report of 1014 cases. *Radiology* **2020**, *295*, E3.
5. Nouvenne, A.; Zani, M.D.; Milanese, G.; Parise, A.; Baciarello, M.; Bignami, E.G.; Odone, A.; Sverzellati, N.; Meschi, T.; Ticinesi, A. Lung Ultrasound in COVID-19 Pneumonia: Correlations with Chest CT on Hospital admission. *Respiration* **2020**, *99*, 617–624. [CrossRef] [PubMed]
6. Yoon, S.H.; Lee, K.H.; Kim, J.Y. Chest radiographic and CT findings of the 2019 novel coronavirus disease (COVID-19): Analysis of nine patients treated in Korea. *Korean J. Radiol.* **2020**, *21*, 494–500. [CrossRef] [PubMed]

7. Winkler, M.; Touw, H.; van de Ven, P. Diagnostic accuracy of chest radiograph, and when concomitantly studied lung ultrasound, in critically ill patients with respiratory symptoms: A systematic review and meta-analysis. *Crit. Care Med.* **2018**, *46*, e707–e714. [CrossRef] [PubMed]
8. Buonsenso, D.; Piano, D.; Raffaelli, A.; Bonadia, F.; Donati, K.D.G.; Franceschi, F. Point-of-care lung ultrasound findings in novel coronavirus disease-19 pnemoniae: A case report and potential applications during COVID-19 outbreak. *Eur. Rev. Med. Pharmacol. Sci.* **2020**, *24*, 2776–2780.
9. Peng, Q.Y.; Wang, X.T.; Zhang, L.N.; Chinese Critical Care Ultrasound Study Group (CCUSG). Findings of lung ultrasonography of novel corona virus pneumonia during the 2019–2020 epidemic. *Intensive Care Med.* **2020**, *46*, 849–850. [CrossRef]
10. Buonsenso, D.; Pata, D.; Chiaretti, A. COVID-19 outbreak: Less stethoscope, more ultrasound. *Lancet Respir. Med.* **2020**, *8*, e27. [CrossRef]
11. Testa, A.; Soldati, G.; Copetti, R.; Giannuzzi, R.; Portale, G.; Gentiloni-Silveri, N. Early recognition of the 2009 pandemic influenza A (H1N1) pneumonia by chest ultrasound. *Crit. Care* **2012**, *16*, R30. [CrossRef] [PubMed]
12. Soldati, G.; Smargiassi, A.; RInchingolo, R.; Buonsenso, D.; Perrone, T.; Briganti, D.F.; Perlini, S.; Torri, E.; Mariani, A.; Mossolani, E.E.; et al. Is There a Role for Lung Ultrasound During the COVID-19 Pandemic? *J. Ultrasound Med.* **2020**, *39*, 1459–1462. [CrossRef]
13. Moore, S.; Gardiner, E. Point of care and intensive care lung ultrasound: A reference guide for practitioners during COVID-19. *Radiography (Lond.)* **2020**, *26*, e297–e302. [CrossRef] [PubMed]
14. Giovannetti, G.; De Michele, L.; De Ceglie, M.; Pierucci, P.; Mirabile, A.; Vita, M.; Palmieri, V.O.; Carpagnano, G.E.; Scardapane, A.; D'Agostino, C. Lung ultrasonography for long-term follow-up of COVID-19 survivors compared to chest CT scan. *Respir. Med.* **2021**, *181*, 106384. [CrossRef]
15. World Health Organisation. Coronavirus Disease 2019 (COVID-19) Clinical Management of Severe Acute Respiratory Infection (SARI) When COVID-19 Disease Is Suspected. Available online: https://apps.who.int/iris/handle/10665/331446 (accessed on 8 November 2021).
16. Buda, N.; Cylwik, J.; Mróz, K.; Rudzińska, R.; Dubik, P.; Malczewska, A.; Oraczewska, A.; Skoczyński, S.; Suska, A.; Górecki, T.; et al. Lung Ultrasound Examination in Patients with SARS-CoV-2 Infection: Multicenter Study. *J. Clin. Med.* **2021**, *10*, 3255. [CrossRef] [PubMed]
17. Skopljanac, I.; Ivelja, M.P.; Barcot, O.; Brdar, I.; Dolic, K.; Polasek, O.; Radic, M. Role of Lung Ultrasound in Predicting Clinical Severity and Fatality in COVID-19 Pneumonia. *J. Personal. Med.* **2021**, *11*, 757. [CrossRef] [PubMed]
18. Mayo, P.H.; Copetti, R.; Feller-Kopman, D.; Mathis, G.; Maury, E.; Mongodi, S.; Mojoli, F.; Volpicelli, G.; Zanobetti, M. Thoracic ultrasonography: A narrative review. *Intensive Care Med.* **2019**, *45*, 1200–1211. [CrossRef] [PubMed]
19. Raiteri, A.; Alvisi, M.; Serio, I.; Stefanini, F.; Tovoli, F.; Piscaglia, F. Lung Ultrasound Is Often, but Not Always, Normal in Healthy Subjects: Considerations for COVID-19 Pandemic. *Diagnostics* **2021**, *11*, 82. [CrossRef]
20. Senter, R.; Capone, F.; Stefano Pasqualin, S.; Cerruti, L.; Molinari, L.; Fonte Basso, E.; Zanforlin, N.; Previato, L.; Toffolon, A.; Sensi, C.; et al. Lung Ultrasound Patterns and Clinical-Laboratory Correlates during COVID-19 Pneumonia: A Retrospective Study from North East Italy. *J. Clin. Med.* **2021**, *10*, 1288. [CrossRef] [PubMed]
21. Bass, C.M.; Sajed, D.R.; Adedipe, A.A.; West, T.E. Pulmonary ultrasound and pulse oximetry versus chest radiography and arterial blood gas analysis for the diagnosis of acute respiratory distress syndrome: A pilot study. *Crit. Care* **2015**, *19*, 282. [CrossRef] [PubMed]
22. Agricola, E.; Bove, T.; Oppizzi, M.; Marino, G.; Zangrillo, A.; Margonato, A.; Picano, E. "Ultrasound comet-tail images": A marker of pulmonary edema; a comparative study with wedge pressure and extravascular lung water. *Chest* **2005**, *127*, 1690–1695. [CrossRef]
23. Soldati, G.; Testa, A.; Silva, F.R.; Carbone, L.; Portale, G.; Silveri, N.G. Chest ultrasonography in lung contusion. *Chest* **2006**, *130*, 533–538. [CrossRef] [PubMed]
24. Heldeweg, M.L.A.; Lieveld, A.W.E.; De Grooth, H.J.; Heunks, L.M.A.; Pieter, R.; Tuinman, P.R. ALIFE study group. Determining the optimal number of lung ultrasound zones to monitor COVID-19 patients: Can we keep it ultra-short and ultra-simple? *Intensive Care Med.* **2021**, *47*, 1041–1043. [CrossRef]
25. Di Serafino, M.; Notaro, M.; Rea, G.; Iacobellis, F.; Paoli, V.D.; Acampora, C.; Ianniello, S.; Brunese, L.; Romano, L.; Vallone, G. The lung ultrasound: Facts or artifacts? In the era of COVID-19 outbreak. *Radiol. Med.* **2020**, *125*, 738–753. [CrossRef] [PubMed]
26. Pérez Pallarés, J.; Flandes Aldeyturriaga, J.; Cases Viedma, E.; Cordovilla Pérez, R. SEPAR-AEER Consensus Recommendations on the Usefulness of the Thoracic Ultrasound in the Management of the Patient with Suspected or Confirmed Infection with COVID-19. *Arch. Bronconeumol.* **2020**, *56* (Suppl. 2), 27–30. [CrossRef]
27. Gargani, L.; Volpicelli, G. How I do it: Lung ultrasound. *Cardiovasc. Ultrasound* **2014**, *12*, 25. [CrossRef]
28. Picano, E.; Scali, M.C.; Ciampi, Q.; Lichtenstein, D. Lung Ultrasound for the Cardiologist. *JACC Cardiovasc. Imaging* **2018**, *11*, 1692–1705. [CrossRef]
29. Lichtenstein, D.A. Lung ultrasound in the critically ill. *Ann. Intensive Care* **2014**, *4*, 1. [CrossRef]
30. Stefanidis, K.; Dimopoulos, S.; Nanas, S. Basic principles and current applications of lung ultrasonography in the intensive care unit. *Respirology* **2011**, *16*, 249–256. [CrossRef]
31. Guarracino, F.; Vetrugno, L.; Forfori, F.; Bove, T. Lung, heart, vascular, and diaphragm ultrasound examination of COVID-19 patients: A comprehensive approach. *J. Cardiothorac. Vasc. Anesth.* **2021**, *35*, 1866–1874. [CrossRef]

32. Jackson, K.; Butler, R.; Aujayeb, A. Lung ultrasound in the COVID-19 pandemic. *Postgrad. Med. J.* **2021**, *97*, 34–39.
33. Soccorsa, S.; Boccatonda, A.; Montanari, M.; Spampinato, M.; D'Ardes, D.; Cocco, G.; Accogli, E.; Cipollone, F.; Schiavone, C. Thoracic ultrasound and SARS-COVID-19: A pictorial essay. *J. Ultrasound* **2020**, *23*, 217–221.
34. Soldati, G.; Smargiassi, A.; Inchingolo, R.; Buonsenso, D.; Perrone, T.; Briganti, D.F.; Perlini, S.; Torri, E.; Mariani, A.; Mossolani, E.E.; et al. On Lung Ultrasound Patterns Specificity in the Management of COVID-19 Patients. *J. Ultrasound Med.* **2020**, *39*, 2283–2284. [CrossRef]
35. Volpicelli, G.; Lamorte, A.; Villén, T. What's new in lung ultrasound during the COVID-19 pandemic. *Intensive Care Med.* **2020**, *46*, 1445–1448. [CrossRef]
36. Changyang, X.; Qiaoying, L.; Hong, D.; Wenzhen, K.; Jianqi, L.; Lijun, Y. Lung ultrasound findings in patients with COVID-19 pneumonia. *Crit. Care* **2020**, *24*, 174.
37. Smith, M.J.; Hayward, S.A.; Innes, S.M.; Miller, A.S.C. Point-of-care lung ultrasound in patients with COVID-19—A narrative review. *Anaesthesia* **2020**, *75*, 1096–1104. [CrossRef] [PubMed]
38. Yang, Y.; Huang, Y.; Gao, F.; Yuan, L.; Wang, Z. Lung ultrasonography versus chest CT in COVID-19 pneumonia: A two-centered retrospective comparison study from China. *Intensive Care Med.* **2020**, *46*, 1761–1763. [CrossRef]
39. Volpicelli, G.; Gargani, L. Sonographic signs and patterns of COVID-19 pneumonia. *Ultrasound J.* **2020**, *12*, 22. [CrossRef] [PubMed]
40. Elhakim, T.S.; Abdul, H.S.; Romero, C.P.; Rodriguez-Fuentes, Y. Spontaneous pneumomediastinum, pneumothorax and subcutaneous emphysema in COVID-19 pneumonia: A rare case and literature review. *BMJ Case Rep.* **2020**, *13*, e239489. [CrossRef] [PubMed]
41. Wimalasena, Y.; Kocierz, L.; Strong, D.; Watterson, J.; Burns, B. Lung ultrasound: A useful tool in the assessment of the dyspnoeic patient in the emergency department. Fact or fiction? *Emerg. Med. J.* **2018**, *35*, 258–266. [CrossRef] [PubMed]
42. Chiumello, D.; Mongodi, S.; Algieri, I.; Vergani, G.L.; Orlando, A.; Via, G.; Crimella, F.; Cressoni, M.; Mojoli, F. Assessment of Lung Aeration and Recruitment by CT Scan and Ultrasound in Acute Respiratory Distress Syndrome Patients. *Crit. Care Med.* **2018**, *46*, 1761–1768. [CrossRef] [PubMed]
43. Dargent, A.; Chatelain, E.; Kreitmann, L.; Quenot, J.P.; Cour, M.; Argaud, L.; COVID-LUS Study Group. Lung ultrasound score to monitor COVID-19 pneumonia progression in patients with ARDS. *PLoS ONE* **2020**, *15*, e0236312. [CrossRef]
44. Zhao, Z.; Jiang, L.; Xi, X.; Jiang, Q.; Zhu, B.; Wang, M.; Xing, J.; Zhang, D. Prognostic value of extravascular lung water assessed with lung ultrasound score by chest sonography in patients with acute respiratory distress syndrome. *BMC Pulm. Med.* **2015**, *15*, 98. [CrossRef] [PubMed]
45. Vetrugno, L.; Bove, T.; Orso, D.; Barbariol, F.; Bassi, F.; Boero, E.; Ferrari, G.; Kong, R. Our Italian experience using lung ultrasound for identification, grading and serial follow-up of severity of lung involvement for management of patients with COVID-19. *Echocardiography* **2020**, *37*, 625–627. [CrossRef] [PubMed]
46. Pisani, L.; Vercesi, V.; Van Tongeren, P.S.I.; Lagrand, W.; Leopold, S.; Huson, M.; Henwood, P.; Walden, A.; Smit, M.; Riviello, E.; et al. The diagnostic accuracy for ARDS of global versus regional lung ultrasound scores—A post hoc analysis of an observational study in invasively ventilated ICU patients. *Intensive Care Med. Exp.* **2019**, *7* (Suppl. 1), 44. [CrossRef] [PubMed]
47. Soldati, G.; Smargiassi, A.; Inchingolo, R.; Buonsenso, D.; Perrone, T.; Briganti, D.F.; Perlini, S.; Torri, E.; Mariani, A.; Mossolani, E.E.; et al. Proposal for International Standardization of the Use of Lung Ultrasound for Patients With COVID-19: A Simple, Quantitative, Reproducible Method. *J. Ultrasound Med.* **2020**, *39*, 1413–1419. [CrossRef]
48. Vetrugno, L.; Mojoli, F.; Cortegiani, A.; Bignami, E.G.; Ippolito, M.; Orso, D.; Francesco Corradi, F.; Cammarota, G.; Mongodi, S.; Boero, E.; et al. Italian Society of Anesthesia, Analgesia, Resuscitation, and Intensive Care expert consensus statement on the use of lung ultrasound in critically ill patients with coronavirus disease 2019 (ITACO). *J. Anesth. Analg. Crit. Care* **2021**, *1*, 16. [CrossRef]
49. Secco, G.; Salinaro, F.; Bellazzi, C.; La Salvia, M.; Delorenzo, M.; Zattera, C.; Barcella, B.; Resta, F.; Vezzoni, G.; Bonzano, M.; et al. Can Alveolar-Arterial Difference and Lung Ultrasound Help the Clinical Decision Making in Patients with COVID-19? *Diagnostics* **2021**, *11*, 761. [CrossRef]
50. Kulkarni, S.; Down, B.; Jha, S. Point-of-care lung ultrasound in intensive care during the COVID-19 pandemic. *Clin. Radiol.* **2020**, *75*, 710.e1–710.e4. [CrossRef]
51. Bouhemad, B.; Brisson, H.; Le-Guen, M.; Arbelot, C.; Lu, Q.; Rouby, J. Bedside ultrasound assessment of positive end-expiratory pressure-induced lung recruitment. *Am. J. Respir. Crit. Care Med.* **2011**, *183*, 341–347. [CrossRef]
52. Prat, G.; Guinard, S.; Bizien, N.; Nowak, E.; Tonnelier, J.M.; Alavi, Z.; Renault, A.; Boles, J.M.; L'Her, E. Can lung ultrasonography predict prone positioning response in acute respiratory distress syndrome patients? *J. Crit. Care* **2016**, *32*, 36–41. [CrossRef]
53. Haddam, M.; Zieleskiewicz, L.; Perbet, S. Lung ultrasonography for assessment of oxygenation response to prone position ventilation in ARDS. *Intensive Care Med.* **2016**, *42*, 1546–1556. [CrossRef] [PubMed]
54. Haaksma, M.E.; Tuinman, P.R.; Heunks, L. Weaning the patient: Between protocols and physiology. *Curr. Opin. Crit. Care* **2021**, *27*, 29–36. [CrossRef] [PubMed]
55. Soummer, A.; Perbet, S.; Brisson, H.; Arbelot, C.; Constantin, J.M.; Lu, Q.; Rouby, J.J. Lung Ultrasound Study Group. Ultrasound assessment of lung aeration loss during a successful weaning trial predicts postextubation distress. *Crit. Care Med.* **2012**, *40*, 2064–2072. [CrossRef]

56. Chang, T.H.; Wu, J.L.; Chang, L.Y. Clinical characteristics and diagnostic challenges of pediatric COVID-19: A systematic review and meta-analysis. *J. Formos. Med. Assoc.* **2020**, *119*, 982–989. [CrossRef] [PubMed]
57. Giorno, E.; De Paulis, M.; Sameshima, Y.; Weerdenburg, K.; Savoia, P.; Nanbu, D.; Couto, T.; Sa, F.; Farhat, S.; Carvalho, W.; et al. Point-of-care lung ultrasound imaging in pediatric COVID-19. *Ultrasound J.* **2020**, *12*, 50. [CrossRef] [PubMed]
58. Musolino, A.M.; Supino, M.C.; Buonsenso, D.; Ferro, V.; Valentini, P.; Magistrelli, A.; Haywood Lombardi, M.; Romani, L.; D'Argenio, P.; Campana, A.; et al. Lung Ultrasound in Children with COVID-19: Preliminary Findings. *Ultrasound Med. Biol.* **2020**, *46*, 2094–2098. [CrossRef] [PubMed]
59. Qiu, H.; Wu, H.; Hong, L.; Luo, Y.; Song, Q.; Chen, D. Clinical and epidemiological features of 36 children with coronavirus disease 2019 (COVID-19) in Zhejiang, China: An observational cohort study. *Lancet Infect. Dis.* **2020**, *20*, 689–696. [CrossRef]
60. Tung-Chen, Y. Lung ultrasound in the monitoring of COVID-19 infection. *Clin. Med. (Lond.)* **2020**, *20*, e62–e65. [CrossRef]
61. George, P.M.; Barratt, S.L.; Condliffe, R.; Desai, S.R.; Devaraj, A.; Forrest, I.; Gibbons, M.A.; Hart, N.; Gisli Jenkins, R.; McAuley, D.F.; et al. Respiratory follow-up of patients with COVID-19 pneumonia. *Thorax* **2020**, *75*, 1009–1016. [CrossRef]
62. Herridge, M.S. Long-term outcomes after critical illness. *Curr. Opin. Crit. Care* **2002**, *8*, 331–366. [CrossRef]

diagnostics

MDPI

Article

One-Year Follow-Up Lung Ultrasound of Post-COVID Syndrome—A Pilot Study

Martin Altersberger [1], Anna Grafeneder [1], Yerin Cho [1], Roland Winkler [2], Ralf Harun Zwick [3], Gebhard Mathis [4] and Martin Genger [1,*]

[1] Department of Cardiology, Nephrology and Intensive Care Medicine, State Hospital Steyr, 4400 Steyr, Austria
[2] Rehabilitation Center Hochegg for Cardiovascular and Respiratory Diseases, 2840 Grimmenstein, Austria
[3] Therme Wien Med, 1100 Vienna, Austria
[4] Praxis of Internal Medicine, 6830 Rankweil, Austria
* Correspondence: martin.genger.1@gmail.com

Abstract: (1) Background: Millions of people worldwide were infected with COVID-19. After the acute phase of the disease, many suffer from prolonged symptoms, the post-COVID syndrome, especially the phenotype with lung residuals. Many open questions regarding lung ultrasound (LUS) have to be answered. One essential question is the means for optimal following-up of patients with post-COVID-19 residuals with LUS; (2) Methods: A retrospective data analysis of patients after acute COVID-19 infection diagnosed with post-COVID syndrome in the state hospital of Steyr and the rehabilitation center of Hochegg was performed. LUS examinations following a 12-zone scanning protocol were performed, and the LUS score quantified comet tail artifacts. A total of 16 patients were evaluated twice with LUS from May 2020 until June 2021. (3) Results: All patients' reverberation artifacts were reduced over time. The initial LUS score of 17.75 (SD 4.84) points was decreased over the duration of the second rehabilitation to 8,2 (SD 5.94). The difference in the Wilcoxon test was significant ($p < 0.001$); (4) Conclusions: Lung ultrasound was a valuable tool in the follow-up of post-COVID-syndrome with lung residuals in the first wave of COVID-19. A reduction in reverberation artifacts was demonstrated. Further studies about the clinical significance have to follow.

Keywords: post-COVID-syndrome; lung ultrasound; COVID-19; LUS

Citation: Altersberger, M.; Grafeneder, A.; Cho, Y.; Winkler, R.; Zwick, R.H.; Mathis, G.; Genger, M. One-Year Follow-Up Lung Ultrasound of Post-COVID Syndrome—A Pilot Study. *Diagnostics* **2023**, *13*, 70. https://doi.org/10.3390/diagnostics13010070

Academic Editors: Gino Soldati and Marcello Demi

Received: 8 October 2022
Revised: 19 December 2022
Accepted: 20 December 2022
Published: 26 December 2022

1. Introduction

The COVID-19 pandemic is an immense burden on healthcare workers [1]. Millions of people have been infected, there are continuously rising numbers, and new virus variants are still being discovered. Likewise, the follow-up after COVID-19 presents some difficulties. Some patients suffer from ongoing symptoms such as dyspnea after acute COVID-19, even though they have a mild form of the disease [2]. In this pilot study of post-COVID syndrome patients, the usage of lung ultrasound (LUS) in the follow-up through identifying the change of reverberation artifacts over the course of approximately one year is evaluated.

LUS can identify persistent reverberation artifacts after a COVID-19 infection, commonly known as B-lines, though the more accurate terminology through etiology is comet tail artifacts [3–5].

1.1. Background Lung Ultrasound

1.1.1. Reverberation Artifacts

Artifacts in LUS are generated by air. Reverberation artifacts show a fluid/air mismatch. An overload of fluid in the interstitium leads to vertical artifacts, so-called B-lines in pulmonary edema, or comet tail artifacts in infectious and interstitial diseases [4–6]. The evaluation of the pleural line is mandatory to differentiate B-lines from comet tail artifacts. A fragmented irregular pleural line points towards inflammation and the presence of comet

tail artifacts. Such an example would be COVID-19 [4,7]. A smooth pleural line with vertical reverberation artifacts can be seen in pulmonary edema. Hence, they are called B-lines (Video S1) [4,5]. Still, there is an active discussion about optimally describing such artifacts, and the current terminology is still insufficient [8].

Comet tail artifacts indicate diffuse alveolar damage and subpleural consolidations, and a reduction in lung sliding can also be observed, indicating inflammatory diseases or diffuse parenchymatous lung diseases (Video S2) [4,9,10]. In the context of critical COVID-19 patients, massive reverberation artifacts were found and described as having a light-beam appearance and seeming like a waterfall [11,12].

1.1.2. Consolidations and Pleural Effusion

Hypoechoic areas have a "tissue-like appearance" or "hepatization" in LUS with small hyperechoic [bronchograms] or hypoechoic (fluid bronchograms) structures within them point toward pneumonia and are described as consolidations and can appear with free fluid [pleural effusion] [7,13–17]. Pleural effusions in COVID-19 are rare and can be seen in bacterial superinfections or other diseases such as heart failure [9,12,18,19]. If the consolidation is present in an entire lung lobe, the borders will be well-defined as a space-consuming entity. In moderate or more significant consolidations, the deeper edges appear irregular and like they were "torn" from the lungs, described as the shred sign [6,20].

1.1.3. COVID-19 LUS, Scoring, Prognosis and Follow-Up

Imaging the lungs is helpful in the follow-up of COVID-19, and LUS can be an add-on tool to chest radiographs and CTs [9,18,21,22]. Significantly, in settings where CTs are not readily available, LUS can assist by means of triage [21,22]. Signs of COVID-19 in lung ultrasound are reverberation artifacts known as comet tail artifacts [4,23,24]. In a setting where lung inflammation is present, these comet tail artifacts can be quantified, and a scoring system can be used to predict outcomes in the acute stage of the disease [21,22,25]. Depending on the scoring system used, different cut-off values are described as markers of poor prognosis [21,25].

The LUS describes a range from 0 to 3 points. 0 points are a typical "physiological" finding of artifacts, meaning normal A-lines and none or few [up to two per intercostal space]. An LUS score of 1 describes a loss of aeration with an irregular pleural line and some comet tails. 2 points is a significant loss of aeration with a markedly irregular pleural line, a reduction in lung sliding, small consolidations located sub-pleural, and many comet tail artifacts. A score of 3 points in the LUS score is given with a large consolidation [25–27] (Figures 1–4).

1.2. Long COVID & Post-COVID Syndrome

There needs to be more data using LUS in post-COVID syndrome patients with lung residuals. The need for rehabilitation is undoubtedly given after critical and severe COVID-19 disease [28,29]. A study by Sonnweber et al. showed that post-COVID-19 patients suffered from persistent symptoms such as dyspnea and impairment in lung function [30]. This study indicated that a follow-up of post-COVID syndrome patients with ongoing dyspnea should include lung imaging with computerized tomography (CT) scans [30].

As the number of symptomatic patients after an acute COVID-19 infection increased, the terms "long COVID" (symptoms after four weeks of acute infection) and "post-COVID syndrome" (symptoms after 12 weeks of acute infection) were introduced and are now used to describe more than 100 different persistent symptoms after acute infection [7,31–33]. Pathologic chest CTs were found in 35% of patients 60 to 100 days after initial presentation, and pathological X-rays were present in approximately two-thirds of hospitalized COVID-19 patients [31,34].

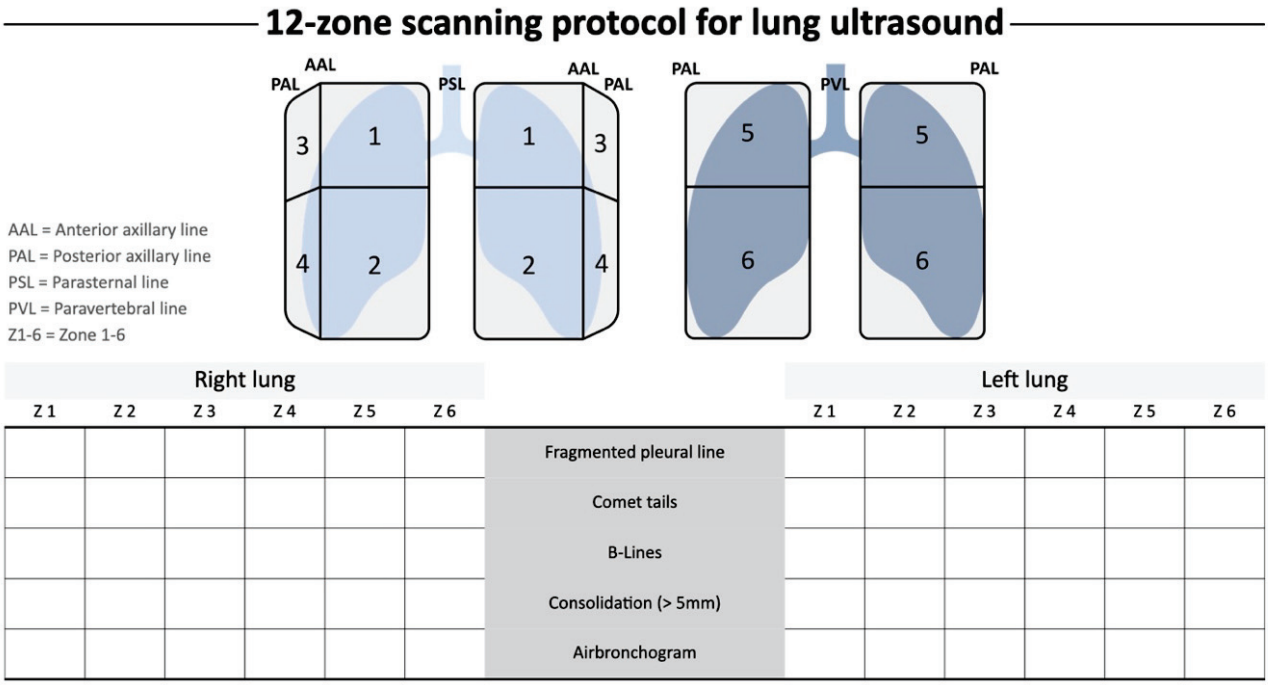

Figure 1. The 12-zone scanning protocol, as suggested by the Austrian Society of Pneumonology and the Austrian Society of Ultrasound in Medicine.

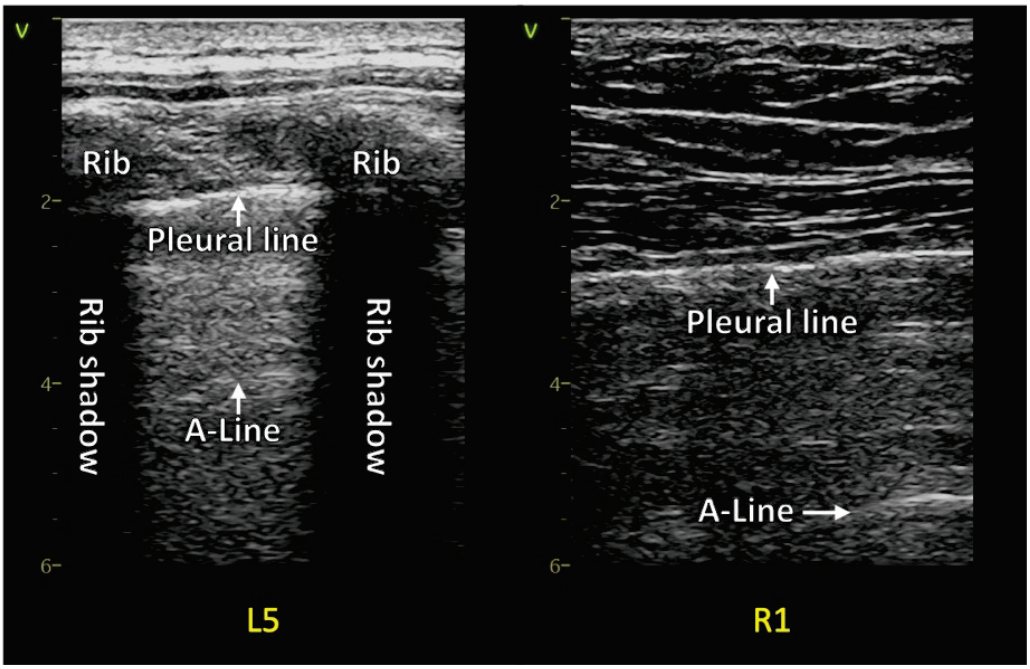

Figure 2. Two normal examples with smooth pleural lines and no reverberation artifacts in post-COVID patients.

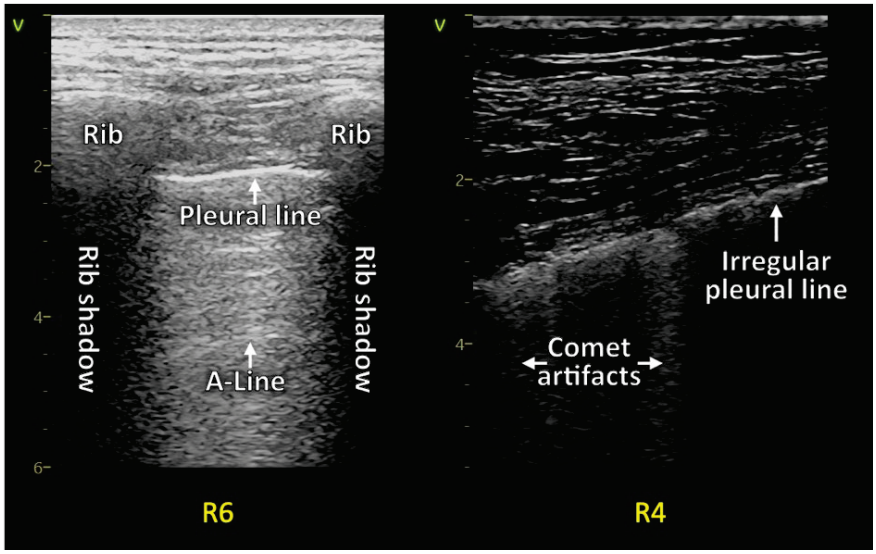

Figure 3. On the left side is a normal image of LUS in post-COVID, and on the right is an irregular pleural line with comet tail artifacts shown.

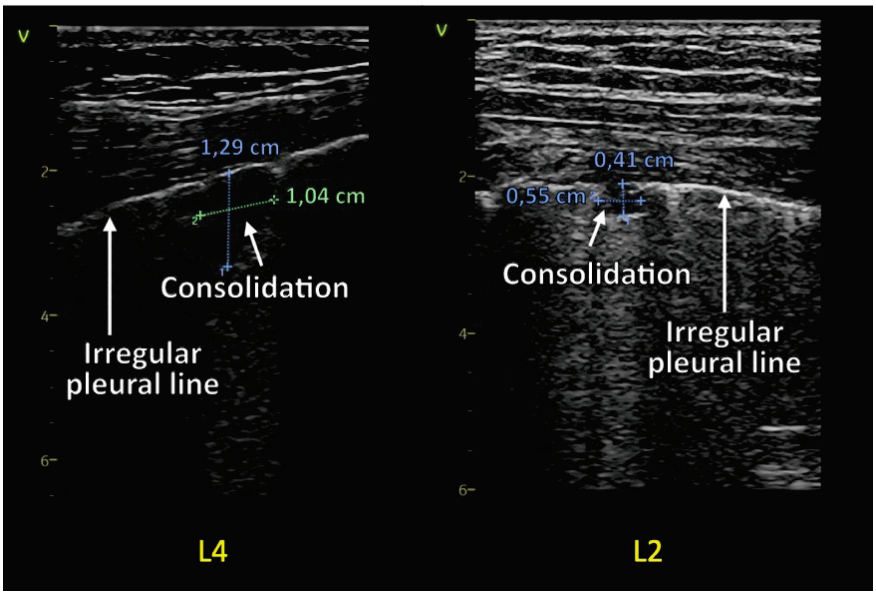

Figure 4. Two areas with small consolidations, including the measurement in the images. On the left side, there is zone four of the left hemithorax (L4), showing an irregular pleural line and a consolidation. On the right side is zone two on the left hemithorax (L2).

2. Materials and Methods

2.1. 12-Zone LUS Scanning Protocol for Follow-Up

A 12-zone scanning protocol for the follow-up was implemented, describing the artifacts and consolidations with the suggested terminology provided in a review endorsed by the Austrian Society of Ultrasound. The Austrian Society of Pulmonology initially described this in a WFUMB position paper, which deals explicitly with the etiologic differentiation of LUS artifacts [4,7]. LUS was implemented during the initial visitation at the treatment center and in the follow-up as a part of the standard ultrasound evaluation in post-COVID syndrome care in combination with a routine echocardiographic exam [7].

The 12-zone scanning protocol was always used and performed with the same standard evaluation. Trained personnel in LUS with at least four years of experience scanned the patients at the respective centers. Additionally, to compare findings over time, the

LUS score was calculated after the exam with a second look at the designated workstation, measuring the size of found consolidations (GE healthcare EchoPAC) [26,27].

The exams were reviewed in echo laboratories certified by the Austrian Society of Cardiology, division of echocardiography. The protocol started in zone one in supine-positioned patients. The anterior and cranial zone of the respective hemothorax was scanned first (Figure 1). Initially, the anterior and lateral right hemithorax was scanned, saving loops of a longitudinal orientation of the transducer [the marker of the transducer pointing cranially] and a transverse orientation [the marker pointing towards the right side of the patient]. There was a particular focus on scanning all the intercostal spaces in two orientations. In the case of pathological findings, loops of reverberation artifacts and their distribution and consolidations were saved as loops. The examiner was always located on the right side of the patient. The midline of the thorax was the border between zone one and two, and the anterior axillary line marked the border between the anterior and the lateral zones (Figure 1). For the posterior zones, patients were moved to an upright position. Zones five and six on the posterior side were examined and documented in the same way as the anterior and lateral zones.

2.2. Image Acquisition

A retrospective data analysis of patients in care after acute COVID-19 infection diagnosed with "long COVID" or "post-COVID syndrome" in the state hospital of Steyr and the rehabilitation center of Hochegg was performed. Lung ultrasound examinations following a 12-zone scanning protocol as priorly described were performed, and the LUS score was quantified utilizing reverberation artifacts (comet tails) and consolidations. Examples are seen in figures two with normal LUS anatomy and three and four with pathologic examples. A specific lung preset with a low mechanical index, single-focal point modality, and without harmonic imaging or other cosmetic filters was set with the focal zone placed at the area of the pleural line [7,35]. The frequency of the LUS preset with a linear transducer was set at 8 to 10 megahertz. The abdominal transducer was set at 4 to 6 megahertz. The VIVID S70 and VIVID T8 ultrasound machines from GE healthcare were used to acquire images.

A linear transducer with a dedicated LUS preset was used in a standard exam. Depth settings were adapted within a range of 4 to 8 cm. A convex transducer with a depth setting of 6 to 15 cm was selected in cases of larger patients and for quantifying pleural effusions or consolidations [7,36]. For larger patients, a cardiac transducer would have been applicable as well. The gain settings were adjusted to optimally visualize pathologic findings (Figures 3 and 4) [8].

2.3. Study Population

A total of 16 patients were included for statistical evaluation. The patients were evaluated twice with LUS from May until June 2020 and in a follow-up visitation around 2021. The mean age was 60 years, ranging from 35–83 years. Out of all the patients, 13 were male, and three were female. Arterial hypertension was present in 11 patients, and diabetes mellitus type II in 3 (Table 1).

Table 1. Patient characteristics of post-COVID syndrome patients.

Age	Range: 35–83
	Mean: 61
Gender	Male: 87.5%
	Female: 12.5%
BMI	Range: 22–38
	Mean: 28.13

0: The mentioned disease is not present. 1: The mentioned disease is present.

Percentages, standard deviation, and mean values were described for descriptive statistics. The Wilcoxon test was applied for the hypothesis that there is no difference in LUS-imaging in two coherent time points in post-COVID syndrome and the alternative

hypothesis that there is a difference. As it was paired and not normally distributed in the follow-up rehabilitation, the Wilcoxon test was chosen over the t-test.

Table 2 displays the minimum and maximum numbers of the individual LUS scores with the mean value of all 16 patients. Table 3 describes the details of evaluating the 12 zones with all the values added for the 16 patients.

Table 2. LUS score at the first and second evaluation.

LUS Score	N	Minimum	Maximum	Mean	Standard Deviation
1st evaluation	16	10.00	27.00	17.7500	4.83735
2nd evaluation	16	2.00	23.00	8.1875	5.93542

Table 3. LUS score of the 12 zones (zone 1 until 6—right (R) hemithorax, zone one until six left (L) hemithorax) during the first and second evaluation of 16 patients. The mean, the median, and the total values are displayed.

Zone	R1		R2		R3		R4		R5		R6	
Evaluation	1st	2nd	1st	2nd	1st	2nd	1st	2nd	1st	2nd	1st	2nd
N	16	16	16	16	16	16	16	16	16	16	16	16
Mean	1.5000	0.8125	1.3750	0.6875	1.6250	0.5000	1.5625	0.8750	1.1875	0.3750	1.9375	0.5625
Median	1.5000	1.0000	1.0000	1.0000	2.0000	0.0000	1.0000	1.0000	1.0000	0.0000	2.0000	0.5000
Total	24.00	13.00	22.00	11.00	26.00	8.00	25.00	14.00	19.00	6.00	31.00	9.00
Zone	**L1**		**L2**		**L3**		**L4**		**L5**		**L6**	
Evaluation	1st	2nd	1st	2nd	1st	2nd	1st	2nd	1st	2nd	1st	2nd
N	16	16	16	16	16	16	16	16	16	16	16	16
Mean	1.3750	0.9375	1.6875	0.8750	1.4375	0.5000	1.5625	0.6875	1.0000	0.3750	1.5625	0.5000
Median	1.0000	1.0000	2.0000	1.0000	1.5000	0.0000	2.0000	1.0000	1.0000	0.0000	1.0000	0.0000
Total	22.00	15.00	27.00	14.00	23.00	8.00	25.00	11.00	16.00	6.00	25.00	8.00

For all the statistical analysis, the statistical software SPSS was used. The statistical software SPSS (Version 28, IBM, New York, NY, USA) was used for data analysis. Informed consent for all published material was obtained.

3. Results

A total of 16 post-COVID patients were evaluated on two occasions. The overall patient characteristics are displayed in Table 1.

The exams took place from the first time in May until June 2020. The follow-up visitation was carried out around 2021. Twelve [75%] of the patients had well-controlled hypertension as a prior known disease. Eight [50%] had LV hypertrophy, three had diabetes mellitus type two, and three had atrial fibrillation [both 18.75%]. None had known lung or other than previously mentioned diseases, and none were smokers. Of the 16 patients, two were female, and 14 were male [Table 1]. The mean BMI was 28.13 ranging from approximately 22 to 38 [Table 1].

The first scan was performed 1–5 months after severe or critical COVID-19 pneumonia. The second evaluation was conducted 5–13 months later.

In our cohort, in all patients, comet tail artifacts and consolidations were quantified by the LUS score. We described a change in pathological findings over 6–13 months. Both times, a standard lung ultrasound approach with a 12-zone scanning protocol was chosen (Figure 1) [7]. All patients did show some mild remaining pathological findings. Two of them had a persistent LUS score above 20 points. The median at the initial scan of 18 was reduced to 8 points in the follow-up. Most consolidations vanished over time, as well. One small anterior consolidation did persist (anterior hemithorax on the right side—zone

one). The detailed occurrence of consolidations is displayed in Table 4. All consolidations were small.

Table 4. Consolidations found in LUS at the first and second visitation, R [right hemithorax], L [left hemithorax].

Zone	N	Consolidations	
		1st Evaluation	2nd Evaluation
1	R	1	1
	L	0	0
2	R	0	0
	L	1	0
3	R	1	0
	L	0	0
4	R	2	0
	L	1	0
5	R	0	0
	L	0	1
6	R	4	0
	L	2	0

Interestingly, in the follow-up scan, one consolidation was found in an area (left posterior hemithorax—zone five) where it was not seen in the initial scan. Due to the anatomical location of the scapula, this small consolidation might have been missed in the initial scan. Pleural effusions were not seen in the evaluated patients after COVID-19.

There were significantly more artifacts and consolidations in the initial evaluation compared to the second evaluation. By means of consolidation, most were found in the posterior basal regions (left and right number six, Table 4).

In Table 4, all consolidations found in LUS at the first and second visitation are displayed in the specific region of scanning in which they appeared.

Table 2 shows the minimum and maximum LUS scores at the first and second evaluations. The mean values in both instances are visualized as well. At the initial assessment, the minimum score of all zones added was 10. The maximum score was 27. In the follow-up, the minimum LUS score was 2, and the maximum score was 23.

Table 3 and Figure 5 show the detailed analysis of the added number of individual patients showing that at the time of the first evaluation, the LUS score was higher compared to the second evaluation, with the highest score at zone six on the right side and zone two at the left hemithorax. In the second evaluation, interestingly, the most points were found at both hemithoraces in anterior regions (zone one and two on the left side and zone one on the right side as well as zone four on the right side).

The reverberation artifacts at the first evaluation displayed in all 16 patients a mean of approximately 17.75 (SD 4.8). In the follow-up, it decreased to 8.19 (SD 5.9) (graphic 2). The overall mean LUS scores were reduced by 46%.

The Wilcoxon test in the evaluation of the first and the second LUS did show a significant reduction in comet tail artifacts utilizing the LUS score ($p \leq 0.001$). Interestingly, none of the included patients showed an entirely normal LUS imaging of the lung. Some reverberation artifacts were persistent in all patients.

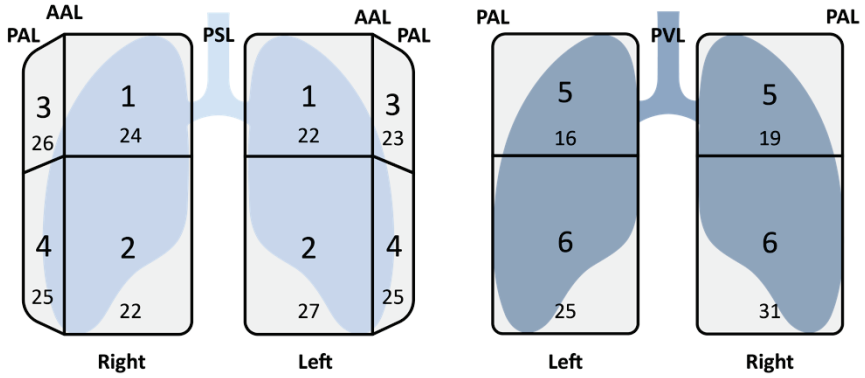

a) Total LUS scores of 16 patients in the respective zones in the first evaluation

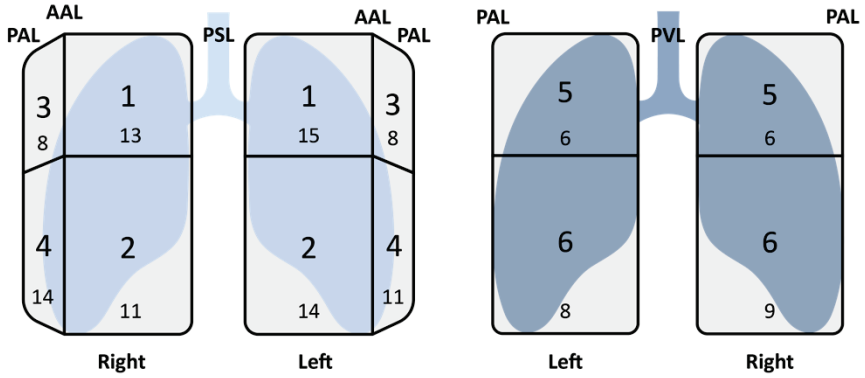

b) Total LUS scores of 16 patients in the respective zones in the follow-up evaluation

Figure 5. (**a**) Total LUS scores of 16 patients in the respective zones in the first evaluation/ (**b**) Total LUS scores of 16 patients in the respective zones in the follow-up evaluation.

4. Discussion

Patients with a post-COVID syndrome can face ongoing symptoms over a long period, including dyspnea [6–8,26]. In a study by Sonnweber et al., it was concluded that serial testing should be considered in patients with persistent symptoms, including serial lung function testing, echocardiography, and CT imaging [30]. LUS has been a more widely used tool in recent years in pulmonary imaging to identify pathological changes in COVID-19 pneumonia in the acute setting [3,5,9,20,36–38]. LUS can function as one of four specified parameters to provide information on hospital admission in acute COVID-19 disease alongside cardiovascular disease, day of illness, and leucocyte count [39].

As there are recommendations for LUS during the acute setting, there are also recommendations for follow-up [3,7].

This pilot study used a 12-zone scanning protocol in LUS to describe comet tail artifacts and consolidations after acute COVID-19 disease. To our knowledge, this is the first study to follow-up patients after a hospital stay or critical COVID-19 from the first COVID-19 wave to demonstrate existing reverberation artifacts as sequelae of lung disease. A recent study did show persisting reverberation artifacts after six months of acute COVID-19 disease and compared it with CT scans of the lungs. It is demonstrated that persistent changes in lung imaging (CT & LUS) are seen after six months, but the clinical relevance is unclear. The authors suggest that LUS might be a screening tool to rule out relevant lung diseases after COVID-19, such as pulmonary fibrosis [40–42]. In an ambulatory setting or rehabilitation, LUS can be a low-cost, easy-to-use, widely available, and radiation-sparing alternative to serial chest radiographs or CT scans for tracking improvement [3,7,40].

By means of prognosis, a score of 26 is considered a cut-off if a patient is scanned in the emergency department to have a 90% specificity of a lethal outcome during this admission. A score of 25 is associated with being admitted to the ICU, with a specificity of

90% in admitted patients due to COVID-19 [25]. In a study by Lichter et al., a LUS score of 18 or more seemed to be a cut-off for the follow-up in terms of mortality and requirement for ventilatory support [22].

The previously mentioned scores are in the case of a 12-zone LUS scanning protocol. As there are several protocols in use and some show 14 zones per each hemithorax, different values have to be known for the cut-off by means of prognosis [21,35]. In a study by Skopljanac et al., it was described that the LUS score was associated with oxygen demand at admission. Similar to a 12-zone scanning protocol, high LUS score values predicted more intensive respiratory care. A score of 29 was a cut-off for high-flow oxygen therapy and 30 for mechanical ventilation [21]. In our cohort, high scores after severe COVID-19 pneumonia were found and significantly reduced in the follow-up.

5. Limitations

Some limitations have to be addressed. First of all, it has to be pointed out that a very heterogeneous group of patients with quite varying time intervals in between scans were evaluated. The initial follow-up time differed by four months. The follow-up exam was conducted with a variation in time by eight months. The time intervals were scheduled in a real-life clinical scenario during the pandemic with limited resources and aimed to find the optimal timing for all individual patients. A third rehabilitation in a follow-up setting was planned. Still, practically all participants were lost to follow-up as the clinical status improved, and the need for another rehabilitation in the next year (2022) was not applicable.

Previously mentioned differences in settings may cause differences in artifact interpretation. That is a pitfall we encourage not to be overseen in daily clinical practice [8].

Another limitation is that this is a study where the data was evaluated retrospectively. The sample size of 16 patients is small, with a relatively broad range of ages. Besides, only two included patients were female, and the other fourteen were male. A healthy control group is missing, as this was in an ambulatory and rehabilitative setting.

We encourage all colleagues fighting against COVID-19 to evaluate patients in rehabilitation or in an ambulatory setting with lung ultrasound.

6. Conclusions

LUS might be an easily available and comparatively cheap tool without side effects that can be used in an ambulatory or hospital setting to follow up on COVID-19 patients that are hospitalized or in intensive care units after severe or critical COVID-19. Possible early detection of long-term complications such as pulmonary fibrosis might be in the scope of a thorough LUS exam using a standardized protocol [7,40,43,44]. In this pilot study, it was shown that LUS could add information regarding imaging. Whether the changes in imaging correlate to outcomes and clinical improvement is a topic for further evaluation.

Supplementary Materials: List of videos https://www.mdpi.com/article/10.3390/diagnostics13010070/s1: Video S1: A normal LUS (scanning one anterior area on the right side (zone r2) in a 12-zone scanning protocol) on the left side of the video with several B-lines in pulmonary congestion on the right side of the video in a heart failure patient. Video S2: A normal LUS (scanning one anterior area on the right side (zone r2) in a 12-zone scanning protocol) on the left side of the video and comet tails adjacent to a small area of consolidation in critical COVID-19 on the right side of the video in a patient without other known diseases. The A-lines have vanished and only comet tails are seen. Video S3: LUS changes in post-COVID syndrome from initial visitation to the second visitation six months later. Initially, there are plenty of comet tail artifacts. After six months, the pleural line looks smooth, and there are one or two reverberation artifacts seen. Both exams show the area of the right anterior hemothorax (zone one on the right hemithorax). Video S4: LUS changes in post-COVID syndrome from initial visitation to the second visitation 11 months later. Initially, there are plenty of comet tail artifacts. After six months, the pleural line looks smooth, and there are one or two reverberation artifacts seen. Both exams show the area of the right anterior hemothorax (zone one on the right hemithorax

Author Contributions: Data curation, M.A. and A.G.; visualization, Y.C.; writing—original draft, M.A.; writing—review & editing, M.A., R.W., R.H.Z., G.M. and M.G.; M.G. is the corresponding author. All authors have read and agreed to the published version of the manuscript.

Funding: This research received no external funding.

Institutional Review Board Statement: Not applicable.

Informed Consent Statement: Written informed consent was obtained from all subjects involved in the study to publish this paper.

Data Availability Statement: Not applicable.

Acknowledgments: For this publication, a special thanks go to the first author Martin Altersberger. He began acquiring images and loops from the first wave of COVID-19 until today. Without his effort and contribution, none of this would have been possible. Other special thanks go to Yerin Cho and her amazing work on editing the videos and creating the graphics.

Conflicts of Interest: The authors declare no conflict of interest.

Abbreviations

LUS	Lung ultrasound
CT	Computerized tomography
LV	Left ventricle
COPD	Chronic obstructive lung disease

References

1. Schneider, M.; Altersberger, M.; Binder, C.; Hengstenberg, C.; Binder, T. The COVID-19 burden for health care professionals: Results of a global survey. *Eur. J. Intern. Med.* **2020**, *83*, 96–98. [CrossRef] [PubMed]
2. Carod-Artal, F.J. Post-COVID-19 syndrome: Epidemiology, diagnostic criteria and pathogenic mechanisms involved. *Rev. Neurol.* **2021**. [CrossRef]
3. Santacroce, L.; Inchingolo, F.; Topi, S.; Del Prete, R.; Di Cosola, M.; Charitos, I.A.; Montagnani, M. Lung Ultrasound in COVID-19 and Post-COVID-19 Patients, an Evidence-Based Approach. *J. Ultrasound Med.* **2021**, *15*, 295–301.
4. Mathis, G.; Horn, R.; Morf, S.; Prosch, H.; Rovida, S.; Soldati, G.; Hoffmann, B.; Blaivas, M.; Dietrich, C.F. WFUMB position paper on reverberation artefacts in lung ultrasound: B-lines or comet-tails? *Med. Ultrason* **2020**, *23*, 70–73. [CrossRef] [PubMed]
5. Demi, L.; Wolfram, F.; Klersy, C.; De Silvestri, A.; Ferretti, V.V.; Muller, M.; Miller, D.; Feletti, F.; Wełnicki, M.; Buda, N.; et al. New International Guidelines and Consensus on the Use of Lung Ultrasound. *J. Ultrasound Med.* **2022**. [CrossRef]
6. Lichtenstein, D. Lung ultrasound in the critically ill. *Curr. Opin. Crit. Care* **2014**. [CrossRef]
7. Altersberger, M.; Goliasch, G.; Khafaga, M.; Schneider, M.; Cho, Y.; Winkler, R.; Funk, G.; Binder, T.; Huber, G.; Zwick, R.; et al. Echocardiography and Lung Ultrasound in Long COVID and Post-COVID Syndrome A Review Document of the Austrian Society of Pneumology and the Austrian Society of Ultrasound in Medicine. *J. Ultrasound Med.* **2022**. Available online: http://www.ncbi.nlm.nih.gov/pubmed/35906952 (accessed on 7 October 2022). [CrossRef]
8. Demi, M.; Buda, N.; Soldati, G. Vertical Artifacts in Lung Ultrasonography: Some Common Clinician Questions and the Related Engineer Answers. *Diagnostics* **2022**, *12*, 215. [CrossRef]
9. Soldati, G.; Smargiassi, A.; Inchingolo, R.; Buonsenso, D.; Perrone, T.; Briganti, D.F.; Perlini, S.; Torri, E.; Mariani, A.; Mossolani, E.E.; et al. Is there a role for lung ultrasound during the COVID-19 pandemic? *J. Ultrasound Med.* **2020**. [CrossRef]
10. Volpicelli, G.; Lamorte, A.; Villén, T. What's new in lung ultrasound during the COVID-19 pandemic. *Intensive Care Med.* **2020**, *46*, 1445–1448. [CrossRef]
11. Volpicelli, G.; Gargani, L. Sonographic signs and patterns of COVID-19 pneumonia. *Ultrasound J.* **2020**, *12*, 1–3. [CrossRef] [PubMed]
12. Huang, Y.; Wang, S.; Liu, Y.; Zhang, Y.; Zheng, C.; Zheng, Y. A Preliminary Study on the Ultrasonic Manifestations of Peripulmonary Lesions of Non-Critical Novel Coronavirus Pneumonia (COVID-19). *SSRN Electron. J.* **2020**. [CrossRef]
13. Gehmacher, O.; Mathis, G.; Kopf, A.; Scheier, M. Ultrasound imaging of pneumonia. *Ultrasound Med. Biol.* **1995**. [CrossRef] [PubMed]
14. Buda, N.; Kosiak, W.; Wełnicki, M.; Skoczylas, A.; Olszewski, R.; Piotrkowski, J.; Skoczyński, S.; Radzikowska, E.; Jassem, E.; Grabczak, E.M.; et al. Recommendations for Lung Ultrasound in Internal Medicine. *Diagnostics* **2020**, *10*, 597. [CrossRef] [PubMed]
15. Mayo, P.H.; Copetti, R.; Feller-Kopman, D.; Mathis, G.; Maury, E.; Mongodi, S.; Mojoli, F.; Volpicelli, G.; Zanobetti, M. Thoracic ultrasonography: A narrative review. *Intensive Care Med.* **2019**, *45*, 1200–1211. [CrossRef] [PubMed]

16. Kiefl, D.; Eisenmann, S.; Michels, G.; Schmid, M.; Ludwig, C.; Pin, M.; Gloeckner, E.; Petersen, P.F.; Damjanovic, D.; Schellhaas, S.; et al. German recommendations on lung and thoracic ultrasonography in patients with COVID-19. *Med. Klin Intensiv. Notfmed.* **2020**, *115*, 654–667. [CrossRef] [PubMed]
17. Abdel Kader, M.; Osman, N.M.M. Implementation of chest ultrasound with color Doppler in diagnosis of pneumonia in adults. *Egypt. J. Radiol. Nucl. Med.* **2016**, *47*, 771–781. [CrossRef]
18. Tung-Chen, Y. Lung ultrasound in the monitoring of COVID-19 infection. Clinical Medicine. *J. R. Coll. Physicians Lond.* **2020**, *20*, e62–e65.
19. Funk, G.C.; Nell, C.; Pokieser, W.; Thaler, B.; Rainer, G.; Valipour, A. Organizing pneumonia following Covid19 pneumonia. *Wien. Klin. Wochenschr.* **2021**, *133*, 979–982. [CrossRef]
20. Altersberger, M.; Schneider, M.; Schiller, M.; Binder-Rodriguez, C.; Genger, M.; Khafaga, M.; Binder, T.; Prosch, H. Point of care echocardiography and lung ultrasound in critically ill patients with COVID-19. *Wien. Klin. Wochenschr.* **2021**, *133*, 1298–1309. [CrossRef]
21. Skopljanac, I.; Ivelja, M.; Barcot, O.; Brdar, I.; Dolic, K.; Polasek, O.; Radic, M. Role of lung ultrasound in predicting clinical severity and fatality in COVID-19 pneumonia. *J. Pers Med.* **2021**, *11*, 757. [CrossRef] [PubMed]
22. Lichter, Y.; Topilsky, Y.; Taieb, P.; Banai, A.; Hochstadt, A.; Merdler, I.; Gal Oz, A.; Vine, J.; Goren, O.; Cohen, B.; et al. Lung ultrasound predicts clinical course and outcomes in COVID-19 patients. *Intensive Care Med.* **2020**. [CrossRef]
23. McElyea, C.; Do, C.; Killu, K. Lung ultrasound artifacts in COVID-19 patients. *J. Ultrasound* **2020**, *25*, 333–338. [CrossRef] [PubMed]
24. Alharthy, A.; Abuhamdah, M.; Balhamar, A.; Faqihi, F.; Nasim, N.; Ahmad, S.; Noor, A.; Tamim, H.; Alqahtani, S.A.; Abdulaziz Al Saud, A.A.; et al. Residual Lung Injury in Patients Recovering From COVID-19 Critical Illness: A Prospective Longitudinal Point-of-Care Lung Ultrasound Study. *J. Ultrasound Med.* **2021**, *40*, 1823–1838. [CrossRef]
25. de Alencar, J.C.G.; Marchini, J.F.M.; Marino, L.O.; Ribeiro, S.C.D.C.; Bueno, C.G.; da Cunha, V.P.; Neto, F.L.; Neto, R.A.B.; Souza, H.P.; COVID U. S. P. Registry Team. Lung ultrasound score predicts outcomes in COVID-19 patients admitted to the emergency department. *Ann. Intensive Care* **2021**, *11*, 6. [CrossRef]
26. Rouby, J.-J.; Arbelot, C.; Gao, Y.; Zhang, M.; Lv, J.; Wang, C.; Chunyao, W.; Bin, D.; Barbas, C.S.V.; Neto, F.L.D.; et al. Training for lung ultrasound score measurement in critically ill patients. *Am. J. Respir Crit Care Med.* **2018**, *198*, 398–401. [CrossRef]
27. Zhao, Z.; Jiang, L.; Xi, X.; Jiang, Q.; Zhu, B.; Wang, M.; Xing, J.; Zhang, D. Prognostic value of extravascular lung water assessed with lung ultrasound score by chest sonography in patients with acute respiratory distress syndrome. *BMC Pulm. Med.* **2015**, *15*, 1–7. [CrossRef]
28. Demeco, A.; Marotta, N.; Barletta, M.; Pino, I.; Marinaro, C.; Petraroli, A.; Moggio, L.; Ammendolia, A. Rehabilitation of patients post-COVID-19 infection: A literature review. *J. Int. Med. Res.* **2020**. [CrossRef]
29. Wade, D.T. Rehabilitation after COVID-19: An evidence-based approach. *Clin. Med.* **2020**, *20*, 359–365. [CrossRef]
30. Sonnweber, T.; Sahanic, S.; Pizzini, A.; Luger, A.; Schwabl, C.; Sonnweber, B.; Kurz, K.; Koppelstätter, S.; Haschka, D.; Petzer, V.; et al. Cardiopulmonary recovery after COVID-19—An observational prospective multi-center trial. *Eur Respir J.* **2020**. [CrossRef]
31. Lopez-Leon, S.; Wegman-Ostrosky, T.; Perelman, C.; Sepulveda, R.; Rebolledo, P.A.; Cuapio, A.; Villapol, S. More than 50 Long-Term Effects of COVID-19: A Systematic Review and Meta-Analysis. *Sci. Rep.* **2021**, *11*, 1–12. [CrossRef] [PubMed]
32. Raveendran, A.V.; Jayadevan, R. Sashidharan; Long COVID: An Overview; Diabetes & Metabolic Syndrome: Clinical Research & Reviews, March 2021. Available online: https://www.swselfmanagement.ca/uploads/ResourceDocuments/Long%20Covid%20Article.pdf (accessed on 7 October 2022).
33. Hayes, L.D.; Ingram, J.; Sculthorpe, N.F. More Than 100 Persistent Symptoms of SARS-CoV-2 (Long COVID): A Scoping Review. *Front. Med.* **2021**, *8*, 750378. [CrossRef] [PubMed]
34. Zhao, Y.M.; Shang, Y.M.; Song, W.B.; Li, Q.Q.; Xie, H.; Xu, Q.F.; Jia, J.L.; Li, L.M.; Mao, H.L.; Zhou, X.M.; et al. Follow-up study of the pulmonary function and related physiological characteristics of COVID-19 survivors three months after recovery. *EClinicalMedicine* **2020**, *25*, 100463. [CrossRef] [PubMed]
35. Soldati, G.; Smargiassi, A.; Inchingolo, R.; Buonsenso, D.; Perrone, T.; Briganti, D.F.; Perlini, S.; Torri, E.; Mariani, A.; Mossolani, E.E.; et al. Proposal for international standardization of the use of lung ultrasound for COVID-19 patients; a simple, quantitative, reproducible method. *J. Ultrasound Med.* **2020**, *39*, 1413–1419. [CrossRef]
36. Gargani, L.; Soliman-Aboumarie, H.; Volpicelli, G.; Corradi, F.; Pastore, M.C.; Cameli, M. Why, when, and how to use lung ultrasound during the COVID-19 pandemic: Enthusiasm and caution. *Eur. Heart J. Cardiovasc. Imaging* **2020**, *21*, 941–948. [CrossRef]
37. Halpin, S.J.; McIvor, C.; Whyatt, G.; Adams, A.; Harvey, O.; McLean, L.; Walshaw, C.; Kemp, S.; Corrado, J.; Singh, R.; et al. Postdischarge symptoms and rehabilitation needs in survivors of COVID-19 infection: A cross-sectional evaluation. *J. Med. Virol.* **2021**, *93*, 1013–1022. [CrossRef]
38. Hoffmann, T.; Bulla, P.; Jödicke, L.; Klein, C.; Bott, S.M.; Keller, R.; Malek, N.; Fröhlich, E.; Göpel, S.; Blumenstock, G.; et al. Can follow up lung ultrasound in Coronavirus Disease-19 patients indicate clinical outcome? *PLoS ONE* **2021**, *16*, e0256359. [CrossRef]
39. Skopljanac, I.; Ivelja, M.P.; Mrsic, D.B.; Barcot, O.; Jelicic, I.; Domjanovic, J.; Dolic, K. Can Lung Imaging Scores and Clinical Variables Predict Severe Course and Fatal Outcome in COVID-19 Pneumonia Patients? A Single-Center Observational Study. *Life* **2022**, *12*, 735. [CrossRef]

40. Russo, G.; Flor, N.; Casella, F.; Ippolito, S.; Leidi, F.; Casazza, G.; Radovanovic, D.; Vezzulli, F.; Santus, P.; Cogliati, C. Lung ultrasound in the follow-up of severe COVID-19 pneumonia: Six months evaluation and comparison with CT. *Intern. Emerg. Med.* **2022**, *17*, 2261–2268. [CrossRef]
41. Manolescu, D.; Oancea, C.; Timar, B.; Traila, D.; Malita, D.; Birsasteanu, F.; Tudorache, V. Ultrasound mapping of lung changes in idiopathic pulmonary fibrosis. *Clin. Respir. J.* **2020**, *14*, 54–63. [CrossRef]
42. Espersen, C.; Platz, E.; Alhakak, A.S.; Sengeløv, M.; Simonsen, J.; Johansen, N.D.; Davidovski, F.S.; Christensen, J.; Bundgaard, H.; Hassager, C.; et al. Lung ultrasound findings following COVID-19 hospitalization: A prospective longitudinal cohort study. *Respir Med.* **2022**, *197*, 106826. [CrossRef] [PubMed]
43. Hernández-Píriz, A.; Tung-Chen, Y.; Jiménez-Virumbrales, D.; Ayala-Larrañaga, I.; Barba-Martín, R.; Canora-Lebrato, J.; Zapatero-Gaviria, A.; Casasola-Sánchez, G.G. Importance of lung ultrasound follow-up in patients who had recovered from coronavirus disease 2019: Results from a prospective study. *J. Clin. Med.* **2021**, *10*, 3196. [CrossRef] [PubMed]
44. Tung-Chen, Y.; Martí de Gracia, M.; Parra-Gordo, M.L.; Díez-Tascón, A.; Agudo-Fernández, S.; Ossaba-Vélez, S. Usefulness of Lung Ultrasound Follow-up in Patients Who Have Recovered From Coronavirus Disease 2019. *J. Ultrasound Med.* **2020**, *40*, 1971–1974. [CrossRef] [PubMed]

diagnostics

MDPI

Article

Pediatric COVID-19 Follow-Up with Lung Ultrasound: A Prospective Cohort Study

Domenico Paolo La Regina [1], Daniela Pepino [2], Raffaella Nenna [1], Elio Iovine [1], Enrica Mancino [1], Gianmarco Andreoli [2], Anna Maria Zicari [1], Alberto Spalice [1], Fabio Midulla [1,*] and on behalf of the Long COVID Research Group [†]

[1] Department of Maternal Infantile and Urological Sciences, Sapienza University of Rome, 00161 Rome, Italy
[2] Department of Diagnostic Medicine and Radiology, Sapienza University of Rome, 00161 Rome, Italy
* Correspondence: midulla@uniroma1.it
† A complete list of group members is provided in the Acknowledgments.

Abstract: During the COVID-19 pandemic, lung ultrasound (LUS) was widely used to assess SARS-CoV-2 infection. To date, there are patients with persistence of symptoms after acute infection. Therefore, it may be useful to have an objective tool to follow these patients. The aim of our study was to evaluate the presence of LUS artifacts after SARS-CoV-2 infection in children and to analyze the associations between time elapsed since infection and symptomatology during acute infection. We conducted an observational study, enrolling 607 children infected with SARS-CoV-2 in the previous twelve months. All patients performed a LUS and medical history of demographic and clinical data. We observed irregular pleural lines in 27.5%, B-lines in 16.9%, and subpleural consolidations in 8.6% of the cases. These artifacts were more frequently observed in the lower lobe projections. We have observed that the frequency of artifacts decreases with increasing time since infection. In symptomatic patients during COVID infection, B-lines ($p = 0.02$) were more frequently found. In our sample, some children, even after months of acute infection, have ultrasound artifacts and showed an improvement with the passage of time from the acute episode. Our study provides additional evidence about LUS in children with previous COVID-19 as a support to follow these patients in the months following the infection.

Keywords: SARS-CoV-2 infection; COVID-19; children; lung ultrasound

Citation: La Regina, D.P.; Pepino, D.; Nenna, R.; Iovine, E.; Mancino, E.; Andreoli, G.; Zicari, A.M.; Spalice, A.; Midulla, F.; on behalf of the Long COVID Research Group. Pediatric COVID-19 Follow-Up with Lung Ultrasound: A Prospective Cohort Study. *Diagnostics* **2022**, *12*, 2202. https://doi.org/10.3390/diagnostics12092202

Academic Editors: Marcello Demi and Gino Soldati

Received: 10 July 2022
Accepted: 6 September 2022
Published: 11 September 2022

1. Introduction

During the coronavirus pandemic, children are less likely to get infected, and typically they have a less severe illness with fewer deaths [1–3]. The most frequent clinical symptom is fever, followed by fatigue, cough, rhinorrhea, sore throat, headache, vomiting, and abdominal pain [4,5]. Although asymptomatic cases in the pediatric population vary in relation to the study analyzed between 15 and 35% [6,7], children with clinical signs of pneumonia represent about 45% of all pediatric cases [8].

In these patients, new evidence from published studies are showing the versatility of lung ultrasound (LUS) from diagnosis to monitoring and follow-up [9,10]. In the last years, this method has been increasingly used and there is growing evidence of its utility in the management of many pediatric lung diseases [11–13].

Moreover, during the COVID-19 pandemic, ultrasound has been widely used to assess the severity of severe acute respiratory syndrome coronavirus 2 (SARS-CoV-2) infection in both adults and children.

Lung ultrasound is able to identify alterations affecting air content in the peripheral lung parenchyma. Normally, the air into the lung reflects ultrasound waves completely. Therefore, healthy lung ultrasounds are characterized by horizontal artifacts beyond the pleural line. When the peripheral airspace of the lung is subverted with a reduced tissue/air

ratio, ultrasound incident waves could enter acoustic channels and be trapped in acoustic microholes on the pleural plane. This determines the generation of vertical artifacts, resulting in the so-called Sonographic Interstitial Syndrome indicative of a hyperdense preconsolidated state of the lungs [14]. If the tissue/air ratio is further reduced, thickening is generated. On the basis of the above, the main ultrasound findings observable in children with COVID-19 are pleural irregularities, vertical artifacts or areas of white lung, and subpleural consolidations [15–17].

It has recently been shown that LUS has a high concordance with the gold standard for diagnosis and assessment of the severity of SARS-CoV-2 pneumonia, computer tomography (CT) of the chest [18–20]. Considering that today many studies show that in children, as in adults, there are patients who report the persistence of symptoms after acute infection, defined as Long-COVID [21–23], it could be useful to have an objective tool to follow the patients after COVID-19.

Thanks to its wide availability, its safety with the absence of ionizing radiation, its low cost, and its rapidity of execution, LUS can represent an optimal method to follow children with previous COVID-19 infection. This can help to exclude the presence of lung sequelae in patients healed from COVID-19, avoiding them to undergo more invasive tests such as CT.

The primary aim of our study was to assess the presence of artifacts on lung ultrasound in children after months of SARS-CoV-2 infection. The secondary aim was to analyze whether the ultrasound artifacts reduced with the time elapsed from the infection and whether there were differences according to the symptoms during the acute infection.

2. Materials and Methods

2.1. Study Population

We conducted an observational prospective, single-centre, study from February to November 2021, at the Department of Maternal Science of a tertiary University hospital in Rome. The local Ethics Committee approved the study protocol and informed parental consent was obtained from all patients (RIF.CE 0399/2021).

We enrolled 607 children, 0 to 18 years old, infected with SARS-CoV-2 one to twelve months before enrollment. The infection was documented by a positive nasopharyngeal swab result, performed outside the hospital. Both symptomatic and asymptomatic patients during acute infection were enrolled.

Patients were divided into 4 groups according to the distance from the infection ($\leq$3 months, 4–6 months, 7–9 months, and >9 months) (Figure 1). For each patient, we performed a medical history. With a structured questionnaire, the following detailed demographic and clinical data were collected: age, gender, body mass index, history of respiratory disease, and exposure to smoke. Moreover, we analysed the presence of blood SARS-CoV-2 antibodies. Exclusion criteria were new respiratory infections between SARS-CoV-2 infection and enrollment, congenital heart diseases, immunodeficiency, and respiratory tract malformation.

2.2. Lung Ultrasound

LUS was performed by a single experienced radiologist blinded to the patient's condition using a high frequency (5–12 MHz) linear probe. Ultrasonographic evaluation was performed according to Copetti et al. [24] and the probe was placed vertically, obliquely, and horizontally to the ribs in three chest projections: anterior, lateral, and posterior. For this, we divided the chest into 12 quadrants (two anterior, two lateral, and two posterior quadrants for each hemithorax) and we have analyzed the following ultrasonographic features:

- pleural line morphology;
- identification of B lines and/or "white lung";
- identification of subpleural consolidations;
- presence of pleural effusion.

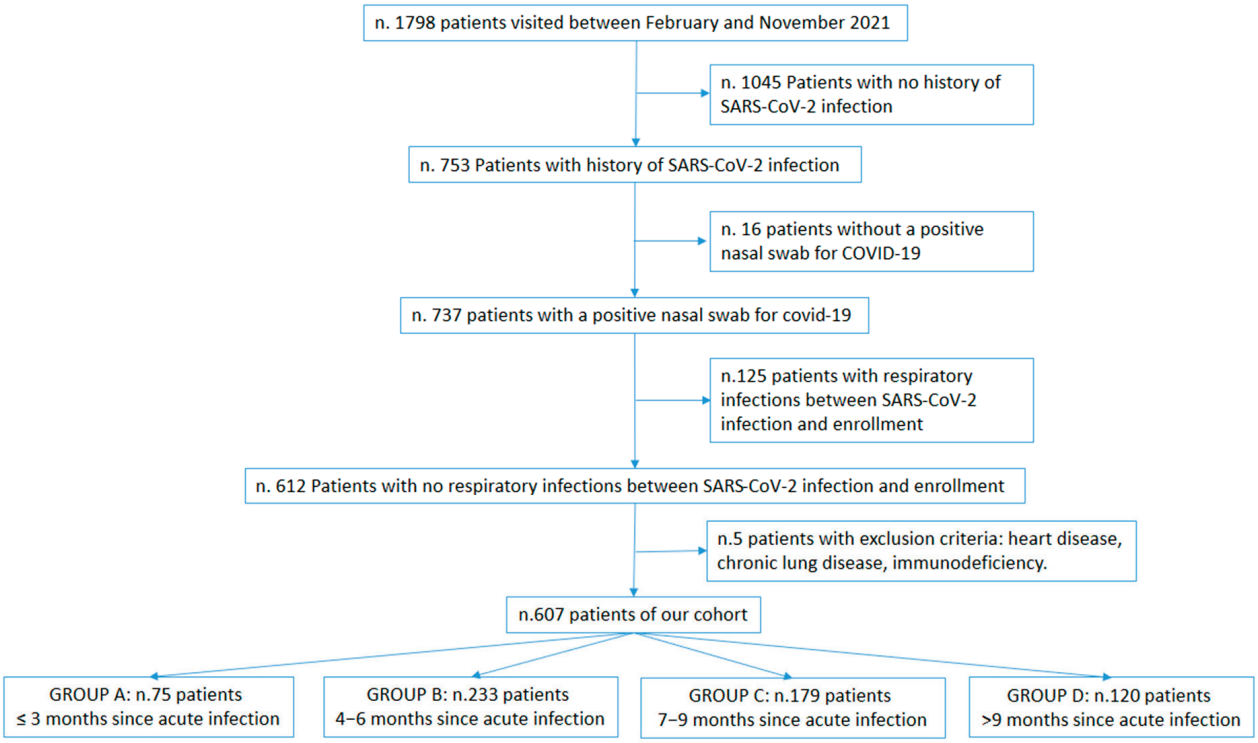

Figure 1. Enrolment flow-chart.

In a normally aerated lung, the only detectable structure is the pleura. It appears as a continuous hyperechogenic line that moves back and forth with the breaths (lung sliding). We considered a pleural line with thickening, granularity, and waviness as pathological. Below the pleural line, the healthy lung is filled with air. This does not allow the direct visualization of the normal pulmonary parenchyma, but you can see the "A-lines". They are horizontal echogenic lines equidistant and parallel to each other and the pleura, representing reverberations of the pleura itself.

B-lines were defined as vertical narrow lines arising from the pleural line. B-lines show a narrow base, extend to the bottom of the screen without fading, and move synchronously with lung sliding.

If the B-lines were less than 3 for quadrant they were not considered pathological. We classified B-lines as multifocal (referring to 3 or more separated B-lines for a quadrant) or confluent.

Finally, the presence of poorly ventilated or solid images near the pleura were identified such as subpleural consolidations. These were divided by size (<0.5 cm, 0.5–1 cm, and >1 cm).

Based on these characteristics we identified a modified Soldati-Volpicelli LUS score [10,25] with five patterns of severity, associated with the degree of pulmonary aeration (Figure 2).

2.3. Statistical Analysis

The statistical software SPSS (version 27.0; IBM, New York, NY, USA) was used for data analysis. For all the variables studied, we performed a descriptive analysis using percentage values for qualitative variables, and mean and standard deviation values for quantitative variables. For qualitative variables, chi-square tests were used. For quantitative variables without normal distribution, non-parametric Mann-Whitney U Tests were used. Results with p-values < 0.05 were considered statistically significant.

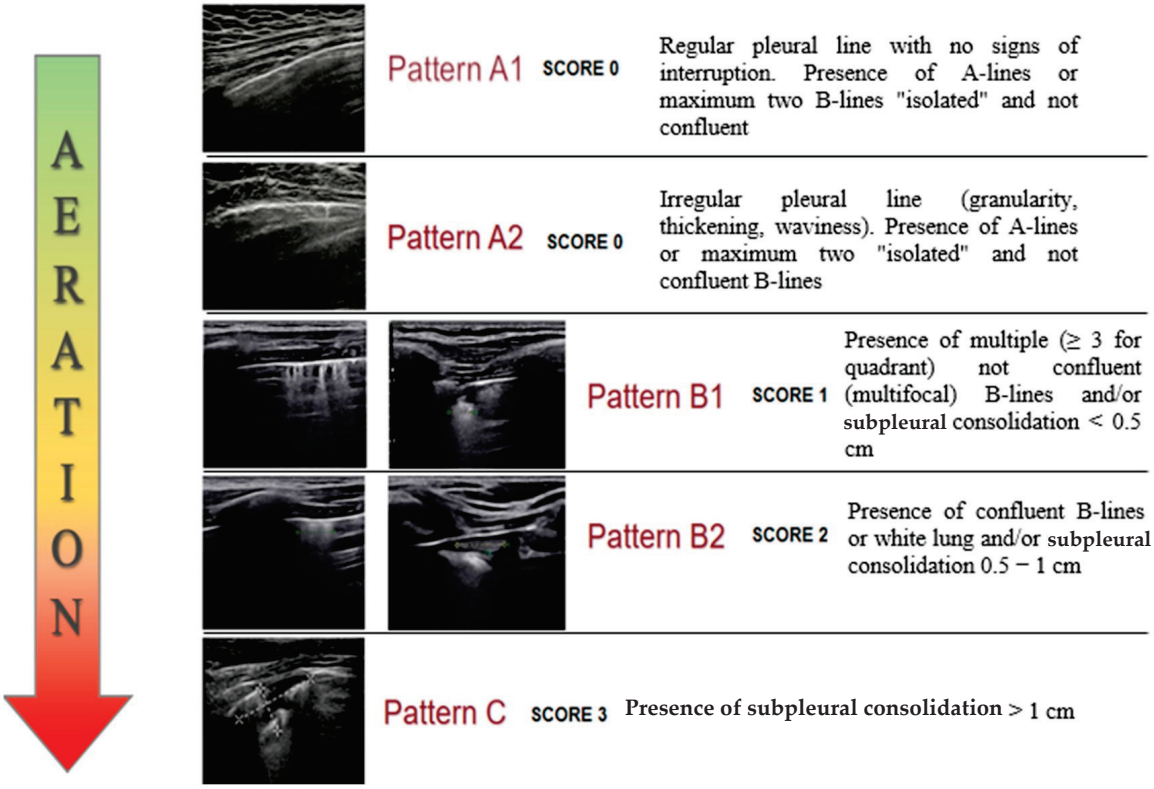

Figure 2. Lung ultrasound patterns with the degree of pulmonary aeration.

3. Results

We evaluated 607 consecutive infants (mean age 9.54 ages ± 4.2, 50.9% males) infected with SARS-CoV-2 in the 12 months before enrollment. Table 1 summarized clinical and epidemiological data of patients. In our sample, the most common symptom during the acute phase was fever (47.5%), followed by headache (36.1%), cough (21.9%), ageusia (19.3%), and anosmia (18.9%).

Table 1. Clinical and demographic characteristics of patients. Variables are expressed as frequencies (percentages) and means (±SD).

Patients with Previous SARS-CoV-2 Infection	**n = 607**
Age at enrollment, years (SD*SD*)	9.54 (±4.2)
<6 years, n (%)	172 (28.3%)
7–12 years, n (%)	291 (47.9%)
>13 years, n (%)	143 (23.6%)
Sex, male, n (%)	309 (50.9%)
Body Mass Index, percentile (SD)	64.5° (±31.14)
Ab SARS-CoV-2, title (SD)	106 (±98.47)
Time elapsed since acute infection, months (SD)	6.26 (± 2.86)
<3 months, n (%)	75 (12.4%)
3–6 months, n (%)	233 (38.4%)
6–9 months, n (%)	179 (29.5%)
>9 months, n (%)	120 (19.8%)
Exposure to smoke, n (%)	164 (27.0%)
Medical history for:	
Bronchiolitis, n (%)	90 (14.8%)
Asthmatic bronchitis, n (%)	109 (18.0%)
Asthma, n (%)	24 (4.0%)
Atopic dermatitis, n (%)	63 (10.4%)
Allergy to inhalants, n (%)	106 (17.5%)

Table 1. *Cont.*

Patients with Previous SARS-CoV-2 Infection	**n = 607**
Symptoms during acute infection, n (%)	478 (78.7%)
Fever, n (%)	289 (47.6%)
Cough, n (%)	133 (21.9%)
Respiratory distress, n (%)	43 (7.1%)
Ageusia, n (%)	117 (19.3%)
Anosmia, n (%)	115 (18.9%)
Vomiting, n (%)	39 (6.4%)
Diarrhea, n (%)	86 (14.2%)
Headache, n (%)	219 (36.1%)

We observed irregular pleural lines in 27.5%, B-lines in 16.9%, and subpleural consolidations in 8.6% of the cases. These artifacts were observed more frequently in the lower lobe projections, particularly patterns B1 and B2 in lower lobes were observed in 80% and 69%, respectively ($p < 0.001$) (Table 2).

Table 2. Rates of patterns and artifacts lung ultrasound at baseline.

Lung Ultrasound Artifacts	**n = 607**
Pleural line	
• Regular	440 (72.5%)
• Irregular	167 (27.5%)
Irregular in only 1 quadrant for hemithorax	57 (9.4%)
- Irregular in >1 quadrant for hemithorax	110 (18.1%)
B-Lines	
• Absence of B-Lines	504 (83.0%)
• Presence of B-lines	103 (17.0%)
- B-lines in only 1 quadrant for hemithorax	81 (13.3%)
- B-lines in >1 quadrant for hemithorax	22 (3.6%)
Subpleural consolidations	
• Absence	555 (91.4%)
• Presence	52 (8.6%)
- <1 cm	52 (8.6%)
- >1 cm	0 (0%)
White Lung	1 (0.2%)
Pleural effusion	2 (0.3%)
Patterns	
• Pattern A2	167 (27.5%)
• Pattern B1	120 (19.8%)
- Lower lobes	96 (80.0%)
- Upper lobes	12 (10.0%)
- Both lobes	13 (10.0%)
• Pattern B2	29 (4.8%)
- Lower lobes	20 (69.0%)
- Upper lobes	9 (31.0%)
- Both lobes	0 (0%)
• Pattern C	0 (0%)

A pulmonary quadrant with the presence of white lung was found in one patient while a pleural effusion flap was found in another two patients. Among the ultrasound patterns, the most represented was the A2 pattern, highlighted in 27.5% of cases, while the C pattern was not found in any patient (Table 2).

We have observed that the frequency of artifacts decreases with increasing time since infection. Patients of "group 4" (infection > 9 months) had fewer ultrasound artifacts than patients of groups with more recent COVID infection (groups 1, 2, and 3) (Figure 3).

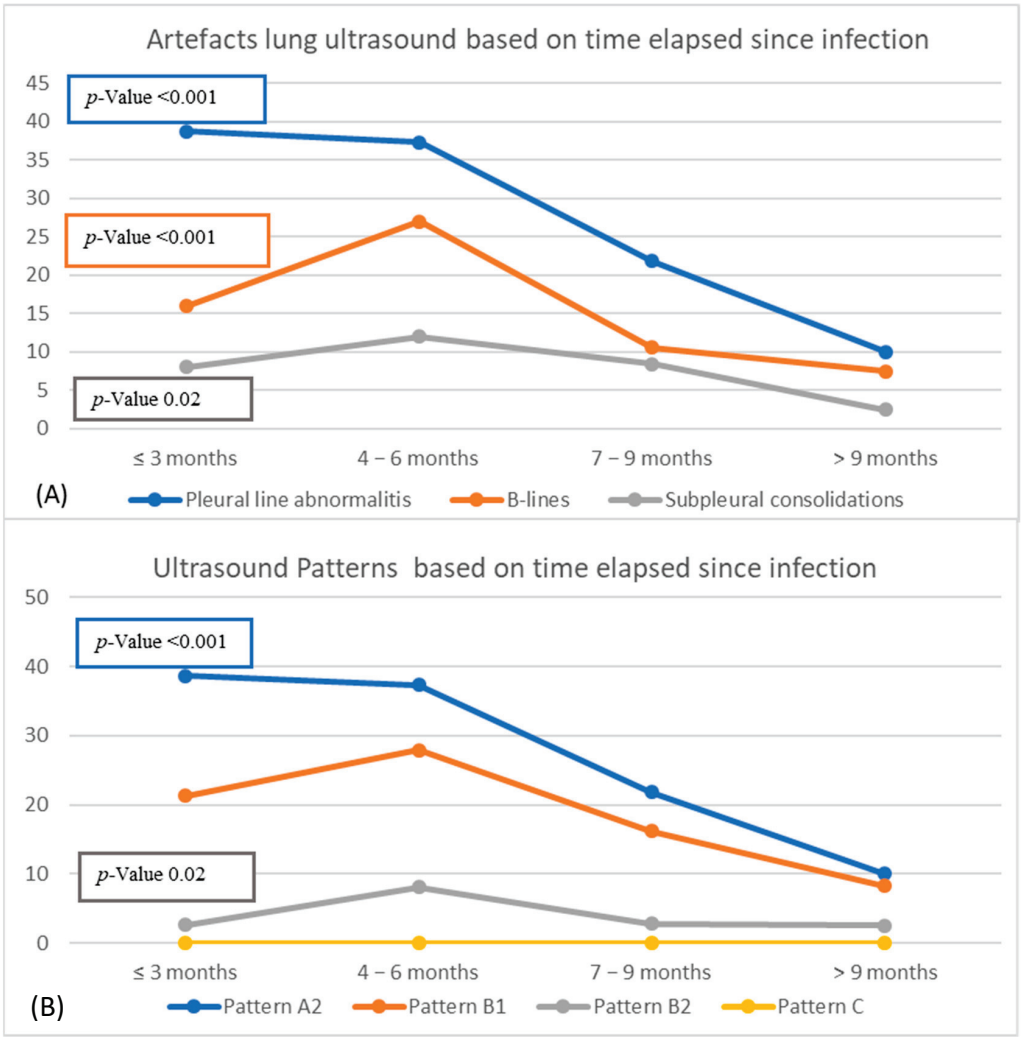

Figure 3. Association between artefacts (**A**) – patterns (**B**) lung ultrasound and time elapsed since infection.

In particular, pleural line abnormalities and B-lines were highlighted in 38.7% and 16% of patients within 3 months from the acute infection and in 10% and 7.5% of patients with infection after 9 months ($p = 0.001$). Finally, subpleural consolidations were found in 8% of patients of "group 1" and in 2.5% of patients of "group 4" ($p = 0.02$). Similar results were found while analyzing lung ultrasound patterns.

In symptomatic patients during COVID infection, B-lines ($p = 0.02$) and pattern B1 ($p = 0.04$) were found more often (Table 3).

Table 3. Association between patterns/artifacts lung ultrasound and symptoms during acute infection.

	Symptoms during Acute Infection		
	Yes (n. 483)	**Not (n. 122)**	***p*-Value**
Pleural line abnormalities	136 (28.1%)	31 (25.4%)	n.s.
B-lines	91 (18.8%)	12 (9.8%)	0.02
Subpleural consolidations	40 (8.3%)	12 (9.8%)	n.s.
White Lung	1 (2.1%)	0 (0%)	n.s.
Pleural effusion	2 (4.2%)	0 (0%)	n.s.
Pattern A2	137 (28.4%)	30 (24.6%)	n.s.
Pattern B1	104 (21.5%)	16 (13.1%)	0.04
Pattern B2	20 (4.1%)	9 (7.4%)	n.s.
Pattern C	0 (0%)	0 (0%)	n.v.

In our sample, males had more B-lines than females but this result has not found statistical significance. We have found that children with a positive history of asthma had more pleural line abnormalities than patients without asthma ($p = 0.04$). No differences were found in the positive history of exposure to smoke, bronchiolitis, and asthmatic bronchitis.

Finally, we observed a significant difference in body mass index between patients with and without lung artifacts. In particular, patients with lung artifacts had a lower mean rank of body mass index percentile than patients without artifacts (Figure 4). We did not find other differences based on epidemiological dates.

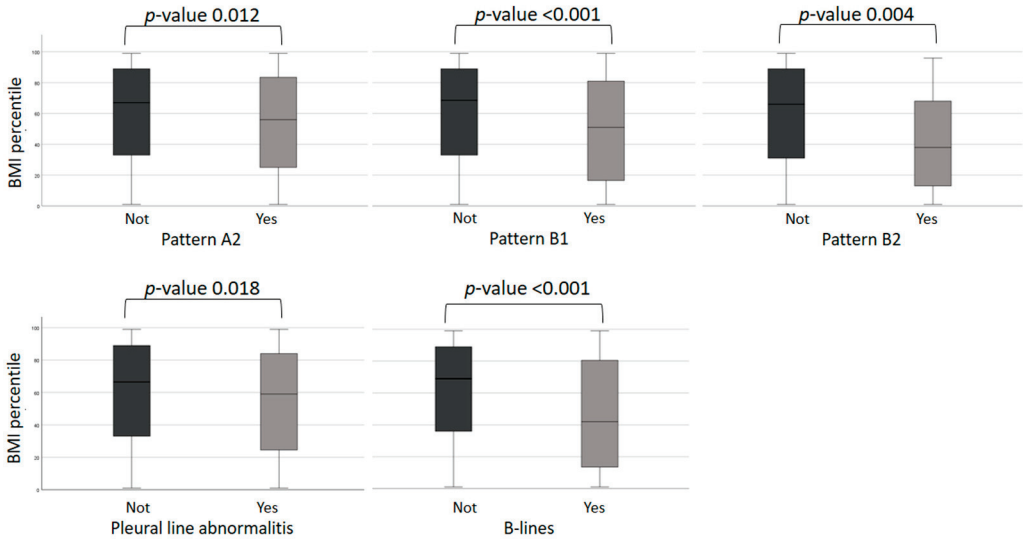

Figure 4. Association between lung ultrasound artifacts and Body Mass Index. Data not statistically significant have not been reported (subpleural consolidation and Pattern C).

4. Discussion

In our study, we found that a small number of children with previous COVID-19, even after months of acute infection, have ultrasound artifacts compatible with a lung involvement during SARS-CoV-2 infection. We have shown that these artifacts are observed less frequently after time from the acute episode, and they were more frequent in the lower lobes than in the upper lobes. Moreover, we have found more often B-lines and pattern B1 in patients with acute symptoms during SARS-CoV-2 infection. On the other hand, there were no particular differences in the clinical characteristics of the patients except for a difference in body mass index between patients with and without lung artifacts and for pleural line abnormalities in patients with a positive history of asthma.

Since the proposal for more frequent use of LUS in COVID-19 patients [26], there has been increasing evidence in adults that LUS is able to detect artifacts of SARS-CoV-2 infection. However, the main patterns are similar to those that we have described in children.

In our sample, the most frequent LUS findings were pleural lines abnormalities, B-lines, and subpleural consolidation. To date, it is clearly reported which are the main lung ultrasound artifacts during SARS-CoV-2 infection in the pediatric population. Ultrasound artifacts described in our patients are analogous to those described by Musolino et al. [16]. In their study, they enrolled 10 children hospitalized for SARS-CoV-2 infection. In all symptomatic cases, LUS revealed signs of lung involvement during COVID-19 infection. In particular, vertical artifacts, areas of white lung and subpleural consolidations, and pleural irregularities were the main findings in pediatric COVID-19 pneumonia. There were no cases of pleural effusions.

Other pediatric studies showed the presence of pulmonary artifacts at the ultrasound ongoing of COVID-19: Denina et al. and Guitart et al. have reported similar artifacts to ours [27,28].

Sawamura et al. [29] showed that in adults 90 days after the acute infectious episode, there were lung lesions detected at HRTC. Of the 91 patients included, 81% had at least one pulmonary lobe with abnormalities 90 days after discharge. Ground-glass opacities (76%) and parenchymal bands (65%) were the predominant abnormalities. This study confirms our results. Even after months of acute infection, lung lesions are still evident with instrumental investigations.

However, it is important to remember that lung ultrasound findings reflect the common abnormal findings of infection pneumonia. Pleural line irregularities, B lines, and subpleural consolidation are also present in other viral infections.

Moreover, we found that lung artifacts are more frequent in the lower lung lobes. This result is similar to that of other studies [30–32]. This may be due to the physiologic regional inhomogeneity of the lung as a result of the influence of gravity [33]. The erect lung is marked by striking regional non-uniformity in perfusion and ventilation resulting in blood flow and ventilation predominating in the lower lobes [34].

The prevalence of lung lesions in the lower regions is not a new concept, but it can also be observed in other viral infections [35].

The secondary aim of our study concerned analyzing possible associations between lung artifacts with time elapsed since the acute infection and the presence of clinical symptoms during acute infection.

We found that the frequency of artifacts decreases with increasing time since infection. The presence of typical viral lung artifacts and the improvement of the ultrasound picture at a distance of time from the infection support the hypothesis that the highlighted artifacts are a direct consequence of a lung involvement during viral infection, still present several months following the acute infection. To avoid mistakes, we have discarded patients with new airway infections in the time elapsed between acute SARS-CoV-2 infection and enrollment.

Our results go in line with the results of Denina et al. [36]. In their study, a clinical-instrumental follow-up was carried out on 25 pediatric patients four months after the acute infection, showing the presence of ultrasound artifacts in the course of follow-up and observing an improvement in ultrasound patterns over time. Although to date there is a lack of studies about the follow-up of SARS-CoV-2 infection in children, taken together, these findings highlight the importance of LUS for pediatric COVID-19 follow-up avoiding the use of ionizing radiation and reducing costs.

In our cohort, we observed B-lines and pattern B1 more often in patients with symptoms during SARS-CoV-2 infection. We also found lung artifacts in asymptomatic patients. This data has already been described in the literature. Ng et al. [37] described CT patterns in 25 asymptomatic young patients who had laboratory-confirmed COVID-19. In their study, chest CT showed abnormalities in six patients (24%), four (16%) had ground glass opacification, one (4%) had a small peripheral subpleural nodule and one (4%) had a dense solitary granuloma. Ng's results are similar to ours. Whereas the coronavirus is a respiratory virus, it seems plausible that, even in the absence of clear respiratory symptomatology, there is an involvement with the pulmonary parenchyma evidenced by the ultrasound.

Further interesting data emerged from our study. In our cohort, males had more B-lines than females. Even if this result is not statistically significant, it is in concord with that reported in the literature about sex differences in COVID-19 infection [38]. In fact, biological sex differences may manifest themselves in susceptibility to infection, early pathogenesis, innate viral control, adaptive immune responses, or the balance of inflammation and tissue repair in the resolution of infection [38].

Moreover, we have found that children with a positive history of asthma had more pleural line abnormalities than patients without asthma. In the literature, it is reported that patients with asthma had predominant A-lines plus lung sliding [39].

In our opinion, pleural line abnormalities could reflect the exaggerated accumulation of air in the lungs in children with asthma who have an efficient inspiratory drive that is not followed by an efficient expiratory phase due to partially occluded bronchi.

Finally, we observed significant differences in body mass index between patients with and without lung artifacts. In particular, patients with lung artifacts had a lower mean rank of body mass index percentile than patients without artifacts. This result is in contrast with other studies published in the literature, that show an association between BMI and both COVID-19 severity and mortality. Obesity was associated with a significantly increased risk of critical COVID-19 and in-hospital mortality [40]. Our difference may be due to the fact that the lean child has less acoustic impedance during the performance of lung ultrasound and this can improve the vision of artifacts.

Our study has some limits. First of all, only one blinded sonographer without a double-blind control performed LUS examinations. Then, in our study only one lung ultrasound was performed for each child, therefore we were not able to evaluate the evolution of ultrasound patterns in each individual patient. Finally, in our study, we did not have a control group of healthy children.

In conclusion, we can speculate that LUS is a valid tool to investigate pediatric populations with previous SARS-CoV-2 infection. This is possible because SARS-CoV-2 lung lesions are peripheral [41], allowing lung lesions to be identified by ultrasound.

Based on our experience, we consider lung ultrasound to be a safe and harmless method. Some studies have shown ultrasound damage in gas-containing tissues (lungs and intestine), but these experiments were performed on animal models and with acoustic intensity significantly higher than the range commonly used in the diagnostic clinic.

In short, the literature indicates that the bio-effects of ultrasound do not reach clinical levels relevant, and their existence is proven only in in vitro studies and animal models.

For this, to date based on current data in the literature, we believe lung ultrasound is safe and repeatable, especially in pediatrics. This reduces the use of radiation that has been shown to be harmful to the maturing lung. Due to its simplicity of execution, ease of learning, and proven usefulness, we believe that every pediatrician should perform it for the management of the acute phase and the follow-up of patients with infectious lung diseases.

In this context, our study provides additional evidence about LUS in children with previous COVID-19 as a support to follow these patients in the months following the infection. In fact, in our sample, some children, even after months of acute infection, have ultrasound artifacts compatible with a previous SARS-CoV-2 infection and showed an improvement with the passage of time from the acute episode.

If our data were confirmed we should consider revisiting the definition of Long COVID, currently based only on the symptomatological aspect, integrating it with the lung ultrasound findings. Further studies are necessary to support our findings because of the lack of data in the literature regarding LUS in the follow-up of children with previous SARS-CoV-2 infection.

Finally, we recommend performing a lung ultrasound in the follow-up of the pediatric patient with a previous SARS-CoV-2 infection.

Author Contributions: Conceptualization: D.P.L.R. and R.N.; Data curation: E.I., E.M. and Long COVID Research Group; Formal analysis: E.B.; Investigation: D.P.L.R., D.P., E.I., E.M., G.A. and Long COVID Research Group; Methodology: D.P.L.R., R.N., A.M.Z., A.S. and F.M.; Resources: D.P., E.I., E.M., G.A. and Long COVID Research Group; Supervision: A.M.Z., A.S. and F.M.; Validation: F.M.; Visualization: A.M.Z., A.S. and F.M.; Writing—Original draft: D.P.L.R.; Writing—Review & editing: R.N. and F.M. All authors have read and agreed to the published version of the manuscript.

Funding: This research received no external funding.

Institutional Review Board Statement: The study was conducted in accordance with the Declaration of Helsinki, and approved by the Ethics Committee of Policlinico Umberto I (protocol code RIF.CE 0399/2021).

Informed Consent Statement: Informed consent was obtained from all subjects involved in the study.

Data Availability Statement: Data available on request due to restrictions. The data presented in this study are available on request from the corresponding author. The data are not publicly available due to privacy.

Acknowledgments: We thank all members of the Long COVID Research Group of the Department of Maternal Sciences, Sapienza University of Rome, Italy, for their contribution: Mattia Spatuzzo, Greta Di Mattia, Luigi Matera, Sara Ialongo, Fabrizio Virgili, Valentina Rizzo, Enea Bonci, Maria Giulia Conti, Laura Petrarca, Antonella Frassanito, Bianca Cinicola.

Conflicts of Interest: The authors declare no conflict of interest.

References

1. COVID-19 Disease in Children and Adolescents: Scientific Brief, 29 September 2021. Available online: https://www.who.int/publications/i/item/WHO-2019-nCoV-Sci_Brief-Children_and_adolescents-2021.1 (accessed on 29 September 2021).
2. La Regina, D.P.; Nenna, R. The use of pediatric flexible bronchoscopy in the COVID-19 pandemic era. *Pediatric Pulmonol.* **2021**, *56*, 1957–1966. [CrossRef] [PubMed]
3. Bi, Q.; Wu, Y. Epidemiology and transmission of COVID-19 in 391 cases and 1286 of their close contacts in Shenzhen, China: A retrospective cohort study. *Lancet Infect. Dis.* **2020**, *20*, 911–919. [CrossRef]
4. She, J.; Liu, L. COVID-19 epidemic: Disease characteristics in 747 children. *J. Med. Virol.* **2020**, *92*, 754. [CrossRef] [PubMed]
5. Nikolopoulou, G.B.; Maltezou, H.C. COVID-19 in Children: Where do we Stand? *Arch. Med. Res.* **2022**, *53*, 1. [CrossRef] [PubMed]
6. Götzinger, F.; Santiago-García, B. COVID-19 in children and adolescents in Europe: A multinational, multicentre cohort study. *Lancet Child Adolesc. Health* **2020**, *4*, 653. [CrossRef]
7. Lu, X.; Zhang, L.; Du, H. SARS-CoV-2 infection in children. *N. Engl. J. Med.* **2020**, *382*, 1663–1665. [CrossRef]
8. Chatziparasidis, G.; Kantar, A. COVID-19 in Children with Asthma. *Lung* **2021**, *199*, 7–12. [CrossRef]
9. Smargiassi, A.; Soldati, G. Lung ultrasonography for early management of patients with respiratory symptoms during COVID-19 pandemic. *J Ultrasound* **2020**, *23*, 449–456. [CrossRef]
10. Soldati, G.; Smargiassi, A. Proposal for International Standardization of the Use of Lung Ultrasound for Patients with COVID-19: A Simple, Quantitative, Reproducible Method. *J. Ultrasound Med.* **2020**, *39*, 1413–1419. [CrossRef]
11. Buonsenso, D.; Musolino, A.M. Lung ultrasound in infants with bronchiolitis. *BMC Pulm. Med.* **2019**, *19*, 159. [CrossRef]
12. Bloise, S.; La Regina, D. Lung ultrasound compared to chest X-ray for the diagnosis of CAP in children. *Pediatr. Int.* **2021**, *63*, 448–453. [CrossRef] [PubMed]
13. Iovine, E.; Nenna, R. Lung Ultrasound: Its Findings and New Applications in Neonatology and Pediatric Diseases. *Diagnostics* **2021**, *11*, 652. [CrossRef] [PubMed]
14. Soldati, G.; Demi, M. The role of ultrasound lung artifacts in the diagnosis of respiratory diseases. *Expert Rev. Respir. Med.* **2019**, *13*, 163–172. [CrossRef]
15. Soldati, G.; Demi, M. What Is COVID 19 Teaching Us about Pulmonary Ultrasound? *Diagnostics* **2022**, *12*, 838. [CrossRef]
16. Musolino, A.M.; Supino, M.C.; Roman Lung Ultrasound Study Team for Pediatric COVID-19 (ROMULUS COVID Team). Lung Ultrasound in Children with COVID-19: Preliminary Findings. *Ultrasound Med. Biol.* **2020**, *46*, 2094–2098. [CrossRef] [PubMed]
17. Caroselli, C.; Blaivas, M. Diagnostic Imaging in Newborns, Children and Adolescents Infected with Severe Acute Respiratory Syndrome Coronavirus 2 (SARS-CoV-2): Is There a Realistic Alternative to Lung High-Resolution Computed Tomography (HRCT) and Chest X-Rays? A Systematic Review of the Literature. *Ultrasound Med. Biol.* **2021**, *47*, 3034–3040. [PubMed]
18. Chung, M.; Bernheim, A. CT imaging features of 2019 novel coronavirus (2019 nCoV). *Radiology* **2020**, *4*, 200–230. [CrossRef]
19. Portale, G.; Ciolina, F. Lung Ultrasound in COVID-19: Clinical Correlates and Comparison with Chest Computed Tomography. *SN Compr. Clin. Med.* **2021**, *3*, 2075–2081. [CrossRef]
20. Zieleskiewicz, L.; Markarian, T. Comparative study of lung ultrasound and chest computed tomography scan in the assessment of severity of confirmed COVID-19 pneumonia. *Intensive Care Med.* **2020**, *46*, 1707–1713. [CrossRef]
21. Thallapureddy, K.; Thallapureddy, K. Long-Term Complications of COVID-19 Infection in Adolescents and Children. *Curr. Pediatr. Rep.* **2022**, *10*, 11–17. [CrossRef]
22. Molteni, E.; Sudre, C.H. Illness duration and symptom profile in symptomatic UK school-aged children tested for SARS-CoV-2. *Lancet Child Adolesc. Health* **2021**, *5*, 708–718. [CrossRef]
23. A Clinical Case Definition of Post COVID-19 Condition by a Delphi Consensus, 6 October 2021. Available online: https://www.who.int/publications/i/item/WHO-2019-nCoV-Post_COVID-19_condition-Clinical_case_definition-2021.1 (accessed on 6 October 2021).
24. Copetti, R.; Cattarossi, L. Lung ultrasound in respiratory distress syndrome: A useful tool for early diagnosis. *Neonatology* **2008**, *94*, 52–59. [CrossRef] [PubMed]
25. Volpicelli, G.; Lamorte, A. What's new in lung ultrasound during the COVID-19 pandemic. *Intensive Care Med.* **2020**, *46*, 1445–1448. [CrossRef] [PubMed]
26. Buonsenso, D.; Pata, D. COVID-19 outbreak: Less stethoscope, more ultrasound. *Lancet Respir. Med.* **2020**, *8*, e27. [CrossRef]
27. Denina, M.; Scolfaro, C. Lung Ultrasound in Children with COVID-19. *Pediatrics* **2020**, *146*, e20201157. [CrossRef]

28. Guitart, C.; Suárez, R. Lung ultrasound findings in pediatric patients with COVID-19. *Eur. J. Pediatr.* **2021**, *180*, 1117–1123. [CrossRef]
29. Sawamura, M.V.Y.; Verrastro, C.G.Y. Post-COVID-19 tomographic abnormalities. *Int. J. Tuberc. Lung Dis.* **2022**, *26*, 629–635. [CrossRef]
30. Salehi, S.; Abedi, A. Coronavirus Disease 2019 (COVID-19): A Systematic Review of Imaging Findings in 919 Patients. *Am. J. Roentgenol.* **2020**, *215*, 87–93. [CrossRef]
31. Palabiyik, F.; Kokurcan, S.O. Imaging of COVID-19 pneumonia in children. *Br. J. Radiol.* **2020**, *93*, 20200647. [CrossRef]
32. Zhang, Y.; Xie, R.M. Clinical and imaging features of pediatric COVID-19. *Ital. J. Pediatr.* **2020**, *46*, 153. [CrossRef]
33. Gurney, J.W.; Schroeder, B.A. Upper lobe lung disease: Physiologic correlates. Review. *Radiology* **1988**, *167*, 359–366. [CrossRef] [PubMed]
34. Yuyun, X.; Lexi, Y. Early Warning Information for Severe and Critical Patients With COVID-19 Based on Quantitative CT Analysis of Lung Segments. *Front. Public Health* **2021**, *9*, 596938. [CrossRef] [PubMed]
35. La Regina, D.P.; Bloise, S. Lung ultrasound in bronchiolitis. *Pediatr. Pulmonol.* **2021**, *56*, 234–239. [CrossRef] [PubMed]
36. Denina, M.; Pruccoli, G. Sequelae of COVID-19 in Hospitalized Children: A 4-Months Follow-Up. *Pediatr. Infect. Dis. J.* **2020**, *39*, e458–e459. [CrossRef] [PubMed]
37. Ng, B.H.; Nuratiqah, N.A. Lung computed tomography patterns of a cluster of asymptomatic young males with COVID-19 admitted to a teaching hospital in Kuala Lumpur. *Med. J. Malaysia* **2020**, *75*, 368–371.
38. Scully, E.P.; Haverfield, J. Considering how biological sex impacts immune responses and COVID-19 outcomes. *Nat. Rev. Immunol.* **2020**, *20*, 442–447. [CrossRef]
39. Lichtenstein, D.A.; Mezière, G.A. Relevance of lung ultrasound in the diagnosis of acute respiratory failure: The BLUE protocol. *Chest* **2008**, *134*, 117–125. [CrossRef]
40. Du, Y.; Lv, Y. Association of body mass index (BMI) with critical COVID-19 and in-hospital mortality: A dose-response meta-analysis. *Metabolism* **2021**, *117*, 154373. [CrossRef]
41. Haseli, S.; Khalili, N. Lobar Distribution of COVID-19 Pneumonia Based on Chest Computed Tomography Findings; A Retrospective Study. *Arch. Acad. Emerg. Med.* **2020**, *8*, e55.

diagnostics

MDPI

Review

Is Lung Ultrasound Helpful in COVID-19 Neonates?—A Systematic Review

Emil Robert Stoicescu [1,2], Ioana Mihaiela Ciuca [3,*], Roxana Iacob [1], Emil Radu Iacob [4], Monica Steluta Marc [5], Florica Birsasteanu [1], Diana Luminita Manolescu [1,6] and Daniela Iacob [2,7]

1 Department of Radiology and Medical Imaging, 'Victor Babes' University of Medicine and Pharmacy Timisoara, Eftimie Murgu Square No. 2, 300041 Timisoara, Romania; stoicescu.emil@umft.ro (E.R.S.); roxana.iacob@umft.ro (R.I.); fbirsasteanu@yahoo.com (F.B.); dmanolescu@umft.ro (D.L.M.)
2 Research Center for Pharmaco-Toxicological Evaluations, 'Victor Babes' University of Medicine and Pharmacy Timisoara, Eftimie Murgu Square No. 2, 300041 Timisoara, Romania; iacob.daniela@umft.ro
3 Pediatric Department, 'Victor Babes' University of Medicine and Pharmacy Timisoara, Eftimie Murgu Square No. 2, 300041 Timisoara, Romania
4 Department of Pediatric Surgery, 'Victor Babes' University of Medicine and Pharmacy, Eftimie Murgu Square 2, 300041 Timisoara, Romania; radueiacob@umft.ro
5 Pulmonology Department, 'Victor Babes' University of Medicine and Pharmacy, Eftimie Murgu Square 2, 300041 Timisoara, Romania; marc.monica@umft.ro
6 Center for Research and Innovation in Precision Medicine of Respiratory Diseases (CRIPMRD), 'Victor Babeș' University of Medicine and Pharmacy, 300041 Timișoara, Romania
7 Department of Neonatology, 'Victor Babes' University of Medicine and Pharmacy Timisoara, Eftimie Murgu Square No. 2, 300041 Timisoara, Romania
* Correspondence: ciuca.ioana@umft.ro

Citation: Stoicescu, E.R.; Ciuca, I.M.; Iacob, R.; Iacob, E.R.; Marc, M.S.; Birsasteanu, F.; Manolescu, D.L.; Iacob, D. Is Lung Ultrasound Helpful in COVID-19 Neonates?—A Systematic Review. *Diagnostics* **2021**, *11*, 2296. https://doi.org/10.3390/diagnostics11122296

Academic Editors: Marcello Demi and Gino Soldati

Received: 18 November 2021
Accepted: 3 December 2021
Published: 8 December 2021

Abstract: Background: The SARS-CoV-2 infection has occurred in neonates, but it is a fact that radiation exposure is not recommended given their age. The aim of this review is to assess the evidence on the utility of lung ultrasound (LUS) in neonates diagnosed with COVID-19. Methods: A systematic literature review was performed so as to find a number of published studies assessing the benefits of lung ultrasound for newborns diagnosed with COVID and, in the end, to make a comparison between LUS and the other two more conventional procedures of chest X-rays or CT exam. The key terms used in the search of several databases were: "lung ultrasound", "sonography", "newborn", "neonate", and "COVID-19′. Results: In total, 447 studies were eligible for this review, and after removing the duplicates, 123 studies referring to LU were further examined, but only 7 included cases of neonates. These studies were considered for the present research paper. Conclusions: As a non-invasive, easy-to-use, and reliable method for lung lesion detection in neonates with COVID-19, lung ultrasound can be used as a useful diagnosis tool for the evaluation of COVID-19-associated lung lesions. The benefits of this method in this pandemic period are likely to arouse interest in opening new research horizons, with immediate practical applicability.

Keywords: lung ultrasound; neonates; newborns; COVID-19; SARS-CoV-2

1. Introduction

From the beginning of the pandemic until now, over 250 million cases of SARS-CoV-2 infections have been reported, according to the Worldometer website [1]. Out of these, a limited number of approximately 15% of cases are infections among children, infants, and newborns, according to the latest data provided by the American Academy of Pediatrics and the Children's Hospital Association, in agreement with the data provided by the CDC. As their results indicate, approximately 7.8% of the newborns from tested COVID-positive mothers showed a positive PCR test at birth [2].

These small numbers of neonates with COVID-19 infection were confirmed by a study from Wuhan, China, where only three cases were reported out of a total of 33 pregnant

women, with an infection rate of 9.09% [3]. In most of the cases, the newborns developed an asymptomatic or mild form of infection [4].

It is a fact that lung ultrasonography (LUS) has the great advantage of being easy to use; it is safe and non-invasive for infants, and at the same time, it is a useful method in the management of pulmonary and cardiac diseases in neonates. Lung artifacts detected by ultrasonography vary slightly with age, so it may be suitable for neonatal respiratory pathology, especially in the SARS-CoV-2 infection [5–7].

A number of studies demonstrate the usefulness of LUS in the evaluation of COVID -19-associated lung lesions in children, indicating that LUS sensitivity was higher than in the case of CT and CXR. Even if CT images present the highest accuracy, CT should not always be recommended for all children with COVID due to its significant irradiation potential. Furthermore, recent studies demonstrated a strong correlation between LUS and CT scores, proving that an ultrasound score higher than 20 (using 12-area score) is associated with an increased risk of complications and death [8,9]. As COVID-19 has become a worldwide disease, in many hospitals, the availability of CT scans for many patients diagnosed with COVID-19 is not widespread. Chest X-rays are more readily available, but they lack the necessary specificity and sensitivity for detecting COVID-19 pneumonia so as to be considered a reliable substitute method for CT scans [10]. Recent studies show the usefulness of LUS in detecting COVID-19, especially for pneumonia detection [11,12].

The findings concerning lung ultrasound procedures in the diagnostic assessment of children with COVID pneumonia are similar to the ones described in the case of adults and children with other types of pneumonia [13,14].

Lung ultrasound showed its utility in many other neonatal respiratory diseases, such as respiratory distress syndrome, transient tachypnea of the newborn, pneumonia, meconium aspiration syndrome, pulmonary hemorrhage and atelectasis of the newborn, pneumothorax, and so on [15,16]. Therefore, the aim of this review is to evaluate the utility of LUS for newborns diagnosed with COVID-19.

2. Materials and Methods

For the current literature review, the PubMed and ScienceDirect databases were searched, with a focus on articles written in English between December 1st 2019 and November 4th 2021. The articles were selected by searching the PRISMA tool (preferred reporting items for systematic reviews and meta-analyses), and in accordance with this, a systematic literature review was conducted. A total of 81 articles published between December 1st 2019 and November 4th 2021, covering the COVID period, were found involving the MeSH Terms ((“Ultrasonography”[Mesh]) AND “Lung”[Mesh]) AND “Infant, Newborn”[Mesh]. After this process, only seven articles were included and discussed in this study, according to the below-mentioned criteria.

The articles under scrutiny were selected according to the following criteria:

- Pathology: COVID-19 pneumonia, SARS-CoV-2 infection;
- Intervention/tool: lung ultrasound;
- Age/population of interest: newborns, neonates, infants, <first 28 days of life.

Inclusion criteria:

1. Original articles, special articles, systematic reviews, case reports, and scientific letters were considered;
2. Studies involving a number of COVID-positive subjects were also included, as well as studies with only some of the participants being newborns;
3. Only studies involving the lung/chest/thoracic ultrasound method were included;
4. There were no exclusions regarding the language of the articles. One article written in Chinese with only the abstract in English was also included.

Only six published articles met the required criteria, and because it was found that the subject is scarcely addressed in the literature, it was necessary to perform two additional

advanced searches on PubMed and ScienceDirect. A total of 133 articles from the reviewed period were found on PubMed, while 233 publications were found on ScienceDirect by searching with the following keywords: "lung", "ultrasound", "sonography", "newborn", "neonate", and "COVID" (Figure 1—PRISMA flowchart). After this extended search, another study was found and was also included in the review. The flowchart below shows the steps that have been followed and the methodology used in deciding upon the eligible articles. From a total of 447 studies initially found, we removed duplicates, and we manually excluded articles with no ultrasound references. Ultimately, articles with no newborn mention were also excluded.

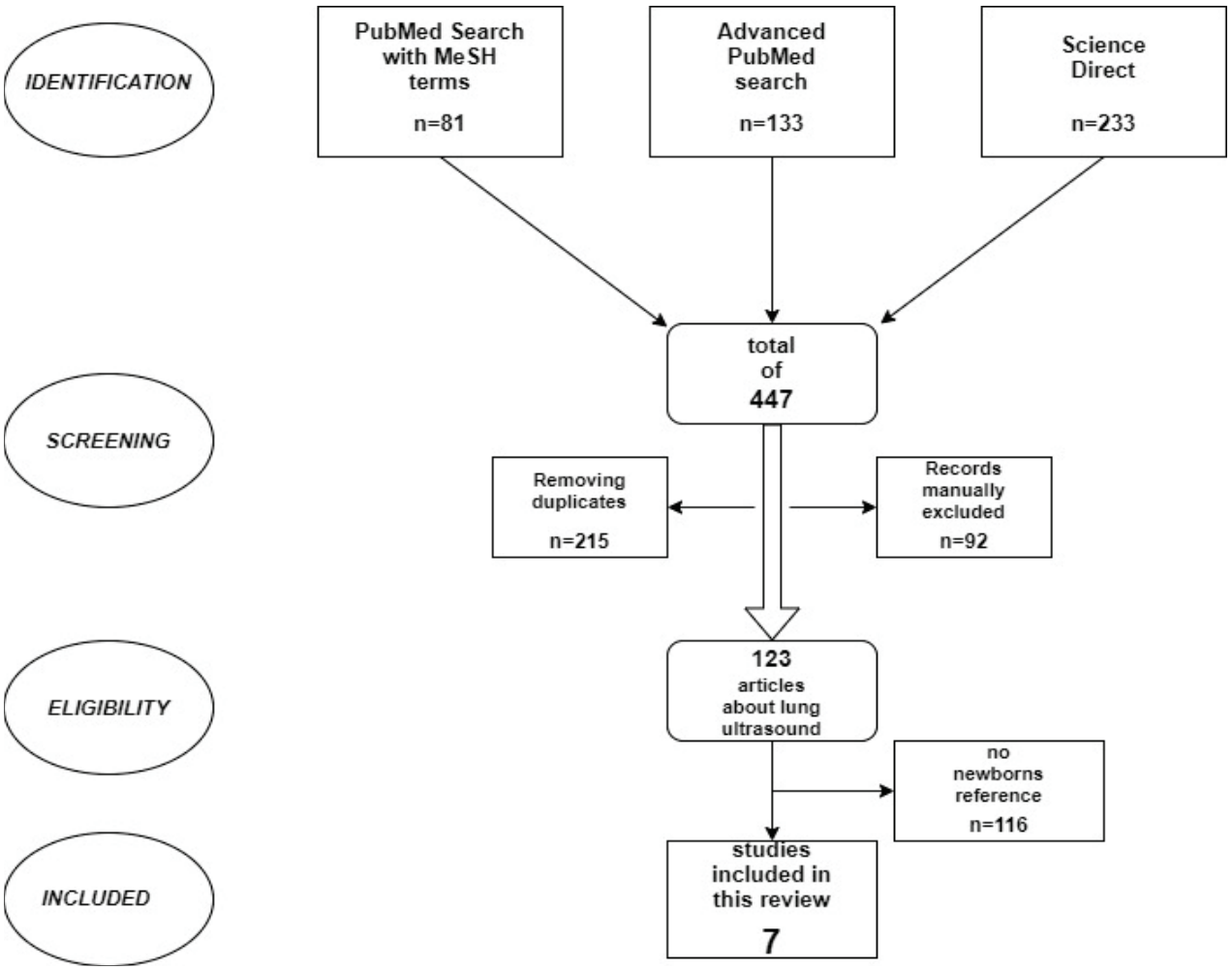

Figure 1. PRISMA flowchart. Literature review.

3. Results

After our search, we found and analyzed seven articles discussing the lung ultrasound method in newborns diagnosed with the SARS-CoV-2 infection, with a total of 58 subjects. The baseline characteristics of the patients were heterogenous; therefore, we underlined the most relevant ones, where data were available. The gender distribution was 41.93% males and 58.06% females, respectively. Regarding the gestational age, 15% of the neonates were preterm, while 85% were born on term. The infection was detected using the Reverse transcription polymerase chain reaction (RT-PCR) in 61.3% of the cases, while for the other subjects, the IgM tests were used. The age (days of life) of the patients when the COVID-19 infection was confirmed varied as follows: two studies with 3.8 ± 5.2 (mean $\pm$ standard deviation), another two studies with the median age of 8 days of life, and one study with the age between 1 and 18 days.

However, with the knowledge gained from the other articles based on this imagistic tool used in the evaluation of neonatal respiratory pathology, we can outline a number of further research directions (Table 1—characteristics of the articles included in the study).

Table 1. Characteristics of the articles included in the study.

No.	Title	Authors	City and Country	Year of Publication	Type	No. of Cases	Observations
1	Quantitative assessment of COVID-19 pneumonia in neonates using lung ultrasound score [17]	Wei Li et al.	Wuhan China	2021	original article	11	
2	Bedside lung ultrasound score (LUSS) on assessing pneumonia in COVID-19 neonates [18]	Wei Li et al.	Wuhan China	2020	original article	11	
3	Point-of-care lung ultrasound in three neonates with COVID-19 [19]	R. Gregorio-Hernández et al.	Toledo Spain	2020	original article	3	
4	Use of lung ultrasound in neonates during the COVID-19 pandemic [20]	Marcia Wang Matsuoka et al.	Sao Paulo Brazil	2020	special article/original article	27	positive and negative COVID neonates
5	Usefulness of chest ultrasound in a neonatal infection due to SARS-CoV-2 [21]	Pineda Caplliure A et al.	Valencia Spain	2021	scientific letter	1	
6	Application of pulmonary ultrasound in the diagnosis of COVID-19 pneumonia in neonates [22]	X Y Feng et al.	Wuhan China	2020	original article	5	abstract in English, article in Chinese
7	Diagnostic Imaging in Newborns, Children and Adolescents Infected with Severe Acute Respiratory Syndrome Coronavirus 2 (SARS-CoV-2): Is There a Realistic Alternative to Lung High-Resolution Computed Tomography (HRCT) and Chest X-Rays? A Systematic Review of the Literature [7]	Costantino Caroselli et al.		2021	review	44	newborns, children and adolescents

3.1. LUS Artifacts

The main changes described after performing ultrasound procedures in the lung fields of newborns were:

- Decrease in and disappearance of A-lines;
- Sparse B-lines;
- Confluent B-lines;
- Abnormal pleural lines;
- Subpleural consolidation (Table 2—lung ultrasound findings and prevalence of the main changes from included studies).

Table 2. Lung ultrasound findings and prevalence of the main changes from included studies.

No.	Title	No. of Cases	Decreasing/Disappearing A-Lines (Total)	Sparse B-Lines	Confluent B-Lines	Abnormal Pleural Lines	Subpleural Consolidation	Predominant Lesions	Myocardial Injury	Observation
1	Quantitative assessment of COVID-19 pneumonia in neonates using lung ultrasound score [17]	11	83/132 regions 62.8%	73/132 regions 55.3%	10/132 regions 7.6%	29/132 regions 21.9%	2/132 regions 1.5%	bilateral inferior and posterior	The majority of patients	12 regions for neonate's chest areas
2	Bedside lung ultrasound score (LUSS) on assessing pneumonia in COVID-19 neonates [18]	11	52 decreased 31 disappear 83/132 regions 62.8%	73/132 regions 55.3%	10/132 regions 7.6%	29/132 regions 21.9%	5/132 regions 3.8%	bilateral lower lobes and right middle lobe	-	12 regions for neonate's chest areas
3	Point-of-care lung ultrasound in three neonates with COVID-19 [19]	3	12/18 regions 66.6%	12/18 regions 66.6%	12/18 regions 66.6%	8/18 regions 44.4%	12/18 regions 66.6%	bilateral posterior areas	-	6 regions for neonate's chest areas
4	Use of lung ultrasound in neonates during the COVID-19 pandemic [20]	27	Present	Present	Present	Present	Present	posterior lung fields	-	positive and negative COVID newborns
5	Usefulness of chest ultrasound in a neonatal infection due to SARS-CoV-2 [21]	1	Present	Present	Present	Present	Present	bilateral posterior areas	-	-
6	Application of pulmonary ultrasound in the diagnosis of COVID-19 pneumonia in neonates [22]	5	5/5 100%	5/5 100%	5/5 100%	5/5 100%	1/5 20%	-	-	-
7	Diagnostic Imaging in Newborns, Children and Adolescents Infected with Severe Acute Respiratory Syndrome Coronavirus 2 (SARS-CoV-2): Is There a Realistic Alternative to Lung High-Resolution Computed Tomography (HRCT) and Chest X-Rays? A Systematic Review of the Literature [7]	44	Present	50%	25%	34.09%	43.18%	posterior lower lung fields	-	review with newborns, children and adolescents

3.1.1. A-Lines Disappearance

The most common ultrasonographic changes found in the analyzed studies were the variations of physiological A-lines from decrease to disappearance, varying between 62.8% and 100% [17,18,22]. A-lines are described as hyperechogenic, horizontal, and equidistant ones that are parallel to the pleura [6]. These are the reflections of the ultrasound waves as they occur as an echo between the pleura and the transducer, similar to a reverberation artifact [6]. These variations of A-lines with some sparse or confluent B-lines can be considered the first sign of an alveolar-interstitial pattern [5].

3.1.2. B-Lines

Sparse B-lines were the next most frequent modification with an occurrence rate between 55.3% and 100%, reported in four reviewed studies [17–19,22].

3.1.3. Abnormalities of Pleural Lines

Abnormal pleural lines, such as thickening, interrupted, or irregular pleural lines, were reported differently in the referenced studies, ranging between 21.9% and 100% [17–19,22].

3.1.4. Consolidations

Subpleural consolidation, recognized as a sign of viral pneumonia in association with variation of B-lines, were reported only in a few cases (between 1.5% and 66.6%) in the lung ultrasound exam in the target group [17–22]. No pleural effusion or pneumothorax was reported.

The predominant lesion distribution was bilateral in the inferior lobes and posterior segments, where the highest scores were recorded (right inferior posterior regions with a score 1.27 ± 0.47) [17].

Wei Li et al. found that most of the neonates included in their study had increased levels of creatine kinase myocardial band (CK-MB) but with no echocardiographic abnormalities [17].

3.2. LUS Scores in Neonates with COVID-19 Pneumonia

Only three articles used a score for the semi-quantitative analyses of the lung lesions. Two studies indicated a 12-area score, while the other one adopted a score with just six segments (anterior, lateral and posterior for each hemithorax) [17–19]. The 12-area score was determined by Mongodi et al., with six regions per hemithorax, the axillary lines as landmarks, placed in anterior and posterior positions, and using the nipple line as a demarcation mark between the upper and lower regions [23].

Two out of the three studies were located in Wuhan, the epicentre of the COVID-19 pneumonia. One compared 11 neonates with the SARS-CoV-2 infection (two preterm and nine babies at term, with asymptomatic or mild forms) with a healthy control group similar in characteristics (age, gender). Lung ultrasound score was higher in the infection group (8.4 ± 1.7 vs. 2.3 ± 1.4), and the most frequent lesions were erased A-lines and sparse/confluent B-lines. Additionally, it is important to note that abnormalities were identified by ultrasound in three of the infected newborns with previous normal radiographic exams. The authors concluded that all pulmonary injuries were bilateral with multiple areas affected, specifically located in the lower lobes and in the middle lobe [17,18].

The other study, which was conducted in Wuhan, China, examined a number of five cases presenting gastrointestinal and respiratory symptoms. In all these cases, the pulmonary ultrasonography showed pleural line abnormalities and pulmonary edema in different conditions, described as confluent B-lines with an interstitial pattern. Additionally, some small areas with pulmonary consolidation were visible. A very important fact to remember is that lung ultrasound has a higher sensitivity rate compared with chest X-ray and thoracic computer tomography in the diagnosis of pulmonary edema [22].

Another article presents the evolution of three neonates during their admission to a neonatology department in Toledo, Spain. They were examined every 48 h using the

ultrasound technique, and the cases were graded by severity following a three-area score for each hemithorax. The highest recorded score was 10/18 in a newborn with severe hypoxic-ischemic encephalopathy and meconium aspiration. These newborns presented a number of comorbidities, such as meconium aspiration pneumonia, bronchopulmonary dysplasia, and Hirschsprung's disease, shown as the limitations of the study. They compared the findings with a previous LU performed in a neonate with bronchopulmonary dysplasia, but with no following results. All neonates described in this report had a mild form of respiratory infection [19].

A significantly larger studied group included 27 neonates from Sao Paulo, Brazil. The study presents the imagistic aspects in patients who tested positive for SARS-CoV-2 or who were highly suspected to be infected. The subjects were divided into two groups, one with respiratory symptoms and the other with no pulmonary manifestations. In the COVID-19 group with respiratory symptoms were reported several coalescent B-lines, pleural irregularities, and some subpleural consolidation [20].

Pineda Caplliure et al. examined a case confirmed with COVID-19 pneumonia that presented a fluctuant evolution with a depreciation at 24 h after admission. The newborn was examined by echocardiography, chest X-ray, and lung ultrasound, which showed the specific subpleural and pleural changes with variation of B-lines [21].

Most of the newborns were asymptomatic or presented mild forms of infection, only 20% of the subjects presenting fever. Additionally, respiratory, gastrointestinal, and cardiac manifestations accompanied the symptomatic forms of the infection. The comorbidities were reported in one study with the above-mentioned examples (Hernández et al.) [19].

4. Discussion

Following the evaluation of the above-mentioned articles, it can be noted that a small number of studies discusses in depth the ultrasound method as a useful instrument of exploration in COVID-positive newborns, a fact that is also confirmed by Caroselli et al. in their review, which found only seven articles about lung ultrasound at newborns, infants, and children with SARS-CoV-2 infection [7].

There is a growing trend in the use of pulmonary ultrasonography, especially in newborns, as evidenced by the numerous recent articles using this imagistic technique, if we compare with the results obtained by conventional radiography or the CT exam [7,24].

Jones et al. note a significant decrease of about 38.8% in the use of chest X-ray procedure, but with very good results in detecting pneumonia with the aid of lung ultrasound. This indicates that ultrasonography is a suitable diagnosis tool that can replace the other more conventional methods that are likely to be more harmful and potentially more invasive [7,25]. Additionally, Feng et al. prove that chest ultrasound has a higher sensitivity and accuracy rate compared to X-ray and CT procedures in the diagnosis of pulmonary edema, suggesting that ultrasonography could be used in the monitoring and evaluation of the lung injuries caused by SARS-CoV-2 infection [22]. LUS findings are directly correlated with CT score at intensive care unit admission and inversely correlated with blood test results (PaO_2, C-reactive protein) [9,26]. Other studies following a similar research line demonstrate that LUS has a higher specificity and sensitivity rate in detecting consolidations, interstitial and alveolar syndromes, and pleural effusion, specific for a pediatric pneumonia, compared to conventional chest radiography [27–29].

Berce et al. underline the importance of LUS as a useful method in a bacterial or viral outbreak or in epidemic times [30]. Lately, several studies have shown a significant role of LUS in the evaluation of COVID-19 pneumonia, not only regarding its accuracy in the detection of lesions, but also in evaluating the risk of death and complications development [8,31].

The majority of patients examined in the referenced studies were asymptomatic or had a mild form of infection, causing pulmonary and gastrointestinal symptoms, but also an unusual symptomatology was described, such as erythema [32]. According to Lingkong Zeng et al., the most frequent manifestation was dyspnea, present in a number of four

neonates, out of a total of 33 cases [3]. The pulmonary symptoms were mentioned by Li et al. in their 11-cohort group, accompanied by digestive complaints [17]. Additionally, Feng et al. report the same manifestations [22]. Both the respiratory and digestive manifestations can be determined by ultrasonography [6,33,34].

Another system with modified parameters was the cardiac one, with reported elevated CK-MB levels and the suspicion of myocardial injury or dysfunction [3,18,35]. The cardiac function was examined using echocardiography, which showed normal parameters in all cases [21,35]. Taking into consideration that all patients are clinically vulnerable and the long-term effects of the SARS-CoV-2 infection are yet to be discover, it would be necessary to have an additional investigating tool, such as the genetic expression of miRNAs, with a higher selectivity and specificity rate than the usual biomarkers [36]. For a better analysis of myocardial dysfunctions, echocardiogram and echocardiography have proven effective, as they are used in the 'SAFE protocol' for critically ill neonates [5,37,38].

According to Volpicelli and Francisco, an interstitial pattern with variation of B-lines with occasional spared areas are indicative of a viral pneumonia. The studies included in this article describe similar changes in lung parenchyma with sparse B-lines as a typically detectable lesion [39]. These changes emerging from viral infections are identified in the findings following CT examinations of the above-mentioned virus infection [7,40,41]. One study concluded that LUS detected all the COVID-19 pneumonia cases compared to the CT exam, with a sensitivity and specificity of 100% and 78.6%, respectively [42].

The peripheral, subpleural area was the front-runner for the ultrasound changes visualized during the SARS-CoV-2 infection due to the small size of the viral particles that easily reach the distal bronchioles and alveoli [17]. The pathological modifications were seen as consolidation spread around the pleura due to the impacting of the alveoli with mucoid material, especially in an immature lung [43,44]. The results of the studies analyzed describe the same topography with a predominance of the lesion in the lower lobes and in the posterior segments [45]. Likewise, Mento et al. conclude that the posterior zones must be explored in all patients with COVID-19 pneumonia, being the most affected area, and they also recommend a 12-area ultrasound examination [46]. In addition, Smargiassi et al. propose a multiple area approach for the lung ultrasound exam [47].

Decrease or disappearance of A-lines is the most common pattern detected by lung ultrasonography, according to the above-mentioned studies, and it is also the first pulmonary change that appears in alveolar–interstitial pathologies [5,48]. For example, Li et al. found variation in A-lines that were even disappearing in the 83 analyzed regions out of a total of 132 regions, based on their 12-area score. It is Feng et al. who discovered these variations in all neonates, but without previously dividing the lung in multiple zones [17,18,22].

On the other hand, 'here to there' B-lines, described as sparse B-lines, were present in varying degrees in all patients examined by lung ultrasonography, ranging between 55.3% and 66.6% [17–19]. These facts are significantly consistent with the results presented by Caroselli et al. in their review of the neonates, children, and adolescents enrolled in their study, indicating the presence of B-lines in a proportion of 50% [7]. These changes result from a fluid collection that expands the interlobular septs and is usually found in pulmonary edema and pneumonia [6,49,50]. Coalescent or confluent B-lines and 'white lung' symptoms were identified in a quarter of the patients [7], but in the studies included in our review, the figures differ from study to study (7.6%, 66%, and 100%, respectively). The higher values were presented by the studies with smaller batches of patients (three and five newborns). For this reason, these results cannot be reproduced and integrated with other pediatric and literature data available [10,51–54].

Another controversial subject concerns the differences between subpleural consolidations and their occurrence rate. Hernandez et al. had the highest percentage of this type of lesions (12/18 affected regions—66.6%), because they examined only three patients in evolution, unlike the other authors that included more subjects in their studies. Therefore, the probability of finding subpleural consolidation is quite low [19]. Thus, the follow-up of the infected neonates can reveal advanced modifications, such as lung consolidations [19].

At the beginning of the COVID-19 pandemic, irregularities and thickenings of the pleura were among the first signs described by lung ultrasonography, accompanied by subpleural consolidations [12]. Abnormalities of the pleura are the hallmarks described by all the reviewed authors discussing pulmonary ultrasound, with a range between 21.9% and 44.4%. The values generated by Caroselli et al. are in the middle of those reported (34.09%) [7,17–19]. This alteration of the pleura is also seen in community-acquired pneumonia [55,56].

Pleural effusions have not been found in SARS-CoV-2 infections, but only in exceptional cases. No pleural effusions were identified in any of the original articles included in this review, while Caroselli et al. report a rate of 6.82% showing the use of LUS. This can be due to the fact that ultrasound is able to detect a small effusion [6,57]. Additionally, the pleural effusion in COVID-19 pneumonia is a rare finding [58].

Given the fact that CT and chest X-ray exams produce irradiation and are harmful, with long-term side effects, especially for newborns, a radiation-free, non-ionizing, real-time, user -riendly, and repeatable tool is necessary [59–61]. Moreover, during this pandemic, hospital circuits have been completely changed, making it more difficult for patients to be transported to radiology departments to be examined by conventional radiography or CT [51]. Furthermore, according to the statistics presented by the World Human Organization, around two-thirds of the world population does not have easy access to a basic radiology or imagistic department [7]. Additionally, ultrasound equipment is readily available in many hospital departments, wards, and small clinics [62]. Unfortunately, this is not the case with radiographs or CTs.

Recently, LUS has proved its efficiency in the dynamic monitoring of COVID-19 pneumonia, as well as in the follow-up of patients recovered from this infection [63,64]. Moreover, a recent review proves the usefulness of hand-held ultrasound equipment, which has the advantage of lower acquisition costs and that is easy to decontaminate, which is a necessary activity nowadays [65]. Lung ultrasonography is the answer to all the demands that have been formulated in the course of this article. Once the lung ultrasound is performed, the procedure could be also used for examining other systems affected by COVID-19, such as the cardiac and gastrointestinal ones.

We must acknowledge the limitation of this review, as only seven studies were reported in our area of interest, with only a small sample size of patients and a lack of data homogeneity. Further multicentric studies are likely to enhance the accuracy of the research results and other important LUS application, as several studies have already showed significant progress in adults and children with COVID-19 pneumonia.

5. Conclusions

LUS proves to be useful in the detection of lung injury in the studies that were reviewed, even if only a small number of publications related to pulmonary ultrasonography in neonates with COVID pneumonia were found. Considering the advantages of lung ultrasound, as well as its utility in this ongoing pandemic period, this method is likely to stir interest in opening new research horizons with increased practical applicability.

Author Contributions: Conceptualization, I.M.C., D.L.M. and F.B.; methodology, E.R.I.; validation, D.L.M., M.S.M. and E.R.I.; formal analysis, M.S.M.; investigation, E.R.S. and R.I.; resources, E.R.S. and R.I.; data curation, E.R.S. and M.S.M.; writing—original draft preparation, E.R.S. and R.I.; writing—review and editing, I.M.C., D.L.M. and D.I.; visualization, F.B. and E.R.I.; supervision, I.M.C., D.L.M., F.B. and D.I.; project administration, D.I. All authors have read and agreed to the published version of the manuscript.

Funding: This research received no external funding.

Institutional Review Board Statement: Not applicable.

Informed Consent Statement: Not applicable.

Acknowledgments: We would like to thank C.A. Dehelean and her Research Center for Pharmaco-Toxicological Evaluations, "Victor Babes" University of Medicine and Pharmacy Timisoara, for support, encouragement and critical review.

Conflicts of Interest: The authors declare no conflict of interest.

References

1. COVID Live Update: 255,225,785 Cases and 5,132,676 Deaths from the Coronavirus—Worldometer. Available online: https://www.worldometers.info/coronavirus/ (accessed on 17 November 2021).
2. CDC COVID Data Tracker. Available online: https://covid.cdc.gov/covid-data-tracker (accessed on 3 November 2021).
3. Zeng, L.; Xia, S.; Yuan, W.; Yan, K.; Xiao, F.; Shao, J.; Zhou, W. Neonatal Early-Onset Infection With SARS-CoV-2 in 33 Neonates Born to Mothers With COVID-19 in Wuhan, China. *JAMA Pediatr.* **2020**, *174*, 722. [CrossRef]
4. Trevisanuto, D.; Cavallin, F.; Cavicchiolo, M.E.; Borellini, M.; Calgaro, S.; Baraldi, E. Coronavirus Infection in Neonates: A Systematic Review. *Arch. Dis. Child.—Fetal Neonatal Ed.* **2021**, *106*, 330–335. [CrossRef]
5. Raimondi, F.; Yousef, N.; Migliaro, F.; Capasso, L.; De Luca, D. Point-of-Care Lung Ultrasound in Neonatology: Classification into Descriptive and Functional Applications. *Pediatr. Res.* **2018**, *90*, 524–531. [CrossRef]
6. Kurepa, D.; Zaghloul, N.; Watkins, L.; Liu, J. Neonatal Lung Ultrasound Exam Guidelines. *J. Perinatol.* **2018**, *38*, 11–22. [CrossRef]
7. Caroselli, C.; Blaivas, M.; Falzetti, S. Diagnostic Imaging in Newborns, Children and Adolescents Infected with Severe Acute Respiratory Syndrome Coronavirus 2 (SARS-CoV-2): Is There a Realistic Alternative to Lung High-Resolution Computed Tomography (HRCT) and Chest X-Rays? A Systematic Review of the Literature. *Ultrasound Med. Biol.* **2021**, *47*, 3034–3040. [CrossRef]
8. Tana, C.; Ricci, F.; Coppola, M.G.; Mantini, C.; Lauretani, F.; Campanozzi, D.; Renda, G.; Gallina, S.; Lugará, M.; Cipollone, F.; et al. Prognostic Significance of Chest Imaging by LUS and CT in COVID-19 Inpatients: The ECOVID Multicenter Study. *Respiration* **2021**, 1–10, in press. [CrossRef]
9. Orlandi, D.; Battaglini, D.; Robba, C.; Viganò, M.; Bergamaschi, G.; Mignatti, T.; Radice, M.L.; Lapolla, A.; Turtulici, G.; Pelosi, P. Coronavirus Disease 2019 Phenotypes, Lung Ultrasound, Chest Computed Tomography and Clinical Features in Critically Ill Mechanically Ventilated Patients. *Ultrasound Med. Biol.* **2021**, *47*, 3323–3332. [CrossRef]
10. Musolino, A.M.; Supino, M.C.; Buonsenso, D.; Ferro, V.; Valentini, P.; Magistrelli, A.; Lombardi, M.H.; Romani, L.; D'Argenio, P.; Campana, A.; et al. Lung Ultrasound in Children with COVID-19: Preliminary Findings. *Ultrasound Med. Biol.* **2020**, *46*, 2094–2098. [CrossRef]
11. Soldati, G.; Smargiassi, A.; Inchingolo, R.; Buonsenso, D.; Perrone, T.; Briganti, D.F.; Perlini, S.; Torri, E.; Mariani, A.; Mossolani, E.E.; et al. Is There a Role for Lung Ultrasound During the COVID-19 Pandemic? *J. Ultrasound Med. Off. J. Am. Inst. Ultrasound Med.* **2020**, *39*, 1459–1462. [CrossRef]
12. Peng, Q.-Y.; Wang, X.-T.; Zhang, L.-N.; Chinese Critical Care Ultrasound Study Group (CCUSG). Findings of Lung Ultrasonography of Novel Corona Virus Pneumonia during the 2019-2020 Epidemic. *Intensive Care Med.* **2020**, *46*, 849–850. [CrossRef]
13. Volpicelli, G.; Lamorte, A.; Villén, T. What's New in Lung Ultrasound during the COVID-19 Pandemic. *Intensive Care Med.* **2020**, *46*, 1445–1448. [CrossRef]
14. Guitart, C.; Suárez, R.; Girona, M.; Bobillo-Perez, S.; Hernández, L.; Balaguer, M.; Cambra, F.J.; Jordan, I.; On behalf of the KIDS-Corona Study Group, Kids Corona Platform. Lung Ultrasound Findings in Pediatric Patients with COVID-19. *Eur. J. Pediatr.* **2021**, *180*, 1117–1123. [CrossRef]
15. Liu, J.; Copetti, R.; Sorantin, E.; Lovrenski, J.; Rodriguez-Fanjul, J.; Kurepa, D.; Feng, X.; Cattaross, L.; Zhang, H.; Hwang, M.; et al. Protocol and Guidelines for Point-of-Care Lung Ultrasound in Diagnosing Neonatal Pulmonary Diseases Based on International Expert Consensus. *J. Vis. Exp.* **2019**, *145*, e58990. [CrossRef]
16. Wu, J.; Wang, Y.; Zhao, A.; Wang, Z. Lung Ultrasound for the Diagnosis of Neonatal Respiratory Distress Syndrome: A Meta-Analysis. *Ultrasound Q.* **2020**, *36*, 102–110. [CrossRef]
17. Li, W.; Fu, M.; Qian, C.; Liu, X.; Zeng, L.; Peng, X.; Hong, Y.; Zhou, H.; Yuan, L. Quantitative Assessment of COVID-19 Pneumonia in Neonates Using Lung Ultrasound Score. *Pediatric Pulmonol.* **2021**, *56*, 1419–1426. [CrossRef]
18. Li, W.; Fu, M.; Qian, C.; Liu, X.; Zeng, L.; Zhou, H.; Yuan, L. Bedside Lung Ultrasound Score (LUSS) on Assessing Pneumonia in COVID-19 Neonates. *Preprints* **2020**. [CrossRef]
19. Gregorio-Hernández, R.; Escobar-Izquierdo, A.B.; Cobas-Pazos, J.; Martínez-Gimeno, A. Point-of-Care Lung Ultrasound in Three Neonates with COVID-19. *Eur. J. Pediatr.* **2020**, *179*, 1279–1285. [CrossRef]
20. Matsuoka, M.W.; da Rocha, S.M.S.; Gibelli, M.A.B.C.; Nicolau, C.M.; de Carvalho, W.B.; Suzuki, L. Use of Lung Ultrasound in Neonates during the COVID-19 Pandemic. *Radiol. Bras.* **2020**, *53*, 401–404. [CrossRef]
21. Pineda Caplliure, A.; Porcar Almela, M.; Navarro Albert, A.; Muñoz Vicente, E.; Mansilla Roig, B. Usefulness of Chest Ultrasound in a Neonatal Infection Due to SARS-CoV-2. *An. Pediatr. Engl. Ed.* **2021**, *94*, 412–413. [CrossRef]
22. Feng, X.Y.; Tao, X.W.; Zeng, L.K.; Wang, W.Q.; Li, G. [Application of pulmonary ultrasound in the diagnosis of COVID-19 pneumonia in neonates]. *Zhonghua Er Ke Za Zhi Chin. J. Pediatr.* **2020**, *58*, 347–350. [CrossRef]
23. Mongodi, S.; Bouhemad, B.; Orlando, A.; Stella, A.; Tavazzi, G.; Via, G.; Iotti, G.A.; Braschi, A.; Mojoli, F. Modified Lung Ultrasound Score for Assessing and Monitoring Pulmonary Aeration. *Ultraschall Med. Stuttg. Ger. 1980* **2017**, *38*, 530–537. [CrossRef]

24. Pare, J.; Camelo, I.; Mayo, K.; Leo, M.; Dugas, J.; Nelson, K.; Baker, W.; Shareef, F.; Mitchell, P.; Schechter-Perkins, E. Point-of-Care Lung Ultrasound Is More Sensitive than Chest Radiograph for Evaluation of COVID-19. *West. J. Emerg. Med.* **2020**, *21*, 771. [CrossRef]
25. Jones, B.P.; Tay, E.T.; Elikashvili, I.; Sanders, J.E.; Paul, A.Z.; Nelson, B.P.; Spina, L.A.; Tsung, J.W. Feasibility and Safety of Substituting Lung Ultrasonography for Chest Radiography When Diagnosing Pneumonia in Children. *Chest* **2016**, *150*, 131–138. [CrossRef]
26. Volpicelli, G.; Gargani, L. Sonographic Signs and Patterns of COVID-19 Pneumonia. *Ultrasound J.* **2020**, *12*, 22. [CrossRef] [PubMed]
27. Wang, J.; Loh, S.W.; Lee, J.H. Paediatric Acute Respiratory Distress Syndrome: Progress over the Past Decade. *J. Emerg. Crit. Care Med.* **2018**, *2*, 24. [CrossRef]
28. Ord, H.L.; Griksaitis, M.J. Fifteen-Minute Consultation: Using Point of Care Ultrasound to Assess Children with Respiratory Failure. *Arch. Dis. Child. Educ. Pract. Ed.* **2019**, *104*, 2–10. [CrossRef] [PubMed]
29. Mateos González, M.; García de Casasola Sánchez, G.; Muñoz, F.J.T.; Proud, K.; Lourdo, D.; Sander, J.-V.; Jaimes, G.E.O.; Mader, M.; Canora Lebrato, J.; Restrepo, M.I.; et al. Comparison of Lung Ultrasound versus Chest X-Ray for Detection of Pulmonary Infiltrates in COVID-19. *Diagnostics* **2021**, *11*, 373. [CrossRef] [PubMed]
30. Berce, V.; Tomazin, M.; Gorenjak, M.; Berce, T.; Lovrenčič, B. The Usefulness of Lung Ultrasound for the Aetiological Diagnosis of Community-Acquired Pneumonia in Children. *Sci. Rep.* **2019**, *9*, 17957. [CrossRef]
31. Hernández-Píriz, A.; Tung-Chen, Y.; Jiménez-Virumbrales, D.; Ayala-Larrañaga, I.; Barba-Martín, R.; Canora-Lebrato, J.; Zapatero-Gaviria, A.; García De Casasola-Sánchez, G. Usefulness of Lung Ultrasound in the Early Identification of Severe COVID-19: Results from a Prospective Study. *Med. Ultrason.* **2021**, in press. [CrossRef]
32. Dima, M.; Enatescu, I.; Craina, M.; Petre, I.; Iacob, E.R.; Iacob, D. First Neonates with Severe Acute Respiratory Syndrome Coronavirus 2 Infection in Romania: Three Case Reports. *Medicine* **2020**, *99*, e21284. [CrossRef]
33. Athamnah, M.N.; Masade, S.; Hamdallah, H.; Banikhaled, N.; Shatnawi, W.; Elmughrabi, M.; Al Azzam, H.S.O. COVID-19 Presenting as Intussusception in Infants: A Case Report with Literature Review. *J. Pediatr. Surg. Case Rep.* **2021**, *66*, 101779. [CrossRef]
34. Sharma, D.; Farahbakhsh, N. Role of Chest Ultrasound in Neonatal Lung Disease: A Review of Current Evidences. *J. Matern.-Fetal Neonatal Med.* **2019**, *32*, 310–316. [CrossRef]
35. Sharma, M.; Gorstein, S.; Aldrich, M.L.; Hsu, D.T.; Choueiter, N.F. Reversible Myocardial Injury Associated With SARS-CoV-2 in an Infant. *JACC Case Rep.* **2020**, *2*, 2348–2352. [CrossRef]
36. Rogobete, A.F.; Bedreag, O.H.; Popovici, S.E.; Sas, A.M.; Stan, A.T.; Stoicescu, E.R.; Sandesc, D. Detection of Myocardial Injury Using MiRNAs Expression as Genetic Biomarkers in Acute Cardiac Care. *J. Cardiovasc. Emergencies* **2016**, *2*, 169–172. [CrossRef]
37. Mertens, L.; Seri, I.; Marek, J.; Arlettaz, R.; Barker, P.; McNamara, P.; Moon-Grady, A.J.; Coon, P.D.; Noori, S.; Simpson, J.; et al. Targeted Neonatal Echocardiography in the Neonatal Intensive Care Unit: Practice Guidelines and Recommendations for Training. Writing Group of the American Society of Echocardiography (ASE) in Collaboration with the European Association of Echocardiography (EAE) and the Association for European Pediatric Cardiologists (AEPC). *J. Am. Soc. Echocardiogr. Off. Publ. Am. Soc. Echocardiogr.* **2011**, *24*, 1057–1078. [CrossRef]
38. De Boode, W.P.; Singh, Y.; Gupta, S.; Austin, T.; Bohlin, K.; Dempsey, E.; Groves, A.; Eriksen, B.H.; van Laere, D.; Molnar, Z.; et al. Recommendations for Neonatologist Performed Echocardiography in Europe: Consensus Statement Endorsed by European Society for Paediatric Research (ESPR) and European Society for Neonatology (ESN). *Pediatr. Res.* **2016**, *80*, 465–471. [CrossRef]
39. Volpicelli, G.; Frascisco, M.F. Sonographic Detection of Radio-Occult Interstitial Lung Involvement in Measles Pneumonitis. *Am. J. Emerg. Med.* **2009**, *27*, 128.e1–128.e3. [CrossRef]
40. Iovine, E.; Nenna, R.; Bloise, S.; La Regina, D.P.; Pepino, D.; Petrarca, L.; Frassanito, A.; Lubrano, R.; Midulla, F. Lung Ultrasound: Its Findings and New Applications in Neonatology and Pediatric Diseases. *Diagnostics* **2021**, *11*, 652. [CrossRef]
41. Xia, W.; Shao, J.; Guo, Y.; Peng, X.; Li, Z.; Hu, D. Clinical and CT Features in Pediatric Patients with COVID-19 Infection: Different Points from Adults. *Pediatr. Pulmonol.* **2020**, *55*, 1169–1174. [CrossRef] [PubMed]
42. Tung-Chen, Y.; Martí de Gracia, M.; Díez-Tascón, A.; Alonso-González, R.; Agudo-Fernández, S.; Parra-Gordo, M.L.; Ossaba-Vélez, S.; Rodríguez-Fuertes, P.; Llamas-Fuentes, R. Correlation between Chest Computed Tomography and Lung Ultrasonography in Patients with Coronavirus Disease 2019 (COVID-19). *Ultrasound Med. Biol.* **2020**, *46*, 2918–2926. [CrossRef]
43. Jiehao, C.; Jin, X.; Daojiong, L.; Zhi, Y.; Lei, X.; Zhenghai, Q.; Yuehua, Z.; Hua, Z.; Ran, J.; Pengcheng, L.; et al. A Case Series of Children with 2019 Novel Coronavirus Infection: Clinical and Epidemiological Features. *Clin. Infect. Dis. Off. Publ. Infect. Dis. Soc. Am.* **2020**, *71*, 1547–1551. [CrossRef]
44. Lu, X.; Zhang, L.; Du, H.; Zhang, J.; Li, Y.Y.; Qu, J.; Zhang, W.; Wang, Y.; Bao, S.; Li, Y.; et al. SARS-CoV-2 Infection in Children. *N. Engl. J. Med.* **2020**, *382*, 1663–1665. [CrossRef]
45. Xiang, C.; Lu, J.; Zhou, J.; Guan, L.; Yang, C.; Chai, C. CT Findings in a Novel Coronavirus Disease (COVID-19) Pneumonia at Initial Presentation. *BioMed Res. Int.* **2020**, *2020*, 5436025. [CrossRef]
46. Mento, F.; Perrone, T.; Macioce, V.N.; Tursi, F.; Buonsenso, D.; Torri, E.; Smargiassi, A.; Inchingolo, R.; Soldati, G.; Demi, L. On the Impact of Different Lung Ultrasound Imaging Protocols in the Evaluation of Patients Affected by Coronavirus Disease 2019: How Many Acquisitions Are Needed? *J. Ultrasound Med. Off. J. Am. Inst. Ultrasound Med.* **2021**, *40*, 2235–2238. [CrossRef] [PubMed]

47. Smargiassi, A.; Soldati, G.; Torri, E.; Mento, F.; Milardi, D.; Del Giacomo, P.; De Matteis, G.; Burzo, M.L.; Larici, A.R.; Pompili, M.; et al. Lung Ultrasound for COVID-19 Patchy Pneumonia: Extended or Limited Evaluations? *J. Ultrasound Med. Off. J. Am. Inst. Ultrasound Med.* **2021**, *40*, 521–528. [CrossRef] [PubMed]
48. Liang, H.-Y.; Liang, X.-W.; Chen, Z.-Y.; Tan, X.-H.; Yang, H.-H.; Liao, J.-Y.; Cai, K.; Yu, J.-S. Ultrasound in Neonatal Lung Disease. *Quant. Imaging Med. Surg.* **2018**, *8*, 535–546. [CrossRef]
49. Volpicelli, G.; Caramello, V.; Cardinale, L.; Mussa, A.; Bar, F.; Frascisco, M.F. Detection of Sonographic B-Lines in Patients with Normal Lung or Radiographic Alveolar Consolidation. *Med. Sci. Monit. Int. Med. J. Exp. Clin. Res.* **2008**, *14*, CR122–CR128.
50. Xing, C.; Li, Q.; Du, H.; Kang, W.; Lian, J.; Yuan, L. Lung Ultrasound Findings in Patients with COVID-19 Pneumonia. *Crit. Care* **2020**, *24*, 174. [CrossRef]
51. Denina, M.; Scolfaro, C.; Silvestro, E.; Pruccoli, G.; Mignone, F.; Zoppo, M.; Ramenghi, U.; Garazzino, S. Lung Ultrasound in Children With COVID-19. *Pediatrics* **2020**, *146*, e20201157. [CrossRef]
52. Parri, N.; Lenge, M.; Buonsenso, D. Children with COVID-19 in Pediatric Emergency Departments in Italy. *N. Engl. J. Med.* **2020**, *383*, 187–190. [CrossRef]
53. Scheier, E.; Levick, N.; Peled, J.; Balla, U. Could It Be Pneumonia? Lung Ultrasound in Children with Low Clinical Suspicion for Pneumonia. *Pediatr. Qual. Saf.* **2020**, *5*, e326. [CrossRef]
54. Vazquez Martínez, J.L.; Pérez-Caballero Macarrón, C.; Coca Pérez, A.; Tapia Moreno, R.; Otheo de Tejada, E. Short Report—Usefulness of Point-of-Care Ultrasound in Pediatric SARS-CoV-2 Infection. *Eur. Rev. Med. Pharmacol. Sci.* **2020**, *24*, 7801–7803. [CrossRef] [PubMed]
55. Caiulo, V.A.; Gargani, L.; Caiulo, S.; Fisicaro, A.; Moramarco, F.; Latini, G.; Picano, E.; Mele, G. Lung Ultrasound Characteristics of Community-Acquired Pneumonia in Hospitalized Children. *Pediatr. Pulmonol.* **2013**, *48*, 280–287. [CrossRef]
56. Liu, J.; Liu, F.; Liu, Y.; Wang, H.-W.; Feng, Z.-C. Lung Ultrasonography for the Diagnosis of Severe Neonatal Pneumonia. *Chest* **2014**, *146*, 383–388. [CrossRef]
57. Lichtenstein, D.A.; Mauriat, P. Lung Ultrasound in the Critically Ill Neonate. *Curr. Pediatr. Rev.* **2012**, *8*, 217–223. [CrossRef] [PubMed]
58. Chong, W.H.; Saha, B.K.; Conuel, E.; Chopra, A. The Incidence of Pleural Effusion in COVID-19 Pneumonia: State-of-the-Art Review. *Heart Lung* **2021**, *50*, 481–490. [CrossRef]
59. Hall, E.J. Lessons We Have Learned from Our Children: Cancer Risks from Diagnostic Radiology. *Pediatr. Radiol.* **2002**, *32*, 700–706. [CrossRef] [PubMed]
60. Liu, J.; Cao, H.-Y.; Wang, X.-L.; Xiao, L.-J. The Significance and the Necessity of Routinely Performing Lung Ultrasound in the Neonatal Intensive Care Units. *J. Matern.-Fetal Neonatal Med.* **2016**, *29*, 4025–4030. [CrossRef]
61. Chen, S.-W.; Fu, W.; Liu, J.; Wang, Y. Routine Application of Lung Ultrasonography in the Neonatal Intensive Care Unit. *Medicine* **2017**, *96*, e5826. [CrossRef]
62. Cogliati, C.; Bosch, F.; Tung-Chen, Y.; Smallwood, N.; Torres-Macho, J. Lung Ultrasound in COVID-19: Insights from the Frontline and Research Experiences. *Eur. J. Intern. Med.* **2021**, *90*, 19–24. [CrossRef]
63. Torres-Macho, J.; Sánchez-Fernández, M.; Arnanz-González, I.; Tung-Chen, Y.; Franco-Moreno, A.I.; Duffort-Falcó, M.; Beltrán-Romero, L.; Rodríguez-Suaréz, S.; Bernabeu-Wittel, M.; Urbano, E.; et al. Prediction Accuracy of Serial Lung Ultrasound in COVID-19 Hospitalized Patients (Pred-Echovid Study). *J. Clin. Med.* **2021**, *10*, 4818. [CrossRef]
64. Hernández-Píriz, A.; Tung-Chen, Y.; Jiménez-Virumbrales, D.; Ayala-Larrañaga, I.; Barba-Martín, R.; Canora-Lebrato, J.; Zapatero-Gaviria, A.; Casasola-Sánchez, G.G.D. Importance of Lung Ultrasound Follow-Up in Patients Who Had Recovered from Coronavirus Disease 2019: Results from a Prospective Study. *J. Clin. Med.* **2021**, *10*, 3196. [CrossRef]
65. Haji-Hassan, M.; Lenghel, L.M.; Bolboacă, S.D. Hand-Held Ultrasound of the Lung: A Systematic Review. *Diagnostics* **2021**, *11*, 1381. [CrossRef]

diagnostics

MDPI

Article

Hospitalist Perceptions of Barriers to Lung Ultrasound Adoption in Diverse Hospital Environments

Anna M. Maw [1,*], P. Michael Ho [2], Megan A. Morris [3], Russell E. Glasgow [3], Amy G. Huebschmann [4], Juliana G. Barnard [3], Robert Metter [1], David M. Tierney [5], Benji K. Mathews [6], Edward P. Havranek [7], Mark Kissler [1], Michelle Fleshner [1], Barbara K. Burian [8], Elke Platz [9] and Nilam J. Soni [10]

1 Division of Hospital Medicine, University of Colorado School of Medicine, Aurora, CO 80045, USA; robert.metter@cuanschutz.edu (R.M.); mark.kissler@cuanschutz.edu (M.K.); michelle.fleshner@cuanschutz.edu (M.F.)
2 Division of Cardiology, University of Colorado School of Medicine, Aurora, CO 80045, USA; michael.ho@cuanschutz.edu
3 Adult and Child Consortium for Health Outcomes Research and Delivery Science (ACCORDS), University of Colorado School of Medicine, Aurora, CO 80045, USA; megan.a.morris@cuanschutz.edu (M.A.M.); russell.glasgow@cuanschutz.edu (R.E.G.); juliana.barnard@cuanschutz.edu (J.G.B.)
4 Division of General Internal Medicine, University of Colorado School of Medicine, Aurora, CO 80045, USA; amy.huebschmann@cuanschutz.edu
5 Medical Education Department, Abbott Northwestern Hospital, Minneapolis, MN 55407, USA; David.Tierney@allina.com
6 Department of Hospital Medicine, HealthPartners, Bloomington, MI 55420, USA; benji@umn.edu
7 Department of Medicine, Denver Health, Denver, CO 80204, USA; ed.havranek@dhha.org
8 Human Systems Integration Division NASA Ames Research Center, Mountain View, CA 94043, USA; barbara.k.burian@nasa.gov
9 Cardiovascular Division, Brigham and Women's Hospital, Harvard Medical School, Boston, MA 02115, USA; eplatz@bwh.harvard.edu
10 Division of Pulmonary and Critical Care Medicine and Division of General & Hospital Medicine, University of Texas Health San Antonio, San Antonio, TX 78229, USA; sonin@uthscsa.edu
* Correspondence: anna.maw@cuanschutz.edu

Citation: Maw, A.M.; Ho, P.M.; Morris, M.A.; Glasgow, R.E.; Huebschmann, A.G.; Barnard, J.G.; Metter, R.; Tierney, D.M.; Mathews, B.K.; Havranek, E.P.; et al. Hospitalist Perceptions of Barriers to Lung Ultrasound Adoption in Diverse Hospital Environments. *Diagnostics* **2021**, *11*, 1451. https://doi.org/10.3390/diagnostics11081451

Academic Editors: Marcello Demi and Gino Soldati

Received: 30 June 2021
Accepted: 6 August 2021
Published: 11 August 2021

Abstract: Despite the many advantages of lung ultrasound (LUS) in the diagnosis and management of patients with dyspnea, its adoption among hospitalists has been slow. We performed semi-structured interviews of hospitals from four diverse health systems in the United States to understand determinants of adoption within a range of clinical settings. We used the diffusion of innovation theory to guide a framework analysis of the data. Of the 27 hospitalists invited, we performed 22 interviews from four hospitals of diverse types. Median years post-residency of interviewees was 10.5 [IQR:5-15]. Four main themes emerged: (1) There are important clinical advantages to LUS despite operator dependence, (2) LUS enhances patient and clinician experience, (3) Investment of clinician time to learn and perform LUS is a barrier to adoption but yields improved efficiency for the health system and (4) Mandated training and use may be necessary to achieve broad adoption as monetary incentives are less effective. Despite the perceived benefits of LUS for patients, clinicians and health systems, a significant barrier to broad LUS adoption is the experience of time scarcity by hospitalists. Future implementation strategies should focus on changes to the clinical environment that address clinician barriers to learning and adoption of new skills.

Keywords: lung ultrasound; implementation science; point-of-care ultrasound

1. Introduction

In recent years, there has been increasing interest in integrating point-of-care ultrasound (POCUS), ultrasound that is performed and interpreted at the bedside by a treating clinician, into diagnostic pathways within internal medicine. In particular, point-of-care

lung ultrasound (LUS) has emerged as an accurate and practical imaging modality for the assessment of undifferentiated dyspnea and for the monitoring of volume status in patients with heart failure [1–8]. LUS has been shown to have multiple advantages over the current first-line imaging modality, chest x-ray, including increased accuracy and avoidance of ionizing radiation in diagnosis of some of the most common causes of dyspnea [1]: pleural effusion [9], pneumonia [10], pulmonary edema [11] and pneumothorax [12]. The COVID pandemic has underscored the many clinical advantages of LUS, as it is an accurate diagnostic tool for the diagnosis and monitoring of COVID-pneumonia with the added potential benefit of reducing the risk of COVID exposure for radiology staff [13,14]. In light of the growing evidence of its utility, multiple professional societies now endorse LUS use in acute care settings [1,15].

Despite its many advantages and increasing availability, adoption of diagnostic POCUS applications, including LUS, remains low. Prior studies have found lack of access to equipment and training to be the biggest barriers to implementation [16]. However, given the falling costs of portable ultrasound machines and increasing opportunities for training, determinants of adoption are likely changing.

The purpose of this study was to understand how internal medicine hospitalists, internist physicians who care for hospitalized adults [17], perceived LUS as a clinical tool through the lens of diffusion of innovations (DOI) theory [18] in order to identify current determinants of implementation and develop strategies to facilitate use among hospitalists. In addition to understanding how environmental factors such as access to machines and training affect adoption, we also sought to identify determinants of use once those fundamental elements were in place. For this reason, we included settings in which clinicians had easy access to equipment and training.

2. Methods

2.1. Study Design

Conceptual Frameworks

We used the DOI theory to frame our investigation [18]. DOI is a theory that seeks to explain how and at what pace new ideas and technology are adopted. DOI has been applied in numerous disciplines, particularly in the study of adoption of medical innovations by health systems [19]. This theory proposes that one of the elements that influences the spread of an innovation is the potential adopter's perception of the innovation. Key attributes of innovations that can affect the rate of adoption and adopter categories per DOI are outlined in Table 1. Adopter categories classify individuals within a social system based on how and when they decide to adopt an innovation. Understanding adopter categories can aid in efforts to facilitate adoption. DOI also proposes that the social system or context influences the uptake of new technology.

To capture elements of the environment that may affect adoption of LUS by hospitalists, we used the Pragmatic Robust Implementation and Sustainability Model (PRISM) to guide development of interview questions. PRISM is a pragmatic multi-level contextual model that includes relatively specific domains relevant to LUS and is tied to implementation outcomes in the RE-AIM framework [20–22]. The RE-AIM [22] framework was developed to promote external validity and equity in research on health interventions and assesses both implementation and effectiveness outcomes. The contextual domains of PRISM include known drivers of implementation [21] in the external environment (i.e., national policies, guidelines, and incentives) and the internal setting (i.e., multi-level organizational characteristics, perspectives, implementation and sustainability infrastructure). Use of PRISM has been recommended for the planning stages of implementation of health interventions to help identify determinants (i.e., barriers and facilitators) that will inform the creation and selection of implementation strategies, thereby enhancing adoption, implementation, and maintenance of evidence-based practices [20,22].

Use of theorical models and frameworks, like DOI and PRISM, is a recommended practice in implementation science [23,24] as they provide a lens with which to understand

determinants of implementation and select strategies that are likely to facilitate implementation. In this study, we selected DOI to better capture the determinants of adoption at the clinician level and PRISM to capture elements of the environment that may influence adoption by clinicians.

Table 1. Diffusion of Innovations Theory Domains.

Attributes of Innovations	Description
Relative Advantage	Advantage offered over traditional approach or tools (strongest predictor of adoption)
Compatibility	Alignment of the intervention with values and needs of the group adopting it (positively correlated with rate of adoption)
Complexity	How difficult the innovation is to use (negatively correlated with rate of adoption)
Trialability	Degree to which an innovation may be used experimentally on a limited basis (positively correlated with rate of adoption)
Observability	Visibility of an innovation's results to others (positively correlated with rate of adoption)
Categories of Adopters	**Description**
Innovators	Risk takers; role is to launch a new idea into the system
Early Adopters	Respected members of a group of potential adopters who are perceived as skilled in selecting new ideas that should be adopted
Early Majority	Need to see some peers successfully using an innovation prior to adopting it
Late Majority	Will adopt innovation if it becomes inconvenient to not adopt it
Laggards	Must be certain an innovation will not fail prior to adopting it

2.2. Study Sample and Setting

This study was approved by the Institutional Review Board at University of Colorado. Verbal consent was obtained from all participants. We interviewed hospitalists from four diverse hospital settings in which LUS was used by some clinicians. Site 1 was a 700-bed private hospital in Minneapolis, Minnesota. Site 2 was a 465-bed private hospital in St. Paul, Minnesota. Site 3 was a 268-bed government hospital in San Antonio, Texas. Site 4 was a 700-bed safety net teaching hospital in San Antonio, Texas. Sites 2, 3 and 4 are University affiliated. All hospitals trained internal medicine resident physicians. Hospitalists from all sites were interviewed to capture their experiences, perceptions, and opinions regarding LUS use in their respective hospitals. We used purposeful sampling for initial study recruitment and snowball sampling to complete enrollment. Purposeful sampling is a non-random sampling technique that is used to recruit participants who can provide in-depth and detailed information about the phenomenon being studied. Snowball sampling occurs when enrolled study participants identify possible future study participants among individuals they know [25].

2.3. Data Collection

Between November 2020 and January 2021, the study team conducted semi-structured interviews with hospitalists at the four study sites to assess their perspectives on LUS implementation in their local setting. The interview questions (see Supplementary Materials) were guided by PRISM [20,21] in order to capture contextual factors that may affect the perception of LUS by hospitalists and evolved over the course of data collection. Participants were asked questions related to determinants of LUS for multiple indications including some questions specifically related to COVID as data collection occurred during

the pandemic. Because the data suggested that there were many determinants of adoption unique to the pandemic and, in light of the decreasing impact of COVID in high resource inpatient settings relative to the time of data collection, responses to questions specific to COVID will be presented separately, so that the data and themes more representative of usual practice circumstances can be fully described and discussed here. Data acquired from questions addressing determinants of LUS adoption unique to the COVID pandemic will be presented in future writing. Qualitatively trained interviewers (AMM, MF and JGB) conducted all interviews by phone or video conferencing. Data collection continued until preliminary analyses indicated thematic saturation, when no additional themes were emerging from the interviews.

2.4. Data Analysis

The interviews were audio recorded and transcribed verbatim. We applied DOI to develop a deductive coding framework [18,26]. We allowed for new codes to inductively arise during the data analysis. Members of the research team (AMM and RM) began the analysis by immersing in the data and then met to develop the initial coding framework and definitions based on the DOI domains. A subset of transcripts was independently coded, and the research team subsequently met to reconcile coding differences and further refine and develop the coding framework. This process continued until a final coding framework was agreed upon and finalized. A member of the research team (AMM) applied the framework to the remaining transcripts with a second member (RM) double coding 20% of the transcripts to ensure consistency in coding across the transcripts. All discrepancies were reconciled through consensus. The codebook and analysis were reviewed by another team member (MF) and a doctoral-trained qualitative expert (MAM). Coded data were analyzed within and across different hospitals to identify themes that represent the participants' perceptions of the LUS adopter categories through the lens of DOI.

3. Results

Of the 27 hospitalists invited to interview, a total of 22 (15 adopters, 7 non-adopters) were enrolled and participated in interviews that lasted 30 to 45 min (Table 2). Median years post-residency of participants was 10.5 [IQR:5-15]. Recruited hospitalists had a broad spectrum of LUS experience ranging from novices to experts who routinely used LUS for diagnosis of multiple disease processes, including pneumothorax, pneumonia, pleural effusion, and pulmonary edema. Adopter status and training experience was determined by qualitative data. Participants were designated adopters if they considered diagnostic LUS a tool they had integrated into their usual care of patients. The site-specific data presented in Table 3 were collected in qualitative interviews of POCUS leaders from each site. Participants at site 1 completed a residency with an established three-year POCUS curriculum that required demonstration of LUS competency before residency graduation or completed a 7-day POCUS course in which participants received 7 full days of POCUS didactics and supervised scanning with LUS being one of the included applications. Some participants at sites 2 and 4 had completed or were in the process of completing the Society of Hospital Medicine (SHM) POCUS certificate of completion program which consists of on-line didactics, in person conferences with supervised hands-on scanning, completion of an imaging portfolio as well as a written and practical examination, with LUS being one of the required applications. The data fit well within the DOI framework and all attributes of innovation domains were used.

Table 2. Characteristics of Participants.

Study Participant and Site	Years Post-Residency	General ** POCUS Training in Which # LUS was an Included Application	Adopter Status
Site 1			
1-1	6	7-day course	Adopter
1-2	20	7-day course	Adopter
1-3	1	3-year residency curriculum	Adopter
1-4	15	** POCUS program founder	Adopter
1-5	6	7-day course	Non-adopter
Site 2			
2-1	10	Completed * SHM certifiation	Adopter
2-2	3	Residency and post-residency training	Adopter
2-3	5	Residency and post-residency training	Adopter
2-4	12	Completed * SHM certification	Adopter
2-5	4	Local certification process	Adopter
2-6	15	** POCUS program founder	Adopter
2-7	3	Residency, locally certified	Adopter
Site 3			
3-1	8	Residency and post-residency training	Adopter
3-2	25	2-day course	Non-adopter
3-3	18	2-day course	Non-adopter
3-4	17	** POCUS program founder	Adopter
3-5	12	Brief simulation training and bedside teaching from an expert	Non-adopter
Site 4			
4-1	2	Completing * SHM certification	Adopter
4-2	11	2-day course	Non-adopter
4-3	15	2-day course	Non-adopter
4-4	15	None	Non-adopter
4-5	9	Completing * SHM certification	Adopter

LUS, * SHM—Society of Hospital Medicine, ** POCUS—Point-of-Care Ultrasound.

Table 3. Description of Study Sites.

Site	Hospital Type	Number of Hospitalists	Number of Hospitalists Who Have Received Training	Number of Hospitalists Who Have Adopted LUS	Estimated Number of LUS Exams Performed Annually	Incentives Offered to Hospitalists	LUS Credentialing Process in Place	External Funding for Training
1	Private	78	78	30	3700	yes	no	yes
2	Private	100	70	10	1000	yes	yes	no
3	Government	24	19	3	312	no	no	no
4	Safety Net	68	16	3	468	no	no	no

3.1. Overview of Themes

Four main themes emerged from these data (Table 4): (1) There are important clinical advantages to LUS despite operator dependence, (2) LUS enhances patient and clinician experience, (3) Investment of clinician time to learn and perform LUS is a barrier to adoption but yields improved efficiency for the health system and (4) Mandated training and use may be necessary to achieve broad adoption as monetary incentives are less effective. Themes were similar across adopter status and study sites.

Table 4. Themes and subthemes.

Theme	Subtheme	Exemplar Quotes
Important clinical advantages of LUS despite operator dependence	Increased accuracy and expedited diagnosis Perceived advantage of LUS among nonadopters Operator-dependence	***2-2:*** *I feel that I'm better able to pick up when I have dried out their lungs and gotten all the extra fluid out sooner with lung ultrasound than other modalities.* ***1-3:*** *If I come around on rounds at 9:00 a.m. and I say, "Let's get a chest x-ray," the chest x-ray comes back at 11:00. Now I'm gonna give 'em one dose of diuretic if they're overloaded. Versus if I come around at 9:00 a.m. and I check, and I see they're overloaded. I can give 'em two doses. That's humane, as opposed to making them be up all night peeing.* ***3-2:*** *I think ultrasound is much more convenient. You can do it yourself. The problem is comfort level with it. . . . I feel very comfortable with X-ray whereas ultrasound, it's just not as familiar to me.* ***2-1:*** *I think it's a sharp object. You can hurt yourself and your patients if you do it wrong.*
Enhanced patient & provider experience		***3-3:*** *By definition, you're going to be at the bedside. You're often, as you're getting set up, gonna be making small talk about maybe not even the ultrasound but something else. They might be asking you questions about the ultrasound machine, and you're answering them. It just creates a conversation, which can only, in my opinion, benefit everyone.* ***1-1:*** *just by doing an ultrasound, you have to be in that room for 10, 15 min. These days, if you watch any hospital environment, if you put up some kind of tracker device, the physicians barely spend eight minutes in a patient's room. The rest of time goes into your coordination, your—the typing notes, all those things. I think that, first of all, you're spending significantly more time in patient's room, which they realize it, that this doctor's been here for a while.*
Investment of clinician time yields improved efficiency for the health system	Time to master Time to perform Replacement of chest x-rays with LUS Improved efficiency for the health system	***4-1:*** *I think there's interest, but again, it's just a lot of—I think people get scared off by the commitment of having to go through all of that, the time that's dedicated to it.* ***2-3:*** *We're limited by time. We have many patients to see. Even if you want to ultrasound more, we're limited by the amount of time we can spend at bedside, unfortunately.* ***1-1:*** *My x-ray use . . . over the last two years has dropped by 70 percent for acute shortness of breath in the hospital. Any time I get a call, and it's like, "Oh, this patient is on oxygen, now four liters, and they're short of breath," I immediately just go there with my ultrasound and try to figure things out rather than just—reflexively, previously I have always ordered an x-ray before I even leave my area where I'm working.* ***1-3:*** *Yeah, its [LUS] ability to replace x-ray and CT in many areas will be very helpful. Additionally, in an outpatient setting, I think that it has huge future implications for monitoring, preventing the need for people to be getting all these tests just to return to their primary doctor to discuss things. . . . .., I think, [LUS] has a real big future in reducing that need for multiple different imaging tests over the course of days.*
Mandated training and use may be necessary to achieve broad adoption as monetary incentives are less effective		***3-4:*** *I think the implementation has been slow for a host of reasons. What's the incentive for anybody to take this on aside from being a good doctor or being able to not miss certain findings? There's really not a lotta personal incentive . . . . How do you get to the guy who says, "I hate technology. I don't wanna change. I've been doin' my way for the last 20 years. What's so much better about your way?" You could say your length of stay and your diagnoses will be better, but what does that really mean to me? The hospital already harasses me for so many other things. Length of stay is really their problem, not mine.* ***2-7:*** *The way that our group compensates is about 80 percent, roughly, base salary and then 20 percent that's production-based in some way or another. A component of that production is RVU driven. I think a point-of-care lung gets 2.4 RVU . . . It's not a huge incentive, I would say. I think there are probably easier ways to add some to your bottom line.*

Participants perceived important clinical advantages of LUS including increased accuracy and expedited diagnoses. However, they acknowledged that ensuring LUS competency was a prerequisite to improving patient outcomes with its use. Some participants also perceived LUS as improving both patient and clinician experience.

Participants reported the investment of their personal time to become proficient and perform LUS exams was one of the biggest barriers to adoption but felt that adoption had important potential benefits for the health system (i.e., reduced length of stay and diagnostic testing).

Despite both adopters and non-adopters acknowledging the benefits of LUS, only a minority of clinicians had adopted LUS, even in environments where portable or handheld ultrasound machines were easily accessible and training was incentivized. POCUS leaders interviewed felt that mandated training and use may be necessary to achieve broad implementation.

3.2. Important Clinical Advantages of LUS despite Operator Dependence

Increased accuracy and expedited diagnosis: Participants perceived multiple clinical advantages of LUS over chest x-ray including expedited diagnosis, improved accuracy, and reduced radiation exposure to patients. Many hospitalists felt LUS outperformed chest x-rays for multiple common diagnoses including decompensated heart failure, one of the most common reasons for hospitalization in adults. Hospitalist 1-3 said: *you can see pulmonary edema much better on ultrasound [than chest x-ray].*

Both users and nonusers of LUS reported expedited clinical decision-making was an important clinical advantage of LUS use. Hospitalist 2-3 said: *If I have a question 'Why is this patient hypoxic?' and I wanna know it now, I get my ultrasound, and I'm in their room, and I'd do it right there. Chest x-rays, even if I ordered it stat, will take maybe another 15, 20 min.*

Perceived advantage of LUS among nonadopters: All participants regardless of adoption status perceived potential benefits of LUS use. For example, hospitalist 1-5 who had undergone extensive LUS training for which he had received a monetary incentive, but had not yet integrated LUS into his practice said: *It's a better tool than the stethoscope and if I were training today, I doubt I would be using only a stethoscope*. Another nonadopter, hospitalist 4-2 said: *I don't think I need to be convinced. Honestly, I am convinced. It's more how do I get the training?*

Operator-dependence: A concern expressed by some participants was that the accuracy of LUS is operator dependent and inadequate training could result in patient harm. Although this was acknowledged as a potential risk, it was not necessarily considered a reason to avoid adoption. Hospitalist 3-3 said: "*It could also be pretty inaccurate, just like the physical exam, just like a poorly done history. When it is more operator-dependent, more human-centered, it's gonna have that variability. That's never been a reason, in my mind, not to... That just means you need to train up to it and learn it and develop confidence*."

3.3. Enhanced Patient and Clinician Experience:

Participants reported perception of improved patient experience and enhanced therapeutic rapport with LUS use, in part because patients received more time and attention from their clinician. Hospitalist 3-3 said: *It gives you more time with the patients, and they really feel like you're examining them in a meaningful way.* Participants perceived LUS as also having a clinical advantage of offering an additional and powerful opportunity for patient education. Hospitalist 1-3 said: *I'm looking for a big pleural effusion that I'm gonna tap, I get to review that effusion with them [the patient], and they're often like, "Whoa, my gosh." I say, "If you take your diuretics and you lay off salt, a lotta this can be avoided."*

Many clinicians reported LUS use improved their own practice experience. Hospitalist 3-3, who had some experience using LUS but was still in the process of deciding whether to adopt said: *[LUS] benefits you in the enjoyment of your job. [It] benefits the patients and their feeling of a therapeutic alliance . . . although it's a technology, some of the . . . more human-centered aspects of it are, to me, the biggest advantages.* In addition, even when LUS findings

didn't change management, many participants reported it significantly reduced diagnostic uncertainty which they felt was valuable. Hospitalist 1-3 said: *It makes me have much more peace of mind when I'm making clinical decisions.* And gives them a feeling they are providing better care: Hospitalist 3-5 said: *"I feel like it allows me to help care for my patients better."*

Clinicians also reported enjoying the ability to answer urgent clinical questions quickly at the beside without relying on traditional imaging services which have an inherent delay. Hospitalist 3-3 said: *There's a number of advantages that come with something being point-of-care that you control, as opposed to having to rely on others. If you have a need for a stat chest x-ray, that stat can be minutes or it could be an hour or sometimes longer. I think that level of control over the process, not being reliant on other people, being able to do it yourself, I think is huge*.

3.4. Investment of Clinician Time to Perform LUS Is a Barrier to Adoption but Yields Improved Efficiency for the Health System

Time to learn and perform LUS: Hospitalists describe the investment of clinician time as the most important disadvantage of LUS adoption. Even at sites 1 and 2 where training is easily available and even incentivized, the time clinicians needed to invest to attain proficiency, optimize efficiency and perform LUS once scanning efficiency was optimized was considered the most important barrier to adoption by both adopters and nonadopters. Hospitalist 2-1 said: *It comes down to time and you have to be extremely self-motivated. I've seen people whose enthusiasm flares up and then it washes away. It happens so, so commonly. That's the reason why there's only so few of us have been able to cross the finish line.*

Even after optimal efficiency is obtained, clinicians describe the extra time it takes at the bedside to perform a LUS exam is a barrier to LUS use. Hospitalist 3-1 said: *No. I think it's really just the time I think is the biggest factor with it. Yeah, that's really the biggest disadvantage I think.*

Replacement of chest X-ray with LUS: Multiple clinicians at sites 1 and 2 reported using LUS as initial imaging in patients with worsening respiratory status and reported greatly decreased use of chest x-rays since adopting LUS because they felt it was more accurate and helped them expedite appropriate management. Hospitalist 2-1 stated: *In the setting of a patient whose respiratory status is acutely worsening, I don't even bother with chest x-ray. I usually just go with the ultrasound machine.*

Reducing the number of chest x-rays was perceived by many participants as one of the potential advantages of LUS implementation at a system level and consistent with high-value care. Hospitalist 1-1 said: *I do think there's cost advantage if there's a reduction in use . . . because x-ray is a multilevel thing, where somebody comes, takes the patient. Somebody takes the picture. Somebody reads the picture. Somebody uploads it. There's like five people going in the background, giving a bunch of time . . . versus an ultrasound, you have the bedside person just going there, making a decision right there.*

Improved efficiency for the health system: Despite the additional cost of clinician time, many participants felt adoption of LUS could improve hospital efficiency by expediting and improving accuracy of diagnoses. Hospitalist 2-2 said: *Cost savings is clearly there as far as doing point-of-care ultrasound during my rounding and making a decision. It may shorten the length of stay, as far as being able to not wait a half day to get a CAT scan and get a CAT scan read if you are able to do the lung ultrasound and reassure yourself that the patient—that things are doing fine and they're ready for discharge. It also, just the sheer cost of CAT scans is there, so I think there's cost savings.*

3.5. Mandated Training and Use May Be Necessary to Achieve Broad Adoption as Monetary Incentives Are Less Effective

At site 1 and 2 where ultrasound equipment and training were easily accessible, participants reported only partial adoption. A large number of hospitalists in both groups had undergone training but still had not adopted LUS use in clinical practice.

POCUS leaders at sites 1 and 2 reported using monetary incentives to encourage clinicians to train and perform POCUS. However, these incentives were perceived as

having limited utility. Hospitalist 1-4: *It [monetary incentives] are not the solution. People that don't want to do it, still don't want to do it with money involved.*

Clinicians who had received training but had not yet adopted LUS stated they were more comfortable with other diagnostic tools and were not sure if their decision-making would be improved by LUS without a significant additional investment in time using LUS in clinical practice. Adopters speculated on the reasons why trained clinicians had not adopted LUS. Many adopters felt that curiosity, perseverance, and younger age predicted clinicians who were more likely to adopt LUS. POCUS leaders at sites 1 and 2 speculated that graduate medical education (GME) training requirements or a mandate from leadership would likely be necessary to increase uptake of LUS broadly to the early majority and late majority adopters.

Hospitalist 1-4 said: *You can't actually get to the endpoint [integration of LUS into actual practice] until GME is at a longitudinal three-year point-of-care ultrasound integrated place.*

Hospitalist 2-6: I would anticipate institutionalizing, meaning this needs to be done.

4. Discussion

In this qualitative study of 22 hospitalists who practice in 4 diverse clinical settings, we have captured key perceptions of LUS through the lens of DOI that are likely to influence the rate of adoption by hospitalists. Overall, our findings suggest LUS was perceived by all study participants as offering relative advantages compared to standard tools including increased accuracy, expedited diagnosis, and improved patient and clinician experience. In addition, multiple participants from sites that had easy access to equipment and training reported that LUS had supplanted chest x-ray in their practice, a finding they perceived as consistent with high-value care. Although there have been studies demonstrating introduction of LUS can decrease the use of chest x-rays in intensive care units [27,28], this is a novel finding among hospitalists.

Through the lens of DOI, many participant perceptions of LUS predict rapid adoption of LUS by hospitalists. However, our study shows that this is not the case. In terms of barriers encountered, our findings suggest that in environments in which equipment and training are not readily available, access to these necessary elements of adoption remain the most important barriers to adoption. This finding is consistent with previously published surveys on this topic [16]. In contrast, we found that even in environments in which the barriers of access to machines and training had been removed, only a minority of clinicians adopt. In these environments, the biggest barrier to adoption reported by participants is the clinician time required to attain proficiency and once proficiency is achieved, time to perform the exam. This is a novel finding that has important implications for future implementation efforts.

A possible explanation for these findings through the lens of DOI would be that LUS is highly "complex"; however, this is not consistent with what we know about this tool. Multiple studies have demonstrated that clinicians can achieve proficiency in performing LUS exams with very brief training [7,29] and LUS exams can be performed in less than 5 min by an experienced operator [4]. Indeed, even those who have adopted LUS say that they are unable to utilize it due to time constraints when patient volumes are high. This signals that it is perhaps the *environment* and not the intervention that poses the barrier to adoption.

Our participants describe a practice setting in which a task that takes only a few extra minutes at the bedside, although perceived as inherently valuable on multiple levels and consistent with their professional values, is considered too time consuming to perform. This mandate to maximize efficiency at the expense of connecting with patients and incorporating new skills that are uniformly perceived as an improvement on traditional tools is striking. It suggests that the perceived scarcity of time within the current inpatient environment places physicians at odds with their professional values of performing well considered clinical decisions, life-long learning and building therapeutic rapport with patients. Further, this reality exists in an era of rapidly advancing medical knowledge

and technology. Our findings underscore the current dilemma for individuals in clinical practice: how does a clinician evolve her practice to adhere to changing practice standards if the need to optimize productivity, often measured in relative value units, leaves no time to learn?

Recent studies tying physician burnout to time scarcity [28] raise the question of whether decreased workloads that allow time for incorporation of new skills into practice may actually decrease the cost of care by both improving outcomes and health system efficiency. Reducing clinician burnout reduces its subsequent negative impact on a health system, including poor quality clinical decisions and physician turnover, which are costly [30,31]. The problem of perceived time scarcity also raises the question of how clinicians are to stay abreast of medical advancement if there is no cognitive space in their practice to do so and may in part explain the well documented lag in adoption of evidence-based practices [32].

We must also recognize that although time scarcity was the most commonly cited factor limiting uptake of LUS by hospitalists, it seems possible the word *time* may be a stand-in for a host of factors that serve as barriers to the acquisition of new knowledge and skills in clinical practice. Literature on human factors engineering and the cognitive sciences emphasizes ways that environmental design, cognitive load, attention demands, and task allocation are all elements that contribute to the clinician's sense of being 'pressed for time' [33,34]. This expanded view of the barrier articulated by study participants has the advantage of promoting inquiry that will lead to a better understanding how these factors contribute to the adoption of health innovations by clinicians which in turn can be applied as targeted changes in infrastructure, culture, and procedures to address barriers to clinician learning and evidence-based practice.

Some participants felt mandating LUS use may be necessary to achieve uniform implementation across a department or institution, since monetary incentives were not perceived as effective. However, our findings underscore a current lack of alignment between clinician and health system incentives regarding LUS adoption. Given business models greatly influence decision-making in health care, health system leaders must be convinced of LUS's value as measured by increased efficiency and reduced overall cost before investing in the infrastructure needed to facilitate robust LUS implementation. Until this is achieved, broad adoption by clinicians is likely to remain unrealized.

Limitations and Future Directions

There are important limitations to this study which must be recognized. First, our findings represent the viewpoints of hospitalists at 4 teaching hospitals in the United States. Hospitalists in rural, non-teaching hospitals or hospitals in other countries may have unique perspectives that were not captured by our study. Additionally, our 4 participating institutions had national POCUS leaders among their faculty which likely increased general awareness of LUS among local clinicians. Finally, although we interviewed several nonusers, early adopters were over-represented in our sample, and it should be emphasized that these early adopters represent a minority in their practice groups.

These data help us understand both hospitalist perspectives of LUS and environmental factors that influence their decisions to adopt LUS. These findings will allow us to consider implementation strategies that address the fundamental barriers in different environments. Additionally, we captured hospitalist attitudes and patterns of adoption that mirror the adopter categories proposed in DOI. This observation will allow us to create and test implementation strategies using audience segmentation messaging. However, the major finding of these data is hospitalists interviewed felt that time was such a limited resource in their practice that it precluded integration of LUS use despite acknowledging the multiple benefits to patient care. This suggests implementation strategies that target institutional buy-in and policy will be needed to achieve complete implementation.

5. Conclusions

The hospitalists interviewed perceive LUS as having important benefits for patients, clinicians and health systems. The time required to master and perform LUS was perceived to be an important barrier to its adoption by hospitalists. This finding highlights the crises of perceived time scarcity in clinical practice and its impact on the adoption of health innovations by clinicians.

Supplementary Materials: The following are available online at https://www.mdpi.com/article/10.3390/diagnostics11081451/s1, Supplementary Material File S1. Interview guide for Hospitalists.

Author Contributions: Conceptualization, A.M.M.; methodology, M.A.M., J.G.B., R.E.G. and A.G.H.; formal analysis, A.M.M. and R.M.; investigation, A.M.M., J.G.B., M.F., D.M.T., B.K.M. and N.J.S.; writing—original draft preparation, A.M.M.; writing—review and editing, A.M.M., M.A.M., J.G.B., R.E.G., A.G.H., N.J.S., M.F., P.M.H., B.K.B., E.P., M.K. and E.P.H.; supervision, P.M.H., A.G.H., R.E.G., M.A.M., E.P.H., N.J.S. and M.A.M.; funding acquisition, R.E.G. and A.M.M. All authors have read and agreed to the published version of the manuscript.

Funding: This research was funded by National Heart, Lung, and Blood Institute, K12HL137862.

Institutional Review Board Statement: The study was conducted according to the guidelines of the Declaration of Helsinki, and approved by the Institutional Review Board of University of Colorado (protocol code 20-0904 and April 2020).

Informed Consent Statement: Informed consent was obtained from all subjects involved in the study.

Data Availability Statement: The data presented in this study are available on request from the corresponding author.

Conflicts of Interest: Platz' employer has received support from Novartis for consulting work and she has consulted for scPharmaceuticals outside of the submitted work. She has received research support from NHLBI and NIDDK outside of the submitted work. Tierney is a member of the Medical Advisory Board for EchoNous, Inc. and the Transesophageal Ultrasound Advisory Board for FUJIFILM SonoSite, Inc.

References

1. Qaseem, A.; Etxeandia-Ikobaltzeta, I.; Mustafa, R.A.; Kansagara, D.; Fitterman, N.; Wilt, T.J. Appropriate Use of Point-of-Care Ultrasonography in Patients With Acute Dyspnea in Emergency Department or Inpatient Settings: A Clinical Guideline From the American College of Physicians. *Ann. Intern. Med.* **2021**. [CrossRef]
2. Pivetta, E.; Goffi, A.; Lupia, E.; Tizzani, M.; Porrino, G.; Ferreri, E.; Volpicelli, G.; Balzaretti, P.; Banderali, A.; Iacobucci, A.; et al. Lung Ultrasound-Implemented Diagnosis of Acute Decompensated Heart Failure in the ED: A SIMEU Multicenter Study. *Chest* **2015**, *148*, 202–210. [CrossRef] [PubMed]
3. Araiza-Garaygordobil, D.; Gopar-Nieto, R.; Martinez-Amezcua, P.; Cabello-López, A.; Alanis-Estrada, G.; Herbert, J.A.L.; González-Pacheco, H.; Paredes-Paucar, C.P.; Sierra-Lara, M.D.; la Cruz, J.L.B.-D.; et al. A randomized controlled trial of lung ultrasound-guided therapy in heart failure (CLUSTER-HF study). *Am. Heart J.* **2020**, *227*, 31–39. [CrossRef] [PubMed]
4. Al Deeb, M.; Barbic, S.; Featherstone, R.; Dankoff, J.; Barbic, D. Point-of-care Ultrasonography for the Diagnosis of Acute Cardiogenic Pulmonary Edema in Patients Presenting with Acute Dyspnea: A Systematic Review and Meta-analysis. *Acad. Emerg. Med.* **2014**, *21*, 843–852. [CrossRef]
5. Rivas-Lasarte, M.; Alvarez-Garcia, J.; Fernández-Martínez, J.; Maestro, A.; López-López, L.; Gonzalez, E.S.; Pirla, M.J.; Mesado, N.; Mirabet, S.; Fluvià, P.; et al. Lung ultrasound-guided treatment in ambulatory patients with heart failure: A randomized controlled clinical trial (LUS-HF study). *Eur. J. Heart Fail.* **2019**, *21*, 1605–1613. [CrossRef]
6. Marini, C.; Fragasso, G.; Italia, L.; Sisakian, H.; Tufaro, V.; Ingallina, G.; Stella, S.; Ancona, F.; LoIacono, F.; Innelli, P.; et al. Lung ultrasound-guided therapy reduces acute decompensation events in chronic heart failure. *Heart* **2020**, *106*, 1934–1939. [CrossRef] [PubMed]
7. Noble, V.E.; Lamhaut, L.; Capp, R.; Bosson, N.; Liteplo, A.; Marx, J.-S.; Carli, P. Evaluation of a thoracic ultrasound training module for the detection of pneumothorax and pulmonary edema by prehospital physician care providers. *BMC Med. Educ.* **2009**, *9*, 3. [CrossRef] [PubMed]
8. Cibinel, G.A.; Casoli, G.; Elia, F.; Padoan, M.; Pivetta, E.; Lupia, E.; Goffi, A. Diagnostic accuracy and reproducibility of pleural and lung ultrasound in discriminating cardiogenic causes of acute dyspnea in the Emergency Department. *Intern. Emerg. Med.* **2012**, *7*, 65–70. [CrossRef] [PubMed]
9. Soni, N.J.; Franco, R.; Velez, M.I.; Schnobrich, D.; Dancel, R.; Restrepo, M.I.; Mayo, P.H. Ultrasound in the diagnosis and management of pleural effusions. *J. Hosp. Med.* **2015**, *10*, 811–816. [CrossRef]

10. Ye, X.; Xiao, H.; Chen, B.; Zhang, S. Accuracy of Lung Ultrasonography versus Chest Radiography for the Diagnosis of Adult Community-Acquired Pneumonia: Review of the Literature and Meta-Analysis. *PLoS ONE* **2015**, *10*, e0130066. [CrossRef] [PubMed]
11. Maw, A.M.; Hassanin, A.; Ho, P.M.; McInnes, M.D.F.; Moss, A.; Juarez-Colunga, E.; Soni, N.J.; Miglioranza, M.H.; Platz, E.; De Santo, K.; et al. Diagnostic Accuracy of Point-of-Care Lung Ultrasonography and Chest Radiography in Adults With Symptoms Suggestive of Acute Decompensated Heart Failure: A Systematic Review and Meta-analysis. *JAMA Netw. Open* **2019**, *2*, e190703. [CrossRef]
12. Alrajab, S.; Youssef, A.M.; Akkus, N.I.; Caldito, G. Pleural ultrasonography versus chest radiography for the diagnosis of pneumothorax: Review of the literature and meta-analysis. *Crit. Care* **2013**, *17*, R208. [CrossRef] [PubMed]
13. Sorlini, C.; Femia, M.; Nattino, G.; Bellone, P.; Gesu, E.; Francione, P.; Paternò, M.; Grillo, P.; Ruffino, A.; Bertolini, G.; et al. The role of lung ultrasound as a frontline diagnostic tool in the era of COVID-19 outbreak. *Intern. Emerg. Med.* **2021**, *16*, 749–756. [CrossRef]
14. Gutsche, H.; Lesser, T.; Wolfram, F.; Doenst, T. Significance of Lung Ultrasound in Patients with Suspected COVID-19 Infection at Hospital Admission. *Diagnostics* **2021**, *11*, 921. [CrossRef] [PubMed]
15. Ponikowski, P.; Voors, A.A.; Anker, S.D.; Bueno, H.; Cleland, J.G.F.; Coats, A.J.S.; Falk, V.; González-Juanatey, J.R.; Harjola, V.-P.; Jankowska, E.A.; et al. 2016 ESC Guidelines for the diagnosis and treatment of acute and chronic heart failure: The Task Force for the diagnosis and treatment of acute and chronic heart failure of the European Society of Cardiology (ESC)Developed with the special contribution of the Heart Failure Association (HFA) of the ESC. *Eur. Heart J.* **2016**, *37*, 2129–2200.
16. Wong, J.; Montague, S.; Wallace, P.; Negishi, K.; Liteplo, A.; Ringrose, J.; Dversdal, R.; Buchanan, B.; Desy, J.; Ma, I.W.Y. Barriers to learning and using point-of-care ultrasound: A survey of practicing internists in six North American institutions. *Ultrasound J.* **2020**, *12*, 1–7. [CrossRef] [PubMed]
17. Wachter, R.M.; Goldman, L. Zero to 50,000—The 20th Anniversary of the Hospitalist. *N. Engl. J. Med.* **2016**, *375*, 1009–1011. [CrossRef] [PubMed]
18. Rogers, E. *Diffusion of Innovations*, 5th ed.; Simon and Schuster: New York, NY, USA, 2003.
19. Berwick, D.M. Disseminating innovations in health care. *JAMA* **2003**, *289*, 1969–1975. [CrossRef] [PubMed]
20. McCreight, M.S.; Rabin, B.A.; Glasgow, R.E.; Ayele, R.A.; Leonard, C.A.; Gilmartin, H.M.; Frank, J.W.; Hess, P.L.; Burke, R.E.; Battaglia, C.T. Using the Practical, Robust Implementation and Sustainability Model (PRISM) to qualitatively assess multilevel contextual factors to help plan, implement, evaluate, and disseminate health services programs. *Transl. Behav. Med.* **2019**, *9*, 1002–1011. [CrossRef] [PubMed]
21. Feldstein, A.C.; Glasgow, R.E. A Practical, Robust Implementation and Sustainability Model (PRISM) for Integrating Research Findings into Practice. *Jt. Comm. J. Qual. Patient Saf.* **2008**, *34*, 228–243. [CrossRef]
22. Glasgow, R.E.; Harden, S.M.; Gaglio, B.; Rabin, B.; Smith, M.L.; Porter, G.C.; Ory, M.G.; Estabrooks, P.A. RE-AIM Planning and Evaluation Framework: Adapting to New Science and Practice With a 20-Year Review. *Front. Public Health* **2019**, *7*. [CrossRef]
23. Nilsen, P. Making sense of implementation theories, models and frameworks. *Implement. Sci.* **2015**, *10*, 1–13. [CrossRef] [PubMed]
24. Ridde, V.; Pérez, D.; Robert, E. Using implementation science theories and frameworks in global health. *BMJ Glob. Health* **2020**, *5*, e002269. [CrossRef]
25. Palinkas, L.A.; Horwitz, S.M.; Green, C.A.; Wisdom, J.P.; Duan, N.; Hoagwood, K. Purposeful Sampling for Qualitative Data Collection and Analysis in Mixed Method Implementation Research. *Adm. Policy Ment. Health* **2015**, *42*, 533–544. [CrossRef] [PubMed]
26. Gale, N.K.; Heath, G.; Cameron, E.; Rashid, S.; Redwood, S. Using the framework method for the analysis of qualitative data in multi-disciplinary health research. *BMC Med. Res. Methodol.* **2013**, *13*, 117. [CrossRef] [PubMed]
27. Brogi, E.; Bignami, E.; Sidoti, A.; Shawar, M.; Gargani, L.; Vetrugno, L.; Volpicelli, G.; Forfori, F. Could the use of bedside lung ultrasound reduce the number of chest x-rays in the intensive care unit? *Cardiovasc. Ultrasound* **2017**, *15*, 1–5. [CrossRef] [PubMed]
28. Peris, A.; Tutino, L.; Zagli, G.; Batacchi, S.; Cianchi, G.; Spina, R.; Bonizzoli, M.; Migliaccio, L.; Perretta, L.; Bartolini, M.; et al. The Use of Point-of-Care Bedside Lung Ultrasound Significantly Reduces the Number of Radiographs and Computed Tomography Scans in Critically Ill Patients. *Anesth. Analg.* **2010**, *111*, 687–692. [CrossRef]
29. Mozzini, C.; Pasini, A.M.F.; Garbin, U.; Cominacini, L. Lung ultrasound in internal medicine: Training and clinical practice. *Crit. Ultrasound J.* **2016**, *8*, 1–7. [CrossRef] [PubMed]
30. Tawfik, D.S.; Scheid, A.; Profit, J.; Shanafelt, T.; Trockel, M.; Adair, K.C.; Sexton, J.B.; Ioannidis, J.P.A. Evidence Relating Health Care Provider Burnout and Quality of Care: A Systematic Review and Meta-analysis. *Ann. Intern. Med.* **2019**, *171*, 555–567. [CrossRef]
31. Han, S.; Shanafelt, T.D.; Sinsky, C.A.; Awad, K.M.; Dyrbye, L.N.; Fiscus, L.C.; Trockel, M.; Goh, J. Estimating the Attributable Cost of Physician Burnout in the United States. *Ann. Intern. Med.* **2019**, *170*, 784–790. [CrossRef]
32. Morris, Z.; Wooding, S.; Grant, J. The answer is 17 years, what is the question: Understanding time lags in translational research. *J. R. Soc. Med.* **2011**, *104*, 510–520. [CrossRef] [PubMed]
33. Proctor, R.W.; Trisha, V.Z. *Human Factors in Simple and Complex Systems*, 3rd ed.; CRC Press: Boca Raton, FL, USA, 2017.
34. Lee, J.D.; Kirlik, A. *The Oxford Handbook of Cognitive Engineering*, 3rd ed.; Oxford University Press: New York, NY, USA, 2013.

diagnostics

MDPI

Review

Hand-Held Ultrasound of the Lung: A Systematic Review

Mariam Haji-Hassan [1,2], Lavinia Manuela Lenghel [3,4,*] and Sorana D. Bolboacă [1,*]

1 Department of Medical Informatics and Biostatistics, Iuliu Haţieganu University of Medicine and Pharmacy Cluj-Napoca, Louis Pasteur Str., No. 6, 400349 Cluj-Napoca, Romania; mariam.haji-hassan@umfcluj.ro
2 Department of Anatomy, Iuliu Haţieganu University of Medicine and Pharmacy Cluj-Napoca, Louis Pasteur Str., No. 6, 400349 Cluj-Napoca, Romania
3 Department of Radiology, Iuliu Haţieganu University of Medicine and Pharmacy Cluj-Napoca, Clinicilor Str., No. 3-5, 400006 Cluj-Napoca, Romania
4 Radiology and Medical Imaging Department, County Emergency Clinical Hospital, Clinicilor Str., No. 3-5, 400006 Cluj-Napoca, Romania
* Correspondence: pop.lavinia@umfcluj.ro (L.M.L.); sbolboaca@umfcluj.ro (S.D.B.)

Abstract: Background: The ultrasound examination is a surface technique with an accurate diagnosis of pathological processes adjacent to the pleural line. The purpose of the study was to evaluate the role of hand-held ultrasound devices (visual stethoscopes) in the diagnosis of peripheral lung disease. Methods: We conducted a systematic search of literature comparing the diagnostic accuracy of truly hand-held ultrasound devices compared to conventional high-end ultrasound devices, chest X-rays, thoracic CT (computer tomography), or physical examinations to diagnose peripheral lung lesions. ScienceDirect, PubMed, and PubMed Central bibliographic databases were searched within a time limit of 15 years. Results: The applied search strategy retrieved 439 studies after removing duplicates; 34 were selected for full-text review, and 15 articles met all inclusion criteria and were included in the analysis. When comparing hand-held ultrasound devices to chest X-rays, negative predictive values were above 90%, while positive predictive values tended to be lower (from 35% to 75.8%). Hand-held ultrasound reached a correlation of 0.99 as associated with conventional ultrasound with a Bland–Altman bias close to zero. Conclusions: Being accessible, radiation-free, and comparatively easy to decontaminate, hand-held ultrasound devices could represent a reliable tool for evaluating peripheral lung diseases. This method can be successfully employed as an alternative to repeated X-ray examinations for peripheral lung disease monitoring.

Keywords: lung ultrasound; hand-held ultrasound device; lung disease; COVID-19 (Coronavirus Disease 2019)

Citation: Haji-Hassan, M.; Lenghel, L.M.; Bolboacă, S.D. Hand-Held Ultrasound of the Lung: A Systematic Review. *Diagnostics* **2021**, *11*, 1381. https://doi.org/10.3390/diagnostics11081381

Academic Editor: Philippe A. Grenier

Received: 28 June 2021
Accepted: 28 July 2021
Published: 31 July 2021

1. Introduction

Ultrasound is a medical technique that has recently begun to be used for investigating lung disease, which was a surprising turn for medical imaging technology [1,2]. For years, the method was thought to be of little use in this area because the air in the lung scatters and impedes the transmission of sound waves. However, the lung's surface is a strong reflector of ultrasound waves and thus creates several reverberation artifacts. However, these artifacts contain valuable information and correlate with the current lung pathophysiology [3].

Expert recommendations support the use of ultrasound examination for a vast array of lung diseases such as pleural effusions, interstitial pulmonary lesions, lung consolidations, etc., and in different settings, including at point-of-care [4–7]. Lung ultrasonography gives results comparable to thoracic computer tomography (CT) scanning while having the advantages of portability, repeatability, low cost, and absence of irradiation [8]. Coronavirus Disease 2019 (COVID-19) generally begins in the terminal alveoli, close to the pleura, and can be clearly observed by lung ultrasound [9]. Lung ultrasound is a surface imaging technique useful in cases of acute respiratory failure, and bedside US should be performed

for the early diagnosis of COVID-19 pneumonia in all the patients who present to the emergency department with flu-like symptoms in the era of novel COVID-19 [10].

Several hospitals in COVID hotspots are using hand-held ultrasound. Using these systems, they are examining patients to determine whether they should be admitted and, if so, whether they need intensive care [11]. The absence of ionizing radiations means doctors can use the devices every day to closely track the course of the disease. On the other hand, auscultation presents a high risk of nosocomial transmission because a stethoscope cannot be covered entirely by protective equipment [12].

Several organizations, such as the Canadian Association of Emergency Physicians, and experts recommend using a wireless probe and tablet as the most appropriate ultrasound equipment, as they can be easily wrapped in single-use plastic covers to reduce contamination and promote sterilization. It is possible to put a sheath around the entire system to prevent any pathogens from contaminating it [13–16].

No systematic review regarding the accuracy of hand-held ultrasound devices for scanning peripheral lungs diseases has previously been conducted. Considering the recommendations to use hand-held ultrasound devices because of their portability and reduced risk of contamination, we performed a systematic search of the literature to assess pocket-size devices' performance as a diagnostic method for lung pathology.

2. Materials and Methods

This review was performed in accordance to the PRISMA (Preferred Reporting Items for Systematic Reviews and Meta-Analyses) guidelines. The study protocol was registered in PROSPERO with the registration number CRD42021242620.

2.1. Search Strategy

The search strategy was constructed to address the following:

- Problem: lung disease
- Intervention: hand-held (pocket-sized) ultrasound (US)
- Comparisons: X-ray OR conventional US OR computer tomography (CT)
- Outcome: accuracy
- Study design: any

We conducted the literature search in PubMed, ScienceDirect, and PubMed Central (PMC) bibliographic databases, from 2006 to 8 April 2021, covering the 15-year period that marked hand-held ultrasound devices' appearance and development. The search strategy was designed and carried out with input from all investigators.

The following string was used in searching the PubMed database: (pneumonia[Title/Abstract] OR lung[Title/Abstract] OR respiratory OR coronavirus[Title/Abstract] OR COVID-19[Title/Abstract])[Title/Abstract] AND (portable[Title/Abstract] OR hand-held[Title/Abstract] OR handheld[Title/Abstract] OR pocket-size[Title/Abstract] OR visual stethoscope)[Title/Abstract] AND (ultrasound[Title/Abstract] OR ultrasonography[Title/Abstract] OR visual stethoscope)[Title/Abstract].

2.2. Study Selection

Our predetermined list of exclusions included:

(1) non-English study;
(2) impossible to obtain the full-text considering the university subscription to bibliographic databases or the request submitted to the first or the corresponding author, or payment for the full-text article;
(3) article type (e.g., opinion of the experts, editorials, case reports, abstracts, commentary, book chapters, etc.);
(4) not truly-portable ultrasound devices or portable US devices (at the size of a laptop);
(5) no comparison of hand-held ultrasound examination with physical examination, biological testing or other imaging methods (e.g., X-ray, conventional US, computer tomography (CT), etc.);

(6) lung ultrasound performed by non-doctors (e.g., medical students, nurses) or using portable US devices (small devices compared to the console-style ultrasound machines that can be carried out by hand);
(7) the studies not applied to human subjects. Duplicated studies were excluded during the screening.

The articles' selection involved a two-step screening process and was conducted after eliminating the duplicated titles using the Conditional Formatting features of Microsoft Excel. In the first step of screening, two independent researchers screened each article's titles and abstracts for relevancy to hand-held US screening of peripheral lung diseases. In the second step, the full texts were screened by two independent researchers who assessed the studies for inclusion. In both screening steps, any disagreement was resolved by the intervention of a third independent reviewer, if necessary.

Articles that described hand-held lung ultrasounds performed by non-doctors (e.g., medical students, nurses), those that referred to veterinary medicine, or those that involved were excluded.

2.3. Data Extraction

Data extraction was performed using a self-developed extraction form. The following data were extracted independently by two individual researchers:

(1) study settings (e.g., when?, where?);
(2) study design (e.g., target condition, index test, comparative test, methods to estimate the accuracy of the hand-held US, etc.);
(3) study results (e.g., eligible subjects, evaluated subjects, characteristics of the evaluated patients, accuracy parameters).

2.4. Quality of Reporting Assessment

The quality of the studies included in the systematic review was evaluated by the QUADAS-2 tool (Quality Assessment of Diagnostic Accuracy Studies 2) [17].

2.5. Presentation of the Findings

The results were reported using a narrative method: tabulation of the study characteristics (e.g., year, country/region, condition studied, etc.), diagnosis methods (index test and comparator test), characteristics of the sample (e.g., number of participants, age, gender), and reported accuracy methods. The evaluated risk of bias and applicability was conducted for the following domains: patients selection, index test, reference standard, flow and timing.

3. Results

Four hundred and fifty-three articles were retrieved from all search bibliographic databases and 15 studies were evaluated (Figure 1): Bedetti et al. [18], Kajimoto et al. [19], Lisi et al. [20], Cogliati et al. [21], Filopei et al. [22], Platz et al. [23], Sforza et al. [24], Phillips and Manning [25], Bobbia et al. [26], Bensted et al. [27], Lima et al. [28], Newhouse et al. [29], Jalil et al. [30] Dini et al. [31], Bennett et al. [32].

Five out of the 15 studies were conducted in Italy [15,17,18,25,32,33] and in most cases, eligible subjects on a specific period of time [23–26,28,30–32] were evaluated with a hand-held US device (Table 1). In the majority of cases, the role of the index test (namely HHUS, hand-held ultrasound) was diagnostic [19–24,26,27,30,32,33] followed by screening [28,29,32] and only one study as triage [24]. One of the included studies was a pilot study (Bobbia et al. [26]).

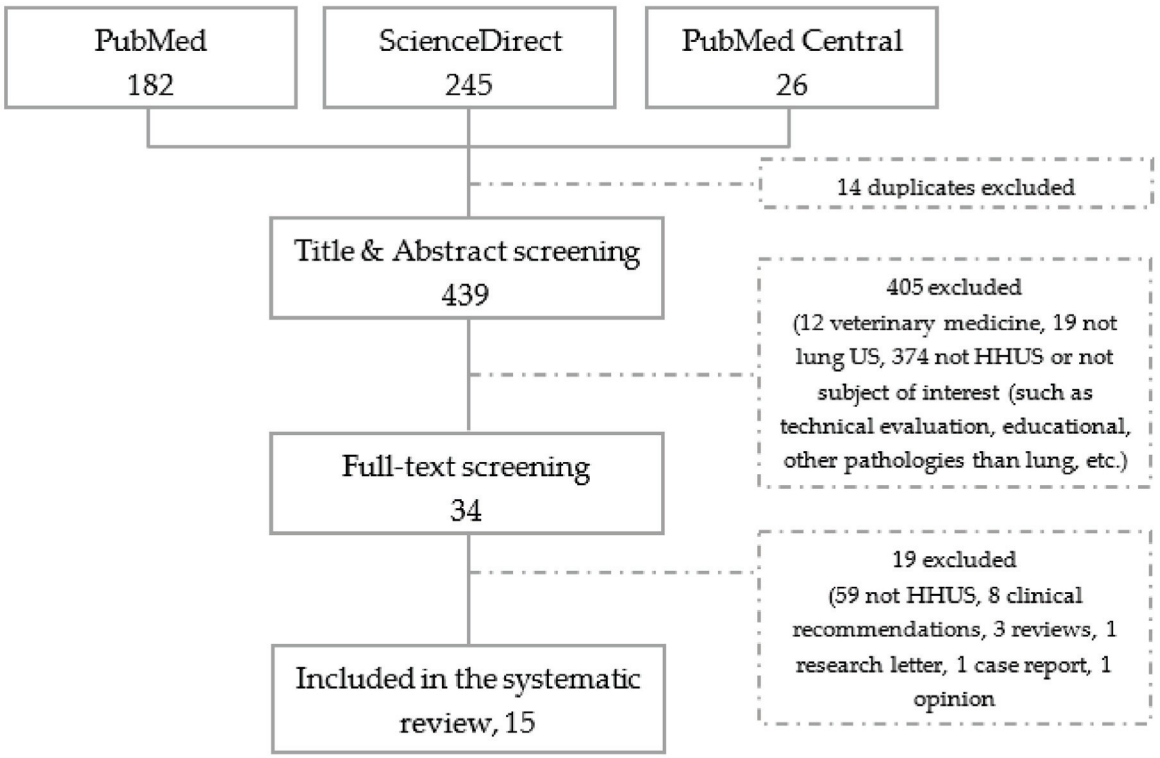

Figure 1. Flowchart of the literature screening (HHUS = Hand-Held UltraSound).

Table 1. Characteristics of the reviewed studies.

Study, Year [Ref.]	Location	Sign/Disease	Index Test Device	Comparator Test
Bedetti et al., 2006 [18]	Pisa, Italy	ultrasound lung comets (ULC) (extravascular lung water)	Optigo (Philips, Andover, MA, USA) ("low-tech beginner")	conventional US
Kajimoto et al., 2012 [19]	Tokyo, Japan	pulmonary disease	Vscan (GE Healthcare, Japan)	chest X-ray
Lisi et al., 2012 [20]	Siena, Italy	pleural effusion	Vscan, Horten, Norway (1.7–3.8 MHz)	chest X-rays
Cogliati et al. 2014 [21]	Milan, Italy	interstitial lung disease in patients with rheumatoid arthritis	VSCAN, GE Healthcare, Fairfield, CT, USA) supporting a phased array transducer (1.7–3.8 MHz).	conventional US, high-resolution CT
Filopei et al., 2014 [22]	New York City, NY, USA	Dyspnea *	Vscan; GE Vingmed Ultrasound, Horten, Norway	chest X-ray, CT
Platz et al., 2015 [23]	unclear	pulmonary edema—heart failure	VScan, General Electric	conventional US
Sforza et al., 2017 [24]	Italy	acute or worsening of chronic dyspnea	Vscan (General Electric Healthcare	chest X-ray

Table 1. *Cont.*

Study, Year [Ref.]	Location	Sign/Disease	Index Test Device	Comparator Test
Phillips and Manning, 2017 [25]	Boston, MA, USA	interstitial edema, pleural effusion, pneumonia, and the presence of a central line	Vscan (GE Vingmed Ultrasound A/S, Horten, Norway)	chest X-ray and conventional transthoracic echocardiography (TTE)
Bobbia et al., 2018 [26]	France	acute respiratory failure	Vscan Dual probe, GE Hea	CT, conventional US
Bensted et al., 2018 [27]	Sydney, Australia	pneumothorax after transbronchial lung biopsy	Vscan; GE Healthcare, Chicago, IL, USA)	chest X-ray
Lima et al., 2019 [28]	Nepal	subclinical pulmonary edema on healthy volunteers	iViz (FUJIFILM SonoSite, Inc)	Ancillary measurements included pulse oximetry (SpO2; %), heart rate (HR; /min), and blood pressure (BP; mmHg)
Newhouse et al. 2020 [29]	Adelaide, SA, Australia	unilateral pleural effusion	Signostics Uscan© hand-held US	conventional US
Jalil et al., 2020 [30]	TX, USA	SARS-CoV-2 pneumonia	Vscan Extend Dual Probe, GE	chest X-ray, SARS-CoV-2 PCR testing
Dini et al. 2020 [31]	Pavia, Italy	COVID-19 pneumonia	CERBERO (ATL, Milano, Italy)	nasopharyngeal swab testing for COVID-19
Bennett et al. 2021 [32]	Siena, Italy	COVID-19 pneumonia	Butterfly iQ	conventional US

* (1) exacerbation of chronic obstructive pulmonary disease or asthma (COPD/asthma), (2) acute pulmonary edema (APE), (3) pneumonia (PNA), (4) pulmonary embolus (PE), (5) pneumothorax (PTX), (6) pleural effusion (PLEFF), and (7) other (OTH), namely anemia, ascites, and dehydration.

The number of eligible participants were reported by four studies and were equal with 39 (Cogliati et al. 2014 [21]), 37 (Platz et al., 2015 [23]), 198 (Bensted et al., 2018 [27]) and 54 (Newhouse et al. 2020 [29]). The evaluated sample ranged from 18 (Bennett et al. 2021 [32]) to 165 (Bensted et al., 2018 [27]) (Table 2). The characteristics of the evaluated subjects and the reported metrics for assessing the accuracy are summarized in Table 2.

Table 2. Demographics of the evaluated subjects and reported accuracy metrics.

Study, Year [Ref.]	Sample Size	Age, Years	Men	Accuracy Metric
Bedetti et al., 2006 [18]	20	66 ± 12	18 (90.0)	Feasibility: 100%; Mean ULCs: 35.7 ± 25.3 ("high-tech veteran") vs. 34.2 ± 26.8 ("low-tech beginner")
Kajimoto et al., 2012 [19]	90	78.1 ± 9.9	45 (50.0)	Se = 96.2%, Sp = 54.0%, NPV = 90.9%, PPV = 75.0%,
Lisi et al., 2012 [20]	73	68.4 ± 9.2	41 (56.2)	AUC = 0.99, Se = 91.7%, Sp = 99.9% for PE (pleural effusion) >100 mL
Cogliati et al., 2014 [21]	29	64.87 ± 9.9 *n* = 39	10 (25.6) *n* = 39	LUS using a PS-USD: Se = 89% (95%CI = [68 to 100]), Sp = 50% [28 to 72], *n* = 29
Filopei et al., 2014 [22]	69	69 ± n.a.	(52.2)	Se = 36% and Sp = 100% for pneumonia—focus training group vs. Se = 89% and Sp = 100% for pulmonary edema—extended training group

Table 2. *Cont.*

Study, Year [Ref.]	Sample Size	Age, Years	Men	Accuracy Metric
Platz et al., 2015 [23]	21	73 (36 to 86)	17 (81)	number of B-lines: Wilcoxon signed-rank test
Sforza et al., 2017 [24]	68	78 ± 12	43 (62)	Se = 92.6% [74.2 to 98.7], Sp = 80.5% [64.6 to 90.6], PPV = 75.8% [57.4 to 88.2], NPV = 94.3% [79.5 to 99], Acc = 85.3% for interstitial syndrome / effusion
Phillips and Manning, 2017 [25]	64 *	70 ± 15	n.a.	Concordance PS-USD—X-rays: 80% (interstitial edema), 77% (pleural effusion), 92% (pneumonia), 81% (central line)
Bobbia et al., 2018 [26]	10	62 ± 16	5 (50)	Kappa coefficient PUD—CT using vascular probe (6–14 MHz): 0.62 [0.37 to 0.86] for experts and 0.68 [0.44 to 0.91] for trained physicians
Bensted et al., 2018 [27]	165	44 (mean value)	80 (48.5)	Se = 75%, Sp = 93%, PPV = 35%, NPV = 99%
Lima et al., 2019 [28]	20	24.7 ± 5.8	9 (45)	B-line Scores at different altitude: 3 (1400m), 0 (3440 m), 1 (3820 m), 17 (4240m), 12 (5160m)
Newhouse et al., 2020 [29]	53	72.9 ± 12.7	27 (50)	No accuracy assessment; image ratings
Jalil et al., 2020 [30]	69	64 ± n.a.	34 (49)	LUS vs. RT-PCR testing: Se = 91%, Sp = 86%, PPV = 86%, NPV = 91%
Dini et al., 2020 [31]	150	88 ± n.a.	n.a. (15)	Se = 79% in predicting positive naso-pharyngeal testing, Sp = 57%, PPV = 74%, NPV = 62%
Bennett et al., 2021 [32]	18	77.6 ± 10	14 (n.a.)	PS-USD vs. conventional US: Pearson correlation coefficient 0.99, Bland–Altman bias close to zero (absolute level of bias—0.016)

Age is reported as mean±standard deviation or median (range), where range = (first quartile to thirs quartile); n.a. = not available; Data regarding the men are reported as number (%); 95% confidence intervals [lower bound to upper bound]; * 108 examinations; ULCs = ultrasound lung comets; Acc = accuracy; Se = sensitivity; Sp = specificity; NPV = negative predictive value; PPV = positive predictive value; PUD = pocket ultrasound device; LUS = lung ultrasound; PS-USD = pocket-size ultrasound device; CT = computed tomography; RT-PCR = reverse transcriptase-polymerase chain reaction.

Seven studies included in the analysis had a low risk of bias, and they had a low risk of applicability concerns (Table 3).

Table 3. QUADAS-2 quality assessments of evaluated studies.

Study, Year [Ref]	Risk of Bias				Applicability Concerns			Comments
	Patient Selection	Index Test	Comparator test	Flow and Timing	Patient Selection	Index Test	Comparator Test	
Bedetti et al., 2006 [18]	unclear	unclear	unclear	low	low	low	low	
Kajimoto et al., 2012 [19]	unclear	low	low	low	low	low	low	
Lisi et al., 2012 [20]	low	low	low	low	low	low	low	X-ray followed by hand-held US

Table 3. *Cont.*

Study, Year [Ref]	Risk of Bias				Applicability Concerns			Comments
	Patient Selection	Index Test	Comparator test	Flow and Timing	Patient Selection	Index Test	Comparator Test	
Cogliati et al., 2014 [21]	low	low	low	low	low	low	low	A short-trained physician, who underwent two sessions of 3h each for recognition of B-lines
Filopei et al., 2014 [22]	low	high	low	low	low	low	low	Brief report
Platz et al., 2015 [23]	low	low	low	low	low	low	low	
Sforza et al., 2017 [24]	low	low	low	low	low	low	low	
Phillips and Manning, 2017 [25]	low	low	unclear	unclear	low	low	low	Different results reported in the abstract and in the body of the manuscript
Bobbia et al., 2018 [26]	low	high	unclear	low	low	low	low	
Bensted et al., 2018 [27]	low	low	low	low	low	low	low	17 patients with pneumothorax
Lima et al., 2019 [28]	low	low	low	low	low	low	low	
Newhouse et al., 2020 [29]	low	low	low	low	low	low	low	
Jalil et al., 2020 [30]	high	low	low	low	low	low	low	
Dini et al., 2020 [31]	low	low	low	unclear	low	low	low	
Bennett et al., 2021 [32]	unclear	low	low	low	low	low	low	Two different operators, both experts in lung ultrasound

4. Discussion

4.1. Main Findings

The studies included in this systematic review have significant heterogeneity regarding the evaluated pathology, sample size, performance metrics, and comparators but indicate the utility of hand-held lung ultrasound. Less than half (seven studies) of the evaluated studies showed a low QUADAS-2 risk of bias, and in most of the cases, the studies with low risk of bias evaluated less than 30 patients with limited generalizability of reported results. As the hand-held US devices emerge towards the point-of-care examination, these technical solutions must be evaluated to show their clinical utility, relevance, and diagnosis accuracy.

4.1.1. Hand-held Ultrasound and Physical Examination

Overall, hand-held ultrasound (HHUS) devices have been shown to have superior accuracy when compared with physical examination. Filopei et al. [22] showed that residents, after undergoing a brief training in lung ultrasound, are significantly better at diagnosing acute pulmonary edema, pneumonia, and pleural effusions than when they use physical examination alone. Melbye [33] and Gustafsson et al. [34] also consider that lung auscultation for rales and crackles, as well as other clinical data, are not reliable and do not have sufficient sensitivity nor specificity for identifying patients with lung disease. Gustafsson et al. [34] also showed the reliability of the HHUS in the identification of the pulmonary congestion signs.

4.1.2. Hand-Held Ultrasound and Thoracic Radiography

Philips and Manning [25] found a good concordance between X-rays and lung HHUS for various lung diseases, such as pneumonia, pleural effusions, and interstitial lung diseases. They also found that lung ultrasound might anticipate the resolution of pulmonary edema faster than chest X-ray [25]. Bensted et al. [27] and Kajimoto et al. [19] reported lower positive predictive values opposite to the negative predictive value, which was very high. A possible explanation is that small subpleural lesions can be seen better with the help of ultrasound while being overlooked by chest X-ray, accounting for a higher rate of false positives if using chest X-ray as a comparator. This finding supported the results reported by Bourcier et al. [35], who used a portable ultrasound device and chest X-ray examinations with patients who had already been diagnosed with acute pneumonia (Se = 95% for ultrasound examination, and 60% for the chest X-ray $p < 0.05$; NPV = 65% for lung ultrasound against 25% for radiography, $p < 0.05$). Filopei et al. [22] showed that peripheral lesions (e.g., Kerley B lines, pleural effusions, subpleural consolidations) could be detected by HHUS with higher accuracy than deeper lesions (e.g., chronic broncho-obstructive pulmonary disease).

In all articles included in this review, only lesions present in the superficial (subpleural) areas of the lung can be visualized with HHUS, which is consistent with prior research. The sensitivity of lung ultrasound may be higher for peripheral lesions than in the case of X-rays, and this makes ultrasound particularly suitable for detecting COVID-19 lesions, which evolve in a centripetal direction (start in the periphery and spread towards the central part of the lung). This means lung involvement in COVID-19 infection could be detected early, possibly with greater sensitivity than with X-ray examination but also with a risk of false positives that needs to be further investigated. These results are in line with the findings reported in a meta-analysis that compared the accuracy of chest X-ray and LUS for diagnosing acute pulmonary edema, reporting that lung ultrasound can diagnose 15 more cases than chest X-ray without an increase in the number of false positives [36]. Future prospective studies would be useful to determine if lung ultrasound in the initial evaluation of suspected acute pulmonary edema patients improves diagnosis, treatment, and outcomes of these patients, even for conventional or pocket-size US devices.

4.1.3. Hand-Held Ultrasound and Computed Tomography

Thoracic CT is usually seen as the gold standard when investigating lung pathology, but it is not always the first choice because of the risk of radioactive exposure, especially in high-risk groups (e.g., children, pregnant women), and the examination requires high costs [37]. Similarly, critically ill patients whose conditions can change rapidly demand repeated examinations. HHUS has proven high sensitivity, and low specificity for identifying interstitial lung disease when comparing lung HHUS with high-resolution CT and with high concordance between HHUS and CT was high [21]. In the same study, pocket-size ultrasound devices were found to provide a diagnostic yield similar to higher-level devices [21]. Bobbia et al. [26] compared the accuracy of various types of ultrasound probes while using CT as a gold standard with both experienced and novice physicians and find a good concordance only with trained and expert physicians. The agreement between

LUS and CT was poor for residents, revealing the necessity for training standards for novices [26]. Buonsenso et al. [38] reported conventional lung ultrasound (LUS) as more sensitive than chest X-ray for diagnosing COVID-19 lesions with a high correlation between LUS and CT on this category of patients.

4.1.4. Hand-Held Ultrasound and High-End Ultrasound

Tight concordance between HHUS and high-end ultrasound evaluations is reported in the scientific literature, even when comparing experts using a high-tech device with beginners using a hand-held ultrasound device [18]. A possible explanation is the fact that lung ultrasound is easier to perform than other types of ultrasound. Furthermore, the HHUS devices incorporate algorithms that guide the users towards the image. Bennett et al. [32] reported an absolute level of bias equal to −0.0016 (995 confidence interval [−0.054 to 0.021], Bland-Altman method) when the LUS score was compared to a pocket-sized ultrasound score on patients with COVID-19. Furthermore, a high concordance was reported between the two methods (0.990, 95%CI [0.980 to 0.995]) [32]. The Bennett et al. [32] study was cited in a NICE (National Institute for Health and Care Excellence) medtech innovation briefing on nice.org.uk [39]. Burleson et al. [40] reported the use of Butterfly iQ+ device in rural east Africa (no comparator) on evaluation of different systems (e.g., pulmonary, cardiac, abdominal, and musculoskeletal). Five emergency physicians evaluated the performance of the Butterfly iQ+. They considered that it performed well and met their needs for point-of-care ultrasound. The use of the same probe for whole-body scanning, good image quality for most indications, and the low cost were the main advantages of the Butterfly iQ+ device. Disadvantages included lower quality for cardiac imaging and frequent overheating, which means the investigator needs to pause the examination to wait for the cooling of the device [40]. In Saudi Arabia, the same device was used by Rajendram et al. [41] to assess the presence of shunts using saline microbubble enhanced transthoracic echocardiography and lung ultrasound, suggesting the usefulness of this combined approach in the identification of the shunt etiology. An ongoing study evaluates the utility of self-administrated LUS under teleguidance from a medical professional of the same device (Butterfly iQ+) on COVID-19 positive subjects [42].

4.2. Lung Ultrasound in Systematic Reviews

Trauer et al. assessed the utility of conventional LUS in COVID-19, showing higher sensitivity than chest X-ray and possibly than CT [43]. The systematic review reported by Hew et al. [44] showed high sensitivity (from 0.91 to 1.00) and moderate specificity (from 0.78 to 1.00) of chest ultrasound examination in the identification of radiological consolidations in patients with acute respiratory failure. However, all evaluated studies were with a high risk of bias and thus questionable regarding the applicability. Hew et al. [44] highlighted the necessity to report the time when the ultrasound examination was performed because the more time elapses before performing the ultrasound examination, the more likely it is that the lesions would progress to a detectable extent without improving patient outcome. This boosts ultrasound sensitivity, overstating its utility as an initial test. Additionally, analyzing lung regions instead of lungs as a whole inflates specificity, giving the misleading appearance of increased precision [44]. Further studies should be conducted using patients as the unit of analysis, since they are the unit of clinical management.

4.3. Key Advantages of Hand-Held Ultrasound Devices for Lung Scanning

Pocket-size ultrasound devices can be adequately cleaned and disinfected from one examination to the next one. In contrast with a high-end ultrasound device, a smaller machine can be fully covered by a protective sheath that can be changed after each use [45]. The use of CT scans and multiple chest X-rays requires the transportation of the patient to the radiology department, increasing the risk of contamination, while pocket-size ultrasound provides point-of-care examinations [46].

Another advantage of lung ultrasound is the monitoring of the disease progression, enabling repeated examinations at every change of the clinical presentation or evaluating treatment efficacy. This is even more important in vulnerable populations, such as pregnant women and children, in whom exposure to radiation can thus be avoided. The performance of hand-held ultrasound devices for lung imaging offers a solution for the challenges posed by traditional imaging methods.

4.4. Technological Advancement in Lung Ultrasound

The developers of conventional and hand-held ultrasound devices currently explore the inclusion of artificial intelligence (AI) to increase image quality and assisted diagnosis. Roy et al. [47] developed and used a deep learning (DP) algorithm to estimate pixel-level segmentation translated in the overall pathological score [16] of LUS images on COVID-19 positive patients. The higher reported accuracy was 0.96, but external validation using a larger database is needed to validate the proposed DP algorithm. Evans et al. [48] reported the LUS evaluation with robotic ultrasound equipment that allows the sonographer to perform an examination using a robotic arm located at the patient's bedside, enabling a minimal exposure to disease.

Artificial intelligence algorithms were also used to automatically count LUS B lines and consolidations, using the data to calculate a lung score that indicates the severity of infection [11]. The same team is also working on advanced apps for its hand-held systems called Vscan [11] allowing inexperienced users to perform high-quality examinations. Philips created the Anatomically Intelligent Ultrasound suite technology, recreating the optimal version of the diagnostic view, automatically computing measurements three to six times faster than manual methods [49].

4.5. Downsides of Hand-Held Ultrasound Devices

Despite their advantages, the hand-held probes also have some disadvantages that must be listed [50]:

- Battery life is reduced (2–3 h), and recharging takes approximately 6 h
- Inability to perform prolonged scanning because of overheating, with temperatures rising after 15–20 min, which freezes all imaging until the device has cooled down
- Inferior image quality reported by a majority of users
- It is impossible to perform a comprehensive ultrasound examination because of the lack of spectral Doppler, tissue Doppler and other specific measurements offered by fully-featured conventional devices. However, this is not necessarily applied for lung ultrasound, which does not usually require advanced US techniques.

4.6. Limitations of the Study

This article provides a comprehensive view of the application of hand-held ultrasound devices in the evaluation of lung lesions, comparing this method with imaging techniques used in clinical practice.

However, some limitations of our study must be listed. First, the used search string did not include all types of lung pathology, limiting the reported findings to the peripheral lung lesions. Thus, the presented results cannot be generalized to all pulmonary diseases. Second, since the technology is still emerging, the number of studies included in the systematic review is limited. Considering the small number of studies and diversity of comparators, the heterogeneity between studies is high. The different parameters that were assessed by each study prevented meta-analysis and limited comparisons between studies. The various lung lesions identified during ultrasound lung examinations, such as B-lines and lung effusion, have relatively low specificity and can be observed in several lung or cardiac diseases. Third, although the risk of bias regarding the patient selection, index test, comparator test, and timing of the investigation was assessed to be low, the QUADAS-2 tool does not evaluate the blinding of the examiners. Unclear or incomplete blinding to clinical or comparator examination may have influenced outcomes. Forth, not all of the

hand-held ultrasound devices listed in our study (e.g., Optigo) are still on the market from when the study was conducted. Another device that was used in one of the presented studies, Uscan, was designed for urological examination and not for pulmonary imaging. Some devices, which have been shown to have very good image quality and for which we have not identified studies conducted on lung pathology, are not present in this review.

5. Conclusions

Being accessible, radiation-free, and—due to its small size—theoretically easy to decontaminate, hand-held ultrasound devices could represent a reliable evaluation method for peripheral lung diseases. However, further research is needed to clarify their accuracy, reliability, and reproducibility. In the case of peripheral lung lesions, hand-held ultrasound can be successfully employed as an alternative to repeated X-ray examinations.

Author Contributions: M.H.-H. Conceptualization; S.D.B. methodology; S.D.B. validation; L.M.L., S.D.B. and M.H.-H. formal analysis; M.H.-H. writing—original draft preparation; S.D.B., L.M.L. writing—review and editing; S.D.B. supervision; S.D.B. project administration. All authors have read and agreed to the published version of the manuscript.

Funding: This research received no external funding.

Institutional Review Board Statement: Not applicable.

Informed Consent Statement: Not applicable.

Conflicts of Interest: The authors declare no conflict of interest.

References

1. Lichtenstein, D.A.; Mezière, G.A. Relevance of Lung Ultrasound in the Diagnosis of Acute Respiratory Failure: The BLUE Protocol. *Chest* **2008**, *134*, 117–125. [CrossRef]
2. Lichtenstein, D.A.; Malbrain, M.L. Lung ultrasound in the critically ill (LUCI): A translational discipline. *Anestezjol. Intens Ter.* **2017**, *49*, 430–436. [CrossRef]
3. Siemens Healthineers. White Paper: Lung Ultrasound in Patients with Coronavirus COVID-19 Disease. Dirk-André Clevert. Available online: https://www.siemens-healthineers.com/ro/ultrasound/lung-ultrasound-covid-19 (accessed on 19 September 2020).
4. Volpicelli, G.; International Liaison Committee on Lung Ultrasound (ILC-LUS) for the International Consensus Conference on Lung Ultrasound (ICC-LUS); Elbarbary, M.; Blaivas, M.; Lichtenstein, D.A.; Mathis, G.; Kirkpatrick, A.W.; Melniker, L.; Gargani, L.; Noble, V.E.; et al. International evidence-based recommendations for point-of-care lung ultrasound. *Intensiv. Care Med.* **2012**, *38*, 577–591. [CrossRef] [PubMed]
5. Buda, N.; Kosiak, W.; Radzikowska, E.; Olszewski, R.; Jassem, E.; Grabczak, E.M.; Pomiecko, A.; PiotrkowskI, J.; Piskunowicz, M.; Sołtysiak, M.; et al. Polish recommendations for lung ultrasound in internal medicine (POLLUS-IM). *J. Ultrason.* **2018**, *18*, 198–206. [CrossRef]
6. Radzina, M.; Biederer, J. Ultrasonography of the Lung. *RöFo* **2019**, *191*, 909–923. [CrossRef] [PubMed]
7. Buda, N.; Kosiak, W.; Wełnicki, M.; Skoczylas, A.; Olszewski, R.; Piotrkowski, J.; Skoczyński, S.; Radzikowska, E.; Jassem, E.; Grabczak, E.M.; et al. Recommendations for Lung Ultrasound in Internal Medicine. *Diagnostics* **2020**, *10*, 597. [CrossRef]
8. Peng, Q.-Y.; Chinese Critical Care Ultrasound Study Group (CCUSG); Wang, X.-T.; Zhang, L.-N. Findings of lung ultrasonography of novel corona virus pneumonia during the 2019–2020 epidemic. *Intensiv. Care Med.* **2020**, *46*, 849–850. [CrossRef]
9. Huang, Y.; Wang, S.; Liu, Y.; Zhang, Y.; Zheng, C.; Zheng, Y.; Zhang, C.; Min, W.; Yu, M.; Hu, M. A Preliminary Study on the Ultrasonic Manifestations of Peripulmonary Lesions of Non-Critical Novel Coronavirus Pneumonia (COVID-19). *SSRN Electron. J.* **2020**, 3544750. [CrossRef]
10. Poggiali, E.; Dacrema, A.; Bastoni, D.; Tinelli, V.; Demichele, E.; Ramos, P.M.; Marcianò, T.; Silva, M.; Vercelli, A.; Magnacavallo, A. Can Lung US Help Critical Care Clinicians in the Early Diagnosis of Novel Coronavirus (COVID-19) Pneumonia? *Radiology* **2020**, *295*, E6. [CrossRef] [PubMed]
11. Zorpette, G. Portable Ultrasound Proves a Potent Weapon in the Fight Against COVID-19. IEEE Spectrum. 2020. Available online: https://spectrum.ieee.org/the-human-os/biomedical/imaging/portable-ultrasound-proves-potent-weapon-fight-against-covid19 (accessed on 22 April 2021).
12. Ong, S.; Tan, Y.K.; Chia, P.Y.; Lee, T.H.; Ng, O.T.; Wong, M.S.Y.; Marimuthu, K. Air, Surface Environmental, and Personal Protective Equipment Contamination by Severe Acute Respiratory Syndrome Coronavirus 2 (SARS-CoV-2) from a Symptomatic Patient. *JAMA* **2020**, *323*, 1610. [CrossRef] [PubMed]
13. Kim, D.J.; Jelic, T.; Woo, M.Y.; Heslop, C.; Olszynski, P. Just the Facts: Recommendations on point-of-care ultrasound use and machine infection control during the Coronavirus Disease 2019 pandemic. *CJEM* **2020**, *22*, 445–449. [CrossRef] [PubMed]

14. Buonsenso, D.; Piano, A.; Raffaelli, F.; Bonadia, N.; de Gaetano Donati, K.; Franceschi, F. Point-of-care lung ultrasound find-ings in novel coronavirus disease-19 pnemoniae: A case report and potential applications during COVID-19 outbreak. *Eur. Rev. Med. Pharmacol. Sci.* **2020**, *24*, 2776–2780. [CrossRef] [PubMed]
15. Buonsenso, D.; Pata, D.; Chiaretti, A. COVID-19 outbreak: Less stethoscope, more ultrasound. *Lancet Respir. Med.* **2020**, *8*, e27. [CrossRef]
16. Soldati, G.; Smargiassi, A.; Inchingolo, R.; Buonsenso, D.; Perrone, T.; Briganti, D.F.; Perlini, S.; Torri, E.; Mariani, A.; Mossolani, E.E.; et al. Proposal for International Standardization of the Use of Lung Ultrasound for Patients With COVID-19. *J. Ultrasound Med.* **2020**, *39*, 1413–1419. [CrossRef]
17. Whiting, P.F.; Rutjes, A.W.S.; Westwood, M.E.; Mallett, S.; Deeks, J.J.; Reitsma, J.B.; Leeflang, M.M.G.; Sterne, J.A.C.; Bossuyt, P.M.M.; The QUADAS-2 Group. QUADAS-2: A Revised Tool for the Quality Assessment of Diagnostic Accuracy Studies. *Ann. Intern. Med.* **2011**, *155*, 529–536. [CrossRef] [PubMed]
18. Bedetti, G.; Gargani, L.; Corbisiero, A.; Frassi, F.; Poggianti, E.; Mottola, G. Evaluation of ultrasound lung comets by hand-held echocardiography. *Cardiovasc. Ultrasound* **2006**, *4*, 34. [CrossRef] [PubMed]
19. Kajimoto, K.; Madeen, K.; Nakayama, T.; Tsudo, H.; Kuroda, T.; Abe, T. Rapid evaluation by lung-cardiac-inferior vena cava (LCI) integrated ultrasound for differentiating heart failure from pulmonary disease as the cause of acute dyspnea in the emergency setting. *Cardiovasc. Ultrasound* **2012**, *10*, 49. [CrossRef]
20. Lisi, M.; Cameli, M.; Mondillo, S.; Luzzi, L.; Zacà, V.; Cameli, P.; Gotti, G.; Galderisi, M. Incremental value of pocket-sized imaging device for bedside diagnosis of unilateral pleural effusions and ultrasound-guided thoracentesis. *Interact. Cardiovasc. Thorac. Surg.* **2012**, *15*, 596–601. [CrossRef]
21. Cogliati, C.; Antivalle, M.; Torzillo, D.; Birocchi, S.; Norsa, A.; Bianco, R.; Costantino, G.; Ditto, M.C.; Battellino, M.; Sarzi-Puttini, P.; et al. Standard and pocket-size lung ultrasound devices can detect interstitial lung disease in rheumatoid arthritis patients. *Rheumatology* **2014**, *53*, 1497–1503. [CrossRef]
22. Filopei, J.; Siedenburg, H.; Rattner, P.; Fukaya, E.; Kory, P. Impact of pocket ultrasound use by internal medicine housestaff in the diagnosis of Dyspnea. *J. Hosp. Med.* **2014**, *9*, 594–597. [CrossRef]
23. Platz, E.; Pivetta, E.; Merz, A.; Peck, J.; Rivero, J.; Cheng, S. Impact of device selection and clip duration on lung ultrasound assessment in patients with heart failure. *Am. J. Emerg. Med.* **2015**, *33*, 1552–1556. [CrossRef] [PubMed]
24. Sforza, A.; Mancusi, C.; Carlino, M.V.; Buonauro, A.; Barozzi, M.; Romano, G.; Serra, S.; De Simone, G. Diagnostic performance of multi-organ ultrasound with pocket-sized device in the management of acute dyspnea. *Cardiovasc. Ultrasound* **2017**, *15*, 16. [CrossRef]
25. Phillips, C.T.; Manning, W.J. Advantages and pitfalls of pocket ultrasound vs daily chest radiography in the coronary care unit: A single-user experience. *Echocardiography* **2017**, *34*, 656–661. [CrossRef]
26. Bobbia, X.; Chabannon, M.; Chevallier, T.; de La Coussaye, J.E.; Lefrant, J.Y.; Pujol, S.; Claret, P.-G.; Zieleskiewicz, L.; Roger, C.; Muller, L. Assessment of five different probes for lung ultrasound in critically ill patients: A pilot study. *Am. J. Emerg. Med.* **2018**, *36*, 1265–1269. [CrossRef]
27. Bensted, K.; McKenzie, J.; Havryk, A.; Plit, M.; Ben-Menachem, E. Lung Ultrasound After Transbronchial Biopsy for Pneumothorax Screening in Post–Lung Transplant Patients. *J. Bronchology Interv. Pulmonol.* **2018**, *25*, 42–47. [CrossRef] [PubMed]
28. Lim, R.; Ma, I.W.; Brutsaert, T.D.; Nysten, H.E.; Nysten, C.N.; Sherpa, M.T.; Day, T.A. Transthoracic sonographic assessment of B-line scores during ascent to altitude among healthy trekkers. *Respir. Physiol. Neurobiol.* **2019**, *263*, 14–19. [CrossRef]
29. Newhouse, S.M.; Effing, T.W.; Dougherty, B.D.; Costa, J.A.D.A.; Rose, A.R. Is Bigger Really Better? Comparison of Ultraportable Handheld Ultrasound with Standard Point-of-Care Ultrasound for Evaluating Safe Site Identification and Image Quality prior to Pleurocentesis. *Respiration* **2020**, *99*, 325–332. [CrossRef]
30. Jalil, B.A.; Khan, A.; Kugasia, I.R.; Ijaz, M. Lung ultrasound in early SARS-CoV-2 pneumonia and the LUS-CoV criteria. *Bayl. Univ. Med. Cent. Proc.* **2021**, *34*, 1–4. [CrossRef] [PubMed]
31. Dini, F.L.; Bergamini, C.; Allegrini, A.; Scopelliti, M.; Secco, G.; Miccoli, M.; Boni, S.; Brigada, R.; Perlini, S. Bedside wireless lung ultrasound for the evaluation of COVID-19 lung injury in senior nursing home residents. *Monaldi Arch. Chest Dis.* **2020**, *90*, 1446. [CrossRef]
32. Bennett, D.; De Vita, E.; Mezzasalma, F.; Lanzarone, N.; Cameli, P.; Bianchi, F.; Perillo, F.; Bargagli, E.; Mazzei, M.A.; Volterrani, L.; et al. Portable Pocket-Sized Ultrasound Scanner for the Evaluation of Lung Involvement in Coronavirus Disease 2019 Patients. *Ultrasound Med. Biol.* **2021**, *47*, 19–24. [CrossRef] [PubMed]
33. Melbye, H. Lungeauskultasjonen–fortsatt en nyttig undersøkelse? [Auscultation of the lungs—Still a useful examination?]. *Tidsskr. Nor. Laegeforen.* **2001**, *121*, 451–454. [PubMed]
34. Gustafsson, M.; Alehagen, U.; Johansson, P. Imaging Congestion With a Pocket Ultrasound Device: Prognostic Implications in Patients With Chronic Heart Failure. *J. Card. Fail.* **2015**, *21*, 548–554. [CrossRef] [PubMed]
35. Bourcier, J.-E.; Braga, S.; Garnier, D. Lung Ultrasound Will Soon Replace Chest Radiography in the Diagnosis of Acute Community-Acquired Pneumonia. *Curr. Infect. Dis. Rep.* **2016**, *18*, 43. [CrossRef] [PubMed]
36. Maw, A.M.; Hassanin, A.; Ho, P.M.; McInnes, M.D.F.; Moss, A.; Juarez-Colunga, E.; Soni, N.J.; Miglioranza, M.H.; Platz, E.; DeSanto, K.; et al. Diagnostic Accuracy of Point-of-Care Lung Ultrasonography and Chest Radiography in Adults With Symptoms Suggestive of Acute Decompensated Heart Failure. *JAMA Netw. Open* **2019**, *2*, e190703. [CrossRef]

37. Xia, Y.; Ying, Y.; Wang, S.; Li, W.; Shen, H. Effectiveness of lung ultrasonography for diagnosis of pneumonia in adults: A systematic review and meta-analysis. *J. Thorac. Dis.* **2016**, *8*, 2822–2831. [CrossRef] [PubMed]
38. Buonsenso, D.; Raffaelli, F.; Tamburrini, E.; Biasucci, D.G.; Salvi, S.; Smargiassi, A.; Inchingolo, R.; Scambia, G.; Lanzone, A.; Testa, A.C.; et al. Clinical role of lung ultrasound for diagnosis and monitoring of COVID-19 pneumonia in pregnant women. *Ultrasound Obstet. Gynecol.* **2020**, *56*, 106–109. [CrossRef] [PubMed]
39. NICE. Butterfly iQ+ for Diagnostic Ultrasound Imaging. Medtech Innovation Briefing. Available online: https://www.nice.org.uk/advice/mib254/resources/butterfly-iq-for-diagnostic-ultrasound-imaging-pdf-2285965693413061 (accessed on 4 March 2021).
40. Burleson, S.L.; Swanson, J.F.; Shufflebarger, E.F.; Wallace, D.W.; Heimann, M.A.; Crosby, J.C.; Pigott, D.C.; Gullett, J.P.; Thompson, M.A.; Greene, C.J. Evaluation of a novel handheld point-of-care ultrasound device in an African emergency department. *Ultrasound J.* **2020**, *12*, 53. [CrossRef]
41. Rajendram, R.; Hussain, A.; Mahmood, N.; Kharal, M. Feasibility of using a handheld ultrasound device to detect and characterize shunt and deep vein thrombosis in patients with COVID-19: An observational study. *Ultrasound J.* **2020**, *12*, 49. [CrossRef]
42. ClinicalTrials.gov Identifier: NCT04591158. Status: Recruiting. Indication: Lung infection, COVID-19. Devices: Butterfly iQ+. Last Updated: October 2020. Country: Canada. Available online: www.clinicaltrials.gov/ct2/show/NCT04591158 (accessed on 10 May 2021).
43. Trauer, M.M.; Matthies, A.; Mani, N.; McDermott, C.; Jarman, R. The utility of lung ultrasound in COVID-19: A systematic scoping review. *Ultrasound* **2020**, *28*, 208–222. [CrossRef]
44. Hew, M.; Corcoran, J.P.; Harriss, E.; Rahman, N.M.; Mallett, S. The diagnostic accuracy of chest ultrasound for CT-detected radiographic consolidation in hospitalised adults with acute respiratory failure: A systematic review. *BMJ Open* **2015**, *5*, e007838. [CrossRef]
45. Smith, M.; Hayward, S.; Innes, S.; Miller, A. Point-of-care lung ultrasound in patients with COVID-19—A narrative review. *Anaesthesia* **2020**, *75*, 1096–1104. [CrossRef]
46. Pillai, K.; Hewage, S.; Harky, A. The Role of the Lung Ultrasound in Coronavirus Disease 2019: A Systematic Review. *J. Med. Ultrasound* **2020**, *28*, 207–212. [PubMed]
47. Roy, S.; Menapace, W.; Oei, S.; Luijten, B.; Fini, E.; Saltori, C.; Huijben, I.; Chennakeshava, N.; Mento, F.; Sentelli, A.; et al. Deep Learning for Classification and Localization of COVID-19 Markers in Point-of-Care Lung Ultrasound. *IEEE Trans. Med. Imaging* **2020**, *39*, 2676–2687. [CrossRef] [PubMed]
48. Evans, K.D.; Yang, Q.; Liu, Y.; Ye, R.; Peng, C. Sonography of the Lungs: Diagnosis and Surveillance of Patients With COVID-19. *J. Diagn. Med. Sonogr.* **2020**, *36*, 370–376. [CrossRef]
49. Anatomical Intelligence—Advanced Quantification and Reproducibility for Ultrasound Exams. © Koninklijke Philips N.V., 2004–2021. Available online: https://www.usa.philips.com/healthcare/resources/feature-detail/anatomical-intelligence-ultrasound (accessed on 24 April 2021).
50. Baribeau, Y.; Sharkey, A.; Chaudhary, O.; Krumm, S.; Fatima, H.; Mahmood, F.; Matyal, R. Handheld Point-of-Care Ultrasound Probes: The New Generation of POCUS. *J. Cardiothorac. Vasc. Anesth.* **2020**, *34*, 3139–3145. [CrossRef] [PubMed]

diagnostics

MDPI

Review

Patient Self-Performed Point-of-Care Ultrasound: Using Communication Technologies to Empower Patient Self-Care

Andrew W. Kirkpatrick [1,2,*], Jessica L. McKee [1], Kyle Couperus [3] and Christopher J. Colombo [4]

[1] TeleMentored Ultrasound Supported Medical Interventions (TMUSMI) Research Group, Calgary AB T3H 3W8, Canada
[2] Departments of Critical Care Medicine and Surgery, University of Calgary, Calgary AB T2N 1N4, Canada
[3] Ready Medic One (RMO) Research Group, Tacoma, WA 98431, USA
[4] Department of Medicine, Uniformed Services University of Health Sciences Bethesda Maryland, Bethesda, MD 20814, USA
* Correspondence: andrew.kirkpatrick@ahs.ca

Abstract: Point-of-Care ultrasound (POCUS) is an invaluable tool permitting the understanding of critical physiologic and anatomic details wherever and whenever a patient has a medical need. Thus the application of POCUS has dramatically expanded beyond hospitals to become a portable user-friendly technology in a variety of prehospital settings. Traditional thinking holds that a trained user is required to obtain images, greatly handicapping the scale of potential improvements in individual health assessments. However, as the interpretation of ultrasound images can be accomplished remotely by experts, the paradigm wherein experts guide novices to obtain meaningful images that facilitate remote care is being embraced worldwide. The ultimate extension of this concept is for experts to guide patients to image themselves, enabling secondary disease prevention, home-focused care, and self-empowerment of the individual to manage their own health. This paradigm of remotely telementored self-performed ultrasound (RTMSPUS) was first described for supporting health care on the International Space Station. The TeleMentored Ultrasound Supported Medical Interventions (TMUSMI) Research Group has been investigating the utility of this paradigm for terrestrial use. The technique has particular attractiveness in enabling surveillance of lung health during pandemic scenarios. However, the paradigm has tremendous potential to empower and support nearly any medical question poised in a conscious individual with internet connectivity able to follow the directions of a remote expert. Further studies and development are recommended in all areas of acute and chronic health care.

Keywords: point-of-care ultrasound; patient self-care; telementoring; informatics; community outreach (Min. 5–Max. 8)

Citation: Kirkpatrick, A.W.; McKee, J.L.; Couperus, K.; Colombo, C.J. Patient Self-Performed Point-of-Care Ultrasound: Using Communication Technologies to Empower Patient Self-Care. *Diagnostics* **2022**, *12*, 2884. https://doi.org/10.3390/diagnostics12112884

Academic Editors: Gino Soldati and Marcello Demi

Received: 31 October 2022
Accepted: 16 November 2022
Published: 21 November 2022

1. Introduction

Point-of-Care ultrasound (POCUS) is an invaluable tool permitting the understanding of critical physiologic and anatomic details wherever and whenever a patient has a medical need. Thus, the utilization of POCUS has dramatically expanded beyond hospitals to become a portable user-friendly technology in a variety of prehospital settings. Traditional thinking holds that a trained user is required to obtain images, greatly handicapping the potential improvement in individual health assessments. However, as the interpretation of ultrasound images can be accomplished remotely by experts, the paradigm wherein experts guide novices to obtain meaningful images that facilitate remote care is also being embraced worldwide. The ultimate extension of this concept is for experts to guide patients to image themselves, enabling secondary disease prevention, home-focused care, and self-empowerment of the individual to manage their own health. This paradigm of remotely telementored self-performed ultrasound (RTMSPU) was first described for supporting

health care on the International Space Station. The TeleMentored Ultrasound Supported Medical Interventions (TMUSMI) Research Group thereafter investigated the utility of this paradigm for terrestrial use. The technique has particular attractiveness in enabling surveillance of lung health during Pandemic scenarios. However, the paradigm also has tremendous potential to empower and support nearly any medical question poised in a conscious individual with Internet connectivity able to follow the directions of a remote expert. Further, studying the interaction between remote experts and local individuals could be utilized to design artificial intelligence algorithms capable of guiding quality image acquisition without connectivity. Images could be sent asynchronously when limited connectivity is re-established and then interpreted, with recommendations from the expert sent back to the individual asynchronously. This approach could potentially further expand the utility of this technology to austere and disconnected environments.

2. Concepts

POCUS is an invaluable diagnostic tool for innumerable diagnostic, interventional, and educational uses. Thus the World Health Organization has long recognized ultrasound as one of the most important technologies the developing world requires and considers its access a minimal global standard [1,2]. Ultrasound technology and equipment have dramatically improved in terms of capability and portability while being ever more economical [3]. This allows powerful ultrasound equipment to be more readily available in many locations where there may not be a trained and experienced ultrasonographer. Fortunately, of all the imaging technologies, ultrasound imaging has long consisted of two linked but separate processes—image generation and image interpretation [4], and even in quaternary care hospitals, these processes are typically performed separately by ultrasound image generating technicians and interpreting radiologists. Thus, this enables the interpreting ultrasonographer to be in almost any location on the planet as long as reasonable two-way communication is permitted, such that a remote expert can guide the person holding the probe to obtain images that can be thus interpreted by the expert. When the person holding the probe is less experienced and is being mentored this concept is designated Remote Telementored Ultrasonography (or sonography) (RTMUS) [5–7]. When the novel person is being remotely mentored to generate images of themself, we have designated this as Remote Telementored Self-Performed Ultrasound (RTMSPUS) [8–10].

3. The Space Medicine Origins of Remote Telementored Self-Performed Ultrasound

Just as ultrasound is an ideal tool in resource limited settings on Earth [11], so it has been appreciated in space [12]. Thus, the only diagnostic imaging capability ever transported off the planet Earth into true space onboard the International Space Station, is diagnostic ultrasound [6,13]. Thus ultrasound has been incorporated as a backbone of space medicine protocols looking at various outside-the-box applications [14]. This paradigm has been accomplished despite the absence of a trained sonographer onboard the ISS through the use of informatics and remote guidance by remote ground-based experts using RTMUS [6,15,16]. In this paradigm, the ground-based expert(s) are responsible for guiding the astronaut in space to move the probe to generate real-time images that the terrestrial expert can see, correct, and evaluate. This experience has typically involved one astronaut imaging another, but it also introduced the RTMSPUS concept.

As there is extreme competition for every minute of time onboard the ISS, it was found to be more efficient to have an astronaut image themselves, as to have them image another crewmember which requires double the human resources. Thus, astronauts were guided and demonstrated the feasibility of RTMSPUS of the peritoneal cavity (Focused Assessment with Sonography for Trauma exam), echocardiography [17], a full urinary system examination of the retroperitoneum and pelvis [18], assessment of the jugular venous pressure (JVP) [19], and even panoramic ultrasound depictions of muscle mass [20], Self-scanning has particular attributes in weightlessness wherein Hamilton commented that it has the advantage of self-stabilization and no concern of the subject floating away

from the operator in microgravity [17]. It was further noted that the sensitivity, specificity, and accuracy of the JVP in weightlessness were higher than those on Earth [19].

With the successful demonstration of RTMUS in general and its adoption within the core of Space Medicine practice and theory, the authors have long sought to translate these benefits for terrestrial care on Earth. The TeleMentored Ultrasound Supported Medical Interventions (TMUSMI) Research group thus initiated clinical work involving a fixed internet connection between a Quaternary care trauma center and a rural emergency room in the Rocky Mountains [21]. This project allowed a trauma surgeon in the receiving center to guide resuscitative ultrasound examinations by inexperienced providers at the small rural emergency. It facilitated remote diagnoses of an occult pneumothorax and cases of traumatic hemothorax including one direct to operating room resuscitation in an unstable patient [21]. Unfortunately, the paradigm was unsustainable due to the time delay required for the responding trauma surgeon to physically travel to a fixed teleultrasound base-station. The TMUSMI group has subsequently endeavored to refine RTMUS on completely mobile handheld platforms and to understand the human factors dynamics of RTMUS [7,22–24]. Through this research, it also became apparent that RTMUS is conceptually just a component of a richer telemedical interaction involving audio, visual, and often vital sign communication, as well as the visual information transmitted as ultrasound images.

4. Terrestrial Concepts of Remote Telementored Self-Performed Ultrasound (RTMSPUS)

If an individual is conscious and physically able to engage and participate in their own healthcare, then RTMUS offers unlimited capacity to dramatically increase the medical information transfer available to a remote expert attempting to guide care remotely. While caregivers have most frequently spoken to patients over the telephone to perform triage, the recent COVID pandemic dramatically increased the global utilization of videoconferencing as a provider-patient relationship [25,26]. However, one current limitation of telehealth is the inability to physically examine the patient remotely which leads to the risk of missed or improper diagnosis. Clinicians are thus appropriately concerned about diagnostic safety in telemedicine encounters, especially from a reduced or complete inability to perform a physical examination to collect information to formulate an accurate diagnosis [27,28].

RTMSPUS not only addresses this problem but improves upon the known limitations of the physical examination. Just as the physical examination dramatically improves the accuracy of a verbal history in confirming suspected diagnoses, so does a focused POCUS examination dramatically improve upon a physical examination [29–31]. Thus, the authors suggest that a self-performed ultrasound examination be considered whenever a patient is perceived to potentially benefit from an improved physical examination during a remote medical encounter. The existing database for self-performed ultrasound to date is summarized in Table 1. This table should be understood as representing current examples that will hopefully rapidly expand. The list of potential indications for RTMSPUS are as unlimited as the pathologies that afflict life on Earth.

Table 1. Indications for Remote TeleMentored Self-Performed Ultrasound (RTMSPUS).

Indication	Existing or Theoretical Status
Space Medicine	RTMSPUS has been performed since the early provision of an ultrasound machine onboard the International Space Station for a multitude of indications
COVID Lung examinations	Reported as case reports and case series during the current COVID 19 pandemic
Maternal Wellness Examination	Reported as case series emphasizing practicality
Heroic Self Preservation	If a severely injured but isolated casualty is conscious then self-diagnosing and providing mentored self-care may be the only option for saving their own life reported as theoretical concepts
Appendicitis	Reported in case report format

5. Remote Telementored Self-Performed Ultrasound (RTMSPUS) as Means of Preserving Social Distancing in Pandemic Conditions

At the time of writing we continue to be in a global pandemic [32], and the world continues to suffer both directly from the diseases induced by the COVID-19 virus and from our societal responses to the challenges of containing a rapidly mutating very transmissible virus. Fortunately, the particular pathophysiology of COVID-19 pneumonia lends itself to screening, diagnosis, prognostication, and clinical follow up by POCUS. Early chest CT has been recommended early detection of suspected COVID-19 pneumonia with better sensitivity than polymerase chain reaction [33], but obtaining a home delivered CT scan is obvious impractical [34]. Fortunately LUS may have comparable results to chest CT with markedly reduced logistical challenges [35]. Thus, lung ultrasound has been recommended for increased use in all these roles [36–41]. Most of the mortality in COVID is due to respiratory failure, typically beginning ten days after exposure with the progression of infection from the nasopharynx to the lungs [42]. Point of care lung ultrasound is excellent for examining the pleural surfaces of the lungs [43], which is where lung swelling begins to accumulate when COVID infection progresses to COVID pneumonia. This is also when patients typically begin to deteriorate with sometimes marked life-threatening disease often despite notable symptoms, the so-called happy hypoxemia that may be disastrous [44,45]. In general, POCUS brings the caregiver performing ultrasound in intimate proximity to the infectious patient; thus, numerous procedures to try and protect the ultrasonographer have been recommended. Throughout the pandemic however, health care providers have often been disproportionately affected as they will likely be in future pandemics when the infective agents and transmission characteristics are most unknown. The World Health Organization estimated midway through the pandemic that between 80,000 and 180,000 health and care workers could have died from COVID-19 in the period between January 2020 to May 2021 [46]. While the effectiveness of societal social distancing remains controversial [47], there is no question that if a health care provider is never physically exposed to a potentially infective patient, then all will be safer. Further, if patients can be adequately assessed and followed in their own homes, this greatly reduces logistics, prevents community spread, and protects caregivers. Early on in the pandemic, physicians in an overwhelmed Northern Italian hospital pleaded with the world to adopt increased telemedical surveillance of self-isolating at risk patients to keep them out of the hospital as a means of preserving resources and saving lives [48]. TMUSMI strongly concurred with this sentiment and proposed that lung RTMSPUS could potentially be performed by willing patients to assess their own lung health remotely and to detect early changes that might prompt the need for earlier in-hospital assessment [9,34,49].

A limited experience suggests that health care professionals can self-image themselves satisfactorily (including for appendicitis) [50]. An emergency physician reported using home ultrasound upon themselves to confirm a COVID diagnosis and thereafter to follow herself to rule out other worrisome conditions, such as deep vein thrombosis, right heart strain from a massive pulmonary embolus, pericardial effusion, and lobar pneumonia [51].

Pivetta also reported a case of a nurse who had previous point-of-care ultrasound training on vascular access and bladder scanning who was "teleguided" by an expert operator to image her own lungs with a 12-zone protocol after she was diagnosed with COVID [52].

Although it is intuitive to take advantage of the existing skill sets of health care providers, it will be necessary to empower the general population during pandemic conditions. TMUSMI recently conducted a pilot trial in Edmonton, Canada wherein lay people without previous experience holding an ultrasound probe were guided by a mentoring expert in Calgary, 300 km distant [8]. It was subsequently demonstrated that all these healthy self-isolating non-medical volunteers were able to receive remote guidance to image themselves successfully. In this study as in all RTMSPUS situations, all interpretation of the LUS findings are the responsibility of the remote mentor. They were thus able to image their anterior, lateral, and bases of their backs with a 99.8% adequacy rate as assessed by blinded lung ultrasound reviewers (Figure 1).

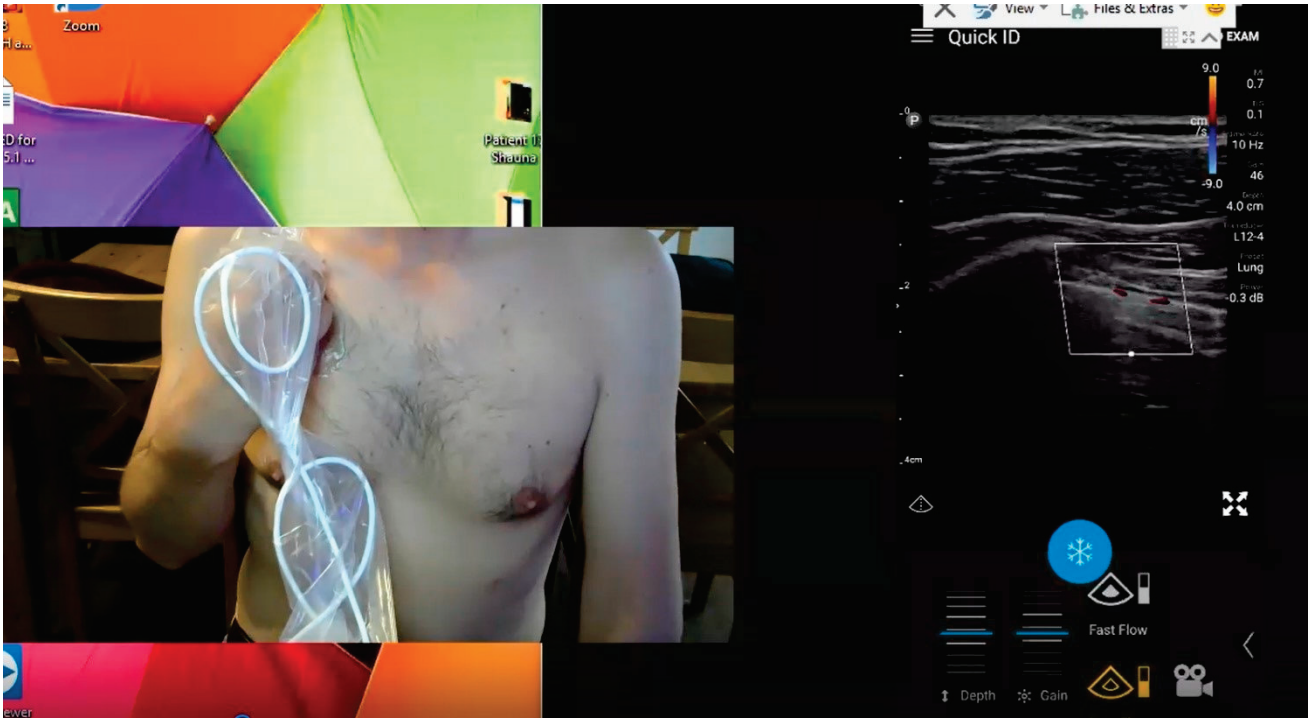

Figure 1. Example of Ultrasound Naïve Volunteer being guided to image their own chest. Figure Legend: Screenshot of the Mentors computer in Calgary viewing the completely novice self-isolating volunteer image their upper right anterior lung field depicting the visceral and parietal pleural interface with movement emphasized with Color Power-Doppler the "Power-Slide" Sign (seen in Supplementary Materials). Note: Lung ultrasound is a dynamic science much better appreciated with real time imaging. The videorecording of the entire mentored Lung examination ca be viewed in Supplementary File S1.

Not unexpectantly, only two-thirds of this population could fully image their backs. While all could image their own low-back, only 70% could image their midback, and only 30% their upper backs for the posterior superior lung fields, in a group of whom 26% self-reported a shoulder injury and 30% upper body musculoskeletal problems [8]. Although anticipated, there was not an obvious difference between sexes. In the case of screening for COVID, this is not a practical limitation as the COVID hot spots at the bases of the lungs could be imaged in 96% of cases [8]. This fact illustrates a factor that does not typically arise in the standard paradigm of a technician performing an ultrasound on a patient, namely the physical ability of a subject to reach their own body parts with an ultrasound probe. Others are considering these facts though, and Kimura and colleagues

also recently published a retrospective analysis of lung ultrasound findings in acutely ill patients with COVID and determined that viewing only the antero-apex of the lungs has had findings in 62% of all patients and associated with death and need for critical care unit admission [42].

One interesting sign that was used to confirm that the true lung bases were being seen, was to identify the liver and lung "points". In this paradigm described by the TMUSMI group, the image under the stationary ultrasound probe can be seen to alternate between a view of the contiguous visceral and parietal pleura and alternatively a view of the underlying liver or spleen depending on which side of the body (Figure 2, Supplementary File S2), as the diaphragm and relative visceral positions alternates with respiration. This sign again 100% confirms that the lung bases are being imaged.

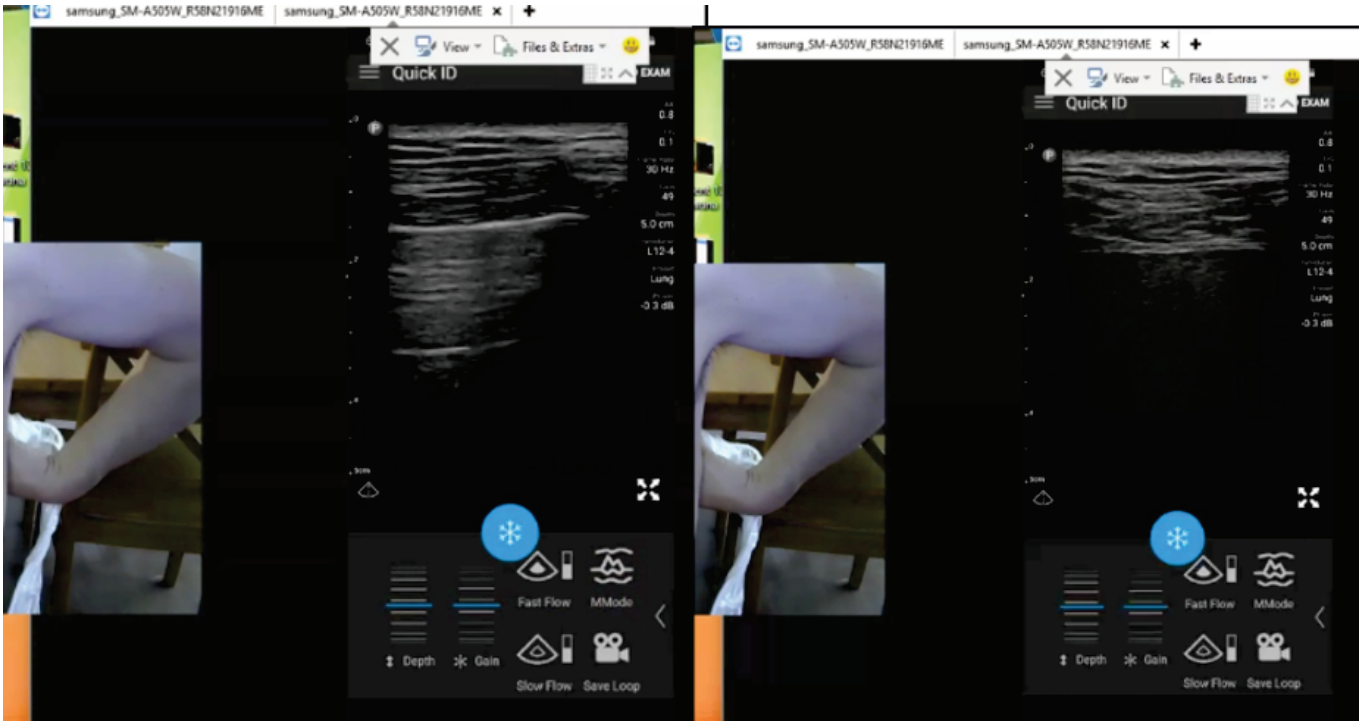

Figure 2. Example of the "Spleen Point" Sign confirming imaging of the Lung Base. Legend: When the ultrasound probe is correctly positioned at the bung base, the image will review the visceral-parietal interface (left) alternating with the parenchyma of the spleen on the left or liver on the right with no probe movement due to the respiratory movement of the diaphragm. Note: Lung ultrasound is a dynamic science much better appreciated with real time imaging. The videorecording of the entire mentored Lung examination ca be viewed in Supplementary File S2.

Resnikoff also recently reported a mixed cohort of 80 COVID confirmed, dyspneic, or cardiology patients who were able to self-image the anterior second intercostal space bilaterally with a 67% sensitivity, 94% specificity, and 88% accuracy for standard lung ultrasound landmarks, with the participants being guided only by a instruction sheet [53]. They also noted that those younger than 80 who used the internet daily were more likely to obtain diagnostic lung images, while being acutely dyspneic was associated with reduced success [53].

Thus, TMUSMI believes it would be possible for large populations of asymptomatic or paucisymptomatic patients at potential but a low risk of deterioration to be screened as frequently as deemed appropriate in their own households. Sanitized lightweight telemedical smart phone supported ultrasound probes can be quickly couriered or even drone delivered to completely obviate human to human contact (Figure 3a,b) [54,55]. In the group of previously asymptomatic patients at risk for COVID, one subject later caught

COVID, with his initial pre-infectious study serving as a baseline for repeated examinations by the same remote mentor providing longitudinal follow-up to detect deterioration at the earliest possible time [10].

(**a**) (**b**)

Figure 3. (**a**) Sanitized Home Ultrasound Delivery Package. Legendz: Sanitized package for home-delivery to patients containing a Philips Lumify Ultrasound probe and dedicated smart phone to support the ultrasound, gloves, masks, and ultrasound jelly. (**b**) Sanitized Home Ultrasound Delivery Package. Figure Legend: Sanitized package ready for home-delivery to self-isolating patients.

6. Self-Performed Home Obstetrical Ultrasound

In 2011, TMUSMI reported early experiences with the transnational remote mentoring of maternal wellness examinations [7]. There have since been remarkable developments including the development of self-scanning algorithms that allow pregnant women to image their own fetus's guided by an app to guide the mothers through self-scanning with the results viewed remotely in either delayed or real-time. Hader reported that among 100 women, there was 95.3% success for detecting fetal heart activity, 88.3% for body movements, and 92% for normal amniotic fluid volume, although only 23% success in detecting fetal breathing. They concluded the system was a potential solution for remote sonographic fetal assessment although further study was required [56].

7. The Potential of Remotely Mentored Teleultrasound for Acute Self Resuscitation

With the dramatically increased availability of ultrasound devices that are now connected and powered by smart phones, it is likely any severely injured victim who is not unconscious, will be able to reach out for potential online remote help, which might include the possibility of remotely directed self-performed ultrasound assessments to assist in triage efforts, or even remotely guided self-care in extreme circumstances when no other options exist. This topic was recently reviewed by TMUSMI in the publication entitled; "Empowering catastrophic far-forward self-care: Nobody should die alone without trying" [57]. Just as it would be strange for a trauma surgeon to function in a trauma resuscitation bay without ultrasound, it may become the norm for a remote rescuer to supplement the basic

"how are you" questions in an emergent medical interaction with a progressive ultrasound vital signs check.

8. The Potential of Remotely Mentored Teleultrasound for Self-Care of Chronic Conditions

While TMUSMI has been focused on acute health events, managing chronic health problems of an aging population challenge is a profound global challenge, and one that may bankrupt publicly funded health care systems. Thus, any solution that can keep the aging safely at home in good health, rather than requiring in hospital assessment or institutionalization will not only dramatically reduce costs but hopefully increase the quality of life. Smart homes are one form of gerontechnological innovation, that designates the augmentation of a residence with sensors and devices/actuators integrated into the residence's infrastructure. While occupants have been satisfied with their residences, they have not been proven to reduce emergency department visits or hospital admission rates [58]. TMUSMI proposes that adding a remote ultrasound capability to the typical smart home infrastructure may provide the ability to improve home care in almost limitless ways. Low-lying fruit already being include remote self-monitoring of cardiac conditions such as congestive heart failure [53]. By potentially using RTMSPUS innumerable conditions such as pneumothorax, pulmonary edema, pleural effusion, aspiration pneumonia, and pneumonia might be remotely diagnosed remotely [59]. As ultrasound is the most versatile imaging technology without side effects; thus it is presumable that almost any medical, nursing, and allied specialty will find some aspect of RTMSPUS to incorporate into their improved telehealth interactions.

9. Future Directions and Conclusions

The COVID pandemic redefined much of Global Societies communicate, including catalyzing the acceptance and demand for remote services including acute and chronic health needs. While remote access is potentially safer and more convenient, the risk of missing important findings due to the lack of in-person assessment is ever present. Enabling patients to examine themselves with smart phone powered and supported ultrasound brings the care giver back to the patient's presence and improves the physical examination, providing immediate answers that can be electronically documented for future analysis or comparison. TMUSMI and others have shown that almost any technique is possible. The potential for impacting triage, diagnosis and treatment decisions extends in the present to high connectivity environments, and in the immediate future to poorly connected environments. The challenge is to make these techniques logistically sustainable, to understand the human factors required to provide optimal mentoring of this technique, and to improve artificial intelligence and machine learning to the point of extending this resource to disconnected environments.

Supplementary Materials: The following supporting information can be downloaded at: https://www.mdpi.com/article/10.3390/diagnostics12112884/s1, Supplementary File S1: Entire recorded video of an Engineer who had never held an ultrasound probe before being remotely mentored to complete their own Remote Telementored Self-Performed Ultrasound Examination of the lungs while self-isolating for COVID; Supplementary File S2: Specifically edited video of an Engineer who had never held an ultrasound probe before being remotely mentored to demonstrate imaging of their lung base both laterally and posteriorly demonstrating the "spleen-point" sign. Of not File 2 is contained within the larger File 1 but was edited to make understanding this concept easier.

Author Contributions: Conception and Design, A.W.K. and J.L.M.; drafting manuscript, A.W.K.; final revision, A.W.K., J.L.M., C.J.C. and K.C.; accountable for the content, A.W.K., J.L.M., C.J.C. and K.C. All authors have read and agreed to the published version of the manuscript.

Funding: This research received no external funding.

Conflicts of Interest: AW Kirkpatrick has consulted for ZOLL Medical, Acelity (3M/KCI), CSL Behring, Innovative Trauma Care, and SAM Medical and the Statesman Group of Companies and is the principal investigator of a randomized trial partially supported by Acelity. He has previously disclosed a personal relationship with JL McKee. JL McKee has consulted for Innovative Trauma Care, SAM Medical, Aceso, Acelity (3M/KCI), ZOLL Medical, and Andrew W. Kirkpatrick Professional Corporation. She has previously disclosed a personal relationship with AW Kirkpatrick. CJ Colombo has no conflicts of interest to disclose. KS Couperus is currently the Director of Learning and Development for 98point6, Inc a virtual healthcare company. At the time of writing this manuscript, there is no active use of ultrasound through this virtual offering.

References

1. The Partnership for Maternal, Newborn & Child Health. From Pledges to Action, New Delhi, India 13–14 November 2010. Available online: http://www.who.int/pmnch/events/2010/2010_pf_innovation_ultrasound/en/ (accessed on 19 May 2011).
2. World Health Organization. Effective choices for diagnostic imaging in clinical practice. In *Report of a WHO Scientific Group*; World Health Organization: Geneva, Switzerland, 1990.
3. Demi, L.; Wolfram, F.; Klersy, C.; De Silvestri, A.; Ferretti, V.V.; Muller, M.; Miller, D.; Feletti, F.; Welnicki, M.; Buda, N.; et al. New International Guidelines and Consensus on the Use of Lung Ultrasound. *J. Ultrasound Med.* **2022**. [CrossRef] [PubMed]
4. Kirkpatrick, A.W.; Hamilton, D.R.; Nicolaou, S.; Sargsyan, A.E.; Campbell, M.R.; Feiveson, A.; Dulchavsky, S.A.; Melton, S.; Beck, G.; Dawson, D.L. Focused Assessment with Sonography for Trauma in weightlessness: A feasibility study. *J. Am. Coll. Surg.* **2003**, *196*, 833–844. [CrossRef]
5. Pian, L.; Gillman, L.M.; McBeth, P.B.; Xiao, Z.; Ball, C.G.; Blaivas, M.; Hamilton, D.R.; Kirkpatrick, A.W. Potential Use of Remote Telesonography as a Transformational Technology in Underresourced and/or Remote Settings. *Emerg. Med. Int.* **2013**, *2013*, 986160. [CrossRef] [PubMed]
6. Sargsyan, A.E.; Hamilton, D.R.; Jones, J.A.; Melton, S.; Whitson, P.A.; Kirkpatrick, A.W.; Martin, D.; Dulchavsky, S.A. FAST at MACH 20: Clinical ultrasound aboard the International Space Station. *J. Trauma* **2005**, *58*, 35–39. [CrossRef]
7. McBeth, P.B.; Crawford, I.; Blaivas, M.; Hamilton, T.; Musselwhite, K.; Panebianco, N.; Melniker, L.; Ball, C.G.; Gargani, L.; Gherdovich, C.; et al. Simple, almost anywhere, with almost anyone: Remote low-cost telementored resuscitative lung ultrasound. *J. Trauma* **2011**, *71*, 1528–1535. [CrossRef]
8. Kirkpatrick, A.W.; McKee, J.L.; Ball, C.G.; Ma, I.W.Y.; Melniker, L.A. Empowering the willing: The feasibility of tele-mentored self-performed pleural ultrasound assessment for the surveillance of lung health. *Ultrasound J.* **2022**, *14*, 2. [CrossRef]
9. Kirkpatrick, A.W.; McKee, J.L.; Volpicelli, G.; Ma, I.W.Y. The Potential for Remotely Mentored Patient-Performed Home Self-Monitoring for New Onset Alveolar-Interstitial Lung Disease. *Telemed. J. E. Health* **2020**, *26*, 1304–1307. [CrossRef]
10. Kirkpatrick, A.W.; McKee, J.L.; Conly, J.M. Longitudinal remotely mentored self-performed lung ultrasound surveillance of paucisymptomatic COVID-19 patients at risk of disease progression. *Ultrasound J.* **2021**, *13*, 27. [CrossRef]
11. Ienghong, K.; Cheung, L.W.; Tiamkao, S.; Bhudhisawasdi, V.; Apiratwarakul, K. Integrating Point of Care Ultrasound Education into Clinical Practice at the Emergency Department. *Tomography* **2022**, *8*, 1052–1059. [CrossRef]
12. Kirkpatrick, A.W.; Jones, J.A.; Sargsyan, A.; Hamilton, D.R.; Melton, S.; Beck, G.; Nicolau, S.; Campbell, M.; Dulchavsky, S. Trauma sonography for use in microgravity. *Aviat. Space Environ. Med.* **2007**, *78*, A38–A42.
13. Martin, D.S.; South, D.A.; Garcia, K.M.; Arbeille, P. Ultrasound in space. *Ultrasound Med. Biol.* **2003**, *29*, 1–12. [CrossRef]
14. Wagner, M.S.; Garcia, K.; Martin, D.S. Point-of-care ultrasound in aerospace medicine: Known and potential applications. *Aviat. Space Env. Med.* **2014**, *85*, 730–739. [CrossRef] [PubMed]
15. Chiao, L.; Sharipov, S.; Sargsyan, A.E.; Melton, S.; Hamilton, D.R.; McFarlin, K.; Dulchavsky, S.A. Ocular examination for trauma; clinical ultrasound aboard the International Space Station. *J. Trauma* **2005**, *58*, 885–889. [CrossRef] [PubMed]
16. Fincke, E.M.; Padalka, G.; Lee, D.; van Holsbeeck, M.; Sargsyan, A.E.; Hamilton, D.R.; Martin, D.; Melton, S.L.; McFarlin, K.; Dulchavsky, S.A. Evaluation of shoulder integrity in space: First report of musculoskeletal US on the International Space Station. *Radiology* **2005**, *234*, 319–322. [CrossRef] [PubMed]
17. Hamilton, D.R.; Sargsyan, A.E.; Martin, D.S.; Garcia, K.M.; Melton, S.L.; Feiveson, A.; Dulchavsky, S.A. On-orbit prospective echocardiography on International Space Station crew. *Echocardiography* **2011**, *28*, 491–501. [CrossRef]
18. Jones, J.A.; Sargsyan, A.E.; Barr, Y.R.; Melton, S.; Hamilton, D.R.; Dulchavsky, S.A.; Whitson, P.A. Diagnostic ultrasound at MACH 20: Retroperitoneal and pelvic imaging in space. *Ultrasound Med. Biol.* **2009**, *35*, 1059–1067. [CrossRef]
19. Zamboni, P.; Sisini, F.; Menegatti, E.; Taibi, A.; Gadda, G.; Tavoni, V.; Malagoni, A.M.; Tessari, M.; Gianesini, S.; Gambaccini, M. Ultrasound Monitoring of Jugular Venous Pulse during Space Missions: Proof of Concept. *Ultrasound Med. Biol.* **2018**, *44*, 726–733. [CrossRef]
20. Scott, J.M.; Downs, M.; Martin, D.S.; Hougland, E.; Sarmiento, L.; Arzeno, N.; Pettit, D.R.; Ploutz-Snyder, R.; Cunningham, D.; Jones, L.W.; et al. Teleguided self-ultrasound scanning for longitudinal monitoring of muscle mass during spaceflight. *iScience* **2021**, *24*, 102344. [CrossRef]
21. Dyer, D.; Cusden, J.; Turner, C.; Boyd, J.; Hall, R.; Lautner, D.; Hamilton, D.R.; Shepherd, L.; Dunham, M.; Bigras, A.; et al. The clinical and technical evaluation of a remote telementored telesonography system during the acute resuscitation and transfer of the injured patient. *J. Trauma* **2008**, *65*, 1209–1216. [CrossRef]

22. McBeth, P.B.; Hamilton, T.; Kirkpatrick, A.W. Cost-effective remote iPhone-teathered telementored trauma telesonography. *J. Trauma* **2010**, *69*, 1597–1599. [CrossRef]
23. McBeth, P.; Crawford, I.; Tiruta, C.; Xiao, Z.; Zhu, G.Q.; Shuster, M.; Sewell, L.; Panebianco, N.; Lautner, D.; Nicolaou, S.; et al. Help is in your pocket: The potential accuracy of smartphone- and laptop-based remotely guided resuscitative telesonography. *Telemed. J. E-Health Off. J. Am. Telemed. Assoc.* **2013**, *19*, 924–930. [CrossRef] [PubMed]
24. Kirkpatrick, A.W.; Blaivas, M.; Sargsyan, A.E.; McBeth, P.B.; Patel, C.; Xiao, Z.; Pian, L.; Panebianco, N.; Hamilton, D.R.; Ball, C.G.; et al. Enabling the Mission Through Trans-Atlantic Remote Mentored Musculoskeletal Ultrasound: Case Report of a Portable Hand-Carried Tele-ultrasound System for Medical Relief Missions. *Telemed. J. E-Health Off. J. Am. Telemed. Assoc.* **2013**, *19*, 530–534. [CrossRef] [PubMed]
25. Garfan, S.; Alamoodi, A.H.; Zaidan, B.B.; Al-Zobbi, M.; Hamid, R.A.; Alwan, J.K.; Ahmaro, I.Y.Y.; Khalid, E.T.; Jumaah, F.M.; Albahri, O.S.; et al. Telehealth utilization during the COVID-19 pandemic: A systematic review. *Comput. Biol. Med.* **2021**, *138*, 104878. [CrossRef] [PubMed]
26. Omboni, S.; Padwal, R.S.; Alessa, T.; Benczur, B.; Green, B.B.; Hubbard, I.; Kario, K.; Khan, N.A.; Konradi, A.; Logan, A.G.; et al. The worldwide impact of telemedicine during COVID-19: Current evidence and recommendations for the future. *Connect. Health* **2022**, *1*, 7–35. [CrossRef]
27. Sharma, A.E.; Khoong, E.C.; Nijagal, M.A.; Lyles, C.R.; Su, G.; DeFries, T.; Sarkar, U. Clinician experience with telemedicine at a safety-net hospital network during COVID-19: A cross sectional survey. *J. Health Care Poor Underserved* **2021**, *32*, 220–240. [CrossRef]
28. Khoong, E.C.; Sharma, A.E.; Gupta, K.; Adler-Milstein, J.; Sarkar, U. The Abrupt Expansion of Ambulatory Telemedicine: Implications for Patient Safety. *J. Gen. Intern. Med.* **2022**, *37*, 1270–1274. [CrossRef]
29. Mehta, M.; Jacobson, T.; Peters, D.; Le, E.; Chadderdon, S.; Allen, A.J.; Caughey, A.B.; Kaul, S. Handheld ultrasound versus physical examination in patients referred for transthoracic echocardiography for a suspected cardiac condition. *JACC Cardiovasc. Imaging* **2014**, *7*, 983–990. [CrossRef]
30. Meyer, R.; Lin, C.; Yenokyan, G.; Ellen, M. Diagnostic Utility of Ultrasound Versus Physical Examination in Assessing Knee Effusions: A Systematic Review and Meta-analysis. *J. Ultrasound Med.* **2022**, *41*, 17–31. [CrossRef]
31. Wu, T.S.; Roque, P.J.; Green, J.; Drachman, D.; Khor, K.N.; Rosenberg, M.; Simpson, C. Bedside ultrasound evaluation of tendon injuries. *Am. J. Emerg. Med.* **2012**, *30*, 1617–1621. [CrossRef]
32. Kimball, S.R. WHO Says COVID Still a Global Public Health Emergency Even as Deaths Fall to Lowest Level in Two Years. Available online: https://www.cnbc.com/2022/04/13/who-says-covid-still-global-health-emergency-even-as-deaths-fall-to-lowest-level-in-two-years.html (accessed on 15 July 2022).
33. Fang, Y.; Zhang, H.; Xie, J.; Lin, M.; Ying, L.; Pang, P.; Ji, W. Sensitivity of Chest CT for COVID-19: Comparison to RT-PCR. *Radiology* **2020**, *296*, 200432. [CrossRef]
34. Kirkpatrick, A.W.; McKee, J.L. Re: "Proposal for International Standardization of the Use of Lung Ultrasound for Patients With COVID-19: A Simple, Quantitative, Reproducible Method"-Could Telementoring of Lung Ultrasound Reduce Health Care Provider Risks, Especially for Paucisymptomatic Home-Isolating Patients? *J. Ultrasound Med.* **2021**, *40*, 211–212. [CrossRef] [PubMed]
35. Peng, Q.Y.; Wang, X.T.; Zhang, L.N.; Chinese Critical Care Ultrasound Study Group. Findings of lung ultrasonography of novel corona virus pneumonia during the 2019-2020 epidemic. *Intensive Care Med.* **2020**, *46*, 849–850. [CrossRef] [PubMed]
36. Gargani, L.; Soliman-Aboumarie, H.; Volpicelli, G.; Corradi, F.; Pastore, M.C.; Cameli, M. Why, when, and how to use lung ultrasound during the COVID-19 pandemic: Enthusiasm and caution. *Eur. Heart J. Cardiovasc. Imaging* **2020**, *21*, 941–948. [CrossRef] [PubMed]
37. Volpicelli, G.; Gargani, L. Sonographic signs and patterns of COVID-19 pneumonia. *Ultrasound J.* **2020**, *12*, 22. [CrossRef] [PubMed]
38. Volpicelli, G.; Gargani, L.; Perlini, S.; Spinelli, S.; Barbieri, G.; Lanotte, A.; Casasola, G.G.; Nogue-Bou, R.; Lamorte, A.; Agricola, E.; et al. Lung ultrasound for the early diagnosis of COVID-19 pneumonia: An international multicenter study. *Intensive Care Med.* **2021**, *47*, 444–454. [CrossRef]
39. Skaarup, S.H.; Aagaard, R.; Ovesen, S.H.; Weile, J.; Kirkegaard, H.; Espersen, C.; Lassen, M.C.H.; Skaarup, K.G.; Posth, S.; Laursen, C.B.; et al. Focused lung ultrasound to predict respiratory failure in patients with symptoms of COVID-19: A multicentre prospective cohort study. *ERJ Open Res.* **2022**, *8*, 00128-2022. [CrossRef] [PubMed]
40. Toraskar, K.; Zore, R.R.; Gupta, G.A.; Gondse, B.; Pundpal, G.; Kadam, S.; Pawaskar, S.; Setia, M.S. Utility and diagnostic test properties of pulmonary and cardiovascular point of care ultra-sonography (POCUS) in COVID-19 patients admitted to critical care unit. *Eur. J. Radiol. Open* **2022**, *9*, 100451. [CrossRef]
41. Ma, I.W.Y.; Hussain, A.; Wagner, M.; Walker, B.; Chee, A.; Arishenkoff, S.; Buchanan, B.; Liu, R.B.; Mints, G.; Wong, T.; et al. Canadian Internal Medicine Ultrasound (CIMUS) Expert Consensus Statement on the Use of Lung Ultrasound for the Assessment of Medical Inpatients With Known or Suspected Coronavirus Disease 2019. *J. Ultrasound Med.* **2020**, *40*, 1879–1892. [CrossRef]
42. Kimura, B.J.; Shi, R.; Tran, E.M.; Spierling Bagsic, S.R.; Resnikoff, P.M. Outcomes of Simplified Lung Ultrasound Exam in COVID-19: Implications for Self-Imaging. *J. Ultrasound Med.* **2022**, *41*, 1377–1384. [CrossRef]

43. Kirkpatrick, A.W.; Sirois, M.; Laupland, K.B.; Liu, D.; Rowan, K.; Ball, C.G.; Hameed, S.M.; Brown, R.; Simons, R.; Dulchavsky, S.A.; et al. Hand-held thoracic sonography for detecting post-traumatic pneumothoraces: The Extended Focused Assessment with Sonography for Trauma (EFAST). *J. Trauma* **2004**, *57*, 288–295. [CrossRef]
44. Busana, M.; Gasperetti, A.; Giosa, L.; Forleo, G.B.; Schiavone, M.; Mitacchione, G.; Bonino, C.; Villa, P.; Galli, M.; Tondo, C.; et al. Prevalence and outcome of silent hypoxemia in COVID-19. *Minerva Anestesiol.* **2021**, *87*, 325–333. [CrossRef] [PubMed]
45. Tobin, M.J.; Laghi, F.; Jubran, A. Why COVID-19 Silent Hypoxemia Is Baffling to Physicians. *Am. J. Respir. Crit. Care Med.* **2020**, *202*, 356–360. [CrossRef] [PubMed]
46. World Health Organization. Health and Care Worker Deaths during COVID-19. Available online: https://www.who.int/news/item/20-10-2021-health-and-care-worker-deaths-during-covid-19 (accessed on 16 July 2022).
47. Sun, K.S.; Lau, T.S.M.; Yeoh, E.K.; Chung, V.C.H.; Leung, Y.S.; Yam, C.H.K.; Hung, C.T. Effectiveness of different types and levels of social distancing measures: A scoping review of global evidence from earlier stage of COVID-19 pandemic. *BMJ Open* **2022**, *12*, e053938. [CrossRef] [PubMed]
48. Nacoti, M.; Ciocca, A.; Giupponi, A.; Brambillasca, P.; Lussana, F.; Pisano, M.; Goisis, G.; Bonacina, D.; Fazzi, F.; Naspro, R.; et al. At the Epicenter of the COVID-19 Pandemic and Humanitarian Crises in Italy: Changing Perspectives on Preparation and Mitigation. *Innov. Care Deliv.* **2020**, *3*, e435. [CrossRef]
49. Kirkpatrick, A.W.; McKee, J.L. Lung ultrasonography in a woman with COVID-19: This examination could be remote. *CMAJ* **2020**, *192*, E435. [CrossRef]
50. Knapp, B.; Feyzeau, K.; Smith, A.; Byars, D.; Goodmurphy, C.; Jones, M. The Evolution of Ultrasound in Medicine: A Case Report of Point-of-care Ultrasound in the Self-diagnosis of Acute Appendicitis. *Clin. Pract. Cases Emerg. Med.* **2020**, *4*, 527–529. [CrossRef]
51. Aminlari, A.; Quenzer, F.; Hayden, S.; Stone, J.; Murchison, C.; Campbell, C. A Case of COVID-19 Diagnosed at Home With Portable Ultrasound and Confirmed With Home Serology Test. *J. Emerg. Med.* **2021**, *60*, 399–401. [CrossRef]
52. Pivetta, E.; Girard, E.; Locascio, F.; Lupia, E.; Martin, J.D.; Stone, M. Self-Performed Lung Ultrasound for Home Monitoring of a Patient Positive for Coronavirus Disease 2019. *Chest* **2020**, *158*, e93–e97. [CrossRef]
53. Resnikoff, P.M.; Shi, R.; Spierling Bagsic, S.R.; Kimura, B.J. The Novel Concept of Patient Self-Imaging: Success in COVID-19 and Cardiopulmonary Disorders. *Am. J. Med.* **2021**, *134*, e360–e361. [CrossRef]
54. Kirkpatrick, A.W.; McKee, J.L.; Moeini, S.; Conly, J.M.; Ma, I.W.Y.; Baylis, B.; Hawkins, W. Pioneering Remotely Piloted Aerial Systems (Drone) Delivery of a Remotely Telementored Ultrasound Capability for Self Diagnosis and Assessment of Vulnerable Populations-the Sky Is the Limit. *J. Digit. Imaging* **2021**, *34*, 841–845. [CrossRef]
55. Flemons, K.; Baylis, B.; Khan, A.Z.; Kirkpatrick, A.W.; Whitehead, K.; Moeini, S.; Schreiber, A.; Lapointe, S.; Ashoori, S.; Arif, M.; et al. The use of drones for the delivery of diagnostic test kits and medical supplies to remote First Nations communities during COVID-19. *Am. J. Infect. Control* **2022**, *50*, 849–856. [CrossRef] [PubMed]
56. Hadar, E.; Wolff, L.; Tenenbaum-Gavish, K.; Eisner, M.; Shmueli, A.; Barbash-Hazan, S.; Bergel, R.; Shmuel, E.; Houri, O.; Dollinger, S.; et al. Mobile Self-Operated Home Ultrasound System for Remote Fetal Assessment During Pregnancy. *Telemed. J. E Health* **2022**, *28*, 93–101. [CrossRef]
57. Kirkpatrick, A.W.; McKee, J.L. Empowering catastrophic far-forward self-care: Nobody should die alone without trying. *J. Mil. Fam. Vet. Health* **2022**, in press. [CrossRef]
58. Liu, P.; Li, G.; Jiang, S.; Liu, Y.; Leng, M.; Zhao, J.; Wang, S.; Meng, X.; Shang, B.; Chen, L.; et al. The effect of smart homes on older adults with chronic conditions: A systematic review and meta-analysis. *Geriatr. Nurs.* **2019**, *40*, 522–530. [CrossRef] [PubMed]
59. Lichtenstein, D.A.; Meziere, G.A. Relevance of lung ultrasound in the diagnosis of acute respiratory distress. *Chest* **2008**, *134*, 117–125. [CrossRef]

diagnostics

MDPI

Article

Clinical Impact of Vertical Artifacts Changing with Frequency in Lung Ultrasound

Natalia Buda [1,*], Agnieszka Skoczylas [2], Marcello Demi [3], Anna Wojteczek [1], Jolanta Cylwik [4] and Gino Soldati [5]

1 Department of Internal Medicine, Connective Tissue Diseases and Geriatric, Medical University of Gdansk, 80-952 Gdansk, Poland; wojteczkowa@vp.pl
2 Department of Geriatrics, National Institute of Geriatrics Rheumatology and Rehabilitation, 02-637 Warsaw, Poland; agnieszka.skoczylas@spartanska.pl
3 Department of Medical Image Procesing, Fondazione Gabriele Monasterio, 56124 Pisa, Italy; demi@ftgm.it
4 Department of Anaesthesiology and Intensive Therapy, Mazovia Regional Hospital in Siedlce, 08-110 Siedlce, Poland; jolacylwik@o2.pl
5 Interventional and Diagnostic Ultrasound Unit, Valle del Serchio, General Hospital Lucca, 55100 Lucca, Italy; gino.soldati@uslnordovest.toscana.it
* Correspondence: natabud@wp.pl

Abstract: Background: This study concerns the application of lung ultrasound (LUS) for the evaluation of the significance of vertical artifact changes with frequency and pleural line abnormalities in differentiating pulmonary edema from pulmonary fibrosis. Study Design and Methods: The study was designed as a diagnostic test. Having qualified patients for the study, an ultrasound examination was performed, consistent with a predetermined protocol, and employing convex and linear transducers. We investigated the possibility of B-line artifact conversion depending on the set frequency (2 MHz and 6 MHz), and examined pleural line abnormalities. Results: The study group comprised 32 patients with interstitial lung disease (ILD) (and fibrosis) and 30 patients with pulmonary edema. In total, 1941 cineloops were obtained from both groups and analyzed. The employment of both types of transducers (linear and convex) was most effective (specificity 91%, specificity 97%, positive predictive value (PPV) 97%, negative predictive value (NPV) 91%, LR(+) 27,19, LR(−) 0.097, area under curve (AUC) = 0.936, $p = 7 \times 10^{-6}$). Interpretation: The best accuracy in differentiating the etiology of B-line artifacts was obtained with the use of both types of transducers (linear and convex), complemented with the observation of the conversion of B-line artifacts to Z-line.

Keywords: B-line; lung ultrasonography; LUS; interstitial lung disease; systemic sclerosis; pulmonary fibrosis; oedema

Citation: Buda, N.; Skoczylas, A.; Demi, M.; Wojteczek, A.; Cylwik, J.; Soldati, G. Clinical Impact of Vertical Artifacts Changing with Frequency in Lung Ultrasound. *Diagnostics* **2021**, *11*, 401. https://doi.org/10.3390/diagnostics11030401

Academic Editor: Philippe A. Grenier

Received: 11 January 2021
Accepted: 24 February 2021
Published: 26 February 2021

1. Introduction:

Lesions affecting the interstitium are most frequently caused by pulmonary edema (cardiogenic and non-cardiogenic) and interstitial lung disease (ILD) [1]. Such lesions are easily detected in a lung ultrasound (LUS), where B-line artifacts are searched for. However, without considering clinical data, differentiating the etiology of lesions affecting the interstitium is much more difficult [2–5]. Consequently, searching for further possibilities for differentiating a pulmonary from cardiogenic etiology of interstitial lesions using LUS is well grounded.

In this study, vertical artifacts were analyzed (depending on the set operating frequency), as well as pleural line abnormalities. The first goal was to compare the length of vertical artifacts evaluated with a convex transducer at two extreme frequencies: 2 MHz, and then 6 MHz. The second goal was to assess pleural line abnormalities, with the employment of a linear transducer in both patient groups.

B-line artifacts are significant in diagnosing many diseases that affect the pulmonary interstitial space and alveoli [1,6]. These artifacts are defined as laser-like vertical re-

verberation artifacts arising from the pleural line, extending to the bottom of the screen (irrespective of the set depth), moving along with the lung slide, and leading to the disappearance of A-lines [7]. Z-line artifacts belong to one family of vertical artifacts, similar to B-line artifacts however, they are much shorter and do not extend to the bottom of the screen [8–10]. The mechanism of B-line and Z-line formation is still not fully examined.

2. Materials and Methods

2.1. Study Design

The study was conducted as a prospective cohort study. Approval from the local ethics committee (number: NKBBN/474/2018 and NKBBN/473/2018) and the informed consent of all participants in the study was duly obtained. Approval date for both 10 October 2018.

2.2. Study Population

Two groups of patients were examined: those patients diagnosed with ILD secondary to systemic sclerosis (group A), and patients diagnosed with pulmonary edema due to the exacerbation of congestive heart failure or to acute heart failure (group B). The exclusion criteria for patients with recognized ILD were as follows: comorbidity of congestive heart failure, pneumonia, and noncardiogenic edema. For patients diagnosed with pulmonary edema, the exclusion criteria were: pulmonary fibrosis, ILD, pneumonia, and noncardiogenic edema. The findings were anonymized and entered into a database by independent members of the research project. Written informed consent was obtained from those patients who agreed to participate. Duration of symptoms, examination findings, comorbidities, treatment, laboratory test results and echocardiography examination results, chest X-rays, and (in the case of ILD) high resolution computed tomography (HRCT) results were recorded. Patients were evaluated with LUS, and findings were recorded on standardized forms.

2.3. Study Protocol

LUS examinations were performed by three independent operators who are clinicians experienced in sonography (4 years, 10 years, and 10 years). Ultrasound examinations were recorded and re-analyzed by clinicians and physics specialists. An ultrasonography device (Philips Sparq, made in Bothell, WA, USA, 2013), with a 2–6 MHz convex curved transducer, and a 4–12 MHz linear transducer, was used. Patients were evaluated with the application of LUS performed in the same manner, and with the same technical criteria: (a) speckle reduction, compound imaging, and tissue harmonic imaging were switched off; (b) the focus of the image was positioned at the pleural line level; (c) imaging depth was set at 15 cm for a convex transducer, and at 6 cm for a linear transducer; (d) gain and time gain compensation (TGC) were adjusted in mid-scale. Moreover, when the lungs were examined with a convex transducer, vertical artifacts were evaluated with two extreme frequencies: 2 MHz, and then 6 MHz. When a convex transducer was employed, the sonomorphology of all artifacts, in both groups, was compared to each other, and analyzed statistically. When a linear transducer was employed, pleural line abnormalities were evaluated. Sonographic examinations were performed in the supine position and through the intercostal spaces on both sides of the chest. The probes were applied at four points over the front of the chest, and eight points over the posterior–lateral part of the chest.

2.4. Statistical Analysis

Data analyses were performed in R statistical software (open source (GNU license) statistical environment available with libraries (stat, pROC, plyr, ggplot2) at www.r-project.org (accessed on 26 February 2021)), version 3.6.0, using the following software: stat, plyr, ggplot2, pROC. The results were presented as the mean (standard deviation) for continuous variables and count (frequency) for discrete data. A p-value < 0.05 was regarded as statistically significant. Discrete data were compared for the groups with Pearson's χ^2 test, with appropriate modifications (i.e., Yates's correction, Fisher's exact test or V^2

test). For ultrasonographic features differentiating pulmonary fibrosis from heart failure, independently and in complex models, a receiver operating characteristic (ROC) curve was plotted, and the area under the curve (AUC) was calculated, determining whether it differed statistically by 0.5 with the application of the DeLong test. AUCs for differentiating parameters and predictive models were compared with the DeLong test. For quasi continuous variables (e.g., a total number of intercoastal spaces containing consolidations) optimal cut-off points were determined with two methods ("closest topleft" and Youden). For all diagnostic parameters, sensitivity, specificity, positive predictive value (PPV), negative predictive value (NPV), and the likelihood ratio for a positive LR(+) and negative result LR(−) were calculated. For statistically significant models, logistic regression was performed, calculating the odds ratio for a positive result of the tested model and a respective Akaike information criterion (AIC) value. AIC allows for the comparison of different models, where the lower its value, the better a given model is adjusted to the experimental data.

2.5. A Differentiating Model's Assumption

A complete predictive model should take into account as many differentiating elements as possible in different chest areas and the examination technique. We considered three complex models:

A—change in the image of the length of the vertical lines artifacts in three or more areas, and lack of consolidation as a fibrotic feature;

B—change in the image of length of the vertical artifacts in three or more areas, lack of: consolidation, irregularity, fragmentation, or blurring of the pleural line in at least two points as a feature of pulmonary fibrosis.

C—change in the image length of the vertical artifacts in three or more areas, or irregularity, fragmentation, or blurring of the pleural line in at least two points, as a feature of pulmonary fibrosis.

All models were created by taking into account the ultrasound protocol: use of the convex transducer to visualize vertical artifacts, followed by a linear one and the assessment of the pleural line. Models were limited to the anterior and posterolateral areas of the chest, which makes it possible to use them in the diagnosis of severe conditions, where ultrasound evaluation of the posterior surface of the chest is impossible. All models require the assessment of vertical artifacts and the pleural line in at least six points: upper, lower, and posterolateral bilaterally. The statistical properties of these models are presented in Table 1.

Table 1. Sensitivity and specificity of findings differentiating pulmonary edema from pulmonary fibrosis in interstitial lung disease (ILD). PLA—pleural line abnormalities, B to Z—Conversion of B-line artifacts to Z-line (with the frequency changed from 2 MHz to 6 MHz), *—single examination zone; SE—sensitivity, SP—specificity, PPV—positive predictive value, NPV—negative predictive value, LR(+)—positive likelihood ratio, LR(−)—negative likelihood ratio, AUC—area under the curve, AIC—Akaike information criterion, OR—odds ratio, CI—confidence interval.

Finding	SE (%)	SP (%)	PPV (%)	NPV (%)	LR(+)	LR(−)	AUC	*p*-Value	AIC	OR (95% CI)
PLA *	68	99	99	68	60	0.32	0.836	0.0002	510.8	184.08 (57.79–586.28)
B to Z *	61	76	80	55	2.58	0.51	0.687	0.03	779.8	5.03 (3.54–7.15)
model A	44	97	93	62	13.13	0.58	0.702	0.035	73.91	22.56 (2.73–186.47)
model B	91	97	97	91	27.19	0.097	0.936	7×10^{-6}	32.68	280.33 (27.52–2855.45)
model C	91	73	78	88	3.40	0.13	0.820	0.0012	60.98	26.58 (6.31–111.97)

3. Results

3.1. Group A Characteristics—Patients with ILD

A total of 32 consecutive patients diagnosed with ILD secondary to systemic sclerosis qualified for the study, 17 females and 15 males, with an average age of 56 (21.2 SD) years. Diagnosis of systemic sclerosis was based on current ACR/EULAR 2013 criteria. ILD in

this patient group was diagnosed on the basis of: patient's clinical picture, abnormalities in immune tests, HRCT as well as pulmonary function tests, bronchofiberoscopy, and echocariography. Infection as the cause of lesions affecting the interstitium was excluded based on microbiological tests.

3.2. Group B Characteristics—Patients with Pulmonary Edema

30 consecutive patients with a clinical diagnosis of exacerbation of left ventricular failure and acute pulmonary edema qualified for the study, 13 females and 17 males, with an average age of 69 (21 SD) years. Pulmonary edema was diagnosed on the basis of clinical symptoms (dyspnea, orthopnea, bilateral abnormalities on auscultation: crackles), high NT-proBNP (N-terminal pro—brain natriuretic protein) level, and typical abnormalities indicating edema visible in a chest X-ray and echocardiography.

3.3. Analysis of LUS Findings

During the study, 789 video clips (cineloops) were obtained and analyzed from patients with pulmonary edema, as well as 1152 cineloops from patients with ILD secondary to systemic sclerosis. While, 876 cineloops containing vertical artifacts evaluated with a convex transducer, and 644 cineloops assessing a specific area with a linear transducer were selected from the collected material, respectively. The recorded cineloops were assessed by clinicians and an engineer specializing in physics. Following the analysis of the video recordings, 128 cineloops were rejected due to inappropriate ultrasound device settings. The remaining cineloops were analyzed as regards the length of the artifacts (convex transducer), and determining whether a given artifact meets the definitional criteria of B-line (long artifact) or Z-line (short artifact). Moreover, the sonomorphology of the pleural line was analyzed in all patient, and evaluated with a linear transducer.

3.4. LUS Findings—Convex Transducer:

B-line artifacts are detected in patients with cardiogenic pulmonary edema and ILD. In this study, B-line artifacts were evaluated with a convex transducer, at a depth of 15 cm, consistently with the settings described in the methodology section. The ultrasound frequency was changed during the examination, and the evaluation was performed at two extreme values: 2 MHz and 6 MHz.

In the cineloops obtained from patients with both pulmonary edema and ILD, B-line artifacts were almost always visualized at the frequency of 2 MHz (consistent with the adopted definition of B-line artifact), in 68% of the examined points in patients with pulmonary edema, and 63% of the examined points in patients with ILD, respectively. Z-lines were visible only in single points: one (0.4%) in heart failure, and 11 (3%) in pulmonary fibrosis, whereas in three cases (0.8%) Z-lines coexisted with B-lines.

At the frequency of 6 MHz, cineloops recorded for patients with ILD presented Z-lines in 62% of the evaluated points and B-lines in 13%, whereas in 10% of the examined points the findings were mixed (Figure 1).

In patients with cardiogenic pulmonary edema, at the frequency of 6 MHz, B-line artifacts were present in 62% of the evaluated points, and Z-lines in 24%, including the mixed profile of B and Z in 16% of the examined areas (Figure 2). Consequently, the change in frequency leads to a change in the profile of vertical artifacts, whereas this phenomenon is much more frequent in patients with pulmonary fibrosis secondary to ILD. Collected data are demonstrated in Table 2.

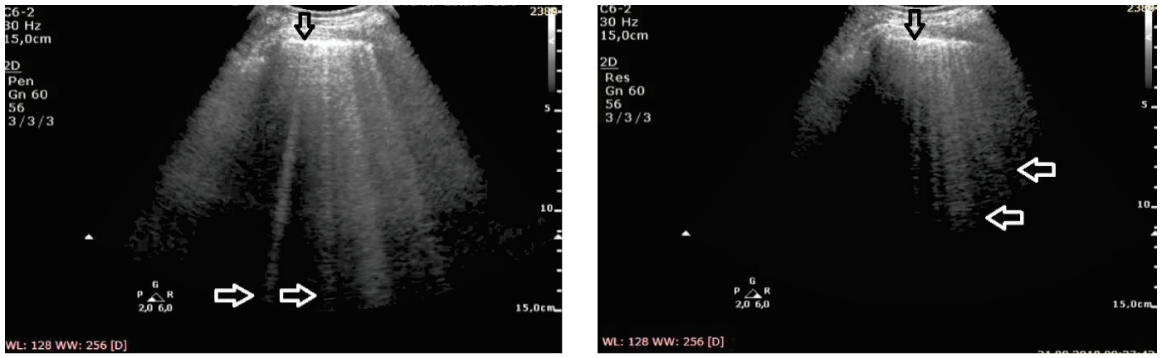

(**a**) (**b**)

Figure 1. Pulmonary fibrosis; (**a**) B-lines at 2 MHz (white arrows), irregular pleural line (black arrow), (**b**) Z-lines at 6 MHz (white arrows), irregular pleural line (black arrow).

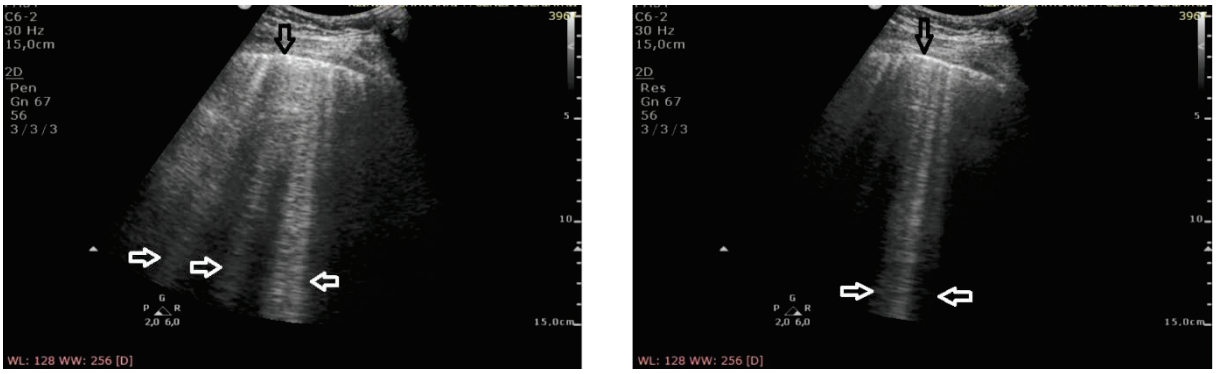

(**a**) (**b**)

Figure 2. Cardiogenic pulmonary edema; (**a**) B-lines at 2 MHz (white arrows), regular pleural line (black arrow), (**b**) B-lines at 6 MHz (white arrow), regular pleural line (black arrow).

Table 2. Conversion of vertical artifacts depending on the set ultrasound frequency.

Conversion of Vertical Artifacts with the Change of the Frequency from 2 MHz to 6 MHz	Pulmonary Edema (n = 250)	Pulmonary Fibrosis (n = 394)	p
B to B and Z	41 (16%)	41(10%)	$<10^{-6}$
B to Z	18 (7%)	193 (49%)	
B to non-verticals (A)	0	1 (<1%)	
B and Z to Z	0	3 (<1%)	
A to B	1 (<1%)	0	
Z to non-verticals (A)	0	2 (<1%)	
No change	190 (76%)	154 (39%)	

The change of the ultrasound frequency from 2 to 6 MHz leads to a shortening or even the disappearance of vertical artifacts (conversion to A lines was observed in three cases), and this phenomenon is more characteristic for pulmonary fibrosis than edema (61% vs. 24% of the examined areas, $p < 10^{-6}$).

Differentiating the etiology of B-line artifacts (pulmonary edema versus pulmonary fibrosis) with the use of extreme frequencies (2 MHz and 6 MHz) is possible, both by detecting Z-lines at the frequency of 6 MHz (sensitivity 76%, specificity 62%, PPV 80%,

NPV 56%, LR(+) 2.57, LR(−) 0.50), and by observing the change of the B-line profile to the Z-line when the frequency is increased (sensitivity 76%, specificity 61%, PPV 80%, NPV 55%, LR(+) 2.58, LR(−) 0.51, AUC= 0.687, $p = 0.03$). Statistically, both methods yield analogous results (to compare: AUC $p = 0.67$).

3.5. LUS Findings—Linear Transducer

Both groups (A and B), having been examined with a convex transducer, were re-evaluated with a linear transducer. Complete data obtained from 641 projections were analyzed statistically.

In patients with cardiogenic pulmonary edema, the pleural line was evaluated in 260 points. In 257 (98.8%) points, no pleural line abnormalities were detected. Only in three (1.2%) points were irregularities in the pleural line observed. Moreover, in 23% (60) of the evaluated areas, subpleural consolidations (up to 2–3 mm in diameter) were found in patients with cardiogenic pulmonary edema. These small consolidations correlated statistically significantly with vertical artifacts that, in the majority of cases, converted from B-lines to Z-lines when the frequency was changed from 2 MHz to 6 MHz in the convex probe (in 85%, $p < 10^{-6}$).

In patients with pulmonary fibrosis, in all 381 points evaluating the pleural line, the following abnormalities were detected: coexisting irregularity and fragmentation of the pleural line in 68% (259 localizations) and blurred pleural line in 22% (84) of all evaluated points; the apparent thickening of the pleural line (>2 mm) was detected in only one (0.26%) area. Irregular and/or fragmented pleural line was present in 97% (230 out of 236) of the patients in the group in which B-lines converted into Z-lines (when the frequency was changed from 2 MHz to 6 MHz) (Figure 3).

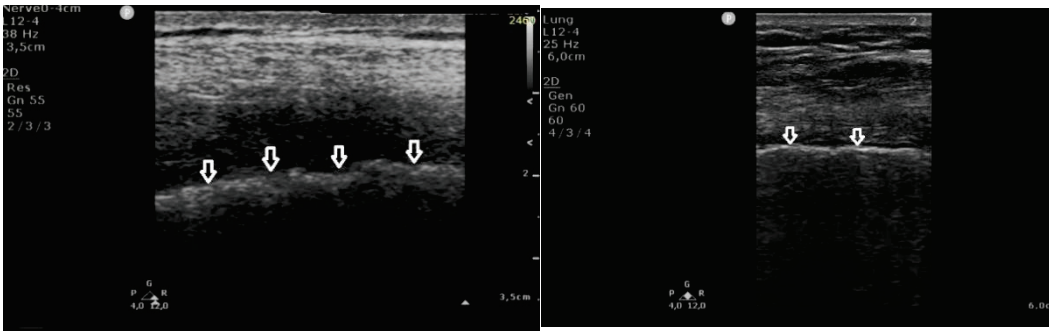

(**a**) (**b**)

Figure 3. Linear transducer used for the evaluation of pleural line abnormalities: (**a**) irregular, blurred pleural line (white arrows), coarse in appearance, in pulmonary fibrosis; (**b**) regular pleural line, with preserved echogenicity (white arrows), in pulmonary edema.

These findings indicate that an irregular and fragmented pleural line is a feature that differentiates pulmonary fibrosis from cardiogenic pulmonary edema. Detection of this feature in a single evaluated point allows for diagnosis of pulmonary fibrosis with a specificity of 99%, a sensitivity of 68%, PPV 99%, NPV 68%, LR(+) 60, and LR(−) 0.32, at AUC = 0.836 and $p = 0.0002$.

An attempt at diagnosis: a differentiating model:

Although both features described above differentiate fibrosis from edema, a single observation point is not sufficient.

We proposed the best final model B, shown in Figure 4, as a decision tree graph. It is characterized not only by excellent Sp, Se, PPV, and NPV, but also the lowest Akaike criterion value. A low negative (<0.1) and high positive (>10) likelihood ratio indicates a high discriminatory value of the model. For example: suppose that a patient has an a priori probability of fibrosis of 50%. If the test result is positive for fibrosis, a posteriori

probability increases to 96%, or else it falls to 9%. A comparative graph of the ROC curves tested is presented in Figure 5.

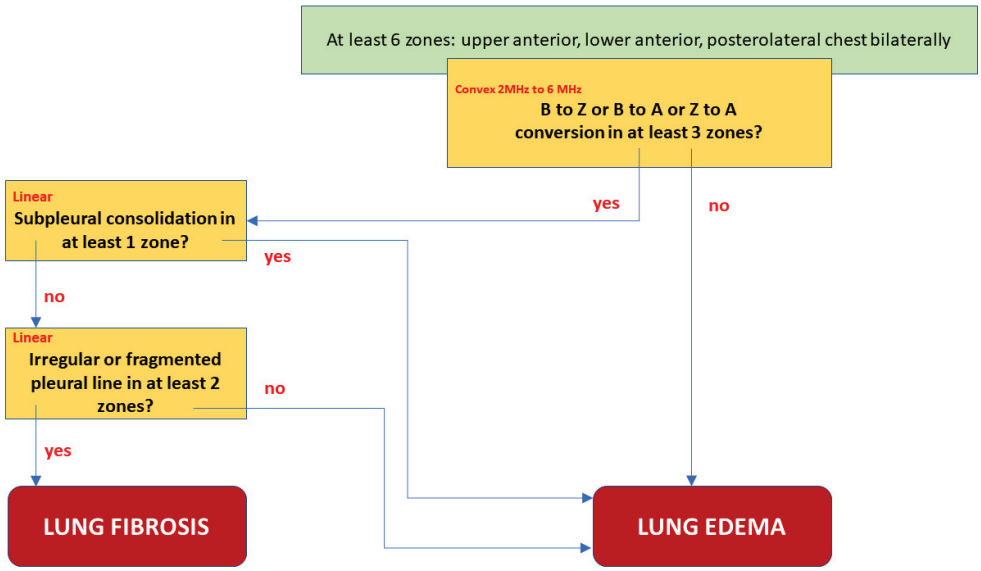

Figure 4. Differentiating between pulmonary fibrosis and cardiogenic lung edema. Decision tree corresponding with model B (in the text).

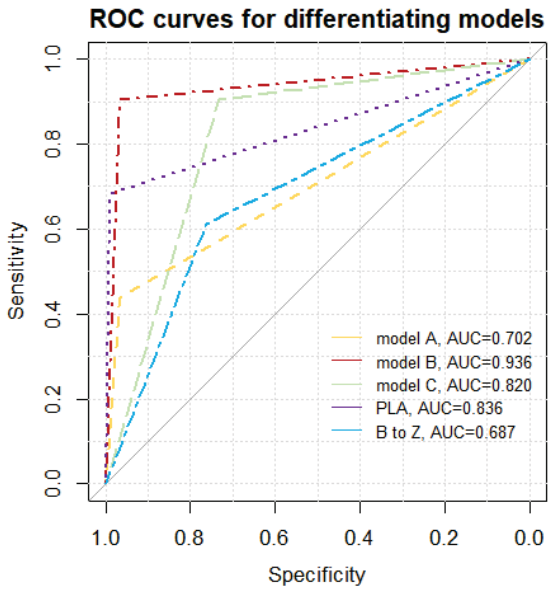

Figure 5. Receiver operating characteristic (ROC) curves for methods of differentiation between pulmonary fibrosis and pulmonary edema. The area under the curve for model B is significantly greater than for other models, with maximal *p*-value of 0.0033 (model B compared to PLA); PLA—pleural line abnormalities in a single examination zone, B to Z—Conversion of B-line artifacts to Z-line (with the frequency changed from 2 MHz to 6 MHz) in a single examination zone; model A—any conversion of vertical artifacts (B to Z, B to A, Z to A with the frequency changed from 2 MHz to 6 MHz) in 3 or more areas, and lack of consolidations, model B—any conversion of vertical artifacts (B to Z, B to A, Z to A with the frequency changed from 2 MHz to 6 MHz) in 3 or more areas, lack of consolidations, and PLA in at least 2 zones, model C—any conversion of vertical artifacts (B to Z, B to A, Z to A with the frequency changed from 2 MHz to 6 MHz) in 3 or more areas, and PLA in at least 2 zones. AUC—area under the curve.

4. Discussion

4.1. Physical Hypothesis

It has been suggested in a previous paper [11,12] that every vertical artifact which can be observed in a LUS image is probably generated by multiple reflections between the walls of the lung aerated spaces. It is highly unlikely that a vertical artifact can be generated by a vibrating air bubble (alveolus or an alveolus partially filled with water) [12]. An acoustic trap is needed to generate a vertical artifact: (a) an acoustic pulse is transmitted from the thoracic wall to the trap through a thickened interstitial space; (b) multiple reflections between the walls of the aerated spaces which surround the trap generate an acoustic perturbation inside the trap; (c) such an acoustic perturbation acts as an ultrasound source, and gradually re-radiates the trapped acoustic energy to the transducer [12,13]. Figure 6 shows two types of acoustic trap. The panel on the left shows a medium (water, blood, tissue, etc.) which is connected to the thoracic wall by means of a single channel. The panel on the right shows a more complex acoustic trap, which is formed by sparse media connected to the thoracic wall by means of multiple channels. In the first case, the aperture of the acoustic trap is given by a single channel, while in the second case by multiple channels.

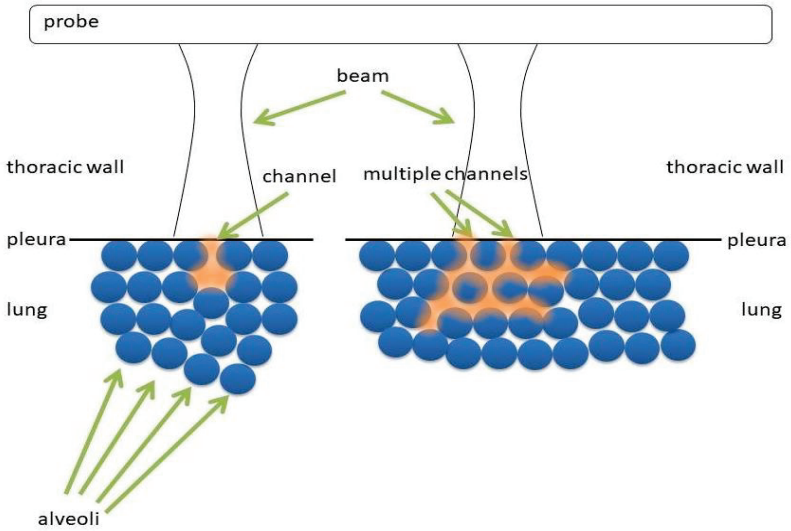

Figure 6. Two types of access channels to the underlying acoustic traps for ultrasound beams.

The characteristics which distinguish vertical artifacts are: brightness, length, lateral width, and internal structure. In this study, only the length of vertical artifacts has been analyzed, depending on the change in ultrasound frequency.

The length of an artifact is an interesting parameter, even though it represents really complex information. It depends on the duration of the trap response which, from a theoretical point of view, is infinite. Once a US pulse has been partially trapped by an acoustic trap, the latter re-radiates the trapped energy during an infinite time interval. Therefore, the question is: Why do we sometimes observe artifacts which reach the bottom of the screen and sometimes shorter artifacts? The answer lies in the signal to noise ratio (SNR). The amplitude of the trap signal decreases during a time interval until the signal is no longer distinguishable from the noise, and there are no possibilities for the time gain compensation (TGC) to make it visible. Therefore, now the question becomes: How much does the trap signal decrease during a time interval? This is an interesting question, and the answer should open our minds to the world of ultrasound artifacts. As an example, Figure 7 shows three different acoustic traps with a single channel aperture at the top. The left panel shows an almost closed trap. Once the acoustic energy is transmitted to this trap, the trapped energy escapes slowly, since there is an impenetrable air barrier everywhere except at the small aperture at the top. In this case, a long artifact is expected. The central

panel displays a trap which is closed at the bottom and opened at the top. Once the acoustic energy is transmitted to the trap, the trapped energy meets an impenetrable barrier at the bottom and at the sides of the trap. However, a large aperture with a low impedance mismatch exists at the top which allows both: a minimal reflection (towards the bottom of the trap), and a significant transmission (towards the transducer) of the trapped energy. In this case, a short artifact is expected. The right panel shows a few traps with single apertures at the top, where traps are connected by secondary channels. Once acoustic energy is transmitted to one of these traps through a single aperture at the top, the trapped energy can escape the trap both through the aperture at the top (by providing in this way the artifact which is visualized by the transducer), and through the secondary channels. Due to the energy loss through the secondary channels, a shorter artifact is expected in this case also.

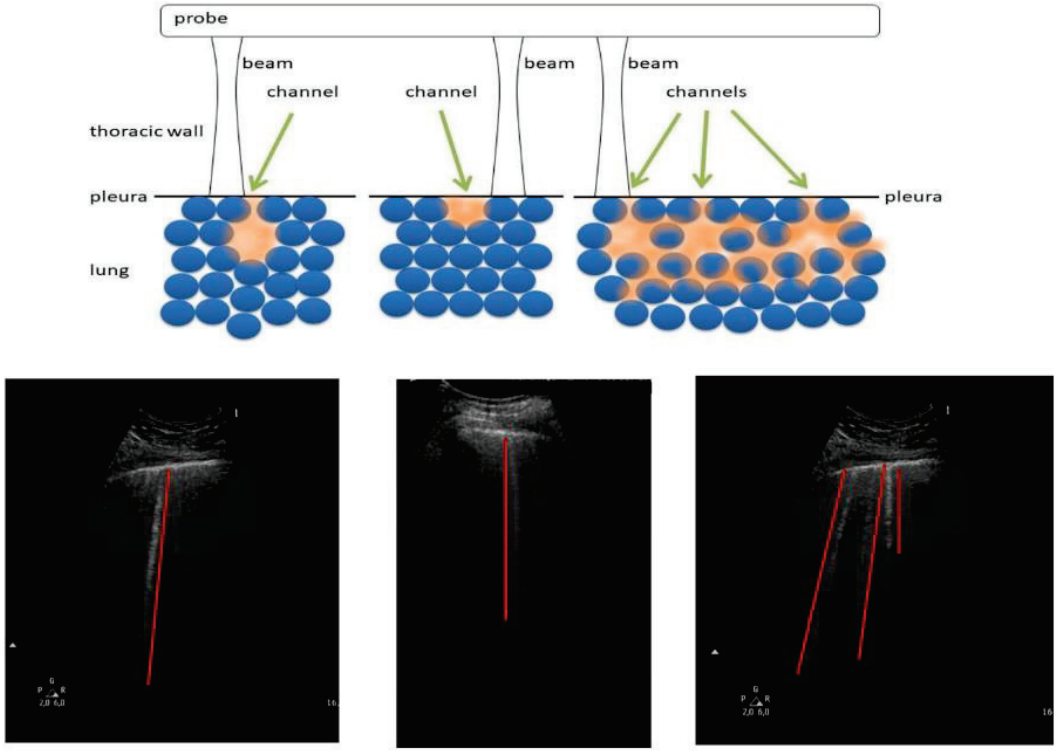

Figure 7. Relations between the length of a vertical artifact and the shape of the acoustic trap.

4.2. From the Physical to the Clinical Significance of the Study Results

The analysis of LUS findings in the case of diseases involving interstitial space presently poses a serious challenge for clinicians. In many diseases that affect the interstitium and alveoli, vertical reverberation artifacts are detected. B-line artifacts are found, for instance, in: cardiogenic pulmonary edema, noncardiogenic pulmonary edema, and ILD (both in the active phase, when ground-glass opacities are found in HRCT, and in the fibrotic phase, in which honeycombing is the corresponding HRCT finding) [10,14–17]. Z-line artifacts have not yet been described as having clinical significance.

So far, the literature in the diagnosis of pulmonary fibrosis has been based mainly on B-line artifacts [18]. It has been proved, inter alia, that the more severe the pulmonary fibrosis, the more B-line artifacts are visible on lung ultrasound images [19–22]. The publications also emphasized the importance of coexistence with B-line artifacts of lesions in the pleural line [23–28]. Consideration should be given here to the diversity of the study protocols, depending on the investigator. The use of convex and linear probes allows for a general and detailed assessment of lesions on the pleural line and the subpleural area [28]. This shows how technical aspects can influence the quality of the ultrasound examination. Optimizing

the settings of the ultrasound machine becomes another link in improving the quality of ultrasound in the diagnosis of diseases that affect the interstitial space of the lungs.

4.3. Pulmonary Fibrosis

We observed a change in the length of vertical artifacts in both examined groups, and the concurrent presence of pleural line abnormalities. In the first examined group (A), conversion of B-lines to Z-lines was usually accompanied with pleural line abnormalities and/or small subpleural lesions. In this patient group, both B-line to Z-line, at two extreme frequencies (2 MHz and 6 MHz) this most likely results from generating artifacts in acoustic traps, that are adjacent to the pleural line, by means of a single large channel and multiple channels. Probably both types of traps are present at the pleural line, given the apparent shape of the pleural line, which appears irregular and blurred.

4.4. Pulmonary Edema

Changes that occurred during the conversion of B-line artifacts in the second patient group (B) were much more diversified. A large number of B-lines did not undergo conversion with a change in ultrasound frequency. Concurrently, some B-line artifacts converted to Z-lines, or B- and Z-lines. However, a correlation between the conversion of B-line artifacts to Z-lines (or B- and Z-lines) and coexisting pleural line abnormalities was observed in this group as well. This was most likely associated with the presence of microconsolidations (for instance, due to small areas of atelectasis caused by pulmonary edema).

This study also demonstrates that differentiating a cardiogenic etiology of B-line artifacts from a pulmonary etiology should be based, both on the analysis of the artifact length after the conversion, and on the evaluation of pleural line abnormalities. Accounting for both findings results in a much higher accuracy in differentiating the causes of lesions affecting the insterstitium.

4.5. Study Limitations

The only analyzed feature was the artifact length. It is possible that more factors (brightness, lateral width, internal structure) are significant in differentiating the etiology of vertical artifacts; however, these factors were not analyzed in this study.

The second limitation is the selection of patients for the study group. Patients with chronic pulmonary congestion, but in a stable clinical condition, were not included in the study.

The third limitation is given by the lack of information on the pulse power spectrum and on the modulation transfer functions of the probes.

5. Conclusions

The visualization and sonomorphological analysis of vertical artifacts with the application of a convex transducer employing two different, extreme frequencies (2 MHz and 6 MHz) may be useful in differentiating lesions affecting the interstitium (cardiogenic pulmonary edema vs lesions due to ILD). However, a higher accuracy is achieved when the pleural line and subpleural lesions are concurrently evaluated with a linear transducer.

Author Contributions: Conceptualization, N.B., A.S. and G.S.; Data curation, N.B., A.W. and J.C.; Formal analysis, N.B., and M.D.; Investigation, N.B. and M.D.; Methodology, N.B., A.S. and G.S.; Supervision, N.B., M.D. All authors have read and agreed to the published version of the manuscript.

Funding: This research received no external funding.

Institutional Review Board Statement: The study was conducted as a prospective cohort study. Approval from the local ethics committee (number: NKBBN/474/2018 and NKBBN/473/2018, approval date for both 10 October 2018) and the informed consent of all participants in the study was duly obtained.

Informed Consent Statement: Informed consent was obtained from all subjects involved in the study.

Data Availability Statement: Data sharing not applicable.

Conflicts of Interest: The authors declare no conflict of interest.

References

1. Buda, N.; Kosiak, W.; Wełnicki, M.; Skoczylas, A.; Olszewski, R.; Piotrkowski, J.; Skoczyński, S.; Radzikowska, E.; Jassem, E.; Grabczak, E.M.; et al. Recommendations for Lung Ultrasound in Internal Medicine. *Diagnostics* **2020**, *10*, 597. [CrossRef]
2. Buessler, A.; Chouihed, T.; Duarte, K.; Bassand, A.; Huot-Marchand, M.; Gottwalles, Y.; Pénine, A.; André, E.; Nace, L.; Jaeger, D.; et al. Accuracy of Several Lung Ultrasound Methods for the Diagnosis of Acute Heart Failure in the ED: A Multicenter Prospective Study. *Chest* **2020**, *157*, 99–110. [CrossRef] [PubMed]
3. Ferreira, A.H.; Pazin-Filho, A. Lung Ultrasound in a Patient with ARDS Secondary to Pancreatitis. *Chest* **2020**, *158*, e85–e87. [CrossRef]
4. Pivetta, E.; Girard, E.; Locascio, F.; Lupia, E.; Martin, J.D.; Stone, M. Self-Performed Lung Ultrasound for Home Monitoring of a Patient Positive for Coronavirus Disease 2019. *Chest* **2020**, *158*, e93–e97. [CrossRef]
5. Goff, C.G.L.; Vivalda, L.; Foligno, S.; Loi, B.; Yousef, N.; De Luca, D. Effect of Different Probes and Expertise on the Interpretation Reliability of Point-of-Care Lung Ultrasound. *Chest* **2020**, *157*, 924–931. [CrossRef] [PubMed]
6. Buda, N.; Andruszkiewicz, P.; Czuczwar, M.; Gola, W.; Kosiak, W.; Nowakowski, P.; Sporysz, K. Consensus of the Study Group for Point-of-Care Lung Ultrasound in the intensive care management of COVID-19 patients. *Anaesthesiol. Intensive Ther.* **2020**, *52*, 83–90. [CrossRef] [PubMed]
7. Lichtenstein, D.A. Current Misconceptions in Lung Ultrasound: A Short Guide for Experts. *Chest* **2019**, *156*, 21–25. [CrossRef] [PubMed]
8. Soldati, G.; Demi, M.; Demi, L. Ultrasound patterns of pulmonary edema. *Ann. Transl. Med.* **2019**, *7* (Suppl. 1), S16. [CrossRef] [PubMed]
9. Goffi, A.; Kruisselbrink, R.; Volpicelli, G. The sound of air: Point-of-care lung ultrasound in perioperative medicine. *Can. J. Anesth. J. Can. D'anesthésie* **2018**, *65*, 399–416. [CrossRef]
10. Lichtenstein, D.; Meziere, G.; Biderman, P.; Gepner, A.; Barre, O. The comet-tail artifact: An ultrasound sign of alveolar interstitialsyndrome. *Am. J. Respir. Crit. Care Med.* **1997**, *156*, 1640–1646. [CrossRef]
11. Soldati, G.; Demi, M.; Inchingolo, R.; Smargiassi, A.; Demi, L. The role of ultrasound lung artefacts in the diagnosis of respiratory diseases. *Expert Rev. Respirat. Med.* **2019**, *13*, 163–172. [CrossRef]
12. Demi, M.; Prediletto, R.; Soldati, G.; Demi, L. Physical mechanisms providing clinical information from ultrasound lung images: Hypotheses and early confirmations. *IEEE Trans. Ultrasound Ferroelectr. Freq. Control.* **2020**, *67*, 612–622. [CrossRef]
13. Soldati, G.; Smargiassi, A.; Demi, L.; Inchingolo, R. Artifactual lung ultrasonography: It is a matter of traps, order, and disorder. *Appl. Sci.* **2020**, *10*, 1570. [CrossRef]
14. Mayo, P.H.; Copetti, R.; Feller-Kopman, D.; Mathis, G.; Maury, E.; Mongodi, S.; Mojoli, F.; Volpicelli, G.; Zanobetti, M. Thoracic ultrasonography: A narrative review. *Intensive Care Med.* **2019**, *45*, 1200–1211. [CrossRef] [PubMed]
15. Van Sloun, R.J.; Demi, L. Localizing B-lines in Lung Ultrasonography by Weakly-Supervised Deep Learning, in-vivo results. *IEEE J. Biomed. Health Inform.* **2019**, *24*, 957–964. [CrossRef]
16. Bekgoz, B.; Kilicaslan, I.; Bildik, F.; Keles, A.; Demircan, A.; Hakoglu, O.; Coskun, G.; AvniDemir, H. BLUE protocol ultrasonography in Emergency Department patients presenting with acute dyspnea. *Am. J. Emerg. Med.* **2019**, *37*, 2020–2027. [CrossRef]
17. Mohanty, K.; Karbalaeisadegh, Y.; Blackwell, J.; Ali, M.; Masuodi, B.; Egan, T.; Muller, M. In-Vivo Assessment of Pulmonary Fibrosis and Pulmonary Edema in Rodents Using Ultrasound Multiple Scattering. *IEEE Trans. Ultrason Ferroelectr. Freq. Control* **2020**, *67*, 2274–2280. [CrossRef] [PubMed]
18. Barskova, T.; Gargani, L.; Guiducci, S.; Randone, S.B.; Bruni, C.; Carnesecchi, G.; Conforti, M.L.; Porta, F.; Pignone, A.; Caramella, D.; et al. Lung ultrasound for the screening of interstitial lung disease in very early systemic sclerosis. *Ann. Rheum. Dis.* **2013**, *72*, 390–395. [CrossRef]
19. Porzezińska, M.; Buda, N.; Osowicka, M.; Kosiak, W.; Rzepko, R.; Radzikowska, E.; Słomiński, J.M.; Jassem, E. Transthoracic lung ultrasonography in pulmonary alveolar proteinosis—case report. *Sarcoidosis Vasc. Diffuse Lung Dis.* **2013**, *30*, 317–320.
20. Gargani, L.; Doveri, M.; D'Errico, L.; Frassi, F.; Bazzichi, M.L.; Delle Sedie, A.; Scali, M.C.; Monti, S.; Mondillo, S.; Bombardieri, S.; et al. Ultrasound lung comets in systemic sclerosis: A chest sonography hallmark of pulmonary interstitial fibrosis. *Rheumatology (Oxford)* **2009**, *48*, 1382–1387. [CrossRef]
21. Buda, N.; Kosiak, W.; Smoleńska, Z.; Zdrojewski, Z. Transthoracic lung ultrasound in the monitoring of interstitial lung disease: A case of scleroderma. *Pol. Arch. Med. Wewn.* **2013**, *123*, 721–722. [CrossRef] [PubMed]
22. Buda, N.; Kosiak, W. Is a linear probe helpful in diagnosing diseases of pulmonary interstitial spaces? *J. Ultrason.* **2017**, *17*, 136–141. [CrossRef]
23. Wohlgenannt, S.; Gehmacher, O.; Gehmacher, U.; Kropf, A.; Mathis, G. Sonographic finding in interstitial lung diseases. *Ultraschall Med.* **2001**, *22*, 27–33. [CrossRef]
24. Mohammadi, A.; Oshnoei, S.; Ghasemi-rad, M. Comparison of a new, modified lung ultrasonography technique with high-resolution CT in the diagnosis of the alveolo-interstitial syndrome of systemic scleroderma. *Med. Ultrason.* **2014**, *16*, 27–31. [CrossRef] [PubMed]
25. Pinal-Fernandez, I.; Pallisa-Nuñez, E.; Selva-O'Callaghan, A.; Castella-Fierro, E.; Simeon-Aznar, C.P.; Fonollosa-Pla, V.; Vilardell-Tarres, M. Pleural irregularity, a new ultrasound sign for the study of interstitial lung disease in systemic sclerosis and antisynthetase syndrome. *Clin. Exp. Rheumatol.* **2015**, *33* (Suppl. 91), S136–S141.

26. Buda, N.; Piskunowicz, M.; Porzezińska, M.; Kosiak, W.; Zdrojewski, Z. Lung Ultrasonography in the Evaluation of Interstitial Lung Disease in Systemic Connective Tissue Diseases: Criteria and Severity of Pulmonary Fibrosis—Analysis of 52 Patients. *Ultraschall Med.* **2016**, *37*, 379–385. [CrossRef]
27. Buda, N.; Masiak, A.; Zdrojewski, Z. Utility of lung ultrasound in ANCA-associated vasculitis with lung involvement. *PLoS ONE* **2019**, *14*, e0222189. [CrossRef] [PubMed]
28. Song, G.G.; Bae, S.C.; Lee, Y.H. Diagnostic accuracy of lung ultrasound for interstitial lung disease in patients with connective tissue diseases: A meta-analysis. *Clin. Exp. Rheumatol.* **2016**, *34*, 11–16.

diagnostics

MDPI

Review

The Mechanisms Underlying Vertical Artifacts in Lung Ultrasound and Their Proper Utilization for the Evaluation of Cardiogenic Pulmonary Edema

Toru Kameda [1,*], Naohisa Kamiyama [2] and Nobuyuki Taniguchi [1]

[1] Department of Clinical Laboratory Medicine, Jichi Medical University, Shimotsuke 329-0498, Japan; taniguch@jichi.ac.jp
[2] Ultrasound Division, GE Healthcare Japan, Hino 191-8503, Japan; naohisa.kamiyama@ge.com
* Correspondence: kamekame@pb3.so-net.ne.jp

Abstract: The recent advances in lung ultrasound for the diagnosis of cardiogenic pulmonary edema are outstanding; however, the mechanism of vertical artifacts known as B-lines used for the diagnosis has not yet been fully elucidated. The theory of "acoustic trap" is useful when considering the generation of vertical artifacts. Basic research in several studies supports the theory. Published studies with pilot experiments indicate that clarification of the relationship between the length and intensity of vertical artifacts and physical or acoustic composition of sources may be useful for differentiating cardiogenic pulmonary edema from lung diseases. There is no international consensus with regard to the optimal settings of ultrasound machines even though their contribution to the configuration of vertical artifacts is evident. In the clinical setting, the configuration is detrimentally affected by the use of spatial compound imaging, the placement of the focal point at a deep level, and the use of multiple focus. Simple educational materials using a glass microscope slide also show the non-negligible impact of the ultrasound machine settings on the morphology of vertical artifacts.

Keywords: lung ultrasound; cardiogenic pulmonary edema; B-line; vertical artifact; spatial compound imaging; focal point

Citation: Kameda, T.; Kamiyama, N.; Taniguchi, N. The Mechanisms Underlying Vertical Artifacts in Lung Ultrasound and Their Proper Utilization for the Evaluation of Cardiogenic Pulmonary Edema. *Diagnostics* **2022**, *12*, 252. https://doi.org/10.3390/diagnostics12020252

Academic Editors: Marcello Demi and Gino Soldati

Received: 21 December 2021
Accepted: 18 January 2022
Published: 20 January 2022

Publisher's Note: MDPI stays neutral with regard to jurisdictional claims in published maps and institutional affiliations.

1. Introduction

In lung ultrasound, the presence and severity of pulmonary edema are evaluated with vertical artifacts known as B-lines. In an international consensus statement published in 2012, B-lines were defined as discrete, laser-like vertical hyperechoic artifacts that arise from the pleural line and extend to the bottom of the screen without fading [1]. The term "multiple B-lines" refers to the presence of three or more B-lines in a longitudinal plane between two ribs. In patients with cardiogenic pulmonary edema, multiple B-lines are usually distributed bilaterally and diffusely [1,2]. A multicenter, prospective study found that the implementation of lung ultrasound in addition to the initial conventional assessment improved the diagnostic accuracy for cardiogenic pulmonary edema [3]. A systematic review and meta-analysis demonstrated that lung ultrasound has higher sensitivity than, and similar specificity to, chest X-ray in the diagnosis of cardiogenic pulmonary edema [4]. Lung ultrasound can also drastically contribute to reducing the time spent on the diagnosis [5]. In addition, the number and spatial extent of B-lines allow the assessment of the severity of pulmonary edema or a semi-quantitative estimation of extravascular lung water [6].

Recent advances in lung ultrasound for the diagnosis of cardiogenic pulmonary edema have been outstanding, as mentioned above. However, the mechanisms underlying the vertical artifacts in cardiogenic pulmonary edema have not been fully elucidated. Furthermore, there is no international consensus with regard to the optimal settings of ultrasound machines even though their contribution to the configuration of vertical artifacts

is evident [7–9]. They may affect the diagnostic accuracy inappropriately [9]. In this article, we review the clinical knowledge and basic research on the generation of vertical artifacts. We then demonstrate how the machine settings impact the configuration of the vertical artifacts.

2. Generation of Vertical Artifacts

2.1. Clinical Implications

In cardiogenic pulmonary edema, a rapid increase in hydrostatic pressure in the pulmonary capillaries leads to increased fluid transfer into the interstitium and alveolar spaces. High capillary pressures can also cause lung injury and barrier disruption which increases permeability and fluid transfer [10].

Chest CT is not a standard imaging modality to diagnose cardiogenic pulmonary edema; however, it is very useful for grasping the distribution of edema in the lung tissue. The findings of interstitial pulmonary edema are ground-glass opacities and interlobular septal and bronchovascular thickening. Alveolar edema appears as airspace consolidation, in addition to the above findings [11,12].

Lichtenstein et al. compared ultrasound images with CT images and indicated that B-lines originate from the thickening of the sub-pleural interlobular septa and ground-glass opacities [13]. Many researchers then reported the association of cardiogenic pulmonary edema and lung diseases with B-lines in their observational studies. Now, B-lines are thought to be generated when the air content decreases and lung density increases due to transudate, exudate, blood, collagen, or hyper-cellularity in the subpleural space [14]. However, the sonographic–pathologic correlation in B-lines and their origin in the sub-pleural space have not yet been fully elucidated with a more scientific method [7]. On top of that, B-lines based on the current definition [1] are not specific for pulmonary edema; therefore, clinicians have to consider their distribution in addition to history and physical examination findings for the diagnosis.

2.2. The Theory of Acoustic Trap

Soldati et al. introduced the interesting theory of "acoustic trap" in the generation of vertical artifacts, including B-lines [15]. An acoustic trap corresponds to a small volume of fluid in cardiogenic pulmonary edema, inflammatory changes in pulmonary diseases, surrounded by aerated alveoli with an acoustic channel on top of the trap at the pleural line. Once an ultrasound beam enters the trap through the channels, it is trapped and reflected by the wall of aerated alveoli multiple times with scattering. The reflection and scattering phenomena act as successive ultrasound sources, with the trapped energy radiated to the transducer little by little. With a larger channel, the ultrasound energy can escape more easily, and opportunities for reflection consequently decrease [7,16].

2.3. Our Basic Research Supporting the Theory

We developed simple experimental models that generate vertical artifacts [7,8]. In one of our previous studies, a long vertical artifact was generated by a spindle-shaped juice sack and a string-shaped glucomannan gel on a phantom of the chest wall and pleura. However, a spot of ultrasound gel did not generate a long vertical artifact; rather, it generated a short vertical artifact. Based on these results, we suspected that the point of contact of the source with the polypropylene sheet corresponding to the visceral pleura was a key factor influencing the generation, configuration and echo intensity of vertical artifacts [8].

In another study, we used an ultrasound gel spot to imitate the source of the vertical artifact and a block of bacon as a chest wall phantom. As the size of the point of contact between the gel spot on the sheet and the phantom decreased when the sheet was peeled, a vertical artifact was generated and/or extended deeper. Next, objects of different shapes made using gel balls were used to observe the generation of vertical artifacts and compare the echo intensity. For a given shape, the intensity was markedly higher in one model with the point of contact than in the other model with the plane of contact. With the same point

or plane of contact, the echo intensity was higher in the taller model. The results obtained from the simple experimental models support the acoustic trap theory [7]. The length and echo intensity of the vertical artifacts depend on the relative size of the channel to the trap volume [7,16]. On top of that, short vertical artifacts, which do not meet the definition of B-lines, may provide clinically significant information about the morphology and structure of the subpleural part [17–19].

In the latter study, we used materials that have similar acoustic properties to water as the sources of vertical artifacts [7]. The model seems to be suitable for considering the mechanism underlying the B-lines in cardiogenic pulmonary edema. If a material with significant sound attenuation is used instead of ultrasound gel or a "pure" gel ball for a given model, it is speculated that the length and intensity of the vertical artifact will be shorter and lower, respectively [7]. This model may be suitable when considering the mechanism underlying B-lines in pulmonary diseases, such as interstitial pneumonia or pulmonary fibrosis. We therefore performed a pilot experiment using a simple model based on this hypothesis. At first, we prepared two tiny hemispherical gel objects of 3.6 mm in diameter that were made of de-aerated water and powdery agar (3%), and a hemispherical gel object of the same size that was made of de-aerated water, powdery agar (3%) and powdery graphite (5%), in which the value of attenuation coefficient was 0.5 dB/cm/MHz. The former and latter object were named "object A" and "object G", respectively. First, the polypropylene sheet was laid onto a block of bacon as a chest wall phantom, which was coated with a thin layer of ultrasound gel. Two objects A and one object G were then placed onto the sheet through a thin layer of ultrasound gel, as shown in Figure 1a,b. The ultrasound image was obtained by LOGIQ S8 scanner (GE Healthcare) with 9 MHz linear transducer (9L-D). Imaging mode was fundamental B-mode with 6.0 MHz with overall gain and dynamic range were 60 and 72, respectively. Time gain compensation (TGC) was flat as used in clinical examinations. The differences in the configurations of vertical artifacts between the two objects A was the same as that in our previous study [7]. The vertical artifact generated from object G was visually attenuated on the deeper side, in line with the hypothesis (Figure 1c). This pilot experiment and published studies [17,20] indicate that clarification of the relationship between the length and intensity of vertical artifacts and the physical or acoustic composition of the sources may be useful for differentiating a cardiogenic pulmonary edema from a lung disease. This notion needs to be verified in future basic and clinical studies.

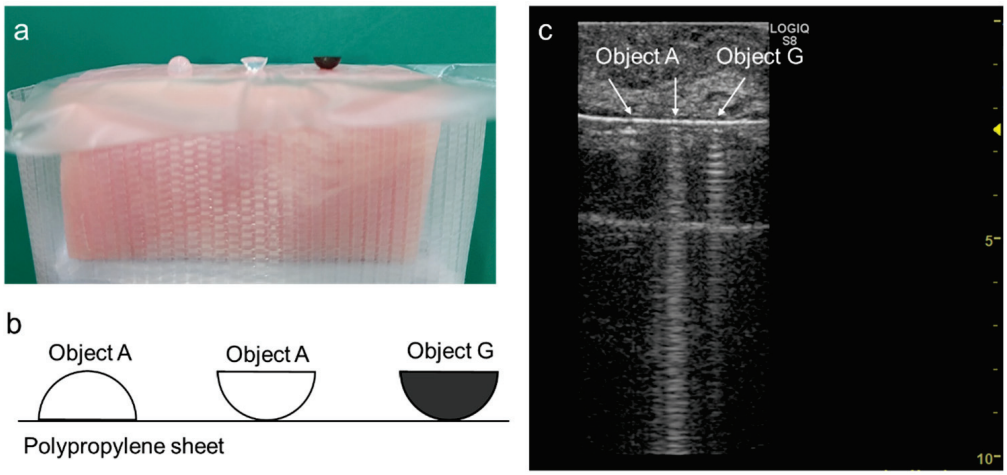

Figure 1. Photograph (**a**) and schematic representation (**b**) of the experimental system and an ultrasound image (**c**) obtained with the system. The object A on the left side generated a short vertical artifact. The object A on the right side generated a long vertical artifact without a qualitative attenuation according to the depth. The object G generated a vertical artifact which was visually attenuated on the deeper side.

3. Influence of Machine Settings and the Selection of Transducers on Vertical Artifacts

The optimal machine settings to visualize B-lines are not completely clear, even in the current situation [9]. Many published studies that used B-lines as a metric do not provide information on the machine settings [9]. In this chapter, we explain several machine settings that have a large impact on the configuration of vertical artifacts based on our basic research [8] and clinical experience with some references [21]

3.1. Spatial Compound Imaging

Spatial compound imaging is now available on most ultrasound machines. The main purposes are to improve contrast resolution and to reduce acoustic shadowing. This method acquires three or more multiple images by multiple transmission with different angles, and creates averaging images by overlaying them incoherently [22] (Figure 2). When a linear probe is used with spatial compound imaging enabled, a single B-line changes to multiple lines starting from the same depth of the pleural line [8] (Figures 3 and 4). This is because the vertical artifact generates associated with the scan line. Thus, the vertex of the multiple lines is considered to be a point of the acoustic trap. The angle made by the lines depends on the machine settings. These multiple lines appear to overlap each other with convex probes in some ultrasound machines. In such cases, the resulting "single" line features a divergent appearance with increasing depth [23] (Figure 5).

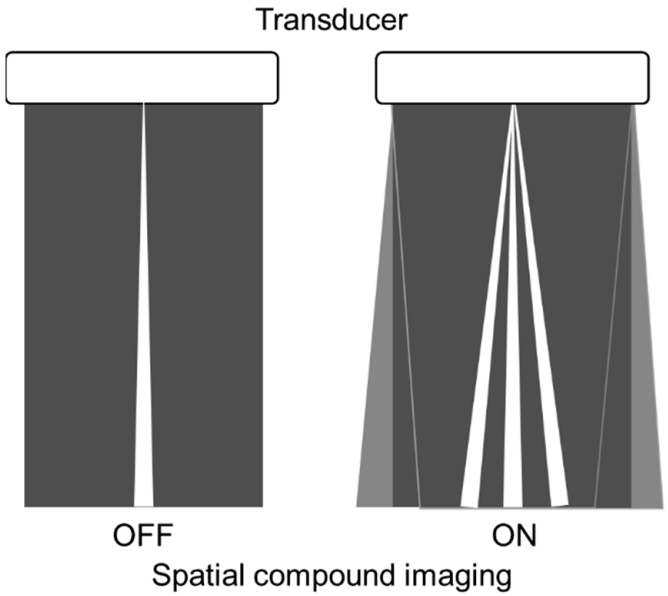

Figure 2. Spatial compound imaging is a method wherein sonographic information is obtained from several different insonation angles and combined to produce a single image.

Many ultrasound machines are now equipped with spatial compound imaging for several applications (e.g., abdominal, breast, thyroid, or vascular ultrasound). If one of the presets for these applications is accidentally selected for the evaluation of B-lines, they may be erroneously counted. To avoid misinterpretation, spatial compound imaging should be set to "off" [8,19,21], or the preset for the lung ultrasound should be selected in advance. In phased array transducers, spatial compound imaging is not mounted; thus, B-lines can be properly evaluated without caution when utilized in addition to echocardiography [9].

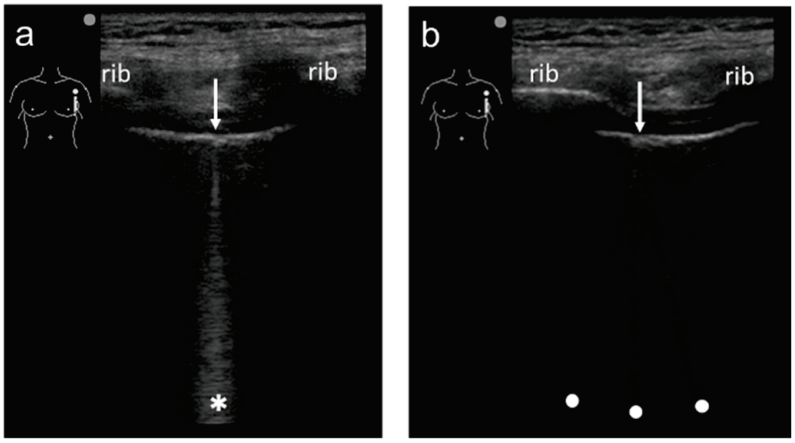

Figure 3. Ultrasound images obtained by MicroMaxx scanner (SonoSite) with a linear transducer without (**a**) and with spatial compound imaging (**b**). A focal point was set as default by the manufacturer, and it is not shown on the screen. With spatial compound imaging enabled, single B-line (asterisk) changes to multiple lines (dots) radiating from the same point (arrows) on the pleural line.

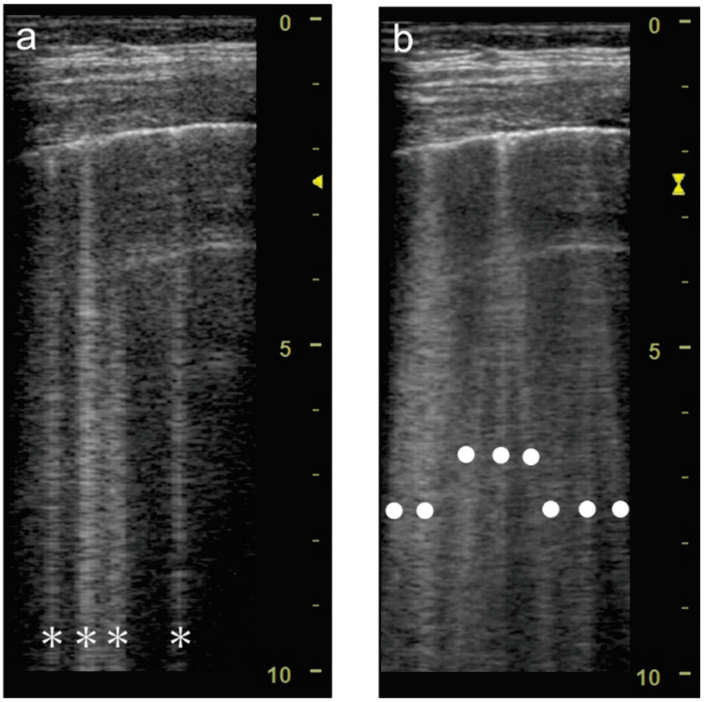

Figure 4. Ultrasound images obtained by LOGIQ V scanner (GE Healthcare) with a linear transducer without (**a**) and with spatial compound imaging (**b**) in cardiogenic pulmonary edema. With spatial compound imaging enabled, each single B-line (asterisks) changes to multiple lines (dots) radiating from the same point on the pleural line.

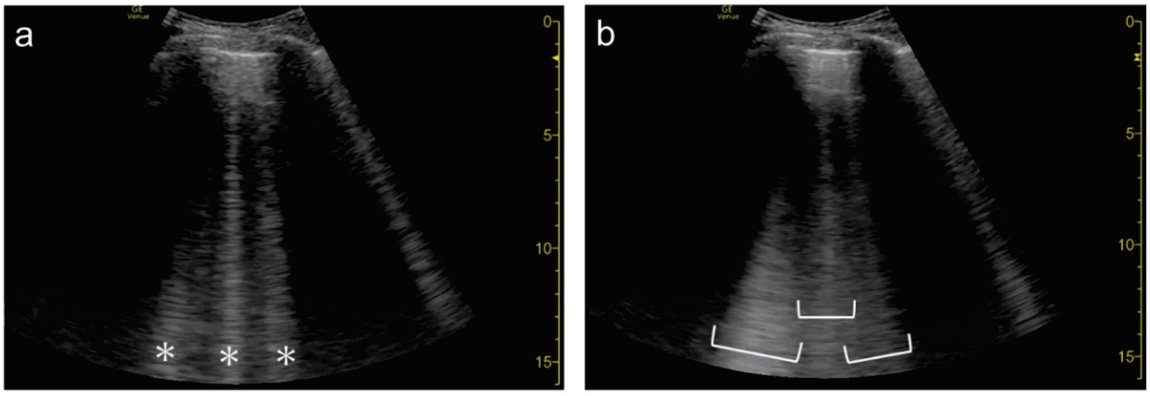

Figure 5. Ultrasound images obtained by Venue scanner (GE Healthcare) with a curvilinear transducer without (**a**) and with spatial compound imaging (**b**) in pulmonary edema. With spatial compound imaging enabled, each B-line (asterisks) becomes divergent with increasing depth, indicating the overlap of multiple lines.

3.2. Focal Point

The focal point can also affect the quantification of B-lines. As the single focal point is shifted from the level of the pleural line to deeper levels, the dispersion of B-lines becomes wider during multiple reflections [8] (Figures 6 and 7). As the focal point is shifted to deeper levels, multiple B-lines become wider and can finally overlap each other (Figures 8 and 9). With focused ultrasound, transmission pulse at the focal point hits a small area, whereas the beam width becomes wider in the de-focused area. That means B-lines can be emphasized if the focal point is set to the same depth of the pleural line [16].

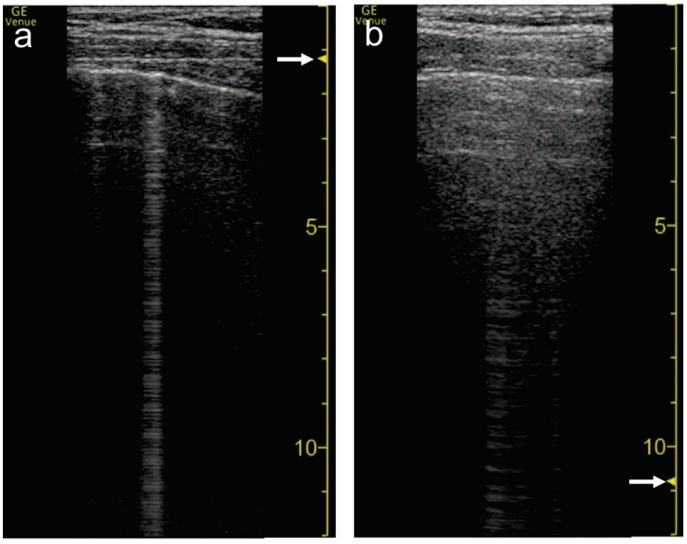

Figure 6. Ultrasound images obtained by Venue scanner (GE Healthcare) with a linear transducer. The B-line becomes wider as the single focal point (arrow) is shifted from the same level as the pleural line (**a**) to a deep level (**b**).

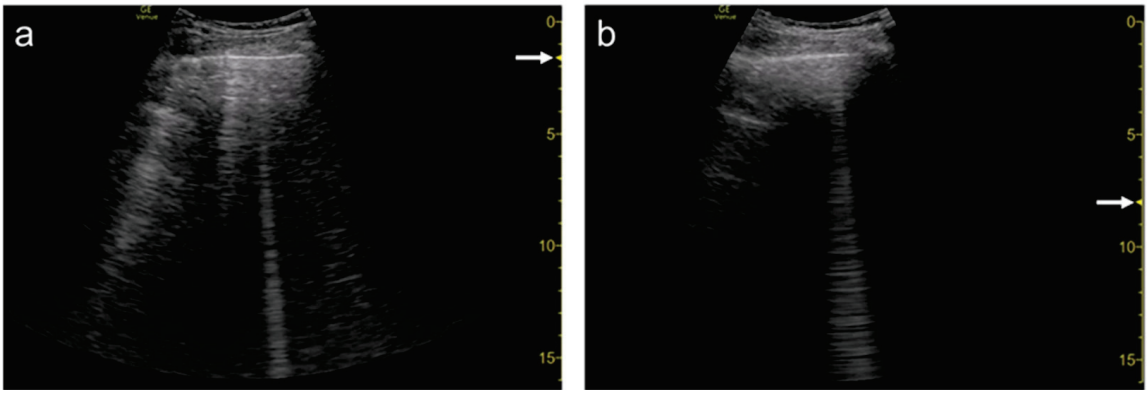

Figure 7. Ultrasound images obtained by Venue scanner (GE Healthcare) with a curvilinear transducer. The B-line becomes wider as the single focal point (arrow) is shifted from the same level as the pleural line (**a**) to a deeper level (**b**).

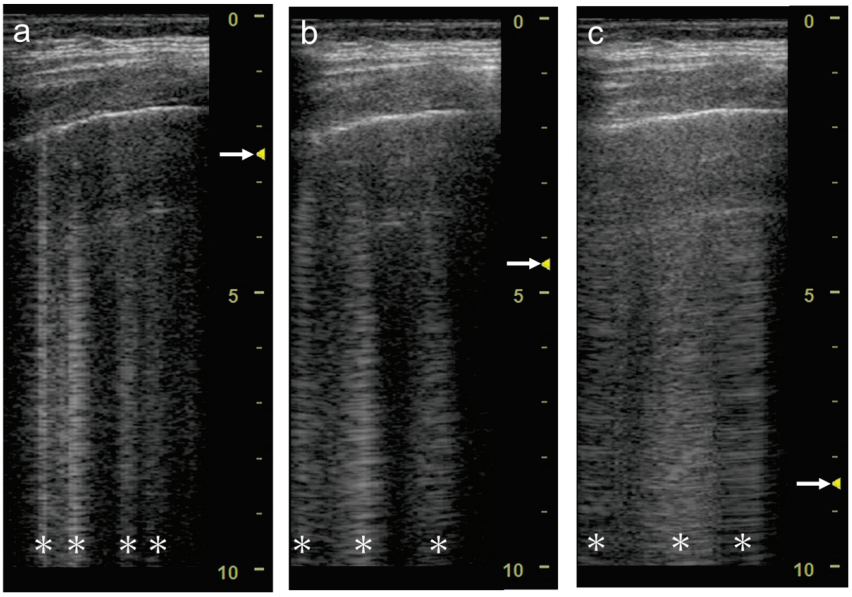

Figure 8. Ultrasound images obtained by LOGIQ V scanner (GE Healthcare) with a linear transducer in cardiogenic pulmonary edema. As the single focal point (arrow) is shifted from a level near the pleural line (**a**) to deeper levels, each B-line becomes wider (**b**), with the B-lines finally overlapping each other (**c**). Asterisks indicate B-lines.

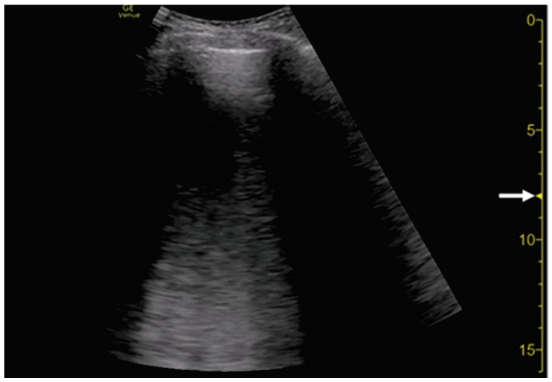

Figure 9. Ultrasound image obtained by Venue scanner (GE Healthcare) with a curvilinear transducer in the same case as Figure 5. As the single focal point (arrow) is shifted to a deeper level, each B-line becomes wider and overlaps each other.

In daily practice, confluent B-lines are often observed in cardiogenic pulmonary edema. The confluent B-lines are also called white lung pattern, especially when they cover the intercostal space [24]. However, at present, the confluent B-lines are not precisely defined in the consensus definitions [25]. For consensus, it is recommended that focal point be set at or near the level of the pleural line to ensure "confluence" and accurate quantification or semi-quantification of B-lines [8,9,19,21]. In some portable or hand-held ultrasound machines, the focal point is fixed to a certain level by default and cannot be moved by the user. The level of the focal point should also be considered in the lung ultrasound presets provided by manufacturers [9]. Some ultrasound machines have a function that allows the number of focal points to be changed. In lung ultrasound, B-lines should be evaluated with a single focal point [26].

3.3. Frequency

Recent in vitro and in vivo studies have revealed the effect of the frequency on vertical artifacts. Demi et al. [27] and Mento et al. [28] conducted in vitro studies using lung-mimicking phantoms with a multifrequency approach, illustrating how the visualization of vertical artifacts depends on frequency and how native frequency correlates with the geometric characteristic of a bubbly structure. In a clinical study, Mento et al. [20] demonstrated that the quantitative evaluation of vertical artifacts using both a multifrequency analysis and the total intensity may have the potential to discriminate pulmonary fibrosis. Buda et al. [17] examined the visualization and morphological analysis of vertical artifacts by employing two different frequencies. The change of the frequency from 2 to 6 MHz led to the shortening or disappearance of vertical artifacts and this phenomenon is more characteristic of pulmonary fibrosis than cardiogenic pulmonary edema (61% vs. 24% of the examined area, $p < 0.001$). As mentioned above, the visualization and length of the artifacts depend on the frequency; thus, the term "vertical artifacts" has been preferred to "B-lines" in recent studies [29,30].

3.4. Selection of Transducers

B-lines are detectable using sector, curvilinear, or linear transducers with low to high central frequencies [1,6]. In sector and curvilinear transducers, multiple B-lines spread radially, whereas in linear probes, multiple B-lines run in parallel (Figure 10).

Many published studies did not mention the presets or used a variety of presets, including cardiac, abdominal, and lung presets set by the manufacturers [9,31,32]; thus, the results should be cautiously interpreted when the performance is compared between the types of transducers. Smit et al. assessed the concordance between a broadband linear transducer (12–4 MHz) and a sector transducer (4–1 MHz) of a handheld ultrasound device in the assessment of lung aeration using B-lines in mechanically ventilated intensive care unit patients. They performed the exams with the lung presets set by the manufacturer in both transducers. There was good concordance between the linear and sector transducers in the assessment; however, a large number of images acquired with the linear probe were of insufficient quality, most likely due to higher attenuation in the subcutaneous tissue layer [33]. The results indicate that a transducer with lower frequency is better for obese and edematous patients.

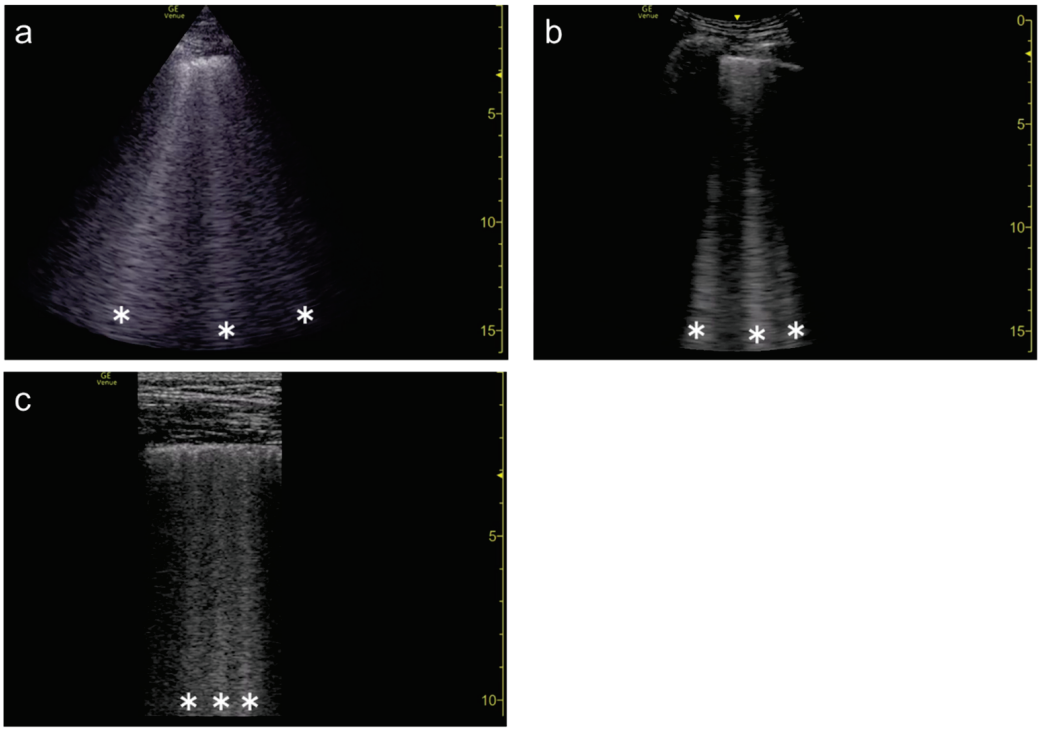

Figure 10. Ultrasound images obtained with Venue scanner (GE Healthcare) with a sector (**a**), curvilinear (**b**), and linear (**c**) transducers in cardiogenic pulmonary edema. Asterisks indicate B-lines.

3.5. Simple Educational Materials

Understanding the influence of the above-mentioned machine settings and the selection of transducers on the configuration of vertical artifacts is crucial for planning clinical research, sharing the appropriate use, and providing education in relation to lung ultrasound. However, the necessity has not been fully shared among users. Furthermore, it is not easy to observe the influence of these factors on 'moving' vertical artifacts in real patients with or without dyspnea and tachypnea.

A more simplified experimental model is useful for the educational purpose. A motionless stable vertical artifact is easily generated by the model using a glass microscopic plate, which is easily obtainable in each medical facility. We herein demonstrate simple educational materials that help users understand the influence of machine settings on the configuration of vertical artifacts [34]. A diagnostic ultrasound scanner (LOGIQ S8, GE Healthcare) with 9 MHz linear transducer (9L-D) and 3.5 MHz curvilinear transducer (C1-5-D) is used in this demonstration. Fundamental B-mode with 5.0 MHz (linear) and 4.0 MHz (curvilinear) is used. The overall gain and dynamic range are 60 and 72, respectively. TGC is flat as used in clinical examinations.

As the preset, spatial compound imaging is turned off and the focal zone is set at the shallowest level. A glass microscope slide of 1 mm in thickness (impedance, 12.7×10^6 Pa s/m) is placed perpendicularly on the footprints with a thin layer of ultrasound gel. The thickness of the slide is made parallel to the scan direction (Figure 11). A single clear vertical artifact with a dense cascade of horizontal lines is shown with both linear and curvilinear transducers, while the width of the artifact is wider with the convex transducer than with the linear transducer.

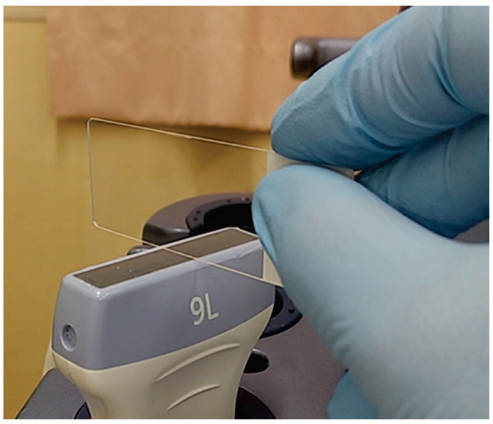

Figure 11. Simple educational materials that help provide an understanding of the influence of machine settings on the configuration of vertical artifacts. A glass microscope slide is placed perpendicularly on the footprint of a linear transducer with a thin layer of ultrasound gel.

We are convinced that ultrasound beam enters the glass slide. We could observe the change of the configuration or the movement of the vertical artifact when we put ultrasound gel on the upper side of the glass slide and moved the gel with the finger. This fact shows that the ultrasound beam enters the glass slide and reaches the upper side. The following description shows the hypothesis of the generation of the vertical artifact with a dense cascade of horizontal lines. Once the ultrasound pulse wave enters the glass slide, it is trapped with countless reflections and scattering inside the "thin" slide glass. These countless reflections and scattering phenomena act as successive ultrasound sources, with trapped energy radiated to the transducer little by little. The propagation speed of the glass, which is more than 5000 m/s, is another reason for the dense cascade. The other cascade of lines in each image is provided by the reverberation inside the acoustic lens of the transducer rather than the reverberation inside the thin layer of ultrasound gel.

As the focal zone is moved from the shallowest level to the deeper levels, the vertical artifact becomes wider with both linear and convex transducers (Figures 12a–e and 13a–c).

When the linear transducer is used with spatial compound imaging enabled, the single vertical artifact changes to three lines radiating from the same point (Figure 12a,f). The three lines become wider as the focal zone is moved to deeper levels (Figure 12 f–j). When the curvilinear transducer is used with spatial compound imaging enabled, the three individual lines appear to overlap each other (Figure 13a,d). These lines become wider as the focal zone is moved to deeper levels (Figure 13d–f).

Some ultrasound scanners have "multiple focus" in B-mode. It transmits ultrasound pulses in the same direction with a different focal depth, synthesizing these scan-line data (mostly applying focal areas) into one scan line image. As a result, the synthesized image has higher spatial resolution due to the multiple focal points. However, this method causes a "patchy" step-wise configuration in the vertical artifact (Figure 14a,b).

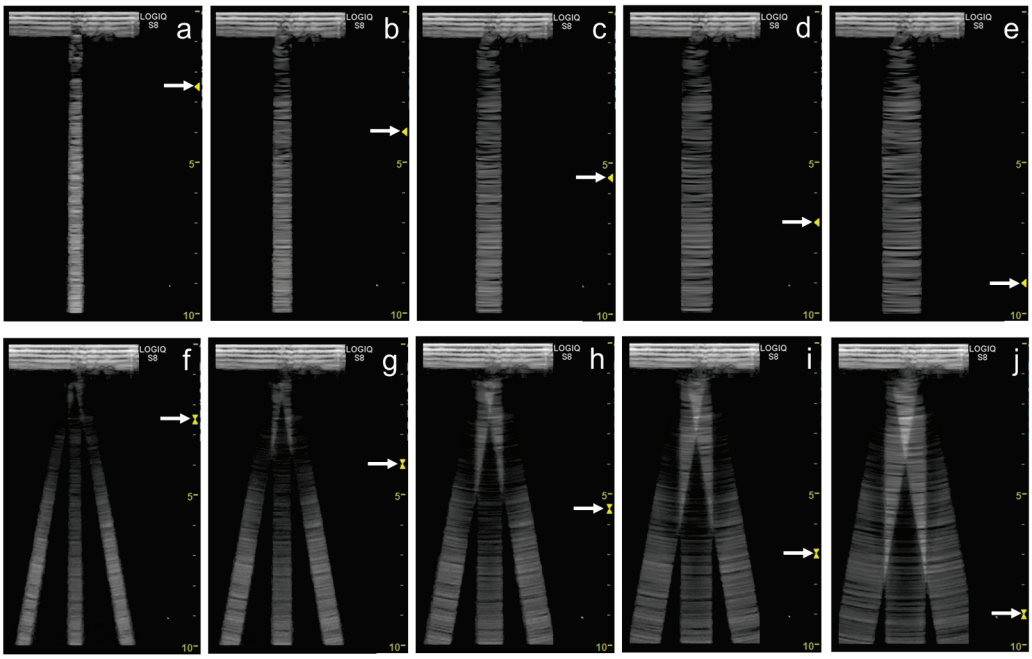

Figure 12. Ultrasound images obtained with the. linear transducer. The vertical artifact becomes wider as the focal point (arrow) is moved to deeper levels (**a**–**e**). When spatial compound imaging is enabled, the single vertical artifact changes to three lines radiating from the same point (**a**,**f**). The three lines become wider as the focal point (arrow) is moved to deeper levels (**f**–**j**).

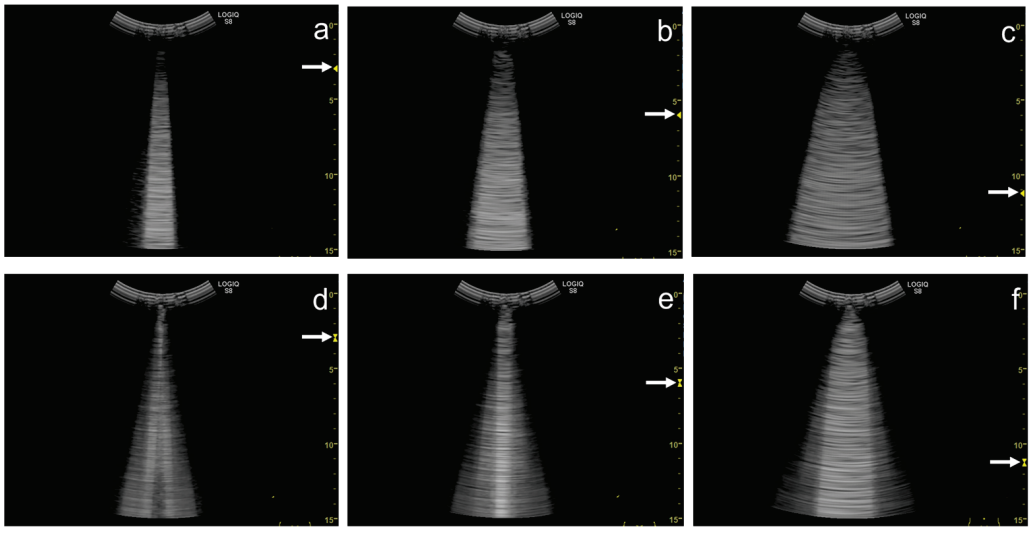

Figure 13. Ultrasound images obtained with the curvilinear transducer. The vertical artifact becomes wider as the focal point (arrow) is moved to deeper levels (**a**–**c**). When spatial compound imaging is enabled, three lines appear to overlap each other (**a**,**d**). The three lines become wider as the focal point (arrow) is moved to deeper levels (**d**–**f**).

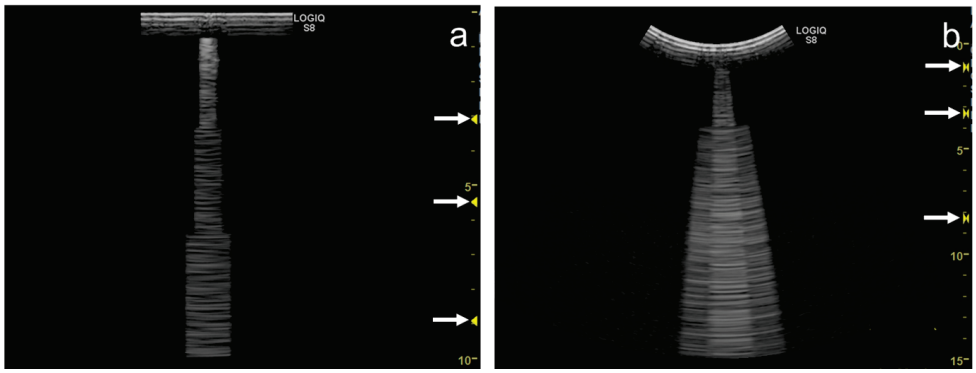

Figure 14. Ultrasound images obtained by a linear transducer (**a**) and a curvilinear transducer (**b**) with multiple focus (arrows), which causes step-wise configuration in a vertical artifact.

As shown with the series of ultrasound images, the configuration of the vertical artifacts is detrimentally affected by the use of spatial compound imaging, the placement of the focal point to at a deep level, and the use of multiple focus. These simple educational materials tell us the non-negligible impact of the ultrasound machine settings on the morphology of vertical artifacts in lung ultrasound.

4. Conclusions

The acoustic trap theory is useful when considering the generation of vertical artifacts in lung ultrasound. Several studies employing basic research support the theory. Published studies with pilot experiments indicate that clarification of the relationship between the length and intensity of the vertical artifacts and the physical or acoustic composition of the sources have potential for differentiating cardiogenic pulmonary edema from lung disease.

In the clinical setting, the configuration of the vertical artifacts is detrimentally affected by the use of spatial compound imaging, the placement of the focal point at a deep level, and the use of multiple focus. Simple educational materials using a glass microscope slide also demonstrate the non-negligible impact of the ultrasound machine settings on the morphology of vertical artifacts. An international consensus needs to be reached on the optimal settings of ultrasound machines, which affect the diagnostic accuracy.

Author Contributions: Conceptualization, T.K. and N.K.; methodology, T.K.; validation, T.K., N.K. and N.T.; resources, T.K., N.K. and N.T.; writing—original draft preparation, T.K.; writing—review and editing, T.K., N.K. and N.T.; supervision, N.T. All authors have read and agreed to the published version of the manuscript.

Funding: This review received no external funding.

Institutional Review Board Statement: Not applicable.

Informed Consent Statement: Informed consent was obtained from subjects involved in the study.

Data Availability Statement: Not applicable.

Conflicts of Interest: Toru Kameda has received a presentation honorarium from GE Healthcare that was unrelated to the submitted work. The other authors declare that there are no conflict of interest.

References

1. Volpicelli, G.; Elbarbary, M.; Blaivas, M.; Lichtenstein, D.A.; Mathis, G.; Kirkpatrick, A.W.; Melniker, L.; Gargani, L.; Noble, V.E.; Via, G.; et al. International evidence-based recommendations for point-of-care lung ultrasound. *Intensive Care Med.* **2012**, *38*, 577–591. [CrossRef] [PubMed]
2. Lichtenstein, D.A.; Mezière, G.A. Relevance of Lung Ultrasound in the Diagnosis of Acute Respiratory Failure: The BLUE Protocol. *Chest* **2008**, *134*, 117–125. [CrossRef]
3. Pivetta, E.; Goffi, A.; Lupia, E.; Tizzani, M.; Porrino, G.; Ferreri, E.; Volpicelli, G.; Balzaretti, P.; Banderali, A.; Iacobucci, A.; et al. Lung ultrasound-implemented diagnosis of acute decompensated heart failure in the ED: A SIMEU multicenter study. *Chest* **2015**, *148*, 202–210. [CrossRef]

4. Maw, A.M.; Hassanin, A.; Ho, P.M.; McInnes, M.D.F.; Moss, A.; Juarez-Colunga, E.; Soni, N.J.; Miglioranza, M.H.; Platz, E.; DeSanto, K.; et al. Diagnostic accuracy of point-of-care lung ultrasonography and chest radiography in adults with symptoms suggestive of acute decompensated heart failure: A systematic review and meta-analysis. *JAMA Netw. Open* **2019**, *2*, e190703. [CrossRef]
5. Pivetta, E.; Goffi, A.; Nazerian, P.; Castagno, D.; Tozzetti, C.; Tizzani, P.; Tizzani, M.; Porrino, G.; Ferreri, E.; Busso, V.; et al. Lung ultrasound integrated with clinical assessment for the diagnosis of acute decompensated heart failure in the emergency department: A randomized controlled trial. *Eur. J. Heart Fail.* **2019**, *21*, 754–766. [CrossRef] [PubMed]
6. Picano, E.; Pellikka, P.A. Ultrasound of extravascular lung water: A new standard for pulmonary congestion. *Eur. Heart J.* **2016**, *37*, 2097–2104. [CrossRef]
7. Kameda, T.; Kamiyama, N.; Taniguchi, N. Simple experimental models for elucidating the mechanism underlying vertical artifacts in lung ultrasound: Tools for revisiting B-Lines. *Ultrasound Med. Biol.* **2021**, *47*, 3543–3555. [CrossRef] [PubMed]
8. Kameda, T.; Kamiyama, N.; Kobayashi, H.; Kanayama, Y.; Taniguchi, N. Ultrasonic B-Line–Like Artifacts Generated with Simple Experimental Models Provide Clues to Solve Key Issues in B-Lines. *Ultrasound Med. Biol.* **2019**, *45*, 1617–1626. [CrossRef]
9. Matthias, I.; Panebianco, N.L.; Maltenfort, M.G.; Dean, A.J.; Baston, C. Effect of Machine Settings on Ultrasound Assessment of B-lines. *J. Ultrasound Med.* **2020**, *40*, 2039–2046. [CrossRef]
10. Nugent, K.; Dobbe, L.; Rahman, R.; Elmassry, M.; Paz, P. Lung morphology and surfactant function in cardiogenic pulmonary edema: A narrative review. *J. Thorac. Dis.* **2019**, *11*, 4031–4038. [CrossRef]
11. Storto, M.L.; Kee, S.T.; Golden, J.A.; Webb, W.R. Hydrostatic pulmonary edema: High-resolution CT findings. *Am. J. Roentgenol.* **1995**, *165*, 817–820. [CrossRef]
12. Parekh, M.; Donuru, A.; Balasubramanya, R.; Kapur, S. Review of the Chest CT Differential Diagnosis of Ground-Glass Opacities in the COVID Era. *Radiology* **2020**, *297*, E289–E302. [CrossRef]
13. Lichtenstein, D.; Mézière, G.; Biderman, P.; Gepner, A.; Barré, O. The comet-tail artifact. An ultrasound sign of alveolar-interstitial syndrome. *Am. J. Respir. Crit. Care Med.* **1997**, *156*, 1640–1646. [CrossRef] [PubMed]
14. Volpicelli, G.; Gargani, L. Interstitial Syndrome. In *Chest Sonography*, 4th ed.; Mathis, G., Ed.; Springer: Cham, Switzerland, 2017; pp. 45–50.
15. Soldati, G.; Demi, M.; Inchingolo, R.; Smargiassi, A.; Demi, L. On the Physical Basis of Pulmonary Sonographic Interstitial Syndrome. *J. Ultrasound Med.* **2016**, *35*, 2075–2086. [CrossRef]
16. Demi, M. The impact of multiple concurrent factors on the length of the ultrasound pulmonary vertical artifacts as illustrated through the experimental and numerical analysis of simple models. *J. Acoust. Soc. Am.* **2021**, *150*, 2106. [CrossRef] [PubMed]
17. Buda, N.; Skoczylas, A.; Demi, M.; Wojteczek, A.; Cylwik, J.; Soldati, G. Clinical Impact of Vertical Artifacts Changing with Frequency in Lung Ultrasound. *Diagnostics* **2021**, *11*, 401. [CrossRef] [PubMed]
18. Demi, M.; Prediletto, R.; Soldati, G.; Demi, L. Physical Mechanisms Providing Clinical Information from Ultrasound Lung Images: Hypotheses and Early Confirmations. *IEEE Trans. Ultrason. Ferroelectr. Freq. Control* **2020**, *67*, 612–623. [CrossRef]
19. Mathis, G.; Horn, R.; Morf, S.; Prosch, H.; Rovida, S.; Soldati, G.; Hoffmann, B.; Blaivas, M.; Dietrich, C.F. WFUMB position paper on reverberation artefacts in lung ultrasound: B-lines or comet-tails? *Med. Ultrason.* **2021**, *23*, 70–73. [CrossRef] [PubMed]
20. Mento, F.; Soldati, G.; Prediletto, R.; Demi, M.; Demi, L. Quantitative lung ultrasound spectroscopy applied to the diagnosis of pulmonary fibrosis: The first clinical study. IEEE Trans. *Ultrason. Ferroelectr. Freq. Control* **2020**, *67*, 2265–2273. [CrossRef]
21. Liu, J.; Guo, G.; Kurepa, D.; Volpicelli, G.; Sorantin, E.; Lovrenski, J.; Alonso-Ojembarrena, A.; Hsieh, K.-S.; Lodha, A.; Yeh, T.F.; et al. Specification and guideline for technical aspects and scanning parameter settings of neonatal lung ultrasound examination. *J. Matern. Fetal Neonatal Med.* **2021**, 1–14. [CrossRef]
22. Kim, M.J.; Kim, J.Y.; Yoon, J.H.; Youk, J.H.; Moon, H.J.; Son, E.J.; Kwak, J.Y.; Kim, E.-K. How to Find an Isoechoic Lesion with Breast US. *RadioGraphics* **2011**, *31*, 663–676. [CrossRef]
23. Blüthgen, C.; Sanabria, S.; Frauenfelder, T.; Klingmüller, V.; Rominger, M. Economical Sponge Phantom for Teaching, Understanding, and Researching A- and B-Line Reverberation Artifacts in Lung Ultrasound. *J. Ultrasound Med.* **2017**, *36*, 2133–2142. [CrossRef]
24. Anderson, K.L.; Fields, J.M.; Panebianco, N.L.; Jenq, K.Y.; Marin, J.; Dean, A.J. Inter-Rater Reliability of Quantifying Pleural B-Lines Using Multiple Counting Methods. *J. Ultrasound Med.* **2013**, *32*, 115–120. [CrossRef] [PubMed]
25. Fischer, E.A.; Minami, T.; Ma, I.W.Y.; Yasukawa, K. Lung Ultrasound for Pleural Line Abnormalities, Confluent B-Lines, and Consolidation: Expert reproducibility and a method of standardization. *J. Ultrasound Med.* **2021**. [CrossRef]
26. Schmickl, C.N.; Menon, A.A.; Dhokarh, R.; Seth, B.; Schembri, F. Optimizing B-lines on lung ultrasound: An in-vitro to in-vivo pilot study with clinical implications. *J. Clin. Monit. Comput.* **2020**, *34*, 277–284. [CrossRef] [PubMed]
27. Demi, L.; Van Hoeve, W.; Van Sloun, R.J.G.; Soldati, G.; Demi, M. Determination of a potential quantitative measure of the state of the lung using lung ultrasound spectroscopy. *Sci. Rep.* **2017**, *7*, 12746. [CrossRef]
28. Mento, F.; Demi, L. On the influence of imaging parameters on lung ultrasound B-line artifacts, in vitro study. *J. Acoust. Soc. Am.* **2020**, *148*, 975–983. [CrossRef] [PubMed]
29. Demi, L. Lung ultrasound: The future ahead and the lessons learned from COVID-19. *J. Acoust. Soc. Am.* **2020**, *148*, 2146–2150. [CrossRef] [PubMed]
30. Soldati, G.; Smargiassi, A.; Demi, L.; Inchingolo, R. Artifactual Lung Ultrasonography: It Is a Matter of Traps, Order, and Disorder. *Appl. Sci.* **2020**, *10*, 1570. [CrossRef]

31. Tasci, O.; Hatipoglu, O.N.; Cagli, B.; Ermis, V. Sonography of the chest using linear-array versus sector transducers: Correlation with auscultation, chest radiography, and computed tomography. *J. Clin. Ultrasound* **2016**, *44*, 383–389. [CrossRef]
32. Bobbia, X.; Chabannon, M.; Chevallier, T.; de La Coussaye, J.E.; Lefrant, J.Y.; Pujol, S.; Claret, P.-G.; Zieleskiewicz, L.; Roger, C.; Muller, L. Assessment of five different probes for lung ultrasound in critically ill patients: A pilot study. *Am. J. Emerg. Med.* **2018**, *36*, 1265–1269. [CrossRef] [PubMed]
33. Smit, M.R.; De Vos, J.; Pisani, L.; Hagens, L.A.; Almondo, C.; Heijnen, N.F.L.; Schnabel, R.M.; Van Der Horst, I.C.C.; Bergmans, D.C.J.J.; Schultz, M.J.; et al. Comparison of Linear and Sector Array Probe for Handheld Lung Ultrasound in Invasively Ventilated ICU Patients. *Ultrasound Med. Biol.* **2020**, *46*, 3249–3256. [CrossRef] [PubMed]
34. Kameda, T. Management of shock using point-of-care ultrasound. *Jpn. J. Med. Ultrason.* **2020**, *47*, 69–80. [CrossRef]

diagnostics

MDPI

Article

On the Replica of US Pulmonary Artifacts by Means of Physical Models

Marcello Demi

Department of Bioengineering, Fondazione Toscana Gabriele Monasterio, 56124 Pisa, Italy; demi@ftgm.it; Tel.: +39-050-3152618

Abstract: Currently, the diagnostic value of the artefactual information provided by lung ultrasound images is widely recognized by physicians. In particular, the existence of a correlation between the visual characteristics of the vertical artifacts, which arise from the pleura line, and the genesis (pneumogenic or cardiogenic) of a pulmonary disorder is commonly accepted. Physicians distinguish vertical artifacts from vertical artifacts which extend to the bottom of the screen (B-lines) and common vertical artifacts from well-structured artifacts (modulated B-lines). However, the link between these visual characteristics and the causes which determine them is still unclear. Moreover, the distinction between short and long artifacts and the distinction between common and structured artifacts are not on/off, and their classification can be critical. In order to derive further information from the visual inspection of the vertical artifacts, the mechanisms which control the artifact formation must be identified. In this paper, the link between the visual characteristics of the vertical artifacts (the observed effect) and the distribution of the aerated spaces at the pleural level (the cause) is addressed. Plausible mechanisms are suggested and illustrated through experimental results.

Keywords: lung ultrasound; B-lines; vertical artifacts; pulmonary artifacts; physical models

Citation: Demi, M. On the Replica of US Pulmonary Artifacts by Means of Physical Models. *Diagnostics* **2021**, *11*, 1666. https://doi.org/10.3390/diagnostics11091666

Academic Editor: Po-Hsiang Tsui

Received: 31 August 2021
Accepted: 10 September 2021
Published: 12 September 2021

1. Introduction

The hypothesis that ultrasound (US) vertical artifacts, which are observed on lung ultrasound images, are generated through multiple reflections between the surfaces of the aerated spaces seems logical and consolidated thanks to both theoretical knowledge and experimental results [1–4]. A distribution of aerated spaces separated by a biological medium (channels) acoustically similar to the chest wall acts as an acoustic trap. Once a US pulse reaches the pleura plane through the chest wall, it is partially reflected towards the probe and partially transmitted to the channels provided by a specific distribution of the aerated spaces which characterizes the outer lung surface. The aerated space distribution can be organized as a compact air wall, and in this case, the acoustic energy is essentially reflected back to the probe. The size of the interalveolar septa is reasonably supposed to be comparable with a capillary lumen (less than 10 microns [5]). However, in the presence of a pathology, the aerated spaces can be separated by wider interstitial channels which are made of media that are acoustically similar to the chest wall [4–7]. In this case, the pulse energy can be partially trapped and subsequently re-radiated towards the probe after multiple reflections between the separated aerated spaces, giving rise to vertical artifacts which arise from the pleura line. A similar effect has been observed with other pairs of materials such as metal immersed in water [8,9]. The imaging parameters play a fundamental role in the formation of the artifacts, and the visibility of a vertical artifact (that is, its brightness, lateral dimension, and length) depends on multiple non-orthogonal factors including the gain, the time gain compensation (TGC), and all the parameters that can be easily set by the operator from the scanner keyboard [10–12]. Therefore, given the intrinsic variability of the artifacts as a function of multiple non-independent factors, including the human factor, making an objective diagnosis on the basis of the artefactual information is a difficult task.

Despite this, the diagnostic value of the artefactual information provided by lung ultrasound images is currently widely recognized by physicians [13–15], and yet it is the information regarding the vertical artifacts that attracts their attention most. The existence of a correlation between the visual characteristics of the vertical artifacts, which arise from the pleura line, and the genesis (pneumogenic or cardiogenic) of a pulmonary disorder is commonly accepted [16–18]. Moreover, it has been observed that the structure and visibility of the vertical artifacts change when varying the pulse central frequency and that this variation can be used to formulate hypotheses on the nature of the pulmonary disease [4,19,20]. Physicians distinguish vertical artifacts from vertical artifacts which extend to the bottom of the screen (B-lines) [15,20,21] and B-lines from well-structured artifacts (modulated B-lines) [7,22]. However, the link between these visual characteristics and the causes which determine them is still unclear. Moreover, the distinction between short and long artifacts and the distinction between common and structured artifacts are not on/off, and their classification can be critical. An effective preliminary diagnosis, based only on the visual inspection of the vertical artifact, is probably possible. However, the mechanisms which control the artifact formation must be identified and rationally used to convert the artefactual information into anatomic information. In the following sections, the link between the visual characteristics of the vertical artifacts (the observed effect) and the distribution of the aerated spaces at the pleural level (the cause) is addressed. Single isolated acoustic traps connected to a lung disorder are introduced and analysed in order to provide a physical explanation for the different forms of vertical artifacts that are usually observed on US lung images.

2. Materials and Methods

Normal aerated lungs are characterized by a distribution of aerated spaces separated by thin interstitial spaces, and in this case, the US pulses are mostly reflected back to the probe by the pleura plane. However, in the presence of pulmonary pathologies, the thickness of the interstitial spaces (for example inter-alveolar and inter-lobular septa) increases, and the US pulses are partially transmitted to the lung surface underneath the pleura through these interstitial channels. In this case, the spatial arrangement of the interstitial spaces can give rise to acoustic traps where the pulse energy can be partially trapped among the aerated spaces. Subsequently, the slow re-radiation of the trapped energy gives rise to the vertical artifacts which are observed on lung images. The spatial configuration of the interstitial and aerated spaces can vary a lot, and many types of acoustic traps can exist, so that an exhaustive description of them is impossible. Obviously, given the numerous types of potential acoustic traps, numerous types of artifacts also exist. Vertical artifacts appear on lung images every time the thickness of the interstitial medium (tissue, blood, water), which separates the aerated spaces, increases over a certain threshold. However, a typical isolated acoustic trap, providing an isolated vertical artifact, can be considered and analysed as a source of important information on the genesis of the vertical artifacts. In this paper interstitial volumes surrounded by aerated spaces and linked to the pleura plane by means of a thickened interstitial space are simulated with some physical models.

The simplest and most immediate idea was to resort to sponges soaked with different volumes of water. Indeed, several papers can be found in the literature by authors who have embarked on this path obtaining interesting results [2,23–26]. Yet, before taking into account random models, other possibilities that allow us to maintain the indisputable advantage of the experiment repeatability can be explored.

In Section 3, a distribution of air cylinders in agar gel is analysed. The idea is to drill corresponding holes on two opposite walls of a box, to insert metallic cylinders in the holes so that they can lie between the two opposite walls of the box, to fill the box with a 3% hot solution of agar in water, to wait until the solution acquires its natural consistency (very similar to that of soft tissues) by means of the cooling process, and then to remove the metallic cylinders [27]. The result is that of placing cylindrical air spaces (mimicking the

alveoli) in a material that simulates the connective tissue of the lung. Boxes of this type can be easily made by distributing metallic cylinders appropriately in order to simulate various acoustic traps.

On the left of Figure 1, the draft of an empty box with a set of eight metallic cylinders lying between the two opposite sides of the box is shown. Seven 5.1 mm holes and an isolated 5.1 mm hole have been drilled on the two opposite sides of a simple wooden box. While the diameter of the holes was 5.1 mm, seven brass rods and one copper tube with a diameter equal to 5 mm were used to make their positioning easier. The seven holes are practically next to each other, except for the two holes at the top, which are separated by about 1 mm. The seven holes, which give rise to seven air cylinders in agar gel by means of the procedure described above, form a classic acoustic trap which is accessible from the aperture between the two air cylinders at the top. A strip of material was removed with a 2 mm diameter mill from the upper part of the copper tube and was subsequently inserted in the isolated 5.1 mm hole. In this case, once the agar solution cooled and the seven brass rods and the copper tube were pushed out, an agar volume (similar to a cylinder) surrounded by seven air cylinders was obtained on the left side of the box, while on the right side, an agar cylinder with a diameter of about 4.5 mm was obtained (the internal diameter of the copper tube). The latter was attached to the rest of the surrounding agar gel by a 2 mm wide and 0.25 mm thick peduncle surrounded by a 0.25 mm thin layer (the wall thickness of the copper tube was equal to 0.25 mm) of air for the remaining part of its surface.

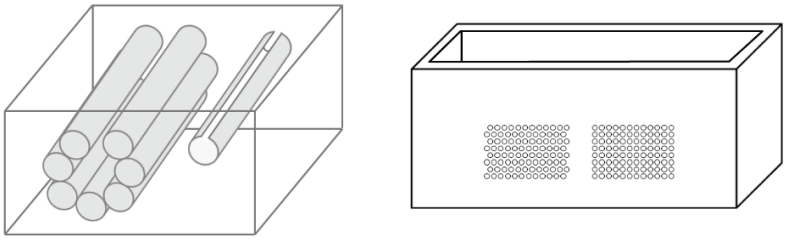

Figure 1. The image on the left shows a draft of an empty box with eight metallic cylinders lying between two opposite sides of the box. The image on the right shows a PVC box where two sets of 1.1 mm holes with a distance of 1.5 mm between their axes have been made using a CNC milling machine.

Due to the significant results obtained with the above phantom, different distributions of air cylinders in agar gel were also simulated by means of a PVC box where two sets of holes had been made using a CNC milling machine. The image on the right in Figure 1 shows the PVC box with two sets of 1.1 mm holes with a distance of 1.5 mm between their axes. In this case, numerous acoustic traps can be simulated by using the same procedure: appropriate distributions of brass rods with a diameter equal to 1 mm are introduced in the holes, the box is subsequently filled with a hot solution of agar in water, and at the end of the cooling process, the brass rods are removed.

The results obtained with these first phantoms led us to develop a device which allowed us to simulate two particular acoustic traps completely surrounded by air: (i) a volume of fluid linked to the chest wall by means of a thickened interalveolar space and (ii) an interlobular septum.

The device is based on two membranes separated by an adjustable air thickness. The two membranes seal the bottom of two cylindrical PVC containers (A and B) which were shaped by means of a lathe. The external diameter of the A container is 2 mm smaller than the internal diameter of the B container, so that the A container can slide inside container B. In so doing, the air thickness between the two membranes, which seal the bottom of the two containers, can vary. The membrane which seals the bottom of the B container (the lower membrane in Figure 2) acts as a simple support of the acoustic trap while the membrane which seals the bottom of the A container (the upper membrane in Figure 2)

simulates the pleura. The two membranes were obtained from two simple polyethylene films which are commonly used for food packaging, and they are secured by means of two O-rings at the throat, which is visible in Figure 2 under the heads of the containers. The A container is filled with 20 mm of purified water in order to simulate the chest wall and to provide an excellent acoustic matching with the probe. The diameter of the top aperture of container A is larger than the head of the probe and makes interfacing the probe and the purified water simple. The acoustic trap under examination (a sample of agar gel) is placed on the lower membrane. Three micrometric M10 fine pitch screws (1 mm for each turn of the screws) fine-tune the air thickness between the two membranes and allow the upper membrane to come close to the acoustic trap in order to ensure an input channel to the ultrasound beam transmitted by the probe through the purified water. Figure 2 shows a drawing of the device with the two membranes which seal the bottom of the two containers A and B and the way it is assembled.

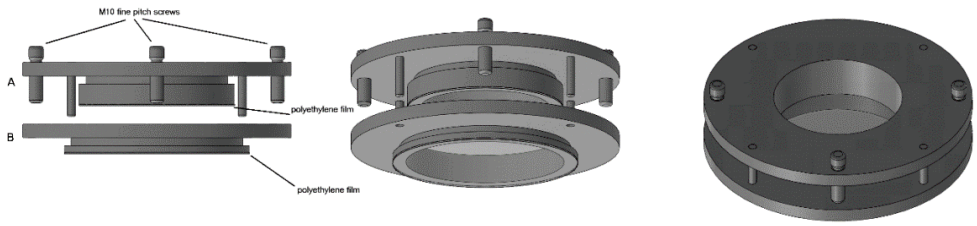

Figure 2. The figure shows a drawing of the device with the two membranes which seal the bottom of two containers A and B and the way it is assembled.

A phantom in the shape of a cusp was chosen to simulate a volume of fluid linked to the chest wall by means of a thickened interstitial space. A 3% hot solution of agar was poured into some moulds which were obtained with a 3D printer, and, once cooled, the agar models were removed from the moulds and checked under a magnifying glass with a digital calliper. Agar cusps such as the one illustrated in Figure 3 with a thickness t varying between 0.1 and 2 mm were obtained. The agar cusps thus obtained are $3 \times (4 + t) \times 10$ mm parallelepipeds with the upper surface which is modelled as a 2 mm high cusp. The agar samples were then placed between the two polyethylene films, taking care to limit the contact of the upper film to the ridge of the agar cusps.

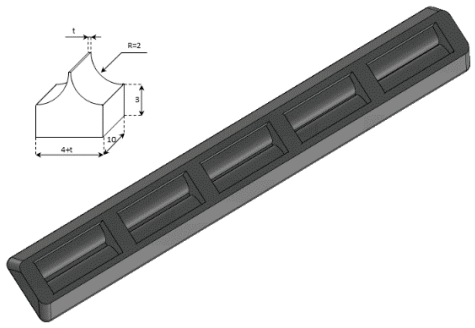

Figure 3. A graphic representation of the agar models with a cusp shape and a drawing of the moulds obtained with the 3D printer are shown.

Another mould was prepared with the 3D printer to simulate an interlobular septum. The aim was to place a micrometric agar septum between the two polyethylene films. The objective is not simple, but it is possible by using two pairs of moulds. The internal pair of moulds is the support for the agar septum. They are separated by means of two washers and assembled by means of two screws which are never removed. The external pair of moulds is pressed against the internal pair of moulds in order to form a thin septum in

their central part. Two calibrated washers limit the minimum distance between the pair of external moulds and set the thickness of the septum. The two pairs of moulds so assembled are subsequently placed in a box that will be filled with an agar solution in hot water. Once the agar solution has assumed its elastic consistency, the assembled pieces are extracted from the box, and the pair of external moulds are gently removed. In so doing the pair of internal moulds are now separated by a calibrated agar septum and can be placed between the two polyethylene films of containers A and B. Here, again, the obtained septa were checked with a digital calliper under a magnifying glass.

Figure 4 shows a drawing of the two pairs of moulds, the way they are assembled, and the agar model of interlobular septum in its support (the pair of internal moulds), which is placed between the two polyethylene films of containers A and B. These pairs of moulds were printed by setting the spatial resolution of the 3D printer to 0.1 mm (the best resolution of our 3D printer). However, in order to simulate a "footprint" that the alveoli can introduce on the walls of the interlobular septa, a second pair of external moulds was also printed by setting the spatial resolution of the 3D printer to 0.280 mm. In so doing, both agar septa with smoother surfaces and agar septa with rough surfaces were obtained, and their response to an ultrasound pulse was analysed.

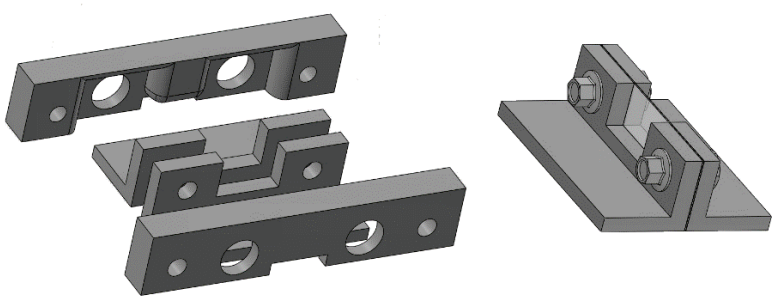

Figure 4. The figure shows a drawing of the two pairs of moulds, the way they are assembled, and the agar model of interlobular septum in its support.

The US phantom images were acquired with a research programmable US scanner, the UlaOp scanner [28] developed by the University of Florence. All images were acquired by using an ultrasound pulse with a 6 MHz central frequency and a duration equal to 3 cycles. A Hanning window was also used as a temporal apodization function, and, in so doing, pulses with a bandwidth of 5.4 MHz at -12 db were obtained. The 6 MHz central frequency was chosen since this is the frequency which in our experience better highlights the modulated B-lines often observed in cardiogenic lung edema [4,7,22]. The maximum amplitude of the pulse allowed by the scanner was used, and the focus position was set at the apertures of the acoustic traps. A 192-element linear probe LA533 from Esaote was used, and 64 elements of the probe were used to transmit the pulses and to receive the echo signals. A Hanning window was also used as a spatial apodization function both in transmission and in reception. In order to reconstruct the images, a propagation speed of 1500 m/s was assumed, and the I- and Q-components of the demodulated RF signals were filtered with low pass filters with a bandwidth of 2.7 MHz at -12 db. The probe was clamped onto an XYZ linear axes electronic positioning system manufactured by IEF-Werner GmbH.

3. Results

3.1. Two Simple Models

Figure 5 shows the two ultrasound vertical artifacts with different zoom degrees, which were obtained on the models that are illustrated in the left image of Figure 1. The seven air cylinders provide two different types of artifacts (a_1 and a_2) which are indicated in Figure 5. The pair of short artifacts a_1 is provided by multiple reflections between the two air cylinders which limit the aperture of the trap. In fact, a distance of about 1 mm

between two replicas of their repetitive patterns can be derived from Figure 5 according to the assumed propagation speed of 1500 m/s. The longer artifact a_2 is generated by the re-radiation of the acoustic energy which has been transmitted to the trap and starts when the beam is reflected from the bottom of the trap. The artifact generated by the agar cylinder has a repetitive pattern that is not seen in the artifact generated by the seven air cylinders and seems to be related to the diameter of the trap. In fact, a distance of about 5 mm between two replicas of the repetitive pattern can be derived from Figure 5 according to the assumed propagation speed of 1500 m/s. This simple example shows how different artifacts can be obtained from acoustic traps with similar volumes and similar shapes. This example also shows how long artifacts can be obtained when an interstitial volume, surrounded by aerated spaces, is linked to the pleura plane by means of a small (as compared to the interstitial volume) channel.

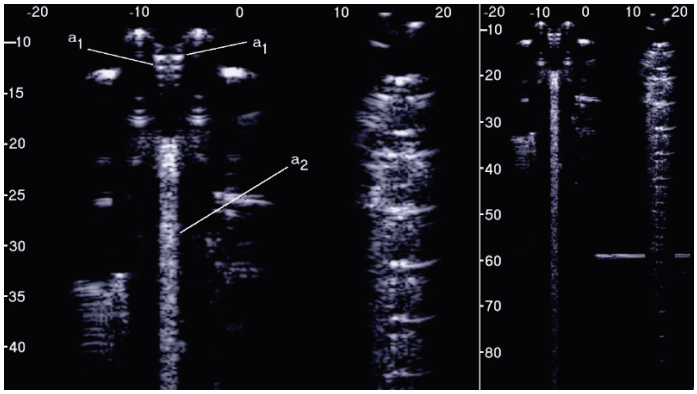

Figure 5. Two ultrasound vertical artifacts with different zoom degrees, which were obtained on the models illustrated in the left image of Figure 1, are shown. The pair of short artifacts a_1 is provided by multiple reflections between the two air cylinders which limit the aperture of the trap. The longer artifact a_2 is generated by the re-radiation of the acoustic energy and starts when the beam is reflected from the bottom of the trap.

3.2. A Distribution of Air Cylinders in Agar Gel

The PVC box, which is shown in the right image of Figure 1, was designed to test the ultrasound response to different distributions of air cylinders. The first test shows what happens when a single row of air cylinders is introduced in the agar gel. The image on the left of Figure 6 shows that in this case, there are no artifacts except the short ones which are generated by multiple reflections between two contiguous air cylinders. In fact, a distance of about 0.5 mm between two replicas of the repetitive pattern can be derived from Figure 6 according to the assumed propagation speed of 1500 m/s. In particular, no artifact is generated by a single air cylinder. The situation changes, however, as a row of air cylinders is added, and increasingly longer artifacts are observed as the number of rows of cylinders increases. The two images in the centre and on the right of Figure 6 show the artifacts which were obtained with two and with four rows of air cylinders, respectively. A repetitive pattern is still perceivable, but it is not clearly quantifiable. The thick white lines at the bottom of the three images are given by the reverberations within the bottom wall of the box.

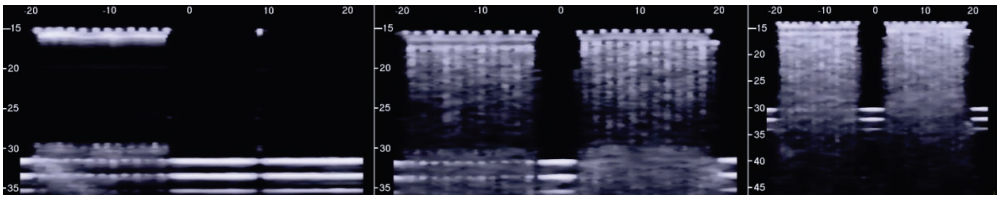

Figure 6. The image on the left shows how a single row of air cylinders does not generate vertical artifacts. The two images in the centre and on the right show the artifacts obtained with two and with four rows of air cylinders. A different zoom degree has been used for the image on the right.

However, the box allows the examination of numerous other configurations. Figure 7 shows some configurations which were tested and the obtained artifacts. Here, it can be observed how traps with the same input channel provide different artifacts as the shape of the trap changes. Artifact A was obtained with three staggered air cylinders. The artifact is short, and it is the only one that shows the characteristic modulation of cardiogenic artifacts [7,22]. The modulation is most likely related to the simplicity of the trap which favours the constructive sum of the echoes, while its length is not easy to interpret. Artifacts B and D are generated by configurations of air cylinders which form two channels with rough lateral surfaces and the different lengths suggest their probable origin. The two artifacts are probably generated by multiple reflections between the walls of the channels during the propagation of the acoustic wave from the top to the bottom of the two channels. Artifact C is generated by a configuration of cylinders similar to that illustrated on the left of Figure 1 with cylinders of a larger diameter. Here, it can be observed how a larger trap with a more complex internal geometry than trap A provides a longer and more confused artifact. Artifact E was generated by a configuration of air cylinders obtained by eliminating the two cylinders that form the input channel of the trap that generated artifact C. This example shows how very different artifacts can be obtained when varying the shape and the size of the access channel. The F artifact is particular since in this case the US energy can be transmitted to the trap through the two small (0.5 mm large) lateral channels and through the larger (2 mm large) central channel. In this case, the artefactual information can be seen as three close but different artifacts or as a single complex artifact.

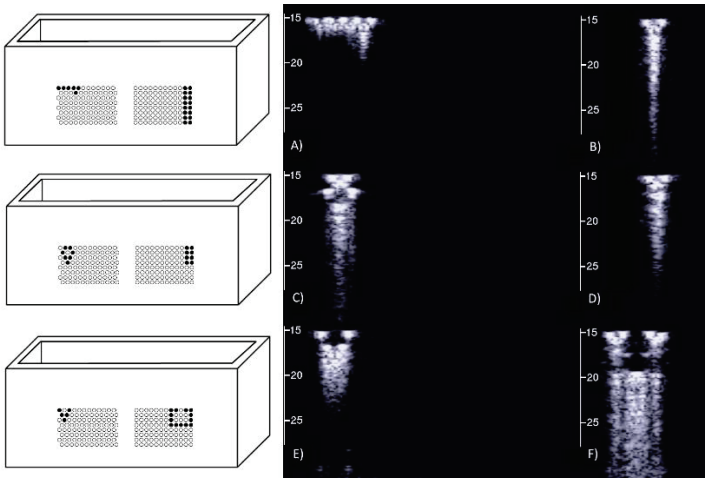

Figure 7. Six different arrangements of air cylinders immersed in agar gel and the obtained artifacts are shown. The black dots indicate the position of the air cylinders.

The above tests on the PVC box provided important indications: first of all, the confirmation that the artifacts observed on the ultrasound pulmonary images are probably generated by multiple reflections between the aerated spaces, since the images acquired on the box in the presence of a single air cylinder did not show any artifacts. The second

indication is that traps with the same input channel can provide different artifacts as the shape of the trap changes. The visual characteristics of a vertical artifact depend on the trap shape and on the input channel. Moreover, tests on simulated single traps did not give rise to artifacts of significant length. Only in the case of the artifact in Figure 5, which was generated by the seven air cylinders, was an artifact of 12 cm observed. Even though the vertical artifacts cannot be objectively split into short and long artifacts, given the great emphasis placed by physicians on their observation regarding artifacts which extend to the bottom of the screen, such a strong indication cannot be neglected. Besides the length of the artifacts, however, another problem arose from the previous tests: none of the artifacts obtained with the air cylinders in agar gel showed those clearly modulated artifacts which are often observed in cardiogenic patients [7,22].

3.3. Agar Gel Samples Completely Surrounded by Air

Figure 8, from left to right, shows the details of the artifacts which were obtained on agar cusps with a thickness *t* equal to 2, 1, 0.5, 0.3, and 0.1 mm, respectively (see Figure 3). A distance of about 4 mm, between the upper polyethylene film and the first reflection generated by the agar cusps, is derived from the figure, according to the assumed propagation speed of 1500 m/s. This means that the US pulse, once it has been transmitted to the ridge of the agar cusps, propagates through the agar sample and reaches the lower polyethylene film before being reflected towards the probe. Figure 8 shows how modulated B-lines are obtained when the thickness *t* of the coupling section is equal to 0.5, 0.3, and 0.1 mm, and how confused artifacts are obtained when the latter increases. A slightly confused modulation was obtained when the thickness of the cusp ridge was equal to 1 mm. Modulated artifacts, such as those observed in cardiogenic pathologies, are finally obtained for the first time on deterministic phantoms, and they seem to be correlated to the size of the acoustic channel which links the acoustic trap to the chest wall.

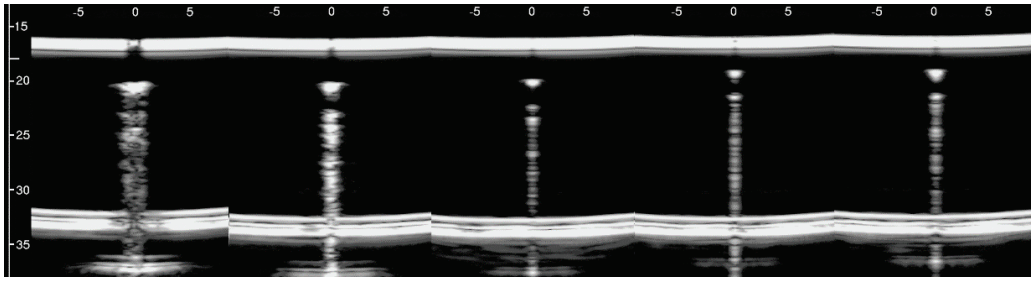

Figure 8. From left to right, the figure shows the vertical artifacts which were obtained with models of agar cusps having a thickness t of the upper part equal to 2, 1, 0.5, 0.3, and 0.1 mm, respectively. The two thick white lines at the top and at the bottom of the images represent the reflection of the upper polyethylene film and its replica, respectively.

Figure 9 shows four lung US images which have been selected from a data set previously acquired by means of a Toshiba Aplio XV scanner in our Respiratory Department during a study which was approved by the local Ethics Committee CEAVNO (study number 1089 approved on January 30, 2017). The two images on the left were acquired with a PVT-375BT convex probe and a central frequency equal to 6 MHz. The two images on the right were acquired with a PLT-704AT linear probe and a central frequency of 7.2 MHz. From left to right, the first image shows two B-lines; the first B-line does not show any modulation, while the second shows a slightly confused modulation. The second image shows a modulated B-line and the third shows a non-modulated B-line. The last image on the right shows a modulated B-line. An analogy with the experimental results illustrated in Figure 8 emerges, and the physicians' hypothesis regarding the progression of a lung disorder supports this thesis. According to their hypothesis, the interstitial spaces between the alveoli gradually increase with the progression of a pathology, and the modulated B-lines are related only to the early stages of the pathology.

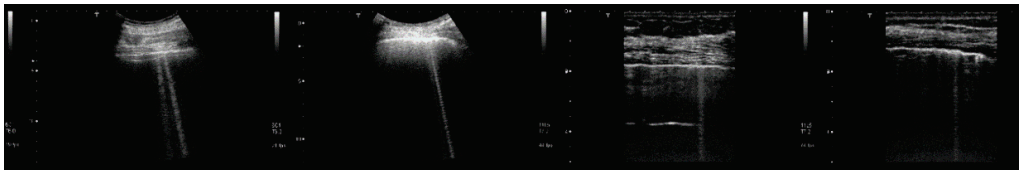

Figure 9. From left to right, the first image shows two B-lines; the first B-line does not show any modulation, while the second shows a slightly confused modulation. The second image shows a modulated B-line, and the third shows a non-modulated B-line. The last image on the right shows a modulated B-line.

3.4. Simulated Interlobular Septa

The simulated septa, which were obtained by using the pair of external moulds printed by setting the spatial resolution of the 3D printer to 0.1 mm, were first analysed. The first four images in Figure 10 from left to right show the artifacts which were obtained on four different simulated septa with smooth lateral surfaces and with thicknesses equal to 1.2, 0.8, 0.6, and 0.4 mm. It is worth noting that in this case, the vertical artifacts begin just below the upper polyethylene film. The septa with a thickness equal to 0.8, 0.6, and 0.4 mm provided modulated artifacts even though the 0.8 mm septum showed a slightly confused modulation. However, Figure 10 also shows an unexpected acoustic sign which is not observed on US lung images. The whiter sign, which is observed within the modulation of the three artifacts, is given by the reflection of the lower polyethylene film. The bottom of the septa gives rise to a reflection which is clearly highlighted in Figure 10, and this experimental result is not consistent with the observations of the physicians. Therefore, the simulated septa, which were obtained by using the pair of external moulds printed by setting the spatial resolution of the 3D printer to 0.280 mm, were also analysed. The vertical artifact which was obtained on a 0.4 mm septum with rough lateral surfaces is shown in the last image on the right of Figure 10. The strong reflection of the bottom of the septum is still perceivable, but this time, it is partially masked within the vertical artifact, and the latter is closer to the artifacts which are observed on US pulmonary images. Modulated vertical artifacts were obtained, and a correlation with the thickness of the septa emerges again, as expected by physicians.

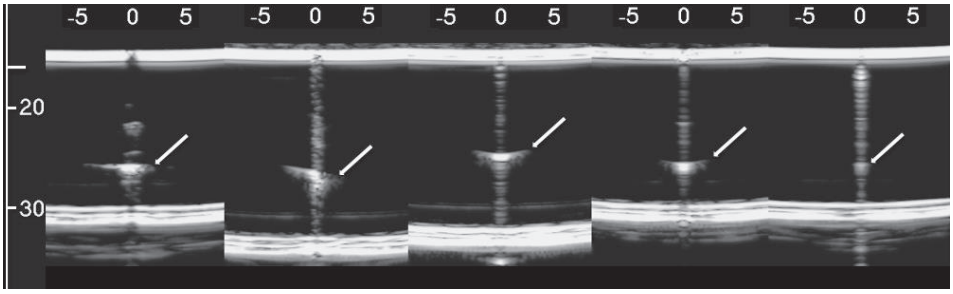

Figure 10. From left to right: the first four images show the vertical artifacts which were obtained with agar septa having smoother lateral surfaces and thickness equal to 1.2, 0.8, 0.6, and 0.4 mm. The last image on the right shows the vertical artifact which was obtained with an agar septum with rough lateral surfaces and a thickness equal to 0.4 mm. The two thick white lines at the top and at the bottom of every image represent the reflection of the upper polyethylene film and its replica, respectively. The arrows indicate the reflection of the lower polyethylene film.

4. Discussion

Some deterministic models have been introduced in this paper in order to replicate the visual characteristics of the vertical artifacts which are often observed on lung US images in the presence of pathologies. In this phase, deterministic models were preferred in order to guarantee the experiment repeatability. The device illustrated in Figure 2 combined with

the agar phantoms and the moulds provided by a 3D printer proved to be an interesting tool, and the technique illustrated in the image on the right of Figure 1 with the PVC box can be further developed. For example, the CNC milling machine can be replaced by laser technology and PVC boxes with aerated space distributions closer to the pulmonary anatomy (smaller holes having smaller distances among their axes) can be obtained. The model of multiple air cylinders arranged in multiple overlapping rows simulates a cloud of alveoli separated by large interstitial spaces which is perhaps what happens when observing the so-called white lung artifact [4]. These experimental models can represent the basis for numerous quantitative studies on vertical artifacts.

In a previous paper [4], the term acoustic trap was introduced. Here, it is illustrated by means of numerical models how a single trap, given by a volume of tissue mimicking medium surrounded by air, can produce a modulated vertical artifact and how its modulation is correlated with the shape and the size of the trap. In this paper, the potential role of the interstitial channel, which allows both the transmission of the acoustic energy of the pulse to the trap and the gradual re-radiation of the trapped energy towards the probe, is highlighted by means of physical experimental models. Modulated artifacts, such as those observed in cardiogenic pathologies, are obtained for the first time on deterministic physical phantoms.

The vertical artifacts which are observed in LUS images have some peculiarities that are probably strictly correlated with important anatomical pathological characteristics of the observed organ and are worth analysing. The length of an isolated vertical artifact is an example. In our experience the artifacts "which start at the pleura line and extend to the bottom of the screen" (the so-called B-lines) are obtained if the trap volume is completely surrounded by air except for a small input/output channel, so that the trapped energy cannot easily leave the trap as in the case of the artifact which is provided by the seven air cylinders (Figure 5). The structure of an isolated artifact is another example. The modulated artifacts were observed on cusps and septa when their link to the polyethylene film of container A was limited to a small acoustic channel. The characteristic modulation of the artifacts gradually disappears when increasing the section of the acoustic channels as shown in Figures 8 and 10. Here, a hypothesis, which should be analysed, can be formulated: when the link between the trap and the polyethylene film is reduced to a small acoustic channel, the trap acts as a point-like source of ultrasound and, consequently, can both re-radiate the trapped energy slowly and eliminate the uneven acoustic perturbation of the particles of the medium at the top of the channel. However, the analysis of this result from a clinical point of view is most important since it seems to match with a physician's focal hypothesis. Physicians relate the presence of modulated B-lines with an early stage of the cardiogenic pulmonary edema or pulmonary inflammation, while they relate the presence of simple B-lines with advanced stages of the two pathologies when the interlobular septa and the interstitial spaces between contiguous alveoli are further enlarged [7,22,29,30]. The experimental results obtained both on simulated interalveolar spaces and interlobular septa provide a rational explanation for the different forms of vertical artifacts that are usually observed on US lung images. The B-line modulation changes and becomes progressively more confused until the artifacts assume a structure which is visually similar to speckle noise in advanced stages of a pathology when the lung density increases.

5. Conclusions

The device illustrated in Figure 2 combined with the moulds provided by a 3D printer and the PVC box are versatile tools and can be used to check models of the outer lung surface that physicians may suggest on the basis of their anatomopathological knowledge. The geometry of the models can also be progressively modified to mimic various degrees of severity of a pathology, as in the case of the cusps and the septa which have been analysed here when varying the size of their link with the water container. The visual inspection of the artifacts obtained on these models can be a helpful guide for physicians in

their interpretation of the clinical data. What is probably most important, however, is the indication provided by the models on the informative content of the visual characteristics of the artefactual information, i.e., an indication of their capability to distinguish two pathologies and estimate their severity. This is another important aspect of the introduced tools; they can be used to investigate the sensitivity of the artifact visual inspection when varying the severity level of a simulated pathology. For example, looking at images in Figure 8, a clear difference among the modulated artifacts obtained when the thickness of the agar cusps varies from 0.5 mm to 0.1 mm does not emerge. According to the experimental results, the visual inspection of these artifacts alone does not allow a physician to distinguish an inter-alveolar space of 0.5 mm (the size of the trap input channel) from an inter-alveolar space of 0.1 mm.

The experimental results obtained on the agar cusps and on the simulated interlobular septa support the physicians' hypothesis, according to which the modulated artifacts are related to the first stages of a pathology, while the presence of simple B-lines is related to advanced stages of the pathology when the interlobular septa and the interstitial spaces between contiguous alveoli are further enlarged.

The experimental results also justify the particular interest of physicians concerning the artifacts which extend to the bottom of the screen, since in our experience, these artifacts can only be provided by particular traps. Very long artifacts are obtained if the trap volume is completely surrounded by air except for a small input/output channel, so that the trapped energy cannot easily leave the trap.

However, the length of a vertical artifact also depends on many imaging parameters (pulse central frequency and bandwidth, pulse amplitude, attenuation, and time gain compensation, just to mention a few), and, consequently, even the same acoustic trap can generate artifacts with different lengths. The artifact length alone does not characterize the trap, and splitting the vertical artifacts into short and long artifacts can be misleading.

Physicians should also carefully consider another experimental result illustrated in this paper. Modulated B-lines have been obtained even with acoustic traps (Figure 3 introduces cusps with a body of 3 mm $\times$ 4 mm $\times$ 10 mm), which are probably much larger than those they expect to find in patients with cardiogenic edema.

The most important problem of the techniques illustrated in this paper is represented by the perishability of the obtained phantoms, which limits their use for the training of physicians. Durable phantoms must be developed for this purpose in the future by professional manufacturers. However, the size of the models is another problem. Agar cusps with a body of 3 mm $\times$ 4 mm $\times$ 10 mm have been used to obtain the results illustrated in Figure 8. Smaller acoustic traps similar to a real pulmonary trap cannot be analysed with this technique. At this stage of our work, a 3D printer is used to print the moulds which are subsequently used to obtain the agar models. Printing the models directly with a 3D printer would be an important step forward, and we are currently working in this direction. A tissue mimicking material with appropriate acoustic properties which is also suitable for feeding a 3D printer is needed.

Funding: This research received no external funding.

Acknowledgments: The author wishes to thank the engineers Antonio Orsini (National Institute of Nuclear Physics, Pisa, Italy), Davide Cini (ReFly Group, Institute of Clinical Physiology, National Research Council, Pisa, Italy), and Rino Rossi for their precious contribution in making the phantoms. Moreover, the author wishes to thank the Fondazione della Cassa di Risparmio di Lucca for its invaluable support.

Conflicts of Interest: The author declares no conflict of interest.

References

1. Avruch, L.; Cooperberg, P.L. The ring down artifact. *J. Ultrasound Med.* **1985**, *41*, 21–28. [CrossRef]
2. Soldati, G.; Copetti, R.; Sher, S. Sonographic interstitial syndrome: The sound of lung water. *J. Ultrasound Med.* **2009**, *28*, 163–174. [CrossRef] [PubMed]

3. Kameda, T.; Kamiyama, N.; Kobayashi, H.; Kanayama, Y.; Taniguchi, N. Ultrasonic B-line-like artifact generated with simple experimental models provide clues to solve key issues in B-lines. *Ultrasound Med. Biol.* **2019**, *45*, 1617–1626. [CrossRef] [PubMed]
4. Demi, M.; Prediletto, R.; Soldati, G.; Demi, L. Physical mechanisms providing clinical information from ultrasound lung images: Hypotheses and early confirmations. *IEEE Trans. Ultrasound Ferroelectr. Freq. Control.* **2020**, *67*, 612–622. [CrossRef]
5. Weibel, E.R. Exploring the Structural Basis for Pulmonary Gas Exchange. In *The Pulmonary Circulation and Gas Exchange*; Wagner, W.W., Jr., Weir, E.K., Eds.; Futura Publishing Co Inc.: Armonk, NY, USA, 1994.
6. Dickinson, R.J.; Nassiri, D.K. *Reflection and Scattering*; Hill, C.R., Bamber, J.C., Haar, G.R., Eds.; Physical Principles of Medical Ultrasonics; Wiley: Chichester, UK, 2004; pp. 191–220.
7. Soldati, G.; Demi, M.; Smargiassi, A.; Inchingolo, R.; Demi, L. The role of ultrasound lung artifacts in the diagnosis of respiratory diseases. *Expert Rev. Respirat. Med.* **2019**, *13*, 163–172. [CrossRef] [PubMed]
8. Faran, J.J. Sound scattering by solid cylinders and spheres. *J. Acoust. Soc. Am.* **1951**, *23*, 405–418. [CrossRef]
9. Wille, J.E. *Analysis of a Cylindrical Acoustic Resonator Sound-Velocity Meter*; United States Naval Postgraduate Study: Monterey, CA, USA, 1957.
10. Bushberg, J.T.; Seibert, J.A.; Leidholdt, E.M., Jr.; Boone, J.M. *The Essential Physics of Medical Imaging*; Williams & Wilkins: Philadelphia, PA, USA, 2002.
11. Cobbold, R.C.S. *Foundations of Biomedical Ultrasound*; Oxford University Press: New York, NY, USA, 2007.
12. Demi, M. The basics of ultrasound. In *Comprehensive Biomedical Physics*; Brahme, A., Ed.; Elsevier: Amsterdam, The Netherlands, 2014; Volume 2, pp. 297–322.
13. Bouhemad, B.; Zhang, M.; Lu, Q.; Rouby, J.J. Clinical review: Bedside lung ultrasound in critical care practice. *Crit. Care* **2007**, *11*, 205. [CrossRef]
14. Koenig, S.J.; Narasimhan, M.; Mayo, P.H. Thoracic ultrasonography for the pulmonary specialist. *Chest* **2011**, *40*, 1332–1341. [CrossRef]
15. Volpicelli, G.; Elbarbary, M.; Blaivas, M.; Lichtenstein, D.A.; Mathis, G.; Kirkpatrick, A.W.; Melniker, L.; Gargani, L.; Noble, V.E.; Via, G.; et al. International evidence-based recommendations for point-of-care lung ultrasound. *Intensive Care Med.* **2012**, *38*, 577–591. [CrossRef]
16. Lichtenstein, D.; Meziere, G. A lung ultrasound sign allowing bedside distinction between pulmonary edema and COPD: The comet-tail artifact. *Intensive Care Med.* **1998**, *24*, 1331–1334. [CrossRef]
17. Copetti, R.; Soldati, G.; Copetti, P. Chest sonography: A useful tool to differentiate acute cardiogenic pulmonary edema from Acute respiratory distress syndrome. *Cardiovasc. Ultrasound* **2008**, *6*, 1–10. [CrossRef]
18. Soldati, G.; Demi, M. The use of lung ultrasound images for the differential diagnosis of pulmonary and cardiac interstitial pathology. *J. Ultrasound* **2017**, *20*, 91–96. [CrossRef]
19. Soldati, G.; Smargiassi, A.; Inchingolo, R.; Sher, S.; Nenna, R.; Valente, S.; Inchingolo, C.D.; Corbo, G.M. Lung ultrasonography may provide an indirect estimation of lung porosity and air space geometry. *Respiration* **2014**, *88*, 458–468. [CrossRef]
20. Buda, N.; Skoczylas, A.; Demi, M.; Wojteczek, A.; Cylwik, J.; Soldati, G. Clinical Impact of Vertical Artifacts Changing with Frequency in Lung Ultrasound. *Diagnostics* **2021**, *11*, 401. [CrossRef]
21. Dietrich, C.F.; Mathis, G.; Blaivas, M.; Volpicelli, G.; Seibel, A.; Wastl, D.; Atkinson, N.S.; Cui, X.W.; Fan, M.; Yi, D. Lung B-line artefacts and their use. *J. Thorac. Dis.* **2016**, *8*, 1356–1365. [CrossRef] [PubMed]
22. Lichtenstein, D.; Mezière, G.; Biderman, P.; Gepner, A.; Barré, O. The comet-tail artifact: An ultrasound sign of alveolar interstitial syndrome. *Am. J. Respir. Crit. Care Med.* **1997**, *156*, 1640–1646. [CrossRef] [PubMed]
23. Soldati, G.; Giunta, V.; Sher, S.; Melosi, F.; Dini, C. Synthetic comets: A new look at lung sonography. *Ultrasound Med. Biol.* **2011**, *37*, 1762–1770. [CrossRef] [PubMed]
24. Spinelli, A.; Vinci, B.; Tirella, A.; Matteucci, M.; Gargani, L.; Ahluwalia, A.; Domenici, C.; Picano, E.; Chiarelli, P. Realization of a poro-elastic ultrasound replica of pulmonary tissue. *Biomatter* **2012**, *2*, 37–42. [CrossRef]
25. Do, H.H.; Lee, S. A low-cost training phantom for lung ultrasonography. *Chest* **2016**, *150*, 1417–1419. [CrossRef]
26. Blüthgen, C.; Sanabria, S.; Frauenfelder, T.; Klingmüller, V.; Rominger, M. Economical sponge phantom for teaching, understanding, and researching A- and B-line reverberation artifacts in lung ultrasound. *J. Ultrasound. Med.* **2017**, *36*, 2133–2142. [CrossRef] [PubMed]
27. Demi, M.; Soldati, G.; Demi, L. On the artefactual information of ultrasound lung images: A lines and B lines. In Proceedings of the 176th Meeting of Acoustical Society of America, Victoria, BC, Canada, 5–9 November 2018.
28. Boni, E.; Bassi, L.; Dallai, A.; Guidi, F.; Ramalli, A.; Ricci, S.; Housden, E.; Tortoli, P. A reconfigurable and programmable FPGA based system for non-standard ultrasound methods. *IEEE Trans. Ultrason. Ferroelectr. Freq. Control.* **2012**, *59*, 1378–1385. [CrossRef] [PubMed]
29. Milne, E.N.; Pistolesi, M.; Miniati, M.; Giuntini, C. The radiologic distinction of cardiogenic and non cardiogenic edema. *AJR Am. J. Roentgenol.* **1985**, *144*, 879–894. [CrossRef] [PubMed]
30. Chiesa, A.M.; Ciccarese, F.; Gardelli, G.; Regina, U.N.; Feletti, F.; Reggiani, M.L.B.; Zompatori, M. Sonography of the normal lung: Comparison between young and elderly subjects. *J. Clin. Ultrasound* **2014**, *43*, 230–234. [CrossRef] [PubMed]

diagnostics

MDPI

Review

Vertical Artifacts in Lung Ultrasonography: Some Common Clinician Questions and the Related Engineer Answers

Marcello Demi [1], Natalia Buda [2,*] and Gino Soldati [3]

[1] Department of Bioengineering, Fondazione Toscana Gabriele Monasterio, 56126 Pisa, Italy; demi@ftgm.it
[2] Department of Internal Medicine, Connective Tissue Diseases and Geriatrics, Medical University of Gdansk, Ul. Smoluchowskiego 17, 80-952 Gdansk, Poland
[3] Ippocrate Medical Center, 55032 Lucca, Italy; soldatigino@yahoo.it
* Correspondence: natabud@wp.pl; Tel.: +48-58-349-46-70

Abstract: Introduction: Vertical artifacts, including B lines, are frequently seen in a variety of lung diseases. Their sonomorphology varies in length, width, shape, and internal reverberations. The reason for this diversity is still unknown and is the cause of discussion between clinicians and ultrasound physics engineers. Aim: The aim of this work is to sum up the most common clinician observations and provide an explanation to each of them derived from ultrasound physics. Materials and Methods: Based on clinical and engineering experiences as well as data collected from relevant literature, the sonomorphology of vertical artifacts was analyzed. Thirteen questions and answers were prepared on the common sonomorphology of vertical artifacts, current nomenclature, and clinical observations. Conclusions: From a clinical standpoint, the analysis of vertical artifacts is very important and requires that further clinical studies be conducted in cooperation with engineers who specialize in physics.

Keywords: lung ultrasonography LUS; B lines; vertical artifacts; sonomorphology of artifacts; cardiac edema; pulmonary fibrosis; interstitial pneumonia

Citation: Demi, M.; Buda, N.; Soldati, G. Vertical Artifacts in Lung Ultrasonography: Some Common Clinician Questions and the Related Engineer Answers. *Diagnostics* **2022**, *12*, 215. https://doi.org/10.3390/diagnostics12010215

Academic Editor: Xavier Muñoz-Berbel

Received: 22 December 2021
Accepted: 14 January 2022
Published: 16 January 2022

Publisher's Note: MDPI stays neutral with regard to jurisdictional claims in published maps and institutional affiliations.

1. Introduction

The utrasound assessment of the lungs involves the analysis of vertical artifacts and consolidations. B-line artifacts are the most frequently described pathology-related vertical artifacts. The definition of a B-line artifact was established many years ago and was based on the first clinical studies which had been conducted on patients with cardiac insufficiency and pulmonary edema. B-line artifacts also occur in many other diseases affecting the interstitial space and alveoli [1,2]. However, the origin of B lines and other vertical artifacts has still not been thoroughly explained. Varied etiology and pathophysiology of diseases that involve the interstitial space and alveoli result in the presence of vertical artifacts, termed B lines, which can be viewed on the display monitor of the ultrasound machine. Recently, studies devoted to varied sonomorphologies of vertical artifacts have appeared [3]. This publication presents the discussion between two clinicians and a physics engineer as regards the differences in the sonomorphology of vertical artifacts and the impact of physical factors and ultrasound machine settings on vertical artifacts.

2. Material and Methods

Some of the terms that will be used in this paper are explained below:

Aerated space/area/volume—air component of the lung (the walls of the alveolar sacs are excluded).

Acoustic medium—includes blood and all other pathological/physiological media that form the barriers that confine air and blood to separate lung compartments.

Acoustic channel—a path given by an acoustic medium surrounded by aerated spaces.

Acoustic trap—a volume of acoustic medium surrounded by aerated spaces that is connected to the pleura plane (and consequently to the thoracic wall) through an acoustic channel.

Aperture—the gap between the aerated spaces that gives rise to an acoustic channel.

Acoustic beam—the area within which the acoustic energy, which is transmitted from the probe to the pleura plane, is mostly constrained through the focusing process. It is characterized by a variable lateral size, which depends on the focus position [4].

Based on clinical and engineering experiences as well as data collected from relevant literature, the sonomorphology of vertical artifacts was analyzed. This work presents examples of clinical observations regarding the presence of vertical artifacts that are manifested in specific clinical conditions, e.g., cardiogenic pulmonary edema, interstitial pneumonia, and pulmonary fibrosis secondary to interstitial lung disease. Questions regarding the reasons for the presence of these related vertical artifacts and the potential impact of the ultrasound machine settings are posed to the engineer who specializes in ultrasound physics.

3. Discussion between the Clinicians and the Engineer

Question 1:

While monitoring the interstitial and alveolar involvement, we observe more and more confluent B lines which can evolve in a so-called white lung artifact which, in turn, can subsequently change to consolidation (see Figure 1) [5,6]. What does the image of B lines and consolidations depend on?

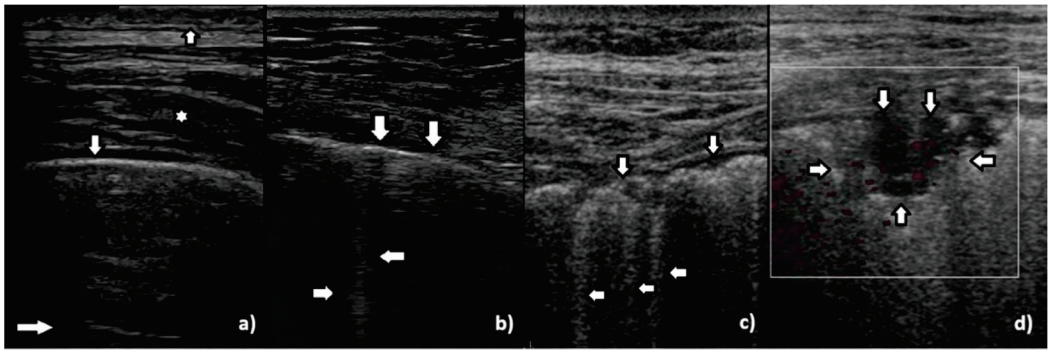

Figure 1. Gradual loss of lung aeration in ultrasound. (**a**) normally aerated lung, (**b**) single vertical artifacts, (**c**) multiple vertical artifacts, and (**d**) subpleural consolidation.

Answer 1:

Isolated B lines are related to isolated acoustic traps and this probably occurs in the first stages of a pathology. When the number of the acoustic traps increases, due to the progression of a pathology, numerous B lines are observed. When their number further increases, they are close to each other and can be even mutually linked. In this case, confluent artifacts logically appear. When the ratio between aerated spaces and interstitial volumes drastically decreases within a lung region, then a lung configuration where small separated aerated spaces are immersed in an interstitial volume is expected. This is probably the lung configuration which is at the basis of the White Lung artifact. Obviously, when the last small aerated spaces also disappear, a clear consolidation naturally emerges.

Question 2:

In healthy individuals, an ultrasound examination of the lungs visualizes only the lung surface, termed the pleural line (see Figure 2a). A-line artifacts are visible below the pleural line. These form horizontal lines that appear at regular intervals, equaling the distance between the body surface and the pleural line (see Figure 2b). Under anatomical

conditions, it is not possible to visualize lung parenchyma and the interstitium. Only when subpleural areas of the lungs lose their aeration due to lesions can vertical artifacts and/or subpleural consolidations be observed [7]. Why is this so?

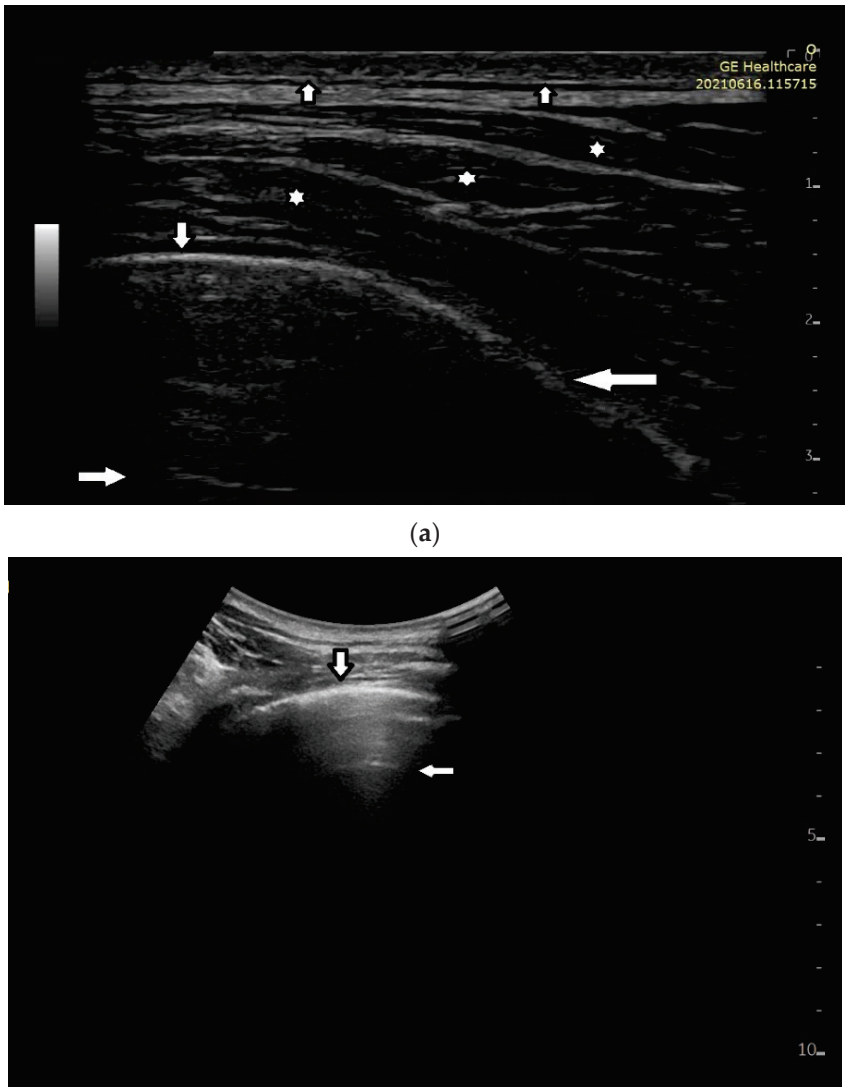

(**a**)

(**b**)

Figure 2. (**a**) Lung ultrasound, linear probe: white stars (*) muscles of the chest wall; down arrow (↓) well-defined pleural line (perpendicular ultrasound beam); left arrow (←) blurred pleural line secondary to the tangential incidence of the ultrasound beam; up arrow (↑) subcutaneous tissue; right arrow (→) A line, horizontal artifact. (**b**) Lung ultrasound, convex probe: down arrow—pleural line, smooth, echoic and regular; left arrow—A-line artifact.

Answer 2:

Once an US pulse reaches the pleura plane through the chest wall, it is partially reflected toward the probe and partially transmitted to the channels provided by a specific distribution of the aerated spaces, which characterizes the outer lung surface. In a healthy lung, the size of the interalveolar septa is, and reasonably so, supposed to be comparable to a capillary lumen (less than 10 microns), and an US pulse "sees" this aerated space distribution as a compact air wall. In this case, the acoustic energy is essentially reflected back to the probe. The lung surface is highlighted with a thick white line (the so-called pleural line), and A-line artifacts are visible below the pleural line thanks to the multiple reflections of the acoustic wave between the lung surface and the probe. Replicas of the

thoracic wall structures are also often well visible between every pair of A lines thanks to the replica and mirror effects as a consequence of the strong reflection of the lung surface. It is worth noting, however, that the affirmation "The A line artifacts form horizontal lines that appear at regular intervals equaling the distance between the body surface and the pleural line" is not entirely correct. Such an affirmation is correct only if the pleural plane is exactly parallel to the head of the probe [8].

On the other hand, in the presence of thickened interstitial spaces, the pulse energy can be partially trapped by the latter. This can subsequently be reradiated toward the probe after multiple reflections between the separated aerated spaces, giving rise to vertical artifacts, which arise from the pleura line. The imaging parameters play a fundamental role in the formation of the artifacts, and the visibility of a vertical artifact (that is, its brightness, lateral dimension, and length) depends on multiple non-orthogonal factors including the gain, the time gain compensation (TGC), and all the parameters that can be easily set by the operator from the scanner keyboard. The clinical information that can be obtained from lung US images is essentially artifactual information except in the case of consolidation when anatomical information is obtained.

Question 3:

The pleural line is an artifact and, in reality, consists of two opposing layers of serous membranes moving against each other. The apparent movement of the pleural line is termed "lung sliding". However, when imaging the lungs with a low-frequency probe, e.g., a convex probe or a low-frequency linear probe, it is not possible to differentiate between the two membranes in the pleural line. Why?

Answer 3:

The thick white line which is visible on lung images, which we usually call pleural line, is given by the reflection of the aerated space distribution, which characterizes the outer lung surface. Such a bright white line cannot be related to the reflection of the pleura (an organ which includes the two parietal and visceral pleurae and the pleural cavity), since its acoustical characteristics are similar to those of the thoracic wall and, consequently, it cannot give rise to strong reflections. Moreover, even though a minimal reflection is conceivable at the border between the chest wall and the pleura (i.e., at the parietal pleura), the latter cannot be easily perceived due to the near and much stronger reflection that occurs at the border between the pleura and the outer lung surface (i.e., at the visceral pleura). As a rule of thumb, two different acoustic discontinuities can be separately perceived if the distance between them (in this case, the pleura thickness) is greater than half the pulse length. Let us suppose the pleura thickness be approximately 0.3 mm–0.4 mm. In theory, a short US pulse (provided for example by a linear probe when using a carrier frequency of 6 MHz) can separately highlight the two pleura borders. However, the reflection which occurs at the parietal pleura is minimal with respect to the reflection that occurs at the visceral pleura. I have never studied the problem in depth, but this is probably why the pleura parietal border is not clearly visible (even with a higher frequency).

Question 4:

The head of the probe should be placed over the patient's body in such a way as to make ultrasound waves perpendicular to the lung's surface. It should be remembered that the surface of the lung is curved. When the ultrasound beam is perpendicular to the lung surface, the pleural line is well defined, echoic, and smooth under normal conditions. In the case of a tangent ultrasound beam, the pleural line is irregular and simultaneously blurred, which should not be interpreted as a pathological sign, but as a result of an incorrect assessment technique. Can you explain this circumstance better?

Answer 4:

The thickness of the bright white line (the so-called pleura thickness), which highlights the outer lung surface, is related to the pulse length. However, even in the case of a healthy

lung, its thickness is theoretically equal to the length of the pulse only if the direction of the acoustic wave propagation is orthogonal to the pleura plane. According to Snell's law, the reflection angle is equal to the incidence angle, and if the direction of the incidence wave is not orthogonal to the pleura plane, then the probe receives only diffuse energy. In this case, a blurred and thicker "pleura line" should be expected. The problem is evident when using a convex probe since the latter transmits the US pulses (and receives the echoes) in a fan-shaped mode. In this way, on the lateral parts of the fan, the US beam does not intersect the lung surface orthogonally, and the pleura line at the border of the fan is mostly blurred.

Question 5:

We observe B lines in many different clinical conditions, e.g., cardiac edema, interstitial pneumonia, ARDS, pulmonary fibrosis, alveolitis, etc. Each time the interstitial space is involved, B lines are observed [9–11]. Which medium could result in visible B lines?

Answer 5:

Whenever the distance among a group of aerated spaces increases, due to the thickening of the barrier that separates them, an acoustic trap develops. An acoustic trap is a volume of non-aerated material and can be a mix of different biological media (water, tissue, blood, exudate, transudate, etc.) with similar acoustic properties. If a reasonably sized acoustic channel, which links the trap to the pleura plane exists, then an acoustic pulse can enter the trap and be gradually reradiated as a vertical artifact. The artifact characteristics are mostly related to the size and shape of the trap and of the linking channel. In my opinion, the impact of the trap medium on the artifact cannot be quantified unless the geometric characteristics of both the trap core and channel are precisely known.

Question 6:

Experts from the World Federation for Ultrasound in Medicine and Biology (WFUMB) differentiate B-line artifacts (BLA) from comet-tail artifacts (CTA) [12]. B-line artifacts arise from the normal pleural line and implicitly result from cardiogenic pulmonary edema. CTA arise from the abnormally changed pleural line, thus they occur in other numerous diseases involving the interstitial space, e.g., pulmonary fibrosis and interstitial pneumonia [13–15].

From a clinical standpoint, it seems that such a division is still not ideal. Active lesions in interstitial lung disease, visualized as the presence of "ground glass" in computed tomography, will also be represented as B lines arising from the normal pleural line in the ultrasound image. This happens in acute hypersensitivity pneumonitis, some cases of sarcoidosis, acute interstitial pneumonia, and alveolar hemorrhage [16,17].

We return, then, to physics and the medium of ultrasound wave propagation. It appears that based on the sonomorphology of comet-tail artifacts per se we are unable to differentiate whether the artifact is of a cardiogenic or pulmonary aetiology. Thus, is the transudate secondary to pulmonary edema the reason for the formation of B lines, or is the artifact caused by the inflammatory fluid?

Answer 6:

A vertical artifact can extend from the pleural line to the bottom of the screen, but it can also be shorter; it can appear as a sequence of alternating white and black horizontal bands or as a vertical bright stripe with a constant gray level, and it can be narrow or wide. The spatial distribution of the gray level bands within the vertical artifact can be the expression of a precise periodic function or an aperiodic function. These vertical artifacts are usually named modulated artifacts even when their modulation is a bit confused (when the horizontal bands are not exactly parallel). Obviously, a vertical artifact is also affected by speckle noise and by the superposition of the replica and mirror effects of the chest wall structures; however, this overlapping alone is not sufficient to explain the different structures of the observed B lines. Their structure can even be that of a completely random gray level distribution (confused vertical artifacts).

The visual aspect of a vertical artifact is not strictly correlated to a pathology. The characteristics of an artifact are related to the mutual distribution of aerated and interstitial

spaces within which the artifact has been generated. For example: (i) A modulated artifact is probably obtained only when the access channel to the trap core is small with respect to the wave length of the carrier frequency. (ii) A confused artifact is obtained when the channel aperture increases. (iii) A long artifact (either confused or modulated) is obtained when the channel cross section is small with respect to the trap internal surface so that the reradiation of the trapped energy can be slowed down, and so on. From a technical point of view, these configurations of aerated and interstitial spaces, which underlie the vertical artifacts, can arise in different pathologies. Vertical artifacts appear on lung images every time the thickness of the interstitial medium (tissue, blood, and effusion caused by either transudate or exudate), which separates the aerated spaces, increases over a certain threshold. The acoustic properties of transudate and exudate are probably similar and do not allow us to distinguish them on the basis of the US response if these two processes give rise to an identical distribution of aerated and interstitial spaces. What I mean is that you should not try to distinguish transudate from exudate fluids. You should focalize your attention on the potential differences between the distributions of aerated spaces originating from different pathological processes, that is, if there is any obvious difference.

Question 7:

Short vertical artifacts (e.g., the so-called I or Z lines) have never been studied thoroughly. The length of vertical artifacts can vary even in the group of artifacts, which does not reach the bottom of the screen (see Figure 3a,b). One example is the early stage of developing atelectasis (during general anesthesia). What are the most important factors that influence the length of vertical artifacts?

Answer 7:

The length of an artifact, as well as its structure and its brightness, depends on so many factors that it is nearly impossible to list them all [18,19]. Generally speaking, the length of a vertical artifact is given by the time an acoustic trap needs to reradiate the pulse energy, which has been partially trapped therein previously. The length of a vertical artifact not only depends on the geometric characteristic of the acoustic trap but also on the imaging parameters. Therefore, the same acoustic trap may give rise to vertical artifacts with different lengths. The imaging parameters play a fundamental role in the formation of the artifacts and the visibility of a vertical artifact (that is, its brightness, lateral dimension, and length) depends on multiple non-orthogonal factors including the gain, the time gain compensation (TGC), and all the parameters that can be easily set by the operator from the scanner keyboard. Therefore, given the intrinsic variability of the artifacts as a function of multiple nonindependent factors, including the human factor, making an objective diagnosis on the basis of the artifactual information is a difficult task. However, going back to your primary question about the length of the shorter artifacts, I can formulate some hypotheses. First of all, we must answer another question: why are they so short with respect to the artifacts that physicians classify them as "artifacts that extend to the bottom of the screen"? Maybe their linking channel is so small that it allows the transmission of a minimal part of the pulse energy, but in this case, a modulated artifact should appear since this is the peculiarity of a small channel [20]. If a confused artifact is generated, then its minimal length can be related to a wide channel with respect to the core of the trap, which allows a quick release of the trapped energy or a dispersion of the trapped energy through lateral doorways. Attenuation can also theoretically account for a minimal length of the artifact, but in this case, I do not have a valid hypothesis on the nature of the medium.

Question 8:

Based on clinical observations, we know that in pulmonary fibrosis, B lines often reduce their length when higher frequencies are used on a convex probe (from 2 MHz up to 6 MHz) (see Figure 4a,b). In the case of cardiac edema, the length of a B line is often stable, irrespective of the frequency modification (see Figure 4c,d) [3]. Why does the length of B

lines sometimes change when varying the pulse central frequency, whereas sometimes the length does not significantly change?

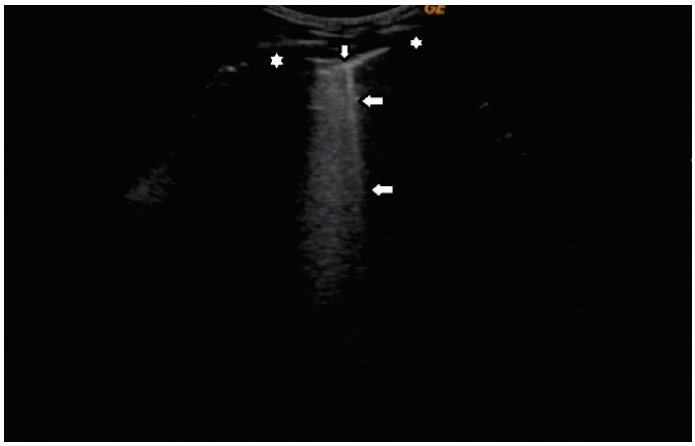

(**a**)

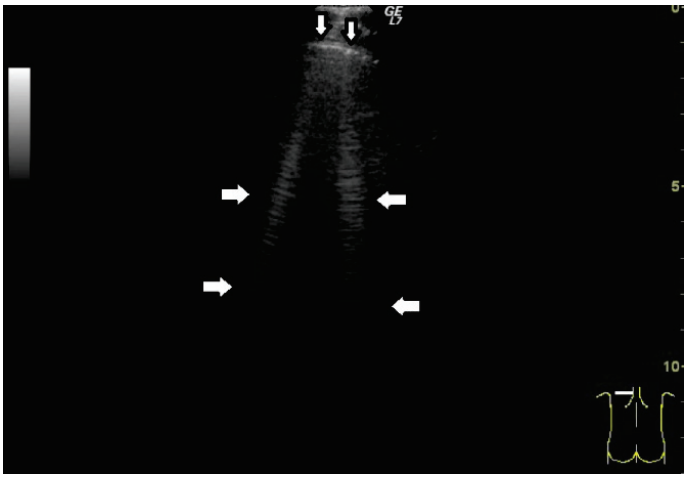

(**b**)

Figure 3. (**a**) Vertical artifact (←) originating from the pleural line (↓), smooth in structure, and ending after a few centimeters (a few centimeters in length). (**b**) Vertical artifacts (←,→) originating from the pleural line (↓), modulated sonomorphology of the artifact, and ending after a few centimeters (a few centimeters in length).

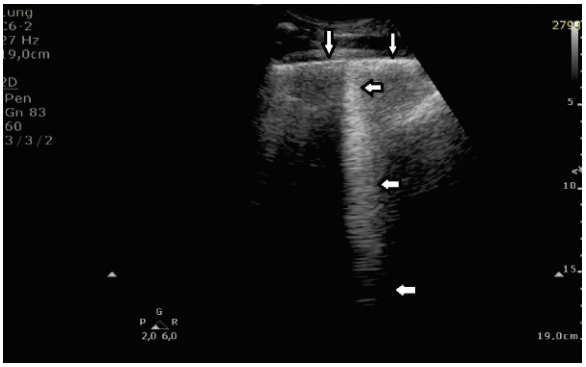

(**a**)

Figure 4. *Cont.*

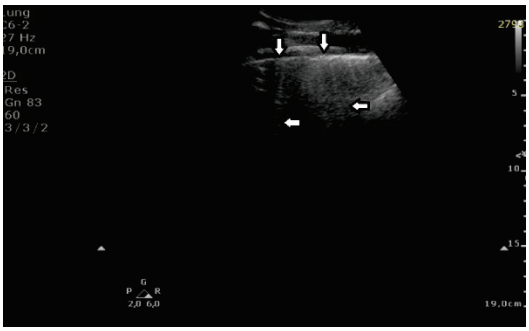

(**b**)

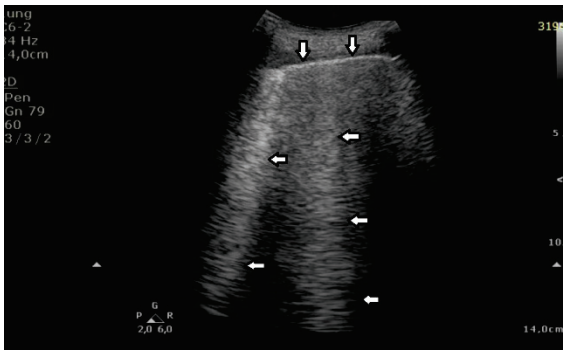

(**c**)

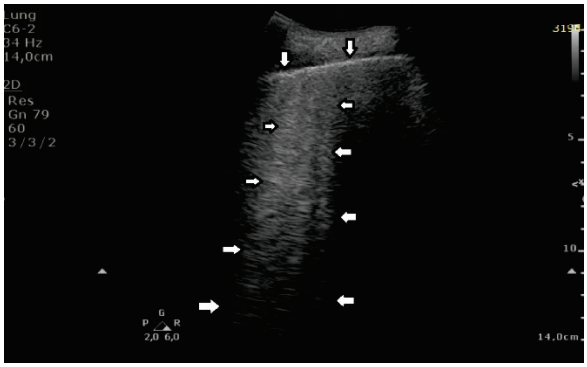

(**d**)

Figure 4. (**a**) Pulmonary fibrosis in the course of interstitial lung disease: down arrows—pleural line; left arrows—B line artifact observed at 2 MHz frequency. (**b**) Pulmonary fibrosis in the course of interstitial lung disease: down arrows—pleural line; left arrows—vertical artifacts observed at 6 MHz frequency. The image was obtained from the same patient and identical assessment site as in Figure 4a. (**c**) Cardiac edema: down arrows—pleural line; left arrows—B-line artifacts observed at 2 MHz frequency. (**d**) Cardiac edema: down arrows—pleural line; left arrows—B-line artifacts observed at 6 MHz frequency. The image was obtained from the same patient and identical assessment site as in Figure 4c.

Answer 8:

Look at the entire image, and you will find the answer. When using the 2 MHz frequency, the image (Figure 4a) is brighter everywhere: the thoracic wall is brighter; the pleura line is brighter; the two lateral sides of the image (where there are no artifacts) are brighter, and the artifacts themselves are brighter. In my opinion, the problem is primarily given by the attenuation, which increases when increasing the frequency. In order to compensate such an effect, you should change the TGC. As a rule of thumb, you can consider an attenuation coefficient of 1 db/cm/Mhz. When varying the frequency from 2 MHz to 6 MHz, you are introducing an additional attenuation of 4db per centimeter.

From a practical point of view, when using the 6 MHz frequency, the probe receives a signal from the depth of half a centimeter, whose amplitude is less than half the amplitude of the signal it would receive from the same depth if a 2 MHz pulse were used. Moreover, it is worth noting that the ratio between the amplitudes of the two temporal signals $s_6(t)$ and $s_2(t)$ (the echoes received by the probe) decreases exponentially when the delay t increases.

The answer is a bit more complex when cardiac edema is considered. In the case of fibrosis, larger acoustic traps and wider linking channels are, in general, expected that reradiate almost the entire power spectrum of the trapped acoustic pulse. In this case, attenuation is probably the main factor that influences the artifact length when varying the frequency. Therefore, the artifact length decreases when increasing the pulse central frequency since attenuation increases when increasing the frequency. On the contrary, in the case of cardiac edema, smaller acoustic traps and narrower linking channels are expected at the early stages of the pathology. Smaller traps can reradiate only a few harmonics, and the overlapping between the pulse spectrum and the spectral signature of the trap affects the artifact length much more than the attenuation factor. In these cases, the trap response to pulses with different frequencies is unpredictable.

Question 9:

Based on clinical observations, we know that vertical artifacts can have different lengths, widths, and shapes (see Figure 5a–c). A modulation of artifacts is also often clearly perceived. Why are they so varied? What does this depend on?

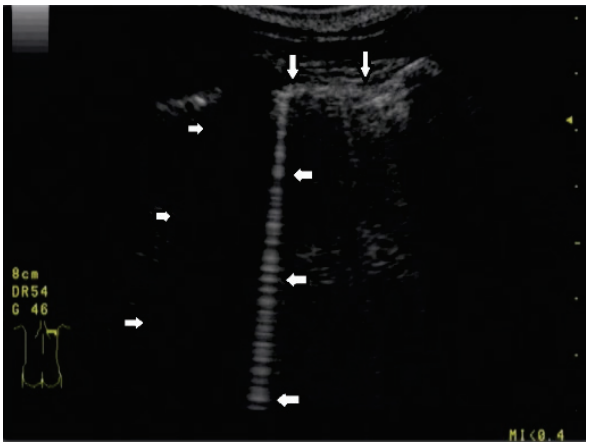

(**a**)

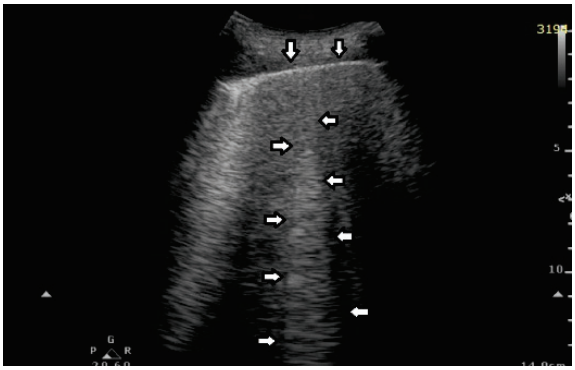

(**b**)

Figure 5. *Cont.*

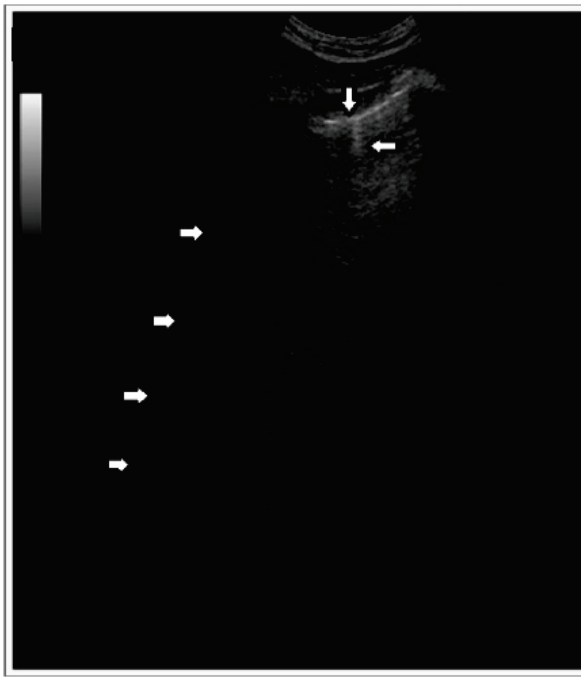

(**c**)

Figure 5. (**a**) Irregular, echoic pleural line (vertical arrows), long vertical artifact (left horizontal arrows), and shadow behind the rib (right horizontal arrows). The vertical artifact is classified as a B line since it originates from the pleural line and reaches the edge of the screen. Multiple small horizontal artifacts (named J artifacts by D. Lichtenstein) are visible inside the B line. (**b**) Smooth, regular, and echoic pleural line (vertical arrows), long vertical artifact, so called B line: narrow at the top and wide at the bottom (left and right horizontal arrows). (**c**) Smooth, regular, and echoic pleural line (vertical arrow), short vertical artifact, so called I line (left horizontal arrow and shadow behind the rib (right horizontal arrows).

Answer 9:

Many types of acoustic traps exist, and, consequently, many types of vertical artifacts exist. Let us consider an isolated acoustic trap. It has its own volume and geometric shape. It is linked to the pleura plane by means of an acoustic channel (typically an interalveolar interstice), and this channel also has its own shape and size represented by its cross-section and length. Every single difference between two acoustic traps affects the visual aspect of the related artifacts. Moreover, you should never forget that even the imaging parameters (pulse central frequency and bandwidth, focus position, TGC, pulse amplitude, etc.) strongly affect the formation and the final shape of an artifact.

Question 10:

B lines that meet the assumptions of the definition may differ from each other. Why do we observe so many sonomorphologies of B lines when we use a convex probe? B lines can be:

(a) Wide at the edge of the screen.
(b) Narrow throughout the entire length.
(c) Modulated.
(d) Smooth.
(e) Frequency dependent or not.

Answer 10:

Usually, when using a convex probe, the lateral size of a vertical artifact naturally increases far from the pleura plane due to the signal/image processing algorithms that the

US system uses to convert RF signals into a two-dimensional image. Moreover, the lateral size of an artifact (provided by a convex probe) at the end of the screen depends on the image depth. A constant narrower artifact is, on the contrary, common when using a linear probe. Modulated artifacts are observed when the cross section of the acoustic channel that links the trap to the pleura plane is small with respect to the wave length of the pulse central frequency. Here, a hypothesis can be formulated: when the link between the trap and the pleura plane is reduced to a small acoustic channel, the trap acts as a point-like source of ultrasound and, consequently, can eliminate the uneven acoustic perturbation of the particles of the medium at the top of the channel [20]. If by "smooth artifact" you mean a vertical artifact with a unique gray level from the beginning to the bottom, this is a particular type of modulation, which is obtained when a trap reradiates a single harmonic. The vertical artifacts are always frequency dependent since this is an intrinsic characteristic of the ultrasound investigation. The variation of the ultrasound response with the frequency may not be always visually perceptible, but such a variation always exists.

Question 11:

The length of vertical artifacts can vary. Consistent with the terminology proposed by Daniel Lichtenstein, B, I, Z, and C lines are differentiated. B, Z, and I lines originate from the pleural line, but have various lengths. Thus far, Z and I lines have not been considered to be clinically significant. C lines originate from the lower edge of subpleural consolidations.

The significance of B lines is related to lesions affecting the interstitial space and alveoli (see Figure 6). Most frequently, the presence of B lines is reported in cardiogenic pulmonary edema, interstitial pneumonia, ARDS, and pulmonary fibrosis secondary to interstitial lung disease. Despite copious clinical observations describing the significance of B-line artifacts, we have still not acquired complete knowledge as regards their origin. The definition of a B line that is presently adopted is as follows:

(a) Well defined.
(b) Originating from the pleural line.
(c) Going to the edge of the screen.
(d) Laser like.
(e) Erasing A lines.
(f) Moving with lung sliding.

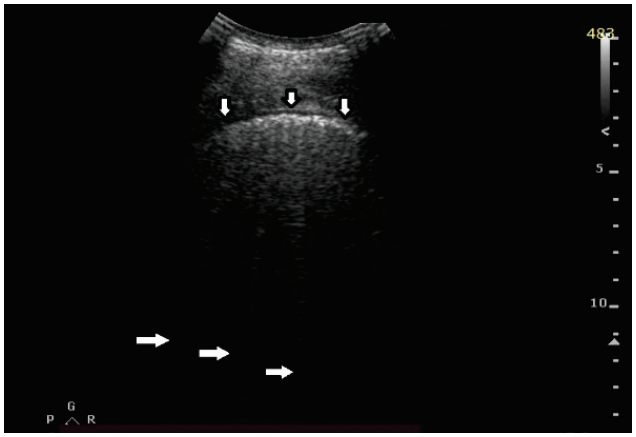

Figure 6. B lines (horizontal arrows) and pleural line (vertical arrows).

Do you agree with this definition of B line? Should we differentiate B lines from other vertical artifacts?

Answer 11:

It is difficult to challenge a definition since a definition is a definition "by definition". What I disagree with is the vagueness of this definition. "Moving with lung sliding" is a specific feature which links the artifact to a precise anatomical position of the outer lung

surface where an acoustic trap developed. However, "well defined" is a subjective and vague characteristic. Moreover, the characteristic of "originating from the pleural line" is not properly formulated since in theory such a definition excludes B lines, which do not originate exactly at the pleural line. Due to both the size of the acoustic trap and the length of the linking acoustic channel, a B line often starts a bit lower than the pleural plane. "Going to the edge of the screen" is also an ambiguous characteristic since the edge of the screen is decided by the operator when he/she sets the acquisition depth. Even the characteristic of "Erasing A lines" is not properly formulated since some modulated B lines do not completely erase the A lines. In particular, the lateral size of B lines does not change a lot when a linear probe is used, and A lines mostly remain visible in the presence of a few B lines. Moreover, "laser like" is an intuitive description, but it is not specific. "Lying on the direction of the acoustic beam propagation" should be used since this is the specific characteristic.

Question 12:

For clinicians the meaning of B lines depends on many factors:

(a) Does it meet the definition of a B line artifact?
(b) Sonomorphology of a B line.
(c) Gravity dependence.
(d) Distribution of interstitial lesions.
(e) Coexisting ultrasound signs.
(f) Ultrasound image with a linear probe.
(g) And the most important factor—clinical context.

What is your proposal (from an engineer's point of view) for the classification of vertical artifacts?

Answer 12:

Why should I classify what I am observing into a limited number of cases? A process of information classification is a delicate process since the risk of losing important information is always present. This is particularly risky in our case since we are dealing with artifactual information, and we do not yet know what is really important and what can be neglected. When using an US probe, a physician actively observes a scene through many video clips. He/she should not observe a single artifact in order to classify it according to a rigid scheme. Different types of artifacts are usually observed even on the same image, and their co-existence is additional information. Moreover, it is also important to analyze how the visual characteristics of the artifactual information change when varying the imaging parameters. Nowadays, the artifactual information should be considered as a unique complete picture, which a physician must interpret on the basis of his/her anatomical knowledge and clinical experience. Our knowledge of the artifactual information is not yet sufficiently mature to be usefully synthetized by means of a classification procedure. In my opinion, a physician should learn to read the artifactual information with the objective of translating it in physioanatomical information. He/she should not give in to the temptation of shortcuts, such as those offered by questionable algorithms derived from AI.

Question 13:

What is the difference between "comet-tail" and "ring-down" artifacts?

Answer 13:

In my opinion, the only difference is in the name. The two names have been proposed in different papers by different authors [21,22] and derive from analogies with similar phenomena suggested by the visual aspect of the examined artifacts. The comet-tail artifact was described as a reverberation effect, i.e., multiple reflections of an acoustic wave between two opposite internal walls of a strong reflector. The ring-down artifact was described as a resonance effect, i.e., when one or more frequency components (multiples of the fundamental frequency) of a transmitted signal are highlighted by a receiving apparatus.

However, they are two sides of the same coin. In any case, they refer to trapped (absorbed, transmitted, etc.) energy which is subsequently released in the form of a periodic signal. A vertical artifact is generated by an acoustic trap that gradually re-radiates previously trapped energy, independently of its given name (ring-down, comet-tail, B-line, etc.).

4. Conclusions

A comparison between US images obtained on the same patient with different imaging parameters (central frequency, bandwidth, focus, etc.) is needed to make the artifactual information significant. The artifactual information depends on so many factors that it is risky to directly translate the visual inspection of a single US cine-loop into clinical information. A classification of the artifactual information on the basis of its visual characteristics can be misleading since the latter is a relative "measure" and must be analyzed by varying the imaging parameters.

Artifactual information must be evaluated along with other clinical information, such as an interview, physical examination, and laboratory and microbiological test results.

The differentiation of vertical artifacts, the assessment of their sonomorphology, the evaluation of the subpleural area with the employment of a lineal probe, the assessment of coexisting lesions visualized in lung ultrasound images, and the interpretation of the detected lesions in the clinical context are crucial for clinicians in the differential diagnosis of the aetiology of lesions affecting the interstitium of the lungs.

From a clinical standpoint, the analysis of vertical artifacts is very important and requires further clinical studies conducted in cooperation with engineers who specialize in physics. Communication between clinicians and engineers is vital considering the further development of lung ultrasound [23].

Funding: No external funding.

Institutional Review Board Statement: Approval from the local ethics committee (number: NKBBN/474/2018 and NKBBN/473/2018, approval date for both 10 October 2018) and the informed consent of all participants in the study was duly obtained.

Informed Consent Statement: Informed consent was obtained from all subjects involved in the study.

Data Availability Statement: Data sharing not applicable.

Conflicts of Interest: The authors declare no conflict of interest.

References

1. Gargani, L.; Bruni, C.; Romei, C.; Frumento, P.; Moreo, A.; Agoston, G.; Guiducci, S.; Bellando-Randone, S.; Lepri, G.; Belloli, L.; et al. Prognostic Value of Lung Ultrasound B-Lines in Systemic Sclerosis. *Chest* **2020**, *158*, 1515–1525. [CrossRef] [PubMed]
2. Lichtenstein, D.A. Lung ultrasound in the critically ill. *Ann. Intensiv. Care* **2014**, *4*, 1. [CrossRef]
3. Buda, N.; Skoczylas, A.; Demi, M.; Wojteczek, A.; Cylwik, J.; Soldati, G. Clinical Impact of Vertical Artifacts Changing with Frequency in Lung Ultrasound. *Diagnostics* **2021**, *11*, 401. [CrossRef]
4. Scali, M.C.; Zagatina, A.; Ciampi, Q.; Cortigiani, L.; D'Andrea, A.; Daros, C.B.; Zhuravskaya, N.; Kasprzak, J.D.; Wierzbowska-Drabik, K.; Pretto, J.L.D.C.E.S.; et al. Lung Ultrasound and Pulmonary Congestion During Stress Echocardiography. *JACC Cardiovasc. Imaging* **2020**, *13*, 2085–2095. [CrossRef]
5. Baldi, G.; Gargani, L.; Abramo, A.; D'Errico, L.; Caramella, D.; Picano, E.; Giunta, F.; Forfori, F. Lung water assessment by lung ultrasonography in intensive care: A pilot study. *Intensiv. Care Med.* **2012**, *39*, 74–84. [CrossRef] [PubMed]
6. Via, G.; Lichtenstein, D.; Mojoli, F.; Rodi, G.; Neri, L.; Storti, E.; Klersy, C.; Iotti, G.; Braschi, A. Whole lung lavage: A unique model for ultrasound assessment of lung aeration changes. *Intensiv. Care Med.* **2010**, *36*, 999–1007. [CrossRef]
7. Soldati, G.; Demi, M.; Smargiassi, A.; Inchingolo, R.; Demi, L. The role of ultrasound lung artifacts in the diagnosis of respiratory diseases. *Expert Rev. Respir. Med.* **2019**, *13*, 163–172. [CrossRef]
8. Demi, M.; Soldati, G.; Demi, L. On the artefactual information of ultrasound lung images: A lines and B lines. In *Proceedings of Meetings on Acoustics 176ASA*; Acoustical Society of America: Melville, NY, USA, 2018; Volume 35, p. 020003. [CrossRef]
9. Staub, L.J.; Biscaro, R.R.M.; Kaszubowski, E.; Maurici, R. Lung Ultrasound for the Emergency Diagnosis of Pneumonia, Acute Heart Failure, and Exacerbations of Chronic Obstructive Pulmonary Disease/Asthma in Adults: A Systematic Review and Meta-analysis. *J. Emerg. Med.* **2019**, *56*, 53–69. [CrossRef]

10. Perrone, T.; Maggi, A.; Sgarlata, C.; Palumbo, I.; Mossolani, E.; Ferrari, S.; Melloul, A.; Mussinelli, R.; Boldrini, M.; Raimondi, A.; et al. Lung ultrasound in internal medicine: A bedside help to increase accuracy in the diagnosis of dyspnea. *Eur. J. Intern. Med.* **2017**, *46*, 61–65. [CrossRef]
11. Buda, N.; Kosiak, W.; Wełnicki, M.; Skoczylas, A.; Olszewski, R.; Piotrkowski, J.; Skoczyński, S.; Radzikowska, E.; Jassem, E.; Grabczak, E.M.; et al. Recommendations for Lung Ultrasound in Internal Medicine. *Diagnostics* **2020**, *10*, 597. [CrossRef] [PubMed]
12. Mathis, G.; Horn, R.; Morf, S.; Prosch, H.; Rovida, S.; Soldati, G.; Hoffmann, B.; Blaivas, M.; Dietrich, C.F. WFUMB position paper on reverberation artefacts in lung ultrasound: B-lines or comet-tails? *Med. Ultrason.* **2021**, *23*, 70–73. [CrossRef]
13. Buda, N.; Kosiak, W. Is a linear probe helpful in diagnosing diseases of pulmonary interstitial spaces? *J. Ultrason.* **2017**, *17*, 136–141. [CrossRef]
14. Buda, N.; Wojteczek, A.; Masiak, A.; Piskunowicz, M.; Batko, W.; Zdrojewski, Z. Lung Ultrasound in the Screening of Pulmonary Interstitial Involvement Secondary to Systemic Connective Tissue Disease: A Prospective Pilot Study Involving 180 Patients. *J. Clin. Med.* **2021**, *10*, 4114. [CrossRef]
15. Buda, N.; Kosiak, W.; Smoleńska, Z.; Zdrojewski, Z. Transthoracic lung ultrasound in the monitoring of interstitial lung disease: A case of scleroderma. *Pol. Arch. Med. Wewn.* **2013**, *123*, 721–722. [CrossRef]
16. Buda, N.; Masiak, A.; Smolenska, Z.; Gałecka, K.; Porzezinska, M.; Zdrojewski, Z. Serial Lung Ultrasonography to Monitor Patient With Diffuse Alveolar Hemorhage. *Ultrasound Q.* **2017**, *33*, 86–89. [CrossRef]
17. Buda, N.; Cylwik, J.; Mróz, K.; Rudzińska, R.; Dubik, P.; Malczewska, A.; Oraczewska, A.; Skoczyński, S.; Suska, A.; Górecki, T.; et al. Lung Ultrasound Examination in Patients with SARS-CoV-2 Infection: Multicenter Study. *J. Clin. Med.* **2021**, *10*, 3255. [CrossRef]
18. Demi, M. The impact of multiple concurrent factors on the length of the US pulmonary vertical artifacts as illustrated through the experimental and numerical analysis of simple models. *J. Acoust. Soc. Am.* **2021**, *150*, 2106–2115. [CrossRef]
19. Kameda, T.; Kamiyama, N.; Taniguchi, N. Simple Experimental Models for Elucidating the Mechanism Underlying Vertical Artifacts in Lung Ultrasound: Tools for Revisiting B-Lines. *Ultrasound Med. Biol.* **2021**, *47*, 3543–3555. [CrossRef]
20. Demi, M. On the Replica of US Pulmonary Artifacts by Means of Physical Models. *Diagnostics* **2021**, *11*, 1666. [CrossRef]
21. Ziskin, M.C.; Thickman, D.I.; Goldenberg, N.J.; Lapayowker, M.S.; Becker, J.M. The comet tail artifact. *J. Ultrasound Med.* **1982**, *1*, 1–7. [CrossRef]
22. Avruch, L.; Cooperberg, P.L. The ring-down artifact. *J. Ultrasound Med.* **1985**, *4*, 21–28. [CrossRef]
23. Demi, M.; Prediletto, R.; Soldati, G.; Demi, L. Physical Mechanisms Providing Clinical Information from Ultrasound Lung Images: Hypotheses and Early Confirmations. *IEEE Trans. Ultrason. Ferroelectr. Freq. Control* **2019**, *67*, 612–622. [CrossRef]

diagnostics

MDPI

Article

B-Lines Lung Ultrasonography Simulation Using Finite Element Method

Fellipe Allevato Martins da Silva [1,*], Eduardo Moreno [2] and Wagner Coelho de Albuquerque Pereira [1]

[1] Engineering Program-COPPE, Federal University of Rio de Janeiro, Rio de Janeiro 21941-901, Brazil
[2] Departamento Física Aplicada, Instituto de Cibernetica Matematica y Fisica-ICIMAF, Habana 10400, Cuba
* Correspondence: fellipe.allevato@peb.ufrj.br

Abstract: Introduction: Lung Ultrasonography (LUS) is a fast technique for the diagnosis of patients with respiratory syndromes. B-lines are seen in response to signal reverberations and amplifications into sites with peripheral lung fluid concentration or septal thickening. Mathematical models are commonly applied in biomedicine to predict biological responses to specific signal parameters. Objective: This study proposes a Finite-Element numerical model to simulate radio frequency ultrasonic lines propagated from normal and infiltrated lung structures. For tissue medium, a randomized inhomogeneous data method was used. The simulation implemented in COMSOL® used Acoustic Pressure and Time-Explicit models, which are based on the discontinuous Galerkin method (dG). Results: The RF signals, processed in MATLAB®, resulted in images of horizontal A-lines and vertical B-lines, which were reasonably similar to real images. Discussion: The use of inhomogeneous materials in the model was good enough to simulate the scattering response, similar to others in the literature. The model is useful to study the impact of the lung infiltration characteristics on the appearance of LUS images.

Keywords: lung ultrasonography; B-lines; simulation; COMSOL; finite element method

Citation: Silva, F.A.M.; Moreno, E.; Pereira, W.C.A. B-Lines Lung Ultrasonography Simulation Using Finite Element Method. *Diagnostics* **2022**, *12*, 2751. https://doi.org/10.3390/diagnostics12112751

Academic Editors: Marcello Demi and Gino Soldati

Received: 1 October 2022
Accepted: 5 November 2022
Published: 10 November 2022

Publisher's Note: MDPI stays neutral with regard to jurisdictional claims in published maps and institutional affiliations.

1. Introduction

Lung Ultrasonography (LUS) is a fast technique for the diagnosis of patients with respiratory syndromes. It is an exam that allows for the evaluation of disease development and response to treatment [1–3]. Pulmonary illnesses with a slow evolution of worsening symptoms cannot be monitored properly by chest X-rays [4,5]. LUS appears to be a reliable bedside exam with good sensitivity to detect pulmonary congestion, cardiogenic pulmonary edema, pneumonia, interstitial lung syndrome (e.g., systemic sclerosis disease), and consolidation [4,6,7]. In the past, lung ultrasound imaging was thought to be useless as a clinical tool due to the high acoustic impedance mismatch between the air inside the lungs and the chest wall tissues [8,9].

B-mode imaging of the lungs does not reproduce the anatomical structure of the aerated organ, but the image artifact patterns formed in this exam correlate well with specific lung conditions [10]. The acoustic impedance of lungs depends on the air proportion inside of them. For the case of a healthy lung filled with air, this impedance is of the order of 0.17 MRayl [11], producing an impedance mismatch that results in a reflection coefficient around 99% on the interface chest muscle/lung pleura. Therefore, ultrasound does not penetrate a healthy aerated lung and the wave reverberates between the pleural and the transducer faces [9,10]. This physical phenomenon is expressed in the ultrasonography as hyperechoic horizontal lines between two acoustic shadows from the ribs. These artifacts are called A-lines (Figure 1).

In interstitial lung syndrome, pulmonary density can be altered by lung congestive diseases (e.g., lung edema and heart failure) or parenchymal diseases (e.g., pneumonia and systemic sclerosis). LUS changes the A-line patterns to the so-called B-line patterns, which

are well-defined vertical hyperechoic lines, and laser beam-like lines that emerge at the pleural level, erasing the A-lines [3,12–14]. They are directly correlated to the level of liquid in the lung parenchyma [1,2,15]. The presence of B-lines on the LUS has been correlated with disease severity by several score protocols, including scores for the identification and classification of COVID-19 [6,7,16–19].

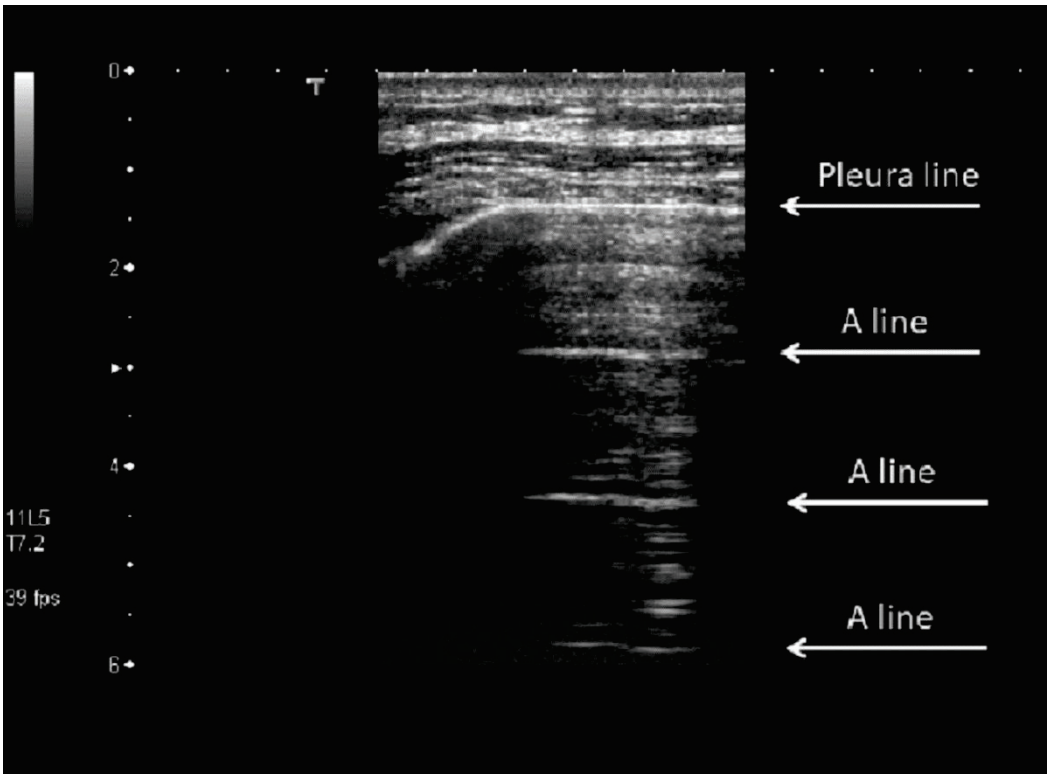

Figure 1. A-lines in a healthy lung. The top image presents a thoracic wall layer (skin, fat and muscles) that ends with the hyperechoic pleural line. Hyperechoic horizontal lines called A-lines, produced by the wave reverberations, are shown beneath. Reprinted/adapted with permission from [10]. 2022, Acoustical Society of America.

The physical explanation of the B-lines' origin has been the aim of some studies [9,10,20]. The main theory is that B-lines are the consequences of signal reverberation and amplification into the peripheral extravascular concentration of lung fluids, or parenchyma septal thickening. Those places become propagation sites that allow for the penetration of the ultrasonic wave in small marginal parts of the lung tissue (Figure 2) [9,10,21].

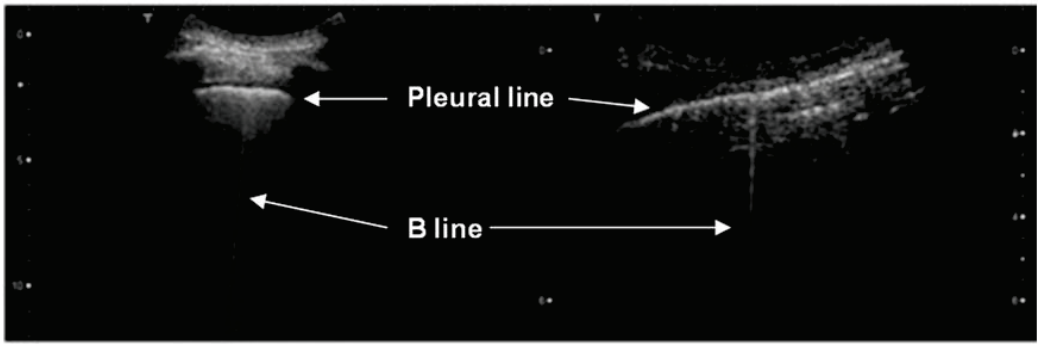

Figure 2. Three examples of B-lines. B-lines are vertical hyperechoic, well-defined and laser beam-like lines that emerge at the pleural level, erasing the A-lines, and move in synchrony with the respiratory cycle. Reprinted/adapted with permission from [10]. 2022, Acoustical Society of America.

Understanding physical phenomena using mathematical models is a commonly applied method in biomedical engineering and similar areas. Ultrasound numerical simulations may be used to infer and predict biological responses to specific signal parameters, and was employed in various studies describing LUS A-line and B-line origins [20,21]. K-wave has been the first-choice software toolbox in LUS simulations to solve the wave equation due to the MATLAB®'s familiarity in the research environment [21,22]. However, the commercial software COMSOL® had more complete tools of the Finite Element Method (FEM). Version 5.5 has specific physics tools, known as acoustic time-explicit methods, that allow for pulse propagations to be simulated in a domain with an acoustic array source. These are based on the discontinuous Galerkin method (dG) [23].

The aim of this study was to develop a mathematical model using the Finite Elements Method (FEM) to simulate RF ultrasonic lines propagated from normal and infiltrated lung structures, to emulate LUS image samples with COMSOL® software and MATLAB® signal processing. The numerical study focuses on the physical factors that originate A-lines and B-lines.

2. Materials and Methods

2.1. Ultrasound Propagation Simulation Techniques

The first step in FEM simulation was the definition of the structural domain. Figure 3 shows a scheme that represents the ultrasonic array probe over a muscle layer that covers the lung domain. A small ellipsoid grey zone just below the muscle layer represents one part of the lung tissue infiltrated by liquid, named Lung Disease Zone (LDZ).

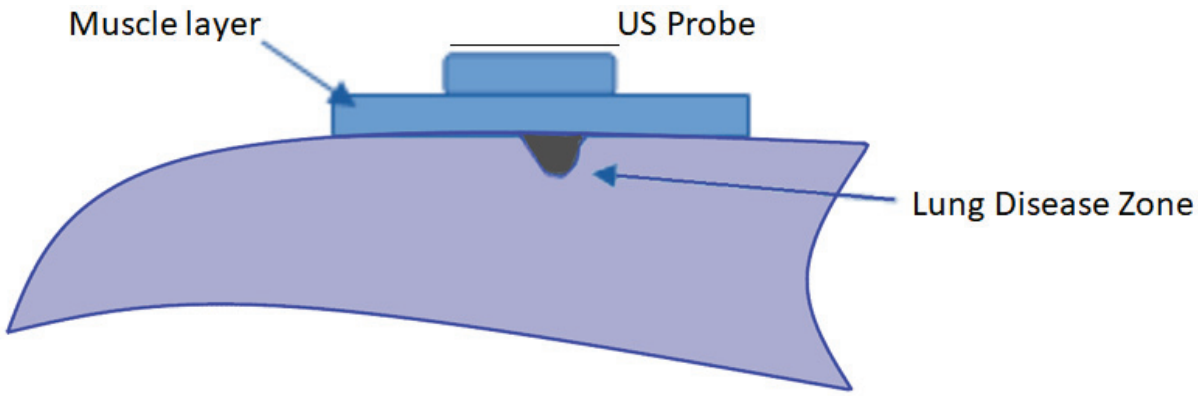

Figure 3. Lung Model Domain. There is a small ellipsoid grey zone of the lung tissue represented as the "lung disease zone" (LDZ).

2.2. COMSOL® Models

COMSOL® version 5.5 was used with Acoustic Pressure and Time-Explicit models. These tools used the dG algorithm for the simulation of ultrasonic pulse propagation. This method, compared to the classic acoustic methods, has the advantage of having less degrees of freedom, leading to a shorter processing time. In this paper, a rectangular base of 66 mm in length and 51 mm in height was used.

In Figure 3, the lung healthy zone assumes the condition of 100% of air, and its acoustic impedance, as mentioned before, is so low (0.17 Mrayl) [6] that only the tissues in the blue zones were taken into consideration in the final COMSOL® domain. Figure 4 shows the domain used for simulation in reversed position (upside down) with respect to Figure 3. In this case, the muscle domain, in a rectangle form, has two perfect matching layer (PML) zones at each lateral side. An ultrasonic linear array with 32 elements (black dots) is shown below. A piece of lung with inhomogeneity is shown at the top and all the area above is lung with 100% air.

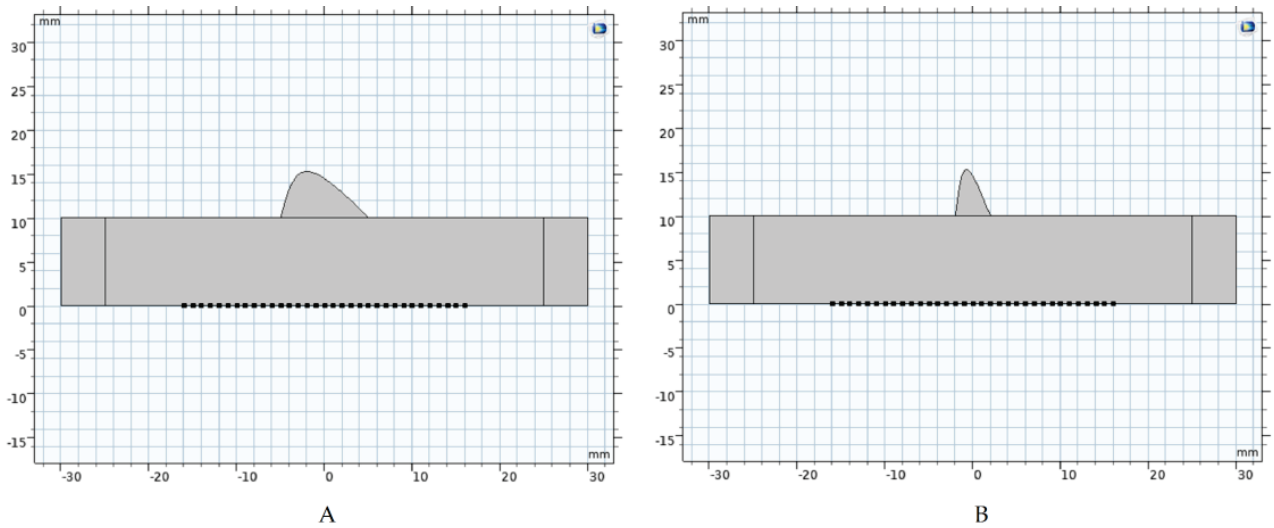

Figure 4. Two COMSOL® domains with 32 array elements (back dots). Domain (**A**) and Domain (**B**). The rectangular area represents the muscle with PML at both left and right sides. The subdomain (in grey) over the rectangle represents the small lung part with inhomogeneity or "Lung disease zone" (LDZ).

The boundary condition in these domains is as follows: 5 mm length and 10 height PML at both sides in the rectangle zone of 50 mm length and 10 mm height. The LDZ was placed in the upper part of the rectangular zone, as an ellipsoid of 5 mm height and two conditions of length: 10 mm (Domain A) and 4 mm (Domain B). A normal sweep velocity with delays is considered for each array element. The array is organized with apertures of five elements, which includes focalization laws at 10 mm in terms of emission. With a sweep step of each five-element group at a time, it is possible to obtain 28 radio frequency (RF) ultrasonic lines.

The superior boundary condition, including the upper part of LDZ, was of Pressure type. Then, it simulates a virtual healthy lung. The other boundaries were "Sound Hard Boundary". Mesh elements were designed according to the recommendations of maximum size of $\lambda/1.5$ [24].

The initial ultrasonic pulse applied to each element with a central frequency of $f_0 = 2$ MHz is shown in Figure 5. The time-domain study was used with a maximum of 50 μs and a step of 0.02 μs. A parametric sweep was necessary to simulate the array emission through 28 steps, where only five elements are allowed for emission each time. The normal sweep velocity mentioned above was made according to the Equation (1):

$$V(i) = A(i) * \text{pulse}(t + B(i)), \text{ for } i = 1 \text{ to } 32, \quad (1)$$

where A(i) = 0 (OFF) or 1 (ON), according to the sweep parameter and the emission organization (five elements ON and the rest OFF). B(i) for each element is the delay at each sweep necessary for focalization in transmission at approximately 10 mm. The function *pulse*, shown in Figure 5, is given by a sinus function with $2\pi f_0 t$ argument modulated by Gaussian envelope.

A workstation with 128 GB RAM, 10 TB HDD, and a microprocessor with 40 cores (Intel® Xeon(R) Gold 6230 CPU @ 2.10 GHz × 40) was used. The time performance was around 5 h depending on the material models at 2-MHz ultrasonic frequency.

Average Nonlocal Coupling was defined for each element to obtain the signals (echoes) at each array element. Then, 28 × 32 = 896 RF signals were obtained (each of them with 2500 samples) and exported to a MATLAB® (MathWorks Inc., Massachusetts, EUA) routine [25] where a visualization program displays B-scan images. The images were built using plot algorithms, with a logarithm amplifier applied to each ultrasonic RF signal first, and then a Hilbert transform was used to obtain the signal envelope, which is

necessary for composing each imaging line. Each line was made from the RF signal that was produced by the 5-element pulse-echo excitation subgroup, and delay focusing was applied at each receiving signal. An interpolation algorithm was employed to increase the lateral imaging size.

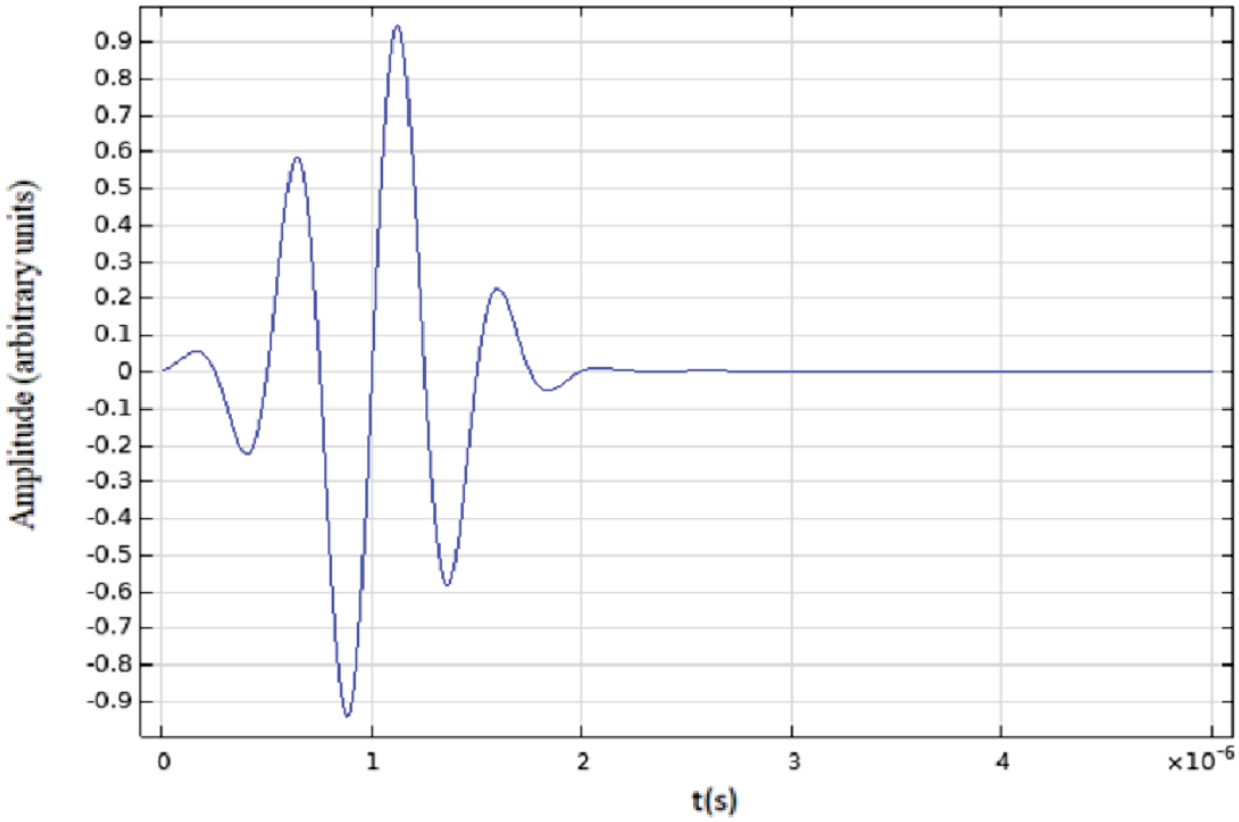

Figure 5. Initial emitted ultrasonic pulse. Sinus function with $2\pi f_0 t$ argument modulated by Gaussian envelope Central and frequency f_0 = 2 MHz.

2.3. COMSOL® Strategy

For tissue medium, a randomized inhomogeneous data method was used according to Sjodin (2017) [26]. This method assumes that each tissue has a random variation in density and ultrasound velocity. The variation could be modeled by a spatial frequency using a cosine transform [26]. This transform has random phase and amplitude functions with parameters that could be adjusted for each material. To achieve that, a random function f(x,y) with the Results Node functions, in a previous short model of COMSOL® 5.5, was obtained. This was then exported using Data Grid for our Lung COMSOL® model, as an interpolation function to use in the Material Node. Figure 6 shows the case for the lung tissue infiltrated subdomain, where f(x,y) oscillates between ± 1 for both velocity and density.

For this domain, the strategy is to define the maximal and minimal values of ultrasonic velocity and density. The maximal value of velocity is 1500 $m \cdot s^{-1}$ and, for density, 1000 $kg \cdot m^{-3}$, which means the lung is modeled as pure water. The minimal values are: vmin = 640 $m \cdot s^{-1}$ and dmin = 430 $kg \cdot m^{-3}$, which corresponds to a lung with 60% of air [11,27]. With these maximal and minimal values, the following equations are obtained for the Material Lung Node for the subdomain of Figure 6:

$$v(x,y) = 1070\ m \cdot s^{-1} + 430 * f(x,y)\ m \cdot s^{-1} \quad (2)$$

$$d(x,y) = 715\ kg \cdot m^{-3} + 285 * f(x,y)\ kg \cdot m^{-3} \quad (3)$$

These equations ensure the interval for velocity and density, as discussed above. This idea could be extended to other intervals.

For the muscle layer, a similar approach was used, with a distribution function g(x,y) obtained as in the previous case, which oscillates between ±1 for both velocity and density. Parameter G defines the variations with values of 0, 5 and 10, for density and velocity, respectively. Figure 7 shows the domain visualization of this function. The distribution is non-symmetric with respect to x–y axes. The idea is to reproduce the muscle fiber structure. Equations (4) and (5) establish the variations in velocity and density for the muscle.

$$v_{muscle}\,(x,y) = 1570\ m{\cdot}s^{-1} + G * g(x,y)\ m{\cdot}s^{-1} \quad (4)$$

$$d_{muscle}\,(x,y) = 1090\ kg{\cdot}m^{-3} + G * g(x,y)\ kg{\cdot}m^{-3} \quad (5)$$

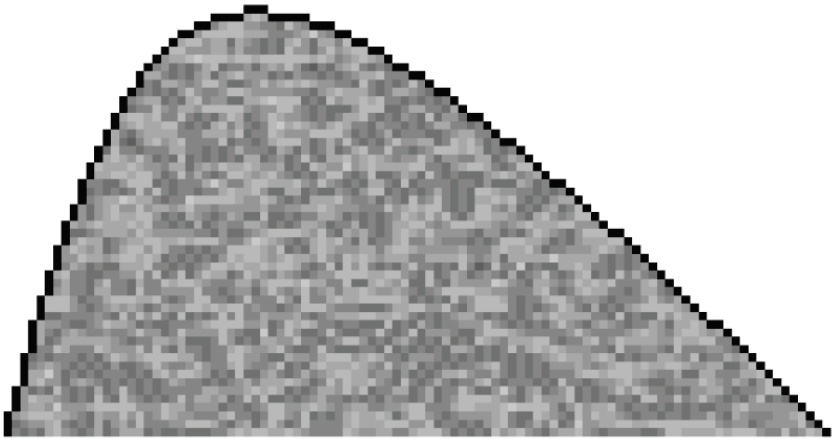

Figure 6. Subdomain distribution function f(x,y) for "lung disease zone" (LDZ). The grey scale indicates the spatial variation in the infiltrated properties of the lung tissue.

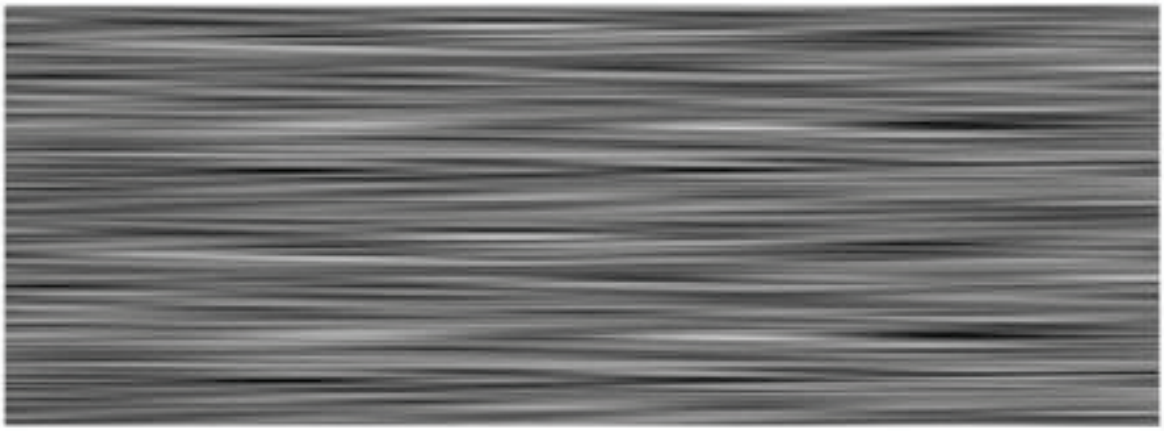

Figure 7. Graphic of the muscle function g(x,y) used on the simulation model. Gray scale indicates the properties of spatial variation for the simulation of muscle fibers.

3. Results

Figure 8 shows one example of a superimposed RF signal obtained from case A of Figure 4. The initial pulse and three well defined echoes from the far boundary of the muscle can be observed. The random echoes between correspond to the multiple scatterings in the subdomain of the lung disease zone (LDZ).

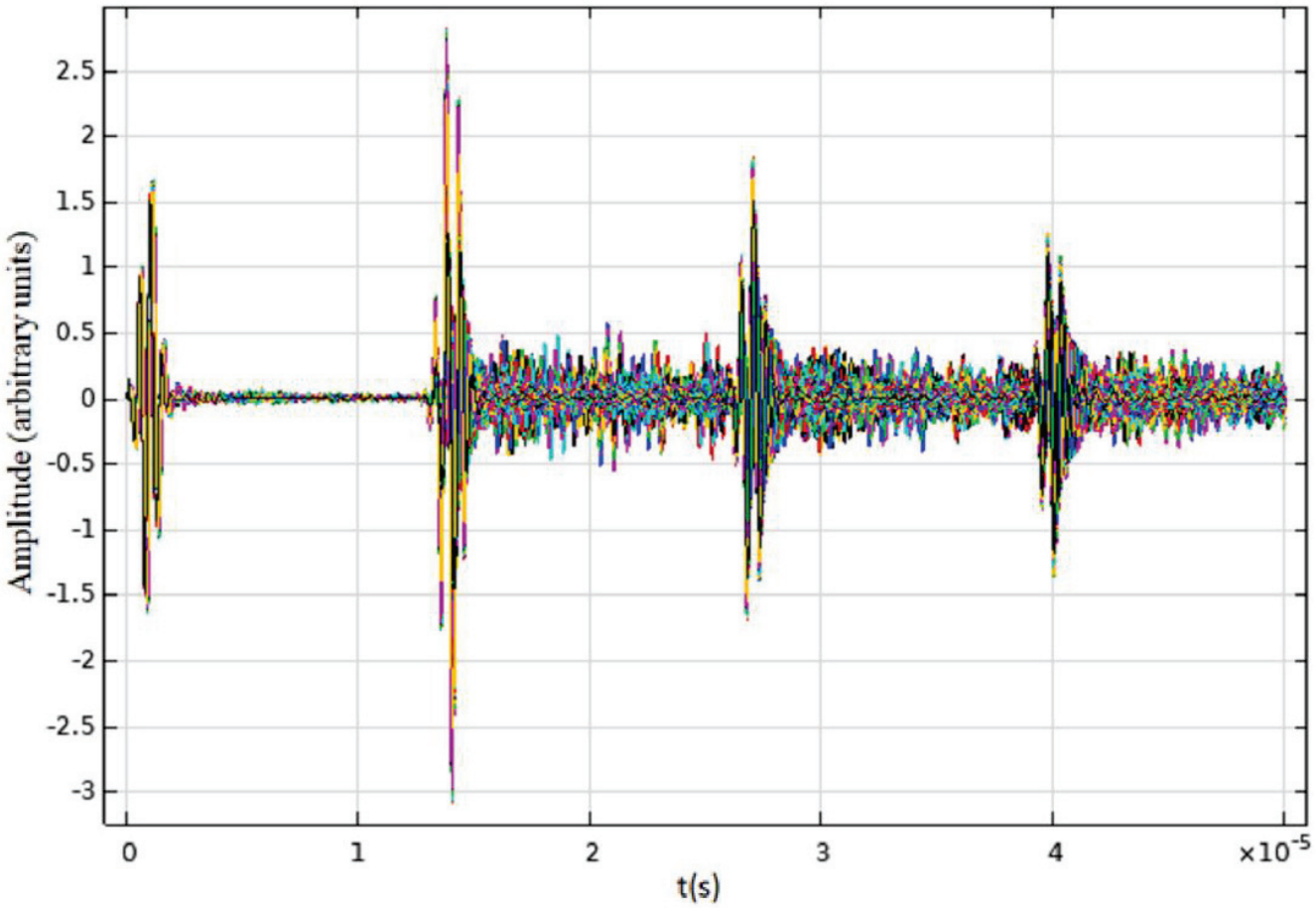

Figure 8. RF signals obtained from COMSOL® corresponding to the domain expressed in Figure 4. The first signal is the emitted pulse, and the others are received echoes.

The following figure, Figure 9A–F, shows the results of the B-Scan imaging obtained in a MATLAB® routine from the RF COMSOL® signals. Subfigures represent three values of the factor of inhomogeneity G (Equations (4) and (5)) for both domains, according to Figure 4.

The horizontal lines for each image correspond to the initial pulse followed by the echoes (top to bottom). The first echo represents the pleural line, while the second and the others are the named A-lines. These lines correspond to repetitions (reverberations) of the first echo between pleura and transducer, as it is possible to observe the muscle fiber image though several micro-horizontal lines.

Vertical patterns also appeared in every simulation, similar to B-lines. Even though these vertical lines do not make A-lines disappear, they are well defined hyperechoic vertical images rising from the pleural line until the image bottom, as in the clinical LUS exam. It is also possible to observe that the LDZ length is directly correlated with the B-line simulation length.

The numerical experiment was also repeated at a frequency of 4 MHz, and with a domain even narrower (1 mm length and 5 mm height). Figure 10 shows the domain and the results with a B-line narrower than the ones obtained previously. This result is more adapted to real medical imaging although it takes about two days to run in our PC computer.

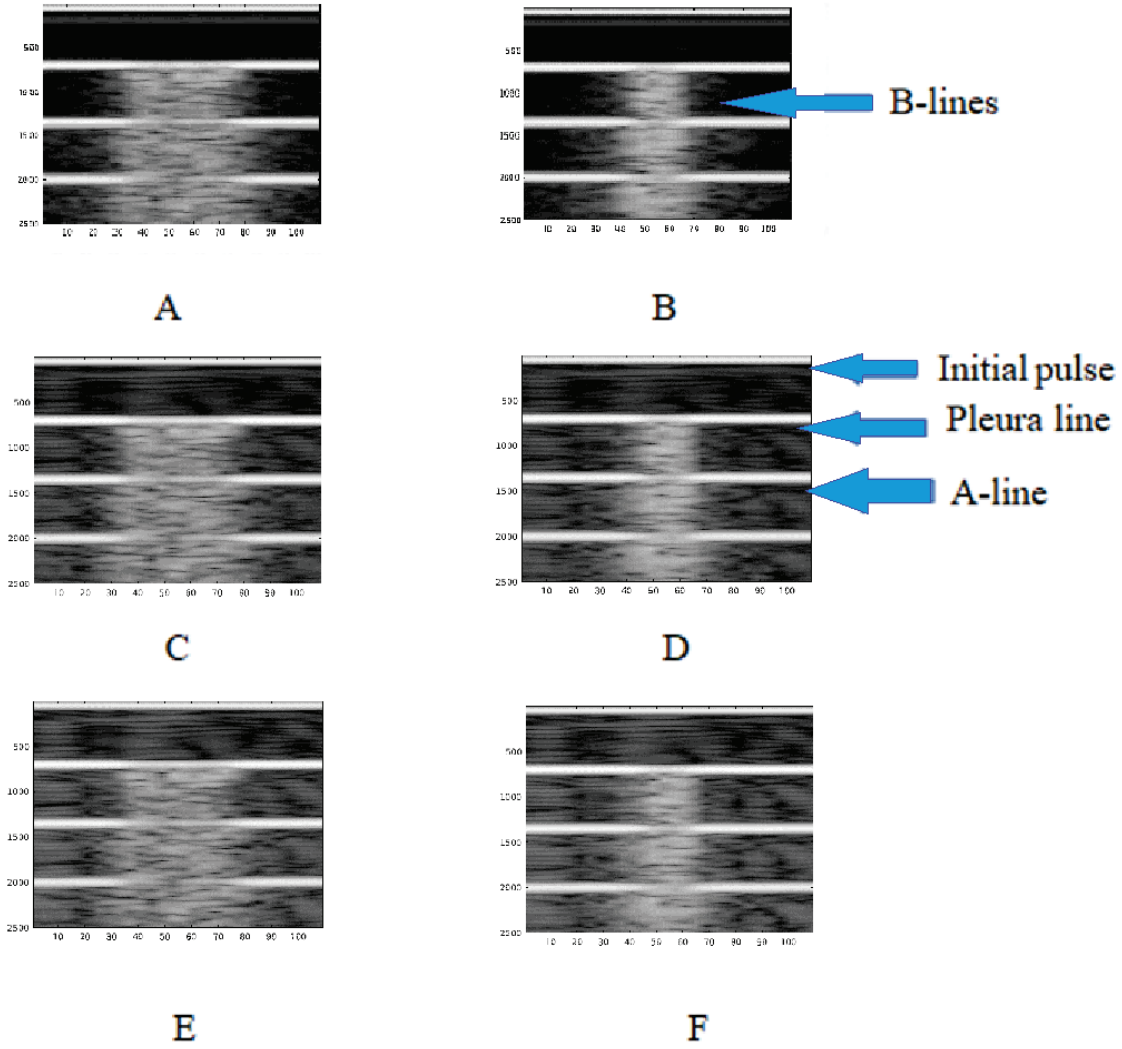

Figure 9. Imaging obtained at different G level and domains. For (**A**) and (**B**), G = 0; (**C**) and (**D**), G = 5; (**E**) and (**F**), G = 10. The left column corresponds to domain A, in Figure 4. The right column corresponds to Domain B in the same figure. The A-lines (horizontal) vs. B-lines (vertical) are shown in B and D, as examples.

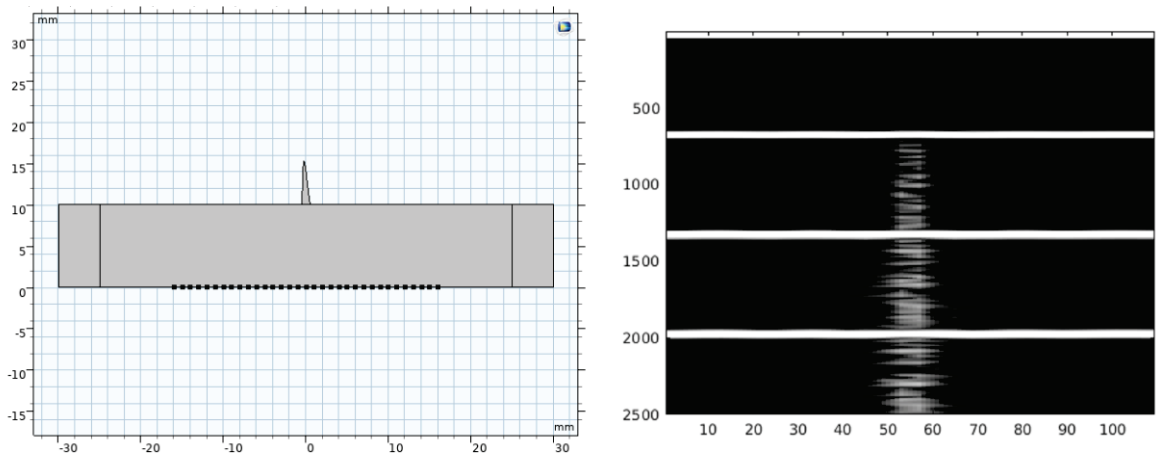

Figure 10. B-Scan imaging obtained at 4 MHz frequency in a new domain with a 1 mm length. Left, it is the simulation domain, and right the image result.

4. Discussion

Lung Ultrasonography has become a central focus of study in the literature since it was shown to be a revolutionary way to diagnose and evaluate different types of lung diseases [15,28]. LUS is a fast, precise, real-time and inexpensive exam that allows for health workers to make better choices regarding patient treatment, with the ability to produce high-sensitivity results to detect pulmonary density changes in interstitial syndrome [2,3,12,14,16,29]. While the formation process of A-lines (horizontal image patterns) is well established, the origin of B-lines (vertical laser-like patterns) still need to be better understood. New numerical studies, with more complete lung models, are important to obtain a better understanding of this topic [3,10,21,30].

The origin and explanations of B-lines has been the subject of several studies. Avruch and Cooperberg (1985) [31] were one of the first to describe what was called a "Ring-Down" artifact, a common ultrasound artifact of either a solid streak or parallel bands, associated with gas collection in the intestinal image exam. It is also theorized for lung image artifacts that fluid collection formed by two layers of bubble tetrahedron would guaranty an oscillator site, which amplifies the RF signal and sends it back to the transducer [32]. Demi et al. (2018) [10] deal with a theoretical model based on signal processing and an experimental model of a phantom made by air rods (as bubble drops) inside and agar-agar matrix. Using B-scan instruments, the authors obtained images that simulate the B-lines.

Peschiera et al. (2021) [21] performed numerical simulations using k-wave MATLAB® toolbox to achieve B-lines simulation. The phantom model involved muscle areas, air areas, and aisle areas with muscle and air circle-like areas. B-line images were generated with satisfactory aspects and were analyzed with intensity parameters features. Low frequencies enabled the formation of B-lines in only the largest interalveolar spacing simulation setting. Then, it is assumed that the lower the frequency at which B-lines appear, the larger the channels formed between alveoli, and more severe the lung condition.

Silva et al. (2022) [22] simulated five configurations of LUS phantom using the k-wave MATLAB® toolbox [33]. Phantom simulations were designed with multiple muscle tissue feature circles lined up above multiple circles with air features, representing muscle fibers and pulmonary alveoli, respectively. Circles with water features were placed over the alveoli in five different configurations, and formed B-line images in all designed phantoms. The arrangement with two close water circles was the one with the clearest laser-like B-line.

Formally, COMSOL® uses a library of material properties that cover several human tissues, such as muscle, fat etc. However, all these models assume homogenous media. To simulate a B-line, it is necessary for part of the domain inside the lung to be represented with multiple scatters. This is a very difficult task using the geometry structure of COMSOL®, because it implies several boundary conditions with their own meshes (grids).

One possible solution is inhomogeneous material models, as described by Sjodin (2017) [26] for thermal properties. The idea is to use random functions as the coefficients and phase of a cosine transform. Inhomogeneous material models with FEM-dG methods describe basic ultrasound-imaging artifacts in lung diseases, with similar results to other numerical studies [21,22], presenting satisfactory image resolution even when a lower central frequency was employed.

The simulation results of the present study show clear B-lines, as a consequence of LDZ inhomogeneity. The results achieved in this mathematical model were very similar to those of Kameda et al. (2019) [34], who simulated in vitro B-lines with B-mode image acquisition at different RF frequencies (6, 8, 11, and 13 MHz) of a lung phantom made of a spindle-shaped juice sac and glucomannan gel. The inhomogeneity models do not need special geometry components for the COMSOL® models; no complex situation is generated with several boundary conditions, and there is no need for independent meshes. The inhomogeneity material avoids these situations and provides a good modeling and understanding of the multiple scattering in this zone. It has been proposed that this zone acts as a trap for the ultrasonic RF, which reverberates and allows for the LDZ to become a secondary RF source [32].

B-lines are then directly correlated with alterations in the lung zone close to the pleura, as water-like fluids and/or lung parenchyma consolidation [10,21,30]. These results are similar to the ones in the literature, indicating that irregular lung surface may generate B-line patterns [6,8,9,15,16,22,29]. The comprehension of the physical phenomena that generate these artifacts is crucial to categorize the different types of B-lines, and to correlate them with both specific diseases and different stages of diseases [35]. The artifacts' signal characterization is also crucial to developing quantitative algorithms dedicated to LUS diagnosis and monitoring [3].

The computational processing speed of the LUS simulations was a limitation of this study, as it proved difficult to use central probe frequencies that are commonly employed in clinical exams (e.g., 4 to 7 MHz). Simulation with other frequencies would allow for a better understanding of its correlation with the formation of B-lines. Another limitation is the simplicity of the lung model. Other conditions, such as parenchyma hepatization and calcifications, have yet to be included.

In our work, B-lines were produced by the inhomogeneity of the LDZ (Figures 9 and 10). The use of inhomogeneous materials based on random components in the model was good enough to simulate the scattering response of the tissue. The dG acoustic model is also one good solution to the simulation of ultrasonic pulse propagation for this kind of scenario. Simulation with narrow LDZ gave a more accurate image result, which was closer to the clinical ones.

5. Conclusions

A mathematical FEM model using randomized inhomogeneous materials was proposed and developed to simulate an LUS image sample and to evaluate the physical origins of A-line and B-line artifacts. The main mechanism theory of B-line formation is assigned to the reverberation of ultrasonic waves in a layer of lung tissue below the pleura with liquids close to the interfaces that cover the lung. The transversal dimension and structure of these B-lines depends on the structure of the LDZ. In any case, the developed model could be used for multiple LDZ zones and other geometrical considerations. It is also possible to obtain results with different ultrasonic array parameters, such as frequency and dimensions, as well as other possible lung conditions that may generate B-lines; thus, this work does not intend to exhaust this subject.

Author Contributions: Software, E.M.; Writing—original draft, F.A.M.d.S.; Writing—review & editing, W.C.d.A.P. All authors have read and agreed to the published version of the manuscript.

Funding: To the Brazilian agencies CNPq, CAPES and FAPERJ and also to the CYTED agency (Project (Ditrecod) for the financial support.

Institutional Review Board Statement: Not applicable.

Informed Consent Statement: Not applicable.

Conflicts of Interest: The authors declare no conflict of interest.

References

1. Lichtenstein, D.A. Lung ultrasound in the critically ill. *Ann. Intensive Care* **2014**, *4*, 1. [CrossRef] [PubMed]
2. Gargani, L. Lung ultrasound: A new tool for the cardiologist. *Cardiovasc. Ultrasound* **2011**, *9*, 6. [CrossRef] [PubMed]
3. Demi, L.; Wolfram, F.; Klersy, C.; De Silvestri, A.; Ferretti, V.V.; Muller, M.; Miller, D.; Feletti, F.; Wełnicki, M.; Buda, N.; et al. New International Guidelines and Consensus on the Use of Lung Ultrasound. *J. Ultrasound Med.* **2022**. [CrossRef] [PubMed]
4. Stassen, J.; Bax, J.J. How to do lung ultrasound. *Eur. Heart J. Cardiovasc. Imaging* **2022**, *23*, 447–449. [CrossRef] [PubMed]
5. Mohamed, M.F.H. The Utility of Ultrasound Extends Beyond Interstitial Pneumonia Assessment in COVID-19 Patients. *Acad. Radiol.* **2020**, *27*, 1332–1333. [CrossRef] [PubMed]
6. Zhao, L.; Yu, K.; Zhao, Q.; Tian, R.; Xie, H.; Xie, L.; Deng, P.; Xie, G.; Bao, A.; Du, J. Lung Ultrasound Score in Evaluating the Severity of Coronavirus Disease 2019 (COVID-19) Pneumonia. *Ultrasound Med. Biol.* **2020**, *46*, 2938–2944. [CrossRef]
7. Soldati, G.; Smargiassi, A.; Inchingolo, R.; Buonsenso, D.; Perrone, T.; Briganti, D.F.; Perlini, S.; Torri, E.; Mariani, A.; Mossolani, E.E.; et al. Proposal for International Standardization of the Use of Lung Ultrasound for Patients with COVID-19: A Simple, Quantitative, Reproducible Method. *J. Ultrasound Med.* **2020**, *39*, 1413–1419. [CrossRef]

8. Volpicelli, G. Lung Sonography. *J. Ultrasound Med.* **2013**, *32*, 165–171. [CrossRef]
9. Soldati, G.; Copetti, R.; Sher, S. Sonographic Interstitial Syndrome: The Sound of Lung Water. *J. Ultrasound Med.* **2009**, *28*, 163–174. [CrossRef]
10. Demi, M.; Soldati, G.; Demi, L. On the artefactual information of ultrasound lung images: A lines and B lines. In Proceedings of the 176th Meeting of Acoustical Society of America 2018 Acoustics Week in Canada, Victoria, BC, Canada, 5–9 November 2018; p. 020003.
11. Oelze, M.L.; Miller, R.J.; Blue, J.P.; Zachary, J.F.; O'Brien, W.D. Estimation of the acoustic impedance of lung versus level of inflation for different species and ages of animals. *J. Acoust. Soc. Am.* **2008**, *124*, 2340–2352. [CrossRef]
12. Buda, N.; Andruszkiewicz, P.; Czuczwar, M.; Gola, W.; Kosiak, W.; Nowakowski, P.; Sporysz, K. Consensus of the Study Group for Point-of-Care Lung Ultrasound in the intensive care management of COVID-19 patients. *Anaesthesiol. Intensive Ther.* **2020**, *52*, 83–90. [CrossRef] [PubMed]
13. Pelosi, P.; Tonelli, R.; Torregiani, C.; Baratella, E.; Confalonieri, M.; Battaglini, D.; Marchioni, A.; Confalonieri, P.; Clini, E.; Salton, F.; et al. Different Methods to Improve the Monitoring of Noninvasive Respiratory Support of Patients with Severe Pneumonia/ARDS Due to COVID-19: An Update. *JCM* **2022**, *11*, 1704. [CrossRef] [PubMed]
14. Ruaro, B.; Baratella, E.; Confalonieri, P.; Confalonieri, M.; Vassallo, F.G.; Wade, B.; Geri, P.; Pozzan, R.; Caforio, G.; Marrocchio, C.; et al. High-Resolution Computed Tomography and Lung Ultrasound in Patients with Systemic Sclerosis: Which One to Choose? *Diagnostics* **2021**, *11*, 2293. [CrossRef] [PubMed]
15. Volpicelli, G.; Elbarbary, M.; Blaivas, M.; Lichtenstein, D.A.; Mathis, G.; Kirkpatrick, A.W.; Melniker, L.; Gargani, L.; Noble, V.E.; Via, G.; et al. International evidence-based recommendations for point-of-care lung ultrasound. *Intensive Care Med.* **2012**, *38*, 577–591. [CrossRef]
16. Bouhemad, B.; Mongodi, S.; Via, G.; Rouquette, I. Ultrasound for "Lung Monitoring" of Ventilated Patients. *Anesthesiology* **2015**, *122*, 437–447. [CrossRef]
17. Dargent, A.; Chatelain, E.; Kreitmann, L.; Quenot, J.-P.; Cour, M.; Argaud, L. The COVID-LUS study group Lung ultrasound score to monitor COVID-19 pneumonia progression in patients with ARDS. *PLoS ONE* **2020**, *15*, e0236312. [CrossRef]
18. Volpicelli, G.; Gargani, L.; Perlini, S.; Spinelli, S.; Barbieri, G.; Lanotte, A.; Casasola, G.G.; Nogué-Bou, R.; Lamorte, A.; Agricola, E.; et al. Lung ultrasound for the early diagnosis of COVID-19 pneumonia: An international multicenter study. *Intensive Care Med.* **2021**, *47*, 444–454. [CrossRef]
19. Lugarà, M.; Tamburrini, S.; Coppola, M.G.; Oliva, G.; Fiorini, V.; Catalano, M.; Carbone, R.; Saturnino, P.P.; Rosano, N.; Pesce, A.; et al. The Role of Lung Ultrasound in SARS-CoV-19 Pneumonia Management. *Diagnostics* **2022**, *12*, 1856. [CrossRef]
20. Demi, M.; Prediletto, R.; Soldati, G.; Demi, L. Physical Mechanisms Providing Clinical Information From Ultrasound Lung Images: Hypotheses and Early Confirmations. *IEEE Trans. Ultrason. Ferroelectr. Freq. Control* **2020**, *67*, 612–623. [CrossRef]
21. Peschiera, E.; Mento, F.; Demi, L. Numerical study on lung ultrasound B-line formation as a function of imaging frequency and alveolar geometriesa. *J. Acoust. Soc. Am.* **2021**, *149*, 2304. [CrossRef]
22. Silva, F.A.M.; Pastrana-Chalco, M.; Teixeira, C.A.; Pereira, W.C.A. Simulation of Lung Ultrasonography Phantom for Acquisition of A-lines and B-lines Artifacts. In *XXVII Brazilian Congress on Biomedical Engineering*; Bastos-Filho, T.F., de Oliveira Caldeira, E.M., Frizera-Neto, A., Eds.; IFMBE Proceedings; Springer International Publishing: Cham, Switzerland, 2022; Volume 83, pp. 2045–2050, ISBN 978-3-030-70600-5.
23. COMSOL Multiphysics®Reference Manual v. 6.1. Available online: http://www.comsol.com (accessed on 30 September 2022).
24. Simulation Software for Analyzing Acoustics and Vibrations. Available online: https://www.comsol.com/acoustics-module (accessed on 30 September 2022).
25. MATLAB Documentation. Available online: https://www.mathworks.com/help/matlab/ (accessed on 30 September 2022).
26. Sjodin, B. How to Generate Randomized Inhomogeneous Material Data | COMSOL Blog. Available online: https://www.comsol.com/blogs/how-to-generate-randomized-inhomogeneous-material-data/ (accessed on 30 September 2022).
27. Dunn, F. Attenuation and speed of ultrasound in lung. *J. Acoust. Soc. Am.* **1986**, *80*, 1248–1250. [CrossRef] [PubMed]
28. Hussain, A.; Via, G.; Melniker, L.; Goffi, A.; Tavazzi, G.; Neri, L.; Villen, T.; Hoppmann, R.; Mojoli, F.; Noble, V.; et al. Multi-organ point-of-care ultrasound for COVID-19 (PoCUS4COVID): International expert consensus. *Crit. Care* **2020**, *24*, 702. [CrossRef] [PubMed]
29. Buonsenso, D.; Piano, A.; Raffaelli, F.; Bonadia, N.; Donati, K.D.G.; Franceschi, F. Point-of-Care Lung Ultrasound findings in novel coronavirus disease-19 pnemoniae: A case report and potential applications during COVID-19 outbreak. *Eur. Rev. Med. Pharmacol. Sci.* **2020**, *24*, 2776–2780. [PubMed]
30. Mento, F.; Demi, L. On the influence of imaging parameters on lung ultrasound B-line artifacts, in vitro study. *J. Acoust. Soc. Am.* **2020**, *148*, 975–983. [CrossRef]
31. Avruch, L.; Cooperberg, P.L. The ring-down artifact. *J. Ultrasound Med.* **1985**, *4*, 21–28. [CrossRef]
32. Louvet, A.; Bourgeois, J.-M. Lung ring-down artifact as a sign of pulmonary alveolar-interstitial disease. *Vet. Radiol. Ultrasound* **2008**, *49*, 374–377. [CrossRef]
33. Treeby, B.E.; Cox, B.T. k-Wave: MATLAB toolbox for the simulation and reconstruction of photoacoustic wave fields. *J. Biomed. Opt.* **2010**, *15*, 021314. [CrossRef]

34. Kameda, T.; Kamiyama, N.; Kobayashi, H.; Kanayama, Y.; Taniguchi, N. Ultrasonic B-Line–Like Artifacts Generated with Simple Experimental Models Provide Clues to Solve Key Issues in B-Lines. *Ultrasound Med. Biol.* **2019**, *45*, 1617–1626. [CrossRef]
35. Soldati, G.; Smargiassi, A.; Demi, L.; Inchingolo, R. Artifactual Lung Ultrasonography: It Is a Matter of Traps, Order, and Disorder. *Appl. Sci.* **2020**, *10*, 1570. [CrossRef]

diagnostics

MDPI

Article

Lung Ultrasound Artifacts Interpreted as Pathology Footprints

Marcello Demi [1], Gino Soldati [2] and Alessandro Ramalli [3,*]

[1] Department of Bioengineering, Fondazione Toscana Gabriele Monasterio, 56126 Pisa, Italy
[2] Ippocrate Medical Center, 55032 Lucca, Italy
[3] Department of Information Engineering, University of Florence, 50139 Florence, Italy
* Correspondence: alessandro.ramalli@unifi.it

Abstract: Background: The original observation that lung ultrasound provides information regarding the physical state of the organ, rather than the anatomical details related to the disease, has reinforced the idea that the observed acoustic signs represent artifacts. However, the definition of artifact does not appear adequate since pulmonary ultrasound signs have shown valuable diagnostic accuracy, which has been usefully exploited by physicians in numerous pathologies. Method: A specific method has been used over the years to analyze lung ultrasound data and to convert artefactual information into anatomical information. Results: A physical explanation of the genesis of the acoustic signs is provided, and the relationship between their visual characteristics and the surface histopathology of the lung is illustrated. Two important sources of potential signal alteration are also highlighted. Conclusions: The acoustic signs are generated by acoustic traps that progressively release previously trapped energy. Consequently, the acoustic signs highlight the presence of acoustic traps and quantitatively describe their distribution on the lung surface; they are not artifacts, but pathology footprints and anatomical information. Moreover, the impact of the dynamic focusing algorithms and the impact of different probes on the visual aspect of the acoustic signs should not be neglected.

Keywords: lung ultrasound; b-lines; vertical artifacts; pulmonary artifacts; physical models

Citation: Demi, M.; Soldati, G.; Ramalli, A. Lung Ultrasound Artifacts Interpreted as Pathology Footprints. *Diagnostics* **2023**, *13*, 1139. https://doi.org/10.3390/diagnostics13061139

Academic Editor: Costin Teodor Streba

Received: 16 February 2023
Revised: 9 March 2023
Accepted: 13 March 2023
Published: 16 March 2023

1. Introduction

More than thirty years ago, Lichtenstein and colleagues described lung ultrasound (US) signs of interstitial lung disease in terms of artifacts [1]. Since then, terms such as A-lines and B-lines have been consistently present in the literature related to the US exploration of the lung. A-lines and B-lines are usually associated with normality and with a sign of interstitial pathology, respectively [2–6]. Over the years, this pathology has included extravascular water of the lung, diffuse interstitial diseases of the lung, contusions and bleeding, and inflammatory states [7], that is, anything that alters the relationship between air and lung tissue without consolidating the organ [8]. The original observation that the US exploration of the still aerated lung informs us about the physical state of the organ rather than the morphological (anatomical) details related to the disease has reinforced the idea that the B-lines represented US artifacts [9]. Obviously, the B-lines do not represent any anatomical part of a pathological lung as, similarly, the A-lines do not represent the anatomy of a normal lung. However, the definition of artifact does not appear adequate in our case. According to the Cambridge dictionary, "an artefact is something observed in a scientific investigation or experiment that is not naturally present but occurs as a result of the preparative or investigative procedure". According to the Merriam-Webster dictionary, "an artifact can be a defect in an image (such as a digital photograph) that appears as a result of the technology and methods used to create and process the image or it can be a product of artificial character (as in a scientific test) due usually to extraneous (such as human) agency". According to Collins, "an artifact is any non-natural feature or structure accidentally introduced into something being observed or studied". All these definitions

lead us to consider the existence of something false, of something wrong, or something conditioned by the process that produces the artifact.

On the contrary, pulmonary US signs have over the years shown considerable diagnostic accuracy, which has been usefully exploited by physicians in numerous pathologies. Although these signs do not explicitly reproduce anatomical details of the lung, they represent practical clinical information. Moreover, recent results provided by numerical simulations and experimental results obtained in the laboratory on physical lung phantoms have increased the robustness of the clinical information contained in the US lung signs [10–15]. Thanks to these results, what was before considered artefactual information has been decoded as physical information of the lung surface. The primary purpose of this paper is to outline how the so-called vertical artifacts are the responses of acoustic traps located on the lung surface and, consequently, to raise these acoustic signs to the level of anatomical information [13,14]. Secondarily, the paper aims to recall the main characteristics of the trap acoustic signs, describe the method that has been used to comprehend their genesis, and highlight their relationship with the surface histopathology of the lung. Moreover, the impact of the US equipment on the visual characteristics of the trap acoustic signs is addressed, and two important sources of potential signal alteration, which remain to be investigated, are illustrated.

2. Materials and Methods

Our interest in lung US as a team began in 2010, and just after a few months, we adopted a precise method of analysis which, in the subsequent years, provided significant results: the four-step method [13,14,16], which is illustrated in Figure 1.

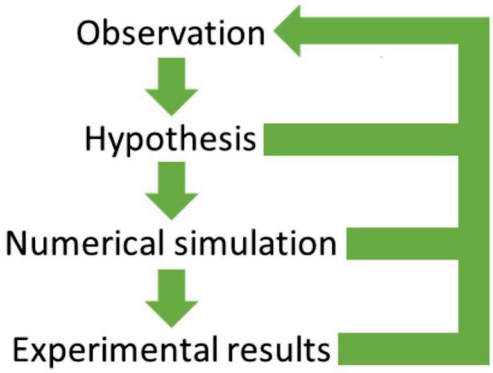

Figure 1. Schematic representation of the methodological approach used to investigate the genesis of the US signs, which are observed on lung US images in the presence of pulmonary pathologies.

The first step is to watch video clips of lung US exams, looking for ideas on the genesis of the observed acoustic signs. The second step is to formulate a reasonable hypothesis derived from, and consequently congruent with, the physics of acoustic wave propagation. The third step is to look for confirmation of the hypotheses by simulating the imaging process on numerical phantoms. The fourth and last step is to verify the hypotheses through experimental results on calibrated physical phantoms. As can be seen in Figure 1, a retroactive role of the previous steps is planned for each single step. For example, once a hypothesis that is based on the observation of numerous video clips is formulated, it is important to conduct a second round of visual analysis of the same video clips. This is because human vision is not limited to simple retinal vision. Important tasks of our vision system are explicated by the brain, and once a hypothesis is formulated, the brain setting changes, and new useful details can be captured on the same video clips.

The visual characteristics of the acoustic signs depend on many imaging parameters [14,17]. However, two important sources of signal alteration, which have never been considered before, have been highlighted during our analysis. Hereinafter, if not differently specified, images were acquired through the US advanced open platform (ULA-OP) [18].

This is a hardware-based research scanner [19] that allows the high programmability and flexibility needed to control and set specific imaging parameters, both in transmission and reception.

3. Results

3.1. The Four-Step Method

At first, we observed that the acoustic signs were oriented along the specific scan/imaging direction [20]. This observation led us to formulate the hypothesis of the acoustic trap [10] as a logical explanation of the acoustic signs observed on lung images: the pulse energy is partially "trapped and repeatedly bounced" in a spot on the lung surface, i.e., the trap, and is subsequently released while the probe and the system are still receiving and processing the RF signal from that direction.

A question, however, was raised: what mechanism, which is congruent with pulmonary anatomy, can trap the pulse energy? Two plausible hypotheses were analyzed: air bubble vibrations and multiple reflections between air bubbles. Both theoretical and experimental results provided the answer. From the Minnaert relationship [21,22], we know that an air bubble (for example, a partially filled alveolar sac) can vibrate once it is excited by an acoustic wave, but cannot re-radiate an US wave at radio frequency (2–6 MHz) unless the bubble is a microbubble with a diameter of a few microns. Experimental results also confirmed that isolated air bubbles do not give rise to acoustic signs [10]. Conversely, numerical simulation and experimental results showed that tissue mimicking volume surrounded by air bubbles (both tissue and bubbles, having sizes compatible with the pulmonary anatomy) can easily give rise to acoustic signs in the range of 2–6 MHz. This second observation suggested the plausible hypothesis that the observed acoustic signs are generated by multiple reflections of an acoustic wave propagating in a non-aerated medium (the interstitial medium) surrounded by aerated structures (the alveoli sacs) [10].

The third observation was related to the length of the trap acoustic signs. Physicians consider those signs that start at the pleura plane and extend to the bottom of the screen to be important [1,5]. Today, we know that this is not true and that the extension of the acoustic signs strongly depends on the imaging parameters [14,17], which often do not extend to the bottom of the screen, and that even those acoustic signs are extremely interesting for clinicians. However, even though they do not extend to the bottom of the screen, their length is an important feature, according to the clinicians' experience. A 12 cm long US sign was obtained for the first time in the laboratory when an agar gel volume completely surrounded by air, except for a 1 mm aperture at the top, was used [14]. However, the illuminating result was casually obtained later when a 2 mm agar disk was used as a phantom. The agar disk was positioned between two polyethylene films; the upper film was covered by a bed of water, which guaranteed a good acoustic matching between the agar disk and the probe, and the lower film, where the agar disk was sitting, separated the latter from the underlying air. The upper film under the weight of the water assumes a convex shape and rests only on the central part of the agar disk (Figure 2a). Figure 2b shows how the agar disk gives rise to a short reverberation in the center and longer reverberations on the periphery, where the agar is partially limited by air, even at its upper wall. Since the beam size is not infinitesimal, once it is reflected by the air underlying the lower film, it is partially intercepted by the air that separates the periphery of the disk from the water laying on the upper film. Consequently, the number of multiple reflections within the agar disk increases and, as a consequence, the length of the acoustic signs also increases. This casual experimental result clearly shows how the length of the trap acoustic sign (i.e., the time interval during which the trapped energy is gradually re-radiated) depends on the shape of the acoustic trap.

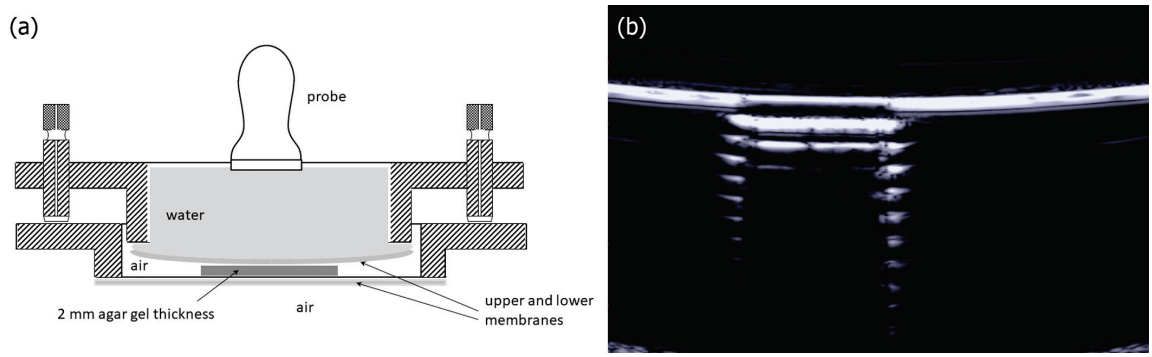

Figure 2. (**a**) Shows an agar disk positioned between two polyethylene films with the upper film that rests only on the central part of the agar disk. (**b**) Shows how the agar disk generates a short reverberation in the center and longer reverberations on the periphery where the agar is partially limited by air even at its upper wall.

In order to further verify the previous hypothesis, a video clip was acquired on a singular phantom, i.e., a drop of water falling from a water container. Initially, the drop is a hemisphere of water attached to the water container by means of a large surface. However, as its weight increases, it assumes the characteristic shape of a drop of water attached to a surface for a peduncle. Such a shape completely changes the response of the drop to the US since it is now limited by air even at the top, apart from a small channel of water that keeps the drop attached to the container. Now, two high acoustic impedance discontinuities (both below and above) reflect the acoustic waves, and the internal reverberation has a longer duration. Let us make a small hole in a polyethylene film that retains a bed of water, and let us acquire a US video clip of a drop of water while it is falling. Figure 3 shows some frames of the video clip. Initially, a short reverberation generated between the bottom of the drop and the polyethylene film is observed. Subsequently, as the size of the drop increases, the distance between the horizontal lines provided by the reverberations increases. The number of visible reverberations also increases until the drop reaches the necessary weight to detach and fall. In these last frames, the acoustic sign changes radically: it appears brighter and much longer. The length of the acoustic sign does not depend only on the volume of the drop, but it also depends on the liquid channel that connects the drop to the polyethylene film. The acoustic trap should be seen as an assembly of two elements: a channel that links the trap to the external medium and the chamber of the trap. The two examples given by the agar disk and by the drop of water show the importance of the experimental results obtained on physical phantoms (the fourth step).

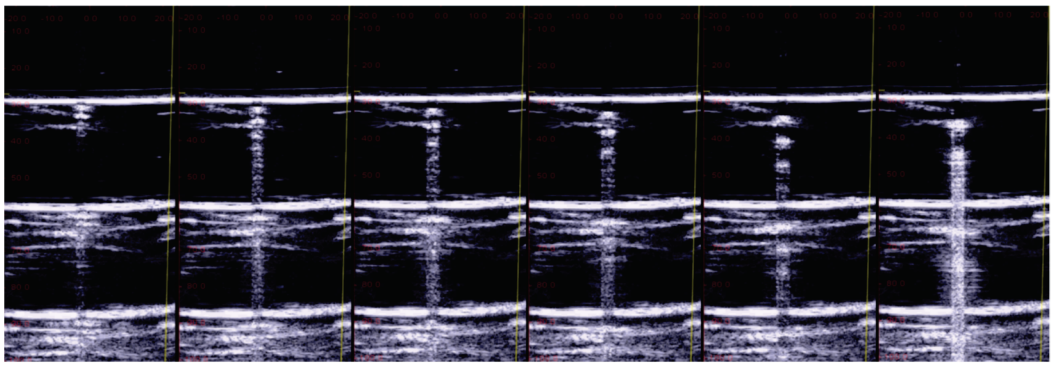

Figure 3. Example frames from a video clip during which a drop of water was acquired, with a linear US probe, while it was falling from a water container. From left to right, the number of observed reverberations and their spacing increase. The last frame shows how the trap acoustic sign changes radically (it appears brighter and much longer) when the drop reaches the necessary weight to detach and fall.

The importance of the third step was highlighted when another observation was analyzed. Physicians distinguish acoustic signs from modulated acoustic signs [23], and great importance is given to this distinction. Mostly, trap acoustic signs have a confused structure, but sometimes they have a clear periodical structure given by a cascade of small horizontal bright segments; these are the signs that physicians call modulated artifacts (Figure 4a). The genesis of these signs has been explained through the modulation transfer function of the acoustic trap (i.e., through its spectral signature). Due to the internal multiple reflections of the acoustic pulse and due to their constructive and destructive summations, the power spectrum of the acoustic signal, which is re-radiated from the trap, is given by a set of regularly spaced harmonics of the pulse spectrum, where the frequency intervals are inversely proportional to the sizes of the trap. For example, if the shape of an acoustic trap could be approximately defined by three dimensions d_1, d_2, and d_3, then its spectral signature would be characterized by the harmonics $f_{n,m,l}$:

$$f_{n,m,l} = \frac{c_0}{2}\sqrt{\left(\frac{n}{d_1}\right)^2 + \left(\frac{m}{d_2}\right)^2 + \left(\frac{l}{d_3}\right)^2} \quad (1)$$

where n, m, and l are integer numbers, and c_0 is the US propagation speed [24]. Equation (1) explains the different modulations that are observed in the lung US signs, which can also be replicated with a simple numerical simulation. The numerical simulation, however, provided an unexpected result. If the three dimensions d_1, d_2, and d_3 were reduced to a single dimension d (for example, if the trap shape was approximately spherical) and d was small, then the set of harmonics $f_{n,m,l}$ could be reduced to a single harmonic (in the frequency range of the probe). If a single harmonic was thus obtained, the image formation process would generate an acoustic sign with a uniform gray level. Such an acoustic sign had never been observed until then, and that challenged our hypothesis. A return to the first step (observation) was mandatory, and while watching the same video clips again, we surprisingly found the acoustic signs we had not previously noticed (Figure 4b). This anecdote illustrates the importance of numerical simulation, which should not be considered a simple verification process. Numerical simulation can provide important and unexpected suggestions that can further validate or reject the hypotheses under examination.

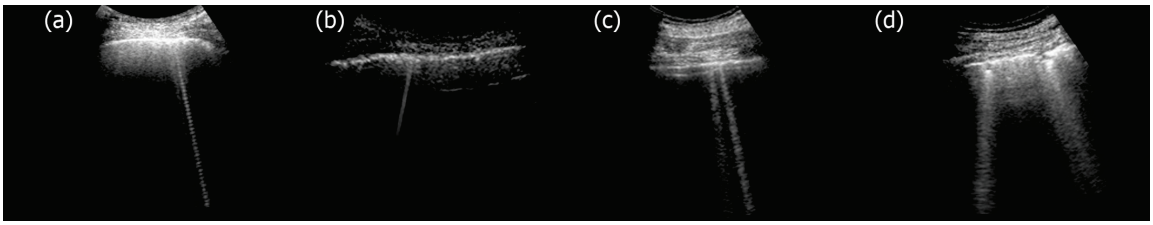

Figure 4. Lung US images acquired with a Toshiba Aplio XV scanner and a PVT-375BT convex probe are shown. From left to right, (**a**) a modulated acoustic sign, (**b**) an acoustic sign with a uniform gray level, (**c**) slight confused acoustic signs, and (**d**) confused acoustic signs starting beyond the pleura line are shown, respectively.

Some acoustic signs, however, are confused (Figure 4c). Often, they do not have the periodical structure of the modulated signs, and this is the fifth observation we analyzed. We do not have a definitive physical explanation for the latter yet. Experimental results on isolated traps and theoretical speculations suggest an explanation that, however, must be further explored. In a previous paper [13], it was shown how a modulated acoustic sign generated by a physical phantom becomes confused when the size of the trap input channel gradually increases (Figure 5). Here, it is suggested that the long modulated acoustic signs are probably generated by isolated acoustic traps that are connected to the thoracic wall through small interstitial channels. In this case, the trap acts as a point-like source of US

and, consequently, can both re-radiate the trapped energy slowly and eliminate the uneven acoustic perturbation of the particles of the medium at the top of the channel.

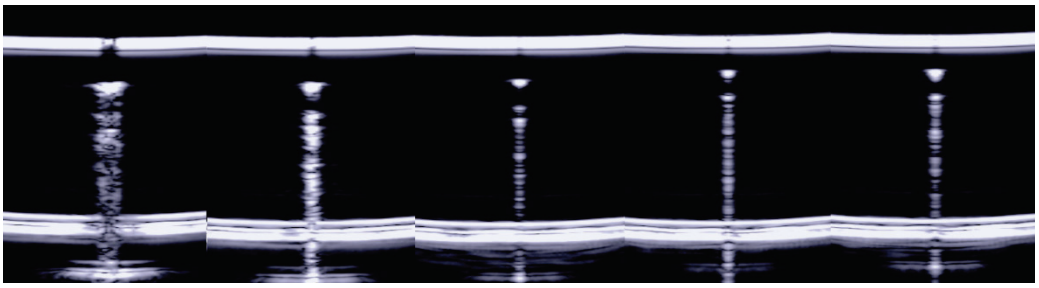

Figure 5. From right to left, the US images show how a modulated acoustic sign generated by a physical phantom becomes confused when the size of the trap input channel gradually increases.

This conclusion, based on theoretical speculations and experimental results, partially contradicts the theory of the spectral signature, according to which the modulated structure of the acoustic signs depends on the size of the traps. Here, we see that the structure of the trap acoustic sign depends also on the size and shape of the input channel. The response of an isolated acoustic trap to an US pulse should be analyzed as a function of both the acoustic channel and the trap chamber. The similitude with the Helmholtz resonator [25] is evident, even though the frequency range is completely different.

A more complex circumstance arises when non-isolated traps or traps having multiple input channels are considered. So far, these traps have not been specifically analyzed, even though a partial explanation has been given as an appendix of the White Lung investigation [10]. The so-called White Lung artifact was investigated through numerical simulation. The hypothesis that was formulated, through the visual analysis of numerous video clips acquired on different patients and the examination of their clinical diagnoses, was that of a distribution of small, aerated spaces, separated by thickened interstitial spaces. A stochastic process where every single reflection inside a distribution of traps was characterized by its own delay and amplitude was assumed. In addition to suggesting a physical explanation of White Lung, the same process also suggests a physical explanation of the local acoustic signs with a confused structure, which are observed, for example, in patients with pulmonary fibrosis or ARDS. The mathematical model provided images and acoustic signs that were very similar to those provided by the clinical cases of White Lung and fibrosis, respectively. Moreover, this is in line with what has been observed both in patients and on phantoms. In patients [26], the lung US images show how the US pattern changes by increasing the alveoli internal pressure and, consequently, their size and dominance with respect to the surrounding lung tissue. Analogously, on phantoms [27], US images show how the US pattern changes by increasing the dominance of the air spaces with respect to water. These articles show how the US pattern changes from White Lung to multiple unstructured acoustic signs and, subsequently, to isolated modulated signs by progressively increasing the dominance of the air spaces.

3.2. The Impact of Wrong Utilization of the Ultrasound Equipment

Every commercial US scanner uses a dynamic focusing algorithm in receive mode [28–31] to increase the quality of the acquired images. Once an US pulse is sent in a direction d_r, a scatterer s_c, located along this direction at a distance d from the probe, partially reflects the acoustic wave and generates an echo signal $s(t)$. Therefore, the N receiving elements, lined up on the head of the probe, receive N signals $s(t–t_i)$, where t_i is the time shift caused by the geometry of the receiving system. Consequently, in order to focalize the response of the scatterer s_c, the signals $s(t–t_i)$ are added by compensating the time shift t_i. However, since the time shift t_i depends on the distance d of the scatterer s_c from the probe, then the time shift t_i changes for every scatterer located along the direction d_r. The idea is to correctly focalize the response of every scatterer located along the scan direction d_r, even if their

distance from the probe varies. Consequently, a dynamic focusing algorithm is used in receive mode to vary the values of the time shift t_i as a function of the time t. The dynamic focusing algorithm (and the dynamic apodization algorithm, too) in receive mode increases the quality of the images when echoes coming from scatterers at different distances from the probe are expected. On the other hand, when a signal that has been radiated by an acoustic trap located at a fixed distance from the probe has to be analyzed, these algorithms should not be used since they introduce artifacts. In this case, the term artifact is correctly used since the two algorithms (the dynamic focusing and the dynamic apodization algorithms) alter the true signal. According to Collins, they accidentally introduce non-natural features into something being observed or studied.

Usually, when the process of beam formation is analyzed, we refer to lateral focusing. Nevertheless, another source of data alteration is introduced by the elevation focus [29]. The latter is typically static (unless probes with active elements arranged in a matrix are used) since it is defined by the probe acoustic lens. This lens is designed to fix the elevation focus at the supposed center of the region of interest, which depends on the application. The problem is not trivial since, in lung US, clinicians use linear, convex, and cardiac probes indifferently. While the linear probe has been designed to study superficial structures, and, consequently, the focus of the acoustic lens is close to the head of the probe, the convex and the cardiac probes have been designed to study deeper structures, and the focus of their acoustic lens is far from the head of the probe. For example, Figures 6 and 7 show the beam profiles in elevation of the LA533 linear array probe from Esaote and of the CA631 convex array probe from Esaote, respectively, when pulses with a central frequency of 4 MHz are used.

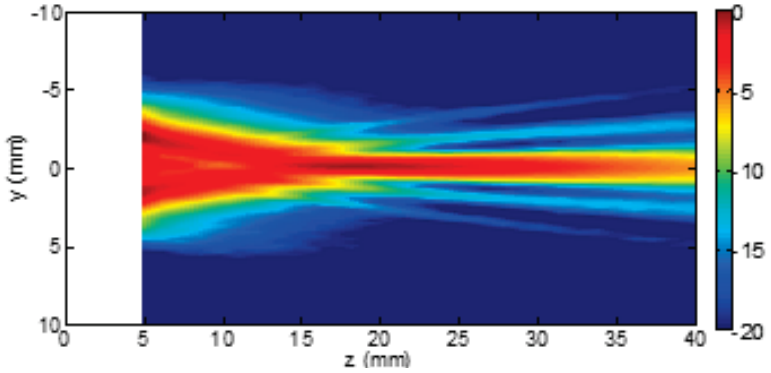

Figure 6. Elevation beam profile of the Esaote LA533 linear array probe when pulses with a central frequency of 4 MHz are used. Figure courtesy of Esaote, Florence, Italy.

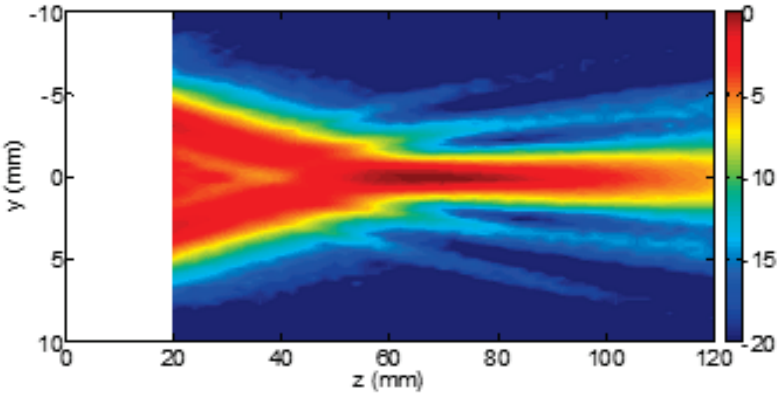

Figure 7. Elevation beam profile of the Esaote CA631 convex array probe when pulses with a central frequency of 4 MHz are used. Figure courtesy of Esaote, Florence, Italy.

Let the distance between the head of the probe and the pleura plane be approximately 20 mm. Then, the difference between the two beam sizes at the pleura plane is evident and substantial. The beam size is 2 mm or 10 mm when the LA533 or the CA631 is used, respectively. The LA533 is correctly used since its acoustic lens focalizes the beam at a mean distance of 20 mm, i.e., the LA533 has been designed and tuned to analyze structures at a mean depth of 20 mm. Convex and cardiac probes are not used correctly when they are used to analyze the pleural plane since they have been designed and tuned to analyze deeper structures. An increased size of the beam decreases the spatial resolution of the probe, and an irregular distribution of the beam energy (as in the case of the CA631 at the depth of 20 mm) alters the response of the pleural plane yielding to artifacts.

4. Discussion

After birth, the surface of the lung shows a porous structure, and in many pathologies, which still allow the aeration of the pulmonary cortex (the so-called interstitial pathology), the lung maintains a superficial porosity, with variable degrees of density and morphology depending on the pathology [32,33]. This also occurs when the lung tissue partially collapses, and the tissue does not show pathological changes. In these contexts, the assumption that the tissue component of the pleural surface may give rise to a distribution of acoustic channels and traps, surrounded by air spaces, is reasonable. In this case, the insonation of the pleural plane locally allows the trapping of the acoustic energy and its gradual re-radiation to the probe. These systems of channels and traps are normally present along the pleura (the normal interstitium), but the small size of the channels (often no more than 10 microns [34]) does not allow the transmission of a significant quantity of acoustic energy to the underlying tissue component. It is only when these channels widen, due to the presence of an interstitial pathology, that they allow the transmission of a quantity of energy that is sufficient to generate a visible acoustic sign during the re-radiation of the trapped energy [35].

A subpleural pathology of the lung, which allows the organ to maintain a certain degree of dispersed aeration, generates acoustic signs, as clinical evidence has repeatedly confirmed [6,36,37]. Similarly, deflation of the lung can produce focal densities in relation to the selective collapse of subpleural peripheral air spaces (folding of air spaces), with a critical reduction of aerated units [38]. Since the distribution of the acoustic traps represents the superficial (pathological or pathologically deflated) interstitium of the lung, a sort of parallelism between the distribution of the trap acoustic signs and the superficial histopathology of the lung sounds realistic.

While the concept of non-consolidated density has already been expressed in previous papers [8,39], no clear clinical interpretation has yet been made regarding the distribution and the visual characteristics of the trap acoustic signs (and, consequently, of the focal thickening of the pulmonary superficial, non-aerated medium). What is known is that different interstitial diseases of the lung may or may not involve the surface, and, consequently, that their US visibility depends on the surface involvement. Moreover, some of these diseases appear to be more evident in specific regions of the lung. Some diseases largely affect the surface of the lungs, while others show a preference for a location or a patchy appearance. These clinical aspects have already been described when focusing on the differential diagnosis between primitive pulmonary processes (fibrogenic diseases) and cardiogenic diseases [40,41]. Recent experiences with pneumonia from COVID-19 have been enlightening, and the distribution of the acoustic traps in these contexts offers a coherent explanation [23]. The acoustic trap theory allows clinicians to estimate the gravity of a specific pathology through the analysis of the distribution of the acoustic signs. Physiological acoustic traps of the normal lung cannot generate visible acoustic signs. Consequently, the more numerous the acoustic signs, the more severe the pathological involvement is. However, apart from the density and the topographic distribution of the trap acoustic signs, apart from their continuous or patched distribution, and apart from the appearance or not of White Lung, the acoustic trap theory suggests that the visual

structure of the acoustic signs may provide information regarding the geometry of the trapping systems. In other words, an acoustic sign can be considered a pathology footprint. The trapping system, with its combinations of acoustic channels and traps with variable characteristics, can roughly indicate groups of defined histopathologies.

The acoustic interaction of US with the surface of a lung when the latter is affected by an interstitial disease involves many traps with variable characteristics, such as size, morphology, and content. According to this, some correlations can be speculated. For example, a regular distribution of acoustic traps with small openings (channels) on the pleural surface is likely to generate images with many extended acoustic signs, starting from the pleura and having a modulated structure. Conversely, large access channels to acoustic traps would tend to produce larger, non-modulated, and often non-extended signs. This clear difference is observed when subjects with initial pulmonary edema (small channels derived from interlobular septa) and subjects with idiopathic pulmonary fibrosis are evaluated (large channels with variable size due to collagenization) [40]. Another aspect that must be considered is the visual localization of the bottom of the acoustic trap. The acoustic signs originate from the bottom of the trap, and, consequently, the depth of the trap can be estimated when they do not appear to originate from the pleural line (Figure 4d). Therefore, a trap acoustic sign that appears as starting beyond the reflection of the pleural line can indicate a primitively pulmonary (even micronodular) genesis because the initial hydrostatic edema (cardiogenic) does not produce acoustic traps with these characteristics [42].

The correlation between surface histopathology and the visual characteristics, distribution, and gray-level intensity of the phenomena currently defined as vertical artifacts will probably strengthen soon. The specificity of the acoustic signs will probably point clinicians toward specific groups of pathologies. In this sense, the epidemic of pneumonia from COVID-19 has taught us a lot [23,43], especially thanks to the variety and the temporal evolution of the finds. In COVID-19, early alveolar aspects appear as discontinuous acoustic signs associated with discontinuous areas of White Lung. Discontinuous acoustic signs are probably generated by discrete distributions of small channels that transmit, trap, and gradually re-radiate the acoustic energy. As for White Lung, its origin from the insonation of groups of homogeneous and closely packed small traps is conceivable. The presence of wide non-modulated signs, originating from the bottom of identifiable larger traps (the micro-consolidations), is only observed with the consolidating evolution of the disease. It is interesting to note that this evolution and the heterogeneity of findings is constant in all situations of alveolar damage (ARDS is the most typical case).

5. Limitations

One limitation of the method that has been introduced and illustrated in Section 2 is the difficulty to produce small durable phantoms. Calibrated physical phantoms with reproduced aerated volumes and tissue-mimicking septa that have dimensions similar to the real lung are needed to further investigate the US signs, but realizing the latter is challenging. Moreover, durable phantoms are also needed to guarantee the repeatability of the experimental step (the fourth step of the method). The agar gel that has been used so far is not suitable since, once exposed to air, it begins to dry, and its acoustic properties change. More complex mathematical models must be developed, and new materials must be explored to realize the physical phantoms [44,45].

The impact of the imaging parameters is another limitation of the methodology [14,17]. For example, it is difficult to distinguish the contribution of the imaging parameters to the length of a trap acoustic sign from the contribution of the trap geometry. Specific acquisition protocols could even be developed where every imaging parameter is exactly defined. However, differences between different US scanners and differences between different probes cannot be avoided.

6. Conclusions

Over the years, different terms have been used to highlight the lung US acoustic signs as opposed to the anatomical information. The terms ring-down artifact, comet-tail artifact, and vertical artifact have also been proposed, in addition to B-line. The two terms ring-down artifact and comet-tail artifact have been proposed in different papers by different authors and derive from analogies with similar phenomena suggested by the visual aspect of the examined acoustic sign. The comet-tail artifact [46] was described as a reverberation effect, and the ring-down artifact [47] was described as a resonance effect. All these terms have a common attribute: they consider trap acoustic signs as artifacts. However, all of them refer to trapped (absorbed, transmitted, etc.) energy that is subsequently released in the form of a periodic or confused signal. The acoustic traps can be seen as secondary sources of US. Consequently, trap acoustic signs highlight the presence of acoustic traps and quantitatively describe their distribution on the lung surface; they are not artifacts, but pathology footprints and anatomical information.

The term artifact does not do justice to the trap acoustic signs that are observed on US images of the lung. These acoustic signs are reproducible in the laboratory [13] and convey important clinical information. Even though they do not represent anatomical details of the lung in the proper sense, they originate from altered spots (acoustic traps) of the lung surface and represent a structural reality of the pathological lung.

It is undeniable that the diagnostic usefulness of lung US is limited to the lung pathologies that surface on the pleural plane. Lung US cannot provide information on deeper layers of the lung unless its aerated component is strongly reduced. However, the methodology that has been adopted to investigate the genesis of the acoustic signs has provided important results. Physical explanations of the main attributes of trap acoustic signs, such as their length, brightness, and shape, have been formulated thanks to the four-step method. Different approaches to the study of the information provided by lung US, such as those derived from artificial intelligence, could not have helped us to develop the physical knowledge of lung US that we have today. This research method is somehow comparable to the methodology that usually guides the clinical use of thoracic US (a practice that is known as Clinical US [48]).

The visibility and the visual characteristics of the acoustic signs, which are potentially generated by the traps once they have been activated by an US pulse, depend both on the trap geometry and the imaging parameters. The impact of the latter on the acoustic signs generated by specific traps is generally known, and, in our opinion, the problem can be partially overcome by analyzing how the response of the acoustic traps varies when varying the imaging parameters. However, two important sources of signal alteration are still ignored: when exploring the pleural plane of the lung, the dynamic focusing and apodization should be switched off. Moreover, given the geometric features of the acoustic lens, the impact of different probes on the visual aspect of trap acoustic signs should not be neglected.

Much work has still to be done, but in our opinion, the diagnostic potential of lung acoustic signs will progressively increase through a better understanding of the relationship between the visual aspects of these signs and the pathological morphology of the lung surface. What has so far been interpreted as an artifact should be perceived as a pathology footprint.

Author Contributions: Conceptualization, G.S. and M.D.; methodology, G.S.; software, A.R.; validation, M.D., G.S. and A.R.; formal analysis, M.D. and A.R.; investigation, M.D., G.S. and A.R.; resources, M.D. and A.R.; data curation, M.D. and G.S.; writing—original draft preparation, M.D. and G.S.; writing—review and editing, M.D. and A.R.; visualization, M.D. All authors have read and agreed to the published version of the manuscript.

Funding: This research received no external funding.

Institutional Review Board Statement: Not applicable.

Informed Consent Statement: Not applicable.

Data Availability Statement: Not applicable.

Acknowledgments: The authors wish to thank the engineer Rino Rossi for his precious contribution in making the phantoms. Moreover, the authors wish to thank the Fondazione della Cassa di Risparmio di Lucca for its invaluable support.

Conflicts of Interest: The authors declare no conflict of interest.

References

1. Lichtenstein, D.; Mezière, G.; Biderman, P.; Gepner, A.; Barré, O. The comet-tail artifact: An ultrasound sign of alveolar interstitial syndrome. *Am. J. Respir. Crit. Care Med.* **1997**, *156*, 1640–1646. [CrossRef]
2. Koegelenberg, C.F.; von Groote-Bidlingmaier, F.; Bolliger, C.T. Transthoracic ultrasonography for the respiratory physician. *Respiration* **2012**, *84*, 337–350. [CrossRef] [PubMed]
3. Vignon, P.; Repessè, X.; Vieillard Baron, A.; Maury, E. Critical care ultrasonography in acute respiratory failure. *Crit. Care* **2016**, *20*, 228. [CrossRef] [PubMed]
4. Rambhia, S.H.; D'Agostino, C.A.; Noor, A.; Villani, R.; Naidich, J.J.; Pellerito, J.S. Thoracic Ultrasound: Technique, Applications, and Interpretation. *Curr. Probl. Diagn. Radiol.* **2017**, *46*, 305–316. [CrossRef] [PubMed]
5. Mayo, P.H.; Copetti, R.; Feller-Kopman, D.; Mathis, G.; Maury, E.; Mongodi, S.; Mojoli, F.; Volpicelli, G.; Zanobetti, M. Thoracic ultrasonography: A narrative review. *Intensive Care Med.* **2019**, *45*, 1200–1211. [CrossRef]
6. Lichtenstein, D.A.; Mezière, G.A. Relevance of lung ultrasound in the diagnosis of acute respiratory failure: The BLUE protocol. *Chest* **2008**, *134*, 117–125. [CrossRef] [PubMed]
7. Volpicelli, G.; Elbarbary, M.; Blaivas, M.; Lichtenstein, D.A.; Mathis, G.; Kirkpatrick, A.W.; Melniker, L.; Gargani, L.; Noble, V.E.; Via, G.; et al. International Liaison Committee on Lung Ultrasound (ILC-LUS) for the International Consensus Conference on Lung Ultrasound (ICC-LUS). International evidence-based recommendations for point-of-care lung ultrasound. *Intensive Care Med.* **2012**, *38*, 577–591. [CrossRef]
8. Soldati, G.; Smargiassi, A.; Inchingolo, R.; Sher, S.; Nenna, R.; Valente, S.; Inchingolo, C.D.; Corbo, G.M. Lung ultrasonography may provide an indirect estimation of lung porosity and airspace geometry. *Respiration* **2014**, *88*, 458–468. [CrossRef]
9. Bushberg, J.T.; Seibert, J.A.; Leidholdt, E.M., Jr.; Boone, J.M. *The Essential Physics of Medical Imaging*; Williams & Wilkins: Philadelphia, PA, USA, 2002.
10. Demi, M.; Prediletto, R.; Soldati, G.; Demi, L. Physical mechanisms providing clinical informations from ultrasound lung images: Hypothesis and early confirmations. *IEEE Trans. Ultrason. Ferroelectr. Freq. Control* **2019**, *67*, 612–623. [CrossRef]
11. Kameda, T.; Kamiyama, N.; Taniguchi, N. The Mechanisms Underlying Vertical Artifacts in Lung Ultrasound and Their Proper Utilization for the Evaluation of Cardiogenic Pulmonary Edema. *Diagnostics* **2022**, *12*, 252. [CrossRef]
12. Allevato Martins da Silva, F.; Moreno, E.; Coelho de Albuquerque Pereira, W. B-Lines Lung Ultrasonography Simulation Using Finite Element Method. *Diagnostics* **2022**, *12*, 2751. [CrossRef] [PubMed]
13. Demi, M. On the Replica of US Pulmonary Artifacts by Means of Physical Models. *Diagnostics* **2021**, *11*, 1666. [CrossRef] [PubMed]
14. Demi, M. The impact of multiple concurrent factors on the length of the ultrasound pulmonary vertical artifacts as illustrated through the experimental and numerical analysis of simple models. *J. Acoust. Soc. Am.* **2021**, *150*, 2106. [CrossRef] [PubMed]
15. Kameda, T.; Kamiyama, N.; Taniguchi, N. The effect of attenuation inside the acoustic traps on the configuration of vertical artifacts in lung ultrasound: An experimental study with simple models. *J. Med. Ultrason.* **2022**, *49*, 545–553. [CrossRef] [PubMed]
16. Demi, M.; Buda, N.; Soldati, G. Vertical Artifacts in Lung Ultrasonography: Some Common Clinician Questions and the Related Engineer Answers. *Diagnostics* **2022**, *12*, 215. [CrossRef]
17. Mento, F.; Demi, L. On the influence of imaging parameters on lung ultrasound B-line artifacts, in vitro study. *J. Acoust. Soc. Am.* **2020**, *148*, 975. [CrossRef]
18. Boni, E.; Bassi, L.; Dallai, A.; Guidi, F.; Ramalli, A.; Ricci, S.; Housden, R.J.; Tortoli, P. A reconfigurable and programmable FPGA-based system for nonstandard ultrasound methods. *IEEE Trans. Ultrason. Ferroelectr. Freq. Control* **2012**, *59*, 1378–1385. [CrossRef]
19. Boni, E.; Yu, A.C.H.; Freear, S.; Jensen, J.A.; Tortoli, P. Ultrasound Open Platforms for Next-Generation Imaging Technique Development. *IEEE Trans. Ultrason. Ferroelectr. Freq. Control* **2018**, *65*, 1078–1092. [CrossRef]
20. Lu, J.-Y.; Zou, H.; Greenleaf, J.F. Biomedical ultrasound beam forming. *Ultrasound Med. Biol.* **1994**, *20*, 403–428. [CrossRef]
21. Minnaert, M. On musical air-bubblesand sounds of running water. *Phil. Mag.* **1933**, *16*, 235–248. [CrossRef]
22. Leighton, T.G. *The Acoustic Bubble*; Academic Press: Cambridge, MA, USA, 1994.
23. Soldati, G.; Demi, M.; Smargiassi, A.; Inchingolo, R.; Demi, L. The role of ultrasound lung artifacts in the diagnosis of respiratory diseases. *Expert Rev. Respir. Med.* **2019**, *13*, 163–172. [CrossRef]
24. Beranek, L.L. *Acoustics*; Acoustical Society of America: New York, NY, USA, 1993.
25. Wikipedia. Available online: https://en.wikipedia.org/wiki/Helmholtz_resonance (accessed on 15 February 2023).
26. Bouhemad, B.; Brisson, H.; Le Guen, M.; Arbelot, C.M.B.; Lu, Q.; Rouby, J.J. Bedside ultrasound assessment of positive end-expiratory pressure-induced lung recruitment. *Am. J. Respirat. Crit. Care Med.* **2011**, *183*, 341–347. [CrossRef] [PubMed]

27. Soldati, G.; Giunta, V.; Sher, S.; Melosi, F.; Dini, C. "Synthetic" comets: A new look at lung sonography. *Ultrasound Med. Biol.* **2011**, *37*, 1762–1770. [CrossRef]
28. Vogel, J.; Bom, N.; Ridder, J.; Lancee, C. Transducer design considerations in dynamic focusing. *Ultrasound Med. Biol.* **1979**, *5*, 187–193. [CrossRef] [PubMed]
29. Szabo, T.L. *Diagnostic Ultrasound Imaging: Inside Out*, 1st ed.; Academic Press: Cambridge, MA, USA, 2004.
30. Thijssen, J.M.; Mischi, M. Ultrasound Imaging Arrays. In *Comprehensive Biomedical Physics*; Elsevier: Amsterdam, The Netherlands, 2014; Volume 506, pp. 323–341.
31. Duck, F.A.; Baker, A.C.; Starritt, H.C. *Ultrasound Medicine*; Institute of Physics Publishing: Bristol, UK, 1998.
32. Weibel, E.R. How to make an alveolus. *Eur. Respir. J.* **2008**, *31*, 483–485. [CrossRef] [PubMed]
33. Leslie, K.O. Pathology of interstitial lung disease. *Clin. Chest Med.* **2004**, *25*, 657–703. [CrossRef]
34. Weibel, E.R. *Morphometry of the Human Lung*; Springer: Berlin/Heidelberg, Germany, 1963.
35. Leslie, K.; Wick, M. *Practical Pulmonary Pathology. A Diagnostic Approach*, 1st ed.; Churchill-Livingstone: Phildelphia, PA, USA, 2005.
36. Hasan, A.A.; Makhlouf, H.A. B-lines: Transthoracic chest ultrasound signs useful in assessment of interstitial lung diseases. *Ann. Thorac. Med.* **2014**, *9*, 99–103.
37. Reissig, A.; Copetti, R.; Kroegel, C. Current role of emergency ultrasound of the chest. *Crit. Care Med.* **2011**, *39*, 839–845. [CrossRef]
38. Scarpelli, E.M. The alveolar surface network: A new anatomy and its physiological significance. *Anat. Rec.* **1998**, *251*, 491–527. [CrossRef]
39. Soldati, G.; Inchingolo, R.; Smargiassi, A.; Sher, S.; Nenna, R.; Inchingolo, C.D.; Valente, S. Ex vivo lung sonography: Morphologic-ultrasound relationship. *Ultrasound Med. Biol.* **2012**, *38*, 1169–1179. [CrossRef]
40. Soldati, G.; Demi, M. The use of lung ultrasound images for the differential diagnosis of pulmonary and cardiac interstitial pathology. *J. Ultrasound* **2017**, *20*, 91–96. [CrossRef] [PubMed]
41. Copetti, R.; Soldati, G.; Copetti, P. Chest sonography: A useful tool to differentiate acute cardiogenic pulmonary edema from acute respiratory distress syndrome. *Cardiovasc. Ultrasound* **2008**, *29*, 6–16. [CrossRef] [PubMed]
42. Soldati, G.; Demi, M. What Is COVID 19 Teaching Us about Pulmonary Ultrasound? *Diagnostics* **2022**, *12*, 838. [CrossRef]
43. Demi, L. Lung Ultrasound: The future ahead and the lessons learned from COVID-19. *J. Acoust. Soc. Am.* **2020**, *148*, 2146. [CrossRef]
44. Spinelli, A.; Vinci, B.; Tirella, A.; Matteucci, M.; Gargani, L.; Ahluwalia, A.; Domenici, C.; Picano, E.; Chiarelli, P. Realization of a poro-elastic ultrasound replica of pulmonary tissue. *Biomatter* **2012**, *2*, 37–42. [CrossRef]
45. Zell, K.; Sperl, J.I.; Vogel, M.W.; Niessner, R.; Haisch, C. Acoustical properties of selected tissue phantom materials for ultrasound imaging. *Phys. Med. Biol.* **2007**, *52*, 475–484. [CrossRef]
46. Ziskin, M.C.; Thickman, D.I.; Goldenberg, N.J.; Lapayowker, M.S.; Becker, J.M. The comet tail artifact. *J. Ultrasound Med.* **1982**, *1*, 1–7. [CrossRef] [PubMed]
47. Avruch, L.; Cooperberg, P.L. The ring-down artifact. *J. Ultrasound Med.* **1985**, *4*, 21–28. [CrossRef]
48. Creditt, A.; Tozer, J.; Vitto, M.; Joyce, M.; Taylor, L. *Clinical Ultrasound: A Pocket Manual*; Springer: Berlin/Heidelberg, Germany, 2018.

MDPI
St. Alban-Anlage 66
4052 Basel
Switzerland
Tel. +41 61 683 77 34
Fax +41 61 302 89 18
www.mdpi.com

Diagnostics Editorial Office
E-mail: diagnostics@mdpi.com
www.mdpi.com/journal/diagnostics

Academic Open
Access Publishing

mdpi.com

ISBN 978-3-0365-8740-0